ISSN 1007-9327 (print)
ISSN 2219-2840 (online)

World Journal of *Gastroenterology*

Weekly Volume 31 Number 21 June 7, 2025

Published by Baishideng Publishing Group Inc

World Journal of Gastroenterology

Contents

Weekly Volume 31 Number 21 June 7, 2025

REVIEW

ORIGINAL ARTICLE

Retrospective Cohort Study

Retrospective Study

Observational Study

Basic Study

META-ANALYSIS

LETTER TO THE EDITOR

World Journal of Gastroenterology

Weekly Volume 31 Number 21 June 7, 2025

Contents

ABOUT COVER

Editorial Board Member of *World Journal of Gastroenterology*, Antonietta Gerarda Gravina, PhD, MD, Associate Professor, Department of Precision Medicine, Gastroenterology Unit, University of Campania "Luigi Vanvitelli", Naples 80138, Italy. antoniettagerarda.gravina@unicampania.it

AIMS AND SCOPE

The primary aim of *World Journal of Gastroenterology* (*WJG*, *World J Gastroenterol*) is to provide scholars and readers from various fields of gastroenterology and hepatology with a platform to publish high-quality basic and clinical research articles and communicate their research findings online. *WJG* mainly publishes articles reporting research results and findings obtained in the field of gastroenterology and hepatology and covering a wide range of topics including gastroenterology, hepatology, gastrointestinal endoscopy, gastrointestinal surgery, gastrointestinal oncology, and pediatric gastroenterology.

INDEXING/ABSTRACTING

The *WJG* is now abstracted and indexed in Science Citation Index Expanded (SCIE), MEDLINE, PubMed, PubMed Central, Scopus, Reference Citation Analysis, China Science and Technology Journal Database, and Superstar Journals Database. The 2025 edition of Journal Citation Reports® cites the 2024 journal impact factor (JIF) for *WJG* as 5.4; Quartile: Q1. The *WJG*'s CiteScore for 2024 is 8.1.

RESPONSIBLE EDITORS FOR THIS ISSUE

NAME OF JOURNAL
World Journal of Gastroenterology

ISSN
ISSN 1007-9327 (print) ISSN 2219-2840 (online)

LAUNCH DATE
October 1, 1995

FREQUENCY
Weekly

PUBLICATION DATE
June 7, 2025

PUBLISHING PARTNER
Shanghai Pancreatic Cancer Institute and Pancreatic Cancer Institute, Fudan University
Biliary Tract Disease Institute, Fudan University

INSTRUCTIONS TO AUTHORS
https://www.wjgnet.com/bpg/gerinfo/204

GUIDELINES FOR ETHICS DOCUMENTS
https://www.wjgnet.com/bpg/GerInfo/287

GUIDELINES FOR NON-NATIVE SPEAKERS OF ENGLISH
https://www.wjgnet.com/bpg/gerinfo/240

PUBLICATION ETHICS
https://www.wjgnet.com/bpg/GerInfo/288

PUBLICATION MISCONDUCT
https://www.wjgnet.com/bpg/gerinfo/208

POLICY OF CO-AUTHORS
https://www.wjgnet.com/bpg/GerInfo/310

ARTICLE PROCESSING CHARGE
https://www.wjgnet.com/bpg/gerinfo/242

STEPS FOR SUBMITTING MANUSCRIPTS
https://www.wjgnet.com/bpg/GerInfo/239

ONLINE SUBMISSION
https://www.f6publishing.com

PUBLISHING PARTNER's OFFICIAL WEBSITE
https://www.shca.org.cn
https://www.zs-hospital.sh.cn

World Journal of Gastroenterology

Submit a Manuscript: https://www.f6publishing.com

World J Gastroenterol 2025 June 7; 31(21): 106964

DOI: 10.3748/wjg.v31.i21.106964

ISSN 1007-9327 (print) ISSN 2219-2840 (online)

REVIEW

Recent advances and challenges in colorectal cancer: From molecular research to treatment

Gao-Xiu Qi, Rui-Xia Zhao, Chen Gao, Zeng-Yan Ma, Shang Wang, Jing Xu

Specialty type: Gastroenterology and hepatology

Provenance and peer review: Unsolicited article; Externally peer reviewed.

Peer-review model: Single blind

Peer-review report's classification

Scientific Quality: Grade A, Grade C, Grade C

Novelty: Grade A, Grade C, Grade C

Creativity or Innovation: Grade A, Grade C, Grade C

Scientific Significance: Grade B, Grade B, Grade C

P-Reviewer: Li HB; Li XY; Yang N

Received: March 12, 2025

Revised: April 22, 2025

Accepted: May 26, 2025

Published online: June 7, 2025

Processing time: 86 Days and 13.8 Hours

Gao-Xiu Qi, Rui-Xia Zhao, Chen Gao, Zeng-Yan Ma, Jing Xu, Department of Pathology, Qingdao Central Hospital, University of Health and Rehabilitation Sciences (Qingdao Central Medical Group), Qingdao 266042, Shandong Province, China

Shang Wang, Department of Pathology, School of Basic Medicine, Qingdao University, Qingdao 266071, Shandong Province, China

Corresponding author: Jing Xu, MD, Chief Physician, Department of Pathology, Qingdao Central Hospital, University of Health and Rehabilitation Sciences (Qingdao Central Medical Group), No. 127 Siliu South Road, Shibei District, Qingdao 266042, Shandong Province, China. katherine_xu@163.com

Abstract

Colorectal cancer (CRC) ranks among the top causes of cancer-related fatalities globally. Recent progress in genomics, proteomics, and bioinformatics has greatly improved our comprehension of the molecular underpinnings of CRC, paving the way for targeted therapies and immunotherapies. Nonetheless, obstacles such as tumor heterogeneity and drug resistance persist, hindering advancements in treatment efficacy. In this context, the integration of artificial intelligence (AI) and organoid technology presents promising new avenues. AI can analyze genetic and clinical data to forecast disease risk, prognosis, and treatment responses, thereby expediting drug development and tailoring treatment plans. Organoids replicate the genetic traits and biological behaviors of tumors, acting as platforms for drug testing and the formulation of personalized treatment approaches. Despite notable strides in CRC research and treatment - from genetic insights to therapeutic innovations - numerous challenges endure, including the intricate tumor microen-vironment, tumor heterogeneity, adverse effects of immunotherapies, issues related to AI data quality and privacy, and the need for standardization in organoid culture. Future initiatives should concentrate on clarifying the pathogenesis of CRC, refining AI algorithms and organoid models, and creating more effective therapeutic strategies to alleviate the global impact of CRC.

Key Words: Colorectal cancer; Molecular; Treatment; Artificial intelligence; Organoid

Core Tip: This study highlights recent advances and challenges in colorectal cancer from molecular research to treatment. Advances in genomics, proteomics, and bioinformatics have significantly enhanced our understanding of colorectal cancer's molecular mechanisms, driving targeted therapies and immunotherapies. However, tumor heterogeneity and drug resistance remain major hurdles. Artificial intelligence and organoid technology offer new opportunities.

Citation: Qi GX, Zhao RX, Gao C, Ma ZY, Wang S, Xu J. Recent advances and challenges in colorectal cancer: From molecular research to treatment. *World J Gastroenterol* 2025; 31(21): 106964
URL: https://www.wjgnet.com/1007-9327/full/v31/i21/106964.htm
DOI: https://dx.doi.org/10.3748/wjg.v31.i21.106964

INTRODUCTION

Colorectal cancer (CRC) is one of the most common malignant tumors in the digestive system, ranking third in incidence (9.6%) and second in mortality rate (9.3%) worldwide in 2022[1,2]. It poses a significant threat to the public[3]. The rising incidence of CRC can be attributed to lifestyle changes, such as reduced physical activity and a higher intake of high-fat foods[4]. By 2030, it is projected that there will be more than 2.2 million new cases of CRC worldwide, with an estimated 1.1 million deaths, further exacerbating the global health burden[5].

CRC progresses from normal epithelial cells through a process of uncontrolled growth, leading to the formation of polyps and ultimately cancer. Adenocarcinoma is the predominant subtype. The genetic landscape of CRC is complex, involving various molecular pathways that contribute to tumor development and metastasis[6]. Current treatment modalities include surgery, chemotherapy, radiotherapy, and targeted therapies[7]. Surgical intervention is typically favored for early-stage CRC, while patients with advanced disease often require a combination of therapies. However, these treatment options have their drawbacks: Chemotherapy can lead to adverse effects such as nausea and hair loss, and tumor cells may develop resistance to drugs. Immunotherapy can boost immune responses but is primarily effective for a limited group of patients[8]. Targeted therapies aim to inhibit specific mutations but are restricted to individuals with particular genetic alterations and may encounter secondary resistance. Overall, existing treatment strategies do not fully address clinical needs, as treatment outcomes remain suboptimal, recurrence rates are high, and patients' survival and quality of life are significantly impacted[9].

"Precision medicine" emphasizes personalized approaches to disease diagnosis, treatment, and prevention by considering individual variations. It employs omics technologies, including genomics and proteomics, to analyze, identify, validate, and apply biomarkers for large populations and specific diseases. The objective is to identify disease causes and therapeutic targets while accurately subclassifying disease states and processes. In 2012, The Cancer Genome Atlas (TCGA) research network published a comprehensive molecular characterization of human CRC in Nature. This marked the third malignant tumor for which cancer genomic information was released by the TCGA project team, heralding the onset of the "precision medicine" era for CRC. The TCGA project utilizes molecular markers to develop models for prognosis and treatment guidance. In the realm of CRC, initial prognostic assessments were based on a limited number of markers, including chromosomal instability (CIN), microsatellite instability (MSI), and the CpG island methylator phenotype (CIMP). Experts have since incorporated genetic mutations, copy number variations, methylation patterns, microRNA profiles, and proteomic data to categorize CRC into four consensus molecular subtypes (CMS)[10]: CMS1 (MSI immune), CMS2 (canonical), CMS3 (metabolic), and CMS4 (mesenchymal). The CMS classification system is now regarded as the most reliable framework for CRC, offering clear biological insights and guiding future clinical stratification and targeted interventions.

The integration of artificial intelligence (AI) in healthcare is rapidly advancing precision medicine[11]. Notable advancements include pathological diagnosis, imaging diagnostics, molecular diagnostics, personalized treatment, and drug discovery[12]. AI identifies new molecular markers and therapeutic targets by analyzing genomic, radiomic, and clinical data, thereby improving diagnostic accuracy and treatment effectiveness. AI can evaluate pathological images using deep learning (DL) algorithms, automatically detecting tumor cells and characteristics of the microenvironment, and assisting clinicians in diagnosis and classification[13]. Furthermore, AI can forecast a patient's response to various treatment options based on their genomic and clinical data, providing valuable insights for clinicians to formulate personalized treatment plans[14].

Despite the array of treatment options available for CRC, including surgery, chemotherapy, radiotherapy, and targeted therapies, these approaches encounter challenges such as drug resistance and insufficient personalized precision. Organoid technology addresses these challenges by accurately mimicking the tumor microenvironment in vitro, preserving tumor heterogeneity, and facilitating high-throughput drug screening[15]. Patient-derived tumor organoids (PDOs) replicate the genetic features of original tumors, improving evaluations of drug sensitivity and resistance while supporting personalized treatment strategies[16]. When combined with advanced techniques like single-cell sequencing and genome analysis, organoids offer a powerful platform for new drug development and predicting therapeutic outcomes, thereby advancing disease research[17]. In summary, organoid technology holds significant potential for enhancing CRC diagnosis and treatment.

With the swift progress in molecular pathology and the emergence of precision medicine, the development of individualized treatment plans has become a crucial priority to improve both survival rates and quality of life for

patients. This paper explores the molecular mechanisms underlying CRC, personalized treatment strategies, and the application of AI and organoids in the management of CRC.

GENETIC AND EPIGENETICS ALTERATIONS IN CRC

At the molecular level, CRC arises from the cumulative effects of polygenic and epigenetic alterations. Similar to other solid tumors, CRC exhibits significant heterogeneity, which can be attributed to at least three major molecular pathways: MSI, CIMP, and CIN[18]. From a therapeutic standpoint, MSI is linked to immunotherapy in CRC, while CIN and CIMP are not direct therapeutic targets; rather, they inform the selection of treatment strategies based on the specific gene mutations they induce. These pathways contribute to the progression of CRC through gene mutations, epigenetic alterations, and abnormal cell signaling mechanisms. The predominant pathway in CRC is CIN, which is present in approximately 85% of sporadic cases[19]. CIN can be divided into two categories: High-level CIN and low-level CIN. CIN is characterized by abnormal chromosome structure and number, loss of heterozygosity at tumor suppressor gene (TSG) loci, and chromosomal rearrangements, resulting in somatic copy number alterations (SCNA). These alterations are often associated with mutations in key genes such as adenomatous polyposis coli (*APC*), Kirsten rat sarcoma viral oncogene homolog (*KRAS*), phosphatidylinositol 4,5-bisphosphate 3-kinase catalytic subunit alpha (*PIK3CA*), B-raf proto-oncogene (*BRAF*), sma and mad homolog (*SMAD)*, and tumor protein 53 (*P53*)[20], which are crucial for regulating cell proliferation and the cell cycle, thus playing a significant role in CRC development. Another important pathway is MSI, which arises from the malfunction of DNA mismatch repair (MMR) genes during DNA replication and repair processes. This malfunction leads to a shift from microsatellite stability (MSS) to instability. MSI is often linked to a genetic predisposition characterized by high variability and can be further classified into high MSI (MSI-H) and low MSI (MSI-L). The third major pathway is CIMP. Tumors classified as CIMP-high (CIMP-H) exhibit *BRAF* mutations, MutL homolog 1 (MLH1) methylation, and silencing of *MGMT* or *CDKN2A*, whereas CIMP-low *(*CIMP-L*)* tumors are associated with *KRAS* mutations[21].

THE MECHANISM OF CRC OCCURRENCE AND DEVELOPMENT

The progression of CRC typically follows an adenoma-carcinoma-metastasis model (Figure 1), evolving from aberrant crypt foci to benign adenomatous polyps and ultimately to sporadic CRC over a span of 10 years to 15 years. This model is observed in 70% to 90% of cases. The malignant transformation involves three critical stages: Stem or epithelial cells acquire driver mutations; mutant cells outcompete wild-type cells to dominate the crypt (clonal fixation); and mutant crypts expand through crypt division (clonal expansion)[22]. These processes are linked to sequential mutations in genes such as *APC*, *KRAS*, and *TP53*. According to the multi-step genetic model proposed by Fearon and Vogelstein[23], the early inactivation of the TSG *APC* located on chromosome 5q21-q22 is essential. Mutations in *APC* lead to aberrant *Wnt/β-catenin* signaling[24,25], which promotes cell proliferation and inhibits apoptosis, a crucial step in benign polyp formation. CRC develops through the activation of proto-oncogenes and the inactivation of TSGs. *KRAS* mutations facilitate continuous signaling for cell growth and survival, driving the formation and expansion of adenomatous polyps. In advanced macroadenomas, additional driver mutations accumulate. The deleted in colorectal carcinoma gene influences cell adhesion pathways, impacting tumor progression. Mutations in *BRAF V600E*, *SMAD4/DPC4*, and alterations in the transforming growth factor beta (*TGF-β*) pathway affect cell migration and invasion. Changes in the phosphatidylinositol 3-kinase (*PI3K*) - protein kinase B (*AKT*) pathway, including mutations in *PIK3CA* and phosphatase and tensin homolog, lead to uncontrolled cell proliferation. Defects in *MMR* genes, such as *MLH1* and *MSH2*, result in MSI, producing tumors with unique clinical features and potentially improved prognosis. Collectively, these genetic alterations transform normal cells into cancer-associated fibroblasts (CAFs) and colon cancer stem cells, creating a signaling environment that fosters tumor growth. The final genetic alteration in the transition from advanced adenomas to aggressive cancers, as outlined in the Vogelstein model, is the inactivation of *P53*. Mutations in *P53* enable cells with accumulating genetic abnormalities to survive and proliferate, promoting the development and metastasis of aggressive cancers. Known as the "guardian of the genome", *P53* plays a vital role in DNA repair, cell cycle regulation, and apoptosis. These genetic changes also induce epigenetic alterations, particularly CIN. Hypermethylation silences TSGs, while hypomethylation leads to the overexpression of proto-oncogenes. The CIMP, characterized by frequent methylation events, is strongly associated with CRC.

Not all CRCs strictly adhere to this conventional pathway. Approximately 15% develop through the serrated pathway and exhibit distinct molecular characteristics (Figure 1). Serrated tumors can progress *via* two primary routes: The traditional serrated pathway and the sessile serrated pathway[26]. The traditional serrated pathway primarily occurs in the proximal colon, beginning with *KRAS* mutations. It progresses from hyperplastic polyps rich in goblet cells to traditional serrated adenomas (TSA). Methylation of *MGMT* and other TSGs leads to TSA with high-grade dysplasia. Further genetic alterations result in serrated adenocarcinoma (SAC), characterized by MSI-L/CIMP-L or MSS/CIMP-L, indicating aggressive CRC[27]. The sessile serrated pathway mainly affects the right-sided colon, starting with *BRAF* mutations. Microvesicular hyperplastic polyps progress to sessile serrated lesions (SSL). This progression involves MLH1 methylation and other TSG methylation events, advancing to SSL with high-grade dysplasia. Continued genetic changes culminate in SAC, characterized by MSI-L/CIMP-H or MSI-H/CIMP-H, which also indicates the presence of invasive CRC. In summary, both the traditional serrated pathway and the sessile serrated pathway are significant routes in colorectal carcinogenesis. These pathways exhibit higher rates of *BRAF* and *KRAS* mutations, increased CIN, and elevated

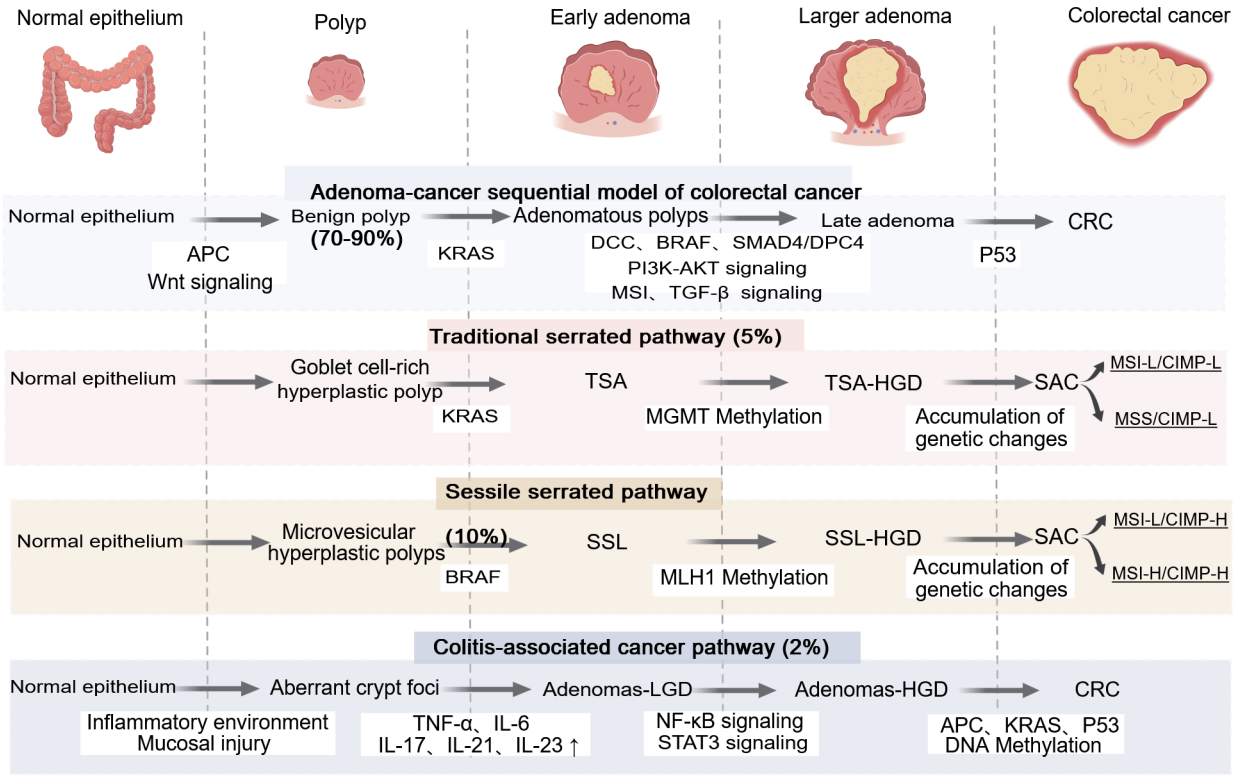

Figure 1 Four distinct pathways of progression from polyps to colorectal cancer, each characterized by specific molecular alterations. Created with MedPeer (medpeer.cn). Copyright permission has been obtained in the Supplementary material. These pathways include the adenoma-carcinoma-metastasis sequence, the traditional serrated pathway, the sessile serrated pathway, and cancers associated with colitis. DCC: Deleted in colorectal cancer; BRAF: B-raf proto-oncogene; SMAD4: Sma and mad homolog; DPC4: Sma and mad homolog family member 4; MGMT: O-6-methylguanine-DNA methyltransferase; MLH1: MutL homolog 1; AKT: Protein kinase B; PI3K: Phosphatidylinositol 3-kinase; TGF-β: Transforming growth factor beta; MSI: Microsatellite instability; TGF: Transforming growth factor; CRC: Colorectal cancer; CIMP-H: CpG island methylator phenotype-high; CIMP-L: CpG island methylator phenotype-low; MSS: Microsatellite stability; MSI-H: High microsatellite instability; MSI-L: Low microsatellite instability; TSA: Traditional serrated adenomas; TSG: Tumor suppressor genes; TSA-HGD: Traditional serrated adenomas with high-grade dysplasia; SSL: Sessile serrated lesions; SSL-HGD: Sessile serrated lesions with high-grade dysplasia; CAC: Colitis-associated cancer; Adenomas-LGD: Adenomas with low-grade dysplasia; Adenomas-HGD: Adenomas with high-grade dysplasia; SAC: Spindle assembly checkpoint; TNF-α: Tumor necrosis factor-α; IL: Interleukin; NF-Kb: Nuclear factor kappa B; APC: Adenomatous polyposis col; KRAS: Kirsten rat sarcoma viral oncogene homolog; STAT3: Signal transducer and activator of transcription 3.

hypermutation rates, but they rarely involve *APC* mutations. Familial and hereditary CRCs, such as Lynch syndrome caused by germline MMR gene mutations, account for about 5% of cases and are often associated with MSI-H.

Colitis-associated cancer (CAC), a specific form of CRC, primarily affects patients with inflammatory bowel disease (Figure 1). CAC constitutes only about 2% of all CRC cases, and most patients with inflammatory bowel disease do not develop it[28]. Compared to sporadic or familial CRC, CAC shares both similarities and distinct features in etiology, genetic alterations, and treatment approaches[29]. Chronic intestinal inflammation, as observed in ulcerative colitis and Crohn's disease, elevates the risk of CAC in proportion to the duration and severity of the inflammation. Ongoing inflammation leads to DNA damage, activates inflammatory pathways such as nuclear factor kappa B (*NF-kappa B*) and signal transducer and activator of transcription 3 (*STAT3*), and induces mutations in critical genes including *P53*, *KRAS*, and *APC*. Epigenetic modifications, such as DNA methylation and alterations in MMR genes, contribute to dysplasia in epithelial cells. The regulation of the immune system fosters an immunosuppressive microenvironment that is conducive to tumor growth. As additional genetic and epigenetic changes accumulate, adenomas with low-grade dysplasia and those with high-grade dysplasia may progressively develop and ultimately progress to CAC.

SIGNIFICANT BIOLOGICAL DISTINCTIONS BETWEEN THE LEFT AND RIGHT-SIDED COLON

The distinction between right and left colon cancer is not uniformly defined. The most common classification identifies cancers located proximally to the splenic flexure as right-sided colon cancer, while those at or distal to the splenic flexure are classified as left-sided colon cancer (Figure 2). According to the CMS classification, left-sided colon cancers predominantly fall under the CMS2 subtype, which is associated with a more favorable prognosis, whereas right-sided colon cancers are primarily classified as CMS1, indicating poorer outcomes[30]. This classification reflects their embryonic origins: The proximal two-thirds of the transverse colon develop from the midgut, while the distal third originates from the hindgut[31]. Right and left colon cancers exhibit differences in embryonic origin, anatomical structure, and physiological function, leading to distinct genetic and epigenetic profiles[32]. These variations influence drug respons-

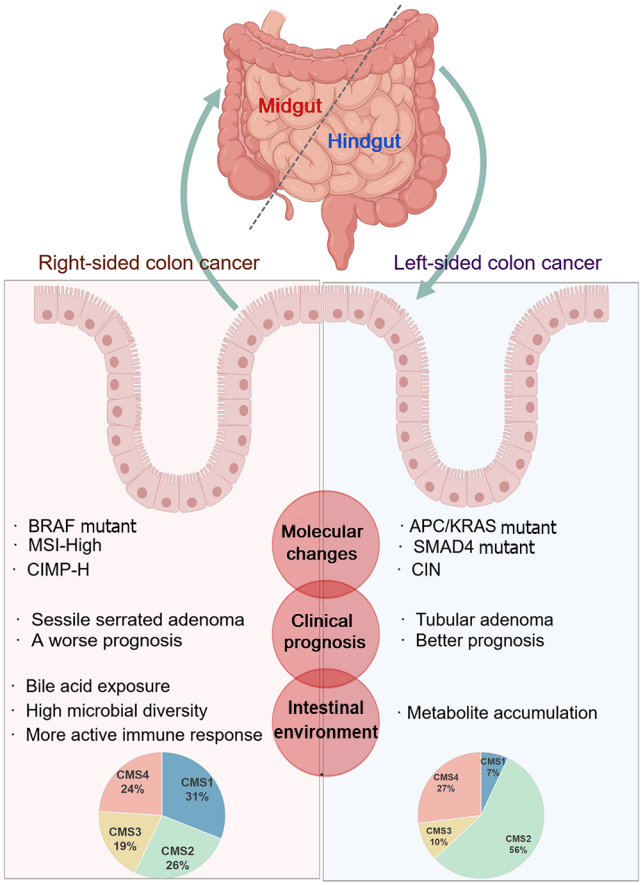

Figure 2 Biological characteristics and molecular distinctions between the left and right - sided colon. Created with MedPeer (medpeer.cn). Copyright permission has been obtained in the Supplementary material. The figure details the differences in the origin, molecular changes, clinical prognosis, and intestinal environment of the left and right-sided colon cancer. CIN: Chromosomal instability; MSI-H: High Microsatellite instability; CIMP-H: CpG island methylator phenotype-high; CMS: Consensus molecular subtypes; APC: Adenomatous polyposis col; KRAS: Kirsten rat sarcoma viral oncogene homolog; SMAD4: Sma and mad homolog; BRAF: B-Raf proto-oncogene.

iveness, treatment strategies, and overall prognosis[33]. Therefore, it is crucial to evaluate right and left colon cancers as separate entities to develop more effective and personalized treatment approaches.

The right-sided colon (Figure 2) features a larger lumen with a thinner wall, primarily designed for the absorption of water and electrolytes, as well as the storage of feces. It receives digestive fluids, bile acids, and partially digested food from the small intestine. Despite the relatively short exposure time of carcinogens to the intestinal mucosa, there is a potential for increased exposure to carcinogens that are ingested through food. The greater microbial diversity in the right-sided colon can influence the immune microenvironment, promoting tumor cell proliferation, invasion, and metastasis[34,35]. The presence of abundant lymphoid tissue and immune cells leads to a more active immune response, which can affect tumor growth and metastasis. Right-sided colon cancer often manifests as sessile serrated adenomas, which are typically detected at later stages and are characterized by poor differentiation, high cellular atypia, frequent mucinous carcinoma, signet-ring cell carcinoma, undifferentiated carcinoma, and strong invasive and metastatic capabilities[36]. This contributes to the limited efficacy of conventional chemotherapy while showing better responsiveness to immunotherapy. Right-sided colon cancer is also associated with *BRAF* mutations, MLH1 hypermethylation, MSI positivity, and CIMP-H[37].

In contrast, the left colon (Figure 2) is smaller in size, has thicker walls, and exhibits faster peristalsis. It forms and transports more solid feces due to increased water absorption, resulting in a longer fecal residence time[38]. This prolonged retention can lead to the accumulation of potentially carcinogenic bacterial metabolites. Consequently, CIN is more prevalent in this region, associated with the inactivation of TSGs such as *APC*, *P53*, and *SMAD4*, as well as frequent mutations in *KRAS* and *PIK3CA*[39]. Left-sided colon cancer generally exhibits better differentiation compared to its right-sided counterpart, with tumor cell growth being more regular and less aggressive. These tumors often begin as tubular adenomas and progress to infiltrating and sclerotic adenocarcinomas with higher differentiation. Patients with left-sided colon cancer typically benefit from 5-fluorouracil (5-FU)-based adjuvant chemotherapy and targeted therapies, resulting in improved overall survival compared to those with right-sided tumors. Notably, anti-epidermal growth factor receptor (*EGFR*) monoclonal antibody therapies (such as cetuximab and panitumumab) demonstrate significantly better responses in left-sided colon cancer[40].

TRANSCRIPTOMICS-BASED CMS OF CRC

The development of cancer arises from complex interactions among multiple genes. TCGA project in the United States aims to uncover the genomic characteristics of cancer, facilitating advancements in diagnosis and treatment. Initially, prognosis relied on markers such as CIN, MSI, or CIMP. However, CRC exhibits significant histological heterogeneity both between and within patients[41]. Subsequent research utilizing Sanger sequencing identified transcriptome molecular subtypes, some of which displayed consistent features, while others lacked uniformity[42]. In 2015, the CRC Typing Consortium combined six classification systems, resulting in the identification of four CMS: CMS1 (MSI immune), CMS2 (classical), CMS3 (metabolic), and CMS4 (mesenchymal)[10]. Approximately 13% of CRC cases remain unclassified due to intratumoral heterogeneity and are categorized as mixed types. This classification aids in recognizing patient-specific disease characteristics and informing treatment decisions.

Key features of the CMS1

CMS1 (MSI immune) represents about 14% of CRC cases and is predominantly observed in females. It typically arises in the right-sided colon and is associated with higher histopathological differentiation. This subtype is linked to non-specific intestinal symptoms, including diarrhea and mucinous stools[43]. CMS1 is characterized by hypermutation but exhibits CIN-L. It encompasses most cases of MSI-H, CIMP-H, and *BRAF* mutations (Figure 3). Furthermore, it demonstrates increased gene expression related to immune cell infiltration and immune escape[44].

CMS1 displays high immunogenicity and significant immune cell infiltration (Figure 4), making it a candidate for immune checkpoint inhibitor therapy. *MMR* genes tend to accumulate mutations at a higher frequency compared to other genomic regions. As a result, MSI-H tumors exhibit a substantially elevated tumor mutational burden, with mutation levels 100 times to 1000 times greater than those in MSS tumors, which correlates with reduced overall survival in patients with a high tumor mutational burden. These mutations generate numerous neoantigens that activate the immune system, eliciting robust immune responses. CMS1 tumors are enriched with various immune cells, including $CD8^+$ cytotoxic T cells, natural killer cells, dendritic cells, regulatory T cells (Tregs), myeloid-derived suppressor cells (MDSC), tumor-associated macrophages, and B lymphocytes. Elevated levels of cytokines such as C-X-C motif chemokine ligands 9 (*CXCL9*), C-X-C motif chemokine ligands 10 (CXCL10), interferon-γ, and interleukin (IL)-15 enhance local immune activity and improve prognosis[45]. Key signaling pathways, including Janus activated kinase (*JAK*) - signal transducer and activator of transcription (*STAT*) (Figure 5)[46], promote inflammatory responses and the recruitment of immune cells. However, tumor cells can suppress T cell activity through the overexpression of immune checkpoint molecules[47]. Initially, CMS1 typically shows a more favorable prognosis, attributed to a high level of immune cell infiltration. However, the increased frequency of somatic mutations in CMS1 Leads to significant tumor heterogeneity. This heterogeneity facilitates the emergence of more aggressive and treatment-resistant mutations, particularly after therapeutic interventions. As a result, the prognosis for CMS1 worsens significantly following recurrence and metastasis.

In CMS1, *EGFR* activation initiates downstream signaling through the rat sarcoma (*RAS*)-rapidly RAF-mitogen-activated extracellular signal-regulated kinase (*MEK*)–extracellular signal-regulated kinase (*ERK*), mitogen-activated protein kinase (*MAPK*), and *PI3K-AKT*-mechanistic target of rapamycin (mechanistic target of rapamycin) pathways (Figure 5), resulting in cell cycle progression, enhanced DNA synthesis, increased cell survival, and morphological changes. Aberrant *EGFR* signaling is closely associated with cancer development, making targeted therapies against *EGFR* and its downstream components a critical focus in anti-cancer strategies[48]. Understanding these mechanisms could pave the way for novel therapeutic interventions for *EGFR*-mediated diseases. The *BRAF V600E* mutation, which substitutes valine with glutamate at position 600, is the most prevalent *BRAF* mutation in CRC, accounting for approximately 90% of all *BRAF* mutations[49]. This mutation leads to sustained activation of *MAPK* signaling, particularly through the *RAS-RAF-MEK-ERK* pathway, promoting tumor proliferation and metastasis[50]. In CMS1, the PIK3CA pathway is aberrantly activated due to gene mutations, resulting in *PI3K* activation, which catalyzes the conversion of phosphatidylinositol 4,5-bisphosphate to phosphatidylinositol (3,4,5)-trisphosphate, subsequently activating AKT and *mTOR*. This promotes cell proliferation, survival, and metabolic reprogramming to support rapid cell growth. The activation of the *PI3K/AKT/mTOR* pathway in CMS1 encourages the secretion of immunosuppressive factors by tumor cells, undermining antitumor immune responses and creating an unfavorable microenvironment. Despite *EGFR* activation in CMS1 CRC, treatment strategies prioritize immunotherapy over traditional targeted therapies due to complex genetics and diverse resistance mechanisms[51].

In CMS1, CIMP-H plays a significant role in tumor biology[52]. CIMP-H induces hypermethylation in gene promoter regions, silencing essential genes such as tumor suppressors and *MMR* genes, which leads to MSI-H[53]. This enhances the expression of immune-related genes, increasing immune cell infiltration and the expression of immune checkpoint genes, making CMS1 more responsive to immunotherapy. CIMP-H frequently co-occurs with *BRAF* mutations, activating the *MAPK* pathway and promoting tumor proliferation and survival.

Key features of the CMS2

CMS2 (canonical) accounts for approximately 37% of CRC cases and is the most prevalent CMS subtype, characterized by a broad range of onset ages and frequent localization in the left-sided colon and rectum[54]. It follows the adenoma-carcinoma progression sequence. Patients with CMS2 generally respond well to standard treatments and have a moderate to favorable prognosis, with high survival rates even after recurrence. Key biological characteristics include CIN, SCNA, elevated *P53* mutation rates, and a CIMP-L rate (Figure 3)[55].

The CMS2 subtype is marked by an immunosuppressive microenvironment with limited immune cell infiltration (Figure 4)[44]. Tumor cells suppress T cell activity through cytokines such as *TGF-β*, IL-10, and IL-6, with stromal cells

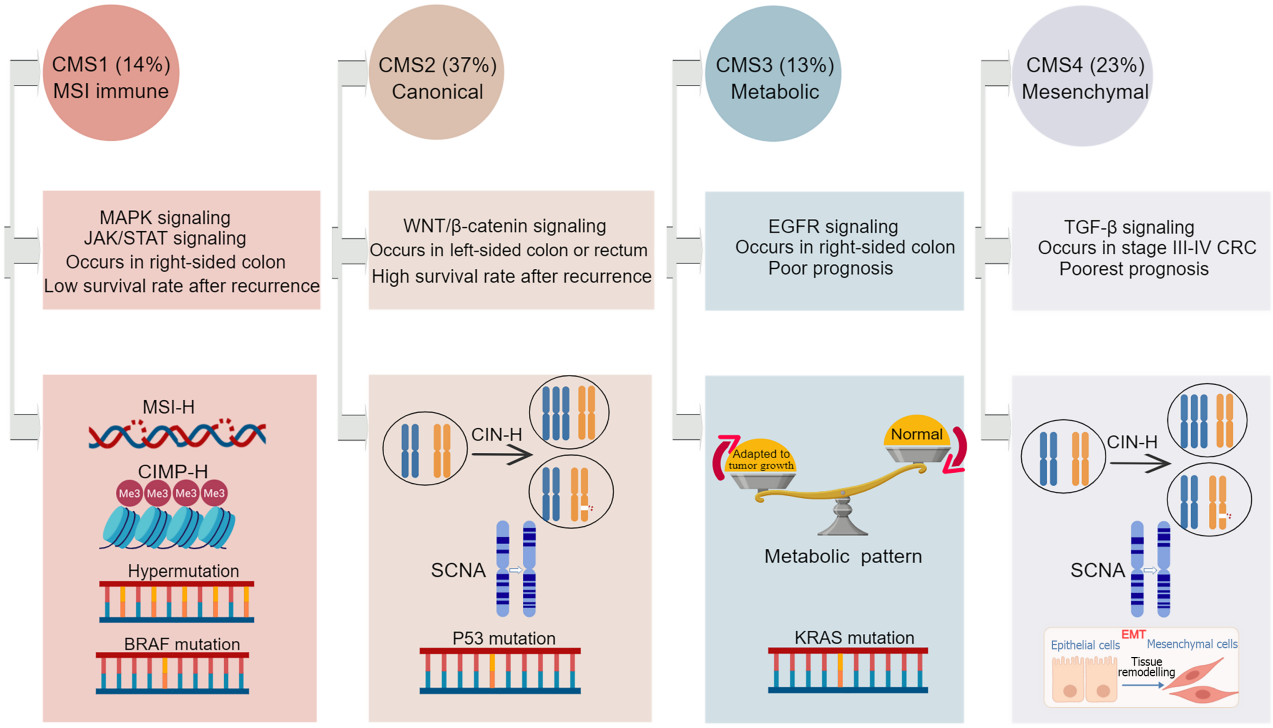

Figure 3 Key features of the four consensus molecular subtypes. Created with MedPeer (medpeer.cn). Copyright permission has been obtained in the Supplementary material. CRC: Colorectal cancer; CMS: Consensus molecular subtypes; CIN-H: High-level chromosome instability; CIMP-H: CpG island methylator phenotype-high; MSI-H: High microsatellite instability; SCNA: Somatic copy number alteration; EMT: Epithelial-mesenchymal transition; TGF-β: Transforming growth factor beta; MAPK: Mitogen-activated protein kinase; STAT: Signal transducer and activator of transcription; EGFR: Epidermal growth factor receptor; JAK: Janus kinase.

also contributing to this immune suppression. Immune cells are largely excluded from the tumor core, with only a few MDSC and Tregs present. This exclusion may result from abnormal molecular expression on tumor cells or altered extracellular matrix components. Additionally, low neoantigen production further restricts the immune response[56].

Activation of the *Wnt/β-catenin* pathway (Figure 5) in CMS2 typically arises from mutations in the *APC* gene or the nuclear accumulation of *β-catenin*[57]. The *Wnt* ligand binds to its frizzled receptor, leading to the inactivation of glycogen synthase kinase 3 beta. Mutated *APC* allows *β-catenin* to evade degradation, accumulate, and translocate into the nucleus, where it interacts with lymphoid enhancer-binding factor/T-cell factor (*TCF*) transcription factors to activate target genes such as the myelocytomatosis oncogene (*MYC*) proto-oncogene and *cyclin D1*[58]. These genes promote cell proliferation, inhibit apoptosis, and maintain stem cell characteristics. Notably, overexpression of *MYC* can induce "*MYC* addiction", making certain tumor cells highly reliant on *MYC* for survival, which provides a rationale for therapeutic targeting[59]. Aberrant activation of the *Wnt/β-catenin* pathway drives the transformation from adenoma to carcinoma and may contribute to the formation of tumor-initiating cell populations, which are potential sources of relapse and drug resistance [60]. Approximately 80% of *APC* mutations, one of the earliest genetic alterations in colorectal carcinogenesis, lead to increased nuclear *β-catenin* levels[61]. This results in the formation of the *TCF/β-catenin* complex, inhibiting epithelial differentiation and promoting tumorigenesis[62]. In CMS2, mutations in *PIK3CA* are common. These mutations in the p110α subunit of *PI3K* can aberrantly activate the *PI3K-Akt-mTOR* signaling pathway, leading to abnormal cell cycle progression, reduced cellular adhesion, decreased apoptosis, and angiogenesis, thereby facilitating tumor initiation and progression[63].

CMS2 tumors are frequently associated with CIN, resulting in abnormal chromosome numbers and structural aberrations due to mutations in key genes such as *P53* and *SMAD4*[64]. Inactivated *P53* impairs the DNA damage response, leading to CIN and increased genomic heterogeneity. CIN also enhances genetic variation within the tumor, affecting drug sensitivities and treatment efficacy. Understanding the role of CIN in CMS2 is crucial for predicting disease progression and developing personalized treatments. CMS2 tumors exhibit high proliferative activity; loss of *TP53* disrupts the balance between proliferation and apoptosis, promoting abnormal cell growth. *TP53* mutations are linked to lymphatic and vascular invasion, enhancing invasive and metastatic capabilities[65]. CRC patients with mutant *P53* demonstrate higher resistance to chemotherapy and poorer prognosis, which likely applies to CMS2 as well[66]. Reactivating *TP53* function shows promise as a therapeutic strategy, with encouraging results observed in cell lines and animal models. Furthermore, CIN manifests as SCNA, increasing genomic instability and enhancing tumor adaptability to environmental changes, impacting disease progression and treatment response.

Key features of the CMS3

CMS3 (metabolic) accounts for about 13% of CRC cases. This subtype primarily affects middle-aged patients in the right-sided colon. Most cases progress from adenoma to carcinoma, exhibiting localized invasive behavior with lower rates of

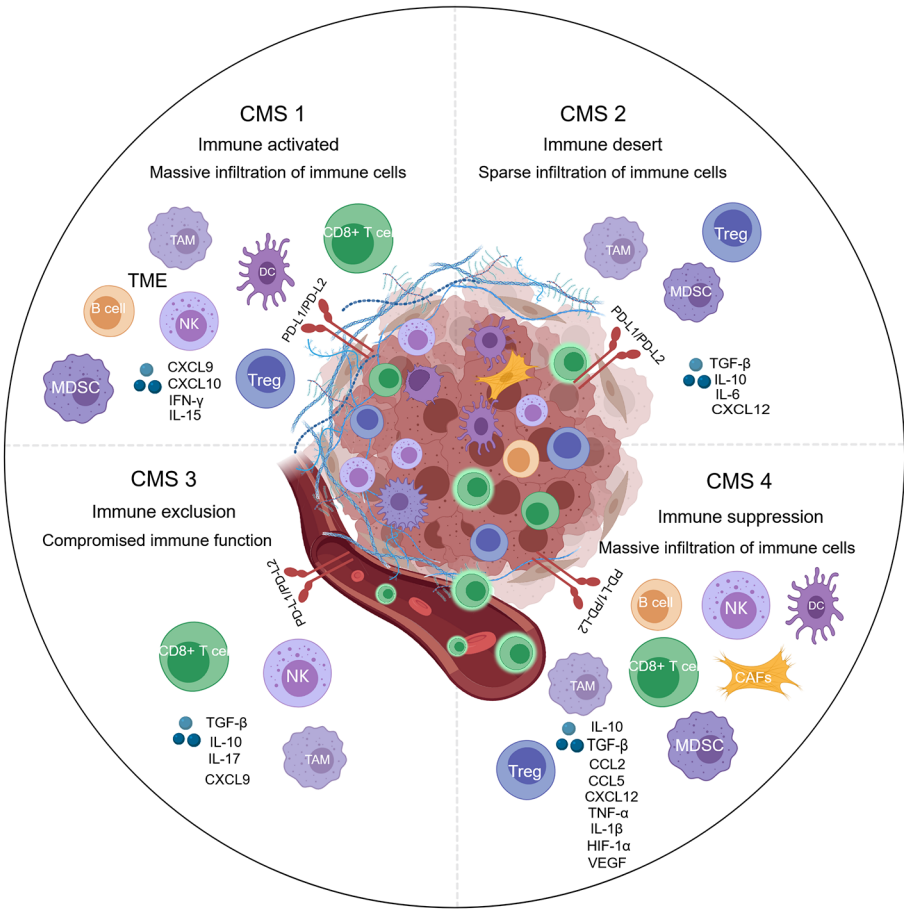

Figure 4 The distinct immune landscapes of the tumor microenvironments across the four consensus molecular subtypes of colorectal cancer. Created with MedPeer (medpeer.cn). Copyright permission has been obtained in the Supplementary material. Consensus molecular subtypes (CMS) 1 is characterized by an "immune activated" environment with massive immune cells. CMS2 is an "immune desert" with sparse infiltration of immune cells. CMS3 is called "immune exclusion", in which immune cells compromised are present and located on the periphery of the tumor nest. CMS4 exhibits "immune suppression", even with an abundance of immune cells. CRC: Colorectal cancer; CMS: Consensus molecular subtypes; DC: Dendritic cells; MDSC: Myeloid-derived suppressor cell; TAM: Tumor-associated macrophages; EMT: Epithelial-mesenchymal transition; PD-L1: Programmed death-ligand 1; PD-L2: Programmed death-ligand 2; IL: Interleukin; TGF-β: Transforming growth factor beta; TME: Tumor microenvironment ; NK: Natural killer; CXCL: C-X-C chemokine ligand; IFN: Interferon; CCL: Chemokine (C-C motif) ligand; HIF-1α: Hypoxia-inducible factor-1α; VEGF: Vascular endothelial growth factor.

lymph node metastasis and poorer overall survival. CMS3 shows fewer instances of CIN, a higher prevalence of CIMP (primarily CIMP-L), and approximately 30% of cases exhibit high mutation rates, enriched with *KRAS* mutations (Figure 3)[67].

The CMS3 subtype is characterized by impaired immune function, reduced immune cell infiltration, and increased levels of immunosuppressive factors (Figure 4)[44]. The metabolic reprogramming of tumor cells leads to immune cell dysfunction, such as inhibiting T-cell activity by consuming glucose and amino acids. Although CMS3 tumors generally show lower levels of immune cell infiltration, small populations of Tregs and MDSCs may still be present in the tumor microenvironment in certain instances. However, the functionality of these immune cells is often compromised, partly due to diminished antigen presentation on tumor cell surfaces or increased expression of immune checkpoint molecules such as programmed death-ligand 1 (*PD-L1*). Additionally, CMS3 tumors secrete various immunosuppressive factors, including IL-10, *TGF-β*, and IL-17, which weaken the host immune system's ability to combat cancer. These factors not only directly inhibit immune cell activity but also promote the proliferation of immunosuppressive cells, such as Tregs and MDSCs, leading to their accumulation within the tumor microenvironment. This creates an environment that is unfavorable for effective anti-tumor immune responses, further suppressing immune reactions[68].

In the intestinal mucosal epithelium, normal cells initially undergo a series of genetic changes, such as the inactivation of the *APC* gene, which is a crucial early event that leads to uncontrolled cell proliferation and the development of adenomas. Over time, additional genetic mutations, including *KRAS* mutations, gradually convert the adenoma into cancer. During this transformation, the metabolic profile undergoes remodeling, shifting from normal metabolic patterns to a tumor-adaptive metabolic phenotype. The most common alteration in CMS3 tumors is an activating *KRAS* mutation, which results in the persistent activation of the *RAS/RAF/MEK/ERK* signaling pathway (Figure 5)[69,70]. *KRAS*, a small guanosine-triphosphate hydrolase, activates a series of downstream effectors, including members of the *RAF* kinase family (*e.g.*, *BRAF*)[71], which subsequently activate *MEK* and *ERK* kinases. This activated pathway also drives metabolic reprogramming to meet the energy demands of rapid cell proliferation. For instance, it enhances glycolysis by regulating key enzymes such as glucose transporters and hexokinases, while simultaneously optimizing oxidative phosphorylation

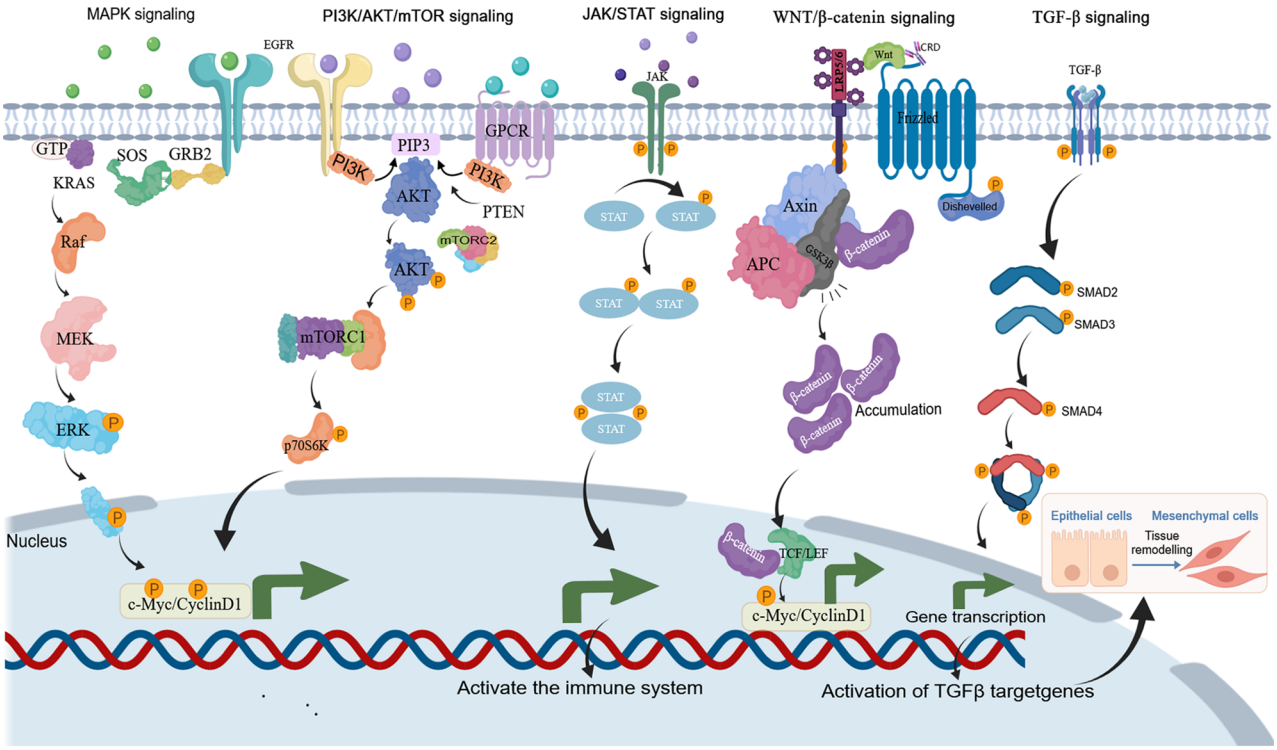

Figure 5 Key signaling pathways in colorectal cancer such as mitogen-activated protein kinase signaling, phosphatidylinositol 3-kinase/protein kinase B/mammalian target of rapamycin signaling, Janus kinase/signal transducer and activator of transcription signaling, Wnt/β-catenin signaling, transforming growth factor beta signaling. Created with MedPeer (medpeer.cn). Copyright permission has been obtained in the Supplementary material. MAPK: Mitogen-activated protein kinase; PI3K: Phosphatidylinositol 3-kinase; AKT: Protein kinase B; mTOR: Mechanistic target of rapamycin; JAK: Janus activated kinase; STAT: Signal transducer and activator of transcription; TGF-β: Transforming growth factor beta; SMAD: Sma and mad homolog; GPT: Guanosine Triphosphate; SOS: Son of sevenless; GRB2: Growth factor receptor-bound protein 2; MEK: Mitogen-activated protein kinase kinase; ERK: Extracellular signal-regulated kinase; AKT: Protein kinase B; PI3K: Phosphatidylinositol 3-kinase; PIP3: Phosphatidylinositol 3,4,5-trisphosphate; TCF: T-cell factor; LEF: Lymphoid enhancer-binding factor; EMT: Epithelial-mesenchymal transition.

by modulating mitochondrial function and fatty acid synthesis to ensure sufficient ATP production[72]. In addition to glycolysis, glutamine metabolism plays a significant role in CMS3. Glutamine, an amino acid and nitrogen source, is widely utilized for synthesizing nucleotides and proteins, and provides fuel for mitochondria through the tricarboxylic acid cycle. CMS3 tumor cells also enhance fatty acid synthesis to meet the demands of membrane structure renewal and signal transduction. At the same time, they maintain a certain level of fatty acid β-oxidation to balance energy needs and provide an additional energy source when required. Furthermore, the PI3K-*AKT*-*mTOR* pathway is central to regulating cell survival, migration, and angiogenesis[73] (Figure 5). In CMS3, *PI3K* catalyzes the production of phosphatidylinositol (3,4,5)-trisphosphate, which subsequently recruits and activates *AKT*. *AKT* then phosphorylates multiple substrates, including Raptor, a key component of the *mTORC1* complex, ultimately leading to the activation of *mTORC1*. *mTORC1* further regulates translation initiation factors, ribosome biogenesis, and other proteins related to cell growth while inhibiting autophagy to ensure an adequate supply of nutrients to sustain rapid tumor proliferation[74].

Key features of the CMS4

CMS4 (mesenchymal) accounts for approximately 23% of CRC cases. The age of onset is relatively younger, with tumors often diagnosed at later stages, commonly in stages III and IV, and a higher proportion of rectal cancer. Overall survival and recurrence-free survival rates are lower, making it the subtype with the poorest prognosis. This type of cancer is frequently associated with significant invasiveness and metastatic potential, particularly to the liver. This often necessitates more aggressive and comprehensive treatment approaches, including a combination of surgery, chemoradiotherapy, and novel targeted therapies to manage the disease. CMS4 is characterized by a high frequency of CIN, a high mutation rate of *P53*, and a low CIMP rate. It features epithelial-mesenchymal transition (EMT), upregulation of *TGF-β*, stromal infiltration, and angiogenesis as major traits (Figure 3). The tumor microenvironment is notably enriched in CAFs and immune cells[75].

The CMS4 subtype is marked by significant immune cell infiltration and an immunosuppressive microenvironment (Figure 4). CMS4 tumors are rich in various immune cell types, including $CD8^+$ T cells, natural killer cells, and TAM. However, the functionality of these immune cells is often suppressed, partly due to reduced antigen presentation on the surface of tumor cells or increased expression of immune checkpoint molecules such as *PD-L1*[76]. CAFs play a crucial role in modifying the tumor microenvironment by releasing cytokines and chemokines, which further suppress immune responses. For example, CMS4 tumors can diminish the host immune system's ability to combat cancer by producing

various immunosuppressive factors, such as *TGF-β* and IL-10, which assist the tumor in escaping immune detection. These factors not only inhibit immune cell function directly but also encourage the buildup of immunosuppressive cell types, including Treg and MDSC, thereby creating an environment that is detrimental to antitumor immune responses [77].

Within the CMS4 tumor microenvironment, CAFs release extracellular matrix components like collagen and fibronectin, along with growth factors such as platelet-derived growth factor, which alter the physical barriers surrounding the tumor. Additionally, CAFs facilitate angiogenesis by secreting vascular endothelial growth factor (*VEGF*) and other pro-angiogenic substances, ensuring the tumor receives adequate oxygen and nutrients. The *TGF-β* signaling pathway (Figure 5) governs various processes, including cell proliferation, differentiation, migration, and adhesion. When *TGF-β* binds to its receptors, it triggers receptor dimerization, forming a complex that activates signaling pathways. This process activates kinase domains that phosphorylate and activate *SMAD2/3* proteins, which then combine with *SMAD4* and move to the nucleus to regulate *TGF-β* target genes[78]. In advanced stages of CRC, elevated *TGF-β* expression leads to EMT. Consequently, increased invasion and cell migration result in diminished immune responses from normal cells. Moreover, the interaction between CAFs and tumor cells can amplify *TGF-β* signaling, prompting CAFs to secrete additional cytokines, thus perpetuating a harmful cycle. The EMT process enhances the migratory and invasive capabilities of tumor cells, facilitating metastasis to distant organs[79]. This process not only boosts migratory ability and invasiveness but also raises the risk of recurrence. Furthermore, the NOTCH pathway intensifies metastatic potential by promoting EMT and neutrophil infiltration[80]. Thus, CMS4 relies not only on inherent genetic changes but also on the contributions of CAFs and immune cells within the tumor microenvironment.

CIN is prevalent in CMS4 and significantly impacts tumor initiation and progression through various mechanisms. It primarily arises from critical gene mutations, including *P53* inactivation, *BUB1B*/*BUBR1*, and *AURKA*, which disrupt the cellular response to DNA damage and the proper distribution of chromosomes, leading to increased genomic heterogeneity[81]. The substantial genetic diversity resulting from CIN enhances the aggressiveness and metastatic potential of CMS4 tumors while facilitating stromal remodeling and EMT, which in turn promotes tumor cell migration and overall malignancy. Additionally, CIN modifies energy metabolism to meet the energy requirements of rapid cell proliferation and may create a microenvironment that is less favorable to anti-tumor immune responses through the generation of neoantigens and the release of immunosuppressive factors. Given the pivotal role of CIN in CMS4, developing therapeutic strategies that target CIN - such as stabilizing microtubules, enhancing spindle assembly checkpoint function, or combining with immunotherapy - has become a significant focus for future research. Accurately identifying and intervening in CIN-related molecular events holds promise for improving clinical outcomes for patients with CMS4.

IMMUNOTHERAPY FOR CRC

Immune checkpoint inhibitor therapy has revolutionized the treatment landscape for various solid tumors, demonstrating the potential for prolonged remission in patients with advanced metastatic disease who have undergone extensive prior therapies[82,83]. The CMS1 subtype is characterized by MSI-H and MMR deficiency (dMMR), showing exceptional responsiveness to immunotherapy. The landmark KEYNOTE-016 trial in 2015 first identified MSI-H/dMMR as a critical biomarker for assessing the effectiveness of immunotherapy, paving the way for future therapeutic advancements. In 2017, the Food and Drug Administration approved pembrolizumab and nivolumab, two anti-programmed cell death protein 1 (*PD-1*) monoclonal antibodies, for treating MSI-H/dMMR metastatic CRC. The pivotal phase III KEYNOTE-177 trial enrolled 307 patients with untreated metastatic MSI-H/dMMR CRC, randomly assigning them in a 1:1 ratio to receive either pembrolizumab or chemotherapy. With a median follow-up of 32.4 months, pembrolizumab showed a significant improvement in progression-free survival (16.5 months compared to 8.2 months). Notably, among patients achieving overall remission, 83% in the pembrolizumab group remained in remission at 24 months, in contrast to only 35% in the chemotherapy group[84,85]. This finding firmly establishes immunotherapy as the standard first-line treatment for MSI-H/dMMR CRC, including for patients who have previously been treated with 5-FU, oxaliplatin, and irinotecan.

Another significant mechanism of immunotherapy focuses on the interaction between *PD-1* and *PD-L1*. Elevated levels of *PD-L1* on tumor cells can serve as a predictive biomarker, suggesting that the tumor has established methods to evade immune responses. Tumors exhibiting high *PD-L1* expression tend to be more aggressive and associated with a poorer prognosis, yet they may also show increased sensitivity to immune checkpoint inhibitor therapies. Immunotherapeutic agents, such as pembrolizumab and nivolumab, which inhibit the *PD-1/PD-L1* interaction, have demonstrated effectiveness in certain *PD-L1*-positive CRC patients. Furthermore, cytotoxic T-lymphocyte-associated protein 4 (CTLA-4) is another crucial immune checkpoint marker in CRC[86]. Similarly, elevated CTLA-4 expression correlates with immune evasion and a worse prognosis, prompting the evaluation of CTLA-4-targeting therapies in clinical trials for their potential advantages. Lenz *et al*[87] reported the effectiveness of nivolumab (an anti-*PD-1* monoclonal antibody) combined with low-dose ipilimumab (an anti-CTLA-4 monoclonal antibody) as a first-line treatment for patients with metastatic MSI-H/dMMR CRC. The study found that this combination therapy achieved an objective response rate (ORR) of 69% and a disease control rate of 84% in untreated MSI-H/dMMR patients. Additionally, a higher presence of activated cytotoxic T cells within tumor-infiltrating lymphocytes often indicates a more favorable prognosis and suggests that the tumor may be more responsive to immune-based therapeutic strategies[88].

Immunotherapy for CRC has shown impressive efficacy in treating dMMR or MSI-H cancers, particularly with *PD-1*/*PD-L1* inhibitors providing long-lasting disease control for some patients. Checkpoint inhibitors enhance survival rates, and combination therapies exhibit promise. However, only about 5% of patients experience benefits, with poor outcomes

in MSS or dMMR cases, alongside immune-related adverse effects and tumor heterogeneity impacting efficacy. Challenges include accurate biomarker screening, treatment optimization, personalized care, accessibility to genomic analysis, and the exploration of combination strategies. Future research aims to identify new biomarkers, investigate synergies with other treatments, and address resistance mechanisms. Technological advancements and cost reductions are anticipated to make immunotherapy more accessible, providing effective personalized treatment to a larger patient population, ultimately improving outcomes, quality of life, and survival rates.

METABOLIC INHIBITORS FOR CRC

In recent years, the use of metabolic inhibitors in CRC treatment has garnered increasing interest. Currently, metabolic inhibitors like the glutaminase inhibitor CB-839 have shown significant antitumor effects in various studies. The CMS3 subtype is marked by considerable metabolic reprogramming, including the upregulation of the glutamine pathway, which is closely linked to *KRAS* mutations[89]. Research indicates that inhibiting specific amino acid transporters, such as amino acid transporter LAT1, can effectively reverse the hyperproliferative phenotype induced by *KRAS* activation, delay adenoma formation, and enhance sensitivity to *mTORC1* inhibitors. Zhao *et al*[90] found that CB-839, when used in conjunction with 5-FU, effectively inhibits the growth of PIK3CA-mutated CRC and induces tumor regression. Treatment with CB-839 increases the conversion of 5-FU to its active metabolite 5-fluoro-2′-deoxyuridine monophosphate by upregulating the expression of uridine phosphorylase 1, thereby intensifying the inhibition of thymidylate synthase by 5-FU. The study also reported that the combination of CB-839 and capecitabine (a prodrug of 5-FU) was well-tolerated in a phase I clinical trial and showed potential clinical benefits for patients with PIK3CA-mutated CRC. This suggests that targeting glutamine metabolism may represent an effective strategy for treating PIK3CA-mutated CRC and warrants further clinical investigation.

TARGETED THERAPY OF CRC

Targeted drugs for BRAF mutations

In the CMS1 subtype of CRC, the frequent presence of *BRAF* mutations, along with distinct characteristics of the tumor microenvironment, leads to unique biological behaviors and therapeutic challenges. Targeted therapies for *BRAF V600E* mutations primarily involve *BRAF* inhibitors and *MEK* inhibitors. Monotherapy with *BRAF* inhibitors has limited effectiveness; thus, combination therapy is necessary to overcome resistance. Clinical trials often combine *BRAF* inhibitors with *EGFR* inhibitors to achieve better outcomes[91]. The BEACON CRC phase III trial demonstrated that the triplet combination of encorafenib (a *BRAF* inhibitor), binimetinib (a *MEK* inhibitor), and cetuximab (an *EGFR* inhibitor), along with the doublet combination of encorafenib and cetuximab, significantly enhanced overall survival and response rates compared to standard treatments (encorafenib combined with irinotecan or FOLFIRI irinotecan, leucovorin, fluorouracil]) [92]. These results present new strategies for managing *BRAF V600E*-mutated CRC, particularly in the poor-prognosis CMS1 subtype. The SWOG S1406 study evaluated irinotecan and cetuximab with or without vemurafenib (a *BRAF* inhibitor) in patients with *BRAF*-mutated metastatic CRC. The findings indicated notable improvements in progression-free survival and ORRs with the addition of vemurafenib[93]. This suggests that combining vemurafenib with irinotecan and cetuximab may provide significant clinical advantages for CRC patients with the *BRAF* V600E mutation, extending this therapeutic benefit beyond the CMS1 subtype. A phase II trial (NCT03668431) investigated the combination of spartalizumab (a *PD-1* inhibitor), dabrafenib (a *BRAF* inhibitor), and trametinib (a *MEK* inhibitor). This combination achieved an ORR of 24.3% in patients with *BRAF V600E*-mutated CRC, surpassing control data[94]. Additionally, single-cell RNA sequencing analysis revealed that patients with favorable therapeutic responses exhibited enhanced activation of intrinsic immune programs within tumor cells and more comprehensive *MAPK* pathway inhibition. The integration of targeted therapy with chemotherapy or immunotherapy not only curtails tumor proliferation but also improves prognosis by bolstering immune responses, paving the way for new avenues in precision therapy. *BRAF*-targeted agents have shown effectiveness in CRC treatment, enhancing both progression-free survival and overall survival. However, challenges persist, including limited efficacy of monotherapy, restricted response rates, resistance issues, and uncertainty regarding the selection of combination therapies. Future advancements in understanding the mechanisms of *BRAF* mutations, developing novel targeted agents, and optimizing combination therapies may improve the effectiveness and applicability of *BRAF*-targeted treatments in CRC.

Targeted drugs for Wnt pathway

The *Wnt/β-catenin* signaling pathway is crucial in CRC, particularly in the CMS2 subtype. Research has investigated targeting this pathway as a therapeutic approach. Porcupine inhibitors, including LGK974, ETC159, and RXC004, inhibit *Wnt* activation by blocking the palmitoylation of *Wnt* ligands, thereby reducing cell proliferation and migration[95]. Approximately 80% of CRC cases display *APC* mutations, leading to abnormal *Wnt* activation, making Porcupine a significant target. SM08502 inhibits CDC-like kinase activity, disrupts spliceosome function, and decreases *Wnt*-related gene expression, demonstrating antitumor effects in gastrointestinal cancer models[96]. NU2058, a ran binding protein 3 inhibitor, selectively inhibits *β-catenin* nuclear translocation and induces senescence in CRC cells with nuclear *β-catenin* activation, effectively suppressing tumor growth in preclinical models. The combination of NU2058 with chemotherapeutic agents like oxaliplatin and irinotecan may enhance antitumor activity[97]. Xiang *et al*[98] identified adavivint a

small-molecule inhibitor that disrupts Zn^{2+} dependent a disintegrin and metalloproteinases 10/*NOTCH2/TCF7 L2* signaling independently of the canonical *Wnt/β-catenin* pathway, effectively suppressing CRC growth in both *in vitro* and *in vivo* models[98]. This highlights the Zn^{2+} dependent a disintegrin and metalloproteinases 10/NOTCH2 axis as a potential therapeutic target. Wu *et al*[99] conducted a detailed analysis of ovo-like zinc finger 2, emphasizing its vital role in regulating stem cell properties and immune cell infiltration, providing new insights into the *Wnt* pathway's role in various cancers[99]. Ovo-like zinc finger 2's regulatory effects on the *Wnt* signaling pathway and its influence on the tumor microenvironment offer potential strategies for targeting the CMS2 subtype of CRC. The *Wnt* signaling pathway is abnormally activated in most CRC cases. Drugs targeting the *Wnt* pathway can inhibit cancer cell growth, with some clinical trials demonstrating tumor reduction and decreased biomarkers. However, challenges include the complexity of the pathway, difficulties in precise inhibition, drug resistance, and a lack of predictive biomarkers. Advanced genomic analysis, high research and development costs, optimized dosing strategies, and clear treatment guidelines are essential. Future efforts may focus on developing precise inhibitors, exploring combination therapies, and identifying effective biomarkers to enhance treatment efficacy and scope.

Targeted drugs for MYC

MYC activation in CRC is influenced by signaling pathways such as *Wnt/β-catenin*, *MAPK*, and *PI3K/AKT/mTOR*, rather than through gene rearrangements or amplifications. This leads to increased *MYC* protein levels, which in turn promotes cancer progression and resistance to treatment. In the CMS2 subtype, the abnormal activation of these pathways is prevalent, making *MYC* a compelling therapeutic target[100]. Considerable advancements have been made in the development of targeted therapies against *MYC*, including MYC-associated factor X inhibitors (SaJM589, MYCi975) that inhibit MYC-dependent transcription; Pin1 inhibitors (such as KPT-6566, developed by Karyopharm Therapeutics) that facilitate *MYC* degradation; and Pim1 inhibitors (such as AZD1208, developed by AstraZeneca Development) that obstruct *MYC*-related oncogenic transcription[101]. Although complete remission has not been achieved in patients, the stabilization of disease progression and the inhibition of *MYC* target gene expression by omomyc-103 suggest potential benefits for CRC patients with ongoing *MYC* activation[102]. Despite the promise of these drugs, their lack of specificity for *MYC* presents a challenge. Further investigation into the underlying mechanisms, suitable patient populations, and combination therapies within the CMS2 subtype is essential for developing more precise and effective treatments, potentially paving the way for new strategies in managing this CRC subtype.

Targeted drugs for KRAS

Historically, *KRAS* has been viewed as an undruggable target; however, recent research has begun to challenge this notion. *KRAS* mutations, particularly at positions G12 and G13, are prevalent drivers in CRC, especially within the CMS3 subtype. These mutations lead to the overactivation of downstream signaling pathways, contributing to tumor initiation and progression. Consequently, the development of specific *KRAS* inhibitors has emerged as a crucial strategy for treating this cancer type[103]. Recent advancements have made significant strides in targeting *KRAS*, both directly and indirectly. Sotorasib (AMG 510), the first *KRAS G12C* inhibitor approved for non-small cell lung cancer, provides insights for treating other malignancies. The *KRAS G12D* mutation involves the substitution of glycine at position 12 with aspartic acid. Unlike G12C, the carboxyl group of G12D has weak nucleophilicity under physiological conditions, necessitating the introduction of basic groups to form a salt bridge with G12D for effective binding. MRTX1133 is the first reported *KRAS* G12D inhibitor, which forms a salt bridge with D12 and occupies the S-II pocket, demonstrating high affinity[104, 105]. Pan-*KRAS* inhibitors aim to target all *KRAS* mutants, with BI-2852 targeting the S-I/S-II pocket to inhibit both KRAS-guanosine triphosphate and *KRAS*-guanosine diphosphate[106]. The development of these inhibitors offers new strategies for addressing various KRAS mutations, showcasing the potential for directly targeting *KRAS* and inspiring further research to overcome resistance challenges. While *KRAS*-targeted drugs have shown efficacy in CRC, they face obstacles such as limited mutation types (affecting only 3%-4% of patients), resistance (including secondary *KRAS* mutations and bypass activation), and toxicity (with a 27.7% incidence of grade 3-4 adverse reactions). Additional challenges include low rates of biomarker testing, optimizing combination therapies, and managing long-term outcomes. Future strategies may focus on developing broad-spectrum inhibitors (targeting G12D and G13D mutations), exploring new combinations (such as immunotherapy), enhancing patient stratification, and improving drug accessibility to refine precision treatment and prognosis.

Directly targeting *KRAS* is precise but challenging, due to the protein's characteristics and the intratumoral heterogeneity present in CRC. Therefore, indirect strategies, such as inhibiting downstream pathways, enhancing immunotherapy, and modulating the immunosuppressive microenvironment, are necessary. *KRAS* mutations primarily drive tumor growth by activating the *MAPK* pathway. *MEK* inhibitors like Trametinib have shown promise in preclinical studies by inhibiting the proliferation and migration of CRC cells with *KRAS* mutations[107]. Additionally, *KRAS* mutations activate the *PI3K-AKT-mTOR* pathway. *mTOR* inhibitors like everolimus and *AKT* inhibitors like capivasertib have demonstrated antitumor activity in both preclinical and clinical studies[108]. Significant progress has been made in developing *PI3K*-targeted therapies for CRC, including *PI3K* inhibitors such as Alpelisib and dual inhibitors like Omipalisib Research on *KRAS* G12C inhibitors is focusing on immune checkpoints such as *PD-1*, lymphocyte activation gene 3, CTLA-4, T cell immunoreceptor with Ig and immunoreceptor tyrosine-based inhibitory motif domains, B and T lymphocyte attenuator, T cell immunoglobulin and mucin domain-3, CD73, indoleamine 2,3-dioxygenase 1, and adenosine A2A receptor[109-111]. These molecules play a significant role in promoting immunosuppression within the tumor microenvironment. *KRAS G12C* inhibitors may lower the expression of these checkpoint molecules, thereby altering cytokine levels, metabolic states, and the composition of immune cells to enhance T-cell activation and boost antitumor immune responses.

In the treatment of CRC, tumor vaccines that target *KRAS* mutation-related antigens have emerged as a key area of research. *KRAS* mutations are prevalent in CRC and are closely associated with tumor aggressiveness and immune evasion. Recent studies have employed vaccine strategies to stimulate the immune system to recognize and attack tumor cells that express *KRAS* mutation-related antigens[112]. For example, DNA methyltransferase inhibitors can induce tumor cells to express cancer testis antigens, which can be combined with granulocyte-macrophage colony-stimulating factor gene-transfected tumor cell vaccine (GVAX) vaccines for treatment, demonstrating enhanced antitumor effects in mouse models[113]. Additionally, a clinical trial investigated the combination of GVAX vaccines with the *PD-1* inhibitor pembrolizumab in patients with MMR advanced CRC. Although the primary endpoint of objective response was not achieved, some patients exhibited biochemical responses, indicating that GVAX vaccines might enhance the efficacy of *PD-1* inhibitors by modulating the tumor immune microenvironment[114]. These findings provide initial evidence for *KRAS*-targeted tumor vaccines in CRC, but further clinical trials are necessary to confirm their efficacy and safety. The combination of *KRAS*-targeted therapies, immunotherapies, and tumor vaccines presents new avenues for treating *KRAS*-mutated CRC. While these therapies have demonstrated antitumor activity in clinical trials, additional research is needed to validate their safety and effectiveness. Their integration may become a crucial strategy for managing *KRAS*-mutated CRC in the future.

Targeted drugs for TGF-β pathway

The *TGF-β* signaling pathway is essential for regulating cell proliferation, apoptosis, migration, and EMT, particularly in the CMS4 subtype of CRC. Researchers have developed small-molecule inhibitors, monoclonal antibodies, and other biologics to inhibit *TGF-β* signaling, aiming to counteract effects such as immune evasion, EMT, and angiogenesis[115]. Studies indicate that combining *TGF-β* receptor I inhibitors like galunisertib with neoadjuvant chemoradiotherapy enhances the complete response rate in locally advanced rectal cancer[116]. The bispecific antibody SHR-1701, which targets both *PD-L1* and *TGF-β*, has shown synergistic effects in first-line treatment for unresectable metastatic CRC by boosting antitumor immune responses[117]. Gulley *et al*[118] investigated the dual inhibition of *TGF-β* and *PD-L1*, noting that TGF-β promotes the production of CAFs and immune evasion. This strategy holds promise for treating CRC, particularly in the CMS4 subtype. Niu *et al*[119] developed a novel anti-*TGF-β*/*VEGF* bispecific antibody, Y332D, which inhibits both *TGF-β* and *VEGF* signaling pathways. When combined with *PD-1* inhibitors, Y332D demonstrated significant synergistic antitumor effects in various mouse models[119]. These findings suggest that targeting *TGF-β* could help overcome resistance to immunotherapy and provide new strategies for treating CMS4 CRC.

Targeted drugs for EMT

EMT plays a vital role in the CMS4 subtype of CRC, contributing to tumor metastasis, drug resistance, and immune evasion[120]. EMT is primarily regulated through signaling pathways such as *TGF-β*, *Wnt/β-catenin*, and Notch, which promote tumor cell migration, invasion, and resistance. Significant advancements have been made in developing drugs that target EMT, including *TGF-β* inhibitors, *Wnt/β-catenin* inhibitors, and netrin-1 blockers[121]. However, challenges persist in clinical applications, such as drug specificity, safety, tumor heterogeneity, and the optimization of combination therapy strategies. Future research should focus on developing biomarkers related to EMT to enable personalized treatment, exploring multi-targeted combination therapy strategies to address tumor heterogeneity and drug resistance, and creating novel drugs to further enhance therapeutic efficacy. By gaining a deeper understanding of the mechanisms underlying EMT and refining targeted therapeutic strategies, it is anticipated that these efforts will significantly improve treatment outcomes for CMS4 CRC.

Targeted drugs for VEGF

Angiogenesis is crucial for supplying nutrients and oxygen to growing tumors, making it a vital target in CRC treatment [122]. *VEGF* is the primary driver of angiogenesis and is frequently overexpressed in CRC. The binding of *VEGF* to its receptors initiates processes that lead to the formation of new blood vessels, thereby promoting tumor growth and metastasis. Anti-angiogenic therapies primarily focus on targeting *VEGF* or its receptors. Bevacizumab, a monoclonal antibody that targets *VEGF*, is extensively utilized in the treatment of CRC. By neutralizing *VEGF*, bevacizumab effectively inhibits angiogenesis, depriving tumors of their blood supply and consequently suppressing growth and metastasis. It is crucial to consider predictive biomarkers in the context of anti-angiogenic therapies within precision medicine. Elevated *VEGF* levels in the tumor microenvironment correlate with poorer prognoses and more aggressive disease. Understanding the molecular mechanisms that drive *VEGF* overexpression is vital for developing personalized treatment strategies[123]. Anti-angiogenic therapies may be particularly effective for patients with specific genotypes or molecular characteristics that indicate a greater reliance on angiogenesis. The combination of anti-angiogenic therapies with other targeted agents, such as *EGFR* inhibitors, has been investigated to enhance efficacy, especially in patients with wild-type *RAS* genes. This approach aims to improve treatment outcomes and provide more tailored therapeutic options [124].

Targeted drugs for APC

Mutations in the *APC* gene are found in more than 80% of sporadic CRC cases. The *APC* protein comprises several functional domains that play roles in cell migration, adhesion, proliferation, differentiation, and chromosomal assembly. Changes in the APC gene represent an early event in the progression of CRC. The CMS2, CMS3, and CMS4 subtypes of CRC show a higher prevalence of *APC* mutations. Therapeutic agents aimed at *APC* in cancer treatment mainly concentrate on altering the *Wnt* signaling pathway (further details are available in section "8.2 targeted drugs for *Wnt* pathway"). Recent studies have provided new insights into targeting *APC*. Research by Shailesh indicated that statins

have a synthetic lethal effect on *APC*-mutated CRC cells by reducing *Wnt* signaling activity and lowering the expression of the anti-apoptotic protein survivin[125]. Wong *et al*[126] discovered that proprotein convertase subtilisin/kexin type 9 is significantly elevated in *APC*/*KRAS*-mutated CRC, promoting tumor cell proliferation *via KRAS/MEK/ERK* signaling. Proprotein convertase subtilisin/kexin type 9 inhibitors significantly inhibit the growth of *APC*/*KRAS*-mutated CRC cells and show synergistic effects when used alongside statins, suggesting that statins may serve as potential treatments for *APC*-mutated CRC. Cen *et al*'s study[127] demonstrated that *APC* mutations enhance the binding of the *β-catenin/TCF4* complex to the *PD-L1* promoter, increasing its transcription and allowing CRC cells to escape $CD8^+$ T-cell-mediated cytotoxicity. This highlights *APC*'s involvement in immune evasion and supports the development of novel therapies targeting *APC*-related immune escape mechanisms, such as inhibitors of *β-catenin* or *TCF4*. Investigational drugs targeting *APC* pathways have shown encouraging results in preclinical studies, including cyclooxygenase-2 inhibitors like celecoxib, which suppress tumor growth, and antibiotics like erythromycin, which restore *APC* function and decrease tumor numbers through nonsense mutation read-through[128]. Organoid technology, which mimics the complexities of the tumor microenvironment, supports research on *APC*-mutated CRC by enabling drug screening and efficacy assessment[129]. Gene therapy holds promise for restoring *APC* function by introducing the normal *APC* gene into cancer cells, thereby inhibiting tumor growth[130,131]. Although still in the experimental stage, encouraging results have been noted in CRC. Future research should focus on exploring *APC* mutations and CRC mechanisms, developing more effective targeted therapies, and integrating various treatment strategies to improve CRC therapeutic outcomes and enhance patient quality of life.

Targeted drugs for P53

The *P53* gene is pivotal in CRC development, with its mutations closely associated with tumor aggressiveness, resistance to chemotherapy, and unfavorable prognosis. Recent progress in *P53*-targeted drug development presents new treatment avenues. Small molecules like analog of PRIMA-1-246 bind to mutant *P53* proteins, restoring their wild-type conformation and tumor-suppressing capabilities. Similarly, maleimide-derived molecule-3 reactivates mutant *P53* by targeting its apoptotic pathways[132]. Another approach involves inhibiting the *P53*-mouse double minute 2 (*MDM2*) interaction, as *MDM2* negatively regulates *P53* by promoting its degradation. *MDM2* inhibitors such as nutlin-3a and AMG 232 disrupt this interaction and enhance *P53* activity, showing potential in tumor suppression[132]. *P53* mutations also lead to increased *PD-L1* expression, facilitating immune evasion, indicating a synergistic potential when combining *P53* reactivators with immune checkpoint inhibitors. Additionally, siRNA can silence mutant *P53* genes, while clustered regularly interspaced short palindromic repeats/clustered regularly interspaced short palindromic repeats-associated protein 9 editing offers the possibility of direct gene repair[133]. Despite promising clinical outcomes, challenges persist: The diversity of *P53* mutations necessitates personalized strategies, and issues such as drug toxicity, side effects, and resistance must be addressed to enhance safety and efficacy.

APPLICATION OF AI IN CRC

AI encompasses theories, methodologies, technologies, and applications that simulate and extend human intelligence through computational means[134]. Machine learning (ML) and DL are fundamental technologies within AI. ML allows computers to learn from data without explicit programming, while DL, a subset of ML, utilizes artificial neural networks to manage complex pattern recognition and prediction tasks through multi-layer abstraction and learning[135]. In medical imaging, DL emulates human cognitive processes to analyze data connections and learn features, emerging as a leading tool for tasks such as molecular prediction and CRC treatment. Prominent DL models include convolutional neural networks (CNN), recurrent neural networks, and Graph neural networks[136]. CNNs excel in image recognition, particularly in analyzing CRC pathology images to identify tumor morphology and immune infiltration. They automatically learn and transform features, simplifying model complexity through techniques like weight sharing. recurrent neural networks are adept at handling sequential data, making them useful for genomic analysis to predict patient responses to treatments. Graph neural networks process unstructured graph data, constructing molecular networks to forecast drug targets and therapeutic pathways[137]. Researchers train and assess DL models utilizing a variety of data types, including genomic, pathological imaging, and clinical information. Data preprocessing steps encompass normalization, feature extraction, and denoising to improve training efficiency and accuracy.

AI technology has extensive applications in the medical domain (Figure 6). In pathology, AI can autonomously identify tumor cells and features of the microenvironment in slides, aiding pathologists in diagnosis and classification. In imaging, AI assists healthcare professionals in analyzing computed tomography, magnetic resonance imaging, and 18F-fluoro-2-deoxyglucose positron emission tomography scans, thereby enhancing diagnostic precision and efficiency. In drug development, AI expedites screening and clinical trial design, leading to reduced costs and shorter timelines. In patient management, AI evaluates electronic medical records and physiological data to forecast disease progression and create personalized care plans[138]. AI presents distinct advantages in healthcare by efficiently processing vast amounts of genomic, radiomic, and clinical data, offering automated decision support to minimize human error. In CRC, AI holds considerable promise, as it can analyze multi-omics data (genomic, transcriptomic, proteomic, metabolomic) to discover new biomarkers and therapeutic targets. Furthermore, AI can formulate personalized treatment strategies based on patients' genomic and clinical profiles, thereby improving treatment outcomes[139].

Application of AI in molecular diagnosis in CRC

Molecular biomarkers are crucial for the diagnosis, treatment, and evaluation of CRC. AI technologies, including ML and

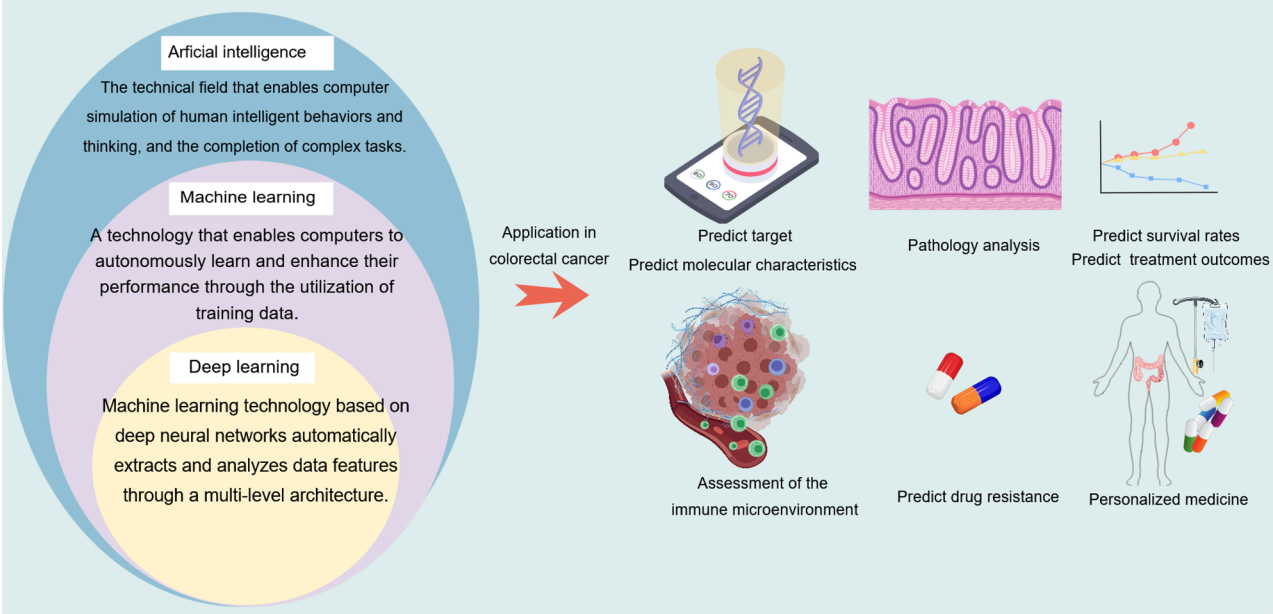

Figure 6 A comparison among artificial intelligence, machine learning, and deep learning, as well as their applications in the molecular diagnosis and treatment of colorectal cancer. Created with MedPeer (medpeer.cn). Copyright permission has been obtained in the Supplementary material.

DL, are increasingly utilized for the detection of molecular biomarkers to enhance efficiency, lower error rates, and improve clinical applicability. AI-driven image analysis and data modeling provide innovative approaches for identifying MSI/dMMR[140]. Specifically, CNNs can predict MSI/dMMR status directly from hematoxylin and eosin (HE)-stained pathological slides by learning from extensive image datasets. This automation minimizes manual intervention, reduces costs, and enhances accuracy compared to conventional methods[141]. Research by Hildebrand *et al*[142] demonstrated high accuracy in predicting MSI/dMMR using ML on high-quality datasets. However, accuracy significantly declines when applied to diverse racial or clinical cohorts. Current studies are focused on refining ML techniques for MSI prediction and comparing them with next-generation sequencing methods. Zamanitajeddin *et al*[143] introduced a novel approach that incorporates cellular network information into DL models. They constructed a cellular graph where cell nuclei serve as nodes and connections form edges, employing social network analysis to extract interpretable features. By integrating social network analysis features with DL in multiple instance learning frameworks, they enhanced predictions for CIN, *P53*, *BRAF*, and MSI status, achieving average area under the receiver operating characteristic increases of 2.4%-4% and area under the precision-recall curve increases of 7%-8.8%.

With advancements in molecular pathology and personalized treatment, CRC diagnosis and treatment have progressed to the molecular subtyping level. The four CRC CMSs (CMS1 to CMS4) provide a research framework, but traditional RNA sequencing for CMS classification is expensive and technically demanding. Recent developments in image analysis and DL facilitate CMS prediction from routine HE-stained slides. Sirinukunwattana *et al*'s team[144] created the Immunotherapy-based Cancer Management System, which, after multi-cohort training, improved model generalization and achieved finer spatial resolution for CMS classification. A NanoCMSer classifier based on NanoString technology also demonstrated high accuracy for fresh-frozen and formalin-fixed paraffin-embedded samples[144]. Bhukdee *et al*[145] utilized a 62-gene panel to identify new subgroups and elucidate CRC molecular mechanisms. These studies investigate AI applications in CRC molecular subtyping, providing technical support and theoretical foundations for precision medicine. Based on DL, this study developed a CRC molecular subtype classification system using high-quality whole-slide images annotated by pathologists. The system performed well on test sets, potentially reducing the workload of pathologists and advancing precise CRC treatments.

Pathological images and genomic data are vital in CRC research. Pathological images reveal tumor morphology, including cellular structure, tissue architecture, and immune infiltration, while genomic data uncover genetic variations and molecular mechanisms. The integration of these data types enhances the understanding of tumor biology, improving predictions of behavior and treatment responses[146]. AI algorithms, particularly DL, serve as effective tools for merging pathological images with genomic data. For instance, CNNs can process pathological images, extract features, and then jointly model these features with gene expression data to predict molecular subtypes or tumor prognosis[147]. This integration leverages both data types to improve prediction accuracy. The combination of digital pathology and AI will propel precision oncology forward, enabling personalized treatments. AI faces several limitations in the molecular diagnosis of CRC. Small sample sizes can lead to overfitting due to challenges in data collection, while inconsistent experimental methods and annotations, along with significant variations in data formats and distributions, hinder algorithm learning. These algorithms require a substantial number of labeled samples, and DL models often lack interpretability. Additionally, existing algorithms struggle to adapt to the dynamic changes in tumor mechanisms, with hyperparameter settings influencing their performance. Clinically, strict regulations, high costs, and lengthy timelines associated with large-scale multicenter trials present significant challenges. Traditional practices can obstruct the integration of new tools, necessitating retraining for healthcare providers, and ensuring data privacy remains a complex

issue.

Application of AI to evaluate tumor immune microenvironment in CRC

The tumor immune microenvironment's composition and its role in CRC progression are intricate. Its significance in predicting prognosis and evaluating immunotherapy is increasing, paving the way for new screening methods for populations sensitive to immunotherapy[148]. Traditional immunohistochemistry often fails to fully capture this complexity. AI algorithms can extract essential features from high-throughput data, such as single-cell sequencing and spatial transcriptomics, to characterize the immune microenvironment[149]. AI can analyze multiplex immunohistochemistry images, identify and quantify immune cells, and assess spatial relationships, leading to more accurate evaluations. Väyrynen *et al*[150] employed DL on HE-stained tissue microarray images to classify and count lymphocytes, plasma cells, neutrophils, and eosinophils in both epithelial and stromal regions of colorectal tumors, demonstrating its potential. Kather *et al*[151] utilized CNNs to identify stromal types in CRC, analyze gene expression profiles, pinpoint genes associated with immunotherapy responses, and create expression scores to predict responses to immune checkpoint inhibitors. AI-driven pathological image analysis will accelerate the assessment of complex tumor immune microenvironments, enhancing objectivity and reproducibility.

Application of AI to predictive models of drug targets and treatment response in CRC

AI algorithms, including ML and DL, are instrumental in identifying potential drug targets and validating their effectiveness through case studies. These models leverage molecular data, such as gene expression profiles and mutation states, to forecast patient responses to specific drugs[152]. Model performance is typically evaluated using metrics like area under the curve, sensitivity, and specificity, and validated through methods such as cross-validation and testing on external datasets. Predicting drug sensitivity remains a significant challenge in precision medicine. By analyzing genomic, transcriptomic, and drug response data from tumors, AI can predict drug responses to inform clinical decisions[153]. AI identifies biomarkers from gene expression, mutations, and copy number variations, uncovering key driver genes and pathways for drug development[154]. Despite AI's potential and efficiency in predicting drug targets for CRC, its application encounters challenges such as data dependency, biological complexity, clinical translation hurdles, and methodological flaws. Interdisciplinary collaboration, interpretable models, and improved experimental validation are essential for clinical progress.

AI algorithms also hold considerable promise in predicting responses to immunotherapy. By analyzing clinical, genomic, transcriptomic, and imaging data, they can forecast responses to immunotherapy and guide treatment decisions [155]. For instance, AI can evaluate tumor mutation burden, MSI, and *PD-L1* levels to predict responses to immune checkpoint inhibitors. Additionally, AI can dynamically monitor immune status to predict long-term efficacy. By analyzing blood samples for circulating tumor DNA, circulating tumor cells, and cytokines, AI can assess treatment responses and adjust therapies accordingly[156]. Schulz *et al*[157] developed a multi-stain DL model trained on over 1000 CRC patients, demonstrating superior prognostic accuracy and aiding in predicting treatment responses for rectal cancer [157]. Such tools facilitate patient stratification and resource allocation.

Application of AI in personalized treatment in CRC

Personalized treatment is crucial for CRC due to its inherent heterogeneity. AI models can integrate clinical history, molecular characteristics, and imaging data to formulate precise treatment plans. AI is utilized in chemotherapy, targeted therapy, and immunotherapy. It can predict chemotherapy efficacy and side effects based on genetic and tumor microenvironment information, optimizing treatment strategies[158]. For targeted therapy, AI assists in selecting appropriate drugs, thereby enhancing efficiency. In immunotherapy, AI predicts responses to immune checkpoint inhibitors, identifying patients most likely to benefit[159]. Sun *et al*[160] developed and validated a radiomics-based biomarker for tumor-infiltrating CD8 cells using ML, predicting responses to *PD-1/PD-L1* therapies based on computed tomography features. In CMS-based treatment for CRC, studies by Lafarge and Domingo highlighted AI's potential. Lafarge *et al*'s study[161] DL-based CMS identified significant correlations between CMS1 and pathological complete response post-long-course chemoradiotherapy by analyzing 1057 whole slide images. Lafarge *et al*[161] examined multi-omics data, confirming the association of CMS1 with radiosensitivity (odds ratio = 3.52, $P = 0.0119$) and created a predictive model for pathological complete response. These results underscore the importance of integrating AI with multi-omics data to accurately identify CMS subtypes and their treatment responses, thereby enhancing personalized care and improving patient outcomes. This progress paves the way for precision medicine based on CMS classification.

Solutions to data privacy and ethical issues of AI in healthcare

In medical AI applications, safeguarding patient data privacy is of utmost importance. Mishandling data can lead to significant legal and reputational repercussions, eroding patient trust. Currently, various strategies are employed to protect sensitive information. Differential privacy obscures individual data by introducing noise while maintaining statistical integrity. Homomorphic encryption allows computations on encrypted data without the need for decryption, thereby preserving privacy[162]. Secure multi-party computation facilitates collaborative computing without disclosing private information. In CRC research, these techniques safeguard genomic data, pathology images, and clinical information while enabling analysis and modeling. Ethical considerations in AI encompass informed consent, algorithmic bias, and accountability. Informed consent ensures that patients are fully aware of the purpose, risks, and benefits associated with the use of AI systems and voluntarily agree to data utilization. Algorithmic bias can lead to discriminatory outcomes, such as diminished diagnostic accuracy for non-white patients if the training data is skewed towards white patients[163]. Accountability issues arise regarding who is liable for AI errors - developers, users, or medical institutions.

These factors directly affect the rights of CRC patients; for instance, if an AI diagnostic system fails to detect a patient's cancer, it may result in delayed treatment.

To address privacy and ethical challenges, a comprehensive framework that encompasses technical, legal, and social dimensions is essential. Stringent regulations should delineate rules for data collection, usage, and sharing, with penalties for violations. Public education initiatives should raise awareness about data privacy and AI ethics, promoting informed consent. Transparency is equally crucial - designs and operations of AI systems should be disclosed for public scrutiny and evaluation[164]. For example, independent ethics committees could evaluate ethical risks associated with medical AI projects and offer guidance.

APPLICATION OF ORGANOIDS IN CRC

The intestinal epithelium, composed of a single layer of columnar cells that includes absorptive and secretory cells, plays a vital role in nutrient absorption and gut protection[165]. It is the fastest self-renewing tissue in adult mammals, with the villus-crypt structure renewing every 4-5 days (Figure 7). Intestinal stem cells located at the base of the crypt, supported by factors such as *Wnt*, R-spondin, epidermal growth factor, NOTCH, and Noggin from Paneth cells, proliferate and differentiate into mature intestinal cells. Sato *et al*[167] identified leucine-rich repeat-containing G-protein-coupled receptor 5 (a *Wnt* target gene) as a marker for intestinal stem cells[166]. Subsequently, Sato *et al*[167] discovered intestinal stem cells at the crypt base in normal mice and differentiated them into self-organizing "mini-gut" organoids with a crypt-villus structure, creating the first 3D organoid that retained crypt characteristics for up to 8 months. Spence *et al* [168] successfully generated human intestinal organoids from pluripotent stem cells by inducing definitive endoderm *via* activin A (a *TGF-β* molecule), treating them with a medium containing fibroblast growth factor 4 and Wnt3A to form hindgut spheroids, and transferring them to an organoid-promoting culture system, resulting in polarized columnar epithelial cells containing goblet, Paneth, and enteroendocrine cells.

Key components for culturing tumor organoids include initial cells, extracellular matrix, and growth regulators. Initial cells can be obtained by isolating cells directly from patient tumor tissues to create PDOs or by utilizing stem cells, such as embryonic, induced pluripotent, and adult stem cells, which self-organize into organoids with specific structures that mimic *in vivo* development (Figure 8). The extracellular matrix provides attachment points and directional growth support for the cells. Growth regulators, including pathway activators or inhibitors, are added to meet the organoid growth requirements at various stages[169]. For CRC organoids, essential factors include, the *Wnt* pathway activator R-spondin-1 protein, the bone morphogenetic proteins inhibitor Noggin protein, nicotinamide, and the tumor necrosis factor inhibitor A83-01[170]. Organoids, as 3D structures cultured in vitro, accurately replicate *in vivo* organ structures, functions, and physiological states, with extensive applications in CRC molecular mechanisms, drug screening, biobanking, and personalized medicine[171,172].

Application of organoids in molecular diagnosis in CRC

Single-cell RNA sequencing highlights the heterogeneity of PDOs, serving as a valuable tool for investigating tumor cell functions and their roles in tumor progression[173]. This technique identifies gene expression profiles across various cellular subpopulations and correlates them with clinical features, facilitating biomarker discovery related to tumor progression and therapeutic responses. In the context of CRC, it can detect diverse cell types, including tumor stem cells, immune cells, and stromal cells, while examining their interactions. This analysis helps elucidate how the tumor microenvironment affects growth and metastasis, thereby guiding targeted therapies. By comparing gene expression variations between drug-sensitive and drug-resistant tumor cells, researchers can uncover molecular mechanisms contributing to drug resistance, providing critical insights for developing strategies to overcome this challenge. For instance, certain subpopulations of tumor cells may display distinct gene expression patterns that make them less responsive to chemotherapy, directing clinicians toward alternative treatment options. The application of single-cell RNA sequencing technology allows for a comprehensive understanding of the intricate heterogeneity of tumors, thus providing essential information for devising more precise treatment strategies[174].

PDOs offer significant advantages in preserving genetic stability and modeling tumor heterogeneity. Compared to conventional 2D cell lines, organoids more effectively maintain the genetic characteristics of the original samples, ensuring the stability of genetic information during extended culture periods and enhancing the reliability of research findings. In cancer research, PDOs retain the genomic, transcriptomic, and epigenetic features of primary tumors, accurately simulating the cellular diversity within tumors[175]. Utilizing advanced techniques like single-cell sequencing, researchers can perform detailed analyses of gene expression profiles across different cell subpopulations within organoids, thereby providing robust support for investigations into tumor evolution, mechanisms of drug resistance, and personalized treatment strategies. Consequently, organoids have become essential tools in cancer research and translational medicine. However, organoids also face several limitations in the molecular diagnosis of CRC. Cultivation can be time-consuming and challenging, with success rates ranging from 30% to 60%, influenced by patient variability, tumor characteristics, and sample quality. Long-term culture poses risks of genetic drift and phenotypic alterations. In molecular detection, current techniques may be incompatible; impurities within organoids can interfere with results, and comprehensive molecular testing can be expensive. Clinically, the processes of organoid cultivation, testing, and result interpretation lack standardized protocols, regulatory approval processes remain unclear, and clinicians may require retraining to effectively utilize these new diagnostic tools.

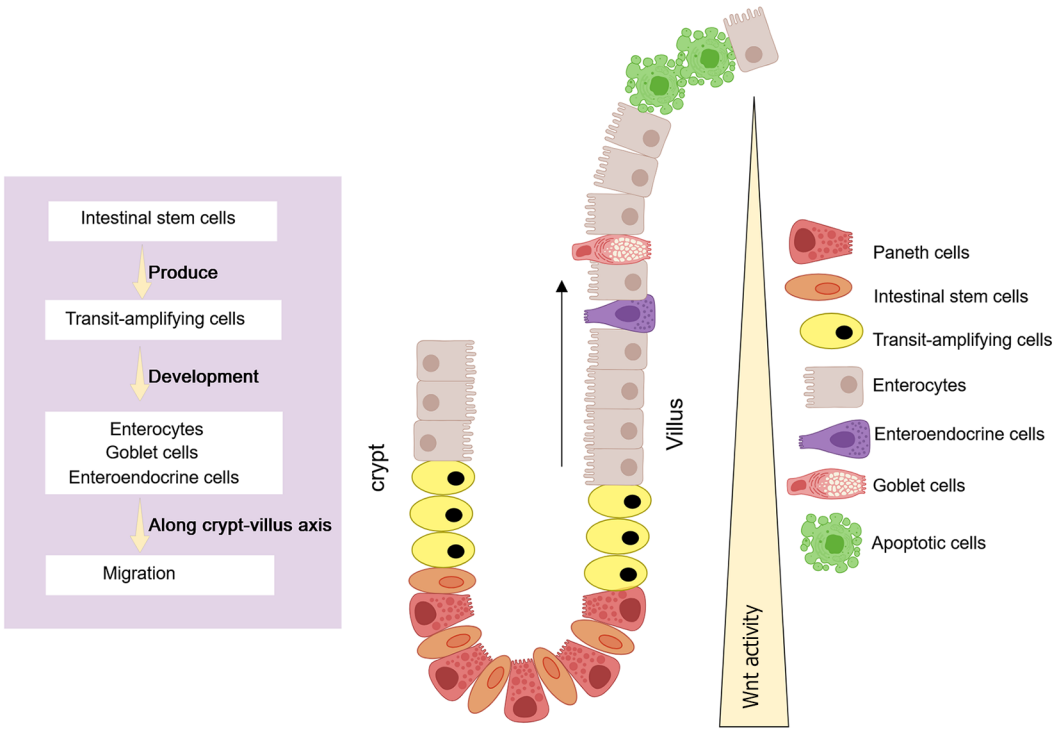

Figure 7 The intestinal crypt is composed of a specialized microenvironment. Created with MedPeer (medpeer.cn). Copyright permission has been obtained in the Supplementary material. Intestinal stem cells drive crypt renewal and give rise to transamplifying cells, whereas Paneth cells secrete critical niche factors, such as Wnt, which is essential for maintaining the stem cell niche.

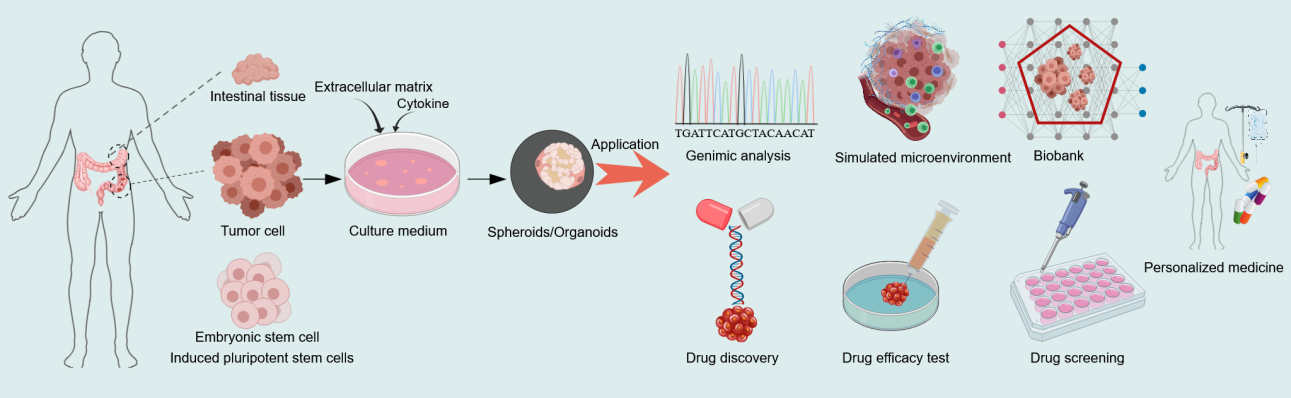

Figure 8 Schematic diagram of the establishment of artificial tissue cultures. Created with MedPeer (medpeer.cn). Copyright permission has been obtained in the Supplementary material. Tumor tissues from human intestines, stem cells from normal intestinal tissues and embryonic stem cells, as well as induced pluripotent stem cells, are embedded in the basement membrane matrix and maintained in the culture medium containing microenvironment factors crucial for proliferation.

Application of organoids in tumor immune microenvironment in CRC

A major advantage of organoids in tumor research is their ability to more accurately simulate the spatial organization and microenvironment of tumors more accurately than traditional 2D cell lines[176]. Organoids, with their three-dimensional structure, replicate the *in vivo* arrangement and interactions of tumor cells, capturing essential cell-cell and cell-matrix interactions that are critical for tumor growth, invasion, and metastasis. They can form various tissue structures, including tumor, stromal, and immune cells, reflecting the complexity of the tumor microenvironment. By manipulating culture conditions, researchers can introduce specific cell types or extracellular matrix components to replicate particular microenvironment features. For instance, incorporating vascular endothelial cells can enhance studies on tumor angiogenesis. Organoids also mimic dynamic tumor changes, such as invasion and metastasis[177]. For example, Qin *et al*[178] discovered that co-culturing mouse intestinal organoids with macrophages and fibroblasts can hyperactivate the *PI3K* signaling pathway in colon epithelial cells harboring *KRAS* and *P53* mutations. Dijkstra *et al*[179] demonstrated that co-culturing autologous tumor organoids with peripheral blood lymphocytes can enrich tumor-reactive T cells from the blood of MMR-deficient CRC patients. Researchers can investigate tumor behavior by observing changes in organoid

morphology, cell migration, and matrix degradation. These capabilities position organoids as a valuable platform for exploring tumor development and treatment, offering new avenues for creating more effective therapies.

Application of organoids in anticancer drug screening and new drug development in CRC

Drug resistance in CRC is a significant factor contributing to treatment failure. Tumor cells can develop resistance to chemotherapy and targeted therapies through mechanisms such as increased drug efflux, mutations in drug targets, pathway activation, and alterations in the tumor microenvironment[180]. PDOs can model the evolution of this resistance through long-term culture. For instance, resistance can be induced by gradually escalating drug concentrations, followed by genomic, transcriptomic, and proteomic analyses to elucidate the underlying resistance mechanisms[181]. Single-cell RNA sequencing can identify resistant subpopulations and highlight key genes and pathways associated with resistance. Research utilizing PDOs has revealed various molecular mechanisms responsible for CRC resistance[182]. The extracellular matrix and immune cells within the tumor microenvironment also play a role in influencing drug sensitivity. PDOs facilitate the examination of these factors, providing insights into overcoming resistance. PDOs, with their 3D structure, more effectively replicate the tumor microenvironment, preserving the heterogeneity and pharmacological characteristics of the original tumor. They excel in evaluating drug sensitivity and facilitate high-throughput screening. Automated platforms and image analysis enable rapid testing of numerous compounds, thereby expediting drug discovery[183]. In clinical settings, PDO-based drug sensitivity assays inform treatment decisions. For example, when resistance to first-line therapies arises, PDOs can assess alternative drugs or combinations to identify the most effective treatment options. Additionally, PDO-based screening aids in new drug development by identifying active compounds and potential therapeutic targets[184]. Despite the high biomimicry and individualized potential of organoid models in drug screening and new drug development for CRC, they encounter significant limitations: Inconsistent cultivation success rates (affected by tumor heterogeneity and sample quality), inadequate clinical relevance in drug sensitivity predictions (due to the absence of standardized evaluation systems), simplified microenvironments (lacking essential components like immune cells and vascular networks), and throughput limitations (making large-scale drug screening challenging). Future efforts should concentrate on optimizing cultivation systems, creating high-throughput platforms, and integrating multi-omics analyses to improve predictive accuracy and translational value.

Application of organoids in personalized treatment in CRC

PDOs play a crucial role in personalized treatment by accurately predicting patient responses through their ability to mimic tumor biology and heterogeneity. Research indicates that PDO drug sensitivity tests correlate strongly with clinical metrics such as ORRs and progression-free survival[185]. For instance, testing CRC PDOs with drugs corresponding to clinical treatments has shown high consistency with patient outcomes[186]. This suggests that PDOs can be employed to anticipate a patient's treatment response before clinical intervention, thereby assisting healthcare providers in selecting the most effective therapeutic strategies. Furthermore, PDOs can compare responses to various treatments, allowing for tailored plans for individual patients. Unlike genomics-based algorithms that rely solely on genetic mutations, PDOs reflect tumor cell function, microenvironment, and interactions, providing a more comprehensive approach to drug response prediction, making them a promising tool for future personalized therapies.

In addition to predicting treatment outcomes, PDOs exhibit significant potential in prognosis prediction and treatment optimization[187]. They can simulate characteristics such as tumor invasion, propensity for metastasis, and drug resistance, aiding physicians in identifying high-risk patients and formulating precise treatment plans. For example, studies have demonstrated that the invasive capabilities of certain PDOs correlate with the risk of tumor metastasis, while their resistance is associated with poor prognosis[188]. Additionally, PDOs can evaluate tumor responses to various therapies, enabling the selection of the most appropriate treatment plan by screening drug combinations or treatment options[189]. In terms of treatment optimization, PDOs can help overcome resistance or minimize side effects, such as identifying drug combinations to counteract resistance or assessing drug toxicity to select less harmful options. Additionally, PDOs facilitate the development of personalized immunotherapy by stimulating tumor PDOs for immune response analysis to identify suitable drugs[190]. However, most studies remain in preclinical phases, necessitating validation in larger clinical trials. Furthermore, PDO culture and analysis techniques require further standardization and refinement to ensure clinical reliability.

Establishment of organoids biobank in CRC

The creation of organoid biobanks is essential for advancing cancer research and facilitating clinical translation[191]. These biobanks provide vital resources for large-scale drug screening, fundamental research, and clinical applications. By establishing organoid libraries that encompass diverse tumor types, pathological features, and genetic backgrounds, researchers can access experimental materials more efficiently, thereby accelerating progress. Tumor organoid biobanks are increasingly important for investigating cancer mechanisms, exploring treatment options, and developing new drugs [192]. Yao *et al*[193] established an organoid biobank from patients enrolled in phase III clinical trials for locally advanced rectal cancer who received neoadjuvant chemoradiotherapy. Their research confirmed that these rectal cancer organoids accurately reflect the pathophysiology and genetic alterations of the corresponding tumors, demonstrating a high degree of concordance between patient responses to chemoradiotherapy and organoid responses. Yan *et al*[194] addressed a gap in existing CRC models by creating an organoid biobank enriched for sporadic early-onset CRC, revealing distinct genetic profiles and novel pathway synergies. The study by Yao *et al*[195] further illustrated the potential of tumor organoids to predict clinical responses to chemotherapy in advanced CRC.

However, the construction of biobanks presents numerous technical challenges. First, the long-term preservation of organoids is problematic, as current cryopreservation methods may compromise their viability and properties,

necessitating the development of more effective techniques. Second, the culture conditions for organoids are complex, requiring stringent quality control systems to ensure consistency[196]. Additionally, a standardized data management system is essential for managing diverse information, and unified data-sharing platforms must resolve inconsistencies across different laboratories. Researchers should investigate advanced cryopreservation methods, automated cultivation systems, and standardized data management solutions to improve the efficiency and reliability of biobanks.

The creation and utilization of organoid biobanks necessitate the protection of patient privacy and strict adherence to ethical guidelines. Since organoids are derived from patient tissue samples that contain genetic and pathological information, it is crucial to implement measures that safeguard patient privacy. First, informed consent must be secured by clearly explaining the purpose, content, and risks associated with organoid research, ensuring that patients have the right to decline participation. Second, patient information should be anonymized, separating personal details from research data to prevent any potential leaks of sensitive information. Furthermore, stringent access control measures must be established, allowing only authorized personnel to access relevant data. Ethical guidelines should strike a balance between scientific research and patient rights, respecting autonomy, informed consent, and privacy. This can be accomplished by drawing from practices in other fields, such as forming ethics review committees to evaluate and oversee research protocols, and implementing regulations to govern organoid biobank management, ensuring transparency and compliance in research. These measures can facilitate scientific advancement while safeguarding patient rights to the fullest extent.

CONCLUSION

CRC, a prevalent and highly lethal malignancy worldwide, has experienced significant advancements in genetics and treatment in recent years. Sequencing technologies have enhanced our understanding of the genetic mechanisms underlying CRC, identifying numerous genetic variants associated with disease risk and molecular subtypes. These subtypes lay the groundwork for precision medicine, enabling tailored predictions of disease progression and treatment responses. On the therapeutic front, targeted therapies, such as anti-*EGFR* and anti-*TGF-β* agents, have improved survival rates and quality of life for patients. Immunotherapy has demonstrated remarkable efficacy in MSI-H/dMMR CRC, providing new hope for patients. Furthermore, multidisciplinary approaches that integrate surgery, chemotherapy, radiotherapy, and emerging methods are achieving personalized and precise treatment outcomes.

In this context, AI and organoid open new paths for CRC research. AI uses ML and DL to analyze complex biological data, such as gene expression profiles and imaging data, thereby accelerating the development of diagnostic models and personalized treatment strategies. AI enhances accuracy and efficiency in early diagnosis, particularly in the analysis of pathology slides, and predicts drug responses to assist in treatment selection. Meanwhile, organoid technology provides a more realistic *in vitro* model that simulates the *in vivo* environment for personalized drug screening and mechanistic studies. Compared to traditional cell lines, organoids more effectively replicate the tumor microenvironment, advancing our understanding of tumor behavior and therapy development.

However, this field faces numerous challenges. Despite significant progress in genetic research, the functions and interaction mechanisms of many genetic variations remain unclear, limiting the translation of genetic information into effective treatments. While targeted therapies and immunotherapies have shown impressive results, both primary and acquired resistance significantly affect long-term efficacy. Additionally, optimizing multidisciplinary treatment plans to ensure seamless integration and synergy among various approaches remains a critical challenge. In AI applications, issues related to data quality, standardization, and privacy protection are pressing concerns. Variability and inconsistencies in genetic and clinical data can hinder the performance of AI models and their widespread adoption. Ensuring patient data privacy is also a fundamental prerequisite for the integration of AI in healthcare. In organoid technology, although organoids can mimic tumor microenvironments, they still fall short of fully replicating human complexity, and challenges such as standardization, long-term stability, and precise environmental matching require further investigation.

Future CRC research and treatment should prioritize understanding genetic mechanisms to develop targeted therapies, explore strategies to overcome resistance, such as combination treatments or drug innovations, and continuously refine multidisciplinary approaches to enhance overall outcomes. The integration of AI, organoid technology, and genetic research holds promise for addressing current challenges. Establishing large-scale, high-quality genetic and organoid databases, combined with AI's analytical capabilities, will advance precision medicine in CRC. At the same time, improving the translation of basic research into clinical applications and expediting the transition of novel technologies from the laboratory to clinical settings will provide more effective treatment options for CRC patients, significantly enhancing their survival rates and quality of life.

FOOTNOTES

Author contributions: Qi GX drafted the manuscript; Zhao RX and Gao C designed the outline; Ma ZY and Wang S reviewed the literature; Xu J revised the article for important intellectual content and was involved in the final approval of the version to be published; and all authors have read and approved the final manuscript.

Supported by the National Human Genetic Resources Sharing Service Platform, No. PT-2024-0303; and Qingdao Medical and Health Research Guidance Project, No. 2023-WJZD202.

Conflict-of-interest statement: All the authors report no relevant conflicts of interest for this article.

Country of origin: China

ORCID number: Gao-Xiu Qi 0009-0005-6170-0523; Jing Xu 0000-0003-2438-3045.

S-Editor: Bai Y
L-Editor: A
P-Editor: Yu HG

REFERENCES

1 **Bray F**, Laversanne M, Sung H, Ferlay J, Siegel RL, Soerjomataram I, Jemal A. Global cancer statistics 2022: GLOBOCAN estimates of incidence and mortality worldwide for 36 cancers in 185 countries. *CA Cancer J Clin* 2024; **74**: 229-263 [PMID: 38572751 DOI: 10.3322/caac.21834] [FullText]

2 **Filho AM**, Laversanne M, Ferlay J, Colombet M, Piñeros M, Znaor A, Parkin DM, Soerjomataram I, Bray F. The GLOBOCAN 2022 cancer estimates: Data sources, methods, and a snapshot of the cancer burden worldwide. *Int J Cancer* 2025; **156**: 1336-1346 [PMID: 39688499 DOI: 10.1002/ijc.35278] [FullText]

3 **Hemminki K**, Försti A, Hemminki A. Survival in colon and rectal cancers in Finland and Sweden through 50 years. *BMJ Open Gastroenterol* 2021; **8**: e000644 [PMID: 34272211 DOI: 10.1136/bmjgast-2021-000644] [FullText]

4 **Burnett-Hartman AN**, Murphy CC, Lee JK. Novel, Emerging Risk Factors for Colorectal Cancer Remain Understudied. *Gastroenterology* 2022; **163**: 574-576 [PMID: 35809616 DOI: 10.1053/j.gastro.2022.06.085] [FullText]

5 **Siegel RL**, Miller KD, Fuchs HE, Jemal A. Cancer statistics, 2022. *CA Cancer J Clin* 2022; **72**: 7-33 [PMID: 35020204 DOI: 10.3322/caac.21708] [FullText]

6 **Li J**, Ma X, Chakravarti D, Shalapour S, DePinho RA. Genetic and biological hallmarks of colorectal cancer. *Genes Dev* 2021; **35**: 787-820 [PMID: 34074695 DOI: 10.1101/gad.348226.120] [FullText]

7 **Patel SG**, Karlitz JJ, Yen T, Lieu CH, Boland CR. The rising tide of early-onset colorectal cancer: a comprehensive review of epidemiology, clinical features, biology, risk factors, prevention, and early detection. *Lancet Gastroenterol Hepatol* 2022; **7**: 262-274 [PMID: 35090605 DOI: 10.1016/S2468-1253(21)00426-X] [FullText]

8 **Fan A**, Wang B, Wang X, Nie Y, Fan D, Zhao X, Lu Y. Immunotherapy in colorectal cancer: current achievements and future perspective. *Int J Biol Sci* 2021; **17**: 3837-3849 [PMID: 34671202 DOI: 10.7150/ijbs.64077] [FullText]

9 **Yazdani A**, Yazdani A, Mendez-Giraldez R, Pillonetto G, Samiei E, Hadi R, Lenz HJ, Venook A, Samiei A, Nixon A, Lucci J, Kopetz S, Bertagnolli M, Perou C, Innocenti F. Gene expression biomarkers differentiate overall survival of colorectal cancer upon targeted therapies. *Res Sq* 2024 [PMID: 38559223 DOI: 10.21203/rs.3.rs-4047331/v1] [FullText]

10 **Guinney J**, Dienstmann R, Wang X, de Reyniès A, Schlicker A, Soneson C, Marisa L, Roepman P, Nyamundanda G, Angelino P, Bot BM, Morris JS, Simon IM, Gerster S, Fessler E, De Sousa E Melo F, Missiaglia E, Ramay H, Barras D, Homicsko K, Maru D, Manyam GC, Broom B, Boige V, Perez-Villamil B, Laderas T, Salazar R, Gray JW, Hanahan D, Tabernero J, Bernards R, Friend SH, Laurent-Puig P, Medema JP, Sadanandam A, Wessels L, Delorenzi M, Kopetz S, Vermeulen L, Tejpar S. The consensus molecular subtypes of colorectal cancer. *Nat Med* 2015; **21**: 1350-1356 [PMID: 26457759 DOI: 10.1038/nm.3967] [FullText]

11 **Shoji F**, Yamashita T, Kinoshita F, Takamori S, Fujishita T, Toyozawa R, Ito K, Yamazaki K, Nakashima N, Okamoto T. Artificial intelligence-derived gut microbiome as a predictive biomarker for therapeutic response to immunotherapy in lung cancer: protocol for a multicentre, prospective, observational study. *BMJ Open* 2022; **12**: e061674 [PMID: 35676015 DOI: 10.1136/bmjopen-2022-061674] [FullText]

12 **Prelaj A**, Miskovic V, Zanitti M, Trovo F, Genova C, Viscardi G, Rebuzzi SE, Mazzeo L, Provenzano L, Kosta S, Favali M, Spagnoletti A, Castelo-Branco L, Dolezal J, Pearson AT, Lo Russo G, Proto C, Ganzinelli M, Giani C, Ambrosini E, Turajlic S, Au L, Koopman M, Delaloge S, Kather JN, de Braud F, Garassino MC, Pentheroudakis G, Spencer C, Pedrocchi ALG. Artificial intelligence for predictive biomarker discovery in immuno-oncology: a systematic review. *Ann Oncol* 2024; **35**: 29-65 [PMID: 37879443 DOI: 10.1016/j.annonc.2023.10.125] [FullText]

13 **Kolisnik T**, Sulit AK, Schmeier S, Frizelle F, Purcell R, Smith A, Silander O. Identifying important microbial and genomic biomarkers for differentiating right- versus left-sided colorectal cancer using random forest models. *BMC Cancer* 2023; **23**: 647 [PMID: 37434131 DOI: 10.1186/s12885-023-10848-9] [FullText]

14 **Kim DH**, Lim Y, Ock CY, Park G, Park S, Song H, Ma M, Mostafavi M, Kang EJ, Ahn MJ, Lee KW, Kwon JH, Yang Y, Choi YH, Kim MK, Ji JH, Yun T, Kim SB, Keam B. Artificial intelligence-powered spatial analysis of tumor-infiltrating lymphocytes as a predictive biomarker for axitinib in adenoid cystic carcinoma. *Head Neck* 2023; **45**: 3086-3095 [PMID: 37828867 DOI: 10.1002/hed.27537] [FullText]

15 **Flood M**, Ramsay R, Heriot A. ASO Author Reflections: Organoid-Based Precision Medicine in Colorectal Cancer-Are We There Yet? *Ann Surg Oncol* 2022; **29**: 60-61 [PMID: 34545532 DOI: 10.1245/s10434-021-10831-3] [FullText]

16 **Razumovskaya A**, Silkina M, Poloznikov A, Kulagin T, Raigorodskaya M, Gorban N, Kudryavtseva A, Fedorova M, Alekseev B, Tonevitsky A, Nikulin S. Predicting patient outcomes with gene-expression biomarkers from colorectal cancer organoids and cell lines. *Front Mol Biosci* 2025; **12**: 1531175 [PMID: 39886381 DOI: 10.3389/fmolb.2025.1531175] [FullText]

17 **Anstett V**, Heinzelmann E, Piraino F, Roch A, Chrisnandy A, Norkin M, Garnier V, Homicsko K, Hoehnel-Ka S, Brandenberg N. In Vitro

Evaluation of the Safety and Efficacy of Cibisatamab Using Adult Stem Cell-Derived Organoids and Colorectal Cancer Spheroids. *Cancers (Basel)* 2025; **17**: 291 [PMID: 39858076 DOI: 10.3390/cancers17020291] [FullText]

18 **Wielandt AM**, Hurtado C, Moreno C M, Villarroel C, Castro M, Estay M, Simian D, Martinez M, Vial MT, Kronberg U, López-Köstner F. Characterization of Chilean patients with sporadic colorectal cancer according to the three main carcinogenic pathways: Microsatellite instability, CpG island methylator phenotype and Chromosomal instability. *Tumour Biol* 2020; **42**: 1010428320938492 [PMID: 32635826 DOI: 10.1177/1010428320938492] [FullText]

19 **Huang Z**, Yang M. Molecular Network of Colorectal Cancer and Current Therapeutic Options. *Front Oncol* 2022; **12**: 852927 [PMID: 35463300 DOI: 10.3389/fonc.2022.852927] [FullText]

20 **Olkinuora AP**, Peltomäki PT, Aaltonen LA, Rajamäki K. From APC to the genetics of hereditary and familial colon cancer syndromes. *Hum Mol Genet* 2021; **30**: R206-R224 [PMID: 34329396 DOI: 10.1093/hmg/ddab208] [FullText]

21 **Ceccon C**, Borga C, Angerilli V, Bergamo F, Munari G, Sabbadin M, Gasparello J, Schiavi F, Zovato S, Scarpa M, Urso EDL, Dei Tos AP, Luchini C, Grillo F, Lonardi S, Parente P, Fassan M. MLH1 gene promoter methylation status partially overlaps with CpG methylator phenotype (CIMP) in colorectal adenocarcinoma. *Pathol Res Pract* 2025; **266**: 155786 [PMID: 39724851 DOI: 10.1016/j.prp.2024.155786] [FullText]

22 **Jiang C**, Zhou Q, Yi K, Yuan Y, Xie X. Colorectal cancer initiation: Understanding early-stage disease for intervention. *Cancer Lett* 2024; **589**: 216831 [PMID: 38574882 DOI: 10.1016/j.canlet.2024.216831] [FullText]

23 **Fearon ER**, Vogelstein B. A genetic model for colorectal tumorigenesis. *Cell* 1990; **61**: 759-767 [PMID: 2188735 DOI: 10.1016/0092-8674(90)90186-i] [FullText]

24 **Huo M**, Gao Z, Wang G, Hou Z, Zheng J. Huaier promotes sensitivity of colorectal cancer to oxaliplatin by inhibiting METTL3 to regulate the Wnt/βcatenin signaling pathway. *Oncol Rep* 2025; **53**: 7 [PMID: 39513580 DOI: 10.3892/or.2024.8840] [FullText]

25 **Gamage CDB**, Kim JH, Zhou R, Park SY, Pulat S, Varlı M, Nam SJ, Kim H. Plectalibertellenone A suppresses colorectal cancer cell motility and glucose metabolism by targeting TGF-β/Smad and Wnt pathways. *Biofactors* 2025; **51**: e2120 [PMID: 39291722 DOI: 10.1002/biof.2120] [FullText]

26 **Nguyen LH**, Goel A, Chung DC. Pathways of Colorectal Carcinogenesis. *Gastroenterology* 2020; **158**: 291-302 [PMID: 31622622 DOI: 10.1053/j.gastro.2019.08.059] [FullText]

27 **Sullivan BA**, Noujaim M, Roper J. Cause, Epidemiology, and Histology of Polyps and Pathways to Colorectal Cancer. *Gastrointest Endosc Clin N Am* 2022; **32**: 177-194 [PMID: 35361330 DOI: 10.1016/j.giec.2021.12.001] [FullText]

28 **Maryńczak K**, Włodarczyk J, Sabatowska Z, Dziki A, Dziki Ł, Włodarczyk M. Colitis-Associated Colorectal Cancer in Patients with Inflammatory Bowel Diseases in a Tertiary Referral Center: A Propensity Score Matching Analysis. *J Clin Med* 2022; **11**: 866 [PMID: 35160321 DOI: 10.3390/jcm11030866] [FullText]

29 **Dougherty MW**, Jobin C. Intestinal bacteria and colorectal cancer: etiology and treatment. *Gut Microbes* 2023; **15**: 2185028 [PMID: 36927206 DOI: 10.1080/19490976.2023.2185028] [FullText]

30 **Asghari-Jafarabadi M**, Wilkins S, Plazzer JP, Yap R, McMurrick PJ. Prognostic factors and survival disparities in right-sided versus left-sided colon cancer. *Sci Rep* 2024; **14**: 12306 [PMID: 38811769 DOI: 10.1038/s41598-024-63143-3] [FullText]

31 **Phipps AI**, Alwers E, Harrison T, Banbury B, Brenner H, Campbell PT, Chang-Claude J, Buchanan D, Chan AT, Farris AB, Figueiredo JC, Gallinger S, Giles GG, Jenkins M, Milne RL, Newcomb PA, Slattery ML, Song M, Ogino S, Zaidi SH, Hoffmeister M, Peters U. Association Between Molecular Subtypes of Colorectal Tumors and Patient Survival, Based on Pooled Analysis of 7 International Studies. *Gastroenterology* 2020; **158**: 2158-2168.e4 [PMID: 32088204 DOI: 10.1053/j.gastro.2020.02.029] [FullText]

32 **Zhong M**, Xiong Y, Ye Z, Zhao J, Zhong L, Liu Y, Zhu Y, Tian L, Qiu X, Hong X. Microbial Community Profiling Distinguishes Left-Sided and Right-Sided Colon Cancer. *Front Cell Infect Microbiol* 2020; **10**: 498502 [PMID: 33324571 DOI: 10.3389/fcimb.2020.498502] [FullText]

33 **Kneis B**, Wirtz S, Weber K, Denz A, Gittler M, Geppert C, Brunner M, Krautz C, Siebenhüner AR, Schierwagen R, Tyc O, Agaimy A, Grützmann R, Trebicka J, Kersting S, Langheinrich M. Colon Cancer Microbiome Landscaping: Differences in Right- and Left-Sided Colon Cancer and a Tumor Microbiome-Ileal Microbiome Association. *Int J Mol Sci* 2023; **24**: 3265 [PMID: 36834671 DOI: 10.3390/ijms24043265] [FullText]

34 **Miyake T**, Mori H, Yasukawa D, Hexun Z, Maehira H, Ueki T, Kojima M, Kaida S, Iida H, Shimizu T, Ohno M, Andoh A, Tani M. The Comparison of Fecal Microbiota in Left-Side and Right-Side Human Colorectal Cancer. *Eur Surg Res* 2021; **62**: 248-254 [PMID: 34198297 DOI: 10.1159/000516922] [FullText]

35 **Pal P**, Shastry RP. Exploring the complex role of gut microbiome in the development of precision medicine strategies for targeting microbial imbalance-induced colon cancer. *Folia Microbiol (Praha)* 2023; **68**: 691-701 [PMID: 37624549 DOI: 10.1007/s12223-023-01085-5] [FullText]

36 **Baran B**, Mert Ozupek N, Yerli Tetik N, Acar E, Bekcioglu O, Baskin Y. Difference Between Left-Sided and Right-Sided Colorectal Cancer: A Focused Review of Literature. *Gastroenterology Res* 2018; **11**: 264-273 [PMID: 30116425 DOI: 10.14740/gr1062w] [FullText]

37 **Su MW**, Chang CK, Lin CW, Chu HW, Tsai TN, Su WC, Chen YC, Chang TK, Huang CW, Tsai HL, Wu CC, Chou HC, Shiu BH, Wang JY. Genomic and Metabolomic Landscape of Right-Sided and Left-Sided Colorectal Cancer: Potential Preventive Biomarkers. *Cells* 2022; **11**: 527 [PMID: 35159336 DOI: 10.3390/cells11030527] [FullText]

38 **Wang ZX**, Wu HX, He MM, Wang YN, Luo HY, Ding PR, Xie D, Chen G, Li YH, Wang F, Xu RH. Chemotherapy With or Without Anti-EGFR Agents in Left- and Right-Sided Metastatic Colorectal Cancer: An Updated Meta-Analysis. *J Natl Compr Canc Netw* 2019; **17**: 805-811 [PMID: 31319395 DOI: 10.6004/jnccn.2018.7279] [FullText]

39 **Siegel RL**, Miller KD, Goding Sauer A, Fedewa SA, Butterly LF, Anderson JC, Cercek A, Smith RA, Jemal A. Colorectal cancer statistics, 2020. *CA Cancer J Clin* 2020; **70**: 145-164 [PMID: 32133645 DOI: 10.3322/caac.21601] [FullText]

40 **Yoshino T**, Hooda N, Younan D, Muro K, Shitara K, Heinemann V, O'neil BH, Herrero FR, Peeters M, Soeda J, Suh M, Reichert H, Mezzi K, Fryzek J, Chia V, Rehn M, Stintzing S. A meta-analysis of efficacy and safety data from head-to-head first-line trials of epidermal growth factor receptor inhibitors versus bevacizumab in adult patients with RAS wild-type metastatic colorectal cancer by sidedness. *Eur J Cancer* 2024; **202**: 113975 [PMID: 38442645 DOI: 10.1016/j.ejca.2024.113975] [FullText]

41 **Valdeolivas A**, Amberg B, Giroud N, Richardson M, Gálvez EJC, Badillo S, Julien-Laferrière A, Túrós D, Voith von Voithenberg L, Wells I, Pesti B, Lo AA, Yángüez E, Das Thakur M, Bscheider M, Sultan M, Kumpesa N, Jacobsen B, Bergauer T, Saez-Rodriguez J, Rottenberg S, Schwalie PC, Hahn K. Profiling the heterogeneity of colorectal cancer consensus molecular subtypes using spatial transcriptomics. *NPJ Precis Oncol* 2024; **8**: 10 [PMID: 38200223 DOI: 10.1038/s41698-023-00488-4] [FullText]

42 **de Back TR**, Wu T, Schafrat PJ, Ten Hoorn S, Tan M, He L, van Hooff SR, Koster J, Nijman LE, Vink GR, Beumer IJ, Elbers CC, Lenos KJ,

Sommeijer DW, Wang X, Vermeulen L. A consensus molecular subtypes classification strategy for clinical colorectal cancer tissues. *Life Sci Alliance* 2024; **7**: e202402730 [PMID: 38782602 DOI: 10.26508/lsa.202402730] [FullText]

43 **Dang Q**, Zuo L, Hu X, Zhou Z, Chen S, Liu S, Ba Y, Zuo A, Xu H, Weng S, Zhang Y, Luo P, Cheng Q, Liu Z, Han X. Molecular subtypes of colorectal cancer in the era of precision oncotherapy: Current inspirations and future challenges. *Cancer Med* 2024; **13**: e70041 [PMID: 39054866 DOI: 10.1002/cam4.70041] [FullText]

44 **Jakab A**, Patai ÁV, Darvas M, Tormássi-Bély K, Micsik T. Microenvironment, systemic inflammatory response and tumor markers considering consensus molecular subtypes of colorectal cancer. *Pathol Oncol Res* 2024; **30**: 1611574 [PMID: 38645565 DOI: 10.3389/pore.2024.1611574] [FullText]

45 **Nunez SK**, Young CD, Griffen TL, Ohandjo AQ, McKinney LP, Kopetz S, Lillard JW Jr. Identification of Gene Co-Expression Networks Associated with Consensus Molecular Subtype-1 of Colorectal Cancer. *Cancers (Basel)* 2021; **13**: 5824 [PMID: 34830978 DOI: 10.3390/cancers13225824] [FullText]

46 **Erdogan F**, Radu TB, Orlova A, Qadree AK, de Araujo ED, Israelian J, Valent P, Mustjoki SM, Herling M, Moriggl R, Gunning PT. JAK-STAT core cancer pathway: An integrative cancer interactome analysis. *J Cell Mol Med* 2022; **26**: 2049-2062 [PMID: 35229974 DOI: 10.1111/jcmm.17228] [FullText]

47 **Housini M**, Dariya B, Ahmed N, Stevens A, Fiadjoe H, Nagaraju GP, Basha R. Colorectal cancer: Genetic alterations, novel biomarkers, current therapeutic strategies and clinical trials. *Gene* 2024; **892**: 147857 [PMID: 37783294 DOI: 10.1016/j.gene.2023.147857] [FullText]

48 **Martins D**, Rodrigues J, Redondo P, Julião I, Faustino C. Evaluating the Optimal Sequence of Treatment With EGFR Inhibitors and Bevacizumab in RAS Wild-Type Metastatic Colorectal Cancer. *Cureus* 2022; **14**: e23543 [PMID: 35494924 DOI: 10.7759/cureus.23543] [FullText]

49 **Kotani D**, Bando H, Taniguchi H, Masuishi T, Komatsu Y, Yamaguchi K, Nakajima T, Satoh T, Nishina T, Esaki T, Nomura S, Takahashi K, Iida S, Matsuda S, Motonaga S, Fuse N, Sato A, Fujii S, Ohtsu A, Ebi H, Yoshino T. BIG BANG study (EPOC1703): multicentre, proof-of-concept, phase II study evaluating the efficacy and safety of combination therapy with binimetinib, encorafenib and cetuximab in patients with BRAF non-V600E mutated metastatic colorectal cancer. *ESMO Open* 2020; **5**: e000624 [PMID: 33551068 DOI: 10.1136/esmoopen-2019-000624] [FullText]

50 **Wu CC**, Wang JH, Lin PC, Liang CA, Huang CY, Lien HC, Chen CY, Chou KJ, Su YC. Tumor sidedness and efficacy of first-line therapy in patients with RAS/BRAF wild-type metastatic colorectal cancer: A network meta-analysis. *Crit Rev Oncol Hematol* 2020; **145**: 102823 [PMID: 31783291 DOI: 10.1016/j.critrevonc.2019.102823] [FullText]

51 **Martelli V**, Pastorino A, Sobrero AF. Prognostic and predictive molecular biomarkers in advanced colorectal cancer. *Pharmacol Ther* 2022; **236**: 108239 [PMID: 35780916 DOI: 10.1016/j.pharmthera.2022.108239] [FullText]

52 **Advani SM**, Swartz MD, Loree J, Davis JS, Sarsashek AM, Lam M, Lee MS, Bressler J, Lopez DS, Daniel CR, Morris V, Shureqi I, Kee B, Dasari A, Vilar E, Overman M, Hamilton S, Maru D, Braithwaite D, Kopetz S. Epidemiology and Molecular-Pathologic Characteristics of CpG Island Methylator Phenotype (CIMP) in Colorectal Cancer. *Clin Colorectal Cancer* 2021; **20**: 137-147.e1 [PMID: 33229221 DOI: 10.1016/j.clcc.2020.09.007] [FullText]

53 **Gebhard C**, Mulet-Lazaro R, Glatz D, Schwarzfischer-Pfeilschifter L, Schirmacher P, Gaedcke J, Weichert W, Reuschel E, Dietmaier W, Rehli M. Aberrant DNA methylation patterns in microsatellite stable human colorectal cancers define a new marker panel for the CpG island methylator phenotype. *Int J Cancer* 2022; **150**: 617-625 [PMID: 34591983 DOI: 10.1002/ijc.33831] [FullText]

54 **Hezi H**, Gelber M, Balabanov A, Maruvka YE, Freiman M. CIMIL-CRC: A clinically-informed multiple instance learning framework for patient-level colorectal cancer molecular subtypes classification from H&E stained images. *Comput Methods Programs Biomed* 2025; **259**: 108513 [PMID: 39581068 DOI: 10.1016/j.cmpb.2024.108513] [FullText]

55 **Nzitakera A**, Uwamariya D, Kato H, Surwumwe JB, Mbonigaba A, Ndoricyimpaye EL, Uwamungu S, Manirakiza F, Ndayisaba MC, Ntakirutimana G, Seminega B, Dusabejambo V, Rutaganda E, Kamali P, Ngabonziza F, Ishikawa R, Watanabe H, Rugwizangoga B, Baba S, Yamada H, Yoshimura K, Sakai Y, Sugimura H, Shinmura K. TP53 mutation status and consensus molecular subtypes of colorectal cancer in patients from Rwanda. *BMC Cancer* 2024; **24**: 1266 [PMID: 39394554 DOI: 10.1186/s12885-024-13009-8] [FullText]

56 **Rejali L**, Seifollahi Asl R, Sanjabi F, Fatemi N, Asadzadeh Aghdaei H, Saeedi Niasar M, Ketabi Moghadam P, Nazemalhosseini Mojarad E, Mini E, Nobili S. Principles of Molecular Utility for CMS Classification in Colorectal Cancer Management. *Cancers (Basel)* 2023; **15**: 2746 [PMID: 37345083 DOI: 10.3390/cancers15102746] [FullText]

57 **Husain K**, Coppola D, Yang CS, Malafa MP. Effect of vitamin E δ-tocotrienol and aspirin on Wnt signaling in human colon cancer stem cells and in adenoma development in APCmin/+ mice. *Carcinogenesis* 2024; **45**: 881-892 [PMID: 38877828 DOI: 10.1093/carcin/bgae041] [FullText]

58 **Tejeda-Muñoz N**, Mei KC. Wnt signaling in cell adhesion, development, and colon cancer. *IUBMB Life* 2024; **76**: 383-396 [PMID: 38230869 DOI: 10.1002/iub.2806] [FullText]

59 **Vishnubhotla R**, Avanthi S, Mitnala S, Guduru VR, Rebala P, Patil SM, Shetty M, Sekaran A, Duvvur NR. Lesser prevalence of polyps/WNT-dysregulation and concomitant upregulation of gamma-catenin/MYC point to alternate pathways in colorectal cancer in India. *Mol Carcinog* 2024; **63**: 361-370 [PMID: 37983720 DOI: 10.1002/mc.23657] [FullText]

60 **Zhu Y**, Du Y, Zhang Y. DHX33 promotes colon cancer development downstream of Wnt signaling. *Gene* 2020; **735**: 144402 [PMID: 32004669 DOI: 10.1016/j.gene.2020.144402] [FullText]

61 **Kelson CO**, Zaytseva YY. Altered lipid metabolism in APC-driven colorectal cancer: the potential for therapeutic intervention. *Front Oncol* 2024; **14**: 1343061 [PMID: 38590663 DOI: 10.3389/fonc.2024.1343061] [FullText]

62 **Bourmoum M**, Radulovich N, Sharma A, Tkach JM, Tsao MS, Pelletier L. β-catenin mediates growth defects induced by centrosome loss in a subset of APC mutant colorectal cancer independently of p53. *PLoS One* 2024; **19**: e0295030 [PMID: 38324534 DOI: 10.1371/journal.pone.0295030] [FullText]

63 **Chen M**, Mashima T, Oishi T, Muramatsu Y, Seto Y, Takamatsu M, Kawata N, Morino S, Nakamura A, Inaba S, Yuan X, Maruyama K, Suzuki M, Sato A, Yoshida H, Jang MK, Mizutani A, Takeuchi K, Yamaguchi K, Shirai F, Nagayama S, Katayama R, Seimiya H. APC/PIK3CA mutations and β-catenin status predict tankyrase inhibitor sensitivity of patient-derived colorectal cancer cells. *Br J Cancer* 2024; **130**: 151-162 [PMID: 37968472 DOI: 10.1038/s41416-023-02484-8] [FullText]

64 **de Back TR**, Wu T, Schafrat PJ, Ten Hoorn S, Tan M, He L, van Hooff SR, Koster J, Nijman LE, Vink GR, Beumer IJ, Elbers CC, Lenos KJ, Sommeijer DW, Wang X, Vermeulen L. Correction: A consensus molecular subtypes classification strategy for clinical colorectal cancer tissues. *Life Sci Alliance* 2024; **7**: e202402889 [PMID: 38936972 DOI: 10.26508/lsa.202402889] [FullText]

65 **Ramos H**, Soares MIL, Silva J, Raimundo L, Calheiros J, Gomes C, Reis F, Monteiro FA, Nunes C, Reis S, Bosco B, Piazza S, Domingues L, Chlapek P, Vlcek P, Fabian P, Rajado AT, Carvalho ATP, Veselska R, Inga A, Pinho E Melo TMVD, Saraiva L. A selective p53 activator and anticancer agent to improve colorectal cancer therapy. *Cell Rep* 2021; **35**: 108982 [PMID: 33852837 DOI: 10.1016/j.celrep.2021.108982] [Full Text]

66 **Liebl MC**, Hofmann TG. The Role of p53 Signaling in Colorectal Cancer. *Cancers (Basel)* 2021; **13**: 2125 [PMID: 33924934 DOI: 10.3390/cancers13092125] [FullText]

67 **Rebersek M**. Consensus molecular subtypes (CMS) in metastatic colorectal cancer - personalized medicine decision. *Radiol Oncol* 2020; **54**: 272-277 [PMID: 32463385 DOI: 10.2478/raon-2020-0031] [FullText]

68 **Wang W**, Kandimalla R, Huang H, Zhu L, Li Y, Gao F, Goel A, Wang X. Molecular subtyping of colorectal cancer: Recent progress, new challenges and emerging opportunities. *Semin Cancer Biol* 2019; **55**: 37-52 [PMID: 29775690 DOI: 10.1016/j.semcancer.2018.05.002] [Full Text]

69 **Zhu G**, Pei L, Xia H, Tang Q, Bi F. Role of oncogenic KRAS in the prognosis, diagnosis and treatment of colorectal cancer. *Mol Cancer* 2021; **20**: 143 [PMID: 34742312 DOI: 10.1186/s12943-021-01441-4] [FullText]

70 **Costigan DC**, Dong F. The extended spectrum of RAS-MAPK pathway mutations in colorectal cancer. *Genes Chromosomes Cancer* 2020; **59**: 152-159 [PMID: 31589789 DOI: 10.1002/gcc.22813] [FullText]

71 **Juszczyk K**, Afzal MZ, Ganguly T, Kelly TL, Zeelie R, Murphy EMA. Evaluating whether KRAS/BRAF mutation status, anaemia and obstruction are associated with recurrence and mortality in non-metastatic colorectal cancer. *ANZ J Surg* 2023; **93**: 2457-2463 [PMID: 37088911 DOI: 10.1111/ans.18470] [FullText]

72 **Huang L**, Guo Z, Wang F, Fu L. KRAS mutation: from undruggable to druggable in cancer. *Signal Transduct Target Ther* 2021; **6**: 386 [PMID: 34776511 DOI: 10.1038/s41392-021-00780-4] [FullText]

73 **Yu L**, Wei J, Liu P. Attacking the PI3K/Akt/mTOR signaling pathway for targeted therapeutic treatment in human cancer. *Semin Cancer Biol* 2022; **85**: 69-94 [PMID: 34175443 DOI: 10.1016/j.semcancer.2021.06.019] [FullText]

74 **Peng Y**, Wang Y, Zhou C, Mei W, Zeng C. PI3K/Akt/mTOR Pathway and Its Role in Cancer Therapeutics: Are We Making Headway? *Front Oncol* 2022; **12**: 819128 [PMID: 35402264 DOI: 10.3389/fonc.2022.819128] [FullText]

75 **Huang TX**, Tan XY, Huang HS, Li YT, Liu BL, Liu KS, Chen X, Chen Z, Guan XY, Zou C, Fu L. Targeting cancer-associated fibroblast-secreted WNT2 restores dendritic cell-mediated antitumour immunity. *Gut* 2022; **71**: 333-344 [PMID: 33692094 DOI: 10.1136/gutjnl-2020-322924] [FullText]

76 **Qiu Q**, Tan D, Chen Q, Zhou R, Zhao X, Wen W, Yang P, Li J, Gong Z, Zhang D, Wang M. Clinical implications of PD-L1 expression and pathway-related molecular subtypes in advanced Asian colorectal cancer patients. *Am J Cancer Res* 2024; **14**: 796-808 [PMID: 38455414 DOI: 10.62347/FSSF9938] [FullText]

77 **González-Montero J**, Rojas CI, Burotto M. Predictors of response to immunotherapy in colorectal cancer. *Oncologist* 2024; **29**: 824-832 [PMID: 38920285 DOI: 10.1093/oncolo/oyae152] [FullText]

78 **Guo H**, Hu Z, Yang X, Yuan Z, Wang M, Chen C, Xie L, Gao Y, Li W, Bai Y, Lin C. Smad4 regulates TGF-β1-mediated hedgehog activation to promote epithelial-to-mesenchymal transition in pancreatic cancer cells by suppressing Gli1 activity. *Comput Struct Biotechnol J* 2024; **23**: 1189-1200 [PMID: 38525105 DOI: 10.1016/j.csbj.2024.03.010] [FullText]

79 **Malki A**, ElRuz RA, Gupta I, Allouch A, Vranic S, Al Moustafa AE. Molecular Mechanisms of Colon Cancer Progression and Metastasis: Recent Insights and Advancements. *Int J Mol Sci* 2020; **22**: 130 [PMID: 33374459 DOI: 10.3390/ijms22010130] [FullText]

80 **Rodríguez Silva J**, Monsalves-Álvarez M, Sepúlveda C, Donoso-Barraza C, Troncoso R, Hirsch S. Folate induces stemness and increases oxygen consumption under glucose deprivation by notch-1 pathway activation in colorectal cancer cell. *Mol Cell Biochem* 2025; **480**: 505-519 [PMID: 38536555 DOI: 10.1007/s11010-024-04987-1] [FullText]

81 **Mouillet-Richard S**, Cazelles A, Sroussi M, Gallois C, Taieb J, Laurent-Puig P. Clinical Challenges of Consensus Molecular Subtype CMS4 Colon Cancer in the Era of Precision Medicine. *Clin Cancer Res* 2024; **30**: 2351-2358 [PMID: 38564259 DOI: 10.1158/1078-0432.CCR-23-3964] [FullText]

82 **Kula A**, Dawidowicz M, Mielcarska S, Kiczmer P, Skiba H, Krygier M, Chrabańska M, Piecuch J, Szrot M, Robotycka J, Ochman B, Strzałkowska B, Czuba Z, Świętochowska E, Waniczek D. Overexpression and Role of HHLA2, a Novel Immune Checkpoint, in Colorectal Cancer. *Int J Mol Sci* 2023; **24**: 5876 [PMID: 36982953 DOI: 10.3390/ijms24065876] [FullText]

83 **Ziranu P**, Pretta A, Pozzari M, Maccioni A, Badiali M, Fanni D, Lai E, Donisi C, Persano M, Gerosa C, Puzzoni M, Bardanzellu F, Ambu R, Pusceddu V, Dubois M, Cerrone G, Migliari M, Murgia S, Spanu D, Pretta G, Aimola V, Balconi F, Murru S, Faa G, Scartozzi M. CDX-2 expression correlates with clinical outcomes in MSI-H metastatic colorectal cancer patients receiving immune checkpoint inhibitors. *Sci Rep* 2023; **13**: 4397 [PMID: 36928082 DOI: 10.1038/s41598-023-31538-3] [FullText]

84 **André T**, Shiu KK, Kim TW, Jensen BV, Jensen LH, Punt C, Smith D, Garcia-Carbonero R, Benavides M, Gibbs P, de la Fouchardiere C, Rivera F, Elez E, Bendell J, Le DT, Yoshino T, Van Cutsem E, Yang P, Farooqui MZH, Marinello P, Diaz LA Jr; KEYNOTE-177 Investigators. Pembrolizumab in Microsatellite-Instability-High Advanced Colorectal Cancer. *N Engl J Med* 2020; **383**: 2207-2218 [PMID: 33264544 DOI: 10.1056/NEJMoa2017699] [FullText]

85 **Ganesh K**. Optimizing immunotherapy for colorectal cancer. *Nat Rev Gastroenterol Hepatol* 2022; **19**: 93-94 [PMID: 34907331 DOI: 10.1038/s41575-021-00569-4] [FullText]

86 **Wang Q**, Shen X, Chen G, Du J. How to overcome resistance to immune checkpoint inhibitors in colorectal cancer: From mechanisms to translation. *Int J Cancer* 2023; **153**: 709-722 [PMID: 36752642 DOI: 10.1002/ijc.34464] [FullText]

87 **Lenz HJ**, Van Cutsem E, Luisa Limon M, Wong KYM, Hendlisz A, Aglietta M, García-Alfonso P, Neyns B, Luppi G, Cardin DB, Dragovich T, Shah U, Abdullaev S, Gricar J, Ledeine JM, Overman MJ, Lonardi S. First-Line Nivolumab Plus Low-Dose Ipilimumab for Microsatellite Instability-High/Mismatch Repair-Deficient Metastatic Colorectal Cancer: The Phase II CheckMate 142 Study. *J Clin Oncol* 2022; **40**: 161-170 [PMID: 34637336 DOI: 10.1200/JCO.21.01015] [FullText]

88 **Moretto R**, Rossini D, Catteau A, Antoniotti C, Giordano M, Boccaccino A, Ugolini C, Proietti A, Conca V, Kassambara A, Pietrantonio F, Salvatore L, Lonardi S, Tamberi S, Tamburini E, Poma AM, Fieschi J, Fontanini G, Masi G, Galon J, Cremolini C. Dissecting tumor lymphocyte infiltration to predict benefit from immune-checkpoint inhibitors in metastatic colorectal cancer: lessons from the AtezoT RIBE study. *J Immunother Cancer* 2023; **11**: e006633 [PMID: 37085190 DOI: 10.1136/jitc-2022-006633] [FullText]

89 **Shi Y**, Zheng H, Wang T, Zhou S, Zhao S, Li M, Cao B. Targeting KRAS: from metabolic regulation to cancer treatment. *Mol Cancer* 2025; **24**: 9 [PMID: 39799325 DOI: 10.1186/s12943-024-02216-3] [FullText]

90 **Zhao Y**, Feng X, Chen Y, Selfridge JE, Gorityala S, Du Z, Wang JM, Hao Y, Cioffi G, Conlon RA, Barnholtz-Sloan JS, Saltzman J, Krishnamurthi SS, Vinayak S, Veigl M, Xu Y, Bajor DL, Markowitz SD, Meropol NJ, Eads JR, Wang Z. 5-Fluorouracil Enhances the Antitumor Activity of the Glutaminase Inhibitor CB-839 against PIK3CA-Mutant Colorectal Cancers. *Cancer Res* 2020; **80**: 4815-4827 [PMID: 32907836 DOI: 10.1158/0008-5472.CAN-20-0600] [FullText]

91 **Van Cutsem E**, Taieb J, Yaeger R, Yoshino T, Grothey A, Maiello E, Elez E, Dekervel J, Ross P, Ruiz-Casado A, Graham J, Kato T, Ruffinelli JC, André T, Carrière Roussel E, Klauck I, Groc M, Vedovato JC, Tabernero J. ANCHOR CRC: Results From a Single-Arm, Phase II Study of Encorafenib Plus Binimetinib and Cetuximab in Previously Untreated BRAF(V600E)-Mutant Metastatic Colorectal Cancer. *J Clin Oncol* 2023; **41**: 2628-2637 [PMID: 36763936 DOI: 10.1200/JCO.22.01693] [FullText]

92 **Kopetz S**, Grothey A, Yaeger R, Van Cutsem E, Desai J, Yoshino T, Wasan H, Ciardiello F, Loupakis F, Hong YS, Steeghs N, Guren TK, Arkenau HT, Garcia-Alfonso P, Pfeiffer P, Orlov S, Lonardi S, Elez E, Kim TW, Schellens JHM, Guo C, Krishnan A, Dekervel J, Morris V, Calvo Ferrandiz A, Tarpgaard LS, Braun M, Gollerkeri A, Keir C, Maharry K, Pickard M, Christy-Bittel J, Anderson L, Sandor V, Tabernero J. Encorafenib, Binimetinib, and Cetuximab in BRAF V600E-Mutated Colorectal Cancer. *N Engl J Med* 2019; **381**: 1632-1643 [PMID: 31566309 DOI: 10.1056/NEJMoa1908075] [FullText]

93 **Kopetz S**, Guthrie KA, Morris VK, Lenz HJ, Magliocco AM, Maru D, Yan Y, Lanman R, Manyam G, Hong DS, Sorokin A, Atreya CE, Diaz LA, Allegra C, Raghav KP, Wang SE, Lieu CH, McDonough SL, Philip PA, Hochster HS. Randomized Trial of Irinotecan and Cetuximab With or Without Vemurafenib in BRAF-Mutant Metastatic Colorectal Cancer (SWOG S1406). *J Clin Oncol* 2021; **39**: 285-294 [PMID: 33356422 DOI: 10.1200/JCO.20.01994] [FullText]

94 **Tian J**, Chen JH, Chao SX, Pelka K, Giannakis M, Hess J, Burke K, Jorgji V, Sindurakar P, Braverman J, Mehta A, Oka T, Huang M, Lieb D, Spurrell M, Allen JN, Abrams TA, Clark JW, Enzinger AC, Enzinger PC, Klempner SJ, McCleary NJ, Meyerhardt JA, Ryan DP, Yurgelun MB, Kanter K, Van Seventer EE, Baiev I, Chi G, Jarnagin J, Bradford WB, Wong E, Michel AG, Fetter IJ, Siravegna G, Gemma AJ, Sharpe A, Demehri S, Leary R, Campbell CD, Yilmaz O, Getz GA, Parikh AR, Hacohen N, Corcoran RB. Combined PD-1, BRAF and MEK inhibition in BRAF(V600E) colorectal cancer: a phase 2 trial. *Nat Med* 2023; **29**: 458-466 [PMID: 36702949 DOI: 10.1038/s41591-022-02181-8] [FullText]

95 **Shah K**, Panchal S, Patel B. Porcupine inhibitors: Novel and emerging anti-cancer therapeutics targeting the Wnt signaling pathway. *Pharmacol Res* 2021; **167**: 105532 [PMID: 33677106 DOI: 10.1016/j.phrs.2021.105532] [FullText]

96 **Ding X**, Huang H, Fang Z, Jiang J. From Subtypes to Solutions: Integrating CMS Classification with Precision Therapeutics in Colorectal Cancer. *Curr Treat Options Oncol* 2024; **25**: 1580-1593 [PMID: 39589648 DOI: 10.1007/s11864-024-01282-5] [FullText]

97 **Zheng CC**, Liao L, Liu YP, Yang YM, He Y, Zhang GG, Li SJ, Liu T, Xu WW, Li B. Blockade of Nuclear β-Catenin Signaling *via* Direct Targeting of RanBP3 with NU2058 Induces Cell Senescence to Suppress Colorectal Tumorigenesis. *Adv Sci (Weinh)* 2022; **9**: e2202528 [PMID: 36270974 DOI: 10.1002/advs.202202528] [FullText]

98 **Xiang Z**, Wang Y, Ma X, Song S, He Y, Zhou J, Feng L, Yang S, Wu Y, Yu B, Xia G, Xu W, Zhao Y, Wang L. Targeting the NOTCH2/ADAM10/TCF7L2 Axis-Mediated Transcriptional Regulation of Wnt Pathway Suppresses Tumor Growth and Enhances Chemosensitivity in Colorectal Cancer. *Adv Sci (Weinh)* 2025; **12**: e2405758 [PMID: 39601111 DOI: 10.1002/advs.202405758] [FullText]

99 **Wu J**, Luo D, Li S. Ovo Like Zinc Finger 2 (OVOL2) Suppresses Breast Cancer Stem Cell Traits and Correlates with Immune Cells Infiltration. *Breast Cancer (Dove Med Press)* 2022; **14**: 211-227 [PMID: 35996562 DOI: 10.2147/BCTT.S363114] [FullText]

100 **Atibalentja DF**, Deutzmann A, Felsher DW. A big step for MYC-targeted therapies. *Trends Cancer* 2024; **10**: 383-385 [PMID: 38580534 DOI: 10.1016/j.trecan.2024.03.009] [FullText]

101 **Saeed H**, Leibowitz BJ, Zhang L, Yu J. Targeting Myc-driven stress addiction in colorectal cancer. *Drug Resist Updat* 2023; **69**: 100963 [PMID: 37119690 DOI: 10.1016/j.drup.2023.100963] [FullText]

102 **Garralda E**, Beaulieu ME, Moreno V, Casacuberta-Serra S, Martínez-Martín S, Foradada L, Alonso G, Massó-Vallés D, López-Estévez S, Jauset T, Corral de la Fuente E, Doger B, Hernández T, Perez-Lopez R, Arqués O, Castillo Cano V, Morales J, Whitfield JR, Niewel M, Soucek L, Calvo E. MYC targeting by OMO-103 in solid tumors: a phase 1 trial. *Nat Med* 2024; **30**: 762-771 [PMID: 38321218 DOI: 10.1038/s41591-024-02805-1] [FullText]

103 **Deming DA**. Development of KRAS Inhibitors and Their Role for Metastatic Colorectal Cancer. *J Natl Compr Canc Netw* 2025; **23**: e247067 [PMID: 39752885 DOI: 10.6004/jnccn.2024.7067] [FullText]

104 **Kataoka M**, Kitazawa M, Nakamura S, Koyama M, Yamamoto Y, Miyazaki S, Hondo N, Tanaka H, Soejima Y. Cetuximab Enhances the Efficacy of MRTX1133, a Novel KRAS(G12D) Inhibitor, in Colorectal Cancer Treatment. *Anticancer Res* 2023; **43**: 4341-4348 [PMID: 37772552 DOI: 10.21873/anticanres.16629] [FullText]

105 **Wei D**, Wang L, Zuo X, Maitra A, Bresalier RS. A Small Molecule with Big Impact: MRTX1133 Targets the KRASG12D Mutation in Pancreatic Cancer. *Clin Cancer Res* 2024; **30**: 655-662 [PMID: 37831007 DOI: 10.1158/1078-0432.CCR-23-2098] [FullText]

106 **Ramalingam PS**, Balakrishnan P, Rajendran S, Jothi A, Ramalingam R, Arumugam S. Identification of Dietary Bioflavonoids as Potential Inhibitors against KRAS G12D Mutant-Novel Insights from Computer-Aided Drug Discovery. *Curr Issues Mol Biol* 2023; **45**: 2136-2156 [PMID: 36975507 DOI: 10.3390/cimb45030137] [FullText]

107 **Ghosh S**, Fan F, Powell R, Park YS, Stephan C, Kopetz ES, Ellis LM, Bhattacharya R. Enhancing efficacy of the MEK inhibitor trametinib with paclitaxel in KRAS-mutated colorectal cancer. *Ther Adv Med Oncol* 2024; **16**: 17588359241303302 [PMID: 39664300 DOI: 10.1177/17588359241303302] [FullText]

108 **Isermann T**, Sers C, Der CJ, Papke B. KRAS inhibitors: resistance drivers and combinatorial strategies. *Trends Cancer* 2025; **11**: 91-116 [PMID: 39732595 DOI: 10.1016/j.trecan.2024.11.009] [FullText]

109 **Desai J**, Alonso G, Kim SH, Cervantes A, Karasic T, Medina L, Shacham-Shmueli E, Cosman R, Falcon A, Gort E, Guren T, Massarelli E, Miller WH Jr, Paz-Ares L, Prenen H, Amatu A, Cremolini C, Kim TW, Moreno V, Ou SI, Passardi A, Sacher A, Santoro A, Stec R, Ulahannan S, Arbour K, Lorusso P, Luo J, Patel MR, Choi Y, Shi Z, Mandlekar S, Lin MT, Royer-Joo S, Chang J, Jun T, Dharia NV, Schutzman JL; GO42144 Investigator and Study Group, Han SW. Divarasib plus cetuximab in KRAS G12C-positive colorectal cancer: a phase 1b trial. *Nat Med* 2024; **30**: 271-278 [PMID: 38052910 DOI: 10.1038/s41591-023-02696-8] [FullText]

110 **Potocki PM**, Wójcik P, Chmura Ł, Goc B, Fedewicz M, Bielańska Z, Swadźba J, Konopka K, Kwinta Ł, Wysocki PJ. Clinical Characterization of Targetable Mutations (BRAF V600E and KRAS G12C) in Advanced Colorectal Cancer-A Nation-Wide Study. *Int J Mol Sci* 2023; **24**: 9073 [PMID: 37240418 DOI: 10.3390/ijms24109073] [FullText]

111 **Ugai S**, Yao Q, Takashima Y, Zhong Y, Matsuda K, Kawamura H, Imamura Y, Okadome K, Mima K, Arima K, Kosumi K, Song M, Meyerhardt JA, Giannakis M, Nowak JA, Ugai T, Ogino S. Clinicopathological, molecular, and prognostic features of colorectal carcinomas

with KRAS c.34G>T (p.G12C) mutation. *Cancer Sci* 2024; **115**: 3455-3465 [PMID: 39039804 DOI: 10.1111/cas.16262] [FullText]

112 **Bever KM**, Thomas DL 2nd, Zhang J, Diaz Rivera EA, Rosner GL, Zhu Q, Nauroth JM, Christmas B, Thompson ED, Anders RA, Judkins C, Liu M, Jaffee EM, Ahuja N, Zheng L, Azad NS. A feasibility study of combined epigenetic and vaccine therapy in advanced colorectal cancer with pharmacodynamic endpoint. *Clin Epigenetics* 2021; **13**: 25 [PMID: 33531075 DOI: 10.1186/s13148-021-01014-8] [FullText]

113 **Kim VM**, Pan X, Soares KC, Azad NS, Ahuja N, Gamper CJ, Blair AB, Muth S, Ding D, Ladle BH, Zheng L. Neoantigen-based EpiGVAX vaccine initiates antitumor immunity in colorectal cancer. *JCI Insight* 2020; **5**: e136368 [PMID: 32376802 DOI: 10.1172/jci.insight.136368] [FullText]

114 **Yarchoan M**, Huang CY, Zhu Q, Ferguson AK, Durham JN, Anders RA, Thompson ED, Rozich NS, Thomas DL 2nd, Nauroth JM, Rodriguez C, Osipov A, De Jesus-Acosta A, Le DT, Murphy AG, Laheru D, Donehower RC, Jaffee EM, Zheng L, Azad NS. A phase 2 study of GVAX colon vaccine with cyclophosphamide and pembrolizumab in patients with mismatch repair proficient advanced colorectal cancer. *Cancer Med* 2020; **9**: 1485-1494 [PMID: 31876399 DOI: 10.1002/cam4.2763] [FullText]

115 **Bakrim S**, El Hachlafi N, Khalid A, Abdalla AN, El Omari N, Aboulaghras S, Sakran AM, Goh KW, Ming LC, Razi P, Bouyahya A. Recent advances and molecular mechanisms of TGF-β signaling in colorectal cancer, with focus on bioactive compounds targeting. *Biomed Pharmacother* 2024; **177**: 116886 [PMID: 38945700 DOI: 10.1016/j.biopha.2024.116886] [FullText]

116 **Yamazaki T**, Gunderson AJ, Gilchrist M, Whiteford M, Kiely MX, Hayman A, O'Brien D, Ahmad R, Manchio JV, Fox N, McCarty K, Phillips M, Brosnan E, Vaccaro G, Li R, Simon M, Bernstein E, McCormick M, Yamasaki L, Wu Y, Drokin A, Carnahan T, To Y, Redmond WL, Lee B, Louie J, Hansen E, Solhjem MC, Cramer J, Urba WJ, Gough MJ, Crittenden MR, Young KH. Galunisertib plus neoadjuvant chemoradiotherapy in patients with locally advanced rectal cancer: a single-arm, phase 2 trial. *Lancet Oncol* 2022; **23**: 1189-1200 [PMID: 35952709 DOI: 10.1016/S1470-2045(22)00446-6] [FullText]

117 **Qiu MZ**, Bai Y, Wang J, Gu K, Yang M, He Y, Yi C, Jin Y, Liu B, Wang F, Chen YK, Dai W, Jiang Y, Huang C, Xu RH, Luo HY. Addition of SHR-1701 to first-line capecitabine and oxaliplatin (XELOX) plus bevacizumab for unresectable metastatic colorectal cancer. *Signal Transduct Target Ther* 2024; **9**: 349 [PMID: 39676137 DOI: 10.1038/s41392-024-02063-0] [FullText]

118 **Gulley JL**, Schlom J, Barcellos-Hoff MH, Wang XJ, Seoane J, Audhuy F, Lan Y, Dussault I, Moustakas A. Dual inhibition of TGF-β and PD-L1: a novel approach to cancer treatment. *Mol Oncol* 2022; **16**: 2117-2134 [PMID: 34854206 DOI: 10.1002/1878-0261.13146] [FullText]

119 **Niu M**, Yi M, Wu Y, Lyu L, He Q, Yang R, Zeng L, Shi J, Zhang J, Zhou P, Zhang T, Mei Q, Chu Q, Wu K. Synergistic efficacy of simultaneous anti-TGF-β/VEGF bispecific antibody and PD-1 blockade in cancer therapy. *J Hematol Oncol* 2023; **16**: 94 [PMID: 37573354 DOI: 10.1186/s13045-023-01487-5] [FullText]

120 **Cassier PA**, Navaridas R, Bellina M, Rama N, Ducarouge B, Hernandez-Vargas H, Delord JP, Lengrand J, Paradisi A, Fattet L, Garin G, Gheit H, Dalban C, Pastushenko I, Neves D, Jelin R, Gadot N, Braissand N, Léon S, Degletagne C, Matias-Guiu X, Devouassoux-Shisheboran M, Mery-Lamarche E, Allard J, Zindy E, Decaestecker C, Salmon I, Perol D, Dolcet X, Ray-Coquard I, Blanpain C, Bernet A, Mehlen P. Netrin-1 blockade inhibits tumour growth and EMT features in endometrial cancer. *Nature* 2023; **620**: 409-416 [PMID: 37532934 DOI: 10.1038/s41586-023-06367-z] [FullText]

121 **Zhang N**, Ng AS, Cai S, Li Q, Yang L, Kerr D. Novel therapeutic strategies: targeting epithelial-mesenchymal transition in colorectal cancer. *Lancet Oncol* 2021; **22**: e358-e368 [PMID: 34339656 DOI: 10.1016/S1470-2045(21)00343-0] [FullText]

122 **Passardi A**, Bittoni A, Bai Z, Zhang Z, Sier C, He Y, Shahini E, Solimando AG. Editorial: Angiogenesis blockade for the treatment of gastrointestinal cancer. *Front Oncol* 2023; **13**: 1147849 [PMID: 36816979 DOI: 10.3389/fonc.2023.1147849] [FullText]

123 **Hong JH**, Woo IS. Metronomic chemotherapy as a potential partner of immune checkpoint inhibitors for metastatic colorectal cancer treatment. *Cancer Lett* 2023; **565**: 216236 [PMID: 37209943 DOI: 10.1016/j.canlet.2023.216236] [FullText]

124 **Zhao M**, Guan P, Xu S, Lu H, Liu Z. Molecularly Imprinted Nanomedicine for Anti-angiogenic Cancer Therapy *via* Blocking Vascular Endothelial Growth Factor Signaling. *Nano Lett* 2023; **23**: 8674-8682 [PMID: 37721331 DOI: 10.1021/acs.nanolett.3c02514] [FullText]

125 **Shailes H**, Tse WY, Freitas MO, Silver A, Martin SA. Statin Treatment as a Targeted Therapy for APC-Mutated Colorectal Cancer. *Front Oncol* 2022; **12**: 880552 [PMID: 35712511 DOI: 10.3389/fonc.2022.880552] [FullText]

126 **Wong CC**, Wu JL, Ji F, Kang W, Bian X, Chen H, Chan LS, Luk STY, Tong S, Xu J, Zhou Q, Liu D, Su H, Gou H, Cheung AH, To KF, Cai Z, Shay JW, Yu J. The cholesterol uptake regulator PCSK9 promotes and is a therapeutic target in APC/KRAS-mutant colorectal cancer. *Nat Commun* 2022; **13**: 3971 [PMID: 35803966 DOI: 10.1038/s41467-022-31663-z] [FullText]

127 **Cen B**, Wei J, Wang D, Xiong Y, Shay JW, DuBois RN. Mutant APC promotes tumor immune evasion *via* PD-L1 in colorectal cancer. *Oncogene* 2021; **40**: 5984-5992 [PMID: 34385594 DOI: 10.1038/s41388-021-01972-6] [FullText]

128 **Noe O**, Filipiak L, Royfman R, Campbell A, Lin L, Hamouda D, Stanbery L, Nemunaitis J. Adenomatous polyposis coli in cancer and therapeutic implications. *Oncol Rev* 2021; **15**: 534 [PMID: 34267890 DOI: 10.4081/oncol.2021.534] [FullText]

129 **Mao Y**, Wang W, Yang J, Zhou X, Lu Y, Gao J, Wang X, Wen L, Fu W, Tang F. Drug repurposing screening and mechanism analysis based on human colorectal cancer organoids. *Protein Cell* 2024; **15**: 285-304 [PMID: 37345888 DOI: 10.1093/procel/pwad038] [FullText]

130 **Shen T**, Sun X, Yang S, Wang W, Chen Z, Lin Y, Li S, Peng H, Zeng L, Li G, Li X, Wang B, Ning J, Wen H, Lei B, Zhang L. Innovative Oral Nano/Gene Delivery System Based on Engineered Modified Saccharomyces cerevisiae for Colorectal Cancer Therapy. *ACS Nano* 2024; **18**: 28212-28227 [PMID: 39363565 DOI: 10.1021/acsnano.4c08044] [FullText]

131 **Wan T**, Pan Q, Liu C, Guo J, Li B, Yan X, Cheng Y, Ping Y. A Duplex CRISPR-Cas9 Ribonucleoprotein Nanomedicine for Colorectal Cancer Gene Therapy. *Nano Lett* 2021; **21**: 9761-9771 [PMID: 34767372 DOI: 10.1021/acs.nanolett.1c03708] [FullText]

132 **Zhao S**, Wen H, Wang B, Xiong Q, Li L, Cheng A. p53: A player in the tumor microenvironment. *Oncol Res* 2025; **33**: 795-810 [PMID: 40191727 DOI: 10.32604/or.2025.057317] [FullText]

133 **Michel M**, Kaps L, Maderer A, Galle PR, Moehler M. The Role of p53 Dysfunction in Colorectal Cancer and Its Implication for Therapy. *Cancers (Basel)* 2021; **13**: 2296 [PMID: 34064974 DOI: 10.3390/cancers13102296] [FullText]

134 **Rompianesi G**, Pegoraro F, Ceresa CD, Montalti R, Troisi RI. Artificial intelligence in the diagnosis and management of colorectal cancer liver metastases. *World J Gastroenterol* 2022; **28**: 108-122 [PMID: 35125822 DOI: 10.3748/wjg.v28.i1.108] [FullText]

135 **Majumder A**, Sen D. Artificial intelligence in cancer diagnostics and therapy: current perspectives. *Indian J Cancer* 2021; **58**: 481-492 [PMID: 34975094 DOI: 10.4103/ijc.IJC_399_20] [FullText]

136 **Repici A**, Spadaccini M, Antonelli G, Correale L, Maselli R, Galtieri PA, Pellegatta G, Capogreco A, Milluzzo SM, Lollo G, Di Paolo D, Badalamenti M, Ferrara E, Fugazza A, Carrara S, Anderloni A, Rondonotti E, Amato A, De Gottardi A, Spada C, Radaelli F, Savevski V, Wallace MB, Sharma P, Rösch T, Hassan C. Artificial intelligence and colonoscopy experience: lessons from two randomised trials. *Gut* 2022; **71**: 757-765 [PMID: 34187845 DOI: 10.1136/gutjnl-2021-324471] [FullText]

137 **Senthil Kumar K**, Miskovic V, Blasiak A, Sundar R, Pedrocchi ALG, Pearson AT, Prelaj A, Ho D. Artificial Intelligence in Clinical Oncology: From Data to Digital Pathology and Treatment. *Am Soc Clin Oncol Educ Book* 2023; **43**: e390084 [PMID: 37235822 DOI: 10.1200/EDBK_390084] [FullText]

138 **Huang S**, Yang J, Fong S, Zhao Q. Artificial intelligence in cancer diagnosis and prognosis: Opportunities and challenges. *Cancer Lett* 2020; **471**: 61-71 [PMID: 31830558 DOI: 10.1016/j.canlet.2019.12.007] [FullText]

139 **Yin Z**, Yao C, Zhang L, Qi S. Application of artificial intelligence in diagnosis and treatment of colorectal cancer: A novel Prospect. *Front Med (Lausanne)* 2023; **10**: 1128084 [PMID: 36968824 DOI: 10.3389/fmed.2023.1128084] [FullText]

140 **Lee SH**, Jang HJ. Deep learning-based prediction of molecular cancer biomarkers from tissue slides: A new tool for precision oncology. *Clin Mol Hepatol* 2022; **28**: 754-772 [PMID: 35443570 DOI: 10.3350/cmh.2021.0394] [FullText]

141 **Ruusuvuori P**, Valkonen M, Latonen L. Deep learning transforms colorectal cancer biomarker prediction from histopathology images. *Cancer Cell* 2023; **41**: 1543-1545 [PMID: 37652005 DOI: 10.1016/j.ccell.2023.08.006] [FullText]

142 **Hildebrand LA**, Pierce CJ, Dennis M, Paracha M, Maoz A. Artificial Intelligence for Histology-Based Detection of Microsatellite Instability and Prediction of Response to Immunotherapy in Colorectal Cancer. *Cancers (Basel)* 2021; **13**: 391 [PMID: 33494280 DOI: 10.3390/cancers13030391] [FullText]

143 **Zamanitajeddin N**, Jahanifar M, Bilal M, Eastwood M, Rajpoot N. Social network analysis of cell networks improves deep learning for prediction of molecular pathways and key mutations in colorectal cancer. *Med Image Anal* 2024; **93**: 103071 [PMID: 38199068 DOI: 10.1016/j.media.2023.103071] [FullText]

144 **Sirinukunwattana K**, Domingo E, Richman SD, Redmond KL, Blake A, Verrill C, Leedham SJ, Chatzipli A, Hardy C, Whalley CM, Wu CH, Beggs AD, McDermott U, Dunne PD, Meade A, Walker SM, Murray GI, Samuel L, Seymour M, Tomlinson I, Quirke P, Maughan T, Rittscher J, Koelzer VH; S:CORT consortium. Image-based consensus molecular subtype (imCMS) classification of colorectal cancer using deep learning. *Gut* 2021; **70**: 544-554 [PMID: 32690604 DOI: 10.1136/gutjnl-2019-319866] [FullText]

145 **Bhukdee D**, Nuwongsri P, Israsena N, Sriswasdi S. Improved Delineation of Colorectal Cancer Molecular Subtypes and Functional Profiles with a 62-Gene Panel. *Mol Cancer Res* 2023; **21**: 240-252 [PMID: 36490322 DOI: 10.1158/1541-7786.MCR-22-0476] [FullText]

146 **Pepe G**, Carrino C, Parca L, Helmer-Citterich M. Dissecting the Genome for Drug Response Prediction. *Methods Mol Biol* 2022; **2449**: 187-196 [PMID: 35507263 DOI: 10.1007/978-1-0716-2095-3_7] [FullText]

147 **Mathema VB**, Sen P, Lamichhane S, Orešič M, Khoomrung S. Deep learning facilitates multi-data type analysis and predictive biomarker discovery in cancer precision medicine. *Comput Struct Biotechnol J* 2023; **21**: 1372-1382 [PMID: 36817954 DOI: 10.1016/j.csbj.2023.01.043] [FullText]

148 **Zhao Y**, Ge X, He J, Cheng Y, Wang Z, Wang J, Sun L. The prognostic value of tumor-infiltrating lymphocytes in colorectal cancer differs by anatomical subsite: a systematic review and meta-analysis. *World J Surg Oncol* 2019; **17**: 85 [PMID: 31118034 DOI: 10.1186/s12957-019-1621-9] [FullText]

149 **Foersch S**, Glasner C, Woerl AC, Eckstein M, Wagner DC, Schulz S, Kellers F, Fernandez A, Tserea K, Kloth M, Hartmann A, Heintz A, Weichert W, Roth W, Geppert C, Kather JN, Jesinghaus M. Multistain deep learning for prediction of prognosis and therapy response in colorectal cancer. *Nat Med* 2023; **29**: 430-439 [PMID: 36624314 DOI: 10.1038/s41591-022-02134-1] [FullText]

150 **Väyrynen JP**, Lau MC, Haruki K, Väyrynen SA, Dias Costa A, Borowsky J, Zhao M, Fujiyoshi K, Arima K, Twombly TS, Kishikawa J, Gu S, Aminmozaffari S, Shi S, Baba Y, Akimoto N, Ugai T, Da Silva A, Song M, Wu K, Chan AT, Nishihara R, Fuchs CS, Meyerhardt JA, Giannakis M, Ogino S, Nowak JA. Prognostic Significance of Immune Cell Populations Identified by Machine Learning in Colorectal Cancer Using Routine Hematoxylin and Eosin-Stained Sections. *Clin Cancer Res* 2020; **26**: 4326-4338 [PMID: 32439699 DOI: 10.1158/1078-0432.CCR-20-0071] [FullText]

151 **Kather JN**, Pearson AT, Halama N, Jäger D, Krause J, Loosen SH, Marx A, Boor P, Tacke F, Neumann UP, Grabsch HI, Yoshikawa T, Brenner H, Chang-Claude J, Hoffmeister M, Trautwein C, Luedde T. Deep learning can predict microsatellite instability directly from histology in gastrointestinal cancer. *Nat Med* 2019; **25**: 1054-1056 [PMID: 31160815 DOI: 10.1038/s41591-019-0462-y] [FullText]

152 **Rafique R**, Islam SMR, Kazi JU. Machine learning in the prediction of cancer therapy. *Comput Struct Biotechnol J* 2021; **19**: 4003-4017 [PMID: 34377366 DOI: 10.1016/j.csbj.2021.07.003] [FullText]

153 **Tanaka I**, Furukawa T, Morise M. The current issues and future perspective of artificial intelligence for developing new treatment strategy in non-small cell lung cancer: harmonization of molecular cancer biology and artificial intelligence. *Cancer Cell Int* 2021; **21**: 454 [PMID: 34446006 DOI: 10.1186/s12935-021-02165-7] [FullText]

154 **Wang C**, Kumar GA, Rajapakse JC. Drug discovery and mechanism prediction with explainable graph neural networks. *Sci Rep* 2025; **15**: 179 [PMID: 39747341 DOI: 10.1038/s41598-024-83090-3] [FullText]

155 **Yang J**, Huang J, Han D, Ma X. Artificial Intelligence Applications in the Treatment of Colorectal Cancer: A Narrative Review. *Clin Med Insights Oncol* 2024; **18**: 11795549231220320 [PMID: 38187459 DOI: 10.1177/11795549231220320] [FullText]

156 **Ginghina O**, Hudita A, Zamfir M, Spanu A, Mardare M, Bondoc I, Buburuzan L, Georgescu SE, Costache M, Negrei C, Nitipir C, Galateanu B. Liquid Biopsy and Artificial Intelligence as Tools to Detect Signatures of Colorectal Malignancies: A Modern Approach in Patient's Stratification. *Front Oncol* 2022; **12**: 856575 [PMID: 35356214 DOI: 10.3389/fonc.2022.856575] [FullText]

157 **Schulz S**, Jesinghaus M, Foersch S. [Multistain deep learning as a prognostic and predictive biomarker in colorectal cancer]. *Pathologie (Heidelb)* 2023; **44**: 104-108 [PMID: 37987821 DOI: 10.1007/s00292-023-01280-8] [FullText]

158 **Das K**, Paltani M, Tripathi PK, Kumar R, Verma S, Kumar S, Jain CK. Current implications and challenges of artificial intelligence technologies in therapeutic intervention of colorectal cancer. *Explor Target Antitumor Ther* 2023; **4**: 1286-1300 [PMID: 38213536 DOI: 10.37349/etat.2023.00197] [FullText]

159 **Kim N**, Lee ES, Won SE, Yang M, Lee AJ, Shin Y, Ko Y, Pyo J, Park HJ, Kim KW. Evolution of Radiological Treatment Response Assessments for Cancer Immunotherapy: From iRECIST to Radiomics and Artificial Intelligence. *Korean J Radiol* 2022; **23**: 1089-1101 [PMID: 36098343 DOI: 10.3348/kjr.2022.0225] [FullText]

160 **Sun R**, Limkin EJ, Vakalopoulou M, Dercle L, Champiat S, Han SR, Verlingue L, Brandao D, Lancia A, Ammari S, Hollebecque A, Scoazec JY, Marabelle A, Massard C, Soria JC, Robert C, Paragios N, Deutsch E, Ferté C. A radiomics approach to assess tumour-infiltrating CD8 cells and response to anti-PD-1 or anti-PD-L1 immunotherapy: an imaging biomarker, retrospective multicohort study. *Lancet Oncol* 2018; **19**: 1180-1191 [PMID: 30120041 DOI: 10.1016/S1470-2045(18)30413-3] [FullText]

161 **Lafarge MW**, Domingo E, Sirinukunwattana K, Wood R, Samuel L, Murray G, Richman SD, Blake A, Sebag-Montefiore D, Gollins S, Klieser E, Neureiter D, Huemer F, Greil R, Dunne P, Quirke P, Weiss L, Rittscher J, Maughan T, Koelzer VH. Image-based consensus

molecular subtyping in rectal cancer biopsies and response to neoadjuvant chemoradiotherapy. *NPJ Precis Oncol* 2024; **8**: 89 [PMID: 38594327 DOI: 10.1038/s41698-024-00580-3] [FullText]

162 **Rezayi S**, R Niakan Kalhori S, Saeedi S. Effectiveness of Artificial Intelligence for Personalized Medicine in Neoplasms: A Systematic Review. *Biomed Res Int* 2022; **2022**: 7842566 [PMID: 35434134 DOI: 10.1155/2022/7842566] [FullText]

163 **Guo J**, Hu J, Zheng Y, Zhao S, Ma J. Artificial intelligence: opportunities and challenges in the clinical applications of triple-negative breast cancer. *Br J Cancer* 2023; **128**: 2141-2149 [PMID: 36871044 DOI: 10.1038/s41416-023-02215-z] [FullText]

164 **Khozin S**. From organs to algorithms: Redefining cancer classification in the age of artificial intelligence. *Clin Transl Sci* 2024; **17**: e70001 [PMID: 39206604 DOI: 10.1111/cts.70001] [FullText]

165 **Kakni P**, Hueber R, Knoops K, López-Iglesias C, Truckenmüller R, Habibovic P, Giselbrecht S. Intestinal Organoid Culture in Polymer Film-Based Microwell Arrays. *Adv Biosyst* 2020; **4**: e2000126 [PMID: 32734713 DOI: 10.1002/adbi.202000126] [FullText]

166 **Li X**, Larsson P, Ljuslinder I, Öhlund D, Myte R, Löfgren-Burström A, Zingmark C, Ling A, Edin S, Palmqvist R. Ex Vivo Organoid Cultures Reveal the Importance of the Tumor Microenvironment for Maintenance of Colorectal Cancer Stem Cells. *Cancers (Basel)* 2020; **12**: 923 [PMID: 32290033 DOI: 10.3390/cancers12040923] [FullText]

167 **Sato T**, Vries RG, Snippert HJ, van de Wetering M, Barker N, Stange DE, van Es JH, Abo A, Kujala P, Peters PJ, Clevers H. Single Lgr5 stem cells build crypt-villus structures in vitro without a mesenchymal niche. *Nature* 2009; **459**: 262-265 [PMID: 19329995 DOI: 10.1038/nature07935] [FullText]

168 **Spence JR**, Mayhew CN, Rankin SA, Kuhar MF, Vallance JE, Tolle K, Hoskins EE, Kalinichenko VV, Wells SI, Zorn AM, Shroyer NF, Wells JM. Directed differentiation of human pluripotent stem cells into intestinal tissue in vitro. *Nature* 2011; **470**: 105-109 [PMID: 21151107 DOI: 10.1038/nature09691] [FullText]

169 **Daoud A**, Múnera JO. Generation of human colonic organoids from human pluripotent stem cells. *Methods Cell Biol* 2020; **159**: 201-227 [PMID: 32586443 DOI: 10.1016/bs.mcb.2020.03.001] [FullText]

170 **Crespo M**, Vilar E, Tsai SY, Chang K, Amin S, Srinivasan T, Zhang T, Pipalia NH, Chen HJ, Witherspoon M, Gordillo M, Xiang JZ, Maxfield FR, Lipkin S, Evans T, Chen S. Colonic organoids derived from human induced pluripotent stem cells for modeling colorectal cancer and drug testing. *Nat Med* 2017; **23**: 878-884 [PMID: 28628110 DOI: 10.1038/nm.4355] [FullText]

171 **Mishra I**, Gupta K, Mishra R, Chaudhary K, Sharma V. An Exploration of Organoid Technology: Present Advancements, Applications, and Obstacles. *Curr Pharm Biotechnol* 2024; **25**: 1000-1020 [PMID: 37807405 DOI: 10.2174/0113892010273024230925075231] [FullText]

172 **Múnera JO**, Kechele DO, Bouffi C, Qu N, Jing R, Maity P, Enriquez JR, Han L, Campbell I, Mahe MM, McCauley HA, Zhang X, Sundaram N, Hudson JR, Zarsozo-Lacoste A, Pradhan S, Tominaga K, Sanchez JG, Weiss AA, Chatuvedi P, Spence JR, Hachimi M, North T, Daley GQ, Mayhew CN, Hu YC, Takebe T, Helmrath MA, Wells JM. Development of functional resident macrophages in human pluripotent stem cell-derived colonic organoids and human fetal colon. *Cell Stem Cell* 2023; **30**: 1434-1451.e9 [PMID: 37922878 DOI: 10.1016/j.stem.2023.10.002] [FullText]

173 **Yoon H**, Lee S. Integration of Genomic Profiling and Organoid Development in Precision Oncology. *Int J Mol Sci* 2021; **23**: 216 [PMID: 35008642 DOI: 10.3390/ijms23010216] [FullText]

174 **Zhang W**, Wu C, Huang H, Bleu P, Zambare W, Alvarez J, Wang L, Paty PB, Romesser PB, Smith JJ, Chen XS. Enhancing Chemotherapy Response Prediction *via* Matched Colorectal Tumor-Organoid Gene Expression Analysis and Network-Based Biomarker Selection. *medRxiv* 2024 [PMID: 38343861 DOI: 10.1101/2024.01.24.24301749] [FullText]

175 **Abd El-Salam MA**, Troulis MJ, Pan CX, Rao RA. Unlocking the potential of organoids in cancer treatment and translational research: An application of cytologic techniques. *Cancer Cytopathol* 2024; **132**: 96-102 [PMID: 37843532 DOI: 10.1002/cncy.22769] [FullText]

176 **Kim SK**, Kim YH, Park S, Cho SW. Organoid engineering with microfluidics and biomaterials for liver, lung disease, and cancer modeling. *Acta Biomater* 2021; **132**: 37-51 [PMID: 33711526 DOI: 10.1016/j.actbio.2021.03.002] [FullText]

177 **Polak R**, Zhang ET, Kuo CJ. Cancer organoids 2.0: modelling the complexity of the tumour immune microenvironment. *Nat Rev Cancer* 2024; **24**: 523-539 [PMID: 38977835 DOI: 10.1038/s41568-024-00706-6] [FullText]

178 **Qin X**, Sufi J, Vlckova P, Kyriakidou P, Acton SE, Li VSW, Nitz M, Tape CJ. Cell-type-specific signaling networks in heterocellular organoids. *Nat Methods* 2020; **17**: 335-342 [PMID: 32066960 DOI: 10.1038/s41592-020-0737-8] [FullText]

179 **Dijkstra KK**, Cattaneo CM, Weeber F, Chalabi M, van de Haar J, Fanchi LF, Slagter M, van der Velden DL, Kaing S, Kelderman S, van Rooij N, van Leerdam ME, Depla A, Smit EF, Hartemink KJ, de Groot R, Wolkers MC, Sachs N, Snaebjornsson P, Monkhorst K, Haanen J, Clevers H, Schumacher TN, Voest EE. Generation of Tumor-Reactive T Cells by Co-culture of Peripheral Blood Lymphocytes and Tumor Organoids. *Cell* 2018; **174**: 1586-1598.e12 [PMID: 30100188 DOI: 10.1016/j.cell.2018.07.009] [FullText]

180 **Li J**, Liu J, Xia W, Yang H, Sha W, Chen H. Deciphering the Tumor Microenvironment of Colorectal Cancer and Guiding Clinical Treatment With Patient-Derived Organoid Technology: Progress and Challenges. *Technol Cancer Res Treat* 2024; **23**: 15330338231221856 [PMID: 38225190 DOI: 10.1177/15330338231221856] [FullText]

181 **Hu LF**, Yang X, Lan HR, Fang XL, Chen XY, Jin KT. Preclinical tumor organoid models in personalized cancer therapy: Not everyone fits the mold. *Exp Cell Res* 2021; **408**: 112858 [PMID: 34600901 DOI: 10.1016/j.yexcr.2021.112858] [FullText]

182 **Toshimitsu K**, Takano A, Fujii M, Togasaki K, Matano M, Takahashi S, Kanai T, Sato T. Organoid screening reveals epigenetic vulnerabilities in human colorectal cancer. *Nat Chem Biol* 2022; **18**: 605-614 [PMID: 35273398 DOI: 10.1038/s41589-022-00984-x] [FullText]

183 **Prieto I**, Barbáchano A, Rodríguez-Salas N, Viñal D, Cortés-Guiral D, Muñoz A, Fernández-Barral A. Tailored chemotherapy for colorectal cancer peritoneal metastases based on a drug-screening platform in patient-derived organoids: a case report. *J Gastrointest Oncol* 2023; **14**: 442-449 [PMID: 36915469 DOI: 10.21037/jgo-22-599] [FullText]

184 **Larsen BM**, Kannan M, Langer LF, Leibowitz BD, Bentaieb A, Cancino A, Dolgalev I, Drummond BE, Dry JR, Ho CS, Khullar G, Krantz BA, Mapes B, McKinnon KE, Metti J, Perera JF, Rand TA, Sanchez-Freire V, Shaxted JM, Stein MM, Streit MA, Tan YC, Zhang Y, Zhao E, Venkataraman J, Stumpe MC, Borgia JA, Masood A, Catenacci DVT, Mathews JV, Gursel DB, Wei JJ, Welling TH, Simeone DM, White KP, Khan AA, Igartua C, Salahudeen AA. A pan-cancer organoid platform for precision medicine. *Cell Rep* 2021; **36**: 109429 [PMID: 34320344 DOI: 10.1016/j.celrep.2021.109429] [FullText]

185 **Sun CP**, Lan HR, Fang XL, Yang XY, Jin KT. Organoid Models for Precision Cancer Immunotherapy. *Front Immunol* 2022; **13**: 770465 [PMID: 35450073 DOI: 10.3389/fimmu.2022.770465] [FullText]

186 **Yi K**, Park SH, Kim DU, Jeon DY, Lee HJ, Song GA, Jo HJ, Baek DH, Han JH, Lee BC. Patient-derived Organoid Model for Predicting the Chemoresponse in Patients With Colorectal Cancer. *In Vivo* 2023; **37**: 1751-1759 [PMID: 37369516 DOI: 10.21873/invivo.13263] [FullText]

187 **Durinikova E**, Buzo K, Arena S. Preclinical models as patients' avatars for precision medicine in colorectal cancer: past and future challenges. *J Exp Clin Cancer Res* 2021; **40**: 185 [PMID: 34090508 DOI: 10.1186/s13046-021-01981-z] [FullText]

188 **Cho YW**, Min DW, Kim HP, An Y, Kim S, Youk J, Chun J, Im JP, Song SH, Ju YS, Han SW, Park KJ, Kim TY. Patient-derived organoids as a preclinical platform for precision medicine in colorectal cancer. *Mol Oncol* 2022; **16**: 2396-2412 [PMID: 34850547 DOI: 10.1002/1878-0261.13144] [FullText]

189 **Yuki K**, Cheng N, Nakano M, Kuo CJ. Organoid Models of Tumor Immunology. *Trends Immunol* 2020; **41**: 652-664 [PMID: 32654925 DOI: 10.1016/j.it.2020.06.010] [FullText]

190 **Yang C**, Xiao W, Wang R, Hu Y, Yi K, Sun X, Wang G, Xu X. Tumor organoid model of colorectal cancer (Review). *Oncol Lett* 2023; **26**: 328 [PMID: 37415635 DOI: 10.3892/ol.2023.13914] [FullText]

191 **Li H**, Liu H, Chen K. Living biobank-based cancer organoids: prospects and challenges in cancer research. *Cancer Biol Med* 2022; **19**: 965-982 [PMID: 35856555 DOI: 10.20892/j.issn.2095-3941.2021.0621] [FullText]

192 **Zhang Y**, Meng R, Sha D, Gao H, Wang S, Zhou J, Wang X, Li F, Li X, Song W. Advances in the application of colorectal cancer organoids in precision medicine. *Front Oncol* 2024; **14**: 1506606 [PMID: 39697234 DOI: 10.3389/fonc.2024.1506606] [FullText]

193 **Yao Y**, Xu X, Yang L, Zhu J, Wan J, Shen L, Xia F, Fu G, Deng Y, Pan M, Guo Q, Gao X, Li Y, Rao X, Zhou Y, Liang L, Wang Y, Zhang J, Zhang H, Li G, Zhang L, Peng J, Cai S, Hu C, Gao J, Clevers H, Zhang Z, Hua G. Patient-Derived Organoids Predict Chemoradiation Responses of Locally Advanced Rectal Cancer. *Cell Stem Cell* 2020; **26**: 17-26.e6 [PMID: 31761724 DOI: 10.1016/j.stem.2019.10.010] [Full Text]

194 **Yan HHN**, Siu HC, Ho SL, Yue SSK, Gao Y, Tsui WY, Chan D, Chan AS, Wong JWH, Man AHY, Lee BCH, Chan ASY, Chan AKW, Hui HS, Cheung AKL, Law WL, Lo OSH, Yuen ST, Clevers H, Leung SY. Organoid cultures of early-onset colorectal cancers reveal distinct and rare genetic profiles. *Gut* 2020; **69**: 2165-2179 [PMID: 32217638 DOI: 10.1136/gutjnl-2019-320019] [FullText]

195 **Yao L**, Zao XL, Pan XF, Zhang HG, Wang FJ, Qiao PF. Application of tumoroids derived from advanced colorectal cancer patients to predict individual response to chemotherapy. *J Chemother* 2023; **35**: 104-116 [PMID: 35285783 DOI: 10.1080/1120009X.2022.2045827] [FullText]

196 **Li Y**, Qin M, Liu N, Zhang C. Organoid development and applications in gynecological cancers: the new stage of tumor treatment. *J Nanobiotechnology* 2025; **23**: 20 [PMID: 39819668 DOI: 10.1186/s12951-024-03086-z] [FullText]

World Journal of Gastroenterology

Submit a Manuscript: https://www.f6publishing.com

World J Gastroenterol 2025 June 7; 31(21): 106939

DOI: 10.3748/wjg.v31.i21.106939

ISSN 1007-9327 (print) ISSN 2219-2840 (online)

ORIGINAL ARTICLE

Retrospective Cohort Study

Chemotherapy plus bevacizumab with or without anti-programmed death 1 immunotherapy as the second-line therapy in colorectal cancer

Zhao Gao, Xiao-Yan Wang, Zhi-Gang Shen, Jia-Hua Liu, Xiao-Yun Wang, Shi-Kai Wu, Xuan Jin

Specialty type: Gastroenterology and hepatology

Provenance and peer review: Unsolicited article; Externally peer reviewed.

Peer-review model: Single blind

Peer-review report's classification

Scientific Quality: Grade A, Grade B, Grade B

Novelty: Grade A, Grade B, Grade B

Creativity or Innovation: Grade A, Grade B, Grade C

Scientific Significance: Grade A, Grade B, Grade B

P-Reviewer: Chen Y; Luo DP; Sheng JP

Received: March 11, 2025

Revised: April 23, 2025

Accepted: May 23, 2025

Published online: June 7, 2025

Processing time: 87 Days and 8.4 Hours

Zhao Gao, Xiao-Yun Wang, Shi-Kai Wu, Xuan Jin, Department of Medical Oncology, Peking University First Hospital, Beijing 100034, China

Xiao-Yan Wang, Zhi-Gang Shen, Jia-Hua Liu, Department of Pharmacy, Jilin Cancer Hospital, Changchun 130012, Jilin Province, China

Co-corresponding authors: Shi-Kai Wu and Xuan Jin.

Corresponding author: Shi-Kai Wu, Department of Medical Oncology, Peking University First Hospital, No. 8 Xishiku Street, Beijing 100034, China. skywu4923@sina.cn

Abstract

BACKGROUND

Patients with microsatellite stable (MSS) metastatic colorectal cancer (mCRC) typically exhibit an immunosuppressive tumor microenvironment and demonstrate a low response rate to immunotherapy. Reports suggest that chemotherapy and anti-angiogenic therapy may have the potential to enhance the response to immunotherapy in these patients. This study aims to evaluate the effectiveness and safety of chemotherapy combined with bevacizumab with or without anti-programmed death 1 (PD-1) immunotherapy as the second-line regimen for MSS mCRC.

AIM

To evaluate the effectiveness and safety of chemotherapy combined with bevacizumab with or without anti-PD-1 immunotherapy as the second-line regimen for MSS mCRC.

METHODS

A retrospective analysis was conducted on patients with MSS mCRC diagnosed at Peking University First Hospital and Jilin Cancer Hospital from January 2020 to December 2024. The patients were divided into two groups: The experimental group receiving second-line chemotherapy combined with bevacizumab and anti-PD-1 immunotherapy, and the control group receiving chemotherapy combined with bevacizumab. Propensity score matching was applied to balance potential prognostic factors, including age, gender, Eastern Cooperative Oncology Group score, number of metastases, and primary tumor site. The progression-free sur-

vival, overall survival, disease control rate, objective response rate, and treatment-related adverse reactions were compared between the two groups. Kaplan-Meier analysis and log-rank test were used to compare survival outcomes. Inverse probability of treatment weighting was used for sensitivity analysis.

RESULTS

Propensity score matching resulted in 103 matched eligible patients. The median follow-up period was 13.9 months in the matched cohort. The objective response rate was 11.5% and 9% for the experimental and control groups, respectively (P = 0.710), while the disease control rate was 76.9% and 53.2%, respectively (P = 0.058). The median progression-free survival in the experimental group was 8.27 months [95% confidence interval (CI): 6.7-14.7 months], significantly higher than that in the control group, which was 4.63 months (95%CI: 3.9-5.67 months) (hazard ratio = 0.4143, 95%CI: 0.2462-0.6972, P = 0.00066). There was a trend towards the higher median overall survival in the experimental group compared to the control group (hazard ratio = 0.4504, 95%CI: 0.1897-1.07, P = 0.064). The incidences of adverse events were similar between the two groups.

CONCLUSION

Compared with the standard second-line chemotherapy combined with bevacizumab regimen, second-line therapy that combines chemotherapy with bevacizumab and anti-PD-1 immunotherapy has demonstrated promising efficacy in the treatment of MSS mCRC, while exhibiting a similar safety profile.

Key Words: Microsatellite stable; *RAS* mutation; Metastatic colorectal cancer; Immune checkpoint inhibitors; Programmed death 1

Core Tip: This manuscript addresses to evaluate the effectiveness and safety of chemotherapy combined with bevacizumab with or without anti-programmed death 1 immunotherapy as the second-line regimen for microsatellite stable metastatic colorectal cancer. As there is currently no clinical data on the second-line treatment of advanced colorectal cancer with the combination of immunotherapy, anti-angiogenic drugs, and anti-programmed death 1 immunotherapy, we conducted a multicenter retrospective cohort clinical study to explore the safety and efficacy of this triplet therapy in second-line treatment of advanced colorectal cancer patients.

Citation: Gao Z, Wang XY, Shen ZG, Liu JH, Wang XY, Wu SK, Jin X. Chemotherapy plus bevacizumab with or without anti-programmed death 1 immunotherapy as the second-line therapy in colorectal cancer. *World J Gastroenterol* 2025; 31(21): 106939
URL: https://www.wjgnet.com/1007-9327/full/v31/i21/106939.htm
DOI: https://dx.doi.org/10.3748/wjg.v31.i21.106939

INTRODUCTION

The latest statistical data show that both the incidence and mortality rates of colorectal cancer are on the rise. In 2022, colorectal cancer ranked third in terms of new cases and second in terms of deaths among all malignant tumors worldwide[1]. For metastatic colorectal cancer (mCRC), the standard first-line recommended regimen currently involves chemotherapy combined with targeted therapy, which can improve tumor control rates in advanced patients to some extent. The first- and second-line chemotherapy options mainly involve sequencing folinic acid, 5-fluorouracil, oxaliplatin (FOLFOX) with folinic acid, 5-fluorouracil, irinotecan (FOLFIRI) or vice versa, with no impact on treatment efficacy[2]. In terms of targeted drug selection, for patients with wild-type *RAS/BRAF* genes, bevacizumab is the standard choice after cetuximab resistance; however, for those with primary resistance to bevacizumab in the first line, current clinical studies suggest that switching to cetuximab does not provide additional benefit compared to continuing bevacizumab[3,4]. Therefore, for second-line treatment of mCRC, regardless of gene status and primary tumor location, bevacizumab combined with second-line chemotherapy is the standard treatment option recommended by current guidelines[5]. Nevertheless, after first-line treatment failure, the overall response rates (ORR) of second-line chemotherapy combined with bevacizumab (doublet regimen) was only 5%-36%, with the median progression-free survival (PFS) of just 4-7 months[6-12]. Therefore, improving the efficacy of second-line treatment for mCRC is a major challenge in current clinical practice.

Immune checkpoint inhibitors have made significant breakthroughs in the treatment of multiple tumors, particularly in microsatellite instability-high mCRC, where anti-programmed death 1 (PD-1) immunotherapy has demonstrated outstanding efficacy[13,14]. However, this patient population accounts for less than 5% of all mCRC cases. For the majority of patients with microsatellite stable (MSS) mCRC, immunotherapy is largely ineffective, limiting their options for chemotherapy and targeted therapy. Therefore, new combination therapy regimens are needed to improve the response to immunotherapy for this subtype. Previous studies have shown that anti-angiogenic therapy can reverse the immunosuppressive tumor microenvironment by normalizing blood vessels and inducing T-cell infiltration and

activation[15]. The phase II CheckMate 9X8 study compared the efficacy of nivolumab combined with modified FOLFOX6 (mFOLFOX6) (plus bevacizumab *vs* standard treatment (mFOLFOX6 plus bevacizumab) in first-line treatment of mCRC patients[16]. Subgroup analysis revealed that patients with consensus molecular subtype (CMS)3[17] could benefit from the addition of nivolumab to mFOLFOX6 plus bevacizumab. The BBCAPX study demonstrated that sintilimab combined with capecitabine and oxaliplatin (CAPEOX) and bevacizumab in first-line treatment improved disease response in patients with *RAS*-mutant MSS mCRC, with controllable adverse reactions and good safety[18]. The METIMMOX study was a phase II clinical trial comparing the efficacy of chemotherapy combined with nivolumab *vs* chemotherapy alone as first-line treatment for MSS mCRC[19]. Results showed a median PFS of 6.6 months in the combination immunotherapy group *vs* 5.6 months in the chemotherapy-alone group. This study suggested that short-course oxaliplatin-based chemotherapy in MSS mCRC patients may alter tumor immunogenicity, potentially inducing responsiveness to immune checkpoint inhibitors.

Based on these findings, chemotherapy combined with bevacizumab and anti-PD-1 immunotherapy (triplet regimen) has a solid theoretical foundation and has shown preliminary efficacy and safety in MSS mCRC patients. Therefore, the optimal combination of these three therapeutic agents - chemotherapy, anti-angiogenic drugs, and anti-PD-1 immunotherapy - should be an important research direction for changing the current treatment landscape of mCRC. As there is currently no clinical data on the second-line treatment of advanced colorectal cancer with the combination of chemotherapy, anti-angiogenic drugs, and anti-PD-1 immunotherapy, we conducted a multicenter retrospective cohort clinical study to explore the safety and efficacy of this triplet therapy in second-line treatment of advanced colorectal cancer patients.

MATERIALS AND METHODS

Study design and participants

This study employed a multicenter retrospective cohort research design. Patients with advanced colorectal cancer who were treated at Peking University First Hospital and Jilin Cancer Hospital between January 1, 2020 and December 30, 2024 were enrolled. The experimental group consisted of patients who received second-line treatment with chemotherapy combined with bevacizumab and anti-PD-1 immunotherapy, while the control group comprised patients who received conventional treatment (chemotherapy combined with bevacizumab).

The inclusion criteria were: (1) Histologically or cytologically confirmed unresectable mCRC (stage IV according to the American Joint Committee on Cancer Staging Manual 8th edition) with measurable lesions based on the Response Evaluation Criteria In Solid Tumors (RECIST) 1.1 criteria; (2) Progression after prior first-line standard two-drug chemotherapy regimen with or without targeted therapy; (3) Proficient mismatch repair (pMMR) or MSS, *BRAF* wild-type; (4) Patients receiving chemotherapy combined with bevacizumab and anti-PD-1 immunotherapy or chemotherapy combined with bevacizumab; (5) Having not undergone radiotherapy or having completed radiotherapy more than 4 weeks ago; and (6) Eastern Cooperative Oncology Group (ECOG) score ≤ 2.

The exclusion criteria were: (1) Patients with deficient DNA mismatch repair or microsatellite instability-high, or *BRAF* mutations; (2) Presence of symptomatic brain metastases; (3) Uncontrolled active infection; (4) Dysphagia, intractable vomiting, or known drug absorption disorders; and (5) Patients with symptomatic or high-risk obstruction, bleeding, or perforation, or those who have undergone intestinal stent placement to relieve intestinal obstruction.

In most cases, the chemotherapy regimen comprised an oxaliplatin-based doublet (FOLFOX, CAPEOX, or raltitrexed and oxaliplatin) or a topoisomerase inhibitor-based (FOLFIRI or CAPEOX: Capecitabine and irinotecan (IRI), or raltitrexed and IRI). anti-PD-1 immunotherapy included penpulimab, pembrolizumab, sintilimab, tislelizumab, and toripalimab. The anti-angiogenic agent was bevacizumab.

This study was conducted in compliance with the postulates of Declaration of Helsinki and approved by the Ethics Committee of Peking University First Hospital and Jilin Cancer Hospital. The requirement for patient approval or informed consent was waived by the Human Ethics Committee of Peking University First Hospital and Jilin Cancer Hospital, owing to the retrospective nature of the study and because the analysis used anonymous clinical data. The flowchart of patient selection is shown in Figure 1.

Procedures

Follow-up data were collected through hospital records, telephone interviews, outpatient visits, and rehospitalizations. The data included age, sex, height, weight, ECOG status, primary tumor location, number of metastatic sites, tumor differentiation grade, percentage reduction in tumor volume, PFS, overall survival (OS), follow-up duration, and survival status. Additionally, peripheral blood indicators within 7 days prior to the initial triplet regimen were collected, encompassing absolute leukocyte count, absolute neutrophil count (ANC), absolute lymphocyte count (ALC), platelet (PLT) count, absolute monocyte count, absolute eosinophil count, albumin (ALB), lactate dehydrogenase (LDH), carcinoembryonic antigen and carbohydrate antigen 199. Neutrophil-to-lymphocyte ratio (NLR) was calculated as ANC/ALC. Lymphocyte-to-monocyte ratio was calculated as the ratio of ALC/absolute monocyte count. Platelet-to-lymphocyte ratio was calculated as the ratio of PLT/ALC, body mass index (BMI) was defined as weight (kg) divided by height squared (m^2) [weight (kg)/height $(m)^2$], advanced lung cancer inflammation index was composed of BMI, ALB, and NLR, with the specific formula being BMI (kg/m^2) × ALB level (g/dL)/NLR. Systemic immune-inflammation index, as an evaluation index of systemic inflammatory response, the calculation formula is PLT × ANC/ALC.

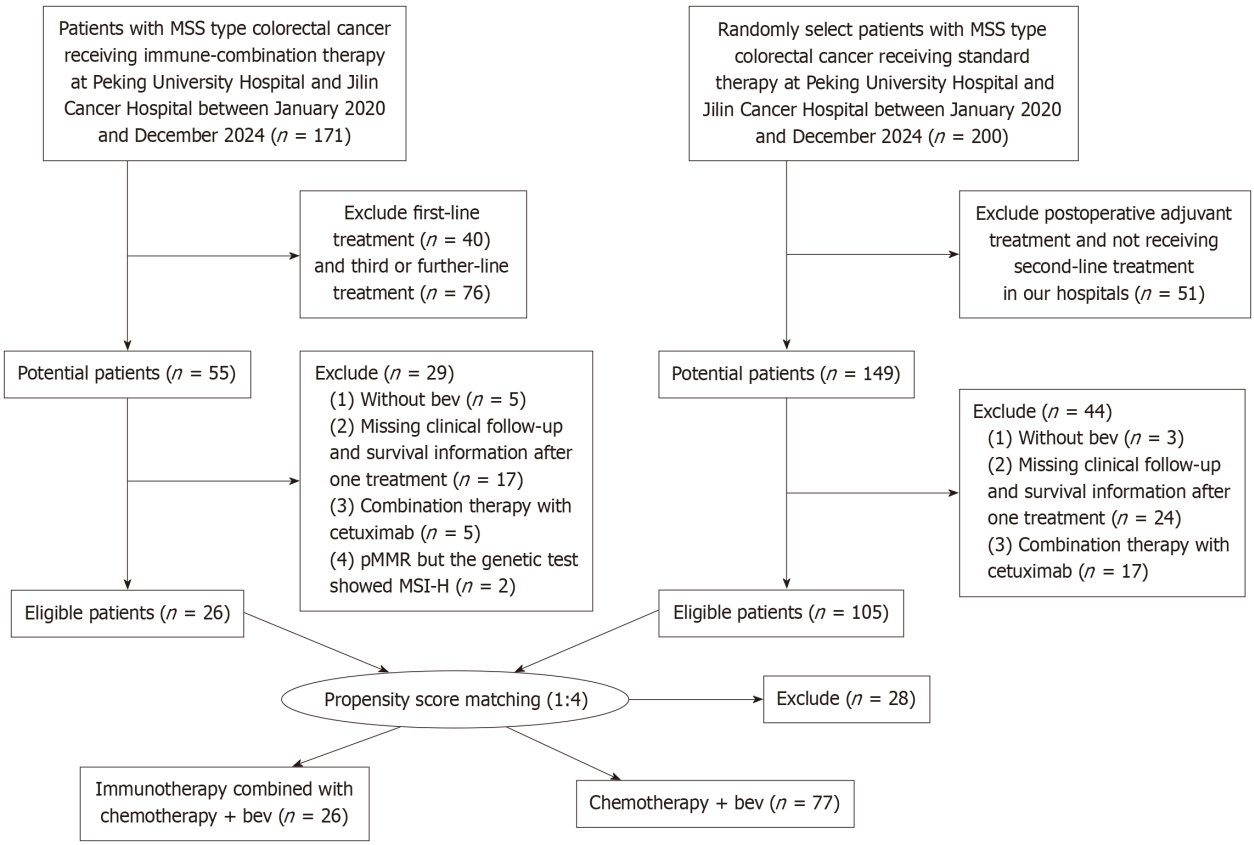

Figure 1 Flow chart of patient inclusion. MSS: Microsatellite stable; bev: Bevacizumab; pMMR: Proficient mismatch repair; MSI-H: Microsatellite instability-high.

The last follow-up date was in January 2025. PFS was the primary outcome, defined as the time from enrollment to the first documented disease progression according to RECIST version 1.1, or death from any cause, whichever occurred first. Secondary outcomes included OS, ORR, disease control rate (DCR), and safety evaluation. OS was calculated from the date of enrollment to the date of death from any cause, with censored cases defined by the last available follow-up. ORR was defined as the proportion of patients with a best objective response of complete response or partial response according to RECIST criteria (version 1.1). DCR was defined as the proportion of patients with complete response, partial response, or stable disease according to RECIST criteria (version 1.1). Treatment-related adverse events were evaluated according to the Common Terminology Criteria for Adverse Events version 4.0.

Statistical analysis

The PSM method was used to eliminate potential confounding factors that could influence the therapeutic effect between the experimental and control groups. PSM analysis was conducted using the nearest-neighbor method with a caliper of 0.018 and a 1:4 matching ratio to balance characteristics such as age, sex, ECOG status, metastasis, and tumor location using the MatchIt package[20]. Categorical variables were compared using the χ^2 test or Fisher's exact test, while continuous variables were assessed using the Mann-Whitney test. Kaplan-Meier estimates were obtained to compare the actuarial survival and the two treatment efficacy endpoints between the two groups. Independent prognostic factors, hazard ratios (HRs), and 95% confidence intervals (CIs) were evaluated using the Cox proportional hazards (PH) model. The cutoff values for continuous variable hematological indicators in predicting patient survival were set at the median. Based on this cutoff value, patients were categorized into high-expression and low-expression groups. The predictive value of hematological indicators for the triplet regimen in MSS mCRC was assessed using receiver operating characteristic curve analysis. A two-sided P value of < 0.050 was considered statistically significant. All statistical analyses in our study were performed using R software (version 4.4.2).

Sensitivity analysis

To address potential biases, three sensitivity analyses were conducted. First, we performed the Schoenfeld residual test on the original data to assess whether the covariates satisfied the PHs assumption, using the cox. zph function from the survival package[21]. If the PH assumption was met, we proceeded with univariate and multivariate regression analyses. Second, PSM analysis with varying matching ratios and inverse probability of treatment weighting are employed to adjust for baseline characteristics and evaluate treatment outcomes of PFS and OS. Third, to evaluate the robustness of the results, we both excluded four patients who received single-agent chemotherapy combined with bevacizumab and immunotherapy, and focused our analysis on patients treated with IRI-based regimens.

Table 1 Baseline characteristics and treatment details of patients in the matched cohort, *n* (%)

Characteristics	Levels	Control group (*n* = 77)	Experiment group (*n* = 26)	*P* value
Age	> 60	33 (42.9)	12 (46.2)	0.949
	≤ 60	44 (57.1)	14 (53.8)	
Gender	Male	55 (71.4)	18 (69.2)	1.000
	Female	22 (28.6)	8 (30.8)	
ECOG	0-1	69 (89.6)	22 (84.6)	0.739
	2	8 (10.4)	4 (15.4)	
Primary tumor location	Right colon	20 (26)	9 (34.6)	0.552
	Left colon and rectum	57 (74)	17 (65.4)	
Primary tumor surgery	No	15 (19.5)	3 (11.5)	0.533
	Yes	62 (80.5)	23 (88.5)	
Number of metastatic organs	1	26 (33.8)	8 (30.8)	0.968
	≥ 2	51 (66.2)	18 (69.2)	
Liver metastasis	No	19 (24.7)	8 (30.8)	0.724
	Yes	58 (75.3)	18 (69.2)	
Lung metastasis	No	41 (53.2)	11 (42.3)	0.461
	Yes	36 (46.8)	15 (57.7)	
RAS mutation type	Unknown	15 (19.5)	5 (19.2)	0.872
	Wild-type	12 (15.6)	3 (11.5)	
	Mutation	50 (64.9)	18 (69.2)	

The control group received chemotherapy combined with bevacizumab; the experimental group received chemotherapy combined with bevacizumab and anti- programmed death 1 immunotherapy. ECOG: Eastern Cooperative Oncology Group.

RESULTS

Patients

After one-to-four lines of PSM, the experimental group receiving triplet regimen included 26 patients, while the control group comprised 77 patients. Among the 103 patients (73 males and 30 females), 45 patients were over 60 years old. There were 29 cases (28.2%) of right-sided colon cancer, 85 patients underwent primary tumor surgery, and 69 patients (67%) had metastases in two or more organs. Sixty-eight patients had *RAS* mutations, and all cases were pMMR (Table 1). The main baseline characteristics of eligible patients were well-balanced between the two groups (Supplementary Figure 1A).

Effectiveness

As of December 2024, the median follow-up period was 13.9 months in the matched cohort. The median PFS was 5.33 months, (95%CI: 4.6-6.33 months), and the median OS was 23 months. In the experimental group, the median PFS was 8.27 months (95%CI: 6.7-14.7 months), and the median OS was 8.6 months. In the control group, the median PFS was 4.63 months (95%CI: 3.9-5.67 months). The PFS in the experimental group was superior to that in the control group (HR = 0.414, 95%CI: 0.2462-0.6972, P = 0.00066) (Figure 2A). There was a trend towards a higher median OS in the experimental group compared to the control group (HR = 0.4504, 95%CI: 0.1897-1.07, P = 0.064) (Figure 2B). The ORR was 11.5% in the experimental group and 9% in the control group (P = 0.710), while the DCR was 76.9% and 53.2%, respectively (P = 0.058) (Table 2).

Sensitivity analysis

For the original cohort, the PFS in the experimental group was superior to that in the control group (HR = 0.414, 95%CI: 0.2462-0.6972, P = 0.0054) (Figure 3A) and the OS did not show a statistically significant difference between the two groups (HR = 0.547, 95%CI: 0.2328-1.287, P = 0.167) (Figure 3B). The independent variables conformed to the PHs assumption model (P > 0.05). Cox univariate and multivariate analyses revealed that immunotherapy combined with chemotherapy (P = 0.004) and patients without liver metastases (P = 0.002) were associated with better PFS (Table 3). Robustness of survival analysis results: insensitivity to changes in PSM ratio, treatment regimen exclusions, and cohort restrictions in PFS and OS (Figures 4 and 5). The inverse probability of treatment weighting also reached the same conclusion for PFS (P = 0.0014) (Figure 4D) and OS (P = 0.1505) (Figure 5D). Meanwhile, after applying weights, the

Table 2 Comparison of short-term efficacy between two groups of microsatellite stable metastatic colorectal cancer

Group	Number	PR	SD	PD	DCR (%)
Control group	77	7	34	36	57.14
Experimental group	26	3	17	6	76.92
χ^2 value	-	-	2.706	3.585	3.5847
P value	-	0.71[1]	0.1	0.058	0.058

[1]Fisher's exact test.

The control group received chemotherapy combined with bevacizumab; the experimental group received chemotherapy combined with bevacizumab and anti- programmed death 1 immunotherapy. PR: Partial response; SD: Stable disease; PD: Progressive disease; DCR: Disease control rate.

Table 3 Univariate and multivariate Cox analysis of the effect of prognostic factors in the original cohort, *n* (%)

Dependent: Survival (PFS/30, status)		All patients (*n* = 131)	HR (univariable)	HR (multivariable)
Gender	Male	76 (58.0)	-	-
	Female	55 (42.0)	0.87 (0.60-1.26, *P* = 0.458)	-
Age	> 60	66 (50.4)	-	-
	≤ 60	65 (49.6)	0.73 (0.50-1.07, *P* = 0.110)	-
ECOG	0-1	116 (88.5)	-	-
	2	15 (11.5)	1.34 (0.73-2.47, *P* = 0.340)	-
Number of metastatic organs	1	55 (42.0)	-	-
	≥ 2	76 (58.0)	1.96 (1.32-2.90, *P* < 0.001)	1.90 (1.27-2.84, *P* = 0.002)
Primary tumor location	Right colon	32 (24.4)	-	-
	Left colon and rectum	99 (75.6)	0.92 (0.61-1.40, *P* = 0.697)	-
Liver metastasis	No	46 (35.1)	-	-
	Yes	85 (64.9)	1.57 (1.04-2.36, *P* = 0.032)	1.28 (0.84-1.96, *P* = 0.254)
Lung metastasis	No	70 (53.4)	-	-
	Yes	61 (46.6)	1.23 (0.85-1.78, *P* = 0.274)	-
RAS mutation type	Unknown	25 (19.1)	-	-
	Wild type	20 (15.3)	0.97 (0.51-1.85, *P* = 0.930)	-
	Mutation	86 (65.6)	1.37 (0.84-2.24, *P* = 0.202)	-
Group	Control group	105 (80.2)	-	-
	Experimental group	26 (19.8)	0.51 (0.31-0.82, *P* = 0.006)	0.49 (0.30-0.80, *P* = 0.004)

n = 131, events = 115, likelihood ratio test = 22.56 on 3 *df* (*P* < 0.001). ECOG: Eastern Cooperative Oncology Group; PFS: Progression-free survival; HR: Hazard ratio.

variables between the two groups maintained a substantial balance at the baseline level (Supplementary Figure 1). Adjusting the PSM ratio in PFS (Figure 5A-C) and OS (Figure 6A-C) did not alter the final results; neither did excluding patients treated with single-agent triplet regimens (Figures 4E and 5E). Similarly, restricting the cohort to IRI-based chemotherapy patients had no effect on the conclusions (Figures 4F and 5F).

Safety

No substantial differences in adverse events were observed between the two groups. The incidence of grade 1-2 fatigue was slightly higher in the experimental group compared to the control group (30.8% *vs* 11.7%, *P* = 0.0332), but the incidence of grade 3-4 adverse events was similar between the two groups (Table 4).

Subgroup analysis

Subgroup analysis showed that patients younger than 60 years old (HR = 0.25, 95%CI: 0.12-0.56, *P* = 0.001), those without liver metastases (HR = 0.14, 95%CI: 0.04-0.48, *P* = 0.002), and those with lung metastases (HR = 0.27, 95%CI: 0.13-0.58, *P* =

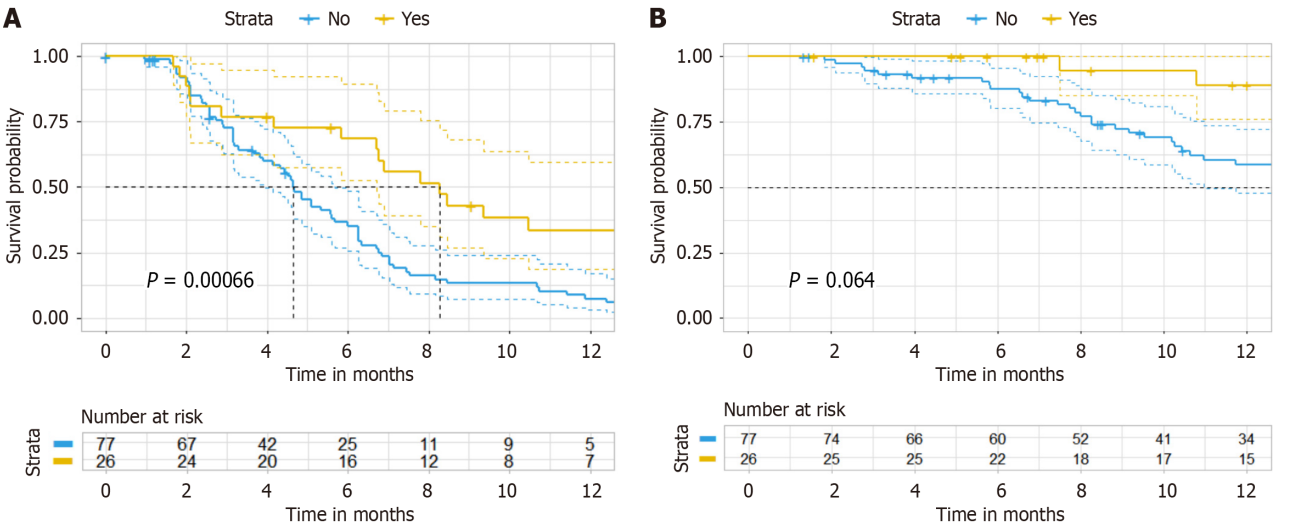

Figure 2 After propensity score-matching analysis of progression-free survival and overall survival. A: After propensity score-matching analysis of PFS (ratio = 4); B: After propensity score-matching analysis of overall survival (ratio = 4).

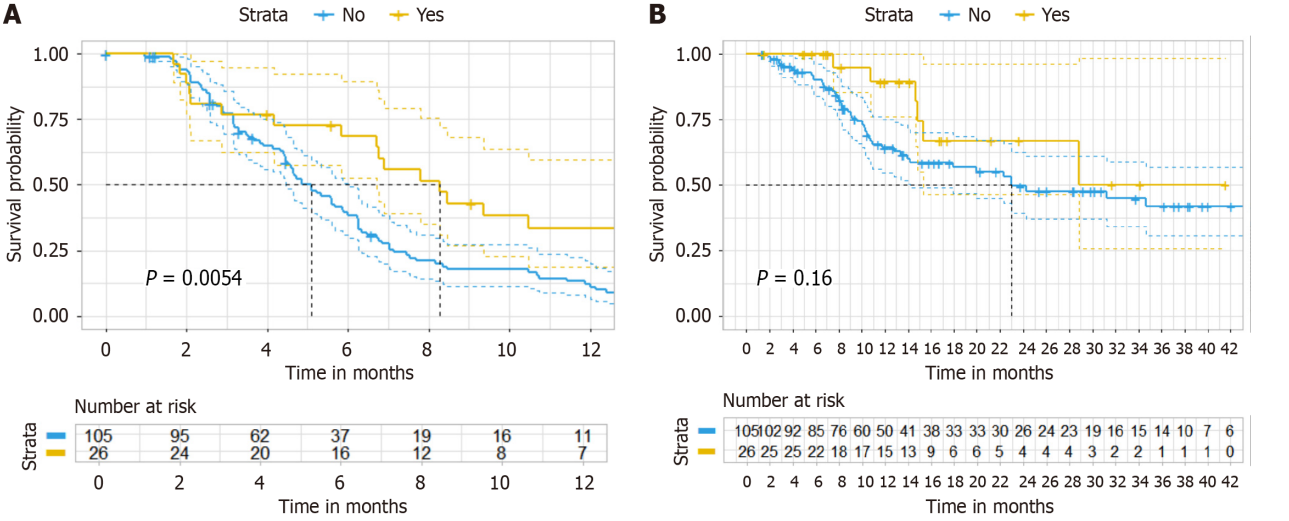

Figure 3 Kaplan-Meier curve of original cohort. A: In the original cohort (progression-free survival); B: In the original cohort (overall survival).

0.001) are more likely to benefit from triplet regimen (Figure 6).

Exploratory biomarker analysis

We analyzed the baseline hematological indicators associated with PFS in patients receiving triplet regimen (Table 5). Univariate analysis revealed that patients with advanced age, right colorectal cancer (CRC), normal carbohydrate antigen 199 levels, high advanced lung cancer inflammation index, and low LDH could benefit from triplet regimen. Multivariate analysis further identified liver metastasis (HR = 8.15, 95%CI: 1.39-47.83, P = 0.020) and LDH (HR = 4.11, 95%CI: 1.02-16.55, P = 0.046) as independent prognostic risk factors (Table 6).

The area under curve values of LDH in predicting the efficacy of second-line triplet regimen for MSS mCRC patients at 6 months, 9 months, and 12 months were 0.80, 0.79, and 0.72 respectively (Figure 7A). Based on the median value of LDH, MSS mCRC patients were divided into high groups and low groups. Survival analysis demonstrated that patients in the high-value group had significantly prolonged PFS compared to those in the low-value group (P = 0.019) (Figure 7B).

DISCUSSION

Multiple Phase III clinical studies have demonstrated that, following the failure of first-line chemotherapy combined with bevacizumab in advanced colorectal cancer, switching the chemotherapy regimen while continuing anti-angiogenic therapy provides additional survival benefits compared to chemotherapy alone[7,8,22]. However, the role of immunotherapy in second-line sequential treatment for mCRC remains unestablished. Previous studies have shown that IRI-

Table 4 Treatment-emergent adverse events in the 103 patients of the matched dataset, *n* (%)

Toxicities	Experimental group (*n* = 26)			Control group (*n* = 77)			*P* value for grade 1-2	*P* value for grade 3-4
	Grade 0	Grade 1-2	Grade 3-4	Grade 0	Grade 1-2	Grade 3-4		
Anemia	8 (30.8)	15 (57.7)	3 (11.5)	47 (61.0)	29 (37.7)	1 (1.3)	0.1197[a]	0.2451[b]
Neutropenia	18 (69.2)	7 (26.9)	1 (3.8)	58 (75.3)	14 (18.2)	5 (6.5)	0.4996[a]	1[b]
Leukocytopenia	14 (53.8)	11 (42.3)	1 (3.8)	55 (71.4)	18 (23.4)	4 (5.2)	0.1088[a]	0.3667[b]
Thrombocytopenia	17 (65.4)	9 (34.6)	0 (0.0)	62 (80.5)	15 (19.5)	0 (0.0)	0.1902[a]	1[b]
Proteinuria	21 (80.8)	5 (19.2)	0 (0.0)	70 (90.9)	7 (9.1)	0 (0.0)	0.2984[a]	1[b]
Aspartate transaminase increased	18 (69.2)	7 (26.9)	1 (3.8)	56 (72.7)	20 (26.0)	1 (1.3)	1[a]	1[b]
Alanine transaminase increased	20 (76.9)	5 (19.2)	1 (3.8)	65 (84.4)	12 (15.6)	0 (0.0)	0.8985[a]	1[b]
Alkaline phosphatase increased	21 (80.8)	5 (19.2)	0 (0.0)	69 (89.6)	7 (9.1)	1 (1.3)	0.1732[b]	1[b]
Blood bilirubin increased	20 (76.9)	5 (19.2)	1 (3.8)	61 (79.2)	16 (20.8)	0 (0.0)	1[a]	1[b]
Triglycerides increased	20 (76.9)	4 (15.4)	2 (7.7)	67 (87.0)	10 (13.0)	0 (0.0)	0.7475[b]	0.4967[b]
Nausea	18 (69.2)	8 (30.8)	0 (0.0)	47 (61.0)	30 (39.0)	0 (0.0)	0.6076[a]	1[b]
Vomiting	19 (73.1)	7 (26.9)	0 (0.0)	61 (79.2)	16 (20.8)	0 (0.0)	0.7054[a]	1[b]
Fatigue	18 (69.2)	8 (30.8)	0 (0.0)	68 (88.3)	9 (11.7)	0 (0.0)	0.0332[b]	1[b]
Fever	24 (92.3)	2 (7.7)	0 (0.0)	73 (94.8)	4 (5.2)	0 (0.0)	0.6407[b]	1[b]
Diarrhea	24 (92.3)	1 (3.8)	1 (3.8)	71 (92.2)	6 (7.8)	0 (0.0)	0.6759[b]	1[b]
Peripheral neurotoxicity	25 (96.2)	1 (3.8)	0 (0.0)	77 (100.0)	0 (0.0)	0 (0.0)	0.2524[b]	1[b]
Hand-foot syndrome	23 (88.5)	3 (11.5)	0 (0.0)	73 (94.8)	4 (5.2)	0 (0.0)	0.3648[b]	1[b]
Hypertension	24 (92.3)	1 (3.8)	1 (3.8)	72 (93.5)	4 (5.2)	1 (1.3)	1[b]	1[b]

[a]*P* values were calculated by χ^2 test.
[b]*P* values were calculated by Fisher's exact test.
The control group received chemotherapy combined with bevacizumab; the experimental group received chemotherapy combined with bevacizumab and anti-programmed death 1 immunotherapy.

Table 5 Baseline hematological prognostic indicators markers for patients receiving chemotherapy combined with bevacizumab and anti-programmed death 1immunotherapy, mean ± SD

Characteristics	Stats	Normal range
Height (cm)	168.3 ± 8.0	140-190
Weight (kg)	67.7 ± 12.0	40-100
ALLC (10^9/L)	6.0 ± 1.9	3.5-9.5
RDW (%)	15.2 ± 3.8	11.6-14.8
PLT (10^9/L)	178.2 ± 63.7	125-350
ANC (10^9/L)	4.1 ± 1.4	1.8-6.3
ALC (10^9/L)	1.4 ± 0.5	1.1-3.2
AMC (10^9/L)	0.4 ± 0.1	0.1-0.6
AEC (10^9/L)	0.2 ± 0.2	0.02-0.52
ALB (g/L)	41.4 ± 4.0	40-55
LDH (IU/L)	240.0 ± 154.9	109-245
FIB (g/L)	3.6 ± 0.7	2-4

Dimer (ng/ml)	257.3 ± 647.3	0-500
CEA (ng/mL), *n* (%)	6 (24.0%)	0-5
	19 (76.0%)	-
CA199 (IU/mL), *n* (%)	13 (52.0%)	0-37
	12 (48.0%)	-

ALLC: Absolute leukocyte count; RDW: Red blood cell distribution width; PLT: Platelet; ANC: Absolute neutrophil count; ALC: Absolute lymphocyte count; AMC: Absolute monocyte count; AEC: Absolute eosinophil count; ALB: Albumin; LDH: Lactate dehydrogenase; FIB: Fibrinogen; CEA: Carcinoembryonic antigen; CA199: Carbohydrate antigen 199.

Table 6 Univariate and multivariate Cox analysis of prognostic factors in microsatellite stable metastatic colorectal cancer patients receiving chemotherapy combined with bevacizumab and anti-programmed death 1 immunotherapy

Dependent: Survival (PFS/30, status)		All	HR (univariable)	HR (multivariable)
Age	> 60	11 (44.0)	-	-
	≤ 60	14 (56.0)	0.20 (0.07-0.62, *P* = 0.005)	0.27 (0.05-1.48, *P* = 0.133)
Gender	Male	18 (72.0)	-	-
	Female	7 (28.0)	1.01 (0.40-2.54, *P* = 0.979)	-
ECOG	1	21 (84.0)	-	-
	2	4 (16.0)	1.01 (0.23-4.55, *P* = 0.985)	-
Location	Right colon	9 (36.0)	-	-
	Left colon and rectum	16 (64.0)	0.73 (0.31-1.74, *P* = 0.477)	-
Liver metastasis	No	7 (28.0)	-	-
	Yes	18 (72.0)	5.23 (1.48-18.50, *P* = 0.010)	8.15 (1.39-47.83, *P* = 0.020)
Lung metastasis	No	10 (40.0)	-	-
	Yes	15 (60.0)	0.62 (0.25-1.51, *P* = 0.291)	-
RAS mutation type	Unknown	5 (20.0)	-	-
	Wild type	3 (12.0)	0.75 (0.13-4.20, *P* = 0.742)	-
	Mutation	17 (68.0)	2.30 (0.74-7.14, *P* = 0.151)	-
CEA	Normal	6 (24.0)	-	-
	Abnormal	19 (76.0)	0.59 (0.21-1.67, *P* = 0.316)	-
CA199	Normal	13 (52.0)	-	-
	Abnormal	12 (48.0)	3.16 (1.12-8.88, *P* = 0.029)	1.06 (0.23-4.90, *P* = 0.942)
NLR	≤ 2.9	13 (52.0)	-	-
	> 2.9	12 (48.0)	1.45 (0.60-3.55, *P* = 0.410)	-
LMR	≤ 3.63	13 (52.0)	-	-
	> 3.63	12 (48.0)	0.57 (0.23-1.39, *P* = 0.216)	-
PLR	≤ 121	13 (52.0)	-	-
	> 121	12 (48.0)	1.43 (0.58-3.48, *P* = 0.436)	-
BMI	≤ 24.9	12 (48.0)	-	-
	> 24.9	13 (52.0)	1.02 (0.43-2.42, *P* = 0.963)	-
ALI	≤ 260.9	13 (52.0)	-	-
	> 260.9	12 (48.0)	0.30 (0.10-0.85, *P* = 0.023)	0.50 (0.15-1.64, *P* = 0.252)
SII	≤ 426.8	13 (52.0)	-	-
	> 426.8	12 (48.0)	1.74 (0.72-4.25, *P* = 0.220)	-

ALLC	≤ 6.0	13 (52.0)	-	-
	> 6.0	12 (48.0)	1.31 (0.53-3.20, *P* = 0.559)	-
ANC	≤ 4.1	13 (52.0)	-	-
	> 4.1	12 (48.0)	1.31 (0.53-3.20, *P* = 0.559)	-
ALC	≤ 1.4	13 (52.0)	-	-
	> 1.4	12 (48.0)	0.61 (0.25-1.50, *P* = 0.285)	-
AMC	≤ 0.4	13 (52.0)	-	-
	> 0.4	12 (48.0)	0.71 (0.28-1.82, *P* = 0.473)	-
AEC	≤ 0.2	13 (52.0)	-	-
	> 0.2	12 (48.0)	1.59 (0.65-3.89, *P* = 0.309)	-
RDW	≤ 15.2	13 (52.0)	-	-
	> 15.2	12 (48.0)	1.04 (0.42-2.57, *P* = 0.938)	-
LDH	≤ 240.0	13 (52.0)	-	-
	> 240.0	12 (48.0)	3.09 (1.16-8.22, *P* = 0.024)	5.72 (1.58-20.72, *P* = 0.008)

n = 25, events = 21, likelihood ratio test = 25.81 on 5 df (*P* < 0.001). ECOG: Eastern Cooperative Oncology Group; PFS: Progression-free survival; HR: Hazard ratio; CEA: Carcinoembryonic antigen; CA199: Carbohydrate antigen 199; NLR: Neutrophil-to-lymphocyte ratio; LMR: Lymphocyte-to-monocyte ratio; PLR: Platelet-to-lymphocyte ratio; BMI: Body mass index; ALI: Advanced lung cancer inflammation index; SII: Systemic immune-inflammation index; ALLC: Absolute leukocyte count; ANC: Absolute neutrophil count; ALC: Absolute lymphocyte count; AMC: Absolute monocyte count; AEC: Absolute eosinophil count; RDW: Red blood cell distribution width; LDH: Lactate dehydrogenase.

based chemotherapy for second-line treatment of advanced CRC yields an ORR of 4%-18.8%, with the median PFS of 2.5-5.8 months and the median OS of 9.9-19.5 months[8,22-25]. When IRI-based chemotherapy is combined with anti-angiogenic targeted therapy for second-line treatment of advanced CRC, the ORR ranges from 14%-19.8%, with median PFS and OS ranging from 3.5-6.9 months and 11.9-13.5 months, respectively[8,22,24]. This study revealed an ORR of 11.5% and a DCR of 76.9% with triplet regimen. The triplet regimen for second-line treatment of advanced CRC showed superior PFS compared to the doublet regimen (*P* = 0.00066). Although our analysis demonstrated a trend toward OS benefit (*P* = 0.064), this finding requires cautious interpretation. Whether PFS improvement and depth of response will ultimately translate into definitive OS gains remains uncertain and necessitates validation through larger sample sizes and prospective cohort studies.

The results of chemotherapy combined with anti-PD-1 immunotherapy for first-line treatment of patients with MSS mCRC are unsatisfactory, with limited overall efficacy improvement. Further consideration is needed regarding the combination and value of this treatment modality. The CHECKMATE-9X8[16] study explored the efficacy of nivolumab plus mFOLFOX6/bevacizumab [nivolumab + standard-of-care (SOC)] *vs* mFOLFOX6/bevacizumab (SOC) alone for first-line treatment of mCRC. The ORR was 60% in the nivolumab group *vs* 46% in the SOC group, with a median PFS of 11.9 months in both groups. The median OS was 29.2 months in the nivolumab group, and not reached in the SOC group. Exploratory subgroup analysis of this study indicated that a higher proportion of patients with CMS1 and CMS3 tumor types remained progression-free at 12 months with nivolumab treatment. The AtezoTRIBE randomized Phase II trial, comparing FOLFOXIRI and bevacizumab with or without atezolizumab, showed that adding atezolizumab prolonged PFS in the overall population[26]. However, in the MSS patient subgroup, the addition of atezolizumab did not significantly improve PFS. In multivariate analysis, high tumor mutational burden and high immune score were independently associated with prolonged PFS with atezolizumab treatment. The KEYNOTE-651 study evaluated the long-term safety and efficacy of pembrolizumab combined with oxaliplatin, leucovorin, and fluorouracil (mFOLFOX7 regimen) for first-line treatment or pembrolizumab combined with IRI, leucovorin, and fluorouracil (FOLFIRI regimen) for second-line treatment of MSS/pMMR mCRC. The results suggested that pembrolizumab combined with chemo-therapy is safe and effective for both first-line and second-line treatment of MSS/pMMR mCRC[27]. The NIVACOR trial assessed the efficacy and safety of nivolumab combined with FOLFOXIRI and bevacizumab in *RAS*/*BRAF*-mutant mCRC patients for first-line treatment. In the MSS patient subgroup analysis, the ORR was 78.9%, the DCR was 96.2%, and the median PFS was 9.8 months (95%CI: 8.18-15.24)[28]. However, there is a lack of data on second-line immune combination therapy for MSS mCRC. We used the triplet regimen and found that it had certain advantages in terms of the median PFS for second-line treatment of MSS mCRC.

Basic studies have shown that liver metastases from CRC are in an immunosuppressive environment[29]. Subgroup analysis of our study found that patients with liver metastases had worse prognoses than those without liver metastases, while patients with lung metastases had better prognoses with triplet regimen. This is similar to the findings of the REGONIVO study[30], which reported better prognoses for patients with lung metastases compared to those with liver metastases. In contrast, subgroup analysis of the bevacizumab and CAPEOX study found that patients with liver metastases had better prognoses in the triplet regimen[18]. Further basic research is needed to explore the efficacy of anti-PD1 immunotherapy in mCRC with different metastatic sites.

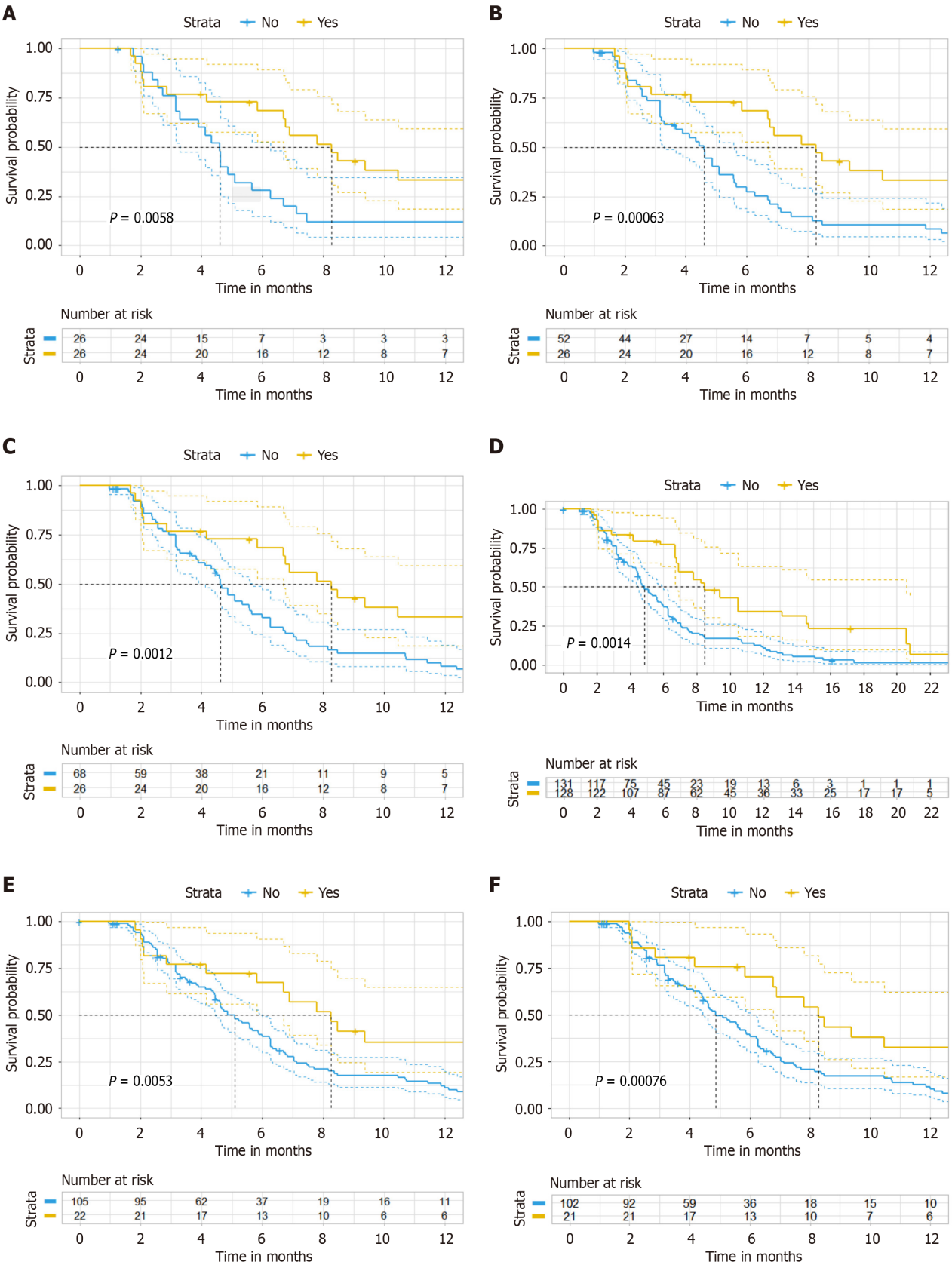

Figure 4 Sensitivity analysis of progression-free survival. A: After propensity score-matching analysis in progression-free survival (PFS) (ratio = 1); B: After propensity score-matching analysis in PFS (ratio = 2); C: After propensity score-matching analysis in PFS (ratio = 3); D: After inverse probability of treatment weighting analysis; E: Kaplan-Meier curve after excluding 4 patients who received single-agent chemotherapy combined with bevacizumab and anti- programmed death 1 immunotherapy in PFS; F: Kaplan-Meier curve restricting the cohort to irinotecan-based chemotherapy patients in PFS.

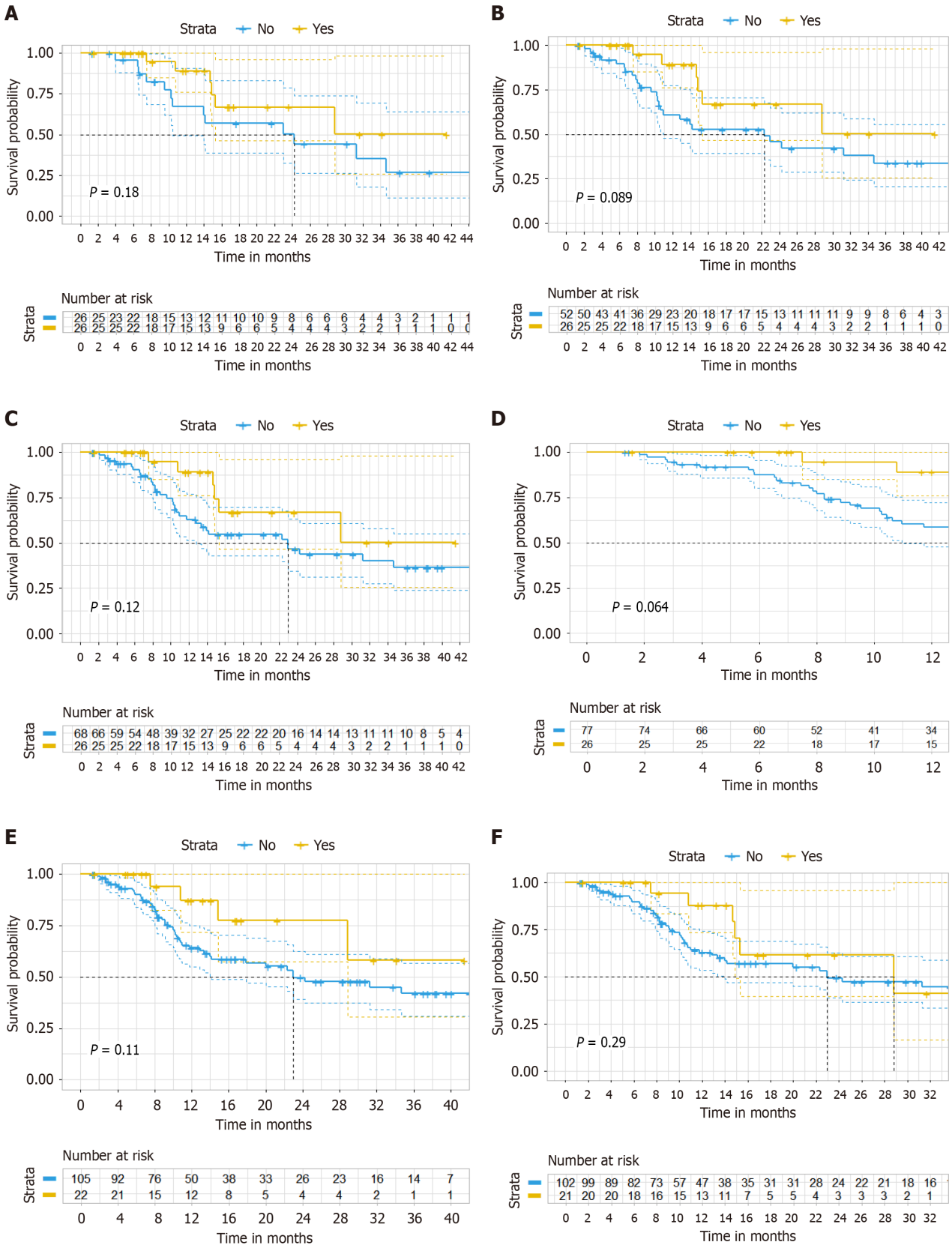

Figure 5 Sensitivity analysis of overall survival. A: After propensity score-matching analysis in overall survival (OS) (ratio = 1); B: After propensity score-matching analysis in OS (ratio = 2); C: After propensity score-matching analysis in OS (ratio = 3); D: After inverse probability of treatment weighting analysis (OS); E: Kaplan-Meier curve after excluding 4 patients who received single-agent chemotherapy combined with bevacizumab and anti-programmed death 1 immunotherapy in OS; F: Kaplan-Meier curve restricting the cohort to irinotecan-based chemotherapy patients in OS.

Variable	Count	Percent	HR (95%CI)	*P* value	*P* for interaction
Overall	103	100	0.41 (0.25 to 0.70)	0.001	
Age					0.02
> 60	45	43.7	0.75 (0.37 to 1.53)	0.432	
≤ 60	58	56.3	0.25 (0.12 to 0.56)	0.001	
Gender					0.995
Male	73	70.9	0.42 (0.23 to 0.79)	0.007	
Female	30	29.1	0.47 (0.18 to 1.21)	0.119	
ECOG					0.844
0-1	91	88.3	0.43 (0.24 to 0.74)	0.002	
2	12	11.7	0.30 (0.06 to 1.51)	0.145	
Primary tumor location					0.469
Right colon	29	28.2	0.54 (0.23 to 1.26)	0.153	
Left colon and rectum	74	71.8	0.35 (0.18 to 0.69)	0.002	
Liver metastasis					0.005
No	27	26.2	0.14 (0.04 to 0.48)	0.002	
Yes	76	73.8	0.69 (0.39 to 1.21)	0.198	
Lung metastasis					0.025
No	52	50.5	0.68 (0.31 to 1.46)	0.316	
Yes	51	49.5	0.27 (0.13 to 0.58)	0.001	
RAS mutation type					0.356
Unknown	20	19.4	0.24 (0.06 to 0.86)	0.029	
Wild_type	15	14.6	0.30 (0.06 to 1.38)	0.121	
Mutation	68	66	0.57 (0.31 to 1.04)	0.068	

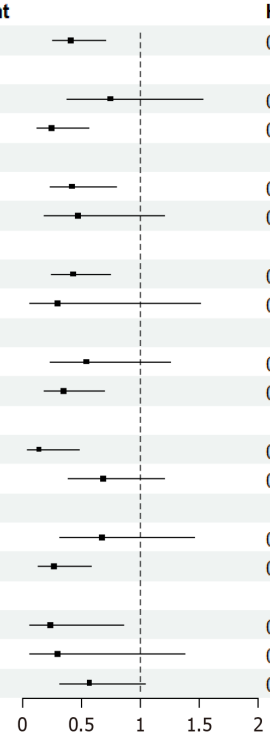

Figure 6 Forest plots depict the hazard ratios and 95% confidence intervals for progression-free survival by subgroup. CI: Confidence interval; ECOG: Eastern Cooperative Oncology Group.

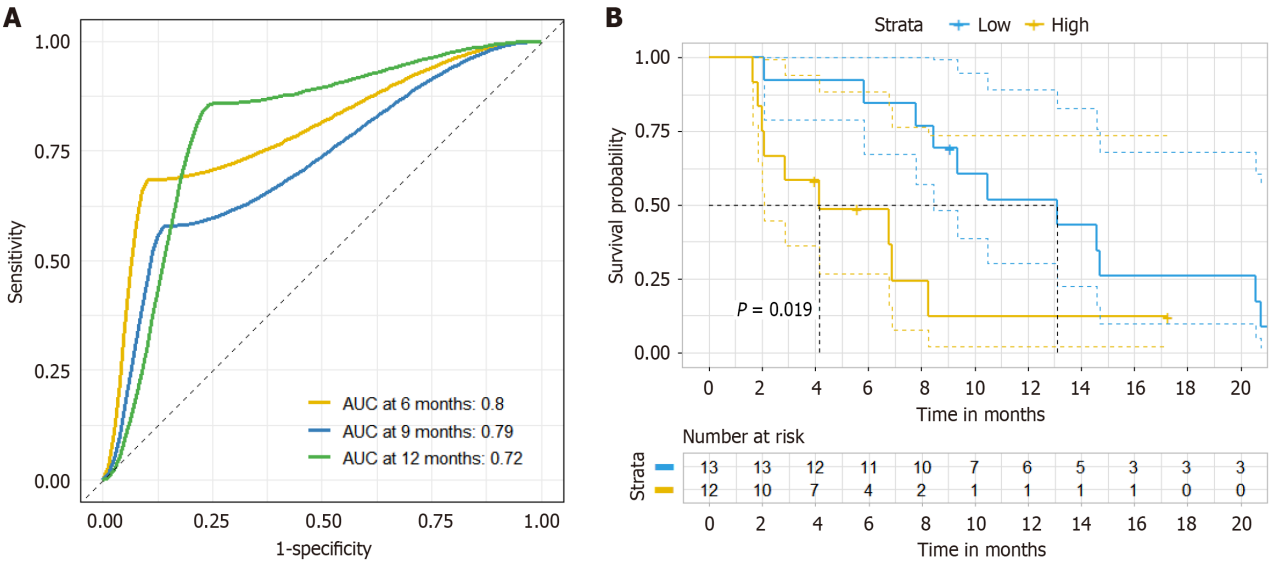

Figure 7 Lactate dehydrogenase as a predictive biomarker of progression-free survival. A: Receiver operating characteristic curves of lactate dehydrogenase (LDH) at 9 months, 12 months, and 15 months before patients receiving chemotherapy combined with bevacizumab and anti-programmed death 1 immunotherapy; B: Survival curves of LDH before patients receiving chemotherapy combined with bevacizumab and anti-programmed death 1 immunotherapy (high group: LDH ≥ 240 mmol/L and low group LDH < 240 mmol/L). ACU: Area under curve.

The results of this study indicate that baseline LDH level is an independent prognostic factor for PFS following the triplet regimen in MSS mCRC. From a metabolic perspective, tumor cells tend to prioritize glycolysis for energy production, where glucose is metabolized to pyruvate and then converted to lactate *via* LDH instead of undergoing aerobic oxidation through the mitochondrial tricarboxylic acid cycle, a phenomenon known as the "Warburg effect"[31]. Research has shown that in metastatic cervical cancer patients receiving combination immunotherapy, higher LDH levels are associated with lower survival rates[32]. Additionally, patients with normal LDH levels before receiving camrelizumab treatment for esophageal squamous cell carcinoma exhibit longer OS[33].

We acknowledge that our multicenter retrospective cohort study has several limitations. First, as a retrospective analysis with a relatively small sample size in the experimental group, data was collected from only two participating

centers, and the findings require validation in larger cohorts and more research institutions. Second, the heterogeneity in treatment regimens - including diverse chemotherapy protocols and five different anti-PD-1 agents - may have confounded efficacy comparisons. The lack of standardization in both chemotherapy and immunotherapy regimens introduces variability that complicates direct comparisons. Third, the immaturity of PFS and OS data in this retrospective analysis, coupled with suboptimal patient management practices, may have introduced biases. Fourth, the study did not evaluate programmed death-ligand 1 expression levels in patients, precluding analysis of the association between programmed death-ligand 1 expression and the efficacy of anti-PD-1 immunotherapy.

CONCLUSION

In the second-line treatment of MSS mCRC, chemotherapy combined with bevacizumab and anti-PD-1 immunotherapy is superior to the traditional regimen of chemotherapy with bevacizumab. This indicates that the triplet regimen is a promising therapeutic strategy, which is expected to provide more clinical benefits. Subgroup analysis shows that patients younger than 60 years old, those without liver metastases, and those with lung metastases may benefit more significantly.

ACKNOWLEDGEMENTS

We are grateful to the patients and their families for supporting the study.

FOOTNOTES

Author contributions: Gao Z collected and analyzed the data; Gao Z and Wang XY wrote the manuscript; Shen ZG, Liu JH, and Jin X analyzed the data; Jin X and Wu SK conceived of the review and edited the manuscript, they contributed equally to this article, they are the co-corresponding authors of this manuscript; and all authors read and approved the final manuscript.

Supported by the National High Level Hospital Clinical Research Funding (Multi-center Clinical Research Project of Peking University First Hospital), No. 2022CR65.

Institutional review board statement: This study was approved by the Medical Ethics Committee of Peking University First Hospital (approval No.2023-505-003) and Jilin Cancer Hospital (approval No. 202501-003-01).

Informed consent statement: The informed consent was waived by the Institutional Review Board.

Conflict-of-interest statement: All the authors report no relevant conflicts of interest for this article.

Data sharing statement: The datasets generated during and/or analyzed during the current study are available from the corresponding author on reasonable request.

STROBE statement: The authors have read the STROBE Statement-checklist of items, and the manuscript was prepared and revised according to the STROBE Statement-checklist of items.

Country of origin: China

ORCID number: Zhao Gao 0009-0007-6128-4042; Shi-Kai Wu 0009-0003-9525-4870; Xuan Jin 0000-0002-9665-5356.

S-Editor: Bai Y
L-Editor: A
P-Editor: Zhao YQ

REFERENCES

1 **Bray F**, Laversanne M, Sung H, Ferlay J, Siegel RL, Soerjomataram I, Jemal A. Global cancer statistics 2022: GLOBOCAN estimates of incidence and mortality worldwide for 36 cancers in 185 countries. *CA Cancer J Clin* 2024; **74**: 229-263 [PMID: 38572751 DOI: 10.3322/caac.21834] [FullText]

2 **Tournigand C**, André T, Achille E, Lledo G, Flesh M, Mery-Mignard D, Quinaux E, Couteau C, Buyse M, Ganem G, Landi B, Colin P,

Louvet C, de Gramont A. FOLFIRI Followed by FOLFOX6 or the Reverse Sequence in Advanced Colorectal Cancer: A Randomized GERCOR Study. *J Clin Oncol* 2023; **41**: 3469-3477 [PMID: 37379692 DOI: 10.1200/JCO.22.02774] [FullText]

3 **Bennouna J**, Hiret S, Bertaut A, Bouché O, Deplanque G, Borel C, François E, Conroy T, Ghiringhelli F, des Guetz G, Seitz JF, Artru P, Hebbar M, Stanbury T, Denis MG, Adenis A, Borg C. Continuation of Bevacizumab vs Cetuximab Plus Chemotherapy After First Progression in KRAS Wild-Type Metastatic Colorectal Cancer: The UNICANCER PRODIGE18 Randomized Clinical Trial. *JAMA Oncol* 2019; **5**: 83-90 [PMID: 30422156 DOI: 10.1001/jamaoncol.2018.4465] [FullText]

4 **Hecht JR**, Cohn A, Dakhil S, Saleh M, Piperdi B, Cline-Burkhardt M, Tian Y, Go WY. SPIRITT: A Randomized, Multicenter, Phase II Study of Panitumumab with FOLFIRI and Bevacizumab with FOLFIRI as Second-Line Treatment in Patients with Unresectable Wild Type KRAS Metastatic Colorectal Cancer. *Clin Colorectal Cancer* 2015; **14**: 72-80 [PMID: 25982297 DOI: 10.1016/j.clcc.2014.12.009] [FullText]

5 **Cervantes A**, Adam R, Roselló S, Arnold D, Normanno N, Taïeb J, Seligmann J, De Baere T, Osterlund P, Yoshino T, Martinelli E; ESMO Guidelines Committee. Electronic address: clinicalguidelines@esmo.org. Metastatic colorectal cancer: ESMO Clinical Practice Guideline for diagnosis, treatment and follow-up. *Ann Oncol* 2023; **34**: 10-32 [PMID: 36307056 DOI: 10.1016/j.annonc.2022.10.003] [FullText]

6 **Peeters M**, Price TJ, Cervantes A, Sobrero AF, Ducreux M, Hotko Y, André T, Chan E, Lordick F, Punt CJ, Strickland AH, Wilson G, Ciuleanu TE, Roman L, Van Cutsem E, Tzekova V, Collins S, Oliner KS, Rong A, Gansert J. Randomized phase III study of panitumumab with fluorouracil, leucovorin, and irinotecan (FOLFIRI) compared with FOLFIRI alone as second-line treatment in patients with metastatic colorectal cancer. *J Clin Oncol* 2010; **28**: 4706-4713 [PMID: 20921462 DOI: 10.1200/JCO.2009.27.6055] [FullText]

7 **Bennouna J**, Sastre J, Arnold D, Österlund P, Greil R, Van Cutsem E, von Moos R, Viéitez JM, Bouché O, Borg C, Steffens CC, Alonso-Orduña V, Schlichting C, Reyes-Rivera I, Bendahmane B, André T, Kubicka S; ML18147 Study Investigators. Continuation of bevacizumab after first progression in metastatic colorectal cancer (ML18147): a randomised phase 3 trial. *Lancet Oncol* 2013; **14**: 29-37 [PMID: 23168366 DOI: 10.1016/S1470-2045(12)70477-1] [FullText]

8 **Van Cutsem E**, Tabernero J, Lakomy R, Prenen H, Prausová J, Macarulla T, Ruff P, van Hazel GA, Moiseyenko V, Ferry D, McKendrick J, Polikoff J, Tellier A, Castan R, Allegra C. Addition of aflibercept to fluorouracil, leucovorin, and irinotecan improves survival in a phase III randomized trial in patients with metastatic colorectal cancer previously treated with an oxaliplatin-based regimen. *J Clin Oncol* 2012; **30**: 3499-3506 [PMID: 22949147 DOI: 10.1200/JCO.2012.42.8201] [FullText]

9 **Giantonio BJ**, Catalano PJ, Meropol NJ, O'Dwyer PJ, Mitchell EP, Alberts SR, Schwartz MA, Benson AB 3rd. Bevacizumab in Combination With Oxaliplatin, Fluorouracil, and Leucovorin (FOLFOX4) for Previously Treated Metastatic Colorectal Cancer: Results From the Eastern Cooperative Oncology Group Study E3200. *J Clin Oncol* 2023; **41**: 3670-3675 [PMID: 37459754 DOI: 10.1200/JCO.22.02761] [FullText]

10 **Sobrero AF**, Maurel J, Fehrenbacher L, Scheithauer W, Abubakr YA, Lutz MP, Vega-Villegas ME, Eng C, Steinhauer EU, Prausova J, Lenz HJ, Borg C, Middleton G, Kröning H, Luppi G, Kisker O, Zubel A, Langer C, Kopit J, Burris HA 3rd. EPIC: phase III trial of cetuximab plus irinotecan after fluoropyrimidine and oxaliplatin failure in patients with metastatic colorectal cancer. *J Clin Oncol* 2008; **26**: 2311-2319 [PMID: 18390971 DOI: 10.1200/JCO.2007.13.1193] [FullText]

11 **Seymour MT**, Brown SR, Middleton G, Maughan T, Richman S, Gwyther S, Lowe C, Seligmann JF, Wadsley J, Maisey N, Chau I, Hill M, Dawson L, Falk S, O'Callaghan A, Benstead K, Chambers P, Oliver A, Marshall H, Napp V, Quirke P. Panitumumab and irinotecan versus irinotecan alone for patients with KRAS wild-type, fluorouracil-resistant advanced colorectal cancer (PICCOLO): a prospectively stratified randomised trial. *Lancet Oncol* 2013; **14**: 749-759 [PMID: 23725851 DOI: 10.1016/S1470-2045(13)70163-3] [FullText]

12 **Peeters M**, Price TJ, Cervantes A, Sobrero AF, Ducreux M, Hotko Y, André T, Chan E, Lordick F, Punt CJ, Strickland AH, Wilson G, Ciuleanu TE, Roman L, Van Cutsem E, Tian Y, Sidhu R. Final results from a randomized phase 3 study of FOLFIRI {+/-} panitumumab for second-line treatment of metastatic colorectal cancer. *Ann Oncol* 2014; **25**: 107-116 [PMID: 24356622 DOI: 10.1093/annonc/mdt523] [Full Text]

13 **Casak SJ**, Marcus L, Fashoyin-Aje L, Mushti SL, Cheng J, Shen YL, Pierce WF, Her L, Goldberg KB, Theoret MR, Kluetz PG, Pazdur R, Lemery SJ. FDA Approval Summary: Pembrolizumab for the First-line Treatment of Patients with MSI-H/dMMR Advanced Unresectable or Metastatic Colorectal Carcinoma. *Clin Cancer Res* 2021; **27**: 4680-4684 [PMID: 33846198 DOI: 10.1158/1078-0432.CCR-21-0557] [FullText]

14 **Overman MJ**, Lonardi S, Wong KYM, Lenz HJ, Gelsomino F, Aglietta M, Morse MA, Van Cutsem E, McDermott R, Hill A, Sawyer MB, Hendlisz A, Neyns B, Svrcek M, Moss RA, Ledeine JM, Cao ZA, Kamble S, Kopetz S, André T. Durable Clinical Benefit With Nivolumab Plus Ipilimumab in DNA Mismatch Repair-Deficient/Microsatellite Instability-High Metastatic Colorectal Cancer. *J Clin Oncol* 2018; **36**: 773-779 [PMID: 29355075 DOI: 10.1200/JCO.2017.76.9901] [FullText]

15 **Qian C**, Liu C, Liu W, Zhou R, Zhao L. Targeting vascular normalization: a promising strategy to improve immune-vascular crosstalk in cancer immunotherapy. *Front Immunol* 2023; **14**: 1291530 [PMID: 38193080 DOI: 10.3389/fimmu.2023.1291530] [FullText]

16 **Lenz HJ**, Parikh A, Spigel DR, Cohn AL, Yoshino T, Kochenderfer M, Elez E, Shao SH, Deming D, Holdridge R, Larson T, Chen E, Mahipal A, Ucar A, Cullen D, Baskin-Bey E, Kang T, Hammell AB, Yao J, Tabernero J. Modified FOLFOX6 plus bevacizumab with and without nivolumab for first-line treatment of metastatic colorectal cancer: phase 2 results from the CheckMate 9X8 randomized clinical trial. *J Immunother Cancer* 2024; **12**: e008409 [PMID: 38485190 DOI: 10.1136/jitc-2023-008409] [FullText]

17 **Guinney J**, Dienstmann R, Wang X, de Reyniès A, Schlicker A, Soneson C, Marisa L, Roepman P, Nyamundanda G, Angelino P, Bot BM, Morris JS, Simon IM, Gerster S, Fessler E, De Sousa E Melo F, Missiaglia E, Ramay H, Barras D, Homicsko K, Maru D, Manyam GC, Broom B, Boige V, Perez-Villamil B, Laderas T, Salazar R, Gray JW, Hanahan D, Tabernero J, Bernards R, Friend SH, Laurent-Puig P, Medema JP, Sadanandam A, Wessels L, Delorenzi M, Kopetz S, Vermeulen L, Tejpar S. The consensus molecular subtypes of colorectal cancer. *Nat Med* 2015; **21**: 1350-1356 [PMID: 26457759 DOI: 10.1038/nm.3967] [FullText]

18 **Fang X**, Zhong C, Weng S, Hu H, Wang J, Xiao Q, Wang J, Sun L, Xu D, Liao X, Dong C, Zhang S, Li J, Ding K, Yuan Y. Sintilimab plus bevacizumab and CapeOx (BBCAPX) on first-line treatment in patients with RAS mutant, microsatellite stable, metastatic colorectal cancer: study protocol of a randomized, open-label, multicentric study. *BMC Cancer* 2023; **23**: 676 [PMID: 37464378 DOI: 10.1186/s12885-023-11139-z] [FullText]

19 **Ree AH**, Šaltytė Benth J, Hamre HM, Kersten C, Hofsli E, Guren MG, Sorbye H, Johansen C, Negård A, Bjørnetrø T, Nilsen HL, Berg JP, Flatmark K, Meltzer S. First-line oxaliplatin-based chemotherapy and nivolumab for metastatic microsatellite-stable colorectal cancer-the randomised METIMMOX trial. *Br J Cancer* 2024; **130**: 1921-1928 [PMID: 38664577 DOI: 10.1038/s41416-024-02696-6] [FullText]

20 **Wang X**, Zhang B, Chen X, Mo H, Wu D, Lan B, Li Q, Xu B, Huang J. Lactate dehydrogenase and baseline markers associated with clinical outcomes of advanced esophageal squamous cell carcinoma patients treated with camrelizumab (SHR-1210), a novel anti-PD-1 antibody. *Thorac Cancer* 2019; **10**: 1395-1401 [PMID: 31017739 DOI: 10.1111/1759-7714.13083] [FullText]

21 **Ho DE**, Imai K, King G, Stuart EA. MatchIt: Nonparametric Preprocessing for Parametric Causal Inference. *J Stat Soft* 2011; **42**: 1-28 [DOI: 10.18637/jss.v042.i08] [FullText]

22 **Lin H**, Zelterman D. Modeling Survival Data: Extending the Cox Model. *Technometrics* 2002; **44**: 85-86 [DOI: 10.1198/tech.2002.s656] [Full Text]

23 **Tabernero J**, Yoshino T, Cohn AL, Obermannova R, Bodoky G, Garcia-Carbonero R, Ciuleanu TE, Portnoy DC, Van Cutsem E, Grothey A, Prausová J, Garcia-Alfonso P, Yamazaki K, Clingan PR, Lonardi S, Kim TW, Simms L, Chang SC, Nasroulah F; RAISE Study Investigators. Ramucirumab versus placebo in combination with second-line FOLFIRI in patients with metastatic colorectal carcinoma that progressed during or after first-line therapy with bevacizumab, oxaliplatin, and a fluoropyrimidine (RAISE): a randomised, double-blind, multicentre, phase 3 study. *Lancet Oncol* 2015; **16**: 499-508 [PMID: 25877855 DOI: 10.1016/S1470-2045(15)70127-0] [FullText]

24 **André T**, Louvet C, Maindrault-Goebel F, Couteau C, Mabro M, Lotz JP, Gilles-Amar V, Krulik M, Carola E, Izrael V, de Gramont A. CPT-11 (irinotecan) addition to bimonthly, high-dose leucovorin and bolus and continuous-infusion 5-fluorouracil (FOLFIRI) for pretreated metastatic colorectal cancer. GERCOR. *Eur J Cancer* 1999; **35**: 1343-1347 [PMID: 10658525 DOI: 10.1016/s0959-8049(99)00150-1] [Full Text]

25 **Peeters M**, Strickland AH, Lichinitser M, Suresh AV, Manikhas G, Shapiro J, Rogowski W, Huang X, Wu B, Warner D, Jain R, Tebbutt NC. A randomised, double-blind, placebo-controlled phase 2 study of trebananib (AMG 386) in combination with FOLFIRI in patients with previously treated metastatic colorectal carcinoma. *Br J Cancer* 2013; **108**: 503-511 [PMID: 23361051 DOI: 10.1038/bjc.2012.594] [FullText]

26 **Muro K**, Boku N, Shimada Y, Tsuji A, Sameshima S, Baba H, Satoh T, Denda T, Ina K, Nishina T, Yamaguchi K, Takiuchi H, Esaki T, Tokunaga S, Kuwano H, Komatsu Y, Watanabe M, Hyodo I, Morita S, Sugihara K. Irinotecan plus S-1 (IRIS) versus fluorouracil and folinic acid plus irinotecan (FOLFIRI) as second-line chemotherapy for metastatic colorectal cancer: a randomised phase 2/3 non-inferiority study (FIRIS study). *Lancet Oncol* 2010; **11**: 853-860 [PMID: 20708966 DOI: 10.1016/S1470-2045(10)70181-9] [FullText]

27 **Antoniotti C**, Rossini D, Pietrantonio F, Salvatore L, Lonardi S, Tamberi S, Marmorino F, Moretto R, Prisciandaro M, Tamburini E, Tortora G, Passardi A, Bergamo F, Raimondi A, Ritorto G, Borelli B, Conca V, Ugolini C, Aprile G, Antonuzzo L, Gelsomino F, Martinelli E, Pella N, Masi G, Boni L, Galon J, Cremolini C. Upfront Fluorouracil, Leucovorin, Oxaliplatin, and Irinotecan Plus Bevacizumab With or Without Atezolizumab for Patients With Metastatic Colorectal Cancer: Updated and Overall Survival Results of the ATEZOTRIBE Study. *J Clin Oncol* 2024; **42**: 2637-2644 [PMID: 38865678 DOI: 10.1200/JCO.23.02728] [FullText]

28 **Chen EX**, Kavan P, Tehfe M, Kortmansky JS, Sawyer MB, Chiorean EG, Lieu CH, Polite B, Wong L, Fakih M, Spencer K, Chaves J, Li C, Leconte P, Adelberg D, Kim R. Pembrolizumab Plus Binimetinib With or Without Chemotherapy for MSS/pMMR Metastatic Colorectal Cancer: Outcomes From KEYNOTE-651 Cohorts A, C, and E. *Clin Colorectal Cancer* 2024; **23**: 183-193 [PMID: 38653648 DOI: 10.1016/j.clcc.2024.03.002] [FullText]

29 **Damato A**, Bergamo F, Antonuzzo L, Nasti G, Iachetta F, Romagnani A, Gervasi E, Larocca M, Pinto C. FOLFOXIRI/Bevacizumab Plus Nivolumab as First-Line Treatment in Metastatic Colorectal Cancer RAS/BRAF Mutated: Safety Run-In of Phase II NIVACOR Trial. *Front Oncol* 2021; **11**: 766500 [PMID: 34970487 DOI: 10.3389/fonc.2021.766500] [FullText]

30 **Wang F**, Long J, Li L, Wu ZX, Da TT, Wang XQ, Huang C, Jiang YH, Yao XQ, Ma HQ, Lian ZX, Zhao ZB, Cao J. Single-cell and spatial transcriptome analysis reveals the cellular heterogeneity of liver metastatic colorectal cancer. *Sci Adv* 2023; **9**: eadf5464 [PMID: 37327339 DOI: 10.1126/sciadv.adf5464] [FullText]

31 **Fakih M**, Raghav KPS, Chang DZ, Larson T, Cohn AL, Huyck TK, Cosgrove D, Fiorillo JA, Tam R, D'Adamo D, Sharma N, Brennan BJ, Wang YA, Coppieters S, Zebger-Gong H, Weispfenning A, Seidel H, Ploeger BA, Mueller U, Oliveira CSV, Paulson AS. Regorafenib plus nivolumab in patients with mismatch repair-proficient/microsatellite stable metastatic colorectal cancer: a single-arm, open-label, multicentre phase 2 study. *EClinicalMedicine* 2023; **58**: 101917 [PMID: 37090438 DOI: 10.1016/j.eclinm.2023.101917] [FullText]

32 **Gatenby RA**, Gillies RJ. Why do cancers have high aerobic glycolysis? *Nat Rev Cancer* 2004; **4**: 891-899 [PMID: 15516961 DOI: 10.1038/nrc1478] [FullText]

33 **Cheng M**, Li G, Liu Z, Yang Q, Jiang Y. Pretreatment Neutrophil-to-Lymphocyte Ratio and Lactate Dehydrogenase Predict the Prognosis of Metastatic Cervical Cancer Treated with Combination Immunotherapy. *J Oncol* 2022; **2022**: 1828473 [PMID: 36304986 DOI: 10.1155/2022/1828473] [FullText]

World Journal of Gastroenterology

Submit a Manuscript: https://www.f6publishing.com

World J Gastroenterol 2025 June 7; 31(21): 105895

DOI: 10.3748/wjg.v31.i21.105895

ISSN 1007-9327 (print) ISSN 2219-2840 (online)

ORIGINAL ARTICLE

Retrospective Study

Longitudinal computed tomography-based delta-radiomics of visceral adipose tissue predicts infliximab secondary loss of response in Crohn's disease patients

Xi Li, Fu-Long Song, Hai-Feng He, Shu-Min Zeng, Zhi-Chao Feng, Peng-Fei Rong

Specialty type: Gastroenterology and hepatology

Provenance and peer review: Unsolicited article; Externally peer reviewed.

Peer-review model: Single blind

Peer-review report's classification

Scientific Quality: Grade A, Grade B, Grade B, Grade C

Novelty: Grade A, Grade B, Grade C, Grade C

Creativity or Innovation: Grade A, Grade B, Grade C, Grade C

Scientific Significance: Grade A, Grade B, Grade B, Grade C

P-Reviewer: Lin Y; Wang CL; Zhu MY

Received: February 10, 2025

Revised: April 5, 2025

Accepted: May 21, 2025

Published online: June 7, 2025

Processing time: 116 Days and 18.3 Hours

Xi Li, Fu-Long Song, Shu-Min Zeng, Zhi-Chao Feng, Peng-Fei Rong, Department of Radiology, The Third Xiangya Hospital, Central South University, Changsha 410013, Hunan Province, China

Hai-Feng He, Department of Radiology, Hunan Cancer Hospital/The Affiliated Cancer Hospital of Xiangya School of Medicine, Central South University, Changsha 410013, Hunan Province, China

Zhi-Chao Feng, Department of Radiology, Department of Medical Imaging, SJTU-Ruijin-UIH Institute for Medical Imaging Technology, Ruijin Hospital, Shanghai Jiao Tong University School of Medicine, Shanghai 200025, China

Zhi-Chao Feng, Department of Medical Imaging, Yueyang Central Hospital, Yueyang 414020, Hunan Province, China

Co-first authors: Xi Li and Fu-Long Song.

Co-corresponding authors: Zhi-Chao Feng and Peng-Fei Rong.

Corresponding author: Peng-Fei Rong, Department of Radiology, The Third Xiangya Hospital, Central South University, No. 138 Tongzipo Road, Changsha 410013, Hunan Province, China. rongpengfei66@163.com

Abstract

BACKGROUND

Visceral adipose tissue (VAT) plays a role in the pathogenesis of Crohn's disease (CD) and is associated with treatment outcomes following infliximab (IFX) therapy. We developed and validated the first delta-radiomics model to quantify VAT heterogeneity as a predictive biomarker for IFX response in patients with CD.

AIM

To develop a longitudinal computed tomography (CT)-based delta-radiomics model of VAT for predicting secondary loss of response (SLR) in patients with CD.

METHODS
This retrospective study included 161 patients with CD who achieved clinical remission following IFX induction therapy between 2015 and 2023. All patients underwent CT enterography before IFX initiation and after completing induction therapy. VAT volume was delineated by two radiologists in consensus. Radiomics features were extracted from pre-treatment and post-induction CT images, and delta-radiomics features were calculated as follows: Delta features = $Feature_{-post}$ - $Feature_{-pre}$. A radiomics model was constructed using logistic regression. Model performance was assessed using discrimination, calibration, and decision curve analyses.

RESULTS
Nine significant delta-radiomics features were used to develop the delta-radiomics model, yielding an area under the receiver operating characteristic curve (AUC) of 0.816 (95%CI: 0.737-0.896) in the training cohort and 0.750 (95%CI: 0.605-0.895) in the validation cohort. Multivariable logistic regression identified platelet count, Montreal behavior classification, and the VAT/subcutaneous adipose tissue volume ratio prior to treatment as independent risk factors for SLR. The combined model integrating clinical predictors and delta-radiomics features achieved superior predictive performance, with an AUC of 0.853 (95%CI: 0.786-0.921) in the training cohort and 0.812 (95%CI: 0.677-0.948) in the validation cohort.

CONCLUSION
We developed a predictive model based on longitudinal changes in VAT, demonstrating significant potential for identifying patients with CD at high risk of SLR to IFX therapy.

Key Words: Crohn's disease; Computed tomography enterography; Infliximab; Delta-radiomics; Secondary loss of response

Core Tip: The treatment response to infliximab in patients with Crohn's disease (CD) is heterogeneous, with approximately 23%-46% of those achieving clinical remission after induction therapy experiencing secondary loss of response (SLR) within the first year. This significantly increases the risk of serious adverse outcomes. In this study, we developed a delta-radiomics model based on longitudinal changes in visceral adipose tissue assessed through computed tomography enterography. This model further integrates clinical and imaging biomarkers to identify patients with CD at high risk of SLR. This non-invasive approach holds promise as a valuable tool for optimizing personalized treatment regimens and guiding monitoring strategies.

Citation: Li X, Song FL, He HF, Zeng SM, Feng ZC, Rong PF. Longitudinal computed tomography-based delta-radiomics of visceral adipose tissue predicts infliximab secondary loss of response in Crohn's disease patients. *World J Gastroenterol* 2025; 31(21): 105895
URL: https://www.wjgnet.com/1007-9327/full/v31/i21/105895.htm
DOI: https://dx.doi.org/10.3748/wjg.v31.i21.105895

INTRODUCTION

Crohn's disease (CD) is a chronic autoimmune inflammatory bowel disease (IBD) characterized by alternating relapsing and remitting symptoms throughout its course, often leading to progressive intestinal damage[1]. The primary clinical objective in managing CD is maintaining long-term asymptomatic remission and preventing serious complications[2,3]. Infliximab (IFX), a monoclonal antibody targeting tumor necrosis factor (TNF), has been shown to significantly improve intestinal mucosal healing and increase clinical remission rates in patients with CD[3,4]. However, approximately 23-46% of patients who achieve clinical remission following IFX induction therapy experience secondary loss of response (SLR) within the first year, increasing the risk of disease exacerbation and serious adverse outcomes[5].

Presently, the efficacy of IFX treatment is primarily monitored through periodic endoscopic evaluations. However, due to limitations such as invasiveness, cost, and patient discomfort, endoscopy is not suitable for all individuals. Although several risk factors-such as disease duration, C-reactive protein (CRP) levels, fecal calprotectin concentration, and the presence of creeping fat-have been identified in relation to IFX treatment response, many of these markers are subjective, and the underlying mechanisms remain poorly understood, which limits their widespread clinical applicability[6-8]. Therefore, there is a need for reliable predictive tools capable of identifying patients at risk of SLR to support personalized management strategies.

Growing evidence suggests that visceral adipose tissue (VAT) plays a critical role in the pathogenesis of CD and is strongly associated with disease complexity, prognosis, and the occurrence of complications[9]. VAT contributes to chronic intestinal inflammation by secreting pro-inflammatory cytokines such as TNF-α and various interleukins[10]. Several studies have employed fat attenuation techniques based on CT imaging to quantitatively assess VAT and derive metrics predictive of CD prognosis[11,12]. However, using single fat parameters to characterize the relationship between

VAT and treatment response in CD has notable limitations. These methods often rely on conventional visual assessment, exhibit inter-observer variability, and lack sensitivity in detecting subtle changes in adipose tissue.

In contrast, more comprehensive analyses that capture microstructural alterations and functional impairments within VAT may offer deeper insights into therapeutic outcomes and disease progression in CD[13].

Radiomics, an emerging technique capable of non-invasively extracting extensive quantitative information from medical images, has demonstrated considerable potential in clinical diagnosis and treatment[14]. Previous studies have confirmed the significant clinical utility of VAT-based radiomic features in predicting CD progression[15]. However, in CD patients undergoing IFX induction therapy and achieving clinical remission, VAT exhibits tissue heterogeneity and subtle pathophysiological alterations that vary temporally and spatially before and after treatment. These changes may be indicative of differential therapeutic outcomes[9].

Delta-radiomic features enable precise quantification of longitudinal variations in subtle structural tissue characteristics between two time points[16], offering enhanced information for assessing the response of CD patients to IFX therapy. Compared to magnetic resonance enterography (MRE), CT provides superior spatial resolution for VAT quantification and broader clinical accessibility in routine practice, rendering it more feasible for delta-radiomic analysis. Despite this, no prior studies have assessed the potential clinical value of VAT radiomic features derived from longitudinal CT enterography for predicting SLR to IFX.

This study aims to develop a delta-radiomics model based on longitudinal changes in VAT and to integrate clinical and imaging biomarkers to investigate its predictive utility in identifying CD patients at high risk for SLR.

MATERIALS AND METHODS

Study patients

This retrospective study was approved by the Institutional Ethics Review Board of the Third Xiangya Hospital, Central South University, with the requirement for informed patient consent waived. Patients diagnosed with CD and treated with IFX between January 2015 and August 2023 at the institution were enrolled. CD diagnosis followed the European Crohn's and Colitis Organization guidelines[3]. IFX was administered intravenously with a dosage of 5-10 mg/kg at weeks 0, 2, and 6, followed by maintenance dosing every 8 weeks.

Inclusion criteria: (1) Initial administration of IFX with subsequent regular continuation of therapy; and (2) Availability of CT enterography scans within two weeks prior to IFX initiation and following induction therapy (*i.e.*, between weeks 0-2 and 2-6, with week 14 evaluation).

Exclusion criteria: (1) History of prior bowel resection or previous treatment of biological agents; (2) Lack of clinical response after IFX induction treatment; (3) Poor CT enterography image quality; and (4) Incomplete clinical baseline data and discontinued IFX treatment for reasons other than SLR.

The patient selection process is detailed in Figure 1. Enrolled patients were randomly assigned to the training or validation cohorts in a 7:3 ratio.

Baseline data included age, sex, height, weight, smoking history, neutrophil, lymphocyte, platelet counts, serum albumin, creatinine, erythrocyte sedimentation rate, and CRP levels. Additionally, CD location and behavior were documented according to the Montreal classification. Body mass index was calculated as weight (kg) divided by height squared (m^2), and the neutrophil-lymphocyte ratio was calculated by dividing the neutrophil count by the lymphocyte count.

Outcomes and definitions

Generally, SLR is defined as the recurrence of clinical symptoms between 14 and 54 weeks following an initial response to IFX[17,18]. In this study, SLR outcomes were evaluated by an experienced multidisciplinary team based on clinical symptoms, radiological and endoscopic findings, and subsequent treatment modifications. These included initiating alternative biological agents, requiring immunosuppressants or corticosteroids, IFX dose escalation, and CD-related surgery. Additional criteria included a CD Activity Index > 150 or a reduction of less than 70% from baseline and/or evidence of mucosal recurrence, defined as a reduction in the Simple Endoscopic Score for CD (SES-CD) of < 50% or an SES-CD ≥ 3.

CT image acquisition

CT enterography examinations were performed using a 64-slice multidetector CT scanner (Philips Brilliance; Philips) or a 256-slice scanner (GE Revolution; GE Healthcare), following standardized bowel preparation protocols. Patients fasted prior to imaging and consumed 1200-1500 mL of 2.5% isotonic mannitol solution in three divided doses at 15-minute intervals before the scan.

Scanning was conducted in the supine position, from the diaphragm to the symphysis pubis. After the acquisition of non-enhanced images, a nonionic contrast agent (320 mg/mL; Loversol, Jiangsu Hengrui Medicine Corp Ltd) was administered intravenously at a dose of 1.5-2.0 mL/kg, with an average injection rate of 3.0-4.0 mL/s. Using automatic bolus-tracking, arterial phase images were obtained either 15 seconds after the attenuation value in the abdominal aorta reached 100 HU or with a fixed delay of 32-35 seconds following contrast administration. Portal venous phase images were acquired 35 seconds after the arterial phase, or with a total delay of 70 seconds post-injection.

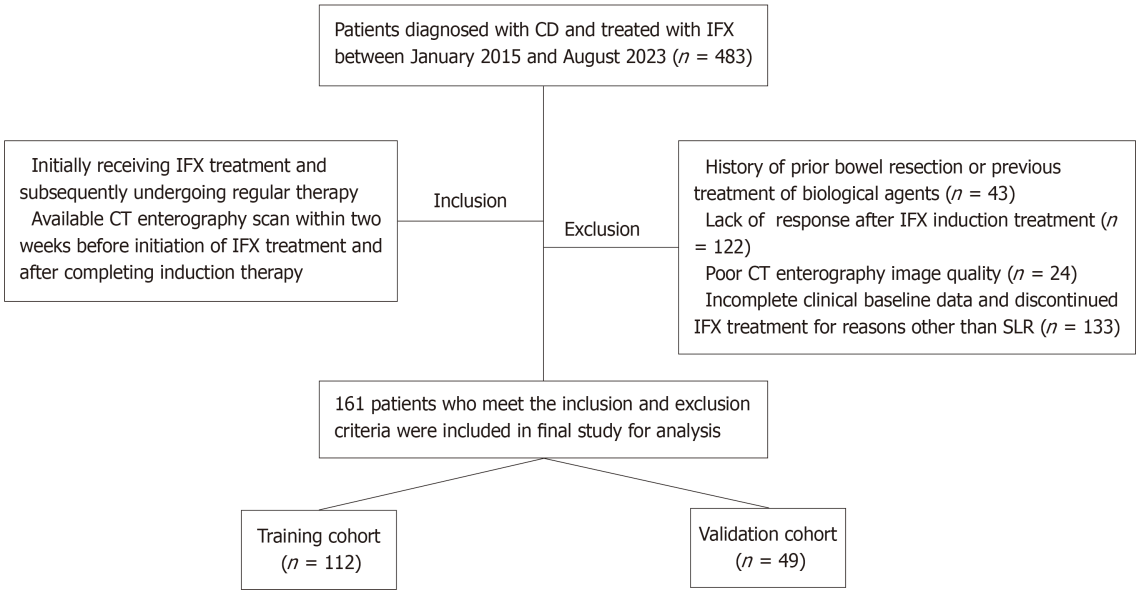

Figure 1 Flowchart of patient recruitment. CD: Crohn's disease; IFX: Infliximab; CT: Computed tomography; SLR: Secondary loss of response.

Detailed scanner parameters are provided in Supplementary Table 1. All CT enterography scans were performed within two weeks before IFX initiation and following the completion of the induction phase. For radiomic analysis, images from the portal venous phase were selected.

Volume of interests segmentation and feature extraction

Volumes of VAT used for radiomics analysis were defined from the top of the diaphragm to the superior margin of the symphysis pubis[15]. Based on tissue-specific attenuation thresholds ranging from -150 to -50 HU[19], two abdominal radiologists-blinded to all clinical information- initially delineated the VAT volumes using the 3D semi-automated segmentation module of an open-source software platform (3D Slicer V4.11.2, https://www.slicer.org/).

Subsequently, manual corrections and verification were performed to finalize the Volume of interests (VOIs). Any discrepancies between the two radiologists were thoroughly reviewed and resolved through consensus. A representative example of the VOI segmentation process is provided in Supplementary Figure 1.

To evaluate reproducibility, the two radiologists independently segmented 30 randomly selected cases after a one-month interval. The intra-class correlation coefficient (ICC) was calculated to assess both intra- and inter-observer reliability, with the methodology illustrated in Figure 2.

The Artificial Intelligent Kit (version 3.2.2; GE Healthcare) was employed to resample CT enterography images. To address differences in voxel resolution across various CT scanners, the voxel dimensions of the portal venous phase images were isotropically resampled to 1 mm × 1 mm × 1 mm (x, y, z) using a linear interpolation algorithm. Hounsfield unit values were discretized into 64 bins to standardize intensity levels.

Subsequently, 1702 radiomics features-including both pre-treatment and post-induction treatment data-were extracted for each patient using the "PyRadiomics" plugin in the 3D Slicer software. To quantify longitudinal changes in VAT, delta-radiomics features were calculated as the relative net differences between the pre-treatment feature values ($Feature_{pre}$) and the post-induction treatment values ($Feature_{post}$) as follows: Delta features = $Feature_{-post}$ - $Feature_{-pre}$. A total of 851 delta-radiomics features could be obtained per patient, encompassing shape features (n = 14), texture features (n = 75), histogram features (n = 18), and wavelet-based features (n = 744).

Measurement of other imaging parameters of adipose tissue

Additional adipose tissue parameters were incorporated into the study, including VAT volume (mm^3), subcutaneous adipose tissue (SAT) volume (mm^3), VAT/SAT volume ratio, VAT area (mm^2) and SAT area (mm^2) measured at the L3 Lumbar vertebral level, and VAT/SAT area ratio prior to treatment initiation and after induction therapy. All measurements were automatically obtained from CT enterography images using 3D slicer software. The VAT/SAT volume or area ratio was calculated as VAT volume or area divided by SAT volume or area. VAT and SAT areas and volumes were normalized by patient height to improve data comparability. The VAT/SAT ratio was further categorized as either < 1.0 or ≥ 1.0.

Model development and validation

To construct the clinical model, univariable and multivariable logistic regression analyses were performed in the training cohort to identify potential clinical predictors. Model performance was assessed using the minimal Akaike Information Criterion (AIC) to optimize fit.

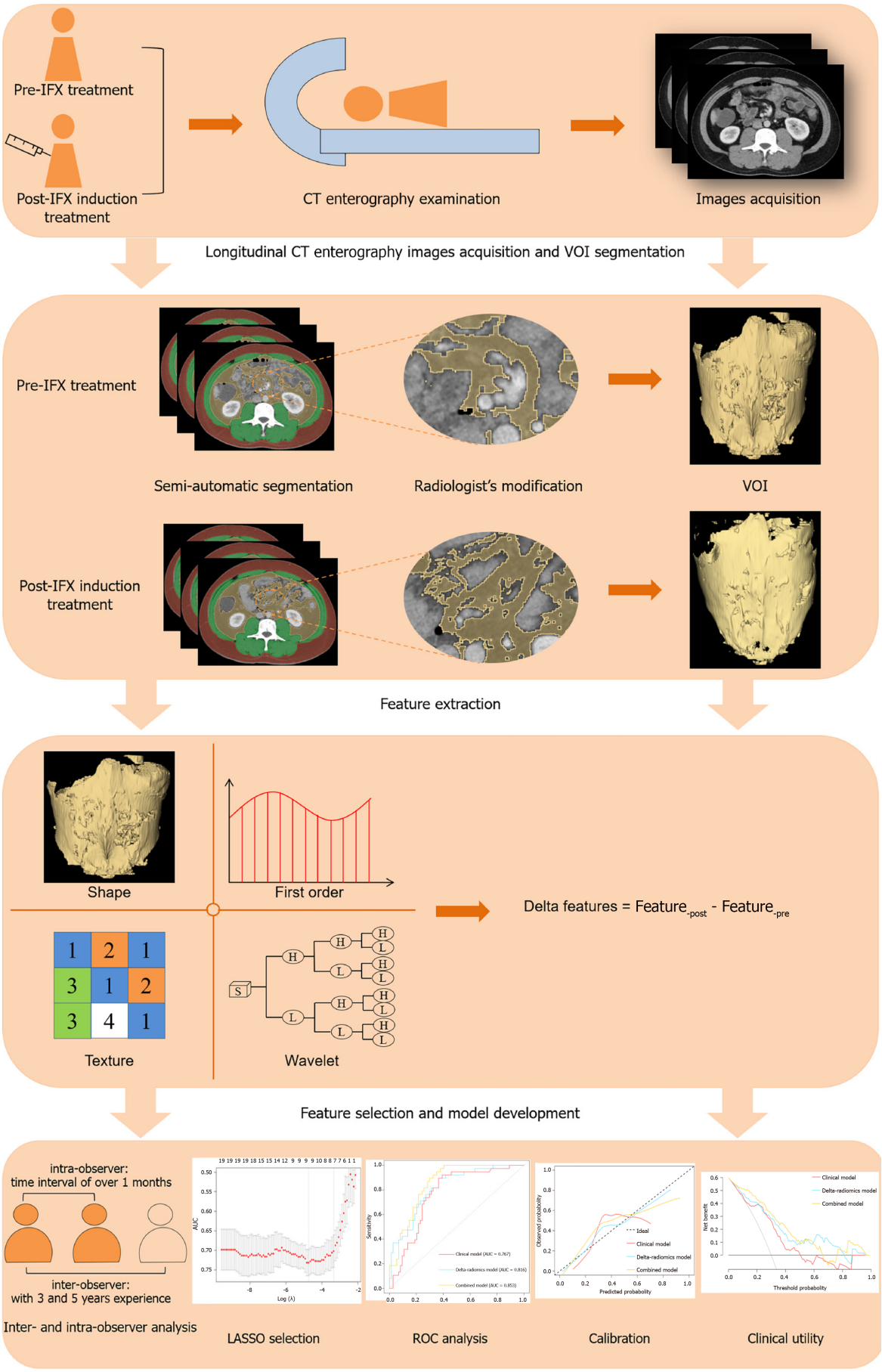

Figure 2 The study design and workflow of radiomics analysis. IFX: Infliximab; CT: Computed tomography; VOI: Volume of interest; LASSO: Least

absolute shrinkage and selection operator; ROC: Receiver operating characteristic curves.

A multi-step feature selection process was implemented to prevent overfitting in the delta-radiomics model. First, all delta-radiomics features were standardized using the *z*-score method to ensure data uniformity. Features with an ICC ≥ 0.75 were retained for further analysis. In the univariable analysis, features with *P* values < 0.05 were selected. The final set of significant features was determined using the least absolute shrinkage and selection operator (LASSO) method with tenfold cross-validation (Supplementary Figure 2), and these were used to construct a delta-radiomics score (delta-radscore).

A nomogram was then developed by integrating the selected clinical predictors with the delta-rad score through logistic regression. Model discrimination was evaluated using receiver operating characteristic (ROC) curve analysis, and the areas under the curves (AUCs) were compared using the DeLong test. Model calibration and clinical utility were assessed with a calibration and decision curve analysis (DCA).

Statistical analysis

Statistical analyses were conducted using R statistical software (version 4.3.1; https//www.r-project.org). Continuous variables were expressed as mean ± SD for normally distributed data or as median with interquartile range for non-normally distributed data. These were analyzed using the Student's *t*-test and the Mann-Whitney *U* test, respectively. Categorical variables were presented as frequencies or percentages and compared using the χ^2 test or Fisher's exact test, as appropriate. A two-sided *P* value < 0.05 was considered statistically significant.

RESULTS

Patient characteristics and construction of the clinical model

A total of 161 eligible patients were included in the final analysis (129 men, 32 women; mean age, 29 years). Demographic and clinical data for the training cohort (n = 112) and validation cohort (n = 49) are summarized in Table 1. Among them, 38 (33.9%) patients in the training cohort and 16 (32.7%) in the validation cohort experienced SLR to IFX during treatment. There were no significant differences in demographic or clinical characteristics between the two cohorts (all P > 0.05).

In the training cohort, multivariable logistic regression analysis identified the following as independent predictors of SLR:

Platelet count [odds ratio (OR) = 1.005, 95%CI: 1.001-1.008, P = 0.011], Montreal behavior classification (OR = 2.307, 95%CI: 1.108-4.803, P = 0.025), VAT/SAT volume ratio before IFX treatment (OR = 3.977, 95%CI: 1.320-11.980, P = 0.014).

These three variables were incorporated into a clinical model developed using logistic regression (Table 2).

Establishment of the delta-radiomics model and clinical-radiomics combined model

A total of 851 delta-radiomics features were extracted from CT enterography images. Following intra- and inter-observer reliability assessment (ICCs > 0.75) and univariate correlation analysis, 193 delta-radiomics features showed statistically significant differences between the SLR and non-SLR groups in the training cohort (P < 0.05).

After applying LASSO selection, 9 delta-radiomics features with nonzero coefficients were obtained to construct a delta-radiomics model based on logistic regression. The model was expressed through the following formula:

Delta-radscore = -1.150
+ 0.452 × Original-Shape-MajorAxisLength
+ 0.448 × Original-Shape-MinorAxisLength
- 1.202 × Wavelet-LHH-Ngtdm-Busyness
- 0.584 × Wavelet-LLH-Gldm-LargeDependenceLowGrayLevelEmphasis
+ 0.436 × Wavelet-LHH-Ngtdm-Contrast
- 0.591 × Wavelet-LHL-Firstorder-Skewness
- 0.193 × Wavelet-HLL-Ngtdm-Contrast
+ 1.118 × Wavelet-HHL-Glcm-JointEnergy
- 0.125 × Wavelet-LLL-Glcm-DifferenceAverage

To integrate significant clinical parameters and delta-radscore, we further established a clinical-radiomics combined model. Based on the combined model, we developed a visual nomogram for simplified application in clinical practice (Figure 3A).

Performance and clinical utility assessment of models

The predictive performance of each model was assessed using ROC analysis, yielding metrics such as the AUC, sensitivity, specificity, positive predictive value, and negative predictive value, as shown in Table 3. In the training cohort (Figure 3B), the AUCs for the clinical model, delta-radiomics model, and combined model in predicting SLR to IFX were 0.767 (95%CI: 0.678-0.857), 0.816 (95%CI: 0.737-0.896), and 0.853 (95%CI: 0.786-0.921), respectively. In the validation cohort (Figure 3C), the corresponding AUCs were 0.707 (95%CI: 0.539-0.876), 0.750 (95%CI: 0.605-0.895), and 0.812 (95%CI: 0.677-0.948), respectively. Among the three models, the combined model exhibited the lowest AIC value (109.28 *vs* 135.10 *vs* 121.61), indicating a superior model fit. The DeLong test demonstrated that the combined model significantly improved

Table 1 Characteristics of patients in the training and validation cohorts, *n* (%)

Variables	Total (*n* = 161)	Training (*n* = 112)	Validation (*n* = 49)	*P* value
Age (years)	29 (22, 38)	27 (21, 38)	31 (24, 38)	0.308
Male gender	129 (80.1)	90 (80.4)	39 (79.6)	0.999
BMI (kg/m²)	18.70 (16.60, 21.50)	19.10 (16.60, 21.50)	17.60 (16.60, 20.10)	0.282
Smoking	49 (30.4)	33 (29.5)	16 (32.7)	0.827
Platelet count (× 10^9 cells/L)	299 (299, 368)	298 (227, 377)	311 (234, 358)	0.834
Albumin (g/dL)	35.2 (32.3, 40.1)	35.2 (32.4, 39.9)	35.0 (31.7, 40.1)	0.827
ESR (mm/hour)	40.0 (22.0, 74.0)	42.0 (22.0,75.0)	37.0 (23.0,70.0)	0.887
CRP (mg/dL)	20.2 (5.0, 50.0)	21.6 (5.4, 49.9)	17.6 (5.0, 51.2)	0.779
Cr (μmol/L)	67 (59, 76)	68 (61, 77)	66 (58, 74)	0.309
NLR	4.3 (2.7, 5.8)	4.3 (2.7, 5.7)	4.0 (2.7, 6.0)	0.977
CDAI	159.0 (107.9, 234.2)	158.7 (99.5, 235.4)	159.0 (118.0, 230.0)	0.786
Montreal location classification				0.380
L1 (ileal disease)	58 (36.0)	41 (36.6)	17 (34.7)	
L2 (colonic disease)	15 (9.3)	13 (11.6)	2 (4.1)	
L3 (ileocolonic disease)	88 (54.7)	58 (51.8)	30 (61.2)	
Montreal behaviour classification				0.554
B1 (non stricturing, non-penetrating)	72 (44.7)	47 (42.0)	25 (51.0)	
B2 (stricturing)	79 (49.1)	58 (51.8)	21 (42.9)	
B3 (penetrating)	10 (6.2)	7 (6.2)	3 (6.1)	
Pre-IFX treatment				
SAT area (cm^2/m^2)	20.0 (7.9, 33.4)	21.7 (8.3, 33.4)	19.2 (7.2, 33.4)	0.511
VAT area (cm^2/m^2)	8.1 (3.2, 25.9)	7.4 (3.2, 24.5)	9.7 (3.1, 28.0)	0.790
SAT volume (cm^3/m^3)	423.2 (166.0, 773.3)	438.2 (170.7, 758.5)	359.8 (155.1, 806.2)	0.901
VAT volume (cm^3/m^3)	187.3 (83.1, 421.4)	169.6 (79.15, 410.3)	214.7 (93.6, 468.1)	0.866
VAT/SAT area ratio (≥ 1)	45 (28.0)	28 (25.0)	17 (34.7)	0.210
VAT/SAT volume ratio (≥ 1)	27 (16.8)	19 (17.0)	8 (16.3)	0.921
Post-IFX treatment				
SAT area (cm^2/m^2)	22.7 (12.9, 35.6)	23.9 (13.7, 39.7)	19.8 (12.1, 31.7)	0.068
VAT area (cm^2/m^2)	11.0 (5.2, 24.9)	11.7 (6.1, 26.7)	9.8 (4.2, 20.3)	0.219
SAT volume (cm^3/m^3)	310.5 (166.1, 596.4)	321.5 (181.8, 627.6)	297.6 (156.8, 535.2)	0.368
VAT volume (cm^3/m^3)	436.2 (244.5, 759.9)	469.1 (272.9, 824.0)	359.6 (214.8, 626.8)	0.131
VAT/SAT area ratio (≥ 1)	37 (23.0)	25 (22.3)	12 (24.5)	0.765
VAT/SAT volume ratio (≥ 1)	18 (11.2)	12 (10.7)	6 (12.2)	0.778

Data are expressed as median (interquartile range), (SD) or number (percentage). BMI: Body mass index; ESR: Erythrocyte sedimentation rate; CRP: C-reactive protein; Cr: Creatinine; NLR: Neutrophil-lymphocyte ratio; CDAI: Crohn's disease activity index; IFX: Infliximab; SAT: Subcutaneous adipose tissue; VAT: Visceral adipose tissue.

predictive performance compared to the clinical model in both the training cohort (P = 0.023) and validation cohort (P = 0.048).

Calibration plots of the combined model showed excellent agreement between the predicted probabilities and observed outcomes in both the training (Figure 4A) and validation (Figure 4B) cohorts. DCA revealed that the combined model outperformed the clinical and delta-radiomics models, offering greater overall net benefit for predicting SLR to IFX treatment in CD patients across the most clinically relevant threshold probability ranges in both the training (Figure 4C)

Table 2 Univariable and multivariable logistic regression analysis for prediction of secondary loss of response to infliximab in Crohn's disease patients in the training cohort, *n* (%)

Variables	Non-SLR (*n* = 74)	SLR (*n* = 38)	Univariable analysis		Multivariable analysis	
			OR (95CI)	*P* value	OR (95%CI)	*P* value
Age (years)	27 (21, 38)	27 (21, 38)	1.004 (0.677-1.489)	0.990		
Male gender	61 (82.4)	29 (76.3)	1.456 (0.323-6.573)	0.603		
BMI (kg/m^2)	19.25 (16.62, 21.10)	18.95 (16.65, 23.02)	0.968 (0.292-3.210)	0.794		
Smoking	23 (31.1)	10 (26.3)	1.263 (0.453-3.521)	0.760		
Platelet count (× 10^9 cells/L)	291 (197, 368)	323 (272, 406)	0.997 (0.021-46.938)	0.049	1.005 (1.001-1.008)	0.011
Albumin (g/dL)	35.7 (32.7, 40.3)	34.3 (32.3, 39.7)	1.020 (0.289-3.593)	0.480		
ESR (mm/hour)	39.5 (24.0, 74.8)	47.0 (18.3, 75.5)	1.000 (0.972-1.029)	0.703		
CRP (mg/dL)	22.1 (6.7, 51.2)	16.1 (5.0, 44.4)	1.006 (0.116-8.735)	0.296		
Cr (μmol/L)	69 (61,78)	65 (58, 74)	1.020 (0.078-13.332)	0.167		
NLR	4.3 (2.7, 5.7)	4.3 (3.1, 5.8)	1.033 (0.360-2.964)	0.825		
CDAI	156.5 (98.5, 242.4)	166.4 (124.8, 233.5)	1.001 (0.590-1.695)	0.890		
Montreal location classification			0.786 (0.090-6.874)	0.401		
L1 (ileal disease)	29 (39.2)	12 (31.5)				
L2 (colonic disease)	8 (10.8)	5 (13.2)				
L3 (ileocolonic disease)	37 (50.5)	21 (55.3)				
Montreal behaviour classification			0.472 (0.007-32.379)	0.031	2.307 (1.108-4.803)	0.025
B1 (non stricturing, non-penetrating)	36 (48.6)	11 (29.0)				
B2 (stricturing)	35 (47.3)	23 (60.5)				
B3 (penetrating)	3 (4.1)	4 (10.5)				
Pre-IFX treatment						
SAT area (cm^2/m^2)	21.2 (7.5, 33.4)	21.7 (9.2, 33.4)	0.999 (0.873-1.143)	0.98		
VAT area (cm^2/m^2)	6.9 (3.0, 21.6)	9.7 (3.6, 26.9)	0.994 (0.320-3.088)	0.405		
SAT volume (cm^3/m^3)	453.3 (165.2, 761.2)	409.8 (179.3, 745.3)	1.000 (0.840-1.190)	0.815		
VAT volume (cm^3/m^3)	168.5 (75.5, 394.8)	234.1 (97.3, 415.2)	0.999 (0.210-4.761)	0.424		
VAT/SAT area ratio (≥ 1)	17 (57.0)	11 (28.9)	1.366 (0.353-5.282)	0.491		
VAT/SAT volume ratio (≥ 1)	8 (10.8)	11 (28.9)	3.361 (0.034-330.690)	0.016	3.977 (1.320-11.980)	0.014
Post-IFX treatment						
SAT area (cm^2/m^2)	26.4 (14.3, 39.8)	20.2 (12.9, 39.3)	1.007 (0.272-3.731)	0.386		
VAT area (cm^2/m^2)	11.8 (6.1, 28.6)	11.1 (6.2, 23.0)	1.009 (0.222-4.577)	0.681		
SAT volume (cm^3/m^3)	481.9 (289.0, 782.3)	408.1 (271.2, 836.1)	1.000 (0.226-4.427)	0.435		
VAT volume (cm^3/m^3)	319.2 (187.9, 624.6)	434.9 (170.6, 612.7)	1.000 (0.544-1.838)	0.975		
VAT/SAT area ratio (≥ 1)	18 (24.3)	7 (18.4)	0.703 (0.175-2.815)	0.479		
VAT/SAT volume ratio (≥ 1)	6 (8.1)	6 (15.8)	2.125 (0.193-23.398)	0.215		

Data are expressed as median (interquartile range), (SD) or number (percentage). IFX: Infliximab; SLR: Secondary loss of response; BMI: Body mass index; ESR: Erythrocyte sedimentation rate; CRP: C-reactive protein; Cr: Creatinine; NLR: Neutrophil-lymphocyte ratio; CDAI: Crohn's disease activity index; SAT: Subcutaneous adipose tissue; VAT: Visceral adipose tissue; OR: Odds ratio.

Table 3 Performance of models for predicting secondary loss of response in the training and validation cohorts

	AUC (95%CI)	Sensitivity	Specificity	PPV	NPV	*P* value[1]	Accuracy
Training cohort (*n* = 112)							
Clinical model	0.767 (0.678-0.857)	85.1% (63/74)	36.8% (14/38)	72.4% (63/87)	56.0% (14/25)	-	68.8% (77/112)
Radiomics model	0.816 (0.737-0.896)	86.5% (64/74)	47.4% (18/38)	76.2% (64/84)	64.3% (18/28)	0.133	73.2% (82/112)
Combined model	0.853 (0.786-0.921)	85.1% (63/74)	52.6% (20/38)	77.8% (63/81)	64.5% (20/31)	0.023	74.1% (83/112)
Validation cohort (*n* = 49)							
Clinical model	0.707 (0.539-0.876)	96.97% (32/33)	31.3% (5/16)	74.4% (32/43)	83.3% (5/6)	-	75.5% (37/49)
Radiomics model	0.750 (0.605-0.895)	84.8% (28/33)	50.0% (8/16)	77.8% (28/36)	61.5% (8/13)	0.204	73.5% (36/49)
Combined model	0.812 (0.677-0.948)	93.9% (31/33)	50.0% (8/16)	79.5% (31/39)	80.0% (8/10)	0.048	79.6% (39/49)

[1]*P* value indicates the significance level of the comparison of areas under the curves with the clinical model as the reference using DeLong test in the training and validation cohort, respectively.

SLR: Secondary loss of response AUC: Area under the curve NPV: Negative predictive value PPV: Positive predictive value.

and validation (Figure 4D) cohorts.

DISCUSSION

Early and accurate identification of SLR to IFX treatment is critical for effectively managing CD. This study utilized baseline clinical parameters and longitudinal delta-radiomics features to develop and validate a predictive model for identifying patients at high risk of SLR. The model demonstrated satisfactory predictive performance in both the training and validation cohorts. Our findings further support the utility of delta-radiomics in capturing temporal and spatial alterations associated with pathophysiological and microstructural changes in VAT, providing valuable insights for predicting treatment response to IFX.

Numerous studies have established that VAT, a complex organ with multifaceted endocrine and immune functions, secretes various pro-inflammatory cytokines and plays a pivotal role in the pathogenesis of CD. It is strongly associated with disease progression and suboptimal therapeutic outcomes[20]. In CD, mesenteric adipose tissue exhibits structural disorganization and functional impairment, characterized by increased deposition of inflammatory mediators and infiltration of immune cells, thereby contributing to intestinal inflammation[21,22]. Radiomics techniques can non-invasively capture these pathophysiological alterations in VAT and transform them into quantifiable imaging features for analysis. A multicenter study by Li *et al*[15] demonstrated that a VAT-based radiomics model accurately identified patients at elevated risk of disease progression. Additionally, a VAT-based deep learning radiomics model effectively differentiated CD from ulcerative colitis[23], showing the presence of distinct microstructural and metabolic characteristics in VAT associated with CD.

Considering that IFX treatment may influence VAT evolution in CD patients[24], we conducted delta-radiomics analysis using CT enterography images obtained before and after IFX induction. Longitudinal changes in VAT between the pre-treatment and post-induction phases were extracted and quantified into nine delta-radiomics features using LASSO regression to predict long-term response to IFX. The resulting delta-radiomics model demonstrated strong predictive capability in identifying high-risk SLR patients. Notably, the nomogram derived from this model offers clinicians a practical tool for optimizing therapeutic strategies, thereby enabling personalized management of CD patients in clinical settings.

In our study, a VAT/SAT volume ratio ≥ 1.0 prior to IFX treatment independently predicted SLR in CD patients. This finding aligns with previous research. Gu *et al*[11] reported that a higher visceral fat index-the ratio of visceral to SAT-was associated with an increased risk of surgery within 6 months of initiating IFX therapy. Other studies have similarly shown that a higher baseline percentage of intra-abdominal VAT relative to total adipose tissue correlates with reduced rates of corticosteroid-free deep remission or endoscopic remission following biologic therapy[9], as well as with increased disease activity and the occurrence of comorbidities[25]. A prospective cohort study also reported that a higher VAT/SAT volume ratio was associated with more severe disease behavior[26].

Despite these findings, our study did not detect a significant correlation between the VAT/SAT area ratio and SLR to IFX. This discrepancy may be attributed to the limitation of measuring fat area from a single axial slice at the L3 vertebral level, which may not fully reflect overall fat distribution[27]. We also observed that patients with complicated disease behaviors, such as stricturing or penetrating phenotypes, were more likely to experience SLR. This is likely because these more complex disease forms are associated with heightened intestinal inflammation, and initiating anti-TNF therapy after developing such phenotypes may result in reduced efficacy and an increased risk of surgical intervention[28,29].

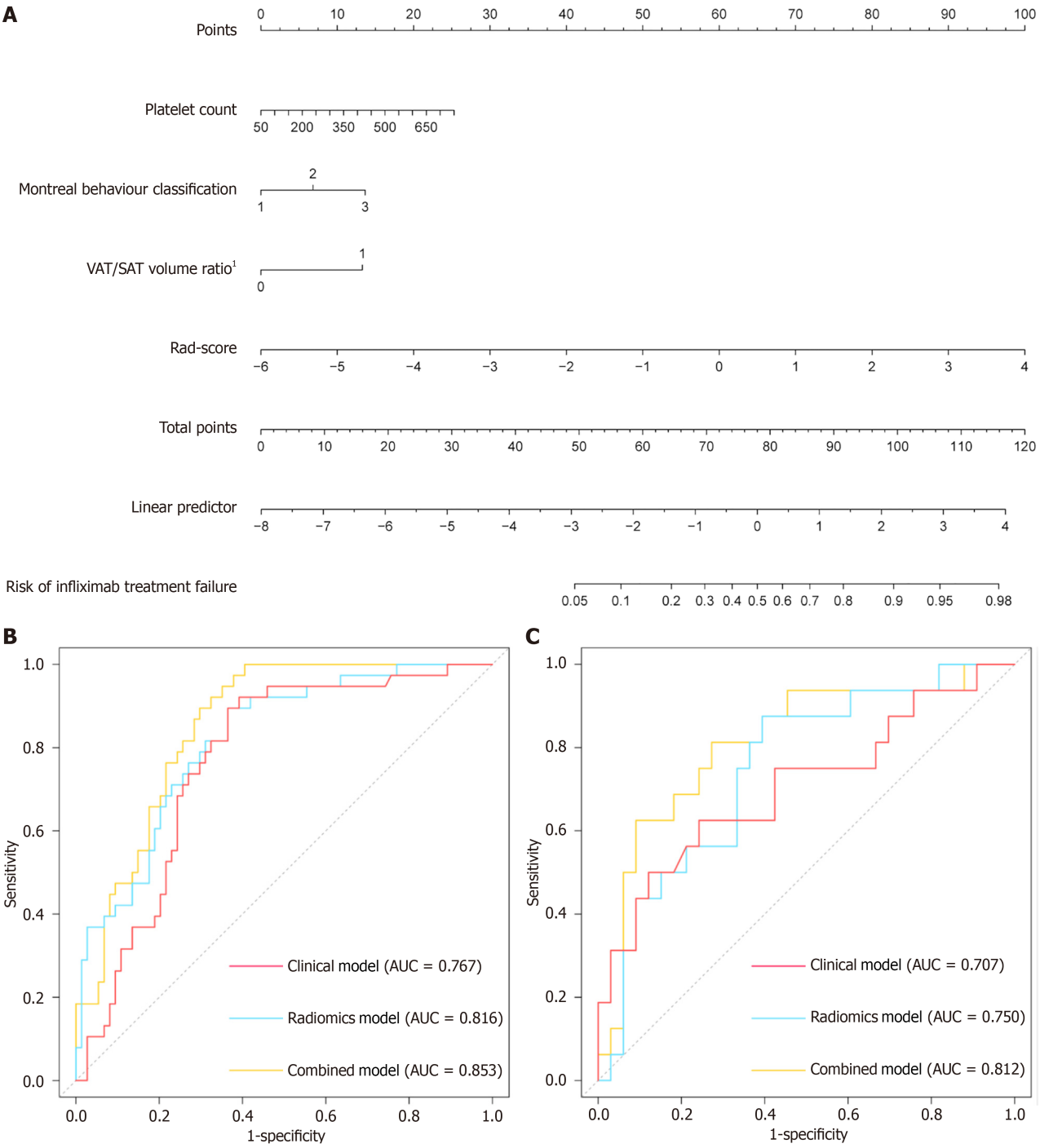

Figure 3 Establishment of the combined model and predictive performance of models for predicting secondary loss of response. A: The developed nomogram of combined model scaled by the proportional regression coefficient of each predictor; B and C: Receiver operating characteristic curves of the clinical model, delta-radiomics model and combined model in the training cohort (B) and the validation cohort (C). VAT: Visceral adipose tissue; SAT: Subcutaneous adipose tissue; AUC: Area under the receiver operating characteristic curve. [1]VAT/SAT volume ratio prior to infliximab treatment.

Abnormalities in platelet number and function have been well documented in IBD[30,31]. As pro-inflammatory cells, platelets release various inflammatory mediators that can initiate or amplify the inflammatory response through diverse cellular and molecular mechanisms, often involving classical immune cells in IBD[30]. Platelets play a critical role in both acute and chronic phases of inflammation. Furthermore, activated platelets secrete profibrogenic factors that contribute to the development of fibrosis in gastrointestinal disorders[32]. In patients with ulcerative colitis who have achieved mucosal healing, elevated platelet counts have been associated with a higher risk of disease recurrence[33].

The platelet-to-lymphocyte ratio has emerged as a promising biomarker for predicting the therapeutic response to anti-TNF treatment in both CD and ulcerative colitis[34,35]. Moreover, an elevated platelet-to-albumin ratio has been identified as an independent risk factor for surgery in CD patients with stricturing disease of the small bowel[36]. In our study, increased platelet count was associated with SLR to IFX, supporting its role as a significant predictive factor in multivariate prediction models. By integrating delta-radiomics features with clinical predictors to construct a combined

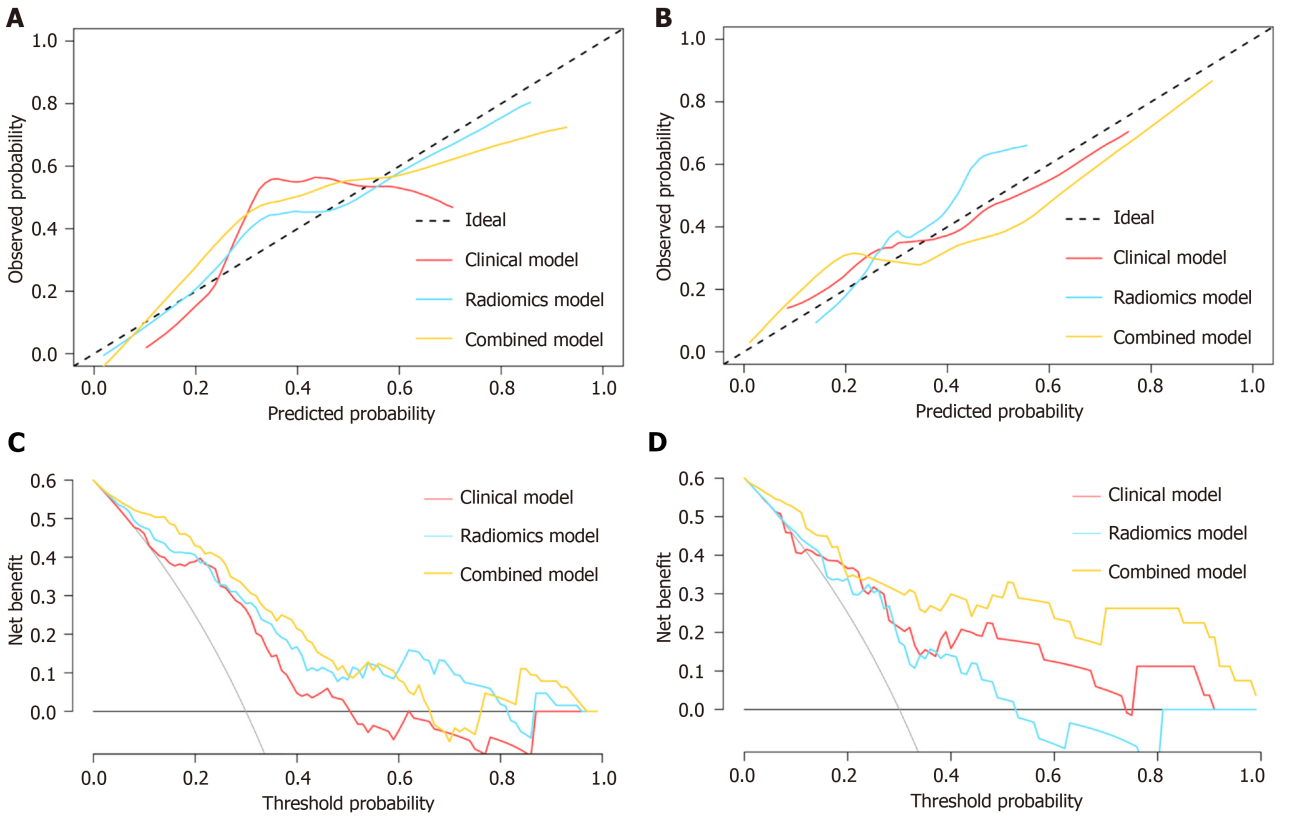

Figure 4 Calibration and clinical utility of models for predicting secondary loss of response to infliximab in patients with Crohn's disease. A and B: Calibration plots for clinical model, delta-radiomics model and combined model in the training cohort (A) and the validation cohort (B); C and D: Decision curve analysis for these three models in the training cohort (C) and the validation cohort (D).

model, we enhanced the overall predictive performance, offering valuable insights for evaluating treatment response to IFX in clinical practice.

Our study has several limitations. First, to enhance the stability and practical applicability of the model, we did not independently include radiomics features extracted from VAT before and after treatment; their clinical utility requires further investigation. Second, although this study confirmed the clinical value of longitudinal VAT changes derived from CT enterography for predicting IFX treatment outcomes using radiomics techniques, CT imaging raises concerns regarding radiation exposure, particularly in adolescent patients. While some studies have utilized MRE to analyze adipose tissue[37], most have been limited to assessments at the level of the third lumbar vertebra. Further research is needed to clarify MRE's potential for evaluating the entire VAT compartment and its feasibility for radiomics applications, thereby helping to reduce radiation-related risks.

Additionally, our study's sample size was relatively limited due to strict inclusion and exclusion criteria. Although the model demonstrated robust performance in internal validation, this limitation may restrict its generalizability to broader patient populations. Multicenter prospective studies with larger cohorts must validate our findings and support clinical translation. Finally, although our LASSO-based model exhibited strong performance and practical utility, exploring alternative feature selection methods may yield further insights and should be considered in future research.

CONCLUSION

We developed and validated a comprehensive model that integrates delta-radiomics features derived from longitudinal changes in VAT with clinical predictors, enabling accurate identification of CD patients at high risk of SLR to IFX treatment. This model holds the potential for guiding individualized treatment planning and monitoring strategies in the clinical management of CD.

FOOTNOTES

Author contributions: Li X, Song FL, He HF, and Zeng SM were tasked with data collection. They gathered information from various clinical sources, carefully extracted key clinical variables such as patient age, disease stage, *etc.*, and assessed images using professional tools. Li X and Song FL conceptualized and designed the research, choosing suitable research methods and setting the direction. They analyzed data using statistical methods and segmented medical images accurately. They also took the lead in writing the manuscript and

are co-first authors. Feng ZC and Rong PF participated in the overall study design and provided valuable suggestions. They supervised data analysis to ensure accuracy and revised the manuscript thoroughly. As co-corresponding authors, they coordinated the whole process. He HF helped with the literature review and looked for relevant studies, while Zeng SM validated the data. They are responsible for patient screening, enrollment, clinical data and imaging index collection. All authors read and approved the final manuscript, ensuring the quality of this research work.

Supported by the National Natural Science Foundation of China, No. 82372072 and No. 82071986.

Institutional review board statement: This retrospective study was reviewed and approved by the Institutional Ethics Review Board of the Third Xiangya Hospital of Central South University, No. Kuai20018.

Informed consent statement: The need for patient consent was waived due to the retrospective nature of the study.

Conflict-of-interest statement: All the authors report no relevant conflicts of interest for this article.

Data sharing statement: Data are available upon reasonable request and pursuant to appropriate agreements from the corresponding author at rongpengfei66@163.com.

Country of origin: China

ORCID number: Zhi-Chao Feng 0000-0001-6651-5195; Peng-Fei Rong 0000-0001-5473-1982.

S-Editor: Li L
L-Editor: A
P-Editor: Yu HG

REFERENCES

1 **Dolinger M**, Torres J, Vermeire S. Crohn's disease. *Lancet* 2024; **403**: 1177-1191 [PMID: 38437854 DOI: 10.1016/S0140-6736(23)02586-2] [FullText]
2 **Cushing K**, Higgins PDR. Management of Crohn Disease: A Review. *JAMA* 2021; **325**: 69-80 [PMID: 33399844 DOI: 10.1001/jama.2020.18936] [FullText]
3 **Gordon H**, Minozzi S, Kopylov U, Verstockt B, Chaparro M, Buskens C, Warusavitarne J, Agrawal M, Allocca M, Atreya R, Battat R, Bettenworth D, Bislenghi G, Brown SR, Burisch J, Casanova MJ, Czuber-Dochan W, de Groof J, El-Hussuna A, Ellul P, Fidalgo C, Fiorino G, Gisbert JP, Sabino JG, Hanzel J, Holubar S, Iacucci M, Iqbal N, Kapizioni C, Karmiris K, Kobayashi T, Kotze PG, Luglio G, Maaser C, Moran G, Noor N, Papamichael K, Peros G, Reenaers C, Sica G, Sigall-Boneh R, Vavricka SR, Yanai H, Myrelid P, Adamina M, Raine T. ECCO Guidelines on Therapeutics in Crohn's Disease: Medical Treatment. *J Crohns Colitis* 2024; **18**: 1531-1555 [PMID: 38877997 DOI: 10.1093/ecco-jcc/jjae091] [FullText]
4 **Singh S**, Fumery M, Sandborn WJ, Murad MH. Systematic review and network meta-analysis: first- and second-line biologic therapies for moderate-severe Crohn's disease. *Aliment Pharmacol Ther* 2018; **48**: 394-409 [PMID: 29920733 DOI: 10.1111/apt.14852] [FullText]
5 **Peyrin-Biroulet L**, Loftus EV Jr, Colombel JF, Sandborn WJ. The natural history of adult Crohn's disease in population-based cohorts. *Am J Gastroenterol* 2010; **105**: 289-297 [PMID: 19861953 DOI: 10.1038/ajg.2009.579] [FullText]
6 **Gisbert JP**, Chaparro M. Predictors of Primary Response to Biologic Treatment [Anti-TNF, Vedolizumab, and Ustekinumab] in Patients With Inflammatory Bowel Disease: From Basic Science to Clinical Practice. *J Crohns Colitis* 2020; **14**: 694-709 [PMID: 31777929 DOI: 10.1093/ecco-jcc/jjz195] [FullText]
7 **Rimola J**, Fernàndez-Clotet A, Capozzi N, Rojas-Farreras S, Alfaro I, Rodríguez S, Masamunt MC, Ricart E, Ordás I, Panés J. Pre-treatment magnetic resonance enterography findings predict the response to TNF-alpha inhibitors in Crohn's disease. *Aliment Pharmacol Ther* 2020; **52**: 1563-1573 [PMID: 32886809 DOI: 10.1111/apt.16069] [FullText]
8 **Yueying C**, Jing F, Qi F, Jun S. Infliximab response associates with radiologic findings in bio-naïve Crohn's disease. *Eur Radiol* 2023; **33**: 5247-5257 [PMID: 36928565 DOI: 10.1007/s00330-023-09542-y] [FullText]
9 **Yarur AJ**, Bruss A, Moosreiner A, Beniwal-Patel P, Nunez L, Berens B, Colombel JF, Targan SR, Fox C, Melmed GY, Abreu MT, Deepak P. Higher Intra-Abdominal Visceral Adipose Tissue Mass Is Associated With Lower Rates of Clinical and Endoscopic Remission in Patients With Inflammatory Bowel Diseases Initiating Biologic Therapy: Results of the Constellation Study. *Gastroenterology* 2023; **165**: 963-975.e5 [PMID: 37499955 DOI: 10.1053/j.gastro.2023.06.036] [FullText]
10 **Bassi M**, Singh S. Impact of Obesity on Response to Biologic Therapies in Patients with Inflammatory Bowel Diseases. *BioDrugs* 2022; **36**: 197-203 [PMID: 35320515 DOI: 10.1007/s40259-022-00522-0] [FullText]
11 **Gu P**, Chhabra A, Chittajallu P, Chang C, Mendez D, Gilman A, Fudman DI, Xi Y, Feagins LA. Visceral Adipose Tissue Volumetrics Inform Odds of Treatment Response and Risk of Subsequent Surgery in IBD Patients Starting Antitumor Necrosis Factor Therapy. *Inflamm Bowel Dis* 2022; **28**: 657-666 [PMID: 34291800 DOI: 10.1093/ibd/izab167] [FullText]
12 **Sehgal P**, Su S, Zech J, Nobel Y, Luk L, Economou I, Shen B, Lewis JD, Freedberg DE. Visceral Adiposity Independently Predicts Time to Flare in Inflammatory Bowel Disease but Body Mass Index Does Not. *Inflamm Bowel Dis* 2024; **30**: 594-601 [PMID: 37307420 DOI: 10.1093/ibd/izad111] [FullText]

13 **Zuo L**, Li Y, Zhu W, Shen B, Gong J, Guo Z, Zhang W, Wu R, Gu L, Li N, Li J. Mesenteric Adipocyte Dysfunction in Crohn's Disease is Associated with Hypoxia. *Inflamm Bowel Dis* 2016; **22**: 114-126 [PMID: 26332309 DOI: 10.1097/MIB.0000000000000571] [FullText]

14 **Gillies RJ**, Kinahan PE, Hricak H. Radiomics: Images Are More than Pictures, They Are Data. *Radiology* 2016; **278**: 563-577 [PMID: 26579733 DOI: 10.1148/radiol.2015151169] [FullText]

15 **Li X**, Zhang N, Hu C, Lin Y, Li J, Li Z, Cui E, Shi L, Zhuang X, Li J, Lu J, Wang Y, Liu R, Yuan C, Lin H, He J, Ke D, Tang S, Zou Y, He B, Sun C, Chen M, Huang B, Mao R, Feng ST. CT-based radiomics signature of visceral adipose tissue for prediction of disease progression in patients with Crohn's disease: A multicentre cohort study. *EClinicalMedicine* 2023; **56**: 101805 [PMID: 36618894 DOI: 10.1016/j.eclinm.2022.101805] [FullText]

16 **Huang Y**, Zhu T, Zhang X, Li W, Zheng X, Cheng M, Ji F, Zhang L, Yang C, Wu Z, Ye G, Lin Y, Wang K. Longitudinal MRI-based fusion novel model predicts pathological complete response in breast cancer treated with neoadjuvant chemotherapy: a multicenter, retrospective study. *EClinicalMedicine* 2023; **58**: 101899 [PMID: 37007742 DOI: 10.1016/j.eclinm.2023.101899] [FullText]

17 **Kennedy NA**, Heap GA, Green HD, Hamilton B, Bewshea C, Walker GJ, Thomas A, Nice R, Perry MH, Bouri S, Chanchlani N, Heerasing NM, Hendy P, Lin S, Gaya DR, Cummings JRF, Selinger CP, Lees CW, Hart AL, Parkes M, Sebastian S, Mansfield JC, Irving PM, Lindsay J, Russell RK, McDonald TJ, McGovern D, Goodhand JR, Ahmad T; UK Inflammatory Bowel Disease Pharmacogenetics Study Group. Predictors of anti-TNF treatment failure in anti-TNF-naive patients with active luminal Crohn's disease: a prospective, multicentre, cohort study. *Lancet Gastroenterol Hepatol* 2019; **4**: 341-353 [PMID: 30824404 DOI: 10.1016/S2468-1253(19)30012-3] [FullText]

18 **Maaser C**, Sturm A, Vavricka SR, Kucharzik T, Fiorino G, Annese V, Calabrese E, Baumgart DC, Bettenworth D, Borralho Nunes P, Burisch J, Castiglione F, Eliakim R, Ellul P, González-Lama Y, Gordon H, Halligan S, Katsanos K, Kopylov U, Kotze PG, Krustinš E, Laghi A, Limdi JK, Rieder F, Rimola J, Taylor SA, Tolan D, van Rheenen P, Verstockt B, Stoker J; European Crohn's and Colitis Organisation [ECCO] and the European Society of Gastrointestinal and Abdominal Radiology [ESGAR]. ECCO-ESGAR Guideline for Diagnostic Assessment in IBD Part 1: Initial diagnosis, monitoring of known IBD, detection of complications. *J Crohns Colitis* 2019; **13**: 144-164 [PMID: 30137275 DOI: 10.1093/ecco-jcc/jjy113] [FullText]

19 **Montano-Loza AJ**, Mazurak VC, Ebadi M, Meza-Junco J, Sawyer MB, Baracos VE, Kneteman N. Visceral adiposity increases risk for hepatocellular carcinoma in male patients with cirrhosis and recurrence after liver transplant. *Hepatology* 2018; **67**: 914-923 [PMID: 29023899 DOI: 10.1002/hep.29578] [FullText]

20 **Eder P**, Adler M, Dobrowolska A, Kamhieh-Milz J, Witowski J. The Role of Adipose Tissue in the Pathogenesis and Therapeutic Outcomes of Inflammatory Bowel Disease. *Cells* 2019; **8**: 628 [PMID: 31234447 DOI: 10.3390/cells8060628] [FullText]

21 **Gonçalves P**, Magro F, Martel F. Metabolic inflammation in inflammatory bowel disease: crosstalk between adipose tissue and bowel. *Inflamm Bowel Dis* 2015; **21**: 453-467 [PMID: 25248003 DOI: 10.1097/MIB.0000000000000209] [FullText]

22 **Weidinger C**, Hegazy AN, Siegmund B. The role of adipose tissue in inflammatory bowel diseases. *Curr Opin Gastroenterol* 2018; **34**: 183-186 [PMID: 29846262 DOI: 10.1097/MOG.0000000000000445] [FullText]

23 **Zhou Z**, Xiong Z, Cheng R, Luo Q, Li Y, Xie Q, Xiao P, Hu D, Hu X, Shen Y, Li Z. Volumetric visceral fat machine learning phenotype on CT for differential diagnosis of inflammatory bowel disease. *Eur Radiol* 2023; **33**: 1862-1872 [PMID: 36255487 DOI: 10.1007/s00330-022-09171-x] [FullText]

24 **Santos JCD**, Malaguti C, Lucca FA, Cabalzar AL, Ribeiro TCDR, Gaburri PD, Chebli LA, Chebli JMF. Impact of biological therapy on body composition of patients with Chron's disease. *Rev Assoc Med Bras (1992)* 2017; **63**: 407-413 [PMID: 28724037 DOI: 10.1590/1806-9282.63.05.407] [FullText]

25 **Büning C**, von Kraft C, Hermsdorf M, Gentz E, Wirth EK, Valentini L, Haas V. Visceral Adipose Tissue in Patients with Crohn's Disease Correlates with Disease Activity, Inflammatory Markers, and Outcome. *Inflamm Bowel Dis* 2015; **21**: 2590-2597 [PMID: 26222339 DOI: 10.1097/MIB.0000000000000527] [FullText]

26 **Bryant RV**, Schultz CG, Ooi S, Goess C, Costello SP, Vincent AD, Schoeman S, Lim A, Bartholomeusz FD, Travis SPL, Andrews JM. Visceral Adipose Tissue Is Associated With Stricturing Crohn's Disease Behavior, Fecal Calprotectin, and Quality of Life. *Inflamm Bowel Dis* 2019; **25**: 592-600 [PMID: 30215805 DOI: 10.1093/ibd/izy278] [FullText]

27 **Shen W**, Punyanitya M, Wang Z, Gallagher D, St-Onge MP, Albu J, Heymsfield SB, Heshka S. Visceral adipose tissue: relations between single-slice areas and total volume. *Am J Clin Nutr* 2004; **80**: 271-278 [PMID: 15277145 DOI: 10.1093/ajcn/80.2.271] [FullText]

28 **Moran GW**, Dubeau MF, Kaplan GG, Yang H, Seow CH, Fedorak RN, Dieleman LA, Barkema HW, Ghosh S, Panaccione R; Alberta Inflammatory Bowel Disease Consortium. Phenotypic features of Crohn's disease associated with failure of medical treatment. *Clin Gastroenterol Hepatol* 2014; **12**: 434-42.e1 [PMID: 23978351 DOI: 10.1016/j.cgh.2013.08.026] [FullText]

29 **Yang T**, Feng J, Yao R, Feng Q, Shen J. CT-based pancreatic radiomics predicts secondary loss of response to infliximab in biologically naïve patients with Crohn's disease. *Insights Imaging* 2024; **15**: 69 [PMID: 38472447 DOI: 10.1186/s13244-024-01637-4] [FullText]

30 **Danese S**, Motte Cd Cde L, Fiocchi C. Platelets in inflammatory bowel disease: clinical, pathogenic, and therapeutic implications. *Am J Gastroenterol* 2004; **99**: 938-945 [PMID: 15128364 DOI: 10.1111/j.1572-0241.2004.04129.x] [FullText]

31 **Menchén L**, Marín-Jiménez I, Arias-Salgado EG, Fontela T, Hernández-Sampelayo P, Rodríguez MC, Butta NV. Matrix metalloproteinase 9 is involved in Crohn's disease-associated platelet hyperactivation through the release of soluble CD40 ligand. *Gut* 2009; **58**: 920-928 [PMID: 19039088 DOI: 10.1136/gut.2008.150318] [FullText]

32 **Ripoche J**. Blood platelets and inflammation: their relationship with liver and digestive diseases. *Clin Res Hepatol Gastroenterol* 2011; **35**: 353-357 [PMID: 21482218 DOI: 10.1016/j.clinre.2011.02.012] [FullText]

33 **Nakarai A**, Kato J, Hiraoka S, Takashima S, Inokuchi T, Takahara M, Sugihara Y, Harada K, Okada H. An Elevated Platelet Count Increases the Risk of Relapse in Ulcerative Colitis Patients with Mucosal Healing. *Gut Liver* 2018; **12**: 420-425 [PMID: 29945423 DOI: 10.5009/gnl17236] [FullText]

34 **Bertani L**, Rossari F, Barberio B, Demarzo MG, Tapete G, Albano E, Baiano Svizzero G, Ceccarelli L, Mumolo MG, Brombin C, de Bortoli N, Bellini M, Marchi S, Bodini G, Savarino E, Costa F. Novel Prognostic Biomarkers of Mucosal Healing in Ulcerative Colitis Patients Treated With Anti-TNF: Neutrophil-to-Lymphocyte Ratio and Platelet-to-Lymphocyte Ratio. *Inflamm Bowel Dis* 2020; **26**: 1579-1587 [PMID: 32232392 DOI: 10.1093/ibd/izaa062] [FullText]

35 **Soufli I**, Hablal A, Bessaad S, Amri M, Labsi M, Boussa RS, Ameur F, Belguendouz H, Younes SA, Idris NS, Touil-Boukoffa C. Nitric Oxide, Neutrophil/Lymphocyte, and Platelet/Lymphocyte Ratios as Promising Inflammatory Biomarkers in Complicated Crohn's Disease: Outcomes of Corticosteroids and Anti-TNF-α Therapies. *Inflammation* 2023; **46**: 1091-1105 [PMID: 36869975 DOI: 10.1007/s10753-023-01796-4] [FullText]

36 **Stidham RW**, Guentner AS, Ruma JL, Govani SM, Waljee AK, Higgins PD. Intestinal Dilation and Platelet:Albumin Ratio Are Predictors of Surgery in Stricturing Small Bowel Crohn's Disease. *Clin Gastroenterol Hepatol* 2016; **14**: 1112-1119.e2 [PMID: 27155551 DOI: 10.1016/j.cgh.2016.04.033] [FullText]

37 **Baum T**, Cordes C, Dieckmeyer M, Ruschke S, Franz D, Hauner H, Kirschke JS, Karampinos DC. MR-based assessment of body fat distribution and characteristics. *Eur J Radiol* 2016; **85**: 1512-1518 [PMID: 26905521 DOI: 10.1016/j.ejrad.2016.02.013] [FullText]

World Journal of Gastroenterology

Submit a Manuscript: https://www.f6publishing.com

World J Gastroenterol 2025 June 7; 31(21): 107029

DOI: 10.3748/wjg.v31.i21.107029

ISSN 1007-9327 (print) ISSN 2219-2840 (online)

ORIGINAL ARTICLE

Retrospective Study

Evaluating log odds of positive lymph nodes as a prognostic tool in differentiated gastric cancer: A retrospective study

Ming-Cong Deng, Ken Chen, Qi-Mei Bao, Yi-Xing Huang, Chun-Kai Zhang, Yu-Ke Zhong, Han-Yi He, Dan Zu, Chen Liang, Hai-Dong Liu, Yang-Chan Hu, Guo-Xia Liu, Yan-Hua He, Wei-Xing Wu, Jing-Nan Zhou, Yao-Shu Teng, Ji Jing, Yin Shi, Clive Yik-Sham Chung, Chen-Huan Yu, Yi-An Du, Zu Ye, Xiang-Dong Cheng

Specialty type: Gastroenterology and hepatology

Provenance and peer review: Unsolicited article; Externally peer reviewed.

Peer-review model: Single blind

Peer-review report's classification

Scientific Quality: Grade A, Grade A, Grade B, Grade B, Grade C

Novelty: Grade A, Grade B, Grade B, Grade B, Grade C

Creativity or Innovation: Grade A, Grade B, Grade B, Grade B, Grade C

Scientific Significance: Grade A, Grade A, Grade A, Grade A, Grade C

P-Reviewer: He ST; Luan SJ; Wang CL

Received: March 13, 2025

Revised: April 23, 2025

Accepted: May 19, 2025

Published online: June 7, 2025

Processing time: 84 Days and 19.9 Hours

Ming-Cong Deng, Ken Chen, Qi-Mei Bao, Yi-Xing Huang, Chun-Kai Zhang, Yu-Ke Zhong, Han-Yi He, Dan Zu, Chen Liang, Hai-Dong Liu, Yang-Chan Hu, Guo-Xia Liu, Yan-Hua He, Wei-Xing Wu, Jing-Nan Zhou, Ji Jing, Chen-Huan Yu, Yi-An Du, Zu Ye, Xiang-Dong Cheng, Zhejiang Cancer Hospital, Hangzhou Institute of Medicine, Chinese Academy of Sciences, Hangzhou 310022, Zhejiang Province, China

Ming-Cong Deng, Hangzhou Medical College, Hangzhou 310013, Zhejiang Province, China

Ken Chen, The Second Clinical Medical College, Zhejiang Chinese Medical University, Hangzhou 310053, Zhejiang Province, China

Ken Chen, Yi-Xing Huang, Yao-Shu Teng, Department of Otorhinolaryngology, Affiliated Hangzhou First People's Hospital, School of Medicine, Westlake University, Hangzhou 310006, Zhejiang Province, China

Yi-Xing Huang, Yin Shi, School of Medicine, Zhejiang University, Hangzhou 310058, Zhejiang Province, China,

Dan Zu, Guo-Xia Liu, School of Life Sciences, Tianjin University, Tianjin 300100, China

Hai-Dong Liu, Yi-An Du, Zu Ye, Xiang-Dong Cheng, Zhejiang Provincial Research Center for Upper Gastrointestinal Tract Cancer, Zhejiang Cancer Hospital, Hangzhou 310022, Zhejiang Province, China

Hai-Dong Liu, Yi-An Du, Zu Ye, Xiang-Dong Cheng, Key Laboratory of Prevention, Diagnosis and Therapy of Upper Gastrointestinal Cancer of Zhejiang Province, Hangzhou 310022, Zhejiang Province, China

Clive Yik-Sham Chung, School of Biomedical Sciences, Li Ka Shing Faculty of Medicine, The University of Hong Kong, Hong Kong, China

Clive Yik-Sham Chung, Department of Pathology, School of Clinical Medicine, Li Ka Shing Faculty of Medicine, The University of Hong Kong, Hong Kong, China

Co-corresponding authors: Xiang-Dong Cheng, Zu Ye, Yi-An Du and Chen-Huan Yu.

Corresponding author: Xiang-Dong Cheng, MD, Professor, Zhejiang Cancer Hospital, Hang-

zhou Institute of Medicine, Chinese Academy of Sciences, No. 1 East Banshan Road, Hangzhou 310022, Zhejiang Province, China. yezuqscx@gmail.com

Abstract

BACKGROUND

The log odds of positive lymph nodes (LODDS) are correlated with survival outcomes in gastric cancer (GC) patients. However, the prognostic value across different tumor differentiation levels remains unclear.

AIM

To evaluate the independent prognostic value of LODDS and the stratified predictive efficacy in GC patients with different histologic differentiations.

METHODS

We conducted a retrospective analysis of 2103 GC patients who underwent radical gastrectomy at Zhejiang Cancer Hospital. The prognostic value of LODDS was compared with that of other lymph node-based metrics, including the pathologic N stage, number of positive lymph nodes, number of total lymph nodes, and lymph node ratio, stratified by tumor differentiation.

RESULTS

LODDS was identified as an independent prognostic factor for overall survival in moderately to poorly differentiated GC patients. LODDS demonstrated superior predictive accuracy over other lymph node metrics. A nomogram incorporating LODDS, age, carbohydrate antigen (CA) 125, carcinoembryonic antigen, and tumor differentiation showed good predictive accuracy (C-index = 0.703). A higher LODDS was significantly associated with an increased risk of recurrence or metastasis, poorly differentiated tumors, advanced cancer, mucinous gastric adenocarcinoma, nerve invasion, and vascular tumor thrombus. Additionally, LODDS was positively correlated with the tumor markers CA19-9, CA72-4, CA125, and CA242 (all $P < 0.05$).

CONCLUSION

LODDS is an independent prognostic indicator for patients with moderately and poorly differentiated GC, and its predictive performance is superior to that of other models.

Key Words: Gastric cancer; Log odds of positive lymph nodes; Tumor differentiation; Tumor marker; Overall survival

Core Tip: This study highlights the log odds of positive lymph nodes (LODDS) as a reliable independent prognostic tool for moderately and poorly differentiated gastric cancer, providing more precise risk stratification than traditional systems such as pathologic N stage. Patients with higher LODDS values, which are associated with more aggressive tumor behavior, may benefit from more frequent follow-ups and intensified treatments. The incorporation of the LODDS into a clinical nomogram is expected to improve individualized survival prediction and the development of therapeutic strategies.

Citation: Deng MC, Chen K, Bao QM, Huang YX, Zhang CK, Zhong YK, He HY, Zu D, Liang C, Liu HD, Hu YC, Liu GX, He YH, Wu WX, Zhou JN, Teng YS, Jing J, Shi Y, Chung CYS, Yu CH, Du YA, Ye Z, Cheng XD. Evaluating log odds of positive lymph nodes as a prognostic tool in differentiated gastric cancer: A retrospective study. *World J Gastroenterol* 2025; 31(21): 107029
URL: https://www.wjgnet.com/1007-9327/full/v31/i21/107029.htm
DOI: https://dx.doi.org/10.3748/wjg.v31.i21.107029

INTRODUCTION

Cancer is one of the most challenging diseases worldwide, with its development governed by a complex interplay of factors. These include intrinsic factors[1-6], such as genetic mutations, genomic instability, and the activation of oncogenes, as well as extrinsic factors[7-12], such as chronic inflammation induced by external stimuli and immune system dysregulation, which collectively contribute to the progression from inflammation to malignancy. Gastric cancer (GC) is the fifth most common cancer worldwide and the third leading cause of cancer-related mortality, following lung and liver cancer[13,14]. According to the GLOBOCAN global cancer burden report, GC causes more than 780000 deaths annually, with its mortality rate remaining high worldwide, especially among patients with advanced disease accompanied by lymph node metastasis, who generally have a poor prognosis[15-17]. In clinical practice, lymph nodes are a primary route of metastasis for GC[18-20]. Cancer cells spread through the lymphatic system to nearby lymph nodes and

may subsequently metastasize to distant lymph nodes or other organs[21-25].

Lymph node metastasis not only reflects the invasiveness and spreading capability of tumor cells but also typically signifies that cancer has progressed to a locally advanced stage[26-28]. Postoperatively, the number and distribution of metastatic lymph nodes directly influence patient survival rates and recurrence risk, and the extent of lymph node metastasis can further inform the staging of GC and potential treatment response[29,30]. Currently, prognosis assessment for GC patients relies primarily on the 8th edition of the American Joint Committee on Cancer (AJCC) tumor-node-metastasis (TNM) staging system[31-33]. Pathologic N stage in this system is determined on the basis of pathologic examination of the lymph nodes removed during surgery, and in particular, the number of metastatic lymph nodes is evaluated to assess the extent of disease progression[34-36]. However, this system does not account for ratio-based lymph node classification, which may provide more precise prognostic insights and better guide personalized treatment strategies.

The grade of tumor differentiation plays a crucial role in GC prognosis[37-39]. Tumor differentiation refers to the degree of similarity between tumor and normal tissue cells and reflects the level of maturation of tumor cells in terms of morphology, structure, and function[40-43]. Poorly differentiated tumors often exhibit higher cellular heterogeneity and invasiveness, which are closely associated with a poor prognosis and a higher risk of recurrence[44-47]. However, in patients with limited lymph node dissection or substantial variation in tumor differentiation, the AJCC pathologic N stage (pN) staging system may fail to accurately reflect individual prognosis, particularly in patients with poorly differentiated and highly invasive tumors[48-50]. Moreover, existing staging systems and prognostic models are often based on the overall GC population and inadequately address the specific impact of tumor differentiation, leading to potential bias in prognostic stratification for patients with moderate to poorly differentiated tumors[51-53]. Therefore, developing tools that can better reflect the true prognosis of such patients is highly important.

In recent years, the log odds of positive lymph nodes (LODDS) - a ratio-based lymph node staging system - has gained attention. By integrating the ratio of positive to negative lymph nodes, LODDS has the potential to overcome the limitations of the traditional pN staging system, which solely depends on the number of positive lymph nodes. Additionally, the LODDS has demonstrated superior prognostic performance, especially in patients with inadequate lymph node dissection[54,55]. Studies across various cancer types have shown the prognostic accuracy of LODDS, which outperforms traditional pN staging in esophageal and colorectal cancers[56,57]. Although the LODDS has been applied in some GC studies, its effectiveness in the context of moderately to poorly differentiated GC remains unclear. This subgroup exhibits unique biological behaviors and a relatively higher recurrence risk, making it crucial to explore tailored staging and prognostic tools for this patient population.

This large-scale retrospective analysis aimed to systematically evaluate the prognostic value and potential applications of the LODDS in patients with moderately to poorly differentiated GC. Additionally, we comprehensively compared the prognostic performance of the pN, number of positive lymph nodes (NPLN), lymph node ratio (LNR), number of total lymph nodes (NTLN), and LODDS systems, identifying a more accurate staging system for predicting survival outcomes in GC patients. Finally, we attempted to develop a prognostic nomogram for GC patients.

MATERIALS AND METHODS

Population

This retrospective cohort study analyzed data from GC patients treated at Zhejiang Cancer Hospital between April 2008 and December 2019. Patients included in the study underwent radical gastrectomy with D1/D2 lymph node dissection and had complete clinical data and follow-up records. The exclusion criteria were other malignant tumors, a lymph node-negative status, palliative care, missing preoperative or postoperative tumor marker data, or unsuccessful surgeries. Ultimately, 2103 GC patients met the inclusion criteria. Tumor staging was performed according to the 8th edition of the AJCC staging manual.

All patients signed informed consent forms. The study was conducted in accordance with the Declaration of Helsinki (as revised in 2013) and was approved by the Ethics Committee of Zhejiang Cancer Hospital, approval No. AF-4.0/34-1.

Data collection

Patient data, including sex, age, body mass index, family history, smoking history, drinking history, tumor differentiation, positive lymph nodes, total lymph nodes, pathological type, nerve invasion, vascular tumor thrombus, surgical method, N stage, pathological TNM (pTNM) stage, survival status, recurrence or metastasis, tumor markers, and overall survival (OS), were collected. OS was defined as the time period from the initiation of treatment or diagnosis to the time of death from any cause. Patients with abnormal tumor marker outpatient levels were excluded from the analysis. All patients underwent regular follow-up after surgery, approximately every 3–6 months, until death or the end of the follow-up period. The median follow-up time was 40 months (range: 1-147 months). Follow-up assessments included computed tomography scans, ultrasound, and endoscopic examinations to assess survival and recurrence status.

Prognostic system and tumor marker grouping

The calculation formula for LODDS is as follows: LODDS = log [(NPLN + 0.5)/(NTLN - NPLN + 0.5)], where an offset of 0.5 is applied to avoid mathematical infinity or division by zero. The formula for the LNR is as follows: LNR = NPLN/NTLN. The optimal cutoff points for the NPLNs, NTLNs, LNR, and LODDS were determined by calculating Youden's index (sensitivity + specificity-1). This index can be used to identify the optimal cutoff point, balance high-risk recognition with low-risk misdiagnosis, and improve survival prediction accuracy. On this basis, the following staging system

was established: NPLN: NPLN1 (1 ≤ NPLN1 < 6) and NPLN2 (6 ≤ NPLN2 ≤ 34); NTLN: NTLN1 (1 ≤ NTLN1 < 33) and NTLN2 (33 ≤ NTLN2 ≤ 73); LNR: LNR1 (0.01 ≤ LNR1 < 0.16) and LNR2 (0.16 ≤ LNR2 ≤ 1.00); LODDS: LODDS1 (-1.68 ≤ LODDS1 < -0.69) and LODDS2 (-0.69 ≤ LODDS2 ≤ 1.40). According to the clinical laboratory standards at our hospital, the cutoff values for the tumor markers carcinoembryonic antigen (CEA), alpha-fetoprotein (AFP), carbohydrate antigen (CA) 19-9, CA72-4, CA125, and CA242 were 5 ng/mL, 10 ng/mL, 37 U/mL, 6.9 U/mL, 35 U/mL, and 15 U/mL, respectively. The values above these thresholds were classified into the high group, whereas the values below the thresholds were classified into the low group.

Study design

This study first employed univariate and multivariate Cox proportional hazards regression models to analyze the hazard ratios (HR) and 95% confidence intervals (CI) of various factors, aiming to identify independent risk factors for OS in GC patients. Independent risk factors were then stratified by tumor differentiation to assess their prognostic value in patients with different tumor differentiation levels. To minimize the influence of confounding factors, a 1:1 propensity score matching (PSM) analysis was performed with a matching tolerance of 0.05. Kaplan–Meier survival analysis was conducted on the matched data to determine survival rate differences among different LODDS groups and pN groups. Additionally, receiver operating characteristic (ROC) analysis was used to compare the prognostic predictive ability of the five staging systems. Finally, independent risk factors for GC patients with different degrees of tumor differentiation were incorporated into a nomogram for prognostic assessment. Decision curve analysis and ROC curve analysis were used to compare the prognostic predictive ability of the nomogram with that of the pTNM system. Calibration curves were used to evaluate the prognostic prediction ability of the model at different postoperative time points. The concordance index (C-index) was used to assess the predictive accuracy of the regression model.

Statistical analysis

Categorical variables in all baseline characteristic data are presented as frequencies and percentages, whereas continuous variables are expressed as mean ± SD. Categorical variables were analyzed *via* the χ^2 test, and continuous variables were analyzed *via* the independent-samples *t* test. Statistical analysis and visualization were performed *via* SPSS 27.0 and R 4.4.1 software, with a two-sided significance level set at $P < 0.05$ for all tests.

RESULTS

The impact of LODDS and tumor differentiation on the prognosis of all patients

After screening, 2103 GC patients who met the inclusion criteria were included in the study (Supplementary Figure 1A). Univariate Cox regression analysis was initially performed to evaluate the impact of various factors on OS, with factors showing $P < 0.05$ included in the multivariate Cox regression analysis. LODDS, pN, LNR, NPLN, and NTLN were analyzed by a variety of covariance analyses, and the variance inflation factor was less than 10 (Supplementary Table 1). The results indicated that both LODDS (HR = 1.515, 95%CI: 1.185-1.938, $P < 0.001$) and tumor differentiation (HR = 1.268, 95%CI: 1.086-1.479, $P = 0.003$) were independent prognostic risk factors for GC patients (Table 1). ROC analysis revealed an area under the curve (AUC) of 0.694 for the LODDS, with an optimal cutoff value of -0.685, achieving a sensitivity of 72.9% and specificity of 56.0% (Supplementary Figure 1B). Kaplan–Meier survival analysis indicated that the OS rate for LODDS2 patients (with higher LODDS) was lower than that for LODDS1 patients (log-rank $P < 0.001$, Supplementary Figure 1C). Furthermore, patients with poorly differentiated tumors had lower survival rates compared to those with moderately differentiated tumors (log-rank $P < 0.001$, Supplementary Figure 1D).

Patient characteristics before and after PSM

Before PSM, the LODDS1 group included 928 patients (44.1%), while the LODDS2 group included 1175 patients (55.9%). As shown in Table 2, significant differences were observed in the distributions of characteristics such as age, surgery method, pathological type, nerve invasion, vascular tumor thrombus, pTNM stage, CEA, CA19-9, CA72-4, CA242, and tumor differentiation between the LODDS1 and LODDS2 groups (all $P < 0.05$). To minimize the impact of distributional differences in confounding factors on the prognostic analysis, 1:1 PSM was performed on the basis of the collected clinical characteristics. After matching, a total of 1472 patients were included, with 736 patients in each group. To ensure the independent prognostic predictive power of the LODDS in patients with different degrees of tumor differentiation, key variables, including tumor differentiation and lymph node-related variables, were excluded from the matching process. After matching, no significant differences in any of the included clinical characteristics were observed between the two groups (all $P \geq 0.05$), indicating a significant improvement in the balance of clinical features between the groups. Notably, owing to the small sample size of patients with well-differentiated tumors, which accounted for only 0.8% of the total cases, these patients were not included in the subsequent analysis.

Accuracy of prognostic prediction by different systems for patients

ROC analysis was used to assess the prognostic prediction accuracy of the NPLN, LNR, LODDS, and N staging systems in GC patients with different degrees of tumor differentiation (Supplementary Figure 2, Supplementary Table 2). The results revealed that within 3 years post-surgery, the LODDS system had the highest predictive accuracy for all patients (AUC = 0.701, $P < 0.001$), as well as for patients with moderately differentiated tumors (AUC = 0.672, $P < 0.001$) and those with poorly differentiated tumors (AUC = 0.607, $P < 0.001$). Between 3-5 years post-surgery, the LODDS system again

Table 1 Univariate and multivariate Cox regression analyses of overall survival prognostic factors in 2103 gastric cancer patients

Patient characteristics		Univariate analysis		Multivariate analysis	
		HR (95%CI)	*P* value	HR (95%CI)	*P* value
Sex	Female	Reference	-	-	-
	Male	1.200 (0.998-1.444)	0.052	-	-
Age	< 60	Reference	-	Reference	-
	≥ 60	1.390 (1.214-1.591)	< 0.001	1.409 (1.198-1.657)	< 0.001
BMI	Normal	Reference	-	Reference	-
	Low	1.406 (1.118-1.768)	0.004	1.018 (0.705-1.470)	0.927
	High	0.810 (0.677-0.971)	0.022	0.843 (0.556-1.279)	0.422
Family history	No	Reference	-	-	-
	Yes	1.034 (0.957-1.118)	0.398	-	-
Smoking history	No	Reference	-	-	-
	Yes	1.104 (0.952-1.279)	0.191	-	-
Drinking history	No	Reference	-	Reference	-
	Yes	1.220 (1.044-1.425)	0.012	1.144 (0.970-1.350)	0.110
Surgery methods	Open	Reference	-	Reference	-
	Laparoscopy	0.531 (0.384-0.739)	< 0.001	0.655 (0.473-0.907)	0.011
Pathological type	NMGC	Reference	-	-	-
	MGC	1.163 (0.857-1.578)	0.322	-	-
Vascular tumor thrombus	No	Reference	-	Reference	-
	Yes	1.435 (1.222-1.684)	< 0.001	1.031 (0.871-1.221)	0.722
Nerve invasion	No	Reference	-	Reference	-
	Yes	1.540 (1.312-1.808)	< 0.001	1.079 (0.912-1.277)	0.374
Differentiation	Moderate	Reference	-	Reference	-
	Poor	1.344 (1.158-1.599)	< 0.001	1.268 (1.086-1.479)	0.003
NPLN	NPLN1	Reference	-	Reference	-
	NPLN2	2.472 (2.122-2.879)	< 0.001	1.466 (1.161-1.851)	0.001
NTLN	NTLN1	Reference	-	Reference	-
	NTLN2	1.200 (1.026-1.404)	0.024	1.073 (0.909-1.267)	0.404
LNR	LNR1	Reference	-	Reference	-
	LNR2	2.573 (2.184-3.032)	< 0.001	1.485 (1.157-1.906)	0.002
LODDS	LODDS1	Reference	-	Reference	-
	LODDS2	2.569 (2.174-3.036)	< 0.001	1.515 (1.185-1.938)	< 0.001
pN	N1 + N2	Reference	-	Reference	-
	N3a + N3b	2.364 (2.0382.742)	< 0.001	1.431 (1.163-1.760)	< 0.001
pTNM	I	Reference	-	Reference	-
	II	2.747 (0.984-7.669)	0.054	2.159 (0.770-6.053)	0.143
	III	8.922 (3.339-23.842)	< 0.001	4.238 (1.558-11.527)	0.005
Recurrence or metastasis	No	Reference	-	Reference	-
	Yes	2.202 (1.800-2.694)	< 0.001	1.792 (1.458-2.201)	< 0.001
CA19-9	Low	Reference	-	Reference	-
	High	1.819 (1.558-2.123)	< 0.001	1.480 (1.213-1.804)	< 0.001

CA125	Low	Reference	-	Reference	-
	High	1.607 (1.239-2.084)	< 0.001	1.718 (1.399-2.109)	< 0.001
AFP	Low	Reference	-	Reference	-
	High	1.536 (1.177-2.004)	0.002	1.289 (1.015-1.638)	0.038
CA242	Low	Reference	-	Reference	-
	High	1.788 (1.515-2.110)	< 0.001	1.123 (0.908-1.390)	< 0.284
CA72-4	Low	Reference	-	Reference	-
	High	1.415 (1.195-1.674)	< 0.001	1.400 (1.209-1.622)	< 0.001
CEA	Low	Reference	-	Reference	-
	High	1.327 (1.179-1.482)	< 0.001	1.430 (1.238-1.653)	< 0.001

CI: Confidence interval; HR: Hazard ratio; BMI: Body mass index; MGC: Mucinous gastric adenocarcinoma; NMGC: Non-mucinous gastric adenocarcinoma; pTNM: Pathological tumor-node-metastasis; NPLN: Number of positive lymph nodes; NTLN: Number of total lymph nodes; LNR: Lymph node ratio; LODDS: Log odds of positive lymph nodes; pN: American Joint Committee on Cancer pathologic N stage; CA: Carbohydrate antigen; AFP: Alpha-fetoprotein; CEA: Carcinoembryonic antigen.

Table 2 Baseline characteristics of patients according to the log odds of positive lymph nodes score before and after propensity score matching, *n* (%)

Patient characteristics	Raw cohort			PSM cohort		
	LODDS1 (*n* = 928)	LODDS2 (*n* = 1175)	*P* value	LODDS1 (*n* = 736)	LODDS2 (*n* = 736)	*P* value
Sex	-	-	0.196	-	-	0.050
Male	732 (78.9)	899 (76.5)	-	580 (78.8)	564 (76.6)	-
Female	196 (21.1)	276 (23.5)	-	156 (21.2)	172 (23.4)	-
Age	-	-	0.041	-	-	0.764
< 60	320 (34.5)	456 (38.8)	-	263 (35.7)	284 (38.6)	-
≥ 60	608 (65.5)	719 (61.2)	-	473 (64.3)	452 (61.4)	-
BMI	-	-	0.072	-	-	0.934
Low	81 (8.7)	115 (9.8)	-	67 (9.1)	72 (9.7)	-
Normal	623 (67.1)	737 (62.7)	-	489 (66.4)	486 (66.0)	-
High	224 (24.2)	323 (27.5)	-	180 (24.5)	17824.3)	-
Family history	-	-	0.428	-	-	0.183
No	607 (65.5)	749 (63.7)	-	479 (65.1)	464 (63.0)	-
Yes	321 (34.5)	426 (36.3)	-	257 (34.9)	272 (37.0)	-
Smoking history	-	-	0.157	-	-	0.780
No	483 (52.0)	648 (55.1)	-	391 (53.1)	395 (53.7)	-
Yes	445 (48.0)	527 (44.9)	-	345 (46.9)	341 (46.3)	-
Drinking history	-	-	0.259	-	-	0.619
No	650 (70.0)	796 (67.7)	-	514 (69.8)	521 (70.8)	-
Yes	278 (30.0)	379 (32.3)	-	222 (30.2)	215 (29.2)	-
Surgery method	-	-	< 0.001	-	-	0.090
Open	786 (84.7)	1080 (91.9)	-	662 (89.9)	646 (87.8)	-
Laparoscopy	142 (15.3)	95 (8.1)	-	74 (10.1)	90 (12.2)	-
Pathological type	-	-	0.042	-	-	0.721

MGC	49 (5.3)	88 (7.5)	-	47 (6.4)	50 (6.8)	-
NMGC	879 (94.7)	1087 (92.5)	-	669 (93.6)	686 (93.2)	-
Nerve invasion	-	-	< 0.001	-	-	0.164
No	469 (50.5)	357 (30.4)		326 (44.3)	311 (42.3)	-
Yes	459 (49.5)	818 (69.6)		410 (55.7)	425 (57.7)	-
Vascular tumor thrombus	-	-	< 0.001	-	-	0.177
No	478 (51.5)	308 (26.2)	-	316 (42.9)	283 (38.5)	-
Yes	450 (48.5)	867 (73.8)	-	420 (57.1)	453 (61.5)	-
pTNM	-	-	< 0.001	-	-	0.086
I	72 (7.8)	6 (0.5)	-	25 (3.4)	6 (0.8)	-
II	241 (26.0)	72 (6.1)	-	173 (23.5)	63 (8.6)	-
III	615 (66.3)	1097 (93.4)	-	538 (73.1)	667 (90.6)	-
CEA	-	-	< 0.001	-	-	0.176
Low	731 (79.1)	840 (71,5)	-	575 (78.1)	508 (69.0)	-
High	194 (20.9)	335 (28.5)	-	161 (21.9)	228 (31.0)	-
AFP	-	-	0.296	-	-	0.110
Low	873 (94.1)	1092 (92.9)		694 (94.3)	685 (93.1)	-
High	55 (5.9)	83 (7.1)		42 (5.7)	51 (6.9)	-
CA19-9	-	-	< 0.001	-	-	0.051
Low	732 (78.9)	793 (67.5)	-	563 (76.5)	504 (68.5)	-
High	196 (21.1)	382 (32.5)	-	173 (23.5)	232 (31.5)	-
CA72-4	-	-	< 0.001	-	-	0.408
Low	760 (81.9)	881 (75.0)	-	594 (80.7)	564 (76.6)	-
High	168 (18.1)	294 (25.0)	-	142 (19.3)	172 (23.4)	-
CA125	-	-	0.053	-	-	0.956
Low	878 (94.6)	1087 (92.5)	-	695 (94.4)	685 (93.1)	-
High	50 (5.4)	88 (7.5)	-	41 (5.6)	51 (6.9)	-
CA242	-	-	< 0.001	-	-	0.120
Low	782 (84.3)	878 (74.7)	-	603 (81.9)	555 (75.4)	-
High	146 (15.7)	297 (25.3)	-	133 (18.1)	181 (24.6)	-
Differentiation	-	-	< 0.001	-	-	-
Well	9 (1.0)	6 (0.6)	-	-	-	-
Moderate	629 (67.7)	655 (55.7)	-	-	-	-
Poor	290 (31.3)	514 (43.7)	-	-	-	-
NPLN	-	-	< 0.001	-	-	-
NPLN1	892 (96.1)	272 (23.1)	< 0.001	-	-	-
NPLN2	36 (3.9)	903 (76.90)	-	-	-	-
NTLN	-	-	0.014	-	-	-
NTLN1	613 (66.1)	835 (71.1)	-	-	-	-
NTLN2	315 (33.9)	340 (28.9)	-	-	-	-
LNR						
LNR1	928 (100)	0	< 0.001	-	-	-
LNR2	0	1175 (100)	-	-	-	-

pN	-	-	< 0.001	-	-	-
N1+N2	603 (65.0)	22 (1.9)	-	-	-	-
N3a+N3b	325 (35.0)	1153 (98.1)	-	-	-	-

PSM: Propensity score matching; BMI: Body mass index; MGC: Mucinous gastric adenocarcinoma; NMGC: Non-mucinous gastric adenocarcinoma; pTNM: Pathological tumor-node-metastasis; NPLN: Number of positive lymph nodes; NTLN: Number of total lymph nodes; LNR: Lymph node ratio; LODDS: Log odds of positive lymph nodes; pN: American Joint Committee on Cancer pathologic N stage; CA: Carbohydrate antigen; AFP: Alpha-fetoprotein; CEA: Carcinoembryonic antigen.

Table 3 Comparison of the prediction performance of different staging systems

	AIC	BIC	C-index	Linear trend χ^2 score
Poor				
LODDS	16.512	25.891	0.607	45.074
pN	16.706	26.086	0.604	41.386
LNR	16.548	25.927	0.605	37.060
NPLN	16.661	26.040	0.606	38.398
Moderate				
LODDS	17.308	27.622	0.651	107.014
pN	17.350	27.664	0.623	97.529
LNR	17.317	27.631	0.646	121.010
NPLN	17.367	27.681	0.640	117.545

AIC: Akaike information criterion; BIC: Bayesian information criterion; C-index: Concordance index; LODDS: Log odds of positive lymph nodes; pN: American Joint Committee on Cancer pathologic N stage; LNR: Lymph node ratio; NPLN: Number of positive lymph nodes.

demonstrated the highest predictive accuracy for all patients (AUC = 0.654, $P < 0.001$), while the NPLN system was most accurate for patients with moderately differentiated tumors (AUC = 0.643, $P < 0.001$). After 5 years, none of the staging systems showed significant prognostic value.

Kaplan–Meier survival analysis after PSM revealed that in moderately differentiated GC patients, both the LODDS2 group and the N3a + N3b group had worse prognoses within 5 years after surgery (Figure 1A-D, all $P < 0.05$). Among poorly differentiated GC patients, those in the LODDS2 group also had a worse prognosis within 5 years (Figure 1E-G, all $P < 0.05$). However, pN stage did not significantly affect survival rates at 3 and 5 years after surgery in poorly differentiated tumor patients (Figure 1H, $P = 0.117$). Further analysis revealed that pN stage had a weak ability to stratify poorly differentiated GC patients (Supplementary Figure 3A), with no significant survival differences among the N1, N2, and N3a groups (Supplementary Table 2, all $P > 0.05$). In moderately differentiated GC patients, there was also no significant difference in survival between the N1 subgroup and the other three N stages (Supplementary Figure 3B, Supplementary Table 3, all $P > 0.05$). Additionally, multivariate Cox regression analysis incorporating the independent risk factors listed in Table 1 showed that age, CA125, CEA, and LODDS were prognostic factors for both moderately and poorly differentiated GC patients (Table 2, all $P < 0.05$).

Patients were stratified by the grade of tumor differentiation, and then LODDS, pN, LNR, and NPLN were subjected to multifactorial Cox regression analyses with other independent prognostic influences separately. The results of the analysis revealed that the LODDS, LNR, pN, and NPLN were all risk factors for the prognosis of patients with moderately and poorly differentiated GC, and among patients with poorly differentiated GC, the HR value of patients with LODDS2 was 1.859, whereas in the group of moderately differentiated patients, the HR value of patients with LODDS2 was 2.391 compared with patients with LODDS1 (Supplementary Table 4), which indicated that the LODDS has a differential prognostic impact in differently differentiated patient groups. In addition, compared with other staging systems, the LODDS system consistently demonstrated higher prognostic predictive ability, with lower Akaike information criterion (AIC) and Bayesian information criterion (BIC) values and higher C-index and linear trend χ^2 scores at different postoperative time points and in different tumor differentiation groups (Table 3). These findings suggest that the LODDS system has significant clinical potential for the prognostic management of GC patients with different levels of tumor differentiation.

LODDS correlation with clinical features and tumor markers in GC

The LODDS value was correlated with various clinicopathological features and tumor markers. Older adult patients aged over 60 years with mucinous gastric adenocarcinoma, vascular tumor thrombus, nerve invasion, or poorly differentiated

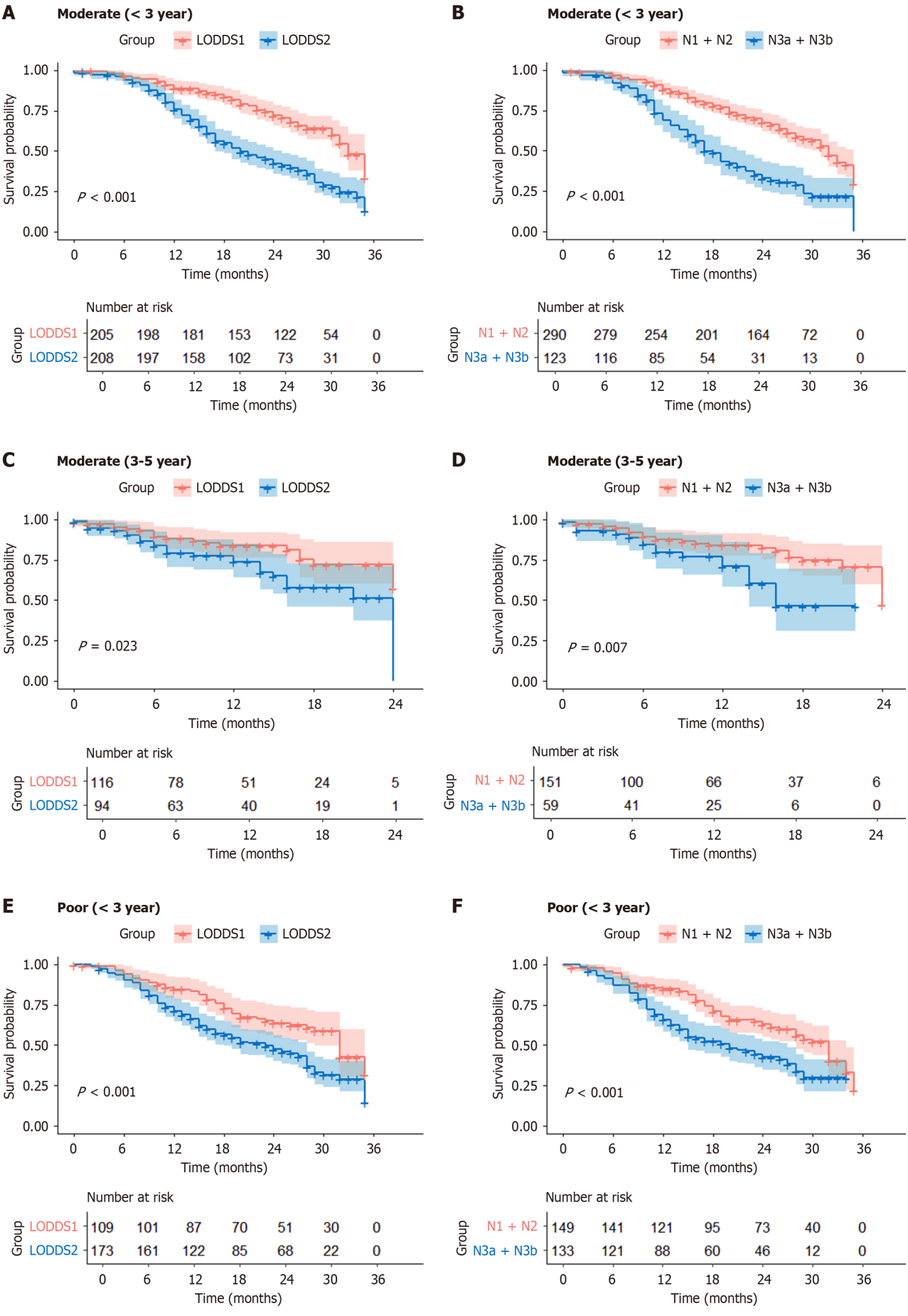
A
Moderate (< 3 year)
Group LODDS1 LODDS2
Survival probability
P < 0.001
Time (months)
Number at risk
LODDS1 205 198 181 153 122 54 0
LODDS2 208 197 158 102 73 31 0
B
Moderate (< 3 year)
Group N1 + N2 N3a + N3b
P < 0.001
N1 + N2 290 279 254 201 164 72 0
N3a + N3b 123 116 85 54 31 13 0
C
Moderate (3-5 year)
P = 0.023
LODDS1 116 78 51 24 5
LODDS2 94 63 40 19 1
D
Moderate (3-5 year)
P = 0.007
N1 + N2 151 100 66 37 6
N3a + N3b 59 41 25 6 0
E
Poor (< 3 year)
P < 0.001
LODDS1 109 101 87 70 51 30 0
LODDS2 173 161 122 85 68 22 0
F
Poor (< 3 year)
P < 0.001
N1 + N2 149 141 121 95 73 40 0
N3a + N3b 133 121 88 60 46 12 0

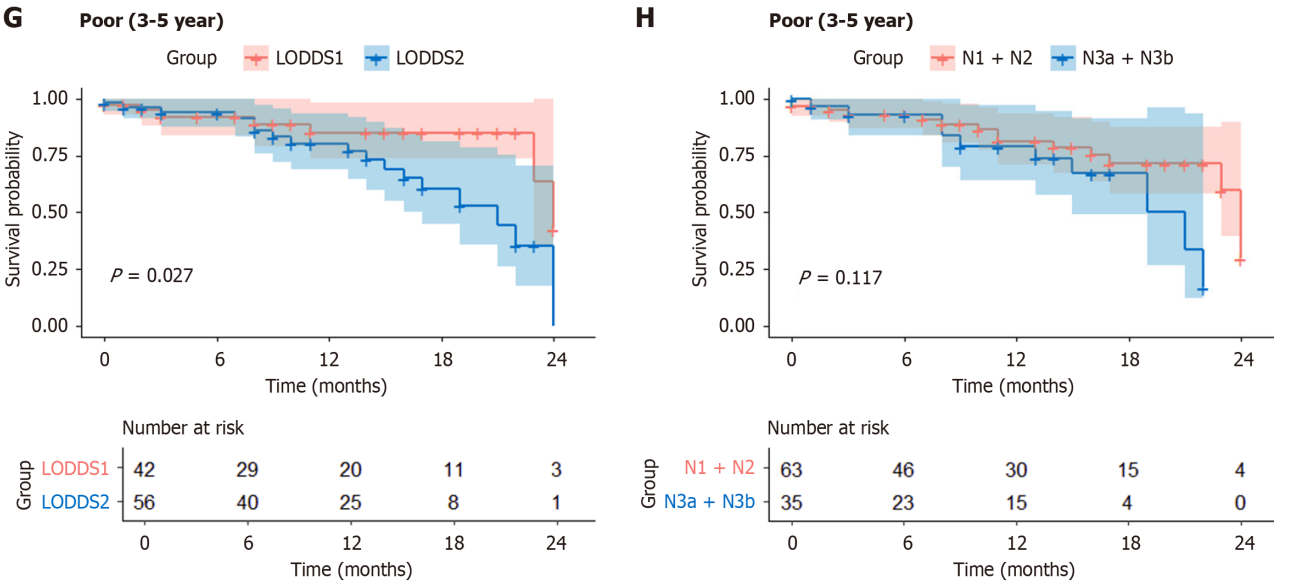

Figure 1 Kaplan–Meier survival analysis after propensity score matching. A: Moderately differentiated gastric cancer (GC) patients 3 years postoperatively log odds of positive lymph nodes (LODDS) 1 *vs* LODDS2; B: Moderately differentiated GC patients 3 years postoperatively N1 + N2 *vs* N3a + N3b; C: Moderately differentiated GC patients 3-5 years postoperatively LODDS1 *vs* LODDS2; D: Moderately differentiated GC patients 3-5 years postoperatively N1 + N2 *vs* N3a + N3b; E: Poorly differentiated GC patients 3 years postoperatively LODDS1 *vs* LODDS2; F: Poorly differentiated GC patients 3 years after surgery N1 + N2 *vs* N3a + N3b; G: Poorly differentiated GC patients 3-5 years after surgery LODDS1 *vs* LODDS2; H: Poorly differentiated GC patients 3-5 years after surgery N1 + N2 *vs* N3a + N3b. LODDS: Log odds of positive lymph nodes.

tumors exhibited significantly higher LODDS values (Figure 2A-F, all $P < 0.05$). The LODDS values did not correlate with patient body mass index (Figure 2D, $P > 0.05$). Furthermore, patients with higher LODDS values were associated with advanced pTNM stages and an increased likelihood of tumor metastasis and recurrence (Figure 2G and H, all $P < 0.05$). Scatter plot analysis revealed positive correlations between the LODDS values and the levels of the tumor markers CA19-9, CA242, CA72-4, and CA125 (Figure 3A, C, D and E, R values = 0.065, 0.095, 0.13, and 0.15, respectively; all $P < 0.01$), and no correlation was detected between the LODDS values and CEA and AFP (Figure 3B and F, all $P > 0.05$).

Construction and validation of a prognostic nomogram for OS in GC patients

In the multivariate Cox regression analysis for patients with different tumor differentiation levels, the LODDS, age, CA125, and CEA were identified as independent prognostic factors for OS in patients with GC (Supplementary Table 4, $P < 0.05$). Tumor differentiation was also included as a risk factor (Table 1, $P < 0.05$). Based on these four factors, a nomogram was constructed to predict 1-year, 3-year, and 5-year OS (Figure 4A). The nomogram demonstrated a C-index of 0.703. The calibration curves demonstrated excellent concordance between the predicted and observed values, confirming that the nomogram provides reliable prognostic predictions (Figure 4B). The AUCs for predicting 1-year, 3-year, and 5-year OS were 0.738, 0.730, and 0.722, respectively, which were higher than those of the pTNM staging system (Figure 4C and Supplementary Figure 4A and B, all $P < 0.001$), confirming that the sensitivity and specificity of this model were superior to those of the pTNM system. The ability of this model to predict patient prognosis was greater than that of individual prognostic indicators (Supplementary Figure 4C-E). The Kaplan–Meier curve successfully distinguished high-risk patients from low-risk patients, with the high-risk group showing poorer OS (Figure 4D, $P < 0.001$). Decision curve analysis revealed that the nomogram provided a greater clinical net benefit in prognostic prediction than did the AJCC 8th edition TNM staging system (Figure 4E). These findings further support the clinical utility of the LODDS in predicting OS in GC patients.

DISCUSSION

Currently, the pN staging system remains the most widely used lymph node staging method in clinical practice. This system, established by the AJCC and the Union for International Cancer Control, evaluates the number and distribution of positive lymph nodes, providing critical information about the extent of tumor spread[58,59]. However, the pN staging system has notable limitations in GC patients, particularly when factors such as insufficient lymph node collection, tumor differentiation, and changes in tumor markers affect its accuracy. These shortcomings potentially lead to reduced staging precision[60]. To address these limitations of the traditional pN system, alternative staging methods, such as the LODDS and LNR, have emerged. By incorporating the ratio of positive to negative lymph nodes, these methods offer more precise prognostic assessments[61].

Existing studies have highlighted the advantages of the LODDS and LNR for prognostic prediction. For example, Fortea-Sanchis *et al*[62] reported that in patients with colorectal cancer, even with a lower number of lymph nodes

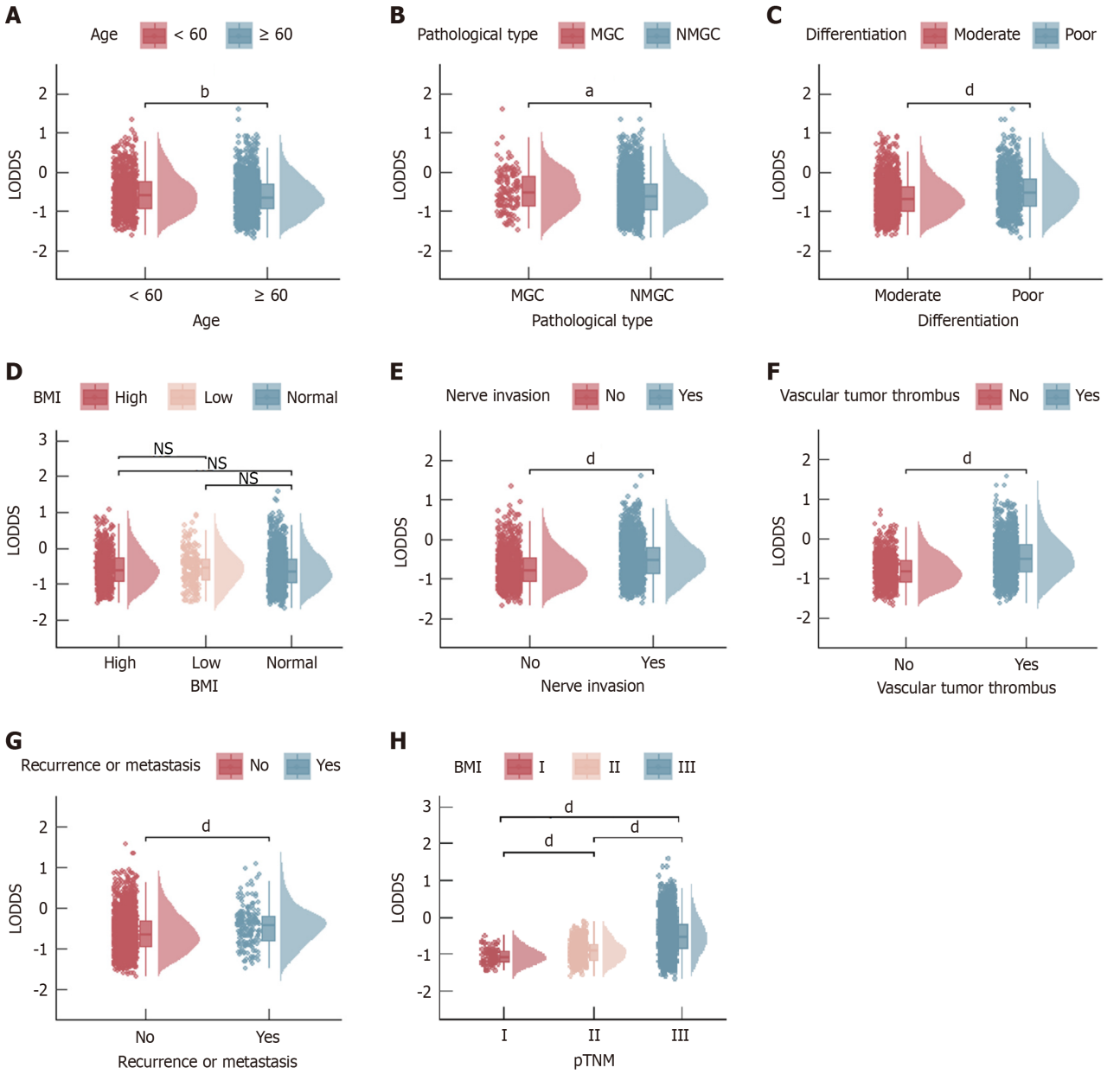

Figure 2 Box plots of the log odds of positive lymph nodes according to clinical features. A: Age; B: Pathological type; C: Differentiation; D: Body mass index; E: Nerve invasion; F: Vascular tumor thrombus; G: Recurrence or metastasis; H: Pathological tumor-node-metastasis. [a]*P* < 0.05; [b]*P* < 0.01; [c]*P* < 0.005; [d]*P* < 0.001. LODDS: Log odds of positive lymph nodes; pTNM: Pathological tumor-node-metastasis; MGC: Mucinous gastric adenocarcinoma; NMGC: Non-mucinous gastric adenocarcinoma; BMI: Body mass index; ns: Not significant.

collected, the LODDS still exhibited high predictive efficacy. Similarly, Teng *et al*[63] noted the significant value of the LNR in predicting OS in breast cancer patients. Despite the abundant evidence supporting the strong prognostic value of the LODDS and LNR, their prognostic ability across different cancers is still debated. Jin *et al*[64] reported that the LODDS more accurately predicts prognosis in muscle-invasive bladder cancer patients than do pN and the LNR, whereas Deng *et al*[65] reported that in non-small cell lung cancer patients, the LODDS and LNR each have their own advantages depending on the NPLN. Thus, our study sought to comprehensively evaluate the prognostic value of various staging systems in GC patients. Through a comprehensive ROC comparison analysis, we found that the LODDS demonstrated superior prognostic ability compared with the N, NPLN, NTLN, and LNR systems in GC patients.

Unlike studies focused on the general GC population, recent research on the LODDS has gradually expanded to include more specific cancer subtypes. For instance, Zhou *et al*[66] compared different staging systems and found that for GC patients with distant metastases, the LODDS and LNR outperformed the PLN in terms of discriminative ability, prognostic homogeneity, and accuracy in predicting 1- or 2-year cancer-specific survival. Similarly, Zhang *et al*[67] demonstrated the significant role of the LODDS in predicting the prognosis of patients with gastric signet-ring cell carcinoma, suggesting that it can serve as an independent prognostic factor. Our study focused on patients with moderately to poorly differentiated GC, a group characterized by more aggressive behaviors and higher recurrence risk. We found that traditional systems, such as pN and the LNR, struggled to stratify prognosis in this subgroup. In contrast, the LODDS provides effective risk stratification across different tumor differentiation levels and postoperative time

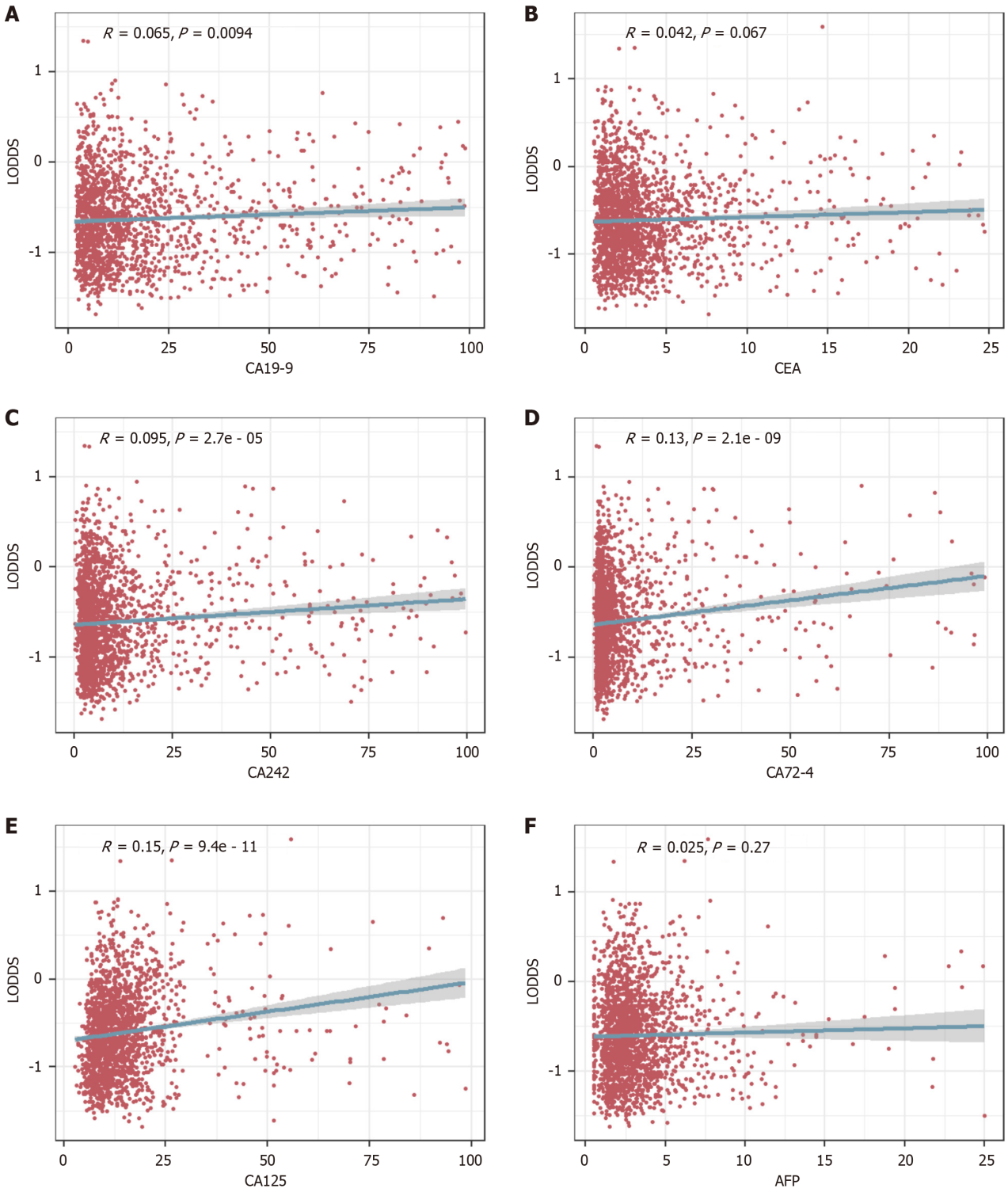

Figure 3 Scatterplot of the correlation of log odds of positive lymph nodes with tumor markers. A: Carbohydrate antigen (CA) 19-9; B: Carcinoembryonic antigen; C: CA242; D: CA72-4; E: CA125; F: Alpha-fetoprotein. LODDS: Log odds of positive lymph nodes; CA: Carbohydrate antigen; CEA: Carcinoembryonic antigen; AFP: Alpha-fetoprotein.

points, underscoring its potential to refine individualized management strategies.

Moreover, our findings revealed a strong association between the LODDS score and clinicopathological features, including nerve invasion, vascular tumor thrombus, mucinous adenocarcinoma, and low tumor differentiation, all of which are linked to an increased risk of postoperative recurrence and poor prognosis[68]. The present study revealed a significant positive correlation between CA family tumor markers (CA19-9, CA72-4, CA125, CA242) and LODDS, whereas AFP and CEA did not show similar associations. This discrepancy may reflect heterogeneity in biological properties and metastatic mechanisms among these markers. CA family markers, as glycosylation-associated antigens, may promote lymph node metastatic microenvironment formation through modulating tumor cell adhesion, metabolic reprogramming (*e.g.*, CA19-9-mediated lactate metabolism), and stromal remodeling (*e.g.*, CA125-activated TGF-β

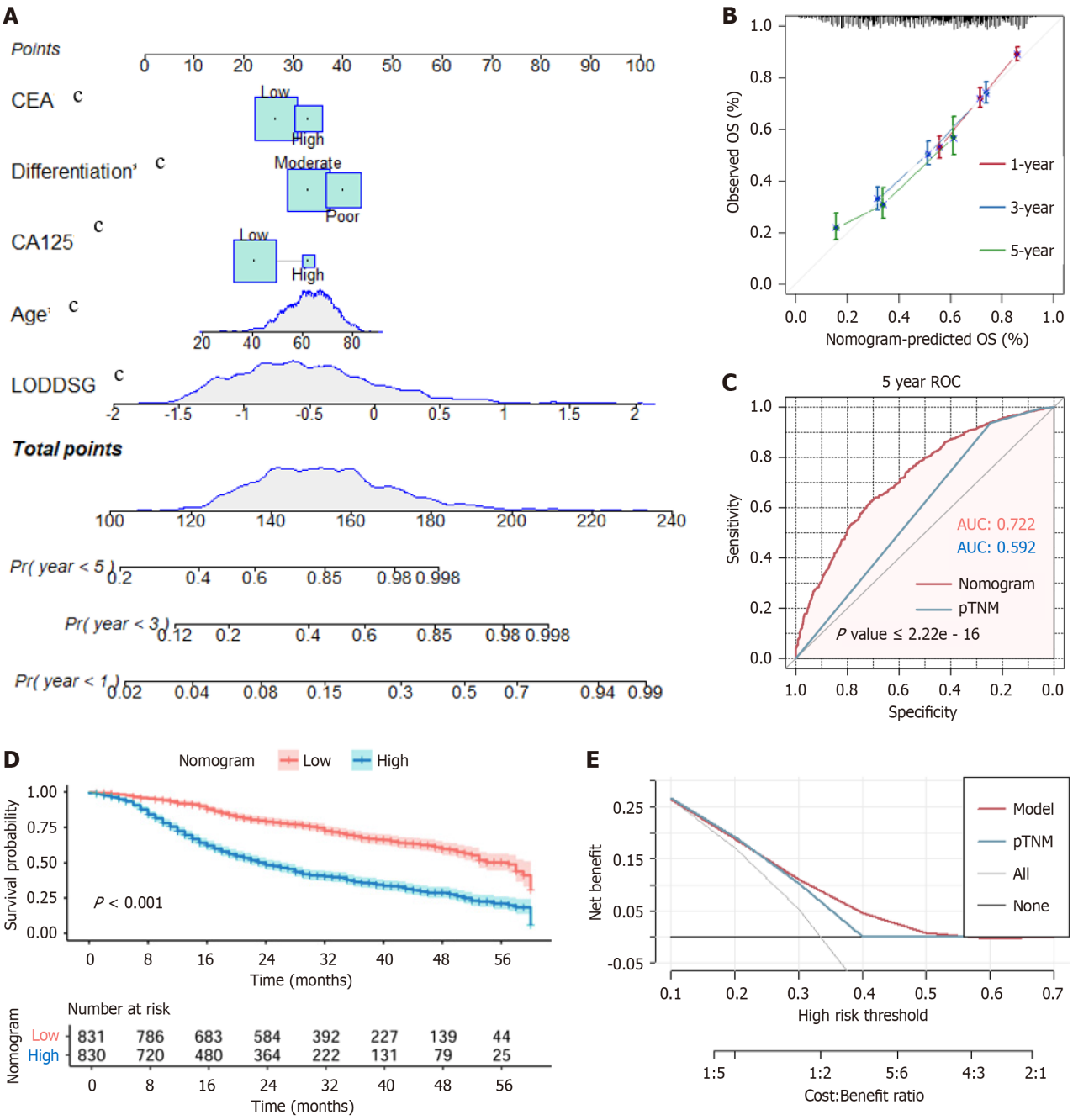

Figure 4 Construction of a nomogram model to predict the prognosis of gastric cancer patients based on log odds of positive lymph nodes, tumor differentiation, and other independent risk factors. A: Nomogram; B: Calibration curve of the nomogram; C: Receiver operating characteristic curves for the nomogram and pathological tumor-node-metastasis staging systems; D: Kaplan–Meier curve of overall survival for the high-risk and low-risk groups based on the nomogram; E: Decision curve analysis comparing the nomogram with the pathological tumor-node-metastasis staging system. ($P < 0.005$). LODDS: Log odds of positive lymph nodes; CA: Carbohydrate antigen; CEA: Carcinoembryonic antigen; pTNM: Pathological tumor-node-metastasis; OS: Overall survival; ROC: Receiver operating characteristic; AUC: Area under the curve.

pathway), thereby evolving synergistically with elevated LODDS. In contrast, the tissue specificity of AFP (*e.g.*, its association with intrahepatic dissemination in hepatocellular carcinoma) and temporal discordance in CEA secretion dynamics (*e.g.*, early-stage elevation misaligned with lymph node metastatic progression) may limit their correlation with LODDS[69,70]. Future studies should incorporate multi-timepoint monitoring and molecular subtyping (*e.g.*, microsatellite instability status or Kirsten rat sarcoma viral oncogene homolog mutations) to evaluate the incremental prognostic value of CA family markers in lymph node metastasis prediction models. Clinically, CA family markers could complement TNM staging to optimize lymph node metastasis risk stratification and immunotherapy response prediction.

To increase the clinical applicability of the LODDS, we developed an individualized prognostic nomogram model specifically designed for GC patients with moderate to poorly differentiated tumors. When five key prognostic risk factors—LODDS, age, CA125, CEA, and tumor differentiation—were incorporated, this nomogram demonstrated superior performance in terms of prediction accuracy, calibration, and clinical applicability compared with the AJCC 8th edition TNM staging system. The model provides precise guidance for clinical follow-up frequency and the formulation

of individualized treatment plans. For example, high-risk patients identified by the model may require more frequent follow-up and intensified adjuvant therapy, whereas low-risk patients can avoid unnecessary overtreatment through personalized strategies. Research by Guo *et al*[71] and He *et al*[72] has also shown that incorporating LODDS into nomograms significantly improves prognostic evaluation accuracy and the practicality of individualized management in patients with colorectal and lung cancers, further confirming the broad potential of LODDS in personalized cancer treatment.

However, this study has some limitations. First, as a retrospective analysis, further prospective studies are needed to validate our findings. Second, there is currently no standardized staging method for systems such as the LODDS and LNR. In this study, we used Youden's index to determine the optimal cutoff value, balancing sensitivity and specificity to predict postoperative survival. Finally, this study included only moderately and poorly differentiated GC patients with positive lymph nodes. Future research should include highly differentiated and lymph node-negative patients to further assess the generalizability of the LODDS. The moderate AUC value (approximately 0.7) of our nomogram model suggests that further improvement in predictive accuracy is possible.

Recent advances in computational methods, particularly deep learning and ensemble modeling, have shown promise in enhancing prognostic performance through several avenues, including the following: (1) More sophisticated feature engineering that integrates additional clinical biomarkers and genomic data; (2) Multimodal data fusion combining imaging, molecular, and pathological inputs; and (3) Personalized model architectures tailored to specific patient subgroups. Integrating these advanced methods with our current model should facilitate the development of more powerful prognostic tools in the future. However, it is also important to acknowledge the trade-offs between model complexity and clinical interpretability. In medical practice, especially in oncology, the adoption of predictive models requires not only accuracy but also transparency and ease of application, which must be carefully balanced in future research.

In conclusion, our study establishes LODDS as an independent and superior prognostic factor for moderately to poorly differentiated GC and that its prognostic value surpasses that of the pN, LNR, NPLN, and NTLN staging systems. Integrating LODDS with tumor differentiation into the GC staging system provides clinicians with a more accurate tool for survival risk stratification for patients undergoing surgical treatment and lymph node dissection, thereby providing stronger support for personalized treatment and prognostic assessment.

CONCLUSION

LODDS has been shown to be a reliable independent prognostic risk factor for patients with GC, providing a more precise risk stratification in patients with moderately and poorly differentiated GC compared to pN, LNR, NPLN, and NTLN. The study showed that LODDS values were significantly associated with several clinical characteristics, including age, pathologic type, degree of differentiation, nerve invasion, vascular tumor thrombosis, recurrence or metastasis, and pTNM staging. In addition, the LODDS was significantly and positively correlated with tumor markers of the CA family. Prognostic models constructed based on the LODDS with other key clinical indicators (*e.g.*, age, tumor differentiation, CEA, CA125) had predictive power beyond the traditional pTNM staging system, showing higher accuracy and potential for clinical application. This finding emphasizes the significant value of LODDS in the prognostic assessment of GC.

ACKNOWLEDGEMENTS

We thank all the laboratory members for insightful discussions.

FOOTNOTES

Author contributions: Deng MC and Chen K wrote the original draft; Deng MC, Chen K, Huang YX, Zhang CK, Zhong YK, Bao QM, Zu D, Liang C, Wu WX, Ten YS, and Liu HD carried out normal analyses, data collation; Deng MC, Chen K, He HY, Hu YC, Liu GX, He YH, Zhou JN, and Jing J made a survey of the manuscript, examining the methodology; Deng MC, Chen K, Shi Y, Chung CYS, Yu CH, Du YA, Ye Z, and Cheng XD conceived and wrote, reviewed, and edited the manuscript; Ye Z and Cheng XD contributed equally to this article, they are the co-corresponding authors of this manuscript; and all authors thoroughly reviewed and endorsed the final manuscript.

Supported by the National Natural Science Foundation of China, No. 82473195 and No. 32370797; the Natural Science Foundation of Zhejiang Province, No. LTGY23H160018; the Zhejiang Medical and Health Science and Technology Program, No. 2024KY789 and No. 2023KY615; the National Research Center for Translational Medicine at Shanghai Program, No. NRCTM(SH)-2025-07; the Beijing Science and Technology Innovation Medical Development Foundation, No. KC2023-JX-0270-07; and the Key Laboratory of Prevention, Diagnosis and Therapy of Upper Gastrointestinal Cancer of Zhejiang Province, No. 2022E10021.

Institutional review board statement: This study was approved by the Medical Ethics Committee of Zhejiang Cancer Hospital, approval No. AF-4.0/34-1.

Informed consent statement: All patients signed informed consent forms. The study was conducted in accordance with the Declaration of

Helsinki (as revised in 2013).

Conflict-of-interest statement: All the authors report no relevant conflicts of interest for this article.

Data sharing statement: The data that support the findings of this study are available from the corresponding author upon reasonable request.

Country of origin: China

ORCID number: Yi-An Du 0000-0002-8250-1209; Zu Ye 0000-0003-0846-7548; Xiang-Dong Cheng 0000-0003-1470-2831.

S-Editor: Bai Y
L-Editor: Filipodia
P-Editor: Zhao YQ

REFERENCES

1 **Kandoth C**, McLellan MD, Vandin F, Ye K, Niu B, Lu C, Xie M, Zhang Q, McMichael JF, Wyczalkowski MA, Leiserson MDM, Miller CA, Welch JS, Walter MJ, Wendl MC, Ley TJ, Wilson RK, Raphael BJ, Ding L. Mutational landscape and significance across 12 major cancer types. *Nature* 2013; **502**: 333-339 [PMID: 24132290 DOI: 10.1038/nature12634] [FullText]

2 **Chen X**, Agustinus AS, Li J, DiBona M, Bakhoum SF. Chromosomal instability as a driver of cancer progression. *Nat Rev Genet* 2025; **26**: 31-46 [PMID: 39075192 DOI: 10.1038/s41576-024-00761-7] [FullText]

3 **Kanda M**, Sugimoto H, Kodera Y. Genetic and epigenetic aspects of initiation and progression of hepatocellular carcinoma. *World J Gastroenterol* 2015; **21**: 10584-10597 [PMID: 26457018 DOI: 10.3748/wjg.v21.i37.10584] [FullText]

4 **Ye Z**, Ng CP, Liu H, Bao Q, Xu S, Zu D, He Y, Huang Y, Al-Aidaroos AQO, Guo K, Li J, Yaw LP, Xiong Q, Thura M, Zheng W, Guan F, Cheng X, Shi Y, Zeng Q. PRL1 and PRL3 promote macropinocytosis *via* its lipid phosphatase activity. *Theranostics* 2024; **14**: 3423-3438 [PMID: 38948056 DOI: 10.7150/thno.93127] [FullText]

5 **Bacolla A**, Sengupta S, Ye Z, Yang C, Mitra J, De-Paula RB, Hegde ML, Ahmed Z, Mort M, Cooper DN, Mitra S, Tainer JA. Heritable pattern of oxidized DNA base repair coincides with pre-targeting of repair complexes to open chromatin. *Nucleic Acids Res* 2021; **49**: 221-243 [PMID: 33300026 DOI: 10.1093/nar/gkaa1120] [FullText]

6 **Ye Z**, Xu S, Shi Y, Bacolla A, Syed A, Moiani D, Tsai CL, Shen Q, Peng G, Leonard PG, Jones DE, Wang B, Tainer JA, Ahmed Z. GRB2 enforces homology-directed repair initiation by MRE11. *Sci Adv* 2021; **7** [PMID: 34348893 DOI: 10.1126/sciadv.abe9254] [FullText]

7 **Xie Y**, Liu F, Wu Y, Zhu Y, Jiang Y, Wu Q, Dong Z, Liu K. Inflammation in cancer: therapeutic opportunities from new insights. *Mol Cancer* 2025; **24**: 51 [PMID: 39994787 DOI: 10.1186/s12943-025-02243-8] [FullText]

8 **Greten FR**, Grivennikov SI. Inflammation and Cancer: Triggers, Mechanisms, and Consequences. *Immunity* 2019; **51**: 27-41 [PMID: 31315034 DOI: 10.1016/j.immuni.2019.06.025] [FullText]

9 **Nigam M**, Mishra AP, Deb VK, Dimri DB, Tiwari V, Bungau SG, Bungau AF, Radu AF. Evaluation of the association of chronic inflammation and cancer: Insights and implications. *Biomed Pharmacother* 2023; **164**: 115015 [PMID: 37321055 DOI: 10.1016/j.biopha.2023.115015] [FullText]

10 **Li X**, Huang Y, Zu D, Liu H, He H, Bao Q, He Y, Liang C, Luo G, Teng Y, Shi Y, Ye Z, Cheng X. PMMA nanoplastics induce gastric epithelial cellular senescence and cGAS-STING-mediated inflammation *via* ROS overproduction and NHEJ suppression. *Ecotoxicol Environ Saf* 2024; **287**: 117284 [PMID: 39515200 DOI: 10.1016/j.ecoenv.2024.117284] [FullText]

11 **Huang Y**, Li X, Xu S, Zu D, Liu H, He H, Bao Q, He Y, Liang C, Shi Y, Cheng X, Teng Y, Ye Z. Polyvinyl chloride nanoplastics suppress homology-directed repair and promote oxidative stress to induce esophageal epithelial cellular senescence and cGAS-STING-mediated inflammation. *Free Radic Biol Med* 2025; **226**: 288-301 [PMID: 39515594 DOI: 10.1016/j.freeradbiomed.2024.11.012] [FullText]

12 **Ye Z**, Xu S, Shi Y, Cheng X, Zhang Y, Roy S, Namjoshi S, Longo MA, Link TM, Schlacher K, Peng G, Yu D, Wang B, Tainer JA, Ahmed Z. GRB2 stabilizes RAD51 at reversed replication forks suppressing genomic instability and innate immunity against cancer. *Nat Commun* 2024; **15**: 2132 [PMID: 38459011 DOI: 10.1038/s41467-024-46283-y] [FullText]

13 **Smyth EC**, Nilsson M, Grabsch HI, van Grieken NC, Lordick F. Gastric cancer. *Lancet* 2020; **396**: 635-648 [PMID: 32861308 DOI: 10.1016/S0140-6736(20)31288-5] [FullText]

14 **Qiu LY**, Kang HY, Yang JL, Zheng YD, Chen AY, Chen CL, Wang XL, Fang QF, Zhu WG, Sha O, Wang YJ. Accurate prediction of stomach adenocarcinomas of poorest and best prognosis with a combination of gene expression and clinical signatures Genome Instab Dis 2022; 3: 227-237 [DOI: 10.1007/s42764-022-00077-y] [FullText]

15 **Thrift AP**, Wenker TN, El-Serag HB. Global burden of gastric cancer: epidemiological trends, risk factors, screening and prevention. *Nat Rev Clin Oncol* 2023; **20**: 338-349 [PMID: 36959359 DOI: 10.1038/s41571-023-00747-0] [FullText]

16 **López MJ**, Carbajal J, Alfaro AL, Saravia LG, Zanabria D, Araujo JM, Quispe L, Zevallos A, Buleje JL, Cho CE, Sarmiento M, Pinto JA, Fajardo W. Characteristics of gastric cancer around the world. *Crit Rev Oncol Hematol* 2023; **181**: 103841 [PMID: 36240980 DOI: 10.1016/j.critrevonc.2022.103841] [FullText]

17 **Huang YX**, He HY, Chen K, Liu HD, Zu D, Liang C, Bao QM, Hu YC, Liu GX, Zhong YK, Zhang CK, Deng MC, He YH, Jing J, Shi Y, Xu SF, Teng YS, Ye Z, Cheng XD. Prognostic impact and reasons for variability by tumor location in gastric cancer. *World J Gastroenterol* 2024;

30: 4709-4724 [PMID: 39610778 DOI: 10.3748/wjg.v30.i44.4709] [FullText]
18 **Deng JY**, Liang H. Clinical significance of lymph node metastasis in gastric cancer. *World J Gastroenterol* 2014; **20**: 3967-3975 [PMID: 24744586 DOI: 10.3748/wjg.v20.i14.3967] [FullText]
19 **Kinami S**, Saito H, Takamura H. Significance of Lymph Node Metastasis in the Treatment of Gastric Cancer and Current Challenges in Determining the Extent of Metastasis. *Front Oncol* 2021; **11**: 806162 [PMID: 35071010 DOI: 10.3389/fonc.2021.806162] [FullText]
20 **Ji H**, Hu C, Yang X, Liu Y, Ji G, Ge S, Wang X, Wang M. Lymph node metastasis in cancer progression: molecular mechanisms, clinical significance and therapeutic interventions. *Signal Transduct Target Ther* 2023; **8**: 367 [PMID: 37752146 DOI: 10.1038/s41392-023-01576-4] [FullText]
21 **Engel J**, Emeny RT, Hölzel D. Positive lymph nodes do not metastasize. *Cancer Metastasis Rev* 2012; **31**: 235-246 [PMID: 22198520 DOI: 10.1007/s10555-011-9343-7] [FullText]
22 **Degiuli M**, De Manzoni G, Di Leo A, D'Ugo D, Galasso E, Marrelli D, Petrioli R, Polom K, Roviello F, Santullo F, Morino M. Gastric cancer: Current status of lymph node dissection. *World J Gastroenterol* 2016; **22**: 2875-2893 [PMID: 26973384 DOI: 10.3748/wjg.v22.i10.2875] [FullText]
23 **Leong SP**, Witte MH. Cancer metastasis through the lymphatic versus blood vessels. *Clin Exp Metastasis* 2024; **41**: 387-402 [PMID: 38940900 DOI: 10.1007/s10585-024-10288-0] [FullText]
24 **Zhou H**, Lei PJ, Padera TP. Progression of Metastasis through Lymphatic System. *Cells* 2021; **10** [PMID: 33808959 DOI: 10.3390/cells10030627] [FullText]
25 **Tian Y**, Pang Y, Yang PG, Guo HH, Liu Y, Zhang Z, Ding PA, Zheng T, Li Y, Fan LQ, Zhang ZD, Wang D, Zhao XF, Tan BB, Liu Y, Zhao Q. Clinical implications of micro lymph node metastasis for patients with gastric cancer. *BMC Cancer* 2023; **23**: 536 [PMID: 37308852 DOI: 10.1186/s12885-023-11023-w] [FullText]
26 **Ri M**, Yamashita H, Gonoi W, Okumura Y, Yagi K, Aikou S, Seto Y. Identifying multiple swollen lymph nodes on preoperative computed tomography is associated with poor prognosis along with pathological extensive nodal metastasis in locally advanced gastric cancer. *Eur J Surg Oncol* 2022; **48**: 377-382 [PMID: 34400037 DOI: 10.1016/j.ejso.2021.08.017] [FullText]
27 **de Jongh C**, Triemstra L, van der Veen A, Brosens LAA, Luyer MDP, Stoot JHMB, Ruurda JP, van Hillegersberg R; LOGICA Study Group. Pattern of lymph node metastases in gastric cancer: a side-study of the multicenter LOGICA-trial. *Gastric Cancer* 2022; **25**: 1060-1072 [PMID: 36103060 DOI: 10.1007/s10120-022-01329-2] [FullText]
28 **Dieterich LC**, Tacconi C, Ducoli L, Detmar M. Lymphatic vessels in cancer. *Physiol Rev* 2022; **102**: 1837-1879 [PMID: 35771983 DOI: 10.1152/physrev.00039.2021] [FullText]
29 **Ba MC**, Ba Z, Long H, Cui SZ, Gong YF, Yan ZF, Lin KP, Wu YB, Tu YN. LncRNA AC093818.1 accelerates gastric cancer metastasis by epigenetically promoting PDK1 expression. *Cell Death Dis* 2020; **11**: 64 [PMID: 31988283 DOI: 10.1038/s41419-020-2245-2] [FullText]
30 **Wang M**, Yu W, Cao X, Gu H, Huang J, Wu C, Wang L, Sha X, Shen B, Wang T, Yao Y, Zhu W, Huang F. Exosomal CD44 Transmits Lymph Node Metastatic Capacity Between Gastric Cancer Cells *via* YAP-CPT1A-Mediated FAO Reprogramming. *Front Oncol* 2022; **12**: 860175 [PMID: 35359362 DOI: 10.3389/fonc.2022.860175] [FullText]
31 **Peyroteo M**, Martins PC, Canotilho R, Correia AM, Baía C, Sousa A, Brito D, Videira JF, Santos LL, de Sousa A. Impact of the 8th edition of the AJCC TNM classification on gastric cancer prognosis-study of a western cohort. *Ecancermedicalscience* 2020; **14**: 1124 [PMID: 33209115 DOI: 10.3332/ecancer.2020.1124] [FullText]
32 **Mranda GM**, Xue Y, Zhou XG, Yu W, Wei T, Xiang ZP, Liu JJ, Ding YL. Revisiting the 8th AJCC system for gastric cancer: A review on validations, nomograms, lymph nodes impact, and proposed modifications. *Ann Med Surg (Lond)* 2022; **75**: 103411 [PMID: 35386808 DOI: 10.1016/j.amsu.2022.103411] [FullText]
33 **Wang J**, Wu Z, Freund JE, de Groot EM, Shan F, Ruurda JP, Li Z, van Hillegersberg R. Comparison between AJCC 8th edition gastric and esophageal ypTNM classification system in Siewert II esophagogastric junction adenocarcinomas: A retrospective study based on Eastern and Western Data. *Eur J Surg Oncol* 2024; **50**: 108730 [PMID: 39357412 DOI: 10.1016/j.ejso.2024.108730] [FullText]
34 **Liu JY**, Peng CW, Yang XJ, Huang CQ, Li Y. The prognosis role of AJCC/UICC 8(th) edition staging system in gastric cancer, a retrospective analysis. *Am J Transl Res* 2018; **10**: 292-303 [PMID: 29423014] [FullText]
35 **Jeon CH**, Park KB, Lee H, Kim DJ, Seo HS, Lee J, Jun KH, Kim JJ, Lee HH. Refining gastric cancer staging: examining the interplay between number and anatomical location of metastatic lymph nodes - a retrospective multi-institutional study. *BMC Cancer* 2023; **23**: 1192 [PMID: 38053052 DOI: 10.1186/s12885-023-11653-0] [FullText]
36 **Yang ZJ**, Yu Y, Chi JR, Guan M, Zhao Y, Cao XC. The combined pN stage and breast cancer subtypes in breast cancer: a better discriminator of outcome can be used to refine the 8th AJCC staging manual. *Breast Cancer* 2018; **25**: 315-324 [PMID: 29353447 DOI: 10.1007/s12282-018-0833-0] [FullText]
37 **Wang Y**, Xu H, Hu C, Yu P, Bao Z, Zhang Y, Zhang R, Zhang S, Li B, Aerts JM, Xu Z, Cheng X. Prognostic value and clinicopathological correlation of the tumor regression grade in neoadjuvant chemotherapy for gastric adenocarcinoma: a retrospective cohort study. *J Gastrointest Oncol* 2022; **13**: 1046-1057 [PMID: 35837180 DOI: 10.21037/jgo-22-537] [FullText]
38 **Guo YX**, Zhang ZZ, Zhao G, Zhao EH. Prognostic and pathological impact of tumor budding in gastric cancer: A systematic review and meta-analysis. *World J Gastrointest Oncol* 2019; **11**: 898-908 [PMID: 31662828 DOI: 10.4251/wjgo.v11.i10.898] [FullText]
39 **Ning FL**, Zhang NN, Wang J, Jin YF, Quan HG, Pei JP, Zhao Y, Zeng XT, Abe M, Zhang CD. Prognostic value of modified Lauren classification in gastric cancer. *World J Gastrointest Oncol* 2021; **13**: 1184-1195 [PMID: 34616522 DOI: 10.4251/wjgo.v13.i9.1184] [FullText]
40 **Jögi A**, Vaapil M, Johansson M, Påhlman S. Cancer cell differentiation heterogeneity and aggressive behavior in solid tumors. *Ups J Med Sci* 2012; **117**: 217-224 [PMID: 22376239 DOI: 10.3109/03009734.2012.659294] [FullText]
41 **Tirosh I**, Suva ML. Cancer cell states: Lessons from ten years of single-cell RNA-sequencing of human tumors. *Cancer Cell* 2024; **42**: 1497-1506 [PMID: 39214095 DOI: 10.1016/j.ccell.2024.08.005] [FullText]
42 **Rakha E**, Toss M, Quinn C. Specific cell differentiation in breast cancer: a basis for histological classification. *J Clin Pathol* 2022; **75**: 76-84 [PMID: 34321225 DOI: 10.1136/jclinpath-2021-207487] [FullText]
43 **Kochetkova M**, Samuel MS. Differentiation of the tumor microenvironment: are CAFs the Organizer? *Trends Cell Biol* 2022; **32**: 285-294 [PMID: 34895986 DOI: 10.1016/j.tcb.2021.11.008] [FullText]
44 **Huang SF**, Chen TC, Hsu JT, Tsai CY, Liu KH, Yeh CN, Yeh TS. Lymph node micrometastasis of poorly differentiated node-negative gastric cancer risks a worse-than-expected survival outcome under standard management algorithm. *Eur J Surg Oncol* 2022; **48**: 783-788 [PMID:

34838393 DOI: 10.1016/j.ejso.2021.11.117] [FullText]
45 **Feng F**, Liu J, Wang F, Zheng G, Wang Q, Liu S, Xu G, Guo M, Lian X, Zhang H. Prognostic value of differentiation status in gastric cancer. *BMC Cancer* 2018; **18**: 865 [PMID: 30176846 DOI: 10.1186/s12885-018-4780-0] [FullText]
46 **Balakrishnan K**. Mitochondrial dysregulation is a key regulator of gastric cancer subtype carcinogenesis. *Genome Instab Dis* 2024; **5**: 210-224 [DOI: 10.1007/s42764-024-00136-6] [FullText]
47 **Liu XY**, Irfan M, Xu XZ, Tay CY, Marshall BJ. Helicobacter pylori infection induced genome instability and gastric cancer. *Genome Instab Dis* 2020; **1**: 129-142 [DOI: 10.1007/s42764-020-00010-1] [FullText]
48 **Hwang SH**, Kim HI, Song JS, Lee MH, Kwon SJ, Kim MG. The Ratio-Based N Staging System Can More Accurately Reflect the Prognosis of T4 Gastric Cancer Patients with D2 Lymphadenectomy Compared with the 7th American Joint Committee on Cancer/Union for International Cancer Control Staging System. *J Gastric Cancer* 2016; **16**: 207-214 [PMID: 28053806 DOI: 10.5230/jgc.2016.16.4.207] [FullText]
49 **Fortea-Sanchis C**, Forcadell-Comes E, Martínez-Ramos D, Escrig-Sos J. Modelling the probability of erroneous negative lymph node staging in patients with colon cancer. *Cancer Commun (Lond)* 2019; **39**: 31 [PMID: 31171042 DOI: 10.1186/s40880-019-0377-5] [FullText]
50 **Margalit O**, Shacham-Shmueli E, Yang YX, Lawerence YR, Levy I, Reiss KA, Golan T, Halpern N, Aderka D, Giantonio B, Mamtani R, Boursi B. Prognostic Implications of Tumor Differentiation in Clinical T1N0 Gastric Adenocarcinoma. *Oncologist* 2021; **26**: e111-e114 [PMID: 32969129 DOI: 10.1002/onco.13542] [FullText]
51 **Zhu J**, Xue Z, Zhang S, Guo X, Zhai L, Shang S, Zhang Y, Lu H. Integrated analysis of the prognostic role of the lymph node ratio in node-positive gastric cancer: A meta-analysis. *Int J Surg* 2018; **57**: 76-83 [PMID: 30103072 DOI: 10.1016/j.ijsu.2018.08.002] [FullText]
52 **Chen ZD**, Zhang PF, Xi HQ, Wei B, Chen L, Tang Y. Recent Advances in the Diagnosis, Staging, Treatment, and Prognosis of Advanced Gastric Cancer: A Literature Review. *Front Med (Lausanne)* 2021; **8**: 744839 [PMID: 34765619 DOI: 10.3389/fmed.2021.744839] [FullText]
53 **Park KB**, Jun KH, Song KY, Chin H, Lee HH. Development of a staging system and survival prediction model for advanced gastric cancer patients without adjuvant treatment after curative gastrectomy: A retrospective multicenter cohort study. *Int J Surg* 2022; **101**: 106629 [PMID: 35460886 DOI: 10.1016/j.ijsu.2022.106629] [FullText]
54 **Li Y**, Wu G, Zhang Y, Han B, Yang W, Wang X, Duan L, Niu L, Chen J, Zhou W, Liu J, Fan D, Hong L. Log odds of positive lymph nodes as a novel prognostic predictor for colorectal cancer: a systematic review and meta-analysis. *BMC Cancer* 2022; **22**: 290 [PMID: 35303818 DOI: 10.1186/s12885-022-09390-x] [FullText]
55 **Li Y**, Wu G, Liu J, Zhang Y, Yang W, Wang X, Duan L, Niu L, Chen J, Zhou W, Han W, Wang J, Zhong H, Ji G, Fan D, Hong L. Log odds of positive lymph nodes as a novel prognostic predictor for gastric cancer: a systematic review and meta-analysis. *BMC Cancer* 2023; **23**: 523 [PMID: 37291493 DOI: 10.1186/s12885-023-10805-6] [FullText]
56 **Wen J**, Chen J, Chen D, Jabbour SK, Xue T, Guo X, Ma H, Ye F, Mao Y, Shu J, Liu Y, Lu X, Zhang Z, Chen Y, Fan M. Comprehensive analysis of prognostic value of lymph node classifications in esophageal squamous cell carcinoma: a large real-world multicenter study. *Ther Adv Med Oncol* 2021; **13**: 17588359211054895 [PMID: 34777583 DOI: 10.1177/17588359211054895] [FullText]
57 **Arrichiello G**, Pirozzi M, Facchini BA, Facchini S, Paragliola F, Nacca V, Nicastro A, Canciello MA, Orlando A, Caterino M, Ciardiello D, Della Corte CM, Fasano M, Napolitano S, Troiani T, Ciardiello F, Martini G, Martinelli E. Beyond N staging in colorectal cancer: Current approaches and future perspectives. *Front Oncol* 2022; **12**: 937114 [PMID: 35928863 DOI: 10.3389/fonc.2022.937114] [FullText]
58 **Subramaniam N**, Balasubramanian D, Kumar N, Murthy S, Vijayan SN, Nambiar A, Vidhyadharan S, Thankappan K, Iyer S. Lymph node staging systems in oral squamous cell carcinoma: A comparative analysis. *Oral Oncol* 2019; **97**: 92-98 [PMID: 31465931 DOI: 10.1016/j.oraloncology.2019.08.002] [FullText]
59 **Zhou Y**, Zhang J, Cao S, Li Y. The evaluation of metastatic lymph node ratio staging system in gastric cancer. *Gastric Cancer* 2013; **16**: 309-317 [PMID: 22945599 DOI: 10.1007/s10120-012-0190-1] [FullText]
60 **Wang W**, Yang YJ, Zhang RH, Deng JY, Sun Z, Seeruttun SR, Wang ZN, Xu HM, Liang H, Zhou ZW. Standardizing the classification of gastric cancer patients with limited and adequate number of retrieved lymph nodes: an externally validated approach using real-world data. *Mil Med Res* 2022; **9**: 15 [PMID: 35387671 DOI: 10.1186/s40779-022-00375-2] [FullText]
61 **Liu H**, Deng J, Zhang R, Hao X, Jiao X, Liang H. The RML of lymph node metastasis was superior to the LODDS for evaluating the prognosis of gastric cancer. *Int J Surg* 2013; **11**: 419-424 [PMID: 23541652 DOI: 10.1016/j.ijsu.2013.03.009] [FullText]
62 **Fortea-Sanchis C**, Martínez-Ramos D, Escrig-Sos J. The lymph node status as a prognostic factor in colon cancer: comparative population study of classifications using the logarithm of the ratio between metastatic and nonmetastatic nodes (LODDS) versus the pN-TNM classification and ganglion ratio systems. *BMC Cancer* 2018; **18**: 1208 [PMID: 30514228 DOI: 10.1186/s12885-018-5048-4] [FullText]
63 **Teng J**, Abdygametova A, Du J, Ma B, Zhou R, Shyr Y, Ye F. Bayesian Inference of Lymph Node Ratio Estimation and Survival Prognosis for Breast Cancer Patients. *IEEE J Biomed Health Inform* 2020; **24**: 354-364 [PMID: 31562112 DOI: 10.1109/JBHI.2019.2943401] [FullText]
64 **Jin S**, Wang B, Zhu Y, Dai W, Xu P, Yang C, Shen Y, Ye D. Log Odds Could Better Predict Survival in Muscle-Invasive Bladder Cancer Patients Compared with pN and Lymph Node Ratio. *J Cancer* 2019; **10**: 249-256 [PMID: 30662545 DOI: 10.7150/jca.27399] [FullText]
65 **Deng W**, Xu T, Wang Y, Xu Y, Yang P, Gomez D, Liao Z. Log odds of positive lymph nodes may predict survival benefit in patients with node-positive non-small cell lung cancer. *Lung Cancer* 2018; **122**: 60-66 [PMID: 30032846 DOI: 10.1016/j.lungcan.2018.05.016] [FullText]
66 **Zhou R**, Zhang J, Sun H, Liao Y, Liao W. Comparison of three lymph node classifications for survival prediction in distant metastatic gastric cancer. *Int J Surg* 2016; **35**: 165-171 [PMID: 27713088 DOI: 10.1016/j.ijsu.2016.09.096] [FullText]
67 **Zhang L**, Ma Y, Liu B. Prognostic Performance of Three Lymph-Node Staging Systems on Gastric Signet-Ring-Cell Carcinoma. *Cancers (Basel)* 2023; **15** [PMID: 37370780 DOI: 10.3390/cancers15123170] [FullText]
68 **Pi H**, Liang S, Liu H, Lu S, Huang L. Anti-PD-1 therapy for advanced colorectal cancer based on intestinal microecology. *J Biochem Mol Toxicol* 2023; **37**: e23438 [PMID: 37421170 DOI: 10.1002/jbt.23438] [FullText]
69 **Fujimura T**, Kinami S, Ninomiya I, Kitagawa H, Fushida S, Nishimura G, Kayahara M, Shimizu K, Ohta T, Miwa K. Diagnostic laparoscopy, serum CA125, and peritoneal metastasis in gastric cancer. *Endoscopy* 2002; **34**: 569-574 [PMID: 12170412 DOI: 10.1055/s-2002-33228] [FullText]
70 **Emoto S**, Ishigami H, Yamashita H, Yamaguchi H, Kaisaki S, Kitayama J. Clinical significance of CA125 and CA72-4 in gastric cancer with peritoneal dissemination. *Gastric Cancer* 2012; **15**: 154-161 [PMID: 21892754 DOI: 10.1007/s10120-011-0091-8] [FullText]
71 **Guo Z**, Li W, Wu K, Fu Y, Yan R, Zhou X. A nomogram based on the log odds of positive lymph nodes for predicting the prognosis of T1 stage rectal cancer. *Am J Cancer Res* 2023; **13**: 1498-1508 [PMID: 37168349] [FullText]
72 **He C**, Ni M, Liu J, Teng X, Ke L, Matsuura Y, Okuda K, Sakairi Y, Cheng J, Yu L, Lv W, Hu J. A survival nomogram model for patients with

resectable non-small cell lung cancer and lymph node metastasis (N1 or N2) based on the Surveillance, Epidemiology, and End Results Database and single-center data. *Transl Lung Cancer Res* 2024; **13**: 573-586 [PMID: 38601448 DOI: 10.21037/tlcr-24-119] [FullText]

World Journal of Gastroenterology

Submit a Manuscript: https://www.f6publishing.com

World J Gastroenterol 2025 June 7; 31(21): 107601

DOI: 10.3748/wjg.v31.i21.107601

ISSN 1007-9327 (print) ISSN 2219-2840 (online)

ORIGINAL ARTICLE

Retrospective Study

Classification of pediatric video capsule endoscopy images for small bowel abnormalities using deep learning models

Yi-Hsuan Huang, Qian Lin, Xin-Yan Jin, Chih-Yi Chou, Jia-Jie Wei, Jiao Xing, Hong-Mei Guo, Zhi-Feng Liu, Yan Lu

Specialty type: Gastroenterology and hepatology

Provenance and peer review: Unsolicited article; Externally peer reviewed.

Peer-review model: Single blind

Peer-review report's classification

Scientific Quality: Grade A, Grade B

Novelty: Grade A, Grade B

Creativity or Innovation: Grade A, Grade B

Scientific Significance: Grade A, Grade B

P-Reviewer: Qiao YF; Tian YJ

Received: March 30, 2025

Revised: April 14, 2025

Accepted: May 19, 2025

Published online: June 7, 2025

Processing time: 68 Days and 22.2 Hours

Yi-Hsuan Huang, Qian Lin, Jia-Jie Wei, Jiao Xing, Hong-Mei Guo, Zhi-Feng Liu, Yan Lu, Department of Gastroenterology, Children's Hospital of Nanjing Medical University, Nanjing 210008, Jiangsu Province, China

Xin-Yan Jin, School of Electronic Science and Engineering, Nanjing University, Nanjing 210023, Jiangsu Province, China

Chih-Yi Chou, College of Medicine, National Taiwan University, Taipei 100, Taiwan

Co-first authors: Yi-Hsuan Huang and Qian Lin.

Co-corresponding authors: Zhi-Feng Liu and Yan Lu.

Corresponding author: Yan Lu, PhD, Associate Research Scientist, Department of Gastroenterology, Children's Hospital of Nanjing Medical University, No. 8 Jiangdong South Road, Jianye District, Nanjing 210008, Jiangsu Province, China. luyan_cpu@163.com

Abstract

BACKGROUND

Video capsule endoscopy (VCE) is a noninvasive technique used to examine small bowel abnormalities in both adults and children. However, manual review of VCE images is time-consuming and labor-intensive, making it crucial to develop deep learning methods to assist in image analysis.

AIM

To employ deep learning models for the automatic classification of small bowel lesions using pediatric VCE images.

METHODS

We retrospectively analyzed VCE images from 162 pediatric patients who underwent VCE between January 2021 and December 2023 at the Children's Hospital of Nanjing Medical University. A total of 2298 high-resolution images were extracted, including normal mucosa and lesions (erosions/erythema, ulcers, and polyps). The images were split into training and test datasets in a 4:1 ratio. Four deep learning models: DenseNet121, Visual geometry group-16, ResNet50, and vision transformer were trained using 5-fold cross-validation, with hyperparameters adjusted for optimal classification performance. The models were

evaluated based on accuracy, precision, recall, F1-score, and area under the receiver operating curve (AU-ROC). Lesion visualization was performed using gradient-weighted class activation mapping.

RESULTS

Abdominal pain was the most common indication for VCE, accounting for 62% of cases, followed by diarrhea, vomiting, and gastrointestinal bleeding. Abnormal lesions were detected in 93 children, with 38 diagnosed with inflammatory bowel disease. Among the deep learning models, DenseNet121 and ResNet50 demonstrated excellent classification performance, achieving accuracies of 90.6% [95% confidence interval (CI): 89.2-92.0] and 90.5% (95%CI: 89.9-91.2), respectively. The AU-ROC values for these models were 93.7% (95%CI: 92.9-94.5) for DenseNet121 and 93.4% (95%CI: 93.1-93.8) for ResNet50.

CONCLUSION

Our deep learning-based diagnostic tool developed in this study effectively classified lesions in pediatric VCE images, contributing to more accurate diagnoses and increased diagnostic efficiency.

Key Words: Deep learning; Video capsule endoscopy; Children; Erosion; Ulcer; Polyp; Convolutional neural network; Vision transformer

Core Tip: This study addresses the challenges clinicians face in manually reviewing video capsule endoscopy (VCE) images, a process that is both time-consuming and labor-intensive. To alleviate this burden, we utilize deep learning models, including DenseNet121, Visual geometry group-16, ResNet50, and vision transformer, to automatically classify small bowel lesions in pediatric VCE images. Our models effectively distinguished between normal tissue, erosions/erythema, ulcers, and polyps with high accuracy. This approach significantly enhances the efficiency and accuracy of diagnosing lesions in pediatric VCE, offering a promising tool for clinical applications.

Citation: Huang YH, Lin Q, Jin XY, Chou CY, Wei JJ, Xing J, Guo HM, Liu ZF, Lu Y. Classification of pediatric video capsule endoscopy images for small bowel abnormalities using deep learning models. *World J Gastroenterol* 2025; 31(21): 107601
URL: https://www.wjgnet.com/1007-9327/full/v31/i21/107601.htm
DOI: https://dx.doi.org/10.3748/wjg.v31.i21.107601

INTRODUCTION

Video capsule endoscopy (VCE) is a noninvasive method that provides detailed visualization of the intestinal mucosa. Since its introduction in 2000, VCE has become a crucial diagnostic technology due to its ability to thoroughly inspect the entire intestine without causing pain, requiring anesthesia, using air insufflation, or emitting radiation, unlike other imaging procedures[1,2]. This innovation marked a significant milestone in the field of endoscopy[3]. The Food and Drug Administration approved the use of VCE as a diagnostic option for adults in 2001, for pediatric patients ten years and above in 2003, and for children over the age of two in 2009[4]. Recently, some studies have reported that VCE could be done safely for children younger than one year or lighter than eight kg[5,6]. After the patient swallows the capsule, it travels smoothly through the gastrointestinal (GI) tract from the mouth to the anus without causing any discomfort, while transmitting videos at the same time[7,8]. Both adult and pediatric patients undergo VCE for similar indications, such as obscure GI bleeding, tumors, iron deficiency anemia, inflammatory bowel disease (IBD) investigation, inherited polyp syndromes, or disease extent assessment[9,10]. However, due to the small bowel's length and location, VCE captures images for over six to eight hours, producing over 50000 images *per* examination[11]. Clinicians must review these images in order, frame by frame, to identify any abnormalities[12]. Even experienced gastroenterologists may require two hours to precisely examine all the images and detect lesions[13].

Therefore, there is a need to develop deep learning methods for automated lesion detection to improve the diagnostic accuracy and efficiency of VCE reviewing work[14-17]. To date, applications of artificial intelligence (AI) for VCE have been well-studied. Deep learning technology has been shown to demonstrate at least 90% accuracy in detecting GI bleeding, angioectasias, esophagus lesions, and small bowel mucosal ulcers[18-23]. In VCE image analysis, various AI-based models for automating GI disease diagnosis have recently been reported. Fan *et al*[24] collected small bowel images from 104 patients and used the AlexNet model to detect ulcers and erosions with an accuracy of 95.16%. Tsuboi *et al*[25] developed a convolutional neural network (CNN)-based model for detecting angioectasia. Trained on 2337 images, the model demonstrated high diagnostic performance with a sensitivity of 98.8% and a specificity of 98.4%. Hwang *et al*[26] trained a Visual geometry group (VGG) Net model to classify hemorrhagic and ulcerative lesions, achieving an overall accuracy of 96.83%. Saito *et al*[27] used 30584 images from 292 patients to train a CNN model for identifying protruding lesions, such as polyps, nodules, epithelial tumors, submucosal tumors, and venous structures, with an accuracy of 98.6%. Ding *et al*[28] collected data from 1970 patients, comprising 158235 images, to develop a CNN-based model for classifying

ten types of lesions, including inflammation, ulcers, polyps, lymphangiectasia, bleeding, vascular disease, protruding lesions, lymphatic follicular hyperplasia, diverticulum, and parasites. The model achieved a sensitivity of 99.90% and a specificity of 100% for the AI-assisted group.

Nevertheless, to date, all studies have focused on building VCE machine-learning models in adults. Compared to adults, children have smaller and more delicate GI tracts, which can affect the capsule's navigation and the interpretation of images. A machine-learning model trained on adult VCE images on pediatric VCE images may not be able to accurately identify lesions. Thus, it is necessary to develop ML models trained on pediatric VCE data to ensure that the algorithms are more accurate and relevant for this population. Therefore, the present study aims to apply deep learning techniques to pediatric VCE images to detect and classify small bowel mucosal lesions, including normal mucosa, erosions/erythema, ulcers, and polyps.

MATERIALS AND METHODS

Study design

This single-center, retrospective study was conducted at the Children's Hospital of Nanjing Medical University (Nanjing, Jiangsu Province, China). Participants with suspected small bowel disorders who have already undergone other imaging exams, like endoscopy and panendoscopy. The study included patients who underwent VCE, managed by the Department of Gastroenterology, between January 2021 and December 2023. The study was approved by the Hospital's Institutional Review Board (No. 202409001-1). Written informed consent was obtained from all patients or their legal guardians before the VCE examinations.

Participants

Participants aged 2 to 18 were eligible for the study if they were recommended for VCE to investigate suspected Crohn's disease (CD), obscure GI bleeding, polyps, tumors, or other conditions. VCE was also recommended following negative gastroscopy and ileocolonoscopy results according to the guidelines of the American and European endoscopic societies and the European Society of Pediatric Gastroenterology, Hepatology, and Nutrition[4,8,29]. Children with contraindications, including suspected obstruction, bowel stricture, bowel fistula, allergy to materials, *etc*., were excluded from the study.

Capsule endoscopy procedure

Two days before the VCE, the children were placed on a liquid diet. The day before the examination, they were given polyethylene glycol electrolyte solution orally. On the examination day, they were required to fast, abstaining from solid foods for 12 hours and liquids for 4 hours prior to the procedure. All VCE procedures were performed using MiroCam® small bowel capsules (IntroMedic, Seoul, South Korea) and reviewed using the MiroView™ Reader software version 2.5 (IntroMedic, Seoul, South Korea).

One hour after swallowing the capsule, the operator, in this case, the gastroenterologist, will verify if the capsule has reached the duodenum by checking the images transmitted in real time. Patients were allowed to drink water after 2 hours and consume a small amount of solid food after 4 hours. If a child has difficulty swallowing the capsule or if the capsule has not reached the duodenum within two hours, the capsule will be transferred to the duodenum manually *via* gastroscopy under anesthesia. The patient can resume their normal diet once the capsule was excreted, typically within 24 to 72 hours, or at the end of the examination. The MiroCam® VCE device captures continuous video data composed of 320 × 320-pixel video frames, which were compressed and stored in JPG format. Representative frames were extracted from the video stream using the MiroView® clinical review platform. Gastroenterology fellows labeled the extracted images. An abdominal X-ray is recommended two weeks after VCE if the video did not show the capsule passing into the colon or if the patient did not observe the natural passage of the capsule.

Dataset and preprocessing

The dataset comprises 2298 images from 162 pediatric patients who underwent VCE. Among these patients, 93 had positive findings indicative of GI abnormalities, and 69 showed no abnormal findings and were considered as the control group. These control patients were diagnosed with conditions unrelated to mucosal pathology, such as disorders of gut-brain interaction, and their VCE images were confirmed to show normal mucosa by expert endoscopists.

All images were categorized into the following four classes: Normal mucosa, erosions/erythema, ulcers, and polyps. These images are divided at random into a training set or a testing set with a 4:1 ratio, respectively. Specifically, 1840 images were allocated for training and 458 images for testing. There is no overlap between the two datasets. Of the 1840 images used for training, 916 images were of normal mucosa, 272 images were of erosions/erythema, 151 images were of ulcers, and 501 images were of polyps. Of the 458 images used for testing, 228 images were of normal mucosa, 68 images were of erosions/erythema, 37 images were of ulcers, and 125 images were of polyps. The data distribution is shown in Table 1.

Development of the deep learning models

For this study, four deep learning models [DenseNet121, VGG16, ResNet50, and vision transformer (ViT)] were developed to classify the VCE images captured by the MiroCam® small bowel capsule, into four categories: Normal mucosa, erosions/erythema, ulcers, and polyps (Figure 1). All four models are pre-trained models, using transfer

Table 1 The data distribution for the classification of normal mucosa, erosions/erythema, ulcers, and polyps

	Training set	Testing set	Total
Normal mucosa	916	228	1144
Erosions/erythema	272	68	340
Ulcers	151	37	188
Polyps	501	125	626
Total images	1840	458	2298

learning to optimize their performance. VGG16 is characterized by its thirteen convolutional layers, three fully connected layers, and the use of 3 × 3 filters with max pooling[30]. ResNet50, a deep CNN architecture, consists of 50 layers and integrates residual connections across its 50 layers, enabling effective training of very deep networks[31]. DenseNet121, another CNN architecture, employs dense connectivity between layers, facilitating feature reuse and parameter efficiency across its 121 layers[32]. ViT has emerged as a transformative approach in image classification by applying the transformer architecture, traditionally used in natural language processing, to large-scale datasets, surpassing CNN[33]. The original ViT framework incorporates patch embedding, position embedding, transformer encoder blocks, a class token, and a classification head[34]. This model usually has a primary dataset of approximately 14 million images but as medical datasets are generally a lot smaller (approximately 500 images)[35], the application of this model in this experiment was adapted using two modules proposed by Lee *et al*[36], shifted patch tokenization (SPT) and locality self-attention (LSA)-as described in their compact transformers framework. SPT improves the model's ability to capture local contextual information by applying small spatial shifts to the input image before patch tokenization, thus preserving fine-grained features typically lost in conventional ViT. LSA introduces a learnable locality bias into the attention mechanism, encouraging attention to nearby patches rather than distant ones, which is especially beneficial when training from scratch on limited data. These adaptations allowed for more effective feature extraction and improved model performance on our pediatric capsule endoscopy dataset. We used both modules to enhance the model's ability to capture local features, thereby enabling effective training of ViT from scratch on smaller datasets. All experiments in this study are conducted using Intel Xeon Gold CPU 5317 @ 3.0 GHz. The analyses were performed on a system with a 3.0 GHz Intel® Xeon® Gold 5317 processor and a double NVIDIA Geforce RTX 4090®.

Table 2 shows the adjusted hyperparameters used for each deep learning model. All models were trained using a 5-fold cross-validation strategy to ensure robust performance estimates and reduce overfitting risk. For the ViT model, we used 300 training epochs, a batch size of 16, a learning rate of 0.006, and the stochastic gradient descent optimizer, along with a dropout rate of 0.3 and transfer learning from pretrained weights. The VGG16, ResNet50, and DenseNet121 models were trained using 100 epochs, a batch size of 32, and a learning rate of 0.001 with the same optimizer and regularization settings (weight decay: 4×10^{-4}, momentum: 0.8). To further address potential overfitting and class imbalance, we applied extensive data augmentation techniques, including horizontal/vertical flipping, color jitter, rotation, and trivial augment wide, with additional augmentation applied to underrepresented classes. Gradient-weighted class activation mapping (Grad-CAM), a widely used explainability method in AI, was employed to visualize abnormal lesion regions in VCE images[37].

Statistical analysis

Clinical data analysis was conducted using SPSS 27.0 software. Due to non-normal distribution confirmed by the Kolmogorov-Smirnov test, non-normally distributed data are presented as medians and interquartile ranges. Model performance analysis utilized Sci-Kit Learn v1.4.0. We performed pairwise comparisons using analysis of variance with Tukey's Honest significant difference post-hoc tests. The models were evaluated on key performance metrics, including accuracy, precision, recall, F1-score, and area under the receiver operating curve (AU-ROC), and the resulting P values were used to determine whether the observed differences between models were statistically significant at $P < 0.05$.

RESULTS

Patient demographic and clinical characteristics

The demographic and baseline clinical characteristics of the patients are shown in Table 3.

This study included 162 patients, with 56 females (35%) and 106 males (65%), between the ages of 9 and 13 years old (median age of 11 years). The most common chief complaint among the patients was abdominal pain, affecting 101 individuals (62%), followed by diarrhea in 31 patients (19%), hematochezia in 18 patients (11%), vomiting in 13 patients (8.0%), and perianal abscess in 10 patients (6.2%). Other symptoms included fever in 8 patients (4.9%), mucocutaneous hyperpigmentation of the mouth and lips in 5 patients (3.1%), oral ulceration in 4 patients (2.5%), and anemia in 2 patients (1.2%). The majority of the patients (137, 85%) swallowed the capsule by themselves, and 25 (15%) patients' capsules were placed in the duodenum manually *via* gastroscopy. The transit time in the stomach was 22 (5, 55) minutes, and in the small bowel was 282 (217, 377) minutes. Of the 162 patients, 93 patients (57%) have positive findings in their VCE images. Among these, 33 patients (20%) had a single lesion, and 60 patients (37%) had multiple lesions. As for the

Table 2 The hyperparameter values of the deep learning models

Type of hyper-parameter	DenseNet121	VGG16	ResNet50	ViT
Number of epochs	100	100	100	300
Batch size	32	32	32	16
Learning rate	1×10^{-3}	1×10^{-3}	1×10^{-3}	6×10^{-3}
Weight decay	4×10^{-4}	4×10^{-4}	4×10^{-4}	4×10^{-4}
momentum	0.8	0.8	0.8	0.8
Optimizer	SGD	SGD	SGD	SGD

VGG: Visual geometry group; ViT: Vision transformer; SGD: Stochastic gradient descent.

enrolled patients' final diagnosis, 36 (22%) had CD, 2 (1.2%) had ulcerative colitis (UC), 30 (19%) were suspected of having IBD, 2 (1.2%) had Behcet disease, 31 (19%) had disorder of gut-brain interaction, 12 (7.4%) had polyps, 35 (22%) had gastroenteritis, and 14 (8.6%) had other conditions.

Deep-learning analysis and model performance

Table 4 presents the overall accuracy and various lesion detection accuracies, with 95% confidence intervals (CI), for the four deep learning models: Densenet121, VGG16, ResNet50, and ViT. The overall accuracy for the DenseNet121, VGG16, ResNet50, and ViT models was 90.6% (95%CI: 89.2-92.0), 88.3% (87.9-88.8), 90.5% (89.9-91.1), and 88.1% (86.7-89.6), respectively. The accuracy in detecting normal mucosa for DenseNet121, VGG16, ResNet50, and ViT were 98.6% (96.0-100), 92.2% (89.7-94.6), 98.1% (96.8-99.4), and 93.2% (88.5-97.9), respectively. The accuracy in detecting ulcers for Densenet121, VGG16, ResNet50, and ViT were 83.3% (75.6-91.1), 91.6% (89.9-93.3), 87.0% (82.3-91.7), and 87.4% (77.6-97.3), respectively. The accuracy in detecting erosions and erythema for Densenet121, VGG16, ResNet50, and ViT were 81.9% (74.2-89.6), 72.1% (63.6-80.6), 77.3% (72.4-82.2), and 73.0% (61.3-84.8), respectively. The accuracy in detecting polyps for Densenet121, VGG16, ResNet50, and ViT were 100% (100-100), 75.0% (66.8-83.2), 100% (100-100), and 87.9% (76.3-99.5), respectively.

A 5-fold cross-validation was performed in the training stage. The performance of the four deep learning models was analyzed using accuracy, precision, recall, F1-score, and AU-ROC with 95%CIs. The DenseNet121 model achieved an accuracy of 90.6% (89.2-92.0), a precision of 91.8% (89.6-94.0), a recall of 91.0% (89.8-92.1), an F1-score of 91.2% (89.4-92.9), and an AU-ROC of 93.7% (92.9-94.5). The ResNet50 model reported an accuracy of 90.5% (89.9-91.2), a precision of 92.5% (91.6-93.3), a recall of 90.7% (90.0-91.3), an F1-score of 91.3% (90.7-91.9), and an AU-ROC of 93.4% (93.1-93.8). The VGG16 model showed an accuracy of 88.3% (87.9-88.8), a precision of 83.0% (80.7-85.3), a recall of 82.8% (81.0-84.6), an F1-score of 82.6% (81.9-83.3), and an AU-ROC of 89.2% (88.1-90.3). The ViT model yielded an accuracy of 88.1% (86.7-89.6), a precision of 84.4% (78.5-90.3), a recall of 85.4% (81.0-89.7), an F1-score of 84.6% (80.0-89.2), and an AU-ROC of 90.4% (88.1-92.7). Table 5 provides the mean performance metrics for each model along with their 95%CIs. Figure 2 shows the Grad-CAMs of the four models with corresponding VCE images.

Furthermore, Table 6 presents the results of pairwise comparisons between models for each metric. These results show that DenseNet121 significantly outperformed VGG16 and ViT across all five evaluation metrics ($P < 0.05$). Meanwhile, ResNet50 also showed statistically significant superiority over VGG16 and ViT ($P < 0.05$). However, no statistically significant difference was observed between DenseNet121 and ResNet50 ($P > 0.05$ across metrics), suggesting their performances are comparable.

Table 7 shows the accuracy, precision, recall, F1-score, and AU-ROC of the deep learning models when used on the testing dataset. The ResNet50 model achieved the highest accuracy at 89.7%, along with a precision of 87.8%, recall of 81.0%, F1-score of 83.8%, and AU-ROC of 88.5%, indicating its strong overall performance. The DenseNet121 model followed closely, with an accuracy of 88.6%, a precision of 87.5%, a recall of 79%, an F1-score of 82.5%, and an AU-ROC of 87.1%. The ViT model also performed well, with an accuracy of 86.6%, a precision of 81.3%, a recall of 80.0%, an F1-score of 80.5%, and an AU-ROC of 87.5%. Finally, the VGG16 model had the lowest metrics, achieving an accuracy of 85.5%, a precision of 87.0%, a recall of 73.3%, an F1-score of 77.3%, and an AU-ROC of 83.6%.

DISCUSSION

AI is becoming more and more prevalent in all industries, including medicine, thanks to its robust capabilities in feature extraction and classification in medical imaging, particularly for VCE[38]. Compared to conventional methods, VCE offers advantages such as radiation-free imaging, non-invasiveness, patient comfort, and high tolerance, making it an indispensable tool in a pediatrician's arsenal. When coupled with AI, VCE can accelerate the process of analyzing the images/videos, leading to faster diagnosis of diseases while standardizing diagnostic criteria. Thus far, deep-learning studies using VCE images have shown results in detecting lesions and abnormalities in the small bowel[26]. While various methods have been explored for identifying bleeding, polyps, ulcers, and other conditions in adults[39,40], the

Table 3 Baseline demographic and clinical characteristics of enrolled patients (*n* = 162), *n* (%)

Patient characteristics	Value
Gender	
Female	56 (35)
Male	106 (65)
Age (year), median (IQR)	11.00 (9.00, 13.00)
Chief complaint	
Abdominal pain	101 (62)
Diarrhea	31 (19)
Anemia	2 (1.2)
Hematochezia	18 (11)
Vomiting	13 (8.0)
Fever	8 (4.9)
Oral ulceration	4 (2.5)
Mucocutaneous hyperpigmentation of the mouth and lips	5 (3.1)
Perianal abscess	10 (6.2)
Swallowed VCE by the patients	137 (85)
Placed VCE by endoscopy	25 (15)
Stomach transit time (minute), median (IQR)	22 (5, 55)
Small bowel transit time (minute), median (IQR)	282 (217, 377)
Number of lesions *per* patient	
None	69 (43)
Single	33 (20)
Multiple	60 (37)
Diagnosis	
Crohn disease	36 (22)
Ulcerative colitis	2 (1.2)
Suspected inflammatory bowel disease	30 (19)
Behcet disease	2 (1.2)
Disorder of gut-brain interaction	31 (19)
Polyps	12 (7.4)
Gastroenteritis	35 (22)
Others	14 (8.6)

IQR: Interquartile range; VCE: Video capsule endoscopy.

full potential of AI in pediatric VCE is yet to be realized. To the best of our knowledge, no previous research has attempted to apply deep learning in classifying normal mucosa, erosions/erythema, ulcers, and polyps using VCE images in children. This study investigates pediatric VCE characteristics among patients admitted to our hospital between 2021 and 2023. Our models demonstrated consistently high accuracy in detecting various types of lesions, resulting in faster but still accurate diagnoses, better patient outcomes, and improved overall care for children.

This study utilizes four deep-learning methods for VCE image classification. The models included classic CNN architectures such as DenseNet121, VGG16, and ResNet50, as well as the recently popular ViT model. We used these models to classify VCE images into four categories: Normal, erosions/erythema, ulcers, and polyps. In our study, models of DenseNet121, VGG16, ResNet50, and ViT demonstrated strong performance overall. Our trained DenseNet121 and ResNet50 models achieved an accuracy of 90%, while VGG16 and ViT models achieved an accuracy of 88%. Recent studies have explored the use of transformers for analyzing and interpreting VCE images in adults[41,42], but their application in pediatric settings remains unexplored. Although our model showed an excellent performance in the overall

Table 4 Accuracy of different deep learning models in detecting lesions of normal mucosa, ulcers, erosions/erythema, and polyps

Model	Overall accuracy (%) (95%CI)	Normal mucosa (%) (95%CI)	Ulcers (%) (95%CI)	Erosions/erythema (%) (95%CI)	Polyps (%) (95%CI)
DenseNet121	90.6 (89.2-92.0)	98.6 (96.0-100)	83.3 (75.6-91.1)	81.9 (74.2-89.6)	100 (100-100)
VGG16	88.3 (87.9-88.8)	92.2 (89.7-94.6)	91.6 (89.9-93.3)	72.1 (63.6-80.6)	75.0 (66.8-83.2)
ResNet50	90.5 (89.9-91.1)	98.1 (96.8-99.4)	87.0 (82.3-91.7)	77.3 (72.4-82.2)	100 (100-100)
ViT	88.1 (86.7-89.6)	93.2 (88.5-97.9)	87.4 (77.6-97.3)	73.0 (61.3-84.8)	87.9 (76.3-99.5)

VGG: Visual geometry group; ViT: Vision transformer; CI: Confidence interval.

Table 5 The overall performances of the deep learning models in the training set

Model	Accuracy (%) (95%CI)	Precision (%) (95%CI)	Recall (%) (95%CI)	F1-score (%) (95%CI)	AU-ROC (%) (95%CI)
DenseNet121	90.6 (89.2-92.0)	91.8 (89.6-94.0)	91.0 (89.8-92.1)	91.2 (89.4-92.9)	93.7 (92.9-94.5)
VGG16	88.3 (87.9-88.8)	83.0 (80.7-85.3)	82.8 (81.0-84.6)	82.6 (81.9-83.3)	89.2 (88.1-90.3)
ResNet50	90.5 (89.9-91.2)	92.5 (91.6-93.3)	90.7 (90.0-91.3)	91.3 (90.7-91.9)	93.4 (93.1-93.8)
ViT	88.1 (86.7-89.6)	84.4 (78.5-90.3)	85.4 (81.0-89.7)	84.6 (80.0-89.2)	90.4 (88.1-92.7)

VGG: Visual geometry group; ViT: Vision transformer; AU-ROC: Area under the receiver operating curve; CI: Confidence interval.

Table 6 Pairwise comparisons of the models' overall performances in the training set (*P* value)

Evaluated metrics	DenseNet121 *vs* VGG16	DenseNet121 *vs* ResNet50	DenseNet121 *vs* ViT	VGG16 *vs* ResNet50	VGG16 *vs* ViT	ResNet50 *vs* ViT
Accuracy	0.004	0.999	0.002	0.006	0.978	0.003
Precision	0.001	0.981	0.003	0.001	0.85	0.001
Recall	0.001	0.995	0.002	0.001	0.212	0.003
F1-score	0.001	0.999	0.001	0.001	0.421	0.001
AU-ROC	0.001	0.984	0.001	0.001	0.304	0.002

VGG: Visual geometry group; ViT: Vision transformer; AU-ROC: Area under the receiver operating curve.

Table 7 The overall performances of the deep learning models in the testing set

Model	Accuracy (%)	Precision (%)	Recall (%)	F1-score (%)	AU-ROC (%)
DenseNet121	88.6	87.5	79.0	82.5	87.1
VGG16	85.5	87.0	73.3	77.3	83.6
ResNet50	89.7	87.8	81.0	83.8	88.5
ViT	86.6	81.3	80.0	80.5	87.5

VGG: Visual geometry group; ViT: Vision transformer; AU-ROC: Area under the receiver operating curve.

classification, the accuracy varies when identifying different lesions, as shown in Table 4. The models demonstrated exceptionally high accuracy in identifying normal mucosa (92% to 99%). However, the accuracy of polyp detection was between 75% and 100%. In particular, the VGG16 model was the worst out of the four, likely due to its less balanced performance when handling smaller datasets. The accuracy of ulcer detection is relatively high (83% to 92%), while the detection of erosions and erythema had the lowest accuracy among all the categories (72% to 82%). The lower accuracy in detecting erosions and erythema compared to other lesions might be attributed to several factors as follows: (1) These lesions often exhibit subtle visual features that may resemble normal mucosa or early-stage ulcers, making them more

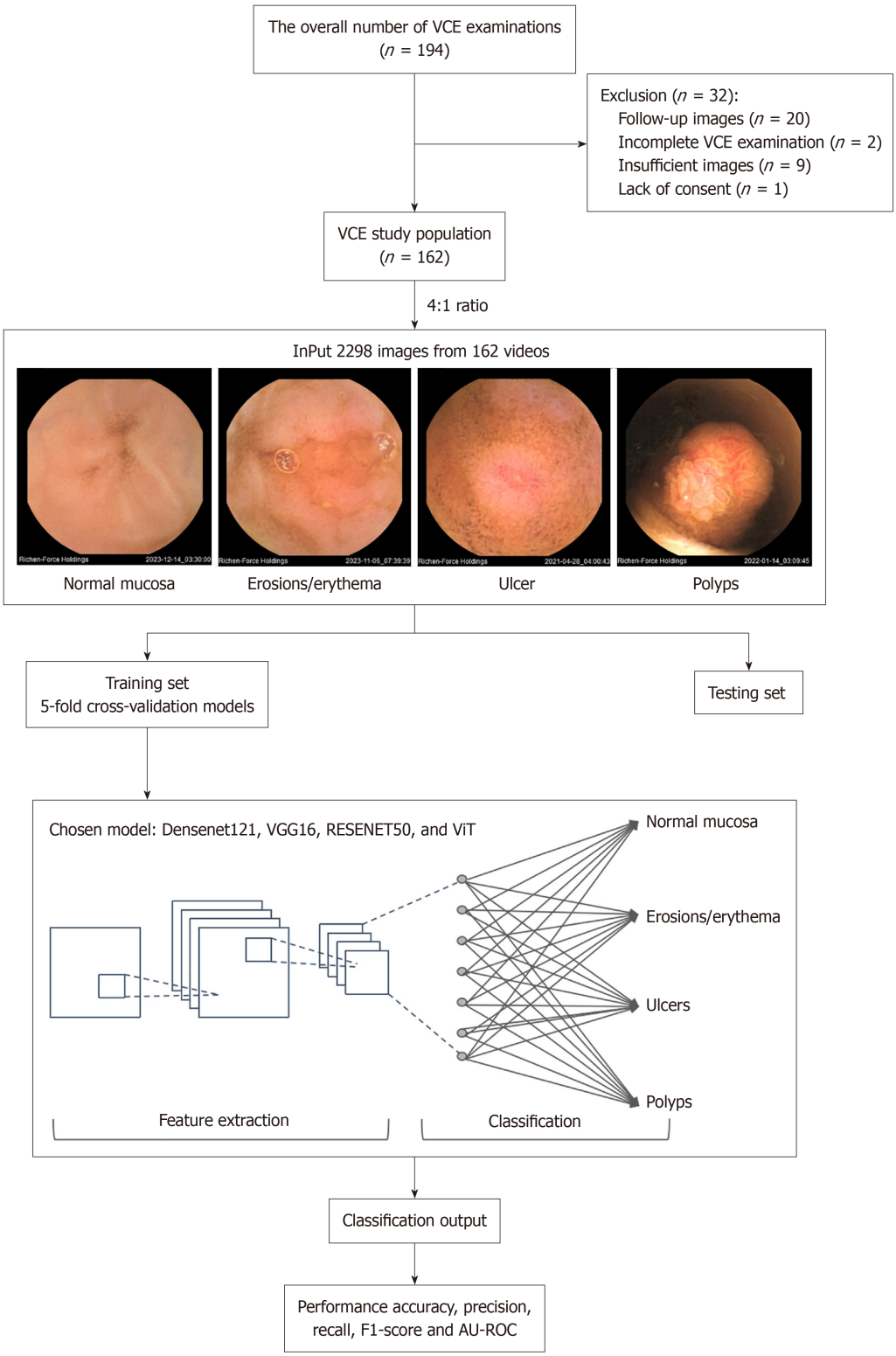

Figure 1 A flowchart illustrating the deep learning models used for lesion classification in video capsule endoscopy images. VCE: Video capsule endoscopy; VGG: Visual geometry group; ViT: Vision transformer; AU-ROC: Area under the receiver operating curve.

difficult to distinguish; (2) Erosions and erythema can vary significantly in size and shape, which might contribute to inconsistencies in detection; (3) The surrounding features around erosions and erythema might be more complex leading to difficulty in recognizing; and (4) Poor quality and fewer images in training data will also affect the accuracy of recognition.

The use of AI can efficiently aid physicians in accurately diagnosing and managing diseases. The healthcare system is heavily burdened by severe diseases that could have been prevented with early detection. Cancers like breast, colorectal, and lung cancers have benefited from early detection, leading to better prognoses for patients and better quality of life as management tends to be less strenuous on the patient in the early stages. On the same basis, using AI to process VCE

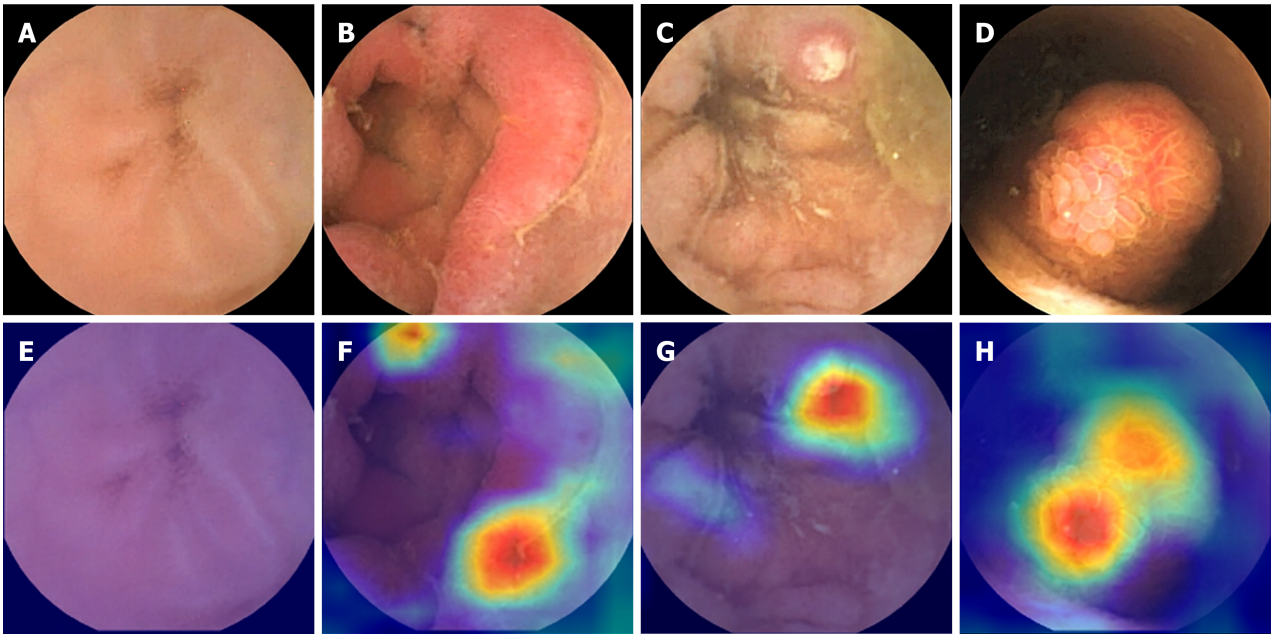

Figure 2 Lesion detection by applying gradient-weighted class activation mapping on representative video capsule endoscopy images, including normal mucosa, erosions/erythema, ulcer, and polyps images. A-D: White-light imaging capsule endoscopic image; E-H: Gradient-weighted class activation mapping image. A and E: Normal mucosa; B and F: Erosions/erythema; C and G: Ulcer; D and H: Polyps. Grad-CAM: Gradient-weighted class activation mapping; VCE: Video capsule endoscopy.

images and differentiate between normal mucosa and lesions like erosions/erythema, ulcers, and polyps can help diagnose diseases like CD, IBD, and UC faster while decreasing the cost of performing the exam as fewer specialists are required to process the same number of images, making the exam more accessible. Malnutrition and anemia can result from various GI diseases and have serious repercussions in children[43-45]. Not only does it decrease a child's quality of life, but it can also cause growth disruptions and psychological distress[46-48]. Timely management improves outcomes. Studies have shown that early intervention in CD has translated well in clinical settings[49,50]. Walters *et al*[50] has found that early treatment with anti-tumor necrosis factor-α has been very effective, with 85.3% of the pediatric patients in the study achieving remission by one year. In addition, as with any technician-dependent exam, the accuracy of the interpretation of images from VCE is operator-dependent. AI can help standardize diagnostic processes by creating more uniform guidelines for interpreting medical data, reducing variability in diagnoses and improving consistency.

Currently, there are limitations to utilizing AI to diagnose diseases. The quality of AI models is entirely dependent on the datasets on which they are trained. Biases will stem from inaccurate representation of populations (incomplete, skewed, or lacking diversity). Our dataset of 2298 VCE images used for model training and testing may not suffice to ensure the suitability of these algorithms for practical clinical use. For VCEs in particular, this exam can be expensive and children in general are not subject to exams unless it were absolutely necessary, leading to smaller sample sizes of data. Smaller sample sizes are also unable to compensate for slight discrepancies. For example, in training, DenseNet121 had the highest accuracy (90.6%), followed by ResNet50 (90.5%). However, in testing, ResNet50 had the highest accuracy (89.7%), while DenseNet121 had the second highest accuracy (88.6%). The slight differences in training are shown to be negligible through pairwise comparisons (Table 6), so both models can be considered to have performed equally well. ResNet50 performing better in testing could have been due to the limited sample size for testing as well as the innate differences between models and how they each respond to the dataset. These fluctuations in performance can be more pronounced in smaller datasets. In the same vein, ViT showed the poorest accuracy in training (88.1%), with VGG16 coming in second to last (88.3%), but ViT performed better in testing with an accuracy of 86.6%, while VGG16 had an accuracy of 85.5%. Pairwise comparisons of ViT and VGG16's performances in training were found to be negligible ($P > 0.05$). Despite the discrepancies between training and testing, the overall trend was maintained. In training, DenseNet121 and ResNet50 performed significantly better than ViT and VGG16 ($P < 0.05$), as shown in Table 6, and this was seen as well in testing. Aside from inaccurate population representation, identifying less obvious lesions or differentiating between lesions will prove challenging without enough training data as some lesion morphology can look very similar to other types of lesions or regular mucosa or even artifacts like bubbles or food. Therefore, further research is needed in order to produce truly viable models. There remains a notable absence of prospective multi-center research in VCE, a prerequisite for integrating this technology into routine clinical workflows. In addition, studies have mainly focused on specific types of VCE, limiting the generalizability of developed models across different VCE platforms. Lastly, our study, like many others, employed datasets composed of selected still frames rather than full-length videos, potentially introducing selection bias. Moving forward, it is imperative to develop deep learning models capable of directly analyzing VCE videos, including techniques for video-to-image conversion and classification of abnormal images by lesion type in the small bowel. Future studies should involve comprehensive analysis using full VCE videos from diverse medical centers to validate the clinical accuracy of proposed models prior to clinical application.

CONCLUSION

This study employed VGG16, ResNet50, DenseNAet121, and ViT models along with Grad-CAM to classify video capsule endoscopic images in children. The four deep learning models effectively differentiated normal tissue, erosions/erythema, ulcers, and polyps with high accuracy. This automated detection approach not only enhances clinical practice by significantly reducing the time required to analyze VCE images but also improves diagnostic accuracy, making it a valuable tool for pediatric gastroenterologists.

FOOTNOTES

Author contributions: Huang YH and Lin Q performed the study, collected the data, carried out the initial analyses, and drafted the original manuscript; Jin XY performed the analysis and interpretation of the data, trained the deep learning models, and revised the manuscript for the intellectual session; Chou CY revised and edited each iteration of the manuscript; Wei JJ, Xing J, and Guo HM collected and interpreted the data; Lu Y and Liu ZF contributed to the design of the study, and critically reviewed and revised the manuscript; All authors have read and approve the final manuscript.

Institutional review board statement: The study protocol was reviewed and approved by the Institutional Review Board of the Children's Hospital of Nanjing Medical University (No. 202409001-1).

Informed consent statement: The need for patient consent was waived due to the retrospective nature of the study.

Conflict-of-interest statement: The authors declare that they have no conflict of interest.

Data sharing statement: No additional data are available.

Country of origin: China

ORCID number: Yi-Hsuan Huang 0009-0008-0654-8639; Yan Lu 0000-0001-6938-9315.

S-Editor: Fan M
L-Editor: A
P-Editor: Yu HG

REFERENCES

1 **Iddan G**, Meron G, Glukhovsky A, Swain P. Wireless capsule endoscopy. *Nature* 2000; **405**: 417 [PMID: 10839527 DOI: 10.1038/35013140] [FullText]
2 **Thomson M**, Fritscher-Ravens A, Mylonaki M, Swain P, Eltumi M, Heuschkel R, Murch S, McAlindon M, Furman M. Wireless capsule endoscopy in children: a study to assess diagnostic yield in small bowel disease in paediatric patients. *J Pediatr Gastroenterol Nutr* 2007; **44**: 192-197 [PMID: 17255830 DOI: 10.1097/01.mpg.0000252196.91707.ff] [FullText]
3 **Cohen SA**, Ephrath H, Lewis JD, Klevens A, Bergwerk A, Liu S, Patel D, Reed-Knight B, Stallworth A, Wakhisi T, Gold BD. Pediatric capsule endoscopy: review of the small bowel and patency capsules. *J Pediatr Gastroenterol Nutr* 2012; **54**: 409-413 [PMID: 21760541 DOI: 10.1097/MPG.0b013e31822c81fd] [FullText]
4 **Friedlander JA**, Liu QY, Sahn B, Kooros K, Walsh CM, Kramer RE, Lightdale JR, Khlevner J, McOmber M, Kurowski J, Giefer MJ, Pall H, Troendle DM, Utterson EC, Brill H, Zacur GM, Lirio RA, Lerner DG, Reynolds C, Gibbons TE, Wilsey M, Liacouras CA, Fishman DS; Endoscopy Committee. NASPGHAN Capsule Endoscopy Clinical Report. *J Pediatr Gastroenterol Nutr* 2017; **64**: 485-494 [PMID: 27642781 DOI: 10.1097/MPG.0000000000001413] [FullText]
5 **Jensen MK**, Tipnis NA, Bajorunaite R, Sheth MK, Sato TT, Noel RJ. Capsule endoscopy performed across the pediatric age range: indications, incomplete studies, and utility in management of inflammatory bowel disease. *Gastrointest Endosc* 2010; **72**: 95-102 [PMID: 20472231 DOI: 10.1016/j.gie.2010.01.016] [FullText]
6 **Nuutinen H**, Kolho KL, Salminen P, Rintala R, Koskenpato J, Koivusalo A, Sipponen T, Färkkilä M. Capsule endoscopy in pediatric patients: technique and results in our first 100 consecutive children. *Scand J Gastroenterol* 2011; **46**: 1138-1143 [PMID: 21615227 DOI: 10.3109/00365521.2011.584900] [FullText]
7 **Eliakim R**. Video capsule endoscopy of the small bowel. *Curr Opin Gastroenterol* 2010; **26**: 129-133 [PMID: 20145540 DOI: 10.1097/MOG.0b013e328334df17] [FullText]
8 **Pennazio M**, Spada C, Eliakim R, Keuchel M, May A, Mulder CJ, Rondonotti E, Adler SN, Albert J, Baltes P, Barbaro F, Cellier C, Charton JP, Delvaux M, Despott EJ, Domagk D, Klein A, McAlindon M, Rosa B, Rowse G, Sanders DS, Saurin JC, Sidhu R, Dumonceau JM, Hassan C, Gralnek IM. Small-bowel capsule endoscopy and device-assisted enteroscopy for diagnosis and treatment of small-bowel disorders: European Society of Gastrointestinal Endoscopy (ESGE) Clinical Guideline. *Endoscopy* 2015; **47**: 352-376 [PMID: 25826168 DOI: 10.1055/s-0034-1391855] [FullText]

9 **ASGE Standards of Practice Committee**, Lightdale JR, Acosta R, Shergill AK, Chandrasekhara V, Chathadi K, Early D, Evans JA, Fanelli RD, Fisher DA, Fonkalsrud L, Hwang JH, Kashab M, Muthusamy VR, Pasha S, Saltzman JR, Cash BD; American Society for Gastrointestinal Endoscopy. Modifications in endoscopic practice for pediatric patients. *Gastrointest Endosc* 2014; **79**: 699-710 [PMID: 24593951 DOI: 10.1016/j.gie.2013.08.014] [FullText]

10 **Cohen SA**, Klevens AI. Use of capsule endoscopy in diagnosis and management of pediatric patients, based on meta-analysis. *Clin Gastroenterol Hepatol* 2011; **9**: 490-496 [PMID: 21440674 DOI: 10.1016/j.cgh.2011.03.025] [FullText]

11 **ASGE Technology Committee**, Wang A, Banerjee S, Barth BA, Bhat YM, Chauhan S, Gottlieb KT, Konda V, Maple JT, Murad F, Pfau PR, Pleskow DK, Siddiqui UD, Tokar JL, Rodriguez SA. Wireless capsule endoscopy. *Gastrointest Endosc* 2013; **78**: 805-815 [PMID: 24119509 DOI: 10.1016/j.gie.2013.06.026] [FullText]

12 **Wang Q**, Pan N, Xiong W, Lu H, Li N, Zou X. Reduction of bubble-like frames using a RSS filter in wireless capsule endoscopy video. *Opt Laser Technol* 2019; **110**: 152-157 [DOI: 10.1016/j.optlastec.2018.08.051] [FullText]

13 **Oliva S**, Cohen SA, Di Nardo G, Gualdi G, Cucchiara S, Casciani E. Capsule endoscopy in pediatrics: a 10-years journey. *World J Gastroenterol* 2014; **20**: 16603-16608 [PMID: 25469028 DOI: 10.3748/wjg.v20.i44.16603] [FullText]

14 **Jia X**, Xing X, Yuan Y, Xing L, Meng MQ. Wireless Capsule Endoscopy: A New Tool for Cancer Screening in the Colon With Deep-Learning-Based Polyp Recognition. *Proc IEEE* 2020; **108**: 178-197 [DOI: 10.1109/jproc.2019.2950506] [FullText]

15 **Kim SH**, Hwang Y, Oh DJ, Nam JH, Kim KB, Park J, Song HJ, Lim YJ. Efficacy of a comprehensive binary classification model using a deep convolutional neural network for wireless capsule endoscopy. *Sci Rep* 2021; **11**: 17479 [PMID: 34471156 DOI: 10.1038/s41598-021-96748-z] [FullText]

16 **Kim SH**, Lim YJ. Artificial Intelligence in Capsule Endoscopy: A Practical Guide to Its Past and Future Challenges. *Diagnostics (Basel)* 2021; **11** [PMID: 34574063 DOI: 10.3390/diagnostics11091722] [FullText]

17 **Oh DJ**, Hwang Y, Lim YJ. A Current and Newly Proposed Artificial Intelligence Algorithm for Reading Small Bowel Capsule Endoscopy. *Diagnostics (Basel)* 2021; **11** [PMID: 34209948 DOI: 10.3390/diagnostics11071183] [FullText]

18 **Xiao Jia**, Meng MQ. A deep convolutional neural network for bleeding detection in Wireless Capsule Endoscopy images. *Annu Int Conf IEEE Eng Med Biol Soc* 2016; **2016**: 639-642 [PMID: 28268409 DOI: 10.1109/EMBC.2016.7590783] [FullText]

19 **Xiao Jia**, Meng MQ. Gastrointestinal bleeding detection in wireless capsule endoscopy images using handcrafted and CNN features. *Annu Int Conf IEEE Eng Med Biol Soc* 2017; **2017**: 3154-3157 [PMID: 29060567 DOI: 10.1109/EMBC.2017.8037526] [FullText]

20 **Aoki T**, Yamada A, Kato Y, Saito H, Tsuboi A, Nakada A, Niikura R, Fujishiro M, Oka S, Ishihara S, Matsuda T, Nakahori M, Tanaka S, Koike K, Tada T. Automatic detection of blood content in capsule endoscopy images based on a deep convolutional neural network. *J Gastroenterol Hepatol* 2020; **35**: 1196-1200 [PMID: 31758717 DOI: 10.1111/jgh.14941] [FullText]

21 **Xing X**, Jia X, Meng MQ. Bleeding Detection in Wireless Capsule Endoscopy Image Video Using Superpixel-Color Histogram and a Subspace KNN Classifier. *Annu Int Conf IEEE Eng Med Biol Soc* 2018; **2018**: 1-4 [PMID: 30440286 DOI: 10.1109/EMBC.2018.8513012] [FullText]

22 **Noya F**, Alvarez-Gonzalez MA, Benitez R. Automated angiodysplasia detection from wireless capsule endoscopy. *Annu Int Conf IEEE Eng Med Biol Soc* 2017; **2017**: 3158-3161 [PMID: 29060568 DOI: 10.1109/EMBC.2017.8037527] [FullText]

23 **Leenhardt R**, Vasseur P, Li C, Saurin JC, Rahmi G, Cholet F, Becq A, Marteau P, Histace A, Dray X; CAD-CAP Database Working Group. A neural network algorithm for detection of GI angiectasia during small-bowel capsule endoscopy. *Gastrointest Endosc* 2019; **89**: 189-194 [PMID: 30017868 DOI: 10.1016/j.gie.2018.06.036] [FullText]

24 **Fan S**, Xu L, Fan Y, Wei K, Li L. Computer-aided detection of small intestinal ulcer and erosion in wireless capsule endoscopy images. *Phys Med Biol* 2018; **63**: 165001 [PMID: 30033931 DOI: 10.1088/1361-6560/aad51c] [FullText]

25 **Tsuboi A**, Oka S, Aoyama K, Saito H, Aoki T, Yamada A, Matsuda T, Fujishiro M, Ishihara S, Nakahori M, Koike K, Tanaka S, Tada T. Artificial intelligence using a convolutional neural network for automatic detection of small-bowel angioectasia in capsule endoscopy images. *Dig Endosc* 2020; **32**: 382-390 [PMID: 31392767 DOI: 10.1111/den.13507] [FullText]

26 **Hwang Y**, Lee HH, Park C, Tama BA, Kim JS, Cheung DY, Chung WC, Cho YS, Lee KM, Choi MG, Lee S, Lee BI. Improved classification and localization approach to small bowel capsule endoscopy using convolutional neural network. *Dig Endosc* 2021; **33**: 598-607 [PMID: 32640059 DOI: 10.1111/den.13787] [FullText]

27 **Saito H**, Aoki T, Aoyama K, Kato Y, Tsuboi A, Yamada A, Fujishiro M, Oka S, Ishihara S, Matsuda T, Nakahori M, Tanaka S, Koike K, Tada T. Automatic detection and classification of protruding lesions in wireless capsule endoscopy images based on a deep convolutional neural network. *Gastrointest Endosc* 2020; **92**: 144-151.e1 [PMID: 32084410 DOI: 10.1016/j.gie.2020.01.054] [FullText]

28 **Ding Z**, Shi H, Zhang H, Meng L, Fan M, Han C, Zhang K, Ming F, Xie X, Liu H, Liu J, Lin R, Hou X. Gastroenterologist-Level Identification of Small-Bowel Diseases and Normal Variants by Capsule Endoscopy Using a Deep-Learning Model. *Gastroenterology* 2019; **157**: 1044-1054.e5 [PMID: 31251929 DOI: 10.1053/j.gastro.2019.06.025] [FullText]

29 **Mishkin DS**, Chuttani R, Croffie J, Disario J, Liu J, Shah R, Somogyi L, Tierney W, Song LM, Petersen BT; Technology Assessment Committee, American Society for Gastrointestinal Endoscopy. ASGE Technology Status Evaluation Report: wireless capsule endoscopy. *Gastrointest Endosc* 2006; **63**: 539-545 [PMID: 16564850 DOI: 10.1016/j.gie.2006.01.014] [FullText]

30 **Sharma A**, Kumar R, Garg P. Deep learning-based prediction model for diagnosing gastrointestinal diseases using endoscopy images. *Int J Med Inform* 2023; **177**: 105142 [PMID: 37422969 DOI: 10.1016/j.ijmedinf.2023.105142] [FullText]

31 **Sahaai MB**, Jothilakshmi GR, Ravikumar D, Prasath R, Singh S. ResNet-50 based deep neural network using transfer learning for brain tumor classification. *AIP Conf Proc* 2022 [DOI: 10.1063/5.0082328] [FullText]

32 **Huang G**, Liu Z, Van Der Maaten L, Weinberger KQ. Densely Connected Convolutional Networks. IEEE 2017: Conference on Computer Vision and Pattern Recognition (CVPR); 2017 July 21-26; Honolulu, HI, United States. 2017: 2261-2269 [DOI: 10.1109/cvpr.2017.243] [Full Text]

33 **Huang G**, Sun Y, Liu Z, Sedra D, Weinberger K. Deep Networks with Stochastic Depth. 2016. Available from: arXiv:1603.09382 [DOI: 10.48550/arXiv.1603.09382] [FullText]

34 **Dosovitskiy A**, Beyer L, Kolesnikov A, Weissenborn D, Zhai X, Unterthiner T, Dehghani M, Minderer M, Heigold G, Gelly S, Uszkoreit J, Houlsby N. An Image is Worth 16x16 Words: Transformers for Image Recognition at Scale. 2021. Available from: arXiv:2010.11929 [DOI: 10.48550/arXiv.2010.11929] [FullText]

35 **Khalil M**, Khalil A, Ngom A. A Comprehensive Study of Vision Transformers in Image Classification Tasks. 2023. Available from: arXiv:2312.01232 [DOI: 10.48550/arXiv.2312.01232] [FullText]

36 **Lee SH**, Lee S, Song BC. Vision Transformer for Small-Size Datasets. 2021. Available from: arXiv:2112.13492 [DOI: 10.48550/arXiv.2112.13492] [FullText]

37 **Selvaraju RR**, Cogswell M, Das A, Vedantam R, Parikh D, Batra D. Grad-CAM: Visual Explanations from Deep Networks *via* Gradient-Based Localization. *Int J Comput Vis* 2020; **128**: 336-359 [DOI: 10.1007/s11263-019-01228-7] [FullText]

38 **Cao Q**, Deng R, Pan Y, Liu R, Chen Y, Gong G, Zou J, Yang H, Han D. Robotic wireless capsule endoscopy: recent advances and upcoming technologies. *Nat Commun* 2024; **15**: 4597 [PMID: 38816464 DOI: 10.1038/s41467-024-49019-0] [FullText]

39 **Li B**, Meng MQ. Computer-based detection of bleeding and ulcer in wireless capsule endoscopy images by chromaticity moments. *Comput Biol Med* 2009; **39**: 141-147 [PMID: 19147126 DOI: 10.1016/j.compbiomed.2008.11.007] [FullText]

40 **Chen Y**, Lee J. Ulcer detection in wireless capsule endoscopy video. MM'12: Proceedings of the 20th ACM international conference on Multimedia; 2012 Oct 29; 2012: 1181-1184 [DOI: 10.1145/2393347.2396413] [FullText]

41 **Bai L**, Wang L, Chen T, Zhao Y, Ren H. Transformer-Based Disease Identification for Small-Scale Imbalanced Capsule Endoscopy Dataset. *Electronics* 2022; **11**: 2747 [DOI: 10.3390/electronics11172747] [FullText]

42 **Subedi A**, Regmi S, Regmi N, Bhusal B, Bagci U, Jha D. Classification of Endoscopy and Video Capsule Images using CNN-Transformer Model. 2024. Available from: arXiv:2408.10733 [DOI: 10.48550/arXiv.2408.10733] [FullText]

43 **Goyal A**, Zheng Y, Albenberg LG, Stoner NL, Hart L, Alkhouri R, Hampson K, Ali S, Cho-Dorado M, Goyal RK, Grossman A. Anemia in Children With Inflammatory Bowel Disease: A Position Paper by the IBD Committee of the North American Society of Pediatric Gastroenterology, Hepatology and Nutrition. *J Pediatr Gastroenterol Nutr* 2020; **71**: 563-582 [PMID: 32947565 DOI: 10.1097/MPG.0000000000002885] [FullText]

44 **Wiskin AE**, Wootton SA, Hunt TM, Cornelius VR, Afzal NA, Jackson AA, Beattie RM. Body composition in childhood inflammatory bowel disease. *Clin Nutr* 2011; **30**: 112-115 [PMID: 20728967 DOI: 10.1016/j.clnu.2010.07.014] [FullText]

45 **Pawłowska-Seredyńska K**, Akutko K, Umławska W, Śmieszniak B, Seredyński R, Stawarski A, Pytrus T, Iwańczak B. Nutritional status of pediatric patients with inflammatory bowel diseases is related to disease duration and clinical picture at diagnosis. *Sci Rep* 2023; **13**: 21300 [PMID: 38042899 DOI: 10.1038/s41598-023-48504-8] [FullText]

46 **Mackner LM**, Greenley RN, Szigethy E, Herzer M, Deer K, Hommel KA. Psychosocial issues in pediatric inflammatory bowel disease: report of the North American Society for Pediatric Gastroenterology, Hepatology, and Nutrition. *J Pediatr Gastroenterol Nutr* 2013; **56**: 449-458 [PMID: 23287808 DOI: 10.1097/MPG.0b013e3182841263] [FullText]

47 **Mikocka-Walus A**, Knowles SR, Keefer L, Graff L. Controversies Revisited: A Systematic Review of the Comorbidity of Depression and Anxiety with Inflammatory Bowel Diseases. *Inflamm Bowel Dis* 2016; **22**: 752-762 [PMID: 26841224 DOI: 10.1097/MIB.0000000000000620] [FullText]

48 **Ishige T**. Growth failure in pediatric onset inflammatory bowel disease: mechanisms, epidemiology, and management. *Transl Pediatr* 2019; **8**: 16-22 [PMID: 30881894 DOI: 10.21037/tp.2018.12.04] [FullText]

49 **Kugathasan S**, Denson LA, Walters TD, Kim MO, Marigorta UM, Schirmer M, Mondal K, Liu C, Griffiths A, Noe JD, Crandall WV, Snapper S, Rabizadeh S, Rosh JR, Shapiro JM, Guthery S, Mack DR, Kellermayer R, Kappelman MD, Steiner S, Moulton DE, Keljo D, Cohen S, Oliva-Hemker M, Heyman MB, Otley AR, Baker SS, Evans JS, Kirschner BS, Patel AS, Ziring D, Trapnell BC, Sylvester FA, Stephens MC, Baldassano RN, Markowitz JF, Cho J, Xavier RJ, Huttenhower C, Aronow BJ, Gibson G, Hyams JS, Dubinsky MC. Prediction of complicated disease course for children newly diagnosed with Crohn's disease: a multicentre inception cohort study. *Lancet* 2017; **389**: 1710-1718 [PMID: 28259484 DOI: 10.1016/S0140-6736(17)30317-3] [FullText]

50 **Walters TD**, Kim MO, Denson LA, Griffiths AM, Dubinsky M, Markowitz J, Baldassano R, Crandall W, Rosh J, Pfefferkorn M, Otley A, Heyman MB, LeLeiko N, Baker S, Guthery SL, Evans J, Ziring D, Kellermayer R, Stephens M, Mack D, Oliva-Hemker M, Patel AS, Kirschner B, Moulton D, Cohen S, Kim S, Liu C, Essers J, Kugathasan S, Hyams JS; PRO-KIIDS Research Group. Increased effectiveness of early therapy with anti-tumor necrosis factor-α vs an immunomodulator in children with Crohn's disease. *Gastroenterology* 2014; **146**: 383-391 [PMID: 24162032 DOI: 10.1053/j.gastro.2013.10.027] [FullText]

World Journal of Gastroenterology

Submit a Manuscript: https://www.f6publishing.com

World J Gastroenterol 2025 June 7; 31(21): 106033

DOI: 10.3748/wjg.v31.i21.106033

ISSN 1007-9327 (print) ISSN 2219-2840 (online)

ORIGINAL ARTICLE

Observational Study

Prevalence and risk factors of *Helicobacter pylori* infection in Xinjiang Uygur Autonomous Region: A cross-sectional study of all age groups

Qi Jiang, Wei-Dong Liu, Wen-Jia Hui, Wen-Jie Kong, Yan Feng, Aihemaijiang Kuerbanjiang, Xiao Ling Huang, Feng Gao

Specialty type: Gastroenterology and hepatology

Provenance and peer review: Unsolicited article; Externally peer reviewed.

Peer-review model: Single blind

Peer-review report's classification

Scientific Quality: Grade A, Grade A, Grade A, Grade B

Novelty: Grade A, Grade A, Grade B, Grade B

Creativity or Innovation: Grade A, Grade B, Grade B, Grade C

Scientific Significance: Grade A, Grade A, Grade B, Grade B

P-Reviewer: Hussein AM; Ullah W

Received: February 17, 2025

Revised: April 14, 2025

Accepted: May 23, 2025

Published online: June 7, 2025

Processing time: 110 Days and 11.3 Hours

Qi Jiang, Wei-Dong Liu, Wen-Jia Hui, Wen-Jie Kong, Yan Feng, Aihemaijiang Kuerbanjiang, Xiao Ling Huang, Feng Gao, Department of Gastroenterology, People's Hospital of Xinjiang Uygur Autonomous Region, Urumqi 830001, Xinjiang Uygur Autonomous Region, China

Co-first authors: Qi Jiang and Wei-Dong Liu.

Corresponding author: Feng Gao, PhD, Professor, Department of Gastroenterology, People's Hospital of Xinjiang Uygur Autonomous Region, No. 91 Tianchi Road, Tianshan District, Urumqi 830001, Xinjiang Uygur Autonomous Region, China. xjgf@sina.com

Abstract

BACKGROUND

Helicobacter pylori (H. pylori) infection rates have been changing with different populations and geographic areas. Currently, there is still a lack of comprehensive survey data on the *H. pylori* infection rate and its risk factors in the natural population of Xinjiang Uygur Autonomous Region.

AIM

To understand the *H. pylori* infection and risk factors in Xinjiang Uygur Autonomous Region for the prevention and control strategies.

METHODS

This study comprehensively collected the survey data on *H. pylori* infection in 15 regions of Xinjiang Uygur Autonomous Region by using the method of stratified random cluster sampling. A total of 4361 individuals from the general population were selected as research subjects, and questionnaire surveys and blood tests for *H. pylori* antibodies were conducted.

RESULTS

The overall *H. pylori* infection rate in Xinjiang Uygur Autonomous Region was 70.79% (3087/4361). The *H. pylori* infection rate showed a trend of first increasing and then decreasing with the increase of age, and the difference was statistically significant ($P < 0.05$). The analysis of the *H. pylori* infection rates among different ethnic groups showed that the infection rates of ethnic minorities such as Uyghur, Kirgiz, and Tajik were significantly higher than those of Han and Hui ethnic

groups, and the difference was statistically significant ($P < 0.01$). Multivariate analysis showed that altitude, regular consumption of beef, mutton, dried nuts, barbecue foods, and drinking river water were positively correlated with the *H. pylori* infection rate.

CONCLUSION
This study indicates that the overall *H. pylori* infection rate in Xinjiang Uygur Autonomous Region is relatively high, with obvious regional and ethnic differences, which are closely related to the sanitation conditions and eating habits.

Key Words: Uygur Autonomous Region; *Helicobacter pylori*; Infection rate; Risk factors; Natural population

Core Tip: The infection rate of *Helicobacter pylori* (*H. pylori*) in China is approximately 49.6%, and there are significant differences in the infection rates among different regions. In-depth exploration of the infection rate of *H. pylori* and its potential risk factors in Xinjiang Uygur Autonomous Region is of crucial reference value for formulating scientific and effective prevention and control strategies against *H. pylori* infection. Studies have shown that the infection rate of *H. pylori* in Xinjiang Uygur Autonomous Region is at a high level, with obvious regional and ethnic differences, and it is closely related to the local sanitation conditions and residents' eating habits.

Citation: Jiang Q, Liu WD, Hui WJ, Kong WJ, Feng Y, Kuerbanjiang A, Huang XL, Gao F. Prevalence and risk factors of *Helicobacter pylori* infection in Xinjiang Uygur Autonomous Region: A cross-sectional study of all age groups. *World J Gastroenterol* 2025; 31(21): 106033
URL: https://www.wjgnet.com/1007-9327/full/v31/i21/106033.htm
DOI: https://dx.doi.org/10.3748/wjg.v31.i21.106033

INTRODUCTION

Helicobacter pylori (*H. pylori*) infection, a chronic infectious disease with a high infection rate, has been classified as a definite Class I carcinogen by the World Health Organization[1-3]. Studies show that the *H. pylori* infection rate has been on a downward trend globally from 1980 to 2022. However, more than 40% of the world's population is still infected with *H. pylori*[4]. Due to differences in socioeconomic development, population density and composition, income levels, and healthcare standards, the prevalence of *H. pylori* exhibits significant regional variations. The prevalence is the lowest in developed countries such as North America and Western Europe, while it remains high in most developing countries[5, 6]. As a developing country, China has regional differences in economic and sanitation levels. The overall *H. pylori* infection rate in China is approximately 49.6%, and there are extensive regional disparities in the infection rate (20.6% to 81.8%)[7]. The *H. pylori* infection rates are relatively higher in the eastern and western regions than in the central region. There are even differences within some provinces[8,9]. Many studies have shown that various factors[9-11], including geographical location, living environment, socioeconomic status, personal habits, and socio-demographic characteristics, may be responsible for the wide variation in *H. pylori* infection rates among regions. Therefore, a comprehensive analysis of the prevalence of *H. pylori* infection and an assessment of regional risk factors are crucial for formulating targeted prevention and treatment strategies. Xinjiang Uygur Autonomous Region is located in the northwest of China, characterized by multi-ethnic aggregation, a vast area, and a scattered population. Currently, there is still a lack of comprehensive survey data on the *H. pylori* infection rate and its risk factors in the natural population of Xinjiang Uygur Autonomous Region. This paper aims to analyze the data from 15 regions in Xinjiang Uygur Autonomous Region, analyze the *H. pylori* infection rate in this region and evaluate the related risk factors, providing evidence - based support for the prevention and treatment of *H. pylori* infection in the population of Xinjiang Uygur Autonomous Region.

MATERIALS AND METHODS

Study subjects

This study was conducted in Xinjiang Uygur Autonomous Region from May 2022 to November 2023. Using the method of stratified random cluster sampling, random cluster sampling was carried out in 15 regions in Xinjiang Uygur Autonomous Region: Altay, Aksu, Börtala Mongol Autonomous Prefecture (Bole), Bayingolin Mongol Autonomous Prefecture (Korla, Yanqi), Changji Hui Autonomous Prefecture (Changji), Hami (Yiwu), Hetian (Hotan), Kashgar (Shule, Tashkurgan Tajike), Kizilsu Kirgiz Autonomous Prefecture (Artouche), Turpan, Tacheng, Ili Kazakh Autonomous Prefecture (Yining). According to "The Announcement of the Seventh National Population Census of Xinjiang Uygur Autonomous Region in 2021" (No. 2), the total population of the above - mentioned regions is 18951708, accounting for 73.31% of the

total population of Xinjiang Uygur Autonomous Region. By simple random sampling, one area was randomly selected within each administrative region, and it was further divided into different standardized census areas according to natural villages or communities. The population of each census area was 200-400 people, and one standardized census area was randomly selected for the survey (the distribution of the survey locations and the number of participants in Xinjiang Uygur Autonomous Region are shown in Figure 1). A total of 4665 people were surveyed, with questionnaire surveys and *H. pylori* antibody blood tests conducted. Of 55 participants with missing basic information and 249 participants with missing blood samples were excluded. Finally, 4361 participants were included (flowchart of participant selection is shown in Figure 2).

Questionnaire

The content of the questionnaire covers demographic and socioeconomic factors [including gender, age, ethnicity, marital status, occupation, family income (China Yuan), educational level, body mass index (BMI, kg/m^2) and the altitude of the place of residence (m)], as well as dietary and lifestyle factors (including eating habits, smoking and drinking situations). The height and weight were measured by trained staff members, and the BMI was defined as the weight (kg) divided by the square of the height (m). According to the altitude standards, the surveyed areas were classified into low - altitude regions (< 1000 m), which included Altay, Bole, Jeminay, Korla, Turpan, Tacheng, and Yining; medium - altitude regions (1000-2000 m), which include Artux, Aksu, Changji, Hotan, Shule, Yiwu, and Yanqi; and medium to high altitude regions (3000-4000 m), with Tashkurgan Tajike being the representative area[12]. Smoking is defined as smoking at least one cigarette per day within the past year or having smoked in the past. Drinking alcohol is defined as consuming at least 1000 g of beer, 150 g of wine, or spirits at least once a week within the past year. The frequency of consumption of foods such as fruits, vegetables, and meats is defined as follows: If they are consumed every day or 3 to 5 times a week, it is considered frequent consumption. Gluttony is defined as consuming food in an amount that reaches or exceeds twice the normal dietary intake, occurring at least once a week and lasting for more than three months. Due to language communication barriers, a noisy on-site environment and time constraints, there is some data missing in the questionnaire survey.

H. pylori antibody detection

Blood samples (2-3 mL) were taken on an empty stomach in the morning. The blood samples were coded with unique identification numbers and analyzed while blinding the identities of the participants. All blood samples were centrifuged, transported with dry ice, and stored at -80 °C. The *H. pylori* antibody kit (Shenzhen Bioloot Biological Products Co., Ltd.) was used for the detection of *H. pylori*. The immunochromatographic method was adopted, and the specific operation was as follows: 75 μL of serum sample was dropped into the sample - adding well, and the test result was interpreted 15 minutes later. The test membrane strip was compared with the standard strip for qualitative determination of the result. Criteria for positive *H. pylori* antibody: Red bands appeared at both the quality control line and the test line. Criteria for negative *H. pylori* antibody: A red band appeared at the quality control line, while no red band appeared at the test line.

Statistical analysis

SPSS 25.0 statistical software was used for statistical analysis of relevant data. Measurement data conforming to the normal distribution were expressed as mean ± SD, and the *t* test was used for comparison between two groups. Measurement data not conforming to the normal distribution were expressed as median (interquartile range) [M (Q1, Q3)], and the non-parametric test was used for comparison between two groups. Enumeration data were described by frequency or constituent ratio, and the χ^2 test was used for comparison between groups. Indicators with statistical significance in the univariate analysis were included in the multivariate Logistic regression analysis. P values < 0.05 were considered to indicate a statistically significant difference.

RESULTS

General data

A total of 4361 participants were included in the study, among whom 1699 were male and 2662 were female. The age range was from 4 to 90 years old, with an average age of 50.1 ± 15.3 years. The overall *H. pylori* infection rate was 70.79% (3087/4361). The *H. pylori* infection rate first increased and then decreased with the increase of age, and the difference was statistically significant (Z = -2.696, P < 0.05) (The *H. pylori* infection rates in different regions are shown in Figure 3). The *H. pylori* infection rate in Hotan was the highest, reaching 88%, while that in Yanqi was the lowest, at 37.21%. The difference was statistically significant (χ^2 = 250.269, P < 0.01). Among different ethnic groups, the *H. pylori* infection rates of Han and Hui ethnic groups were relatively low, at 60.30% and 49.25% respectively, while those of Uyghur, Kirgiz, and Tajik ethnic groups were relatively high, at 77.33%, 77.50%, and 89.05% respectively. The differences in *H. pylori* infection rates among ethnic groups were statistically significant (χ^2 = 182.478, P < 0.01). There was also a significant difference in family income (Z = -2.534, P < 0.01). Among different altitude regions, the *H. pylori* infection rate showed a gradually increasing trend with the increase of altitude, and the difference was statistically significant (Z = -3.914, P < 0.01; Table 1).

Correlation analysis of different lifestyles, dietary habits and H. pylori infection

The analysis results show that the prevalence of *H. pylori* infection is associated with numerous factors. Among the factors related to dietary habits, in descending order of their degree of correlation with the prevalence of infection, are as follows: Frequent consumption of beef (χ^2 = 6.058, P < 0.01), mutton (χ^2 = 17.496, P < 0.01), various common dried nuts, such as

Table 1 Analysis of the demographic characteristics with *Helicobacter pylori* Infection, *n* (%)

Variables	Number	*H. pylori*-positive	*H. pylori*-negative	χ^2	*P* value
Gender	4361				
Male	1699	1214 (71.45)	485 (28.55)	0.599	0.439
Female	2662	1873 (70.36)	789 (29.64)		
Age, years	4361				
≤ 29	478	347 (72.59)	131 (27.41)	-2.601	0.009
30-39	615	450 (73.17)	165 (26.83)		
40-49	855	610 (71.35)	245 (28.65)		
50-59	1179	844 (71.59)	335 (28.41)		
≥ 60	1234	836 (67.75)	398 (32.25)		
Ethnicity	4361				
Han	947	571 (60.30)	376 (39.70)	182.791	< 0.001
Uyghur	1650	1276 (77.33)	374 (22.27)		
Kazak	1053	741 (70.37)	312 (29.63)		
Hui	266	131 (49.25)	135 (50.75)		
Kirgiz	200	155 (77.50)	45 (22.50)		
Tajik	210	187 (89.05)	23 (10.95)		
Other	35	26 (74.29)	9 (25.71)		
Marriage	4177				
Married	3629	2567 (70.74)	1062 (29.26)	3.136	0.371
Unmarried	359	263 (73.26)	96 (26.74)		
Divorced	53	41 (77.36)	12 (22.64)		
Widowed	136	91 (66.91)	45 (33.09)		
Occupation	4361				
Farmer	2201	1558 (70.79)	643 (29.21)	8.378	0.079
Herdsman	366	249 (68.03)	117 (31.97)		
Clerk	655	458 (69.92)	197 (30.08)		
Self-employed and freelance	335	225 (67.16)	110 (32.84)		
Other	804	597 (74.25)	207 (25.75)		
Family income (China Yuan)	3799				
≤ 3000	2408	1747 (72.55)	661 (27.45)	-2.534	0.011
3000-6000	970	677 (69.79)	293 (30.21)		
≥ 6000	421	282 (66.98)	139 (33.02)		
Education level	3618				
Primary education and below	1376	974 (70.78)	402 (29.22)	4.01	0.405
Junior high school	1024	740 (72.27)	284 (27.73)		
Senior high school and secondary vocational school	534	378 (70.79)	156 (29.21)		
Junior college and undergraduate	676	486 (71.89)	190 (28.11)		
Postgraduate	8	8 (100)	0		
BMI, kg/m^2	4161				
< 18.5	227	163 (71.81)	64 (28.19)	-0.081	0.935
18.5-23.9	1482	1042 (70.31)	440 (29.69)		

24.0-27.9	1400	983 (70.21)	417 (29.79)		
≥ 28	1052	746 (70.91)	306 (29.09)		
Altitude of habitation (m)	4361				
Low (< 1000)	2154	1482 (68.80)	672 (31.20)	-3.914	< 0.001
Medium (1000-2000)	1902	1348 (70.87)	554 (29.13)		
Medium to high (2000-4000)	305	257 (84.26)	48 (15.74)		

H. pylori: *Helicobacter pylori*; BMI: Body mass index.

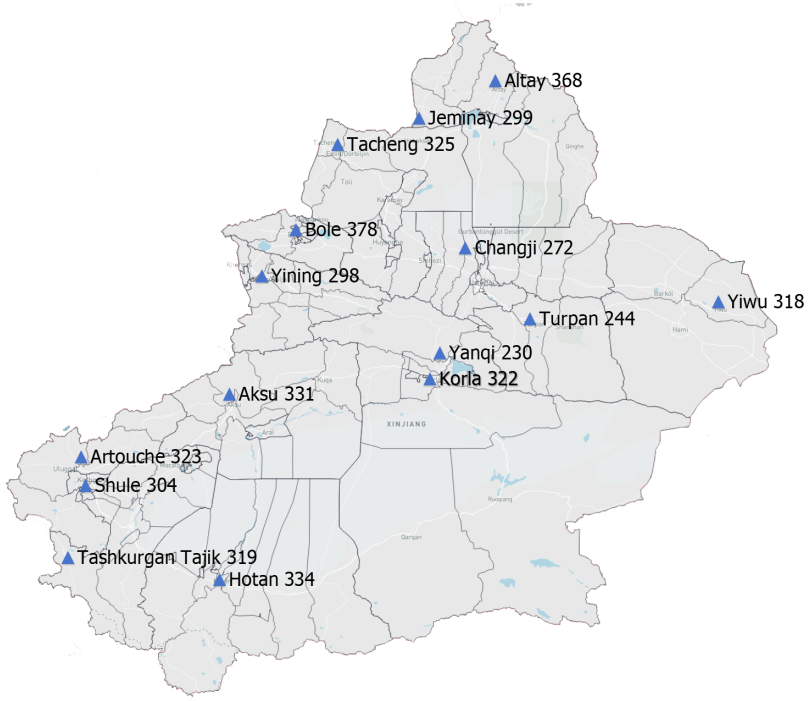

Figure 1 The distribution of the survey locations and the number of participants in Xinjiang Uygur Autonomous Region.

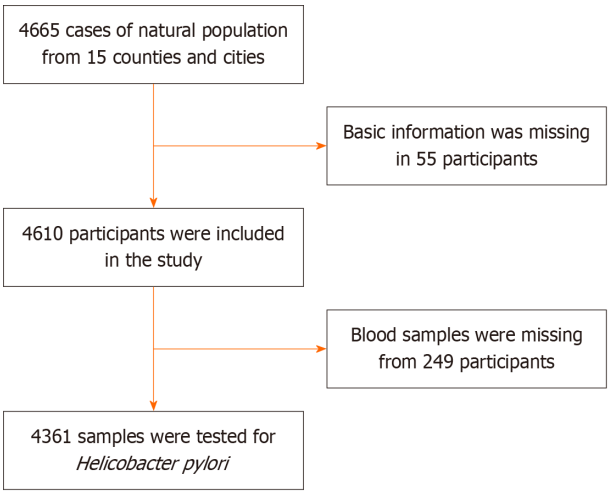

Figure 2 Flowchart of participant selection.

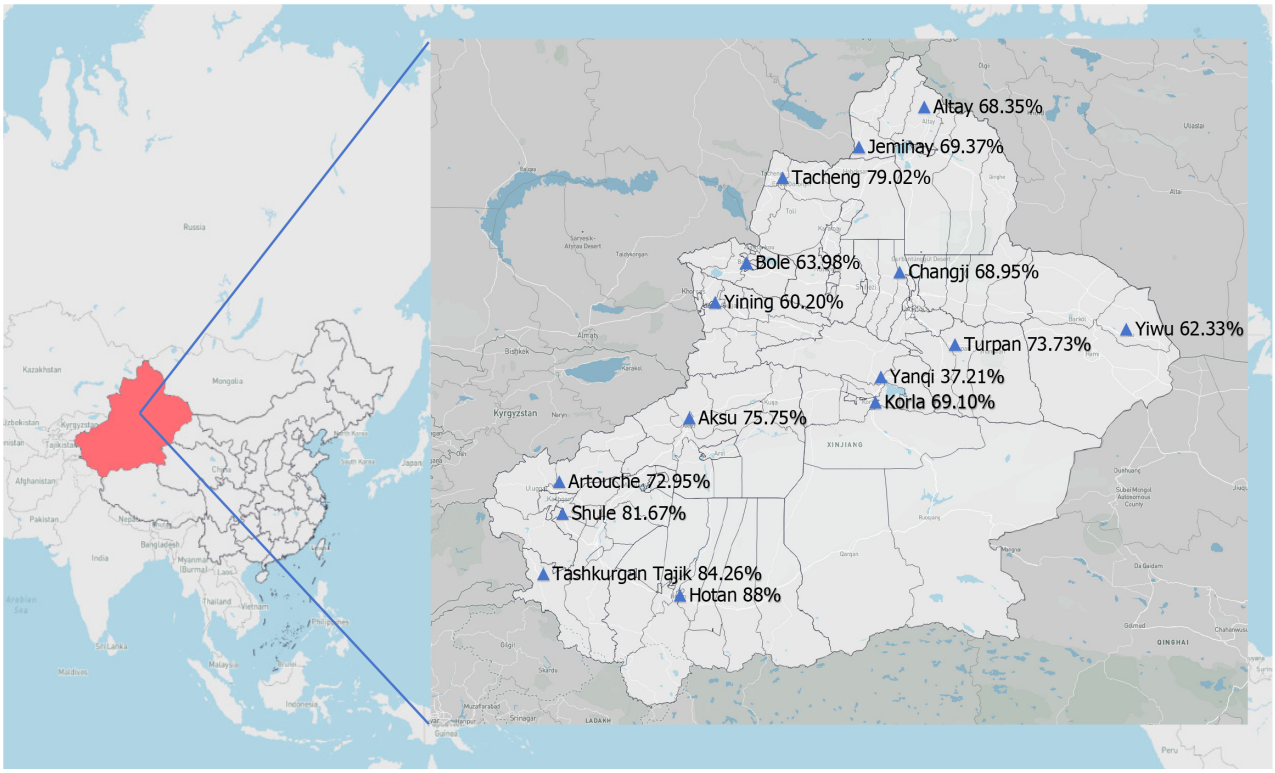

Figure 3 ***Helicobacter pylori*** **infection rates in different regions.**

almonds, apricot kernels, raisins, red dates, walnuts, *etc.*, (χ^2 = 16.688, P < 0.01), barbecue foods (χ^2 = 10.030, P < 0.01), and cured meats, such as cured pork and Chinese sausage (χ^2 = 5.937, P < 0.05). Moreover, the behavior of sharing tableware or not (χ^2 = 6.797, P < 0.01) and the situation of drinking river water or not (χ^2 = 13.734, P < 0.01) are also correlated with the prevalence of *H. pylori* infection (Table 2).

Multivariate logistic regression analysis of factors associated with H. pylori infection

Important variables were included in the multivariate Logistic regression model. Further analysis revealed that altitude [odds ratio (OR): 1.219, 95%CI: 1.068-1.392], regular consumption of beef (OR: 1.327, 95%CI: 1.115-1.580), regular consumption of mutton (OR: 1.351, 95%CI: 1.125-1.622), regular consumption of dried nuts (OR: 1.225, 95%CI: 1.035-1.451), regular consumption of barbecue foods (OR: 1.380, 95%CI: 1.084-1.757), and drinking river water (OR: 2.062, 95%CI: 1.374-3.094) were positively correlated with *H. pylori* infection (Table 3).

DISCUSSION

This study is the first large-scale cross-sectional survey on the prevalence of *H. pylori* and its risk factors in Xinjiang Uygur Autonomous Region. The results show that the *H. pylori* infection rate in the natural population of Xinjiang Uygur Autonomous Region is 70.79%, which is significantly higher than the average *H. pylori* infection rate in China. Studies indicate that the global *H. pylori* infection rate is approximately 48.9%. Regionally, the infection rates are as follows: The Eastern Mediterranean region (59.1%), the African region (58.3%), the European region (47.5%), the Americas region (46.9%), the Western Pacific region (46.8%), and the Southeast Asian region (46.6%)[4]. A meta-analysis spanning from 1990 to 2019 shows that the *H. pylori* infection rate in mainland China is 44.2%, with an estimated 589 million people infected. Regionally, the infection rates are as follows: The Northwest region (51.8%), the East China region (47.7%), and the Southwest region (46.6%)[13]. The analysis of previous relevant research findings in this region indicates that the *H. pylori* infection rate here is at a relatively high level, with significant regional disparities ranging from 51.08% to 61.99% [14,15]. Since this region is situated in the western part of China and covers a vast region, it follows that there are differences in the levels of social and economic development, public health conditions, as well as dietary and living habits among different areas. These factors are highly likely to be the reasons for the relatively high *H. pylori* infection rate in this region. The study found that the *H. pylori* infection rate first increases and then decreases with the increase of age, which is consistent with other reports[16,17].

Many studies suggest that the relatively high *H. pylori* infection rate in Xinjiang Uygur Autonomous Region may be related to lifestyle, medical and health conditions, and economic factors. Based on this, this paper further analyzes the correlation between different lifestyles, dietary habits, and the *H. pylori* infection rate[15,18,19]. Through a random sampling method, this study analyzed the *H. pylori* infection rate in 15 regions of Xinjiang Uygur Autonomous Region and found that there are differences in the *H. pylori* infection rate among different regions, ethnic groups, and altitude regions

Table 2 Correlation analysis of *Helicobacter pylori* infection with lifestyles and dietary habits, *n* (%)

Variables	Number	*H. pylori*-positive	*H. pylori*-negative	χ^2	*P* value
Smoking	4361				
Yes	660	465 (70.45)	195 (29.55)	0.041	0.839
No	3701	2622 (70.85)	1079 (29.15)		
Drinking	4361				
Yes	521	358 (68.71)	163 (31.29)	1.229	0.268
No	3840	2729 (71.07)	1111 (28.93)		
Regular consumption of fruits	4267				
Yes	2798	1973 (70.51)	825 (29.49)	0.318	0.573
No	1469	1048 (71.34)	421 (28.65)		
Regular consumption of vegetables	4267				
Yes	3782	2673 (70.68)	1109 (29.32)	0.241	0.624
No	485	348 (71.75)	137 (28.25)		
Regular consumption of beef	3943				
Yes	1472	1069 (72.62)	403 (27.38)	6.058	0.014
No	2471	1703 (68.92)	768 (31.08)		
Regular consumption of mutton	4100				
Yes	2882	2099 (72.83)	783 (27.17)	17.496	0
No	1218	808 (66.34)	410 (33.66)		
Regular consumption of dairy products	4065				
Yes	685	508 (74.16)	177 (25.84)	3.594	0.058
No	3380	2385 (70.56)	995 (29.44)		
Regular consumption of dried nuts	3799				
Yes	1558	1167 (74.90)	391 (25.10)	16.688	0
No	2241	1542 (68.81)	699 (31.19)		
Regular consumption of spicy and strong-flavored foods	4016				
Yes	751	520 (69.24)	231 (30.76)	2	0.185
No	3265	2340 (71.67)	925 (28.33)		
Regular consumption of barbecued foods	3728				
Yes	633	484 (76.46)	149 (23.54)	10.03	0.002
No	3095	2173 (70.21)	922 (29.79)		
Frequent consumption of preserved meat	3747				
Yes	259	202 (77.99)	57 (22.01)	5.937	0.015
No	3488	2473 (70.90)	1015 (29.10)		
Used tableware in a mixed way	3740				
Yes	2069	1508 (72.89)	561 (27.11)	6.797	0.009
No	1671	1153 (69.00)	518 (31.00)		
Share dental sets	3698				
Yes	159	108 (67.93)	51 (32.07)	0.811	0.368
No	3539	2521 (71.24)	1018 (28.76)		
Drink river water	3812				
Yes	235	193 (82.13)	42 (17.87)	13.734	0

No	3577	2535 (70.87)	1042 (29.13)		
Eat regularly	3830				
Yes	3103	514 (70.70)	213 (29.30)	0.272	0.602
No	727	2224 (71.67)	879 (28.33)		
Engorgement	3834				
Yes	401	274 (68.33)	127 (31.67)	2.198	0.138
No	3433	2467 (71.86)	966 (28.14)		

H. pylori: *Helicobacter pylori*.

Table 3 Multivariate analysis of *Helicobacter pylori* infection

Variable	OR	95%CI	*P* value
Altitude	1.219	1.068-1.392	0.003
Regular consumption of beef	1.327	1.115-1.580	0.001
Regular consumption of mutton	1.351	1.125-1.622	0.001
Regular consumption of dried nuts	1.225	1.035-1.451	0.019
Regular consumption of barbecue foods	1.380	1.084-1.757	0.009
Drink river water	2.062	1.374-3.094	0.000

OR: Odds ratio.

in Xinjiang Uygur Autonomous Region. This may be due to the ethnic differences of the permanent residents in different areas. In the southern regions, ethnic minorities such as Uyghur, Tajik, and Kirgiz are the main groups, while in the northern regions, nomads such as Kazakhs are predominant. And the lack of awareness of the prevention and treatment of *H. pylori* infection, as well as differences in hygiene and economy, result in serious cross - infection and family - clustered infection, which is consistent with previous studies[20-22]. This study shows that family income is related to *H. pylori* infection. The infection rate shows a downward trend with the increase of family income. Currently, relevant domestic and foreign reports suggest that the *H. pylori* infection rate is related to family income, hygiene conditions, and economic resources. The higher the family income, the lower the infection rate, which is consistent with the results of this study[23-26]. This survey shows that the *H. pylori* infection rate is relatively high in those who often consume beef and mutton. As the main sources of meat products in this region, beef and mutton are consumed frequently. Due to the characteristic cooking and eating habits in this region, they are often prepared in ways such as pilaf, boiled lamb, and barbecue, which increases the risk of *H. pylori* infection. This survey found that the frequent consumption of dried nuts snacks such as almonds, raisins, and red dates is related to *H. pylori* infection. Xinjiang Uygur Autonomous Region dried nuts are deeply loved by people because of their rich nutrition and excellent quality. In most families in this region, dried fruits are self - made by natural sun - drying. *H. pylori* are likely to parasitize on the surface of the food, which may increase the risk of infection. Research reports indicate that salt can disrupt the integrity of the gastric mucosa, promote the colonization of *H. pylori*, ultimately triggering inflammation, and accelerate the occurrence of gastric cancer[25].

There are many factors influencing *H. pylori* infection. Besides the factors mentioned above, studies have shown that consuming street snacks and dining out are positively correlated with *H. pylori* infection[27]. The results of this study indicate that the *H. pylori* infection rate is higher among those who frequently consume foods like barbecue and cured meat. It is speculated that this might be related to the relatively high salt content in these foods, as well as the possible generation of carcinogenic substances such as N-nitroso compounds during the processing. These substances can stimulate gastric acid secretion, causing acute damage to the gastric mucosa and increasing the incidence of *H. pylori* infection. Additionally, during the cooking process of barbecue foods, there may be issues such as inadequate heating and sub-standard hygiene conditions[26]. This study found that sharing tableware is associated with *H. pylori* infection. As a chronic infectious disease, *H. pylori* exhibits a family-clustering phenomenon, and sharing tableware may contribute to the transmission of *H. pylori*. An epidemiological review has proposed that drinking well water is a risk factor for *H. pylori* infection, and *H. pylori* DNA has been detected in samples of river water, seawater, well water, and drinking water[27,28]. Some studies also believe that the aquatic environment and sewage sludge potentially play a role in the transmission of *H. pylori* infection[29]. This further supports the findings of this study, namely that the *H. pylori* infection rate is higher among people who drink river water. In Xinjiang Uygur Autonomous Region, many farmers and herdsmen live in mountainous areas where water resources for drinking are limited. The river water they drink may not meet the hygiene standards and may not be adequately heated, both of which can increase the risk of *H. pylori* exposure.

The multivariate Logistic regression analysis of this study shows that the altitude of the regions, a preference for beef and mutton, dried nuts, barbecue foods, and drinking river water are independent risk factors for *H. pylori* infection. Xinjiang's unique geographical feature of "three mountains enclosing two basins" leads to diverse landforms and significant altitude differences. High-altitude areas are inhabited by nomadic ethnic groups. The unique dietary patterns, scarce living resources, and insufficient awareness of disinfection and hygiene all increase the risk of *H. pylori* infection. The multiple poor living and dietary hygiene habits contribute to the relatively high *H. pylori* infection rate in this region. Therefore, more intensive publicity and education on *H. pylori* infection, more accurate screening methods, and more effective eradication strategies should be adopted to reduce the *H. pylori* infection rates among different populations in this region.

This study has certain limitations. Firstly, this study employed the immunochromatographic antibody method to detect *H. pylori* infection. Due to the fact that the antibodies produced by previous infections will persist in the body for a certain period of time, this detection method may lead to the statistical result of the *H. pylori* infection rate being slightly higher than the actual level. Secondly, there are some missing data in the study. After discovering this issue, we carried out a meticulous verification of the original questionnaires and data entry processes, and supplemented the missing data of some variables. However, there is still a small amount of data that cannot be filled. Given that the data sources of this study are real and reliable, the sample size is large, and it has broad representativeness, we judge that the remaining data can still accurately reflect the actual situation and will not have a serious impact on the accuracy of the research results. In conclusion, this study is the first large - scale cross - sectional survey on *H. pylori* infection among the general population in the Xinjiang Uygur Autonomous Region. The research findings not only provide detailed data for understanding the status of *H. pylori* infection and analyzing the risk factors for infection in the Xinjiang Uygur Autonomous Region, but also provide valuable references for the prevention and treatment of *H. pylori* infection in the local area. In addition, the results of this study can also provide guidelines for policymakers, helping to address the problem of the high prevalence of *H. pylori* and promoting the precise formulation and effective implementation of prevention and control measures.

CONCLUSION

In conclusion, this study clearly indicates that the infection rate of *H. pylori* in Xinjiang Uygur Autonomous Region is relatively high, and there are significant differences between regions and ethnic groups. The analysis shows that the altitude of the place of residence, the preference for beef, mutton, dried nuts, barbecued foods, and the consumption of river water are independent risk factors for the infection. In order to reduce the infection rate among different populations, it is necessary to vigorously strengthen the popularization of knowledge about *H. pylori* infection, promote accurate and efficient screening methods, formulate scientific, reasonable, and practical eradication strategies, and safeguard the health of the public in an all-round way.

ACKNOWLEDGEMENTS

We express our gratitude to all individuals who agreed to participate in this study, as well as the medical and technical personnel involved. Additionally, we would like to thank Shenzhen Bioloot Biological Products Co., Ltd. for providing the *H. pylori* antibody detection kit.

FOOTNOTES

Author contributions: Jiang Q, Liu WD, Hui WJ, Kong WJ, and Gao F conceived the experiment; Huang XL, Feng Y, and Kuerbanjiang A conducted the experiment and analyzed the results; Jiang Q, Liu WD, and Hui WJ wrote the manuscript; Gao F supervised the project, administered it, and acquired funding; All authors have read and agreed to the published version of the manuscript.

Supported by Central Government Guide Local Science and Technology Development Special Fund Project, No. ZYYD2024JD11 and No. ZYYD2022A06; and Natural Science Foundation of Xinjiang Uygur Autonomous Region, No. 2024D01C76.

Institutional review board statement: This study was conducted in accordance with the principles of the Declaration of Helsinki, and was approved by the Ethics Committee of People's Hospital of Xinjiang Uygur Autonomous Region, No. KY2022060173.

Informed consent statement: Written informed consent was obtained from each participant.

Conflict-of-interest statement: All the authors report no relevant conflicts of interest for this article.

Data sharing statement: The data supporting the findings of this study are available from the corresponding author upon reasonable request at xjgf@sina.com.

STROBE statement: The authors have read the STROBE Statement—checklist of items, and the manuscript was prepared and revised according to the STROBE Statement—checklist of items.

Country of origin: China

ORCID number: Qi Jiang 0009-0007-6081-905X; Wei-Dong Liu 0000-0002-7384-6651; Wen-Jia Hui 0000-0001-6055-1339; Wen-Jie Kong 0000-0003-1480-9583; Yan Feng 0000-0002-0185-3457; Aihemaijiang Kuerbanjiang 0000-0002-7096-3983; Xiao Ling Huang 0000-0002-1207-9890; Feng Gao 0000-0002-3320-5702.

S-Editor: Li L
L-Editor: A
P-Editor: Wang WB

REFERENCES

1 **Li M**, Gao N, Wang SL, Guo YF, Liu Z. Hotspots and trends of risk factors in gastric cancer: A visualization and bibliometric analysis. *World J Gastrointest Oncol* 2024; **16**: 2200-2218 [PMID: 38764808 DOI: 10.4251/wjgo.v16.i5.2200] [FullText]
2 **Yang L**, Kartsonaki C, Yao P, de Martel C, Plummer M, Chapman D, Guo Y, Clark S, Walters RG, Chen Y, Pei P, Lv J, Yu C, Jeske R, Waterboer T, Clifford GM, Franceschi S, Peto R, Hill M, Li L, Millwood IY, Chen Z; China Kadoorie Biobank Collaborative Group. The relative and attributable risks of cardia and non-cardia gastric cancer associated with Helicobacter pylori infection in China: a case-cohort study. *Lancet Public Health* 2021; **6**: e888-e896 [PMID: 34838195 DOI: 10.1016/S2468-2667(21)00164-X] [FullText]
3 **Sharma R**. Burden of Stomach Cancer Incidence, Mortality, Disability-Adjusted Life Years, and Risk Factors in 204 Countries, 1990-2019: An Examination of Global Burden of Disease 2019. *J Gastrointest Cancer* 2024; **55**: 787-799 [PMID: 38265570 DOI: 10.1007/s12029-023-01005-3] [FullText]
4 **Li Y**, Choi H, Leung K, Jiang F, Graham DY, Leung WK. Global prevalence of Helicobacter pylori infection between 1980 and 2022: a systematic review and meta-analysis. *Lancet Gastroenterol Hepatol* 2023; **8**: 553-564 [PMID: 37086739 DOI: 10.1016/S2468-1253(23)00070-5] [FullText]
5 **Hooi JKY**, Lai WY, Ng WK, Suen MMY, Underwood FE, Tanyingoh D, Malfertheiner P, Graham DY, Wong VWS, Wu JCY, Chan FKL, Sung JJY, Kaplan GG, Ng SC. Global Prevalence of Helicobacter pylori Infection: Systematic Review and Meta-Analysis. *Gastroenterology* 2017; **153**: 420-429 [PMID: 28456631 DOI: 10.1053/j.gastro.2017.04.022] [FullText]
6 **Gong Y**, Luo Y, Chen Z, Sui Y, Zheng Y. Longitudinal analysis of factors related to Helicobacter pylori infection in Chinese adults. *Open Med (Wars)* 2022; **17**: 1742-1749 [PMID: 36407872 DOI: 10.1515/med-2022-0564] [FullText]
7 **Li M**, Sun Y, Yang J, de Martel C, Charvat H, Clifford GM, Vaccarella S, Wang L. Time trends and other sources of variation in Helicobacter pylori infection in mainland China: A systematic review and meta-analysis. *Helicobacter* 2020; **25**: e12729 [PMID: 32686261 DOI: 10.1111/hel.12729] [FullText]
8 **Wang Z**, Hu Y, Fei R, Han W, Wang X, Chen D, She S. Tracking the Helicobacter pylori Epidemic in Adults and Children in China. *Helicobacter* 2024; **29**: e13139 [PMID: 39342457 DOI: 10.1111/hel.13139] [FullText]
9 **Zhang WD**, Hu FL, Xiao SD, Xu ZM. [Prevalence of Helicobacter pylori infection in China]. *Xiandai Xiaohua Ji Jieru Zhenliao* 2010; **15**: 265-270 [DOI: 10.3969/j.issn.1672-2159.2010.05.001] [FullText]
10 **Zhang F**, Pu K, Wu Z, Zhang Z, Liu X, Chen Z, Ye Y, Wang Y, Zheng Y, Zhang J, An F, Zhao S, Hu X, Li Y, Li Q, Liu M, Lu H, Zhang H, Zhao Y, Yuan H, Ding X, Shu X, Ren Q, Gou X, Hu Z, Wang J, Wang Y, Guan Q, Guo Q, Ji R, Zhou Y. Prevalence and associated risk factors of Helicobacter pylori infection in the Wuwei cohort of north-western China. *Trop Med Int Health* 2021; **26**: 290-300 [PMID: 33159827 DOI: 10.1111/tmi.13517] [FullText]
11 **Zhou Y**, Deng Y, You Y, Li X, Zhang D, Qi H, Shi R, Yao L, Tang Y, Li X, Ma L, Li Y, Liu J, Feng Y, Chen X, Hao Q, Li X, Li Y, Niu M, Gao H, Bai F, Hu S. Prevalence and risk factors of Helicobacter pylori infection in Ningxia, China: comparison of two cross-sectional studies from 2017 and 2022. *Am J Transl Res* 2022; **14**: 6647-6658 [PMID: 36247252] [FullText]
12 **Li BY**, Pan BT, Han JF. [Basic terrestrial geomorphological types in China and their circumscriptions]. *Disiji Yanjiu* 2008; **28**: 535-543 [DOI: 10.3321/j.issn:1001-7410.2008.04.004] [FullText]
13 **Ren S**, Cai P, Liu Y, Wang T, Zhang Y, Li Q, Gu Y, Wei L, Yan C, Jin G. Prevalence of Helicobacter pylori infection in China: A systematic review and meta-analysis. *J Gastroenterol Hepatol* 2022; **37**: 464-470 [PMID: 34862656 DOI: 10.1111/jgh.15751] [FullText]
14 **Guo XW**, Wang J, Feng H, Abrikmu, Xu AY, Liao QS. [The epidemiological lunestiqation of Helicobacter Pylori infection in the region of Aksn, Xinjiang]. *Xinjiang Yike Daxue Xuebao* 2009; **32**: 728-730 [DOI: 10.3969/j.issn.1009-5551.2009.06.022] [FullText]
15 **Wang ZF**, Cao W, Yang XM, Hu ZQ. [Helicobacter pylori infection in the population undergoing physical examination in Kashi, Xinjiang Analysis of current situation and related factors]. *Linchuang Neike Zazhi* 2024; **41**: 550-553 [DOI: 10.3969/j.issn.1001-9057.2024.08.012] [FullText]
16 **Cai L**, Yi B, Zhang M, Ni M, Hu JH, Peng Z, Ba S. [Epidemiological investigation of Helicobacter pylori infection in Lhasa region]. *Zhonghua Xiaohua Zazhi* 2018; **38**: 2-6 [DOI: 10.3760/cma.j.issn.0254-1432.2018.01.002] [FullText]
17 **Zou JC**, Wen MY, Huang Y, Chen XZ, Hu JK; SIGES Research Group. Helicobacter pylori infection prevalence declined among an urban health check-up population in Chengdu, China: a longitudinal analysis of multiple cross-sectional studies. *Front Public Health* 2023; **11**: 1128765 [PMID: 38089026 DOI: 10.3389/fpubh.2023.1128765] [FullText]
18 **Fang MZ**, Niu SP, Wang JH, Chu GM, Yuan XR. [Current situation and importance analysis of Helicobacter pylori infection in a certain area]. *Shijie Zuixin Yixue Xinxi Wenzhai* 2018; **18**: 193 [DOI: 10.19613/j.cnki.1671-3141.2018.93.166] [FullText]
19 **Fen Q**, Zuo QQ, Yuan XR. [Investigation and analysis of Helicobacter pylori infection in Karamay area]. *Guoji Jianyan Yixue Zazhi* 2016; **37**:

2913-2915 [DOI: 10.3969/j.issn.1673-4130.2016.20.048] [FullText]

20 **Zhang Y**, Cui YH. [Analysis of Helicobacter pylori infection rate in different population in Turpan area]. *Zhongguo Shiyong Yiyao* 2012; **7**: 75-76 [DOI: 10.14163/j.cnki.11-5547/r.2012.26.114] [FullText]

21 **Bai D**, Liu K, Wang R, Zhang WH, Chen XZ, Hu JK. Prevalence Difference of Helicobacter pylori Infection Between Tibetan and Han Ethnics in China: A Meta-analysis on Epidemiologic Studies (SIGES). *Asia Pac J Public Health* 2023; **35**: 103-111 [PMID: 36321513 DOI: 10.1177/10105395221134651] [FullText]

22 **Li Y**, Li SH, Ma ZQ, Zhan YH, Shen LJ, Wang F, Li CX, Li YH, Zhang MJ, Wang XH. [Prevalence and risk factors of Helicobacter pylori infection in Qinghai Province]. *Zhonghua Xiaohua Zazhi* 2022; **42**: 604-609 [DOI: 10.3760/cma.j.cn311367-20220504-00206] [FullText]

23 **Wang X**, Shu X, Li Q, Li Y, Chen Z, Wang Y, Pu K, Zheng Y, Ye Y, Liu M, Ma L, Zhang Z, Wu Z, Zhang F, Guo Q, Ji R, Zhou Y. Prevalence and risk factors of Helicobacter pylori infection in Wuwei, a high-risk area for gastric cancer in northwest China: An all-ages population-based cross-sectional study. *Helicobacter* 2021; **26**: e12810 [PMID: 33904635 DOI: 10.1111/hel.12810] [FullText]

24 **Chen RX**, Zhang DY, Zhang X, Chen S, Huang S, Chen C, Li D, Zeng F, Chen J, Mo C, Gao L, Zeng J, Xiong J, Chen Z, Bai F. A survey on Helicobacter pylori infection rate in Hainan Province and analysis of related risk factors. *BMC Gastroenterol* 2023; **23**: 338 [PMID: 37777740 DOI: 10.1186/s12876-023-02973-3] [FullText]

25 **She X**, Zhao J, Cheng S, Shi H, Dong L, Zhao P. Prevalence of and risk factors for Helicobacter pylori infection in rural areas of Northwest China: A cross-sectional study in two villages of Yan'an city. *Clinl Epidemiol Glob* 2023; **21**: 101294 [DOI: 10.1016/j.cegh.2023.101294] [FullText]

26 **Cui Y**, Jin Y, Liu XL, Gong M, Wu WJ. [Hp infection rate, antibody typing and logistic regression analysis of 1 111 physical examination people in plateau area]. *Gonggong Weisheng Yu Yufang Yixue* 2024; **35**: 53-56 [DOI: 10.3969/j.issn.1006-2483.2024.02.012] [FullText]

27 **Sjomina O**, Pavlova J, Niv Y, Leja M. Epidemiology of Helicobacter pylori infection. *Helicobacter* 2018; **23** Suppl 1: e12514 [PMID: 30203587 DOI: 10.1111/hel.12514] [FullText]

28 **Monno R**, De Laurentiis V, Trerotoli P, Roselli AM, Ierardi E, Portincasa P. Helicobacter pylori infection: association with dietary habits and socioeconomic conditions. *Clin Res Hepatol Gastroenterol* 2019; **43**: 603-607 [PMID: 30905666 DOI: 10.1016/j.clinre.2018.10.002] [FullText]

29 **Mezmale L**, Coelho LG, Bordin D, Leja M. Review: Epidemiology of Helicobacter pylori. *Helicobacter* 2020; **25** Suppl 1: e12734 [PMID: 32918344 DOI: 10.1111/hel.12734] [FullText]

World Journal of Gastroenterology

Submit a Manuscript: https://www.f6publishing.com

World J Gastroenterol 2025 June 7; 31(21): 107395

DOI: 10.3748/wjg.v31.i21.107395

ISSN 1007-9327 (print) ISSN 2219-2840 (online)

ORIGINAL ARTICLE

Basic Study

Electroacupuncture at ST36 ameliorates gastric dysmotility in rats with diabetic gastroparesis *via* the nucleus tractus solitarius-vagal axis

You Zhang, Yi-Wen Tang, Jin Zhou, Yan-Rong Wei, Yu-Ting Peng, Zi Yan, Zeng-Hui Yue

Specialty type: Gastroenterology and hepatology

Provenance and peer review: Unsolicited article; Externally peer reviewed.

Peer-review model: Single blind

Peer-review report's classification

Scientific Quality: Grade A, Grade A, Grade B

Novelty: Grade A, Grade B, Grade C

Creativity or Innovation: Grade A, Grade B, Grade B

Scientific Significance: Grade A, Grade B, Grade B

P-Reviewer: Tang C; Xie YL

Received: March 23, 2025

Revised: April 11, 2025

Accepted: May 23, 2025

Published online: June 7, 2025

Processing time: 75 Days and 24 Hours

You Zhang, Yi-Wen Tang, Jin Zhou, Yan-Rong Wei, Yu-Ting Peng, Zi Yan, Zeng-Hui Yue, College of Acupuncture, Massage and Rehabilitation, Hunan University of Chinese Medicine, Changsha 410208, Hunan Province, China

Corresponding author: Zeng-Hui Yue, FACE, College of Acupuncture, Massage and Rehabilitation, Hunan University of Chinese Medicine, No. 300 Bachelor Road, Yuelu District, Changsha 410208, Hunan Province, China. yue5381316@126.com

Abstract

BACKGROUND

Diabetic gastroparesis (DGP), characterized by delayed gastric emptying and impaired motility, poses significant therapeutic challenges due to its complex neural and molecular pathophysiology. Emerging evidence suggests that electroacupuncture (EA) at ST36 modulates gastrointestinal function; however, the precise neuromolecular pathways underlying its efficacy in DGP remain incompletely defined.

AIM

To elucidate the neural mechanisms underlying EA at ST36 improving DGP gastric motility through the nucleus tractus solitarius (NTS)-vagal axis.

METHODS

The DGP model was established *via* a single high-dose intraperitoneal injection of 2% streptozotocin combined with an 8-week high-sugar/high-fat diet. Interventions included EA at ST36, pharmacological modulation [choline acetyltransferase (ChAT) agonist polygalacic acid (PA) and inhibitor antagonist alpha-NETA], and subdiaphragmatic vagotomy. Post-intervention observations included body weight and blood glucose levels. Gastric emptying was evaluated using phenol red assays, gastric slow-wave recordings, and dynamic positron emission tomography-computed tomography imaging. Histopathological analysis (hematoxylin-eosin staining) and molecular assessments (Western blot, immunofluorescence) were performed to quantify gastric smooth muscle-associated factors [neuronal nitric oxide synthase (nNOS), cluster of differentiation 117 (C-kit), stem cell factor (SCF)] and vagal targets [ChAT, α7 nicotinic acetylcholine receptor (α7nAChR)] in the ST36 acupoint region, L4-L6 spinal segments, and NTS. Gastrointestinal

peptides [gastrin (Gas), motilin (MLT) and vasoactive intestinal peptide (VIP)] were measured *via* enzyme-linked immunosorbent assay.

RESULTS

The study found that EA significantly increased the rate of gastric emptying, restored the slow-wave rhythms of the stomach, and improved the architecture of the smooth muscles in the stomach. This was evidenced by a reduction in inflammatory infiltration and an increase in the expression of nNOS, C-kit, and SCF. Mechanistically, EA activated vagal targets (ChAT and α7nAChR) at ST36, transmitting signals *via* spinal segments L4-L6 to the NTS, subsequently regulating gastrointestinal peptides (Gas, MLT, VIP) and restoring interstitial cells of Cajal (ICCs) function *via* subdiaphragmatic vagal efferent pathways. It is crucial to note that subdiaphragmatic vagotomy led to the abrogation of EA-induced enhancements in gastric motility and ICC recovery, thereby confirming the indispensable role of vagal efferent signalling.

CONCLUSION

EA provides a novel molecular mechanism for improving gastrointestinal motility in DGP *via* a peripheral stimulation (ST36), spinal afferent (L4-L6), brainstem integration (NTS), vagal efferent (gastric) circuit.

Key Words: Electroacupuncture; Diabetic gastroparesis; Vagus nerve; Gastric motility; Interstitial cells of Cajal; Positron emission tomography-computed tomography imaging

Core Tip: Multimodal validation: Electroacupuncture (EA) significantly enhanced gastric emptying (validated by positron emission tomography-computed tomography), restored gastric slow-wave rhythms, and improved smooth muscle architecture *via* upregulation of neuronal nitric oxide synthase, cluster of differentiation 117, stem cell factor. Mechanistic insight: EA activates cholinergic targets (choline acetyltransferas/α7 nicotinic acetylcholine receptor) at ST36, transmits signals *via* spinal L4-L6 afferents to the nucleus tractus solitarius, and modulates gastrointestinal peptides (ghrelin, motilin, vasoactive intestinal peptide) through subdiaphragmatic vagal efferent, ultimately restoring interstitial cells of Cajal function. Translational relevance: Subdiaphragmatic vagotomy abolished EA's therapeutic effects, unequivocally establishing vagal efferent signaling as indispensable.

Citation: Zhang Y, Tang YW, Zhou J, Wei YR, Peng YT, Yan Z, Yue ZH. Electroacupuncture at ST36 ameliorates gastric dysmotility in rats with diabetic gastroparesis *via* the nucleus tractus solitarius-vagal axis. *World J Gastroenterol* 2025; 31(21): 107395
URL: https://www.wjgnet.com/1007-9327/full/v31/i21/107395.htm
DOI: https://dx.doi.org/10.3748/wjg.v31.i21.107395

INTRODUCTION

In 1958, Kassander[1] was the first to describe the association between diabetes and delayed gastric emptying, and he coined the term 'diabetic gastroparesis' (DGP). DGP has been observed to affect 50%-76% of individuals diagnosed with diabetes, with approximately 10% of these cases manifesting overt clinical symptoms, including nausea, vomiting, constipation, diarrhoea, early satiety and dyspepsia, often exacerbated by dietary triggers[2]. The multifactorial pathogenesis of DGP involves dysregulation of the autonomic and enteric nervous systems, smooth muscle dysfunction, abnormalities in interstitial cells of Cajal (ICCs), and gastrointestinal hormone imbalance, which collectively contribute to delayed gastric emptying[3]. Despite its clinical importance, the underlying pathophysiology remains incompletely understood and current therapeutic outcomes are suboptimal.

Electroacupuncture (EA), a modality integrating traditional acupuncture with electrical stimulation, has emerged as a promising intervention for DGP. The clinical guideline: Management of Gastroparesis by the American Gastroenterological Association emphasizes the efficacy of EA, as evidenced by numerous clinical studies[4,5]. Specifically, EA at the ST36 acupoint (Zusanli) has been shown to enhance gastric peristalsis frequency, modulate smooth muscle activity, and restore intrinsic circular currents function[6]. However, the precise mechanisms by which EA exerts its effect on the improvement of gastric motility remain to be elucidated.

Recent advances in the field have served to emphasize the critical role of the vagal pathways in the regulation of the gastrointestinal system. In mammals, the origin of vagal preganglionic neurons, characterized by choline acetyltransferase (ChAT) and α7 nicotinic acetylcholine receptor (α7nAChR) expression, located in the nucleus tractus solitarius (NTS)[7]. Vagal afferent signals activate NTS neurons prior to their synapsing with the dorsal motor nucleus of the vagus (DMV), which in turn relays information to target organs such as the stomach. Retrograde tracing studies demonstrated that gastric-projecting neurons predominantly localise to the DMV and NTS, with additional clusters in the raphe pallidus and lateral paragigantocellular nuclei[8]. Vagal modulation of gastric motility predominantly involves extrinsic autonomic pathways (*e.g.*, vagovagal reflexes) and intrinsic enteric mechanisms. ChAT, the enzyme responsible for

synthesising acetylcholine, is downregulated in DGP models, exacerbating disease progression through impaired cholinergic neurotransmission[9]. Building on these findings, mechanistic studies on EA at ST36 have identified neural regulation as a pivotal factor. Current research focuses on determining whether EA-mediated improvements in DGP involve the NTS-vagal axis, offering potential therapeutic targets for neuromodulation.

MATERIALS AND METHODS

Animal model and grouping

Seventy specific pathogen-free adult male Sprague-Dawley rats, with a weight range of 180-200 g, were supplied by the Animal Experiment Center of Hunan University of Chinese Medicine. The animals were housed under controlled conditions (temperature: 20-25 °C; humidity: 50%-70%) and fed a high-fat diet with free access to water. The bedding was changed on a daily basis, and the cages were disinfected twice a week. All experimental procedures were approved by the Animal Ethics Committee of Hunan University of Chinese Medicine (Approval No. HNUCM21-2311-08).

The DGP model was established as follows[10]: Rats were subjected to 12 hours of fasting, followed by intraperitoneal injection of 2% streptozotocin (STZ) solution (55 mg/kg). The rats were then maintained on a high-fat, high-sugar diet (composition: The composition of this diet was as follows: 58% basal feed, 15% lard, 20% sucrose, 5% milk powder, and 2% eggs). The rats were subjected to this diet for a period of 8 weeks. The DGP model criteria included: Firstly, non-fasting blood glucose levels of ≥ 16.7 mmol/L and secondly, reduced gastric motility and emptying rates in comparison to the Sham group. The rats in the control group were injected with an equivalent volume of sodium citrate buffer (0.1 mmol) and fed a standard diet. Following an eight-week modelling period, the EA group was administered EA at the ST36 acupoint once daily for a period of two weeks. The EA + antagonist alpha-NETA (AP) group received both EA and intra-acupoint injection of the ChAT antagonist AP (4 mg/kg/day, Abcam, United States) for a period of two weeks. The polygalacic acid (PA) group was injected with the ChAT agonist PA (4 mg/kg/day, MCE, United States) for a period of 2 weeks. The subdiaphragmatic vagotomy (SDV) group underwent SDV under isoflurane an aesthesia 8 weeks post-modeling. A 1 cm longitudinal incision was made approximately 0.2 cm to the left of the midline, below the diaphragm, to sever the anterior and posterior branches of the vagus nerve accompanying the esophagus. This was followed by continued high-fat diet feeding for a period of 2 weeks. The EA + SDV group received EA treatment for a period of two weeks following the same surgical procedure.

Intervention methods

Bilateral ST36 acupoints (from the inferior border of the tibial tuberosity, measure 3 cun distally (where 1 cun is defined as the individual's own thumb width at the interphalangeal joint) were punctured vertically to a depth of 5 mm using 25 mm acupuncture needles. Using an EA apparatus (Model SDZ-II; Hwato, China), a dense-disperse wave (20 Hz for disperse wave, 100 Hz for dense wave) was applied with a current intensity of 1 mA, causing slight skin vibration. The needles were left in place for 20 minutes once per day for a period of two weeks. Rats in other groups were anaesthetised and restrained without EA treatment.

Blood glucose and body weight measurement

Non-fasting blood glucose and body weight were recorded on a weekly basis. The rats were then restrained and their tails were disinfected with alcohol swabs. Following the evaporation of the alcohol, a lancet was used to puncture the tail tip and collect blood. The blood glucose levels were then measured using a blood glucose meter. The puncture site was then meticulously cleansed with a cotton ball to prevent infection. Body weight was measured using an electronic scale, and the values were recorded.

Gastric positron emission tomography-computed tomography imaging

Following the conclusion of all treatment protocols, positron emission tomography (PET) scans were conducted utilizing an Inveon microPET scanner (PingSeng Scientific, China). The rats were fasted for over 12 hours and orally administered a contrast agent [68Ga] Ga-NOTA mixed with 0.2 g black sesame paste and 2 mL saline prior to scanning[11]. Dynamic images were continuously acquired from the time of administration up to 60 minutes post-administration. The dynamic data from each scan were divided into 60 frames (0 second × 10, 600 seconds × 10, 1200 seconds × 10, 1800 seconds × 10, 2400 seconds × 10, 3600 seconds × 10). To enhance the visualisation and anatomical alignment of PET images, micro-computed tomography (CT) scans were performed on the rats. CT scans were conducted from the nasal tip to the distal femur in order to capture the entire rat in the optimal field of view. A manual comparison of the acquired CT images was then performed to identify the frame that most closely matched the position and posture of the PET scan. Finally, the PET images were manually superimposed onto the selected CT images.

Image data analysis

A quantitative analysis of PET images was performed using PMOD software (version 4.3) to accurately measure gastric content volume and total radioactivity. The pixel-based adaptive segmenter module was utilized to automatically extract three-dimensional volumes of interest (VOIs) for the stomach of each rat. Total radioactivity and volume were obtained from these VOIs. The radioactive concentration (RC) was then calculated as RC = total radioactivity/volume. The gastric emptying rate (GER) was subsequently calculated, where GER (t) denotes the percentage of gastric content emptied at a specific time point, using the following formula: GER (t) = [1 - RC (max)/RC (t)] × 100%, where RC (max) is the RC at the

initial time point (*e.g.*, 0 minutes).

Gastric slow wave recording

Following a 12-hour fast, rats were anaesthetized with isoflurane and placed in a supine position. Abdominal hair was then shaved, and the skin was disinfected with iodine. A midline incision was then made below the xiphoid process in order to expose the gastric antrum. Needle electrodes were then inserted into the smooth muscle layer of the antrum, at a point approximately 0.5 cm from the pylorus, in a direction parallel to the longitudinal muscle axis, with an inter-electrode distance of 0.3 cm. The abdomen was then sutured. After a period of 10 minutes had elapsed, the electrode leads were connected to an MP160 multichannel electrophysiological recorder. The following parameters were set for the recording: Sensitivity at a gain of 1000, sampling frequency at 500 Hz, high-pass filter at DC, and low-pass filter at 1 Hz. Continuous slow-wave recordings were then performed for a duration of 30 minutes. Gastric slow wave discharges within 5-minute intervals were analyzed according to Edwards *et al*[12]. Five consecutive 5-minute segments of gastric myoelectric activity were randomly selected, and the number of slow wave discharges was calculated.

GER

Following a 24-hour fast and a 2-hour water restriction, rats were administered 2 mL of a phenol red solution containing 50 mg/dL of the dye *via* oral gavage. Fifteen minutes later, an aesthesia was induced by intraperitoneal injection of 10% sodium pentobarbital (3 mL/kg). The abdominal cavity was then opened, and the entire stomach was excised and cut along the greater curvature. The stomach was then thoroughly rinsed with 20 mL of 0.9% sodium chloride solution, after which the contents were collected into a clean beaker. The contents were then mixed with 20 mL of 0.5 mol/L sodium hydroxide (NaOH) solution and left to stand for 1 hour. Thereafter, 5 mL of the resulting mixture was collected and mixed with 0.5 mL of a 20% trichloroacetic acid (TCA) solution. The mixture was then subjected to centrifugation at 3500 rpm for a period of 10 minutes. Thereafter, 2 mL of the resulting interface was analyzed for its optical density (OD) at 560 nm using a Ultraviolet spectrophotometer. A standard phenol red solution (2 mL phenol red solution, 18 mL distilled water, 20 mL 0.5 mol/L NaOH, and 4 mL 20% TCA) was prepared, and its OD value was measured using the same method. The GER was calculated as follows: GER (%) = (1 - sample OD value/standard phenol red OD value) × 100%[13].

Intestinal propulsive rate

The small intestine was meticulously dissected and positioned in a horizontal position on ice to ascertain its total length. The distal end, which had been stained with phenol red, was identified, and a small incision was made using ophthalmic scissors. A 0.5 mol/L NaOH solution was then added to the incision site, and a pinkish-purple colour change indicated the presence of phenol red. Additional drops of NaOH were applied proximal and distal to this point in order to determine the farthest point reached by phenol red. The intestinal propulsive rate (IPR) was calculated as follows: IPR (in percentage form) was thus calculated by the following method: IPR (in percentage form) = (farthest distance reached by phenol red/total length of the small intestine) × 100%[13].

Hematoxylin and eosin staining

Gastric tissue samples were fixed in 4% paraformaldehyde overnight, followed by paraffin embedding. Following fixation, the tissues were dehydrated, cleared, and embedded in paraffin. Serial sections of 4 μm-5 μm thickness were prepared using a microtome. The sections were then deparaffinized, rehydrated, and stained with hematoxylin and eosin (HE). Following this, the stained sections were dehydrated, cleared, and mounted with neutral balsam. Finally, images were captured under an optical microscope to evaluate morphological changes in the gastric tissues.

Western blotting

The tissues were minced into small fragments, and 20 mg of tissue was homogenised in 150-250 μL of lysis buffer until complete lysis was achieved. The lysate was then subjected to centrifugation at 12000 × g for 15 minutes at 4 °C. The resultant pellet was discarded, and the remaining fluid (supernatant) was collected for protein quantification. The samples were then stored at -80 °C. Polyacrylamide gels (10% or 12%) were prepared based on the molecular weight of target proteins. The gels were then cast into electrophoresis chambers, and an appropriate amount of running buffer was added. Following electrophoresis, proteins were transferred to membranes, which were blocked with 5% bovine serum albumin (BSA) (Elabscience) at 37 °C for 1 hour. Primary antibodies, including neuronal nitric oxide synthase (nNOS) (1:1500, 76067, Abcam), cluster of differentiation 117 (C-kit) (1:1000, 3074, Cell Signaling Technology), stem cell factor (SCF) (1:2500, 52603, Abcam), ChAT (1:1000, 178850, Abcam), α7nAChR (1:1000, 216485, Abcam), and β-actin (1:1000, 4970S, Cell Signaling Technology), were incubated overnight at 4 °C on a shaker. Following a thorough washing step with tris borate sodium tween-20, the membranes were subjected to an incubation with the relevant secondary antibodies (goat anti-rabbit, 1:2000, A-1003, Elabscience) at room temperature for a duration of one hour. Protein bands were detected using chemiluminescence, and band intensities were quantified using ImageJ software.

Immunofluorescence staining

Tissues were fixed in 4% paraformaldehyde and then dehydrated through a graded ethanol series. Following this, they were cleared, embedded in paraffin, and sectioned. The paraffin sections were then deparaffinized, rehydrated, and subjected to antigen retrieval using ethylene diamine tetraacetic acid buffer. Following washing with phosphate buffered saline, autofluorescence quencher was applied, followed by blocking with 5% BSA. Primary antibodies, including rabbit anti-C-kit (1:200, 3074, Cell Signaling Technology), rabbit anti-c-*FOS* (1:200, 2250, Cell Signaling Technology), and mouse anti-ChAT (1:200, MAB5350, Sigma), were incubated overnight at 4 °C. Sections were then incubated with corresponding

secondary antibodies (Alexa Fluor 488-conjugated goat anti-rabbit, 1:200, 11008, Invitrogen; Alexa Fluor 594-conjugated goat anti-mouse, 1:500, A21203, Invitrogen) at room temperature for 60 minutes in the dark. The nuclei were counter-stained with 4′,6-diamidino-2-phenylindole for 10 minutes at room temperature in the dark. Following this, the sections were washed with phosphate buffered saline and mounted with antifade mounting medium. The samples were then observed under a fluorescence microscope. Images from three randomly selected fields *per* section were captured at 400 × magnification.

Enzyme-linked immunosorbent assay

Levels of gastrointestinal peptides [*i.e.*, gastrin (Gas), motilin (MLT) and vasoactive intestinal peptide (VIP)] were measured using enzyme-linked immunosorbent assay kits (purchased from LunChangShuoBiotech, China). Briefly, brain filtrates were subjected to a centrifugation process at 1000 × g for a duration of 10 minutes, with the objective of eliminating particulate matter and aggregates. The measurements were then performed in strict accordance with the instructions provided by the manufacturer. The OD of the samples was subsequently determined at a wavelength of 450 nm, employing a microplate reader.

Statistical analysis

The analysis of the data was conducted utilising Prism 9 (GraphPad Software). Quantitative data are presented as mean ± SD. The differences between the groups were assessed using one-way analysis of variance, followed by Bonferroni's post hoc test. For non-normally distributed data, Dunnett's multiple comparison test was applied. A P value less than 0.05 was considered to be statistically significant.

RESULTS

EA significantly improves GER by enhancing gastric motility in DGP rats

Longitudinal weight monitoring was conducted to evaluate diabetes-associated body weight dynamics (Figure 1A). The Sham group demonstrated progressive weight gain throughout the 10-week study period. In contrast, the STZ-induced diabetic rats (DGP and EA groups) demonstrated a less pronounced weight gain trajectory post-diabetes induction (week 1). The intervention of EA at week 8 led to a significant mitigation of diabetes-related weight loss, with the final body mass of EA-treated rats being 11.4% higher than that of the DGP controls at week 10 ($P < 0.05$). Metabolic profiling confirmed sustained hyperglycaemia (> 16.7 mmol/L, non-fasting) in the DGP and EA groups, with no significant glucose modulation by EA treatment (Figure 1B). Gastric motility was assessed *via* electrogastrography (Figure 1C and D). In comparison to the Sham group, DGP rats exhibited significantly reduced gastric slow wave discharges ($P < 0.05$), while EA intervention restored slow wave frequency to near-normal levels ($P < 0.05$). Further functional assessments revealed impaired gastric emptying and intestinal propulsion in DGP rats ($P < 0.05$), both of which were significantly improved by EA ($P < 0.05$) (Figure 1E and F). Furthermore, the gold standard for diagnosing DGP rats was employed to assess the efficacy of EA through the use of confirmatory PET-CT imaging with quantitative contrast tracking[11]. This revealed that EA-treated rats exhibited accelerated gastric emptying, with only 66.1% radioactivity remaining at 3600 seconds post-administration, in comparison to 80.9% in DGP and 54.5% in Sham controls ($P < 0.05$; Figure 1G-J). This multimodal validation, encompassing electrophysiological, functional, and imaging modalities, provides substantial evidence supporting the efficacy of EA as a robust intervention for restoring gastric motility in DGP.

EA improves gastric dysmotility through structural and functional restoration of smooth muscle

Having established the regulatory effects of EA on gastric emptying, the subsequent focus was on gastric smooth muscle dynamics, which are the primary driver of gastric contractility. Histopathological evaluation *via* HE staining (Figure 2A) revealed distinct morphological profiles across the experimental groups. Sham controls displayed preserved gastric architecture, with intact mucosal layers and orderly smooth muscle arrangement. In contrast, DGP rats exhibited marked mucosal degeneration, characterized by glandular atrophy, inflammatory infiltrates, submucosal fibrosis, and disrupted smooth muscle organization. The administration of EA significantly mitigated these pathological manifestations, as evidenced by the restoration of glandular density, the attenuation of inflammatory infiltration, and the enhancement of smooth muscle alignment. In order to investigate the molecular mechanisms underlying these morphological improvements, a study was conducted on the key regulators of smooth muscle function. Western blot analysis demonstrated significant EA-mediated upregulation of nNOS, C-kit, and SCF protein expression compared to DGP controls ($P < 0.05$, Figure 2B-E). Given the critical role of C-kit in the function of ICC, which are essential for gastric pace making and neuromuscular signalling, its expression was further validated. The quantification of immunofluorescence confirmed EA-induced restoration of C-kit expression patterns (Figure 2F), which is in alignment with the immunoblot findings. Collectively, these results indicate that EA ameliorates DGP through dual mechanisms: Namely, structural preservation of gastric smooth muscle and molecular restoration of key regulatory proteins.

EA improves gastric dysmotility through activation of vagal targets

The vagus nerve is the principal neural regulator of gastrointestinal motility. In order to elucidate its role in EA-mediated improvements, a comprehensive analysis was conducted on key vagal targets in gastric tissues. The results of the immunoblot analysis revealed that EA induced upregulation of the cholinergic markers ChAT and α7nAchR in comparison with DGP controls ($P < 0.05$, Figure 3A-C). Furthermore, immunofluorescence co-localization analysis

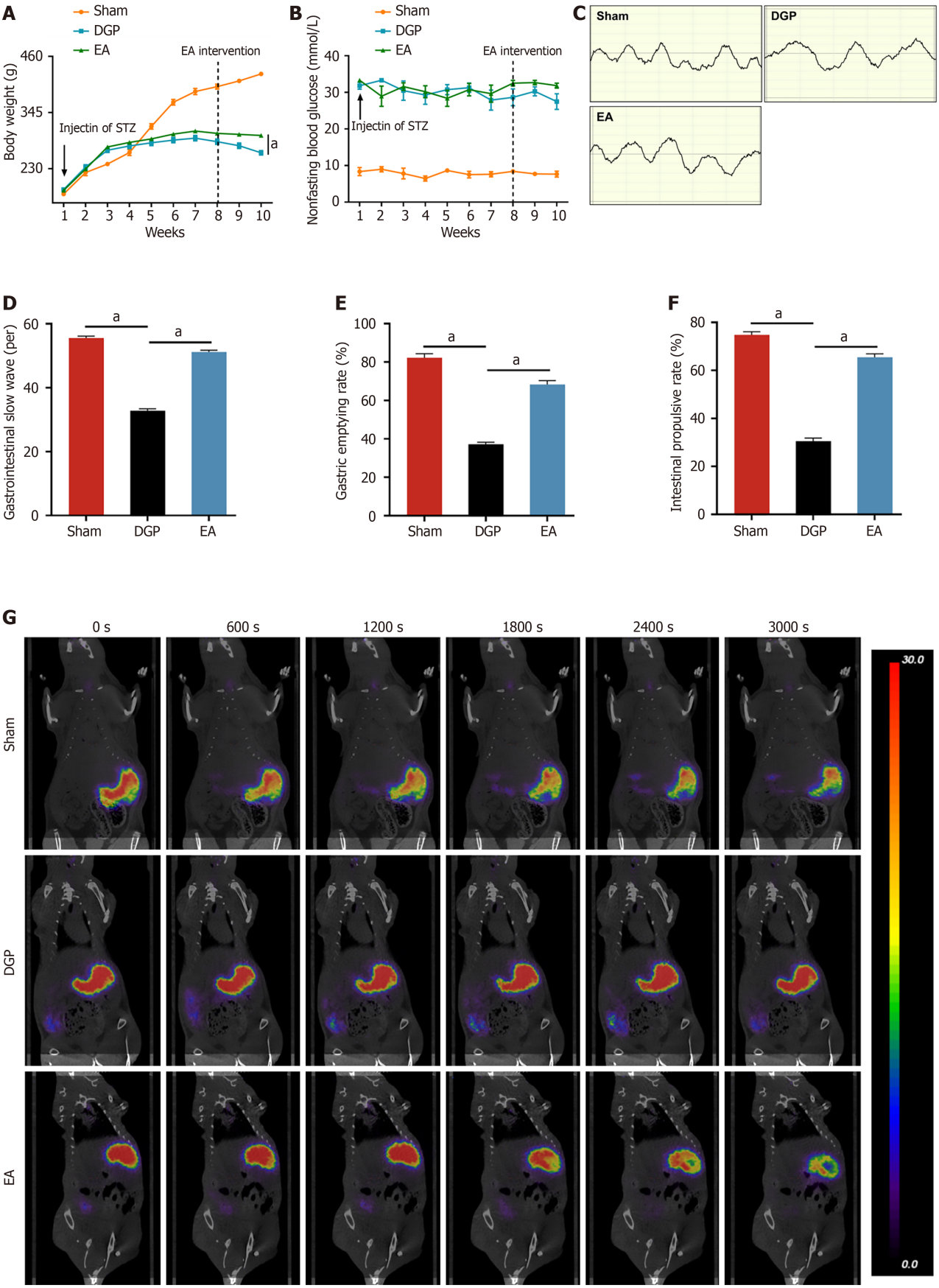
A
Sham
DGP
EA
EA intervention
Body weight (g)
460
345
230
Injectin of STZ
a
1 2 3 4 5 6 7 8 9 10
Weeks
B
Sham
DGP
EA
EA intervention
Nonfasting blood glucose (mmol/L)
40
30
20
10
0
Injectin of STZ
1 2 3 4 5 6 7 8 9 10
Weeks
C
Sham
DGP
EA
D
Gastrointestinal slow wave (per)
60
40
20
0
a
a
Sham DGP EA
E
Gastric emptying rate (%)
100
80
60
40
20
0
a
a
Sham DGP EA
F
Intestinal propulsive rate (%)
80
60
40
20
0
a
a
Sham DGP EA
G
0 s
600 s
1200 s
1800 s
2400 s
3000 s
Sham
DGP
EA
30.0
0.0

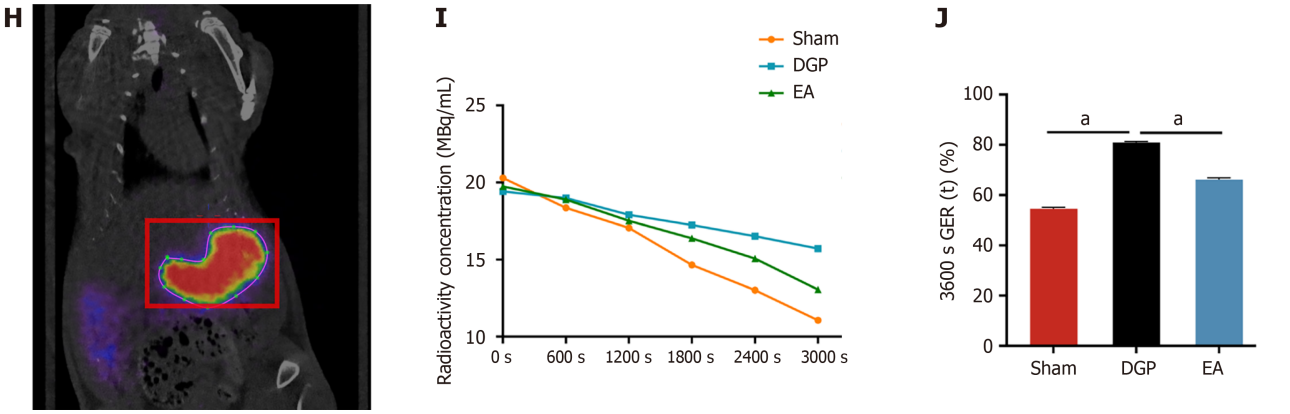

Figure 1 Electroacupuncture has been demonstrated to promote gastric emptying in diabetic gastroparesis rats. A: Body weight (n = 10); B: Non-fasting blood glucose level (n = 10); C: Electrographic recording of gastric motor activity; D: Number of slow wave discharges in the gastric antrum within 5 minutes (n = 5); E: Gastric emptying rate (n = 5); F: Small intestine propulsion rate (n = 5); G: Representative positron emission tomography images; H: Region of interest in the stomach; I: Radioactive concentration in the region of interest in the stomach (n = 5); J: Gastric emptying rate at 3600 seconds (n = 5). Data are expressed as the mean ± SD. $^{a}P < 0.05$. STZ: Streptozotocin; DGP: Diabetic gastroparesis; EA: Electroacupuncture.

demonstrated parallel restoration of C-kit +/ChAT + expression patterns, with EA-treated rats showing distribution characteristics comparable to the Sham group (Figure 3D). This suggests that the vagus nerve target ChAT may be involved in the regulatory effect of EA on ICC. Assessment of gastrointestinal peptides further revealed characteristic alterations. Compared with the Sham group, DGP rats exhibited significant suppression of stimulatory mediators (Gas and MLT), accompanied by a concomitant paradoxical elevation in inhibitory VIP levels ($P < 0.05$). However, the EA intervention led to the normalization of these peptide profiles, with a significant increase in Gas and MLT levels ($P < 0.05$) and a reduction in VIP levels ($P < 0.05$) (Figure 3E-G). The EA intervention appears to have restored gastric motility in DGP rats by coordinating the activation of the vagal cholinergic pathway to regulate ICC cells and rebalance neuroendocrine signals.

EA activates vagal targets at ST36 acupoint via spinal L4-L6 afferent pathways to modulate NTS function

In order to elucidate the afferent neural pathways underlying EA-mediated gastric motility modulation in DGP rats, the ChAT inhibitor AP or the agonist PA was injected into the ST36 acupoint area and ChAT and α7nAChR protein expression was quantified across three key sites (Figures 4, 5 and 6): The ST36 acupoint skin, the spinal L4-L6 segments and the NTS (Figures 4A, 5A and 6A). Western blot analysis revealed significantly elevated ChAT levels in DGP rats compared to Sham controls across all sites ($P < 0.05$), with EA further amplifying ChAT expression ($P < 0.05$), mirroring trends observed in the PA group. However, the co-administration of AP with EA (EA + AP group) led to the abolition of this activation ($P < 0.05$; Figures 4B, 5B and 6B). In addition, EA induced an increase in α7nAChR expression in the ST36 skin, L4-L6 spinal region, and NTS ($P < 0.05$), an effect that was attenuated by AP co-treatment ($P < 0.05$; Figures 4C, 5C and 6C). Immunofluorescence analysis corroborated these observations. DGP rats exhibited reduced ChAT expression in ST36 skin, whereas EA and PA groups showed marked increases. AP administration nullified EA's effects (Figure 4D). In the spinal L4-L6 segments, c-*FOS* immunostaining revealed robust neuronal activation in the EA and PA groups ($P < 0.05$), which was suppressed in the EA + AP rats ($P < 0.05$; Figure 5D). c-*FOS* +/ChAT + co-localization further confirmed that this activation was ChAT-dependent (Figure 5E). In the NTS, c-FOS expression was significantly elevated in the EA and PA groups ($P < 0.05$), with EA + AP rats showing reduced activation ($P < 0.05$; Figure 6D). c-*FOS* +/ChAT + co-expression mirrored these trends, demonstrating EA's dual modulation of neuronal activity and cholinergic signalling (Figure 6E). The data taken together indicate that EA activates vagal ChAT/α7nAChR targets at ST36, transmitting signals *via* spinal L4-L6 afferents to NTS neurons, thereby restoring vagal tone in DGP.

EA promotes gastric emptying via the peripheral vagal efferent pathway

Utilizing the preceding evidence that EA activates the NTS through vagal afferent pathways, the present study investigated the role of vagal efferent signalling in EA-mediated gastric motility restoration by performing SDV in DGP rats. The results of the western blot analysis revealed a significant reduction in the expression of ChAT and α7nAChR in the stomach of the rats in the SDV group compared to the DGP group ($P < 0.05$). In contrast, EA significantly increased the expression of both proteins ($P < 0.05$). Crucially, SDV abolished EA-induced ChAT/α7nAChR activation ($P < 0.05$), confirming that EA's therapeutic effects require intact vagal efferent signaling (Figure 7A-C). Electrogastrography demonstrated that EA restored gastric slow wave discharges in DGP rats ($P < 0.05$), an effect that was attenuated by SDV ($P < 0.05$; Figure 7D and E). The findings were corroborated by functional assessments: EA improved both gastric emptying and small intestinal propulsion rates ($P < 0.05$), whereas SDV negated these improvements ($P < 0.05$; Figure 7F and G). Dynamic PET-CT imaging further validated the prokinetic effects of EA, showing accelerated gastric radioactivity clearance in rats treated with EA (67.8% retention at 3600 seconds) compared to rats treated with DGP (90.9% retention; $P < 0.05$; Figure 7H and I). Post-spontaneous duodenal vagus stimulation (SDV), the efficacy of EA was significantly diminished, with residual gastric content increasing to 82.2% ($P < 0.05$; Figure 7J). The collective findings of this study

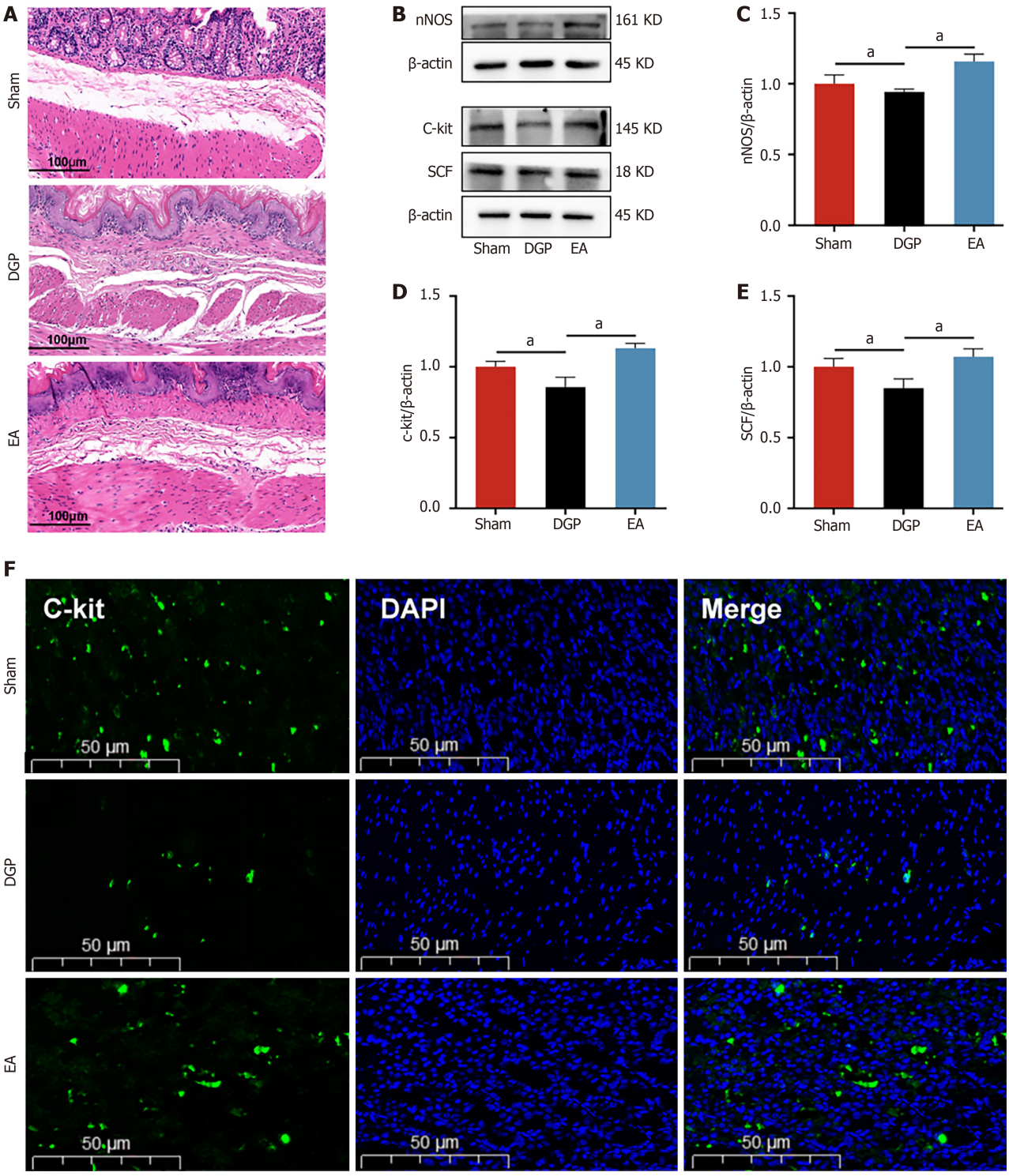

Figure 2 Electroacupuncture improves the dysfunction of gastric smooth muscle in diabetic gastroparesis rats. A: Representative images of hematoxylin-eosin in the stomach. Scale bar: 100 μm; B-E: Western blotting analysis and quantification of neuronal nitric oxide synthase, cluster of differentiation 117 (C-kit) and stem cell factor protein levels in stomach tissue (n = 5); F: Representative immunofluorescence images of C-kit. Scale bar: 50 μm. Data are expressed as the mean ± SD. $^{a}P < 0.05$. DGP: Diabetic gastroparesis; EA: Electroacupuncture; nNOS: Neuronal nitric oxide synthase; C-kit: Cluster of differentiation 117; SCF: Stem cell factor; DAPI: 4',6-diamidino-2-phenylindole.

demonstrate that EA enhances gastric motility *via* the subdiaphragmatic vagus nerve, thereby establishing it as a critical efferent pathway for neuromodulation in DGP.

EA improves gastric dyskinesia by modulating smooth muscle function via peripheral vagal efferent pathway

Histological analysis *via* HE staining revealed that EA ameliorated gastric pathology in DGP rats, characterized by reduced inflammatory infiltration and restored smooth muscle alignment. Conversely, SDV appeared to counteract these benefits, sustaining submucosal collagen deposition and mild smooth muscle disorganization (Figure 8A). In addition, the results of the western blotting analysis demonstrated that EA significantly increased the expression of nNOS, C-Kit,

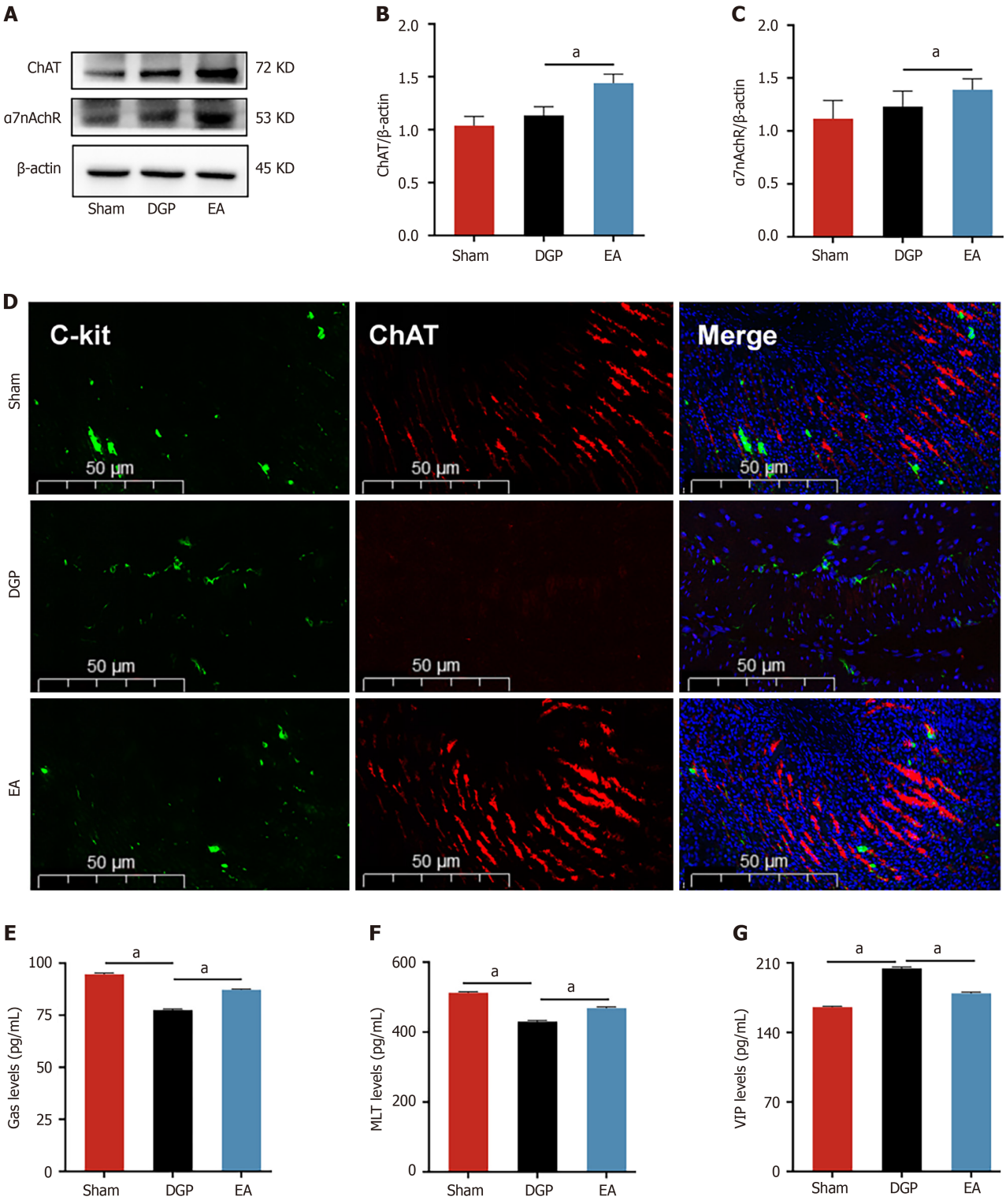

Figure 3 Electroacupuncture improves gastric motility and is associated with vagus nerve targets. A-C: Western blotting analysis and quantification of choline acetyltransferase (ChAT) and α7 nicotinic acetylcholine receptor protein levels in stomach tissue (n = 5); D: Expression of cluster of differentiation 117 +/ChAT + in the stomach in each group. Scale bar: 50 μm; E-G: Enzyme-linked immunosorbent assay to detect the concentration of gastrin, motilin and vasoactive intestinal peptide in supernatant (n = 5). Data are expressed as the mean ± SD. $^{a}P < 0.05$. C-kit: Cluster of differentiation 117; DGP: Diabetic gastroparesis; EA: Electroacupuncture; ChAT: Choline acetyltransferase; α7nAchR: α7 nicotinic acetylcholine receptor; Gas: Gastrin; MLT: Motilin; VIP: Vasoactive intestinal peptide.

and SCF, while SDV significantly reduced the expression of these proteins in comparison with rats treated with EA (P < 0.05; Figure 8B-E). Immunofluorescence corroborated these findings: EA enhanced C-Kit expression, which was suppressed by SDV (P < 0.05; Figure 8F). Furthermore, the co-localization of C-Kit and ChAT further confirmed EA's activation of vagal-ICC interactions, an effect that was attenuated by SDV (P < 0.05; Figure 8G). Furthermore, gastrointestinal peptide profiling revealed that EA-mediated upregulation of Gas and MLT was accompanied by suppression of VIP, with SDV reversing these trends (P < 0.05; Figure 8H-J). Collectively, these results establish that EA

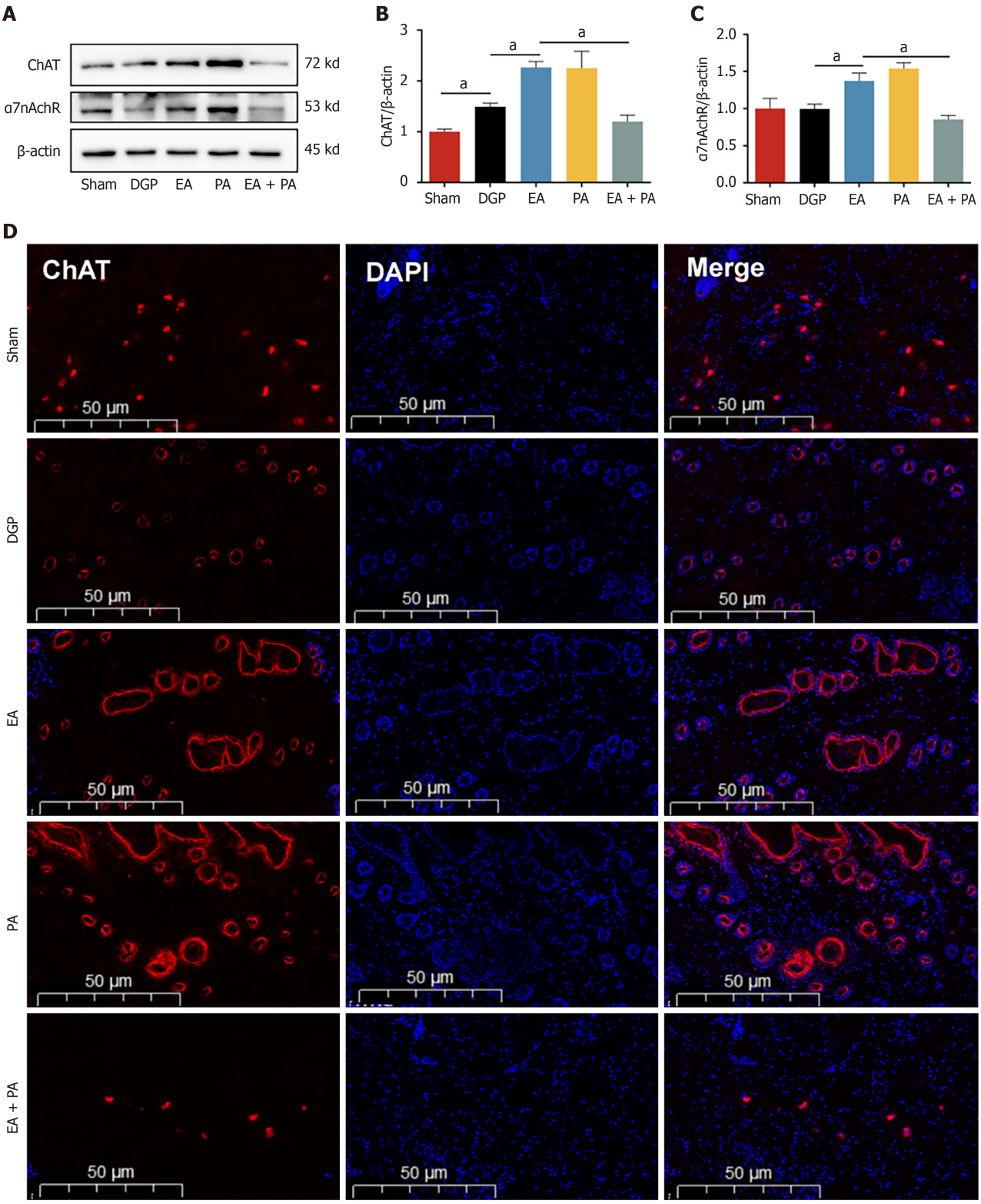

Figure 4 Electroacupuncture activates the vagus nerve target in the ST36 acupoint area. A-C: Western blotting analysis and quantification of choline acetyltransferase (ChAT) and α7 nicotinic acetylcholine receptor protein levels in acupoint skin (n = 5); D: Representative immunofluorescence images of ChAT. Scale bar: 50 μm. Data are expressed as the mean ± SD. $^{a}P < 0.05$. DGP: Diabetic gastroparesis; EA: Electroacupuncture; ChAT: Choline acetyltransferase; α 7nAchR: α7 nicotinic acetylcholine receptor; PA: Agonist polygalacic acid; AP: Antagonist alpha-NETA; DAPI: 4',6-diamidino-2-phenylindole.

improves gastric dysmotility by activating subdiaphragmatic vagal efferent pathways, which regulate smooth muscle integrity, ICC function, and neuropeptide balance in DGP.

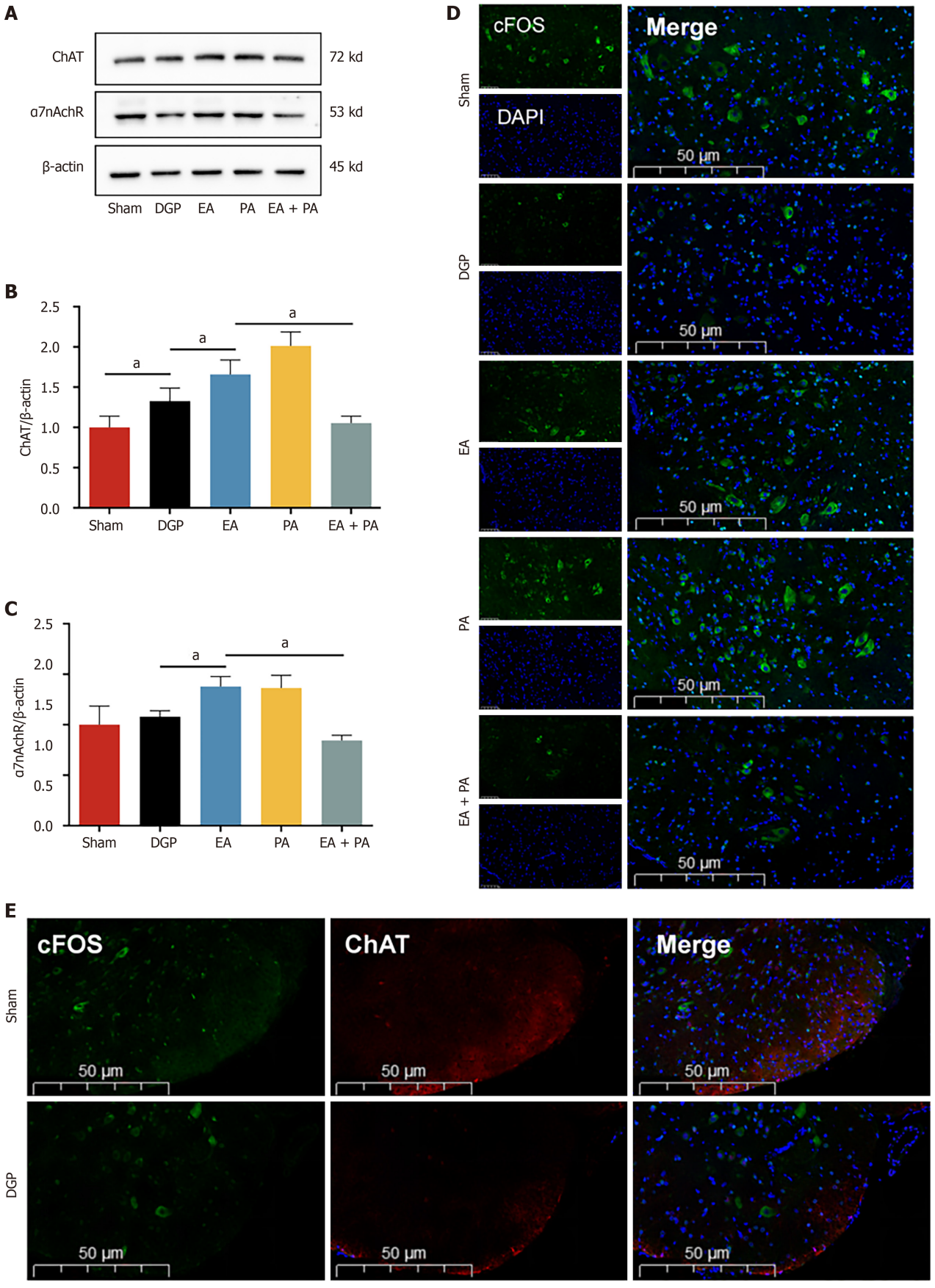
A
ChAT
α7nAchR
β-actin
72 kd
53 kd
45 kd
Sham DGP EA PA EA + PA
B
ChAT/β-actin
2.5
2.0
1.5
1.0
0.5
0.0
a
a
a
Sham DGP EA PA EA + PA
C
α7nAchR/β-actin
2.5
2.0
1.5
1.0
0.5
0.0
a
a
Sham DGP EA PA EA + PA
D
cFOS
Merge
DAPI
Sham
DGP
EA
PA
EA + PA
50 μm
E
cFOS
ChAT
Merge
Sham
DGP
50 μm

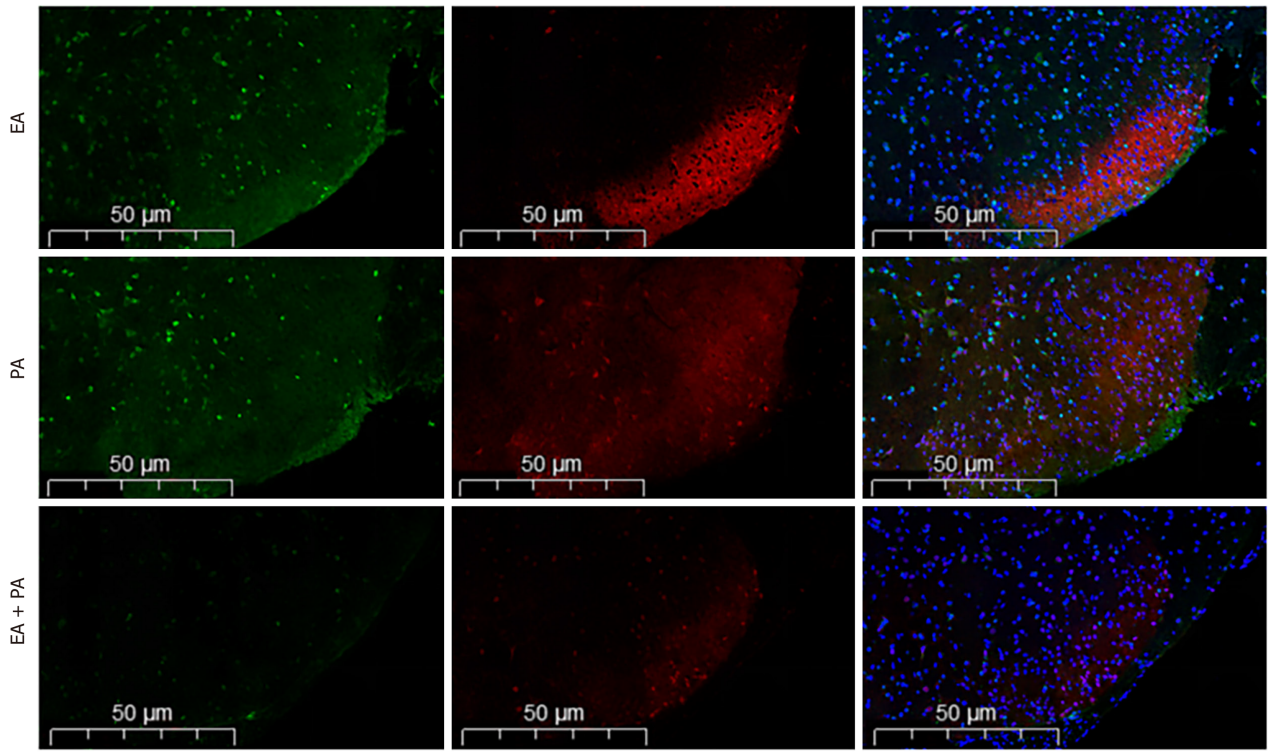

Figure 5 Electroacupuncture activates the vagus nerve target at the L4-L6 segment. A-C: Western blotting analysis and quantification of choline acetyltransferase (ChAT) and α7 nicotinic acetylcholine receptor protein levels in L4-L6 (n = 5); D: Representative immunofluorescence images of c-*FOS*. Scale bar: 50 μm; E: Expression of c-*FOS* +/ChAT + in the stomach in each group. Scale bar: 50 μm. Data are expressed as the mean ± SD. $^{a}P < 0.05$. DGP: Diabetic gastroparesis; EA: Electroacupuncture; ChAT: Choline acetyltransferase; α7nAchR: α7 nicotinic acetylcholine receptor; PA: Agonist polygalacic acid; AP: Antagonist alpha-NETA; DAPI: 4',6-diamidino-2-phenylindole.

DISCUSSION

DGP is a chronic complication of diabetes characterized by impaired gastric motility, delayed gastric emptying and gastric dysrhythmia, which severely compromises patients' quality of life[14]. Current pharmacological strategies targeting gastric prokinetic effects and glycemic control remain limited by adverse effects, drug resistance, and insufficient therapeutic efficacy[15]. EA, a traditional Chinese medical therapy, has demonstrated potential in improving gastrointestinal motility due to its high safety profile and cost-effectiveness, as evidenced by recent studies[16]. In this study, EA alleviated weight loss in DGP rats but did not significantly ameliorate hyperglycaemia. These findings suggest that a 14-day EA regimen may selectively stabilize body weight regulation, whereas chronic hyperglycemia-a hallmark of advanced diabetes-likely necessitates prolonged therapeutic interventions to achieve glycemic normalization, consistent with prior evidence on metabolic inertia in diabetic models[15]. The study found that EA significantly enhanced gastric emptying, as measured by the phenol red method, which is a diagnostic criterion for the DGP model. Electrogastrography revealed that EA markedly increased gastrointestinal slow wave activity, providing direct evidence of its prokinetic effects. Notably, a pioneering approach involved the use of PET-CT imaging, a gold-standard modality renowned for its superior quantitative accuracy and imaging resolution[17], to assess gastric emptying. The dynamic tracking based on PET-CT further validated the therapeutic potential of EA in DGP rats by demonstrating its robust promotion of gastric motility.

Mounting evidence indicates that smooth muscle pathology plays a pivotal role in the pathogenesis of DGP[18]. Of particular note is the finding that the downregulation of nNOS expression, a dimerized enzyme that is critical for inhibitory neurotransmission and gastric smooth muscle relaxation, is a hallmark of DGP. Its reduction has been shown to correlate closely with impaired nitrergic innervation and delayed intestinal transit[19,20]. In a seminal study, Han *et al* [16] demonstrated that EA mitigates nNOS loss in the enteric nervous system, thereby restoring neuro-mediated muscle responses and significantly accelerating gastric emptying. The present findings are in alignment with these observations: In DGP rats, EA resulted in the upregulation of gastric nNOS expression and a significant amelioration of gastric dysmotility. Beyond nNOS, ICCs dysfunction has been shown to be strongly associated with DGP. ICCs are essential for generating gastric slow waves and setting smooth muscle membrane potentials[21]. Clinical studies have revealed markedly reduced ICC density in gastric antral biopsies of DGP patients, with antral changes being more pronounced than those in the gastric body[22,23]. In addition, experimental studies on animals have corroborated these observations, demonstrating a decrease in the expression of the ICC markers C-kit and its receptor SCF in both the antrum and corpus of DGP rats[24]. This supports the hypothesis that ICC loss contributes to delayed gastric emptying. Lin *et al*[25] further validated this mechanism through EA intervention: EA-treated rats exhibited increased ICC populations, enhanced neuro-smooth muscle connectivity, and restored interactions between intrinsic nerves and ICCs compared to DGP

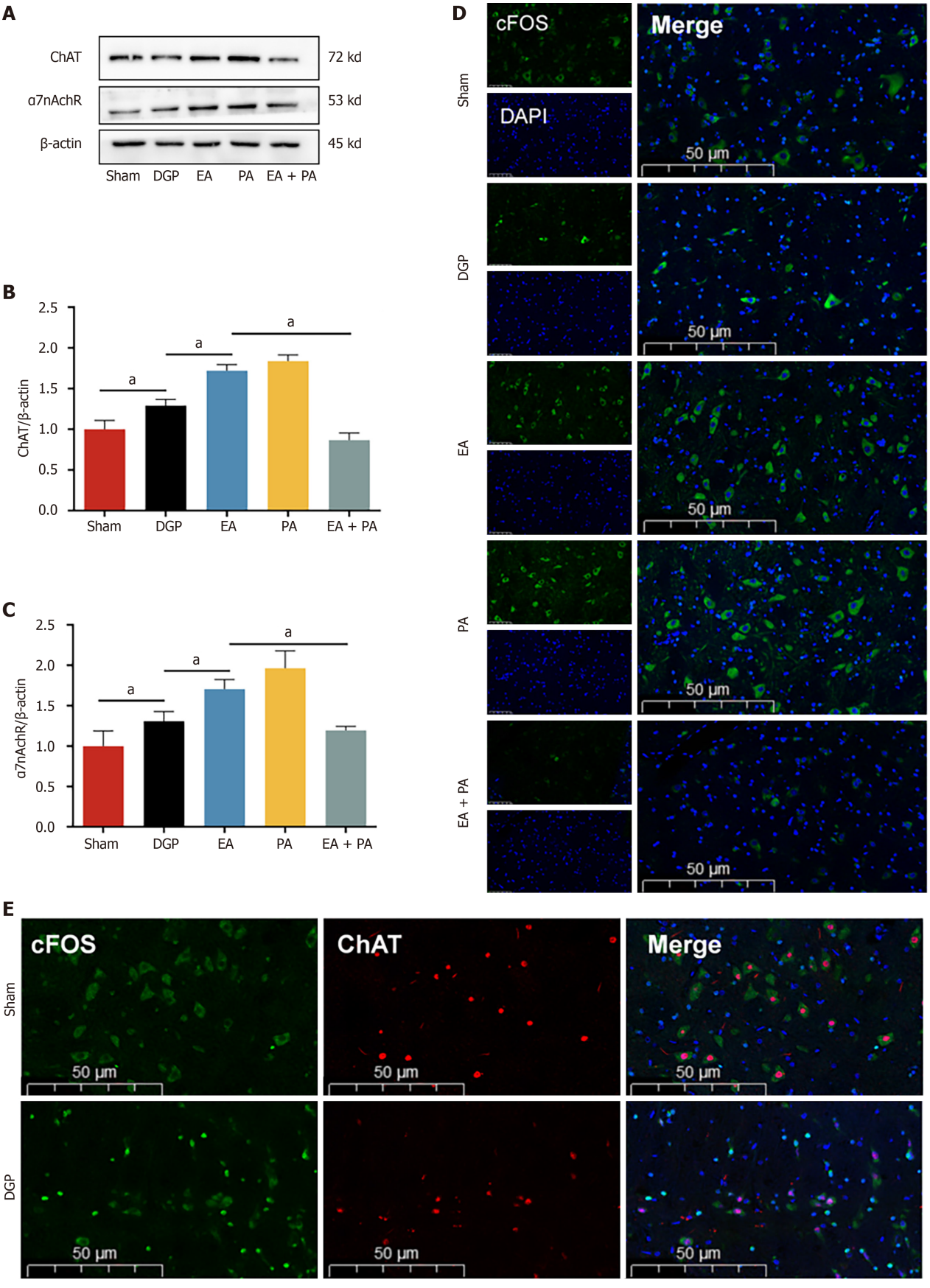
A
ChAT
α7nAchR
β-actin
72 kd
53 kd
45 kd
Sham DGP EA PA EA + PA
B
ChAT/β-actin
2.5
2.0
1.5
1.0
0.5
0.0
a
a
a
Sham DGP EA PA EA + PA
C
α7nAchR/β-actin
2.5
2.0
1.5
1.0
0.5
0.0
a
a
a
Sham DGP EA PA EA + PA
D
cFOS
Merge
DAPI
Sham
DGP
EA
PA
EA + PA
50 μm
E
cFOS
ChAT
Merge
Sham
DGP
50 μm

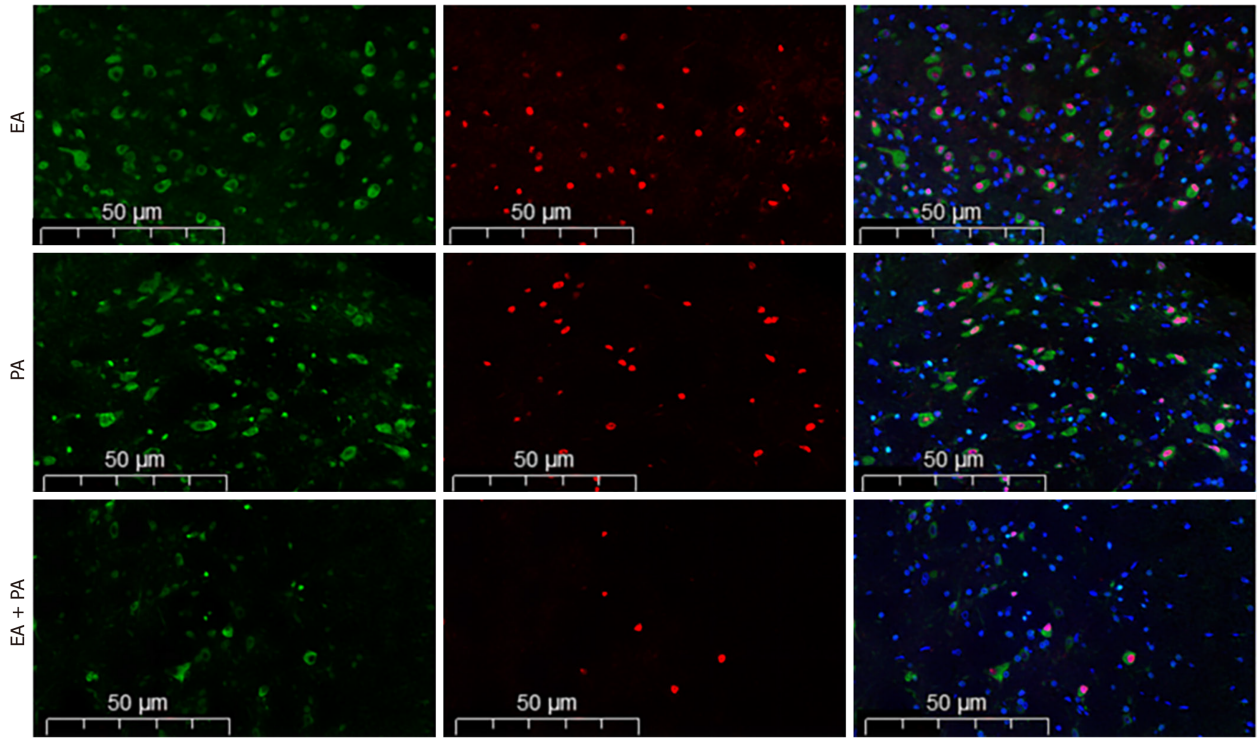

Figure 6 Electroacupuncture activates the vagus nerve target of nucleus tractus solitarius. A-C: Western blotting analysis and quantification of choline acetyltransferase (ChAT) and α7 nicotinic acetylcholine receptor protein levels in nucleus tractus solitarius (n = 5); D: Representative immunofluorescence images of c-*FOS*. Scale bar: 50 μm; E: Expression of c-*FOS* +/ChAT + in the stomach in each group. Scale bar: 50 μm. Data are expressed as the mean ± SD. ^{a}P < 0.05. DGP: Diabetic gastroparesis; EA: Electroacupuncture; ChAT: Choline acetyltransferase; α7nAchR: α7 nicotinic acetylcholine receptor; PA: Agonist polygalacic acid; AP: Antagonist alpha-NETA; DAPI: 4',6-diamidino-2-phenylindole.

models. Quantitative analysis confirmed that EA significantly increased C-kit and SCF expression, consistent with these morphological findings. Importantly, a positive correlation was observed between C-kit and ChAT expression, suggesting that vagal ChAT signalling may mediate EA's regulatory effects on ICCs.

The present study investigates the association between vagal nerve dysfunction and DGP, given its status as the primary autonomic regulator of gastrointestinal motility. The role of the vagus nerve in modulating gastrointestinal smooth muscle contraction and glandular secretion is well-documented, and its contribution to enhancing gastrointestinal transit by maintaining autonomic nervous system balance is also well-established[26]. Evidence indicates that acupuncture exerts therapeutic effects through vagal pathway activation: EA applied to somatic acupoints transmits signals *via* peripheral sensory nerves to the central nervous system, subsequently regulating gastrointestinal motility through autonomic pathways[27]. Liu *et al*[28] demonstrated that EA at ST36 significantly enhances vagal excitability, as evidenced by increased vagal nerve electrical activity. In the present experiments, EA significantly elevated ChAT expression in the ST36 dermal region, thus confirming vagal activation. Neuroanatomical studies further reveal that ST36 stimulation signals are transmitted *via* the sciatic nerve to the L4-L6 spinal segments. Notably, stem cells injected locally at ST36 were observed to distribute along the sciatic nerve to these spinal segments[29]. Notably, stem cells injected locally at ST36 were observed to distribute along the sciatic nerve to these spinal segments. Importantly, our results demonstrated significant c-*FOS* activation in the L4-L6 spinal cord following EA intervention, with a positive correlation between c-*FOS* and ChAT expression, suggesting this region participates in vagal afferent signaling during EA-mediated gastric motility improvement.

Hierarchical vagal regulatory pathways involve brainstem nuclei, particularly the DMV and the NTS, which serve as central hubs for integrating gastrointestinal signals (*e.g.*, stretch reflexes and satiety) and coordinating gastrointestinal motility. EA at ST36 has been shown to modulate neuronal activity in these regions through vagal afferent pathways[27,30]. For instance, retrograde tracing using cholera toxin or pseudorabies virus injected at ST36 revealed abundant labeled neurons in the NTS and DMV, confirming direct neural connectivity between ST36 and these nuclei[31]. Fang *et al*[32] demonstrated that EA at ST36 activates NTS neurons, subsequently enhancing vagal efferent activity to promote gastrointestinal peristalsis. Consistent with this, our findings showed EA-induced activation of c-*FOS*-labeled neurons in the NTS accompanied by synchronized ChAT upregulation, further supporting the cascade activation of vagal central circuits. It is crucial to note that the efficacy of these EA-induced effects is contingent on the integrity of the vagus nerve. SDV abolished EA's therapeutic benefits on gastric emptying and gastrointestinal peptide secretion[33]. In a similar manner, Song *et al*[34] reported that vagal denervation negated EA's efficacy in ameliorating post-burn gastric dysfunction. The present study revealed that vagotomy not only blocked EA's prokinetic effects but also attenuated its regulation of smooth muscle-related factors and gastrointestinal peptides. Most notably, vagal ablation completely abolished EA-induced ChAT upregulation, underscoring the indispensable role of vagal efferent pathways in EA's anti-DGP mechanisms.

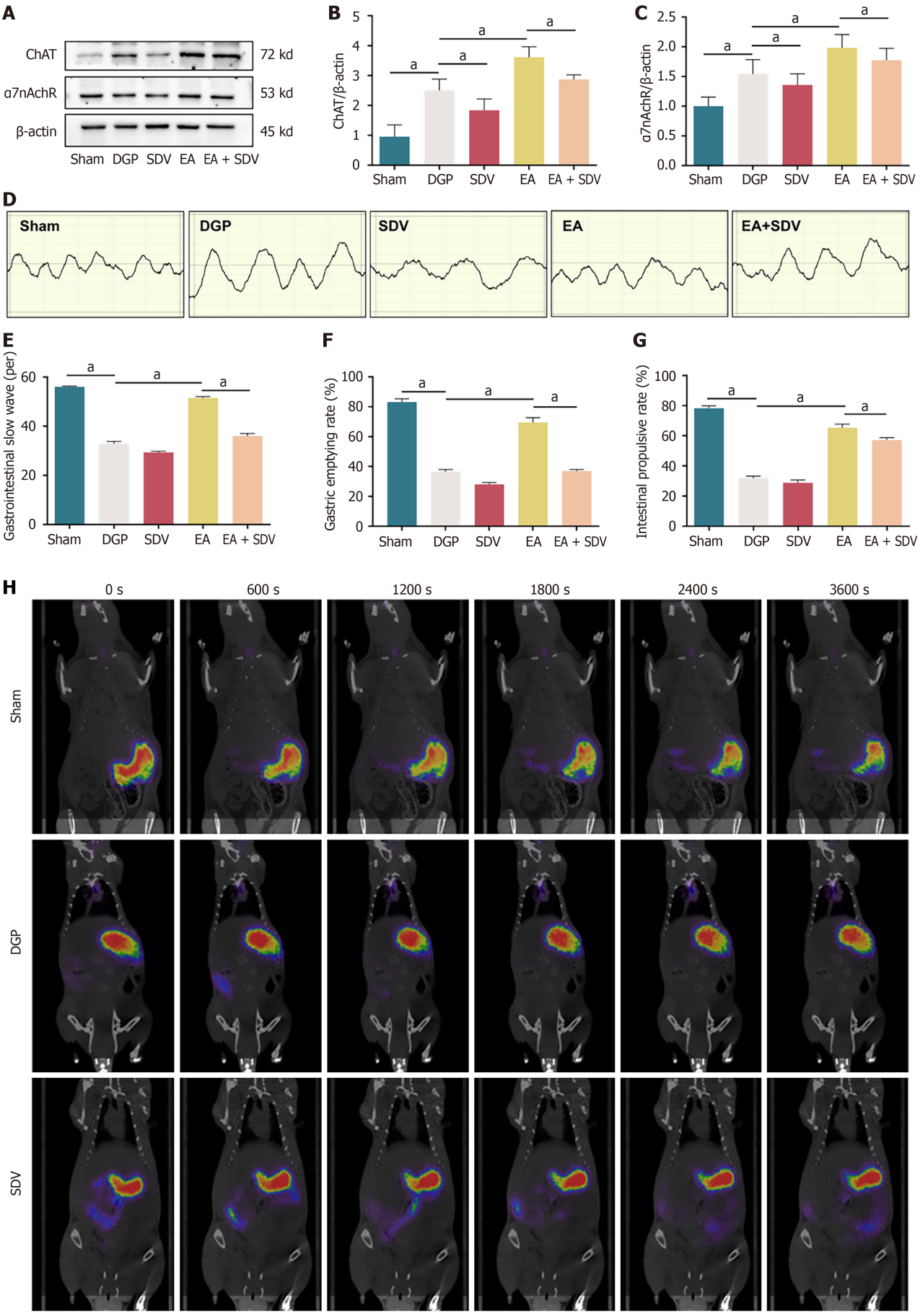
A
ChAT
α7nAchR
β-actin
72 kd
53 kd
45 kd
Sham DGP SDV EA EA + SDV
B
ChAT/β-actin
C
α7nAchR/β-actin
D
Sham
DGP
SDV
EA
EA+SDV
E
Gastrointestinal slow wave (per)
F
Gastric emptying rate (%)
G
Intestinal propulsive rate (%)
H
0 s
600 s
1200 s
1800 s
2400 s
3600 s
Sham
DGP
SDV

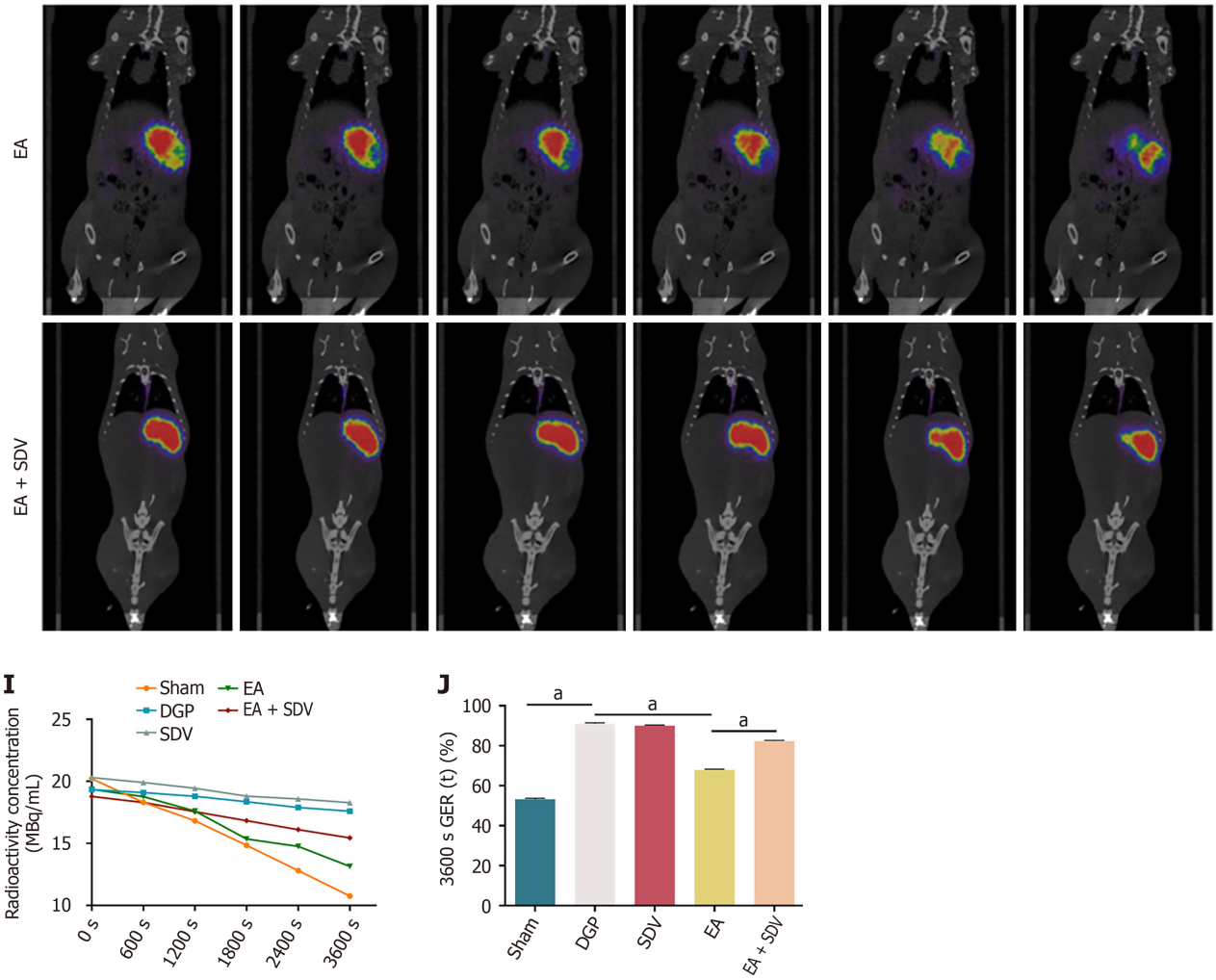

Figure 7 The regulatory effect of electroacupuncture stimulation on gastric emptying after subdiaphragmatic vagotomy. A-C: Western blotting analysis and quantification of choline acetyltransferase (ChAT) and α7 nicotinic acetylcholine receptor protein levels in stomach tissue (n = 5); D: Electromyogram of the rat stomach; E: Number of slow wave discharges in the antrum of the stomach within 5 minutes (n = 5); F: Gastric emptying rate (n = 5); G: Small intestine propulsion rate (n = 5); H: Representative positron emission tomography images; I: Radioactive concentration in the gastric region of interest (n = 5); J: Gastric emptying rate at 3600 seconds (n = 5). Data are expressed as the mean ± SD. $^{a}P < 0.05$. ChAT: Choline acetyltransferase; α7nAchR: α7 nicotinic acetylcholine receptor; DGP: Diabetic gastroparesis; EA: Electroacupuncture; GER: Gastric emptying rate; SDV: Subdiaphragmatic vagotomy.

In summary, EA has been shown to ameliorate DGP through a multi-level neural pathway involving peripheral acupoint (ST36), spinal cord (L4-L6), brainstem nuclei (NTS), target organ (stomach), with therapeutic efficacy strictly dependent on intact vagal circuitry. These findings provide novel insights into the neural mechanisms underlying EA's improvement of gastric dysmotility in DGP, advancing research directions for non-pharmacological interventions. However, this study has limitations. While the investigation focused on elucidating the role of the NTS-vagal axis in EA-mediated improvements, alternative regulatory pathways, such as sympathetic innervation and inflammatory cascades-were not systematically explored, which may overlook potential cross-talk mechanisms between neural and immune systems in DGP pathogenesis. Future studies will prioritize dissecting these interactions to comprehensively map the neuromodulatory network underlying EA therapy.

CONCLUSION

This study elucidates the mechanism by which EA improves gastric dysmotility in DGP rats through multi-tiered validation of vagal pathways. Firstly, EA at the ST36 acupoint activates peripheral vagal targets, specifically ChAT, transmitting signals *via* spinal L4-L6 afferents to the central nervous system. Subsequently, at the brainstem level, these signals enhance vagal central drive by activating c-*FOS*-expressing neurons in the NTS. Finally, EA upregulates smooth muscle-related factors (nNOS, C-kit, SCF) and promotes gastrointestinal peptide secretion, ultimately restoring gastric emptying (Figure 9). In this study, we systematically revealed for the first time the mechanism by which EA improves gastrointestinal motility in DGP through an integrated regulatory circuit of peripheral stimulation, spinal afferents, brainstem integration, vagal efferent, which provides a novel molecular mechanism for the treatment of DGP by EA.

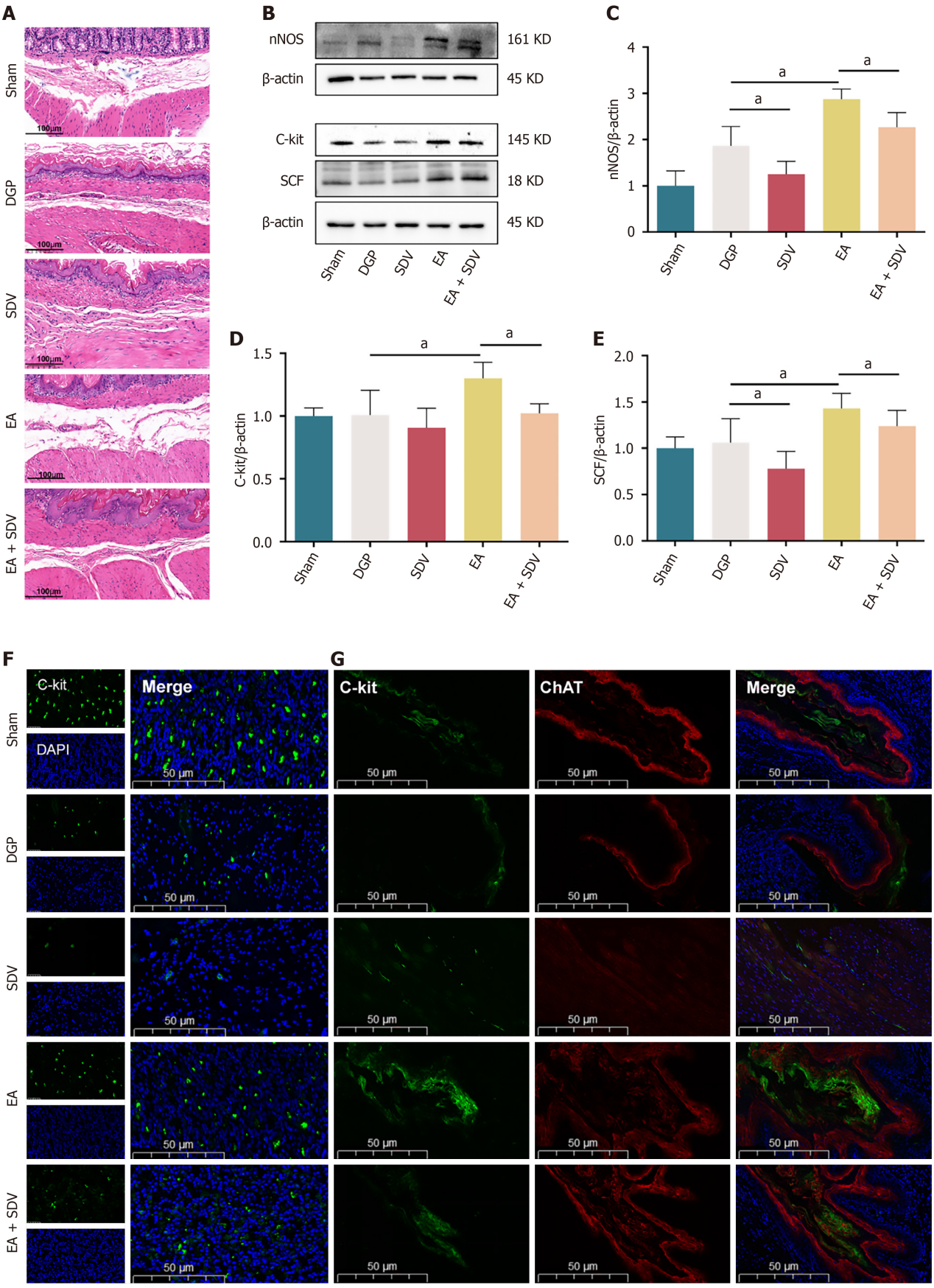
A
Sham
DGP
SDV
EA
EA + SDV
100 μm
B
nNOS
161 KD
β-actin
45 KD
C-kit
145 KD
SCF
18 KD
β-actin
45 KD
Sham
DGP
SDV
EA
EA + SDV
C
nNOS/β-actin
a
a
a
D
C-kit/β-actin
a
a
E
SCF/β-actin
a
a
a
F
C-kit
DAPI
Merge
50 μm
G
C-kit
ChAT
Merge
50 μm

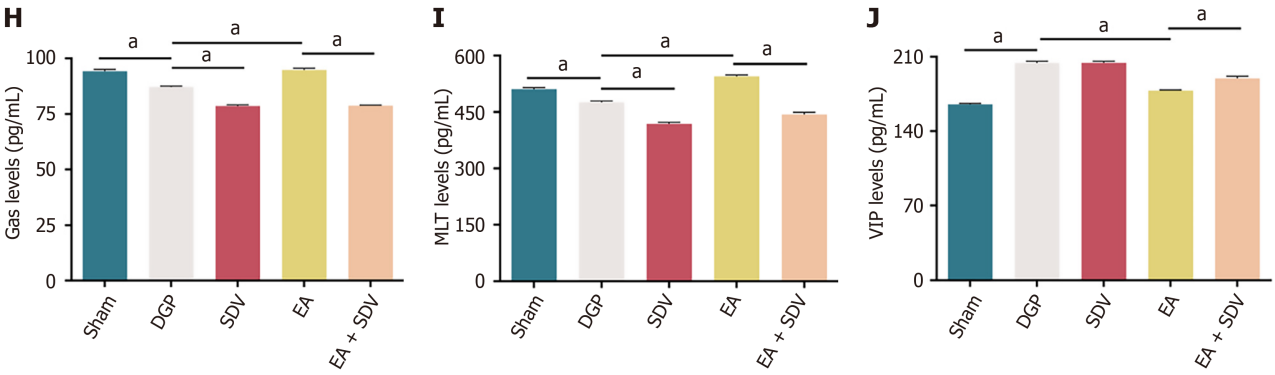

Figure 8 The effect of electroacupuncture on the function of smooth muscle after subdiaphragmatic vagotomy. A: Representative images of hematoxylin-eosin in the stomach. Scale bar: 100 μm; B-E: Western blotting analysis and quantification of neuronal nitric oxide synthase, cluster of differentiation 117 (C-kit) and stem cell factor protein levels in stomach tissue (n = 5); F: Representative immunofluorescence images of C-kit. Scale bar: 50 μm; G: Expression of C-kit +/choline acetyltransferase + in the stomach in each group. Scale bar: 50 μm; H-J: Enzyme-linked immunosorbent assay to detect the concentration of gastrin, motilin and vasoactive intestinal peptide in supernatant (n = 5). Data are expressed as the mean ± SD. $^{a}P < 0.05$. DGP: Diabetic gastroparesis; EA: Electroacupuncture; SDV: Subdiaphragmatic vagotomy; nNOS: Neuronal nitric oxide synthase; C-kit: Cluster of differentiation 117; SCF: Stem cell factor; ChAT: Choline acetyltransferase; DAPI: 4',6-diamidino-2-phenylindole; Gas: Gastrin; MLT: Motilin; VIP: Vasoactive intestinal peptide.

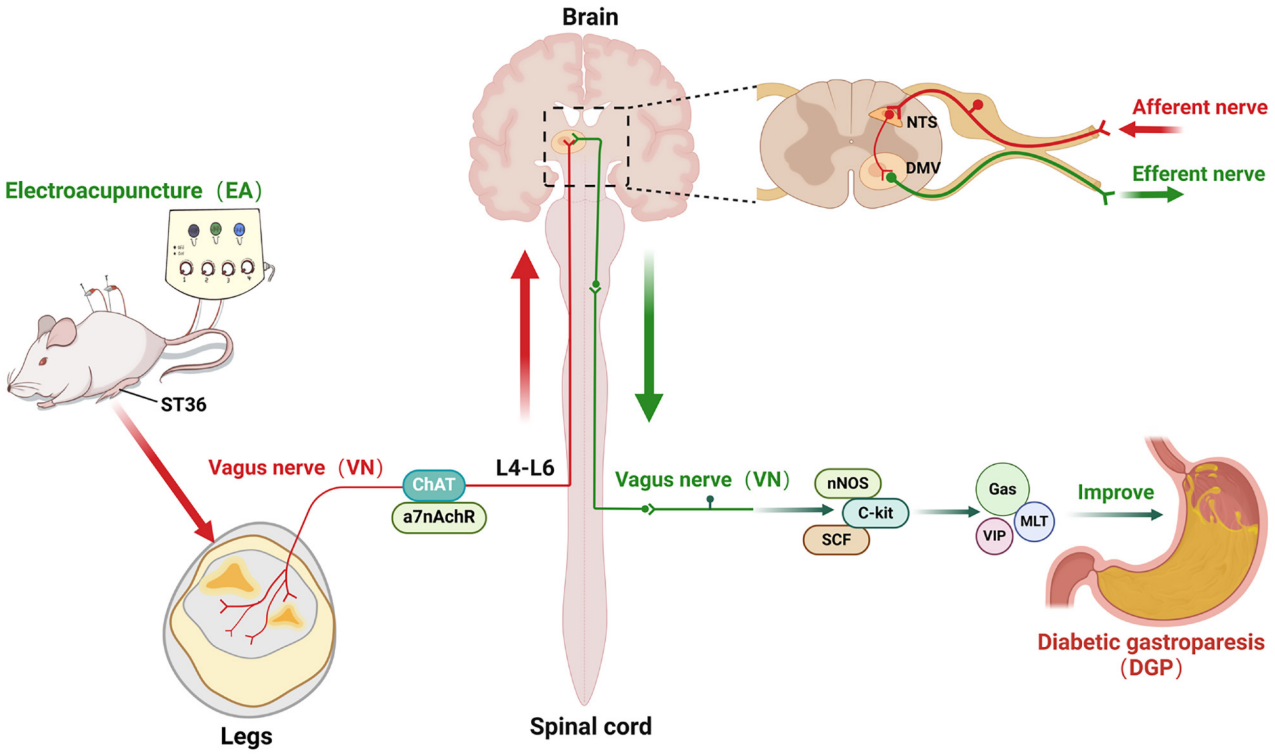

Figure 9 This schematic diagram illustrates the vagus nerve pathway through which electroacupuncture at ST36 enhances diabetic gastroparesis. Electroacupuncture activates the choline acetyltransferase target of the vagus nerve by intervening in the ST36 acupoint area, which is transmitted up the spinal cord from L4-L6 to the intracranial nucleus tractus solitarius. This, in turn, regulates the gastric smooth muscle-related factors neuronal nitric oxide synthase, cluster of differentiation 117 and stem cell factor, as well as gastrointestinal peptides, through the subdiaphragmatic vagus nerve. This, in turn, improves the gastric motility disorder of diabetic gastroparesis. ChAT: Choline acetyltransferase; α7nAchR: α7 nicotinic acetylcholine receptor; nNOS: Neuronal nitric oxide synthase; C-kit: Cluster of differentiation 117; SCF: Stem cell factor; Gas: Gastrin; MLT: Motilin; VIP: Vasoactive intestinal peptide; NTS: Nucleus tractus solitarius; DMV: Dorsal motor nucleus of the vagus.

FOOTNOTES

Author contributions: Zhang Y and Yue ZH designed the study; Zhang Y, Tang YW and Zhou J performed the experiments; Tang YW, Zhou J, Wei YR, Peng YT and Yan Z conducted a survey and search; Zhang Y analyzed the results and wrote the article; All authors read and approved the final version.

Supported by the Natural Science Foundation of Hunan Province, China, No. 2023JJ30462; Hunan Provincial Department of Science and Technology, No. 2023SK2045, No. 22JBZ007 and No. Z2023JB01; and Graduate Research and Innovation Projects of Hunan Province, No.

2024CX031.

Institutional review board statement: This study does not involve any human experiments.

Institutional animal care and use committee statement: All animal studies were approved by the Medical Ethics Committee of Hunan University of Traditional Chinese Medicine (No. HNUCM21-2311-08).

Conflict-of-interest statement: The authors declare that they have no conflict of interest.

Data sharing statement: The datasets used and/or analyzed during the current study are available from the corresponding author on reasonable request.

ARRIVE guidelines statement: The authors have read the ARRIVE guidelines, and the manuscript was prepared and revised according to the ARRIVE guidelines.

Country of origin: China

ORCID number: Zeng-Hui Yue 0000-0002-9234-3056.

S-Editor: Fan M
L-Editor: A
P-Editor: Yu HG

REFERENCES

1 **Kassander P**. Asymptomatic gastric retention in diabetics (gastroparesis diabeticorum). *Ann Intern Med* 1958; **48**: 797-812 [PMID: 13521605 DOI: 10.7326/0003-4819-48-4-797] [FullText]
2 **Ahmed MSO**, Forde H, Smith D. Diabetic gastroparesis: clinical features, diagnosis and management. *Ir J Med Sci* 2023; **192**: 1687-1694 [PMID: 36266392 DOI: 10.1007/s11845-022-03191-8] [FullText]
3 **Bharucha AE**, Kudva YC, Prichard DO. Diabetic Gastroparesis. *Endocr Rev* 2019; **40**: 1318-1352 [PMID: 31081877 DOI: 10.1210/er.2018-00161] [FullText]
4 **Camilleri M**, Parkman HP, Shafi MA, Abell TL, Gerson L; American College of Gastroenterology. Clinical guideline: management of gastroparesis. *Am J Gastroenterol* 2013; **108**: 18-37; quiz 38 [PMID: 23147521 DOI: 10.1038/ajg.2012.373] [FullText]
5 **Schol J**, Huang IH, Carbone F, Fernandez LMB, Gourcerol G, Ho V, Kohn G, Lacy BE, Colombo AL, Miwa H, Moshiree B, Nguyen L, O'Grady G, Siah KTH, Stanghellini V, Tack J. Rome Foundation and international neurogastroenterology and motility societies' consensus on idiopathic gastroparesis. *Lancet Gastroenterol Hepatol* 2025; **10**: 68-81 [PMID: 39674226 DOI: 10.1016/S2468-1253(24)00284-X] [FullText]
6 **Yu B**, Sun M, Wang Z, Zhu B, Xue J, Yang W, Gao X, Zhi M, Cao J, Zhao J, Zhao X, Liu W, Wang F, Li T. Effects of Stimulating Local and Distal Acupoints on Diabetic Gastroparesis: A New Insight in Revealing Acupuncture Therapeutics. *Am J Chin Med* 2021; **49**: 1151-1164 [PMID: 34049477 DOI: 10.1142/S0192415X21500555] [FullText]
7 **Zaman A**, Özçelik H, Yücel E, Su Akkan S, Onsinejad T, Mert Yüksel S, Bülbül M. Effect of sex on chronic stress induced alterations in hindbrain catecholaminergic system and autonomic dysfunction resulting in gastrointestinal dysmotility. *Brain Res* 2024; **1842**: 149112 [PMID: 38969083 DOI: 10.1016/j.brainres.2024.149112] [FullText]
8 **Travagli RA**, Anselmi L. Vagal neurocircuitry and its influence on gastric motility. *Nat Rev Gastroenterol Hepatol* 2016; **13**: 389-401 [PMID: 27251213 DOI: 10.1038/nrgastro.2016.76] [FullText]
9 **Chen Y**, Zhang S, Li Y, Yan H, Ba Y, Wang X, Shi N, Liu C. Gastric Electrical Stimulation Increases the Proliferation of Interstitial Cells of Cajal and Alters the Enteric Nervous System in Diabetic Rats. *Neuromodulation* 2022; **25**: 1106-1114 [PMID: 35088751 DOI: 10.1016/j.neurom.2021.10.003] [FullText]
10 **Huang H**, Peng Y, Xiao L, Wang J, Xin YH, Zhang TH, Li XY, Wei X. Electroacupuncture Promotes Gastric Motility by Suppressing Pyroptosis *via* NLRP3/Caspase-1/GSDMD Signaling Pathway in Diabetic Gastroparesis Rats. *Chin J Integr Med* 2025; **31**: 448-457 [PMID: 39470921 DOI: 10.1007/s11655-024-3821-6] [FullText]
11 **Chen X**, Liu Y, Pan D, Cao M, Wang X, Wang L, Xu Y, Wang Y, Yan J, Liu J, Yang M. (68)Ga-NOTA PET imaging for gastric emptying assessment in mice. *BMC Gastroenterol* 2021; **21**: 69 [PMID: 33581729 DOI: 10.1186/s12876-021-01642-7] [FullText]
12 **Edwards FR**, Hirst GD. An electrical analysis of slow wave propagation in the guinea-pig gastric antrum. *J Physiol* 2006; **571**: 179-189 [PMID: 16357016 DOI: 10.1113/jphysiol.2005.100743] [FullText]
13 **Wei X**, Lin Y, Zhao D, Xiao X, Chen Q, Chen S, Peng Y. Electroacupuncture Relieves Suppression of Autophagy in Interstitial Cells of Cajal of Diabetic Gastroparesis Rats. *Can J Gastroenterol Hepatol* 2020; **2020**: 7920715 [PMID: 32211350 DOI: 10.1155/2020/7920715] [FullText]
14 **Jalleh RJ**, Marathe CS, Jones KL, Horowitz M, Rayner CK. Digesting the pathogenesis of diabetic gastroparesis. *J Diabetes Complications* 2021; **35**: 107992 [PMID: 34389236 DOI: 10.1016/j.jdiacomp.2021.107992] [FullText]
15 **Camilleri M**, Chedid V, Ford AC, Haruma K, Horowitz M, Jones KL, Low PA, Park SY, Parkman HP, Stanghellini V. Gastroparesis. *Nat Rev Dis Primers* 2018; **4**: 41 [PMID: 30385743 DOI: 10.1038/s41572-018-0038-z] [FullText]

16 **Han X**, Chen X, Wang X, Gong M, Lu M, Yu Z, Xu B, Yuan J. Electroacupuncture at ST36 Improve the Gastric Motility by Affecting Neurotransmitters in the Enteric Nervous System in Type 2 Diabetic Rats. *Evid Based Complement Alternat Med* 2021; **2021**: 6666323 [PMID: 34221088 DOI: 10.1155/2021/6666323] [FullText]

17 **Maalouf E**, Khasawneh H, Karbhari A, AlAsfoor S, Breen-Lyles M, Bernard C, Rajan E, Farrugia G, Lowe V, Goenka A, Grover M. Preliminary study on the dynamic positron emission tomography imaging with (11)C-ER176 to delineate macrophage activation in diabetic gastroparesis. *Neurogastroenterol Motil* 2024; **36**: e14762 [PMID: 38376247 DOI: 10.1111/nmo.14762] [FullText]

18 **Petri M**, Singh I, Baker C, Underkofler C, Rasouli N. Diabetic gastroparesis: An overview of pathogenesis, clinical presentation and novel therapies, with a focus on ghrelin receptor agonists. *J Diabetes Complications* 2021; **35**: 107733 [PMID: 32948398 DOI: 10.1016/j.jdiacomp.2020.107733] [FullText]

19 **Edwards PT**, Soni KG, Conner ME, Fowler SW, Foong JPP, Stavely R, Cheng LS, Preidis GA. Site-specific pathophysiology in a neonatal mouse model of gastroparesis. *Neurogastroenterol Motil* 2023; **35**: e14676 [PMID: 37772676 DOI: 10.1111/nmo.14676] [FullText]

20 **Sprouse J**, Sampath C, Gangula P. 17β-Estradiol Suppresses Gastric Inflammatory and Apoptotic Stress Responses and Restores nNOS-Mediated Gastric Emptying in Streptozotocin (STZ)-Induced Diabetic Female Mice. *Antioxidants (Basel)* 2023; **12**: 758 [PMID: 36979006 DOI: 10.3390/antiox12030758] [FullText]

21 **Foong D**, Zhou J, Zarrouk A, Ho V, O'Connor MD. Understanding the Biology of Human Interstitial Cells of Cajal in Gastrointestinal Motility. *Int J Mol Sci* 2020; **21**: 4540 [PMID: 32630607 DOI: 10.3390/ijms21124540] [FullText]

22 **Grover M**, Farrugia G, Lurken MS, Bernard CE, Faussone-Pellegrini MS, Smyrk TC, Parkman HP, Abell TL, Snape WJ, Hasler WL, Ünalp-Arida A, Nguyen L, Koch KL, Calles J, Lee L, Tonascia J, Hamilton FA, Pasricha PJ; NIDDK Gastroparesis Clinical Research Consortium. Cellular changes in diabetic and idiopathic gastroparesis. *Gastroenterology* 2011; **140**: 1575-85.e8 [PMID: 21300066 DOI: 10.1053/j.gastro.2011.01.046] [FullText]

23 **Grover M**, Bernard CE, Pasricha PJ, Parkman HP, Gibbons SJ, Tonascia J, Koch KL, McCallum RW, Sarosiek I, Hasler WL, Nguyen LAB, Abell TL, Snape WJ, Kendrick ML, Kellogg TA, McKenzie TJ, Hamilton FA, Farrugia G; NIDDK Gastroparesis Clinical Research Consortium (GpCRC). Diabetic and idiopathic gastroparesis is associated with loss of CD206-positive macrophages in the gastric antrum. *Neurogastroenterol Motil* 2017; **29** [PMID: 28066953 DOI: 10.1111/nmo.13018] [FullText]

24 **Li H**, Cao W, Zhang XB, Zhang XX, Gu C, Gu LM, Pan CY, Tian YZ, Lu M. Atractylenolide-1 alleviates gastroparesis in diabetic rats by activating the stem cell factor/ckit signaling pathway. *Mol Med Rep* 2021; **24**: 691 [PMID: 34368880 DOI: 10.3892/mmr.2021.12331] [FullText]

25 **Lin G**, Zhang J, Li L, Zou Z, Chen C, Xue L, Zhao L. Effect of electroacupuncture on gastric interstitial cells of Cajal in a rat model of diabetic gastroparesis. *Exp Ther Med* 2016; **11**: 2489-2494 [PMID: 27284337 DOI: 10.3892/etm.2016.3185] [FullText]

26 **Yu Y**, Hu L, Xu Y, Wu S, Chen Y, Zou W, Zhang M, Wang Y, Gu Y. Impact of blood glucose control on sympathetic and vagus nerve functional status in patients with type 2 diabetes mellitus. *Acta Diabetol* 2020; **57**: 141-150 [PMID: 31367992 DOI: 10.1007/s00592-019-01393-8] [FullText]

27 **Jin Z**, Shen Z, Yan S, Chen G, Yin Y, Zhang Y, Wu X. Electroacupuncture ameliorates gastrointestinal dysfunction by modulating DMV cholinergic efferent signals to drive the vagus nerve in p-MCAO rats. *Heliyon* 2024; **10**: e29426 [PMID: 38638995 DOI: 10.1016/j.heliyon.2024.e29426] [FullText]

28 **Liu S**, Wang Z, Su Y, Qi L, Yang W, Fu M, Jing X, Wang Y, Ma Q. A neuroanatomical basis for electroacupuncture to drive the vagal-adrenal axis. *Nature* 2021; **598**: 641-645 [PMID: 34646018 DOI: 10.1038/s41586-021-04001-4] [FullText]

29 **Jung SJ**, Kook MG, Kim S, Kang KS, Soh KS. Homing of the Stem Cells from the Acupoint ST-36 to the Site of a Spinal Cord Injury: A Preliminary Study. *J Acupunct Meridian Stud* 2018; **11**: 133-136 [PMID: 29879473 DOI: 10.1016/j.jams.2018.05.007] [FullText]

30 **Lu MJ**, Yu Z, He Y, Yin Y, Xu B. Electroacupuncture at ST36 modulates gastric motility *via* vagovagal and sympathetic reflexes in rats. *World J Gastroenterol* 2019; **25**: 2315-2326 [PMID: 31148903 DOI: 10.3748/wjg.v25.i19.2315] [FullText]

31 **Lee CH**, Jung HS, Lee TY, Lee SR, Yuk SW, Lee KG, Lee BH. Studies of the central neural pathways to the stomach and Zusanli (ST36). *Am J Chin Med* 2001; **29**: 211-220 [PMID: 11527064 DOI: 10.1142/S0192415X01000241] [FullText]

32 **Fang JF**, Fang JQ, Shao XM, Du JY, Liang Y, Wang W, Liu Z. Electroacupuncture treatment partly promotes the recovery time of postoperative ileus by activating the vagus nerve but not regulating local inflammation. *Sci Rep* 2017; **7**: 39801 [PMID: 28051128 DOI: 10.1038/srep39801] [FullText]

33 **Zhang MT**, Liang YF, Dai Q, Gao HR, Wang H, Chen L, Huang S, Wang XY, Shen GM. A spinal neural circuit for electroacupuncture that regulates gastric functional disorders. *J Integr Med* 2025; **23**: 56-65 [PMID: 39694773 DOI: 10.1016/j.joim.2024.11.005] [FullText]

34 **Song J**, Yin J, Sallam HS, Bai T, Chen Y, Chen JD. Electroacupuncture improves burn-induced impairment in gastric motility mediated *via* the vagal mechanism in rats. *Neurogastroenterol Motil* 2013; **25**: 807-e635 [PMID: 23848593 DOI: 10.1111/nmo.12183] [FullText]

World Journal of Gastroenterology

Submit a Manuscript: https://www.f6publishing.com

World J Gastroenterol 2025 June 7; 31(21): 105753

DOI: 10.3748/wjg.v31.i21.105753

ISSN 1007-9327 (print) ISSN 2219-2840 (online)

META-ANALYSIS

Artificial intelligence for reducing missed detection of adenomas and polyps in colonoscopy: A systematic review and meta-analysis

Sheng-Yu Wang, Jia-Cheng Gao, Shuo-Dong Wu

Specialty type: Gastroenterology and hepatology

Provenance and peer review: Unsolicited article; Externally peer reviewed.

Peer-review model: Single blind

Peer-review report's classification

Scientific Quality: Grade B, Grade B, Grade C

Novelty: Grade B, Grade B, Grade C

Creativity or Innovation: Grade A, Grade B, Grade C

Scientific Significance: Grade A, Grade B, Grade C

P-Reviewer: Issa IA; Musat EC; Satiya J

Received: February 6, 2025

Revised: March 21, 2025

Accepted: May 19, 2025

Published online: June 7, 2025

Processing time: 120 Days and 15.8 Hours

Sheng-Yu Wang, The Second Department of General Surgery, Shengjing Hospital of China Medical University, Shenyang 110004, Liaoning Province, China

Jia-Cheng Gao, Department of Orthopedic Surgery, The First Hospital of China Medical University, Shenyang 110001, Liaoning Province, China

Shuo-Dong Wu, Department of General Surgery, Shengjing Hospital of China Medical University, Shenyang 110004, Liaoning Province, China

Co-first authors: Sheng-Yu Wang and Jia-Cheng Gao.

Corresponding author: Shuo-Dong Wu, MD, Chief, Professor, Department of General Surgery, Shengjing Hospital of China Medical University, No. 36 Sanhao Street, Heping District, Shenyang 110004, Liaoning Province, China. 13909824526@163.com

Abstract

BACKGROUND

Colorectal cancer has a high incidence and mortality rate, and the effectiveness of routine colonoscopy largely depends on the endoscopist's expertise. In recent years, computer-aided detection (CADe) systems have been increasingly integrated into colonoscopy to improve detection accuracy. However, while most studies have focused on adenoma detection rate (ADR) as the primary outcome, the more sensitive adenoma miss rate (AMR) has been less frequently analyzed.

AIM

To evaluate the effectiveness of CADe in colonoscopy and assess the advantages of AMR over ADR.

METHODS

A comprehensive literature search was conducted in PubMed, Embase, and the Cochrane Central Register of Controlled Trials using predefined search strategies to identify relevant studies published up to August 2, 2024. Statistical analyses were performed to compare outcomes between groups, and potential publication bias was assessed using funnel plots. The quality of the included studies was evaluated using the Cochrane Risk of Bias tool and the Grading of Recommendations, Assessment, Development, and Evaluation approach.

RESULTS

Five studies comprising 1624 patients met the inclusion criteria. AMR was significantly lower in the CADe-assisted group than in the routine colonoscopy

group (147/927, 15.9% *vs* 345/960, 35.9%; $P < 0.01$). However, CADe did not provide a significant advantage in detecting advanced adenomas or lesions measuring 6-9 mm or ≥ 10 mm. The polyp miss rate (PMR) was also lower in the CADe-assisted group [odds ratio (OR), 0.35; 95% confidence interval (CI): 0.23-0.52; $P < 0.01$]. While the overall ADR did not differ significantly between groups, the ADR during the first-pass examination was higher in the CADe-assisted group (OR, 1.37; 95%CI: 1.10-1.69; $P = 0.004$). The level of evidence for the included randomized controlled trials was graded as moderate.

CONCLUSION

CADe can significantly reduce AMR and PMR while improving ADR during initial detection, demonstrating its potential to enhance colonoscopy performance. These findings highlight the value of CADe in improving the detection of colorectal neoplasms, particularly small and histologically distinct adenomas.

Key Words: Artificial intelligence; Computer-aided detection; Colonoscopy; Neoplasms; Prevention and control

Core Tip: Artificial intelligence is being increasingly used in colonoscopy, with more and more studies reporting its potential benefits. However, most studies have focused on adenoma detection rate (ADR) as the primary outcome and assessed only short-term effects. Recently, adenoma miss rate (AMR) has gained more attention, and based on this, we designed this meta-analysis to evaluate the effect of computer-aided detection on AMR, compared it with ADR, and assessed its long-term impact.

Citation: Wang SY, Gao JC, Wu SD. Artificial intelligence for reducing missed detection of adenomas and polyps in colonoscopy: A systematic review and meta-analysis. *World J Gastroenterol* 2025; 31(21): 105753
URL: https://www.wjgnet.com/1007-9327/full/v31/i21/105753.htm
DOI: https://dx.doi.org/10.3748/wjg.v31.i21.105753

INTRODUCTION

Colorectal cancer (CRC) is the fourth most common malignancy worldwide, accounting for 6.1% of all cancer cases, and is the second leading cause of cancer-related mortality (9.2%) after lung cancer[1]. Although colonoscopy remains one of the most effective methods for diagnosing and managing gastrointestinal diseases[2], its effectiveness is largely dependent on the endoscopist's skill, and the low detection rate of adenomas and polyps in conventional colonoscopy contributes to the high incidence of CRC, increasing both patient burden and healthcare costs[3].

With advancements in medical technology, artificial intelligence (AI) has been increasingly integrated into clinical practice. AI-assisted colonoscopy has demonstrated high diagnostic accuracy, with one study reporting an accuracy of 98% and a specificity of 100% for detecting colorectal neoplasms[4]. By enhancing visual recognition, AI can improve the detection of both subtle and advanced adenomas, thereby reducing the risk of misclassifying non-neoplastic lesions. Thus, it may help lower the rate of unnecessary resections and decrease complications such as intestinal bleeding and perforation[5,6].

In 2019, the computer-aided polyp detection (CADe) system was introduced into clinical practice, and it demonstrated a significant improvement in adenoma detection rate (ADR) compared to conventional colonoscopy (29.1% *vs* 20.3%, $P < 0.001$)[7]. This system is based on convolutional neural networks (CNNs) or self-learning algorithms that integrate visual recognition with diagnostic criteria, providing real-time alerts to endoscopists regarding suspicious lesions.

Until now, most studies that have evaluated AI-assisted colonoscopy have used ADR as the primary outcome measure [8,9]. However, AI-based systems may generate false positives by detecting non-adenomatous lesions, leading to an overestimation of ADR[10,11]. To address this limitation, adenoma miss rate (AMR) has been proposed as a more reliable metric, as it accounts for lesions that are missed during the initial examination and are subsequently detected upon repeat colonoscopy. AMR provides a more accurate assessment of AI performance, as it directly reflects the system's ability to reduce missed lesions. While previous studies have explored AMR in colonoscopy, most have been limited to short-term evaluations due to time constraints[12-14].

Herein, we designed this study using latest research to determine the long-term effects of AI in colonoscopy, which have not been extensively explored in previous studies. Specifically, we analyzed the impact of the CADe system on AMR and provided a comprehensive overview of advancements in AI-assisted colorectal disease detection. By highlighting the advantages of AMR over ADR, this study further demonstrates the potential of AI to enhance colonoscopy performance and improve diagnostic accuracy.

MATERIALS AND METHODS

Data sources and search strategy

A comprehensive literature search was conducted in PubMed, Embase, and the Cochrane Central Register of Controlled Trials to identify studies published up to August 2, 2024. The search was restricted to randomized controlled trials (RCTs), although studies involving the CADe system were also reviewed. The detailed search strategy is provided in Supplementary materials, and the study flow chart is illustrated in Figure 1.

Outcomes and inclusion and exclusion criteria

Primary outcome: The primary outcome was the AMR, defined as the number of adenomas detected during the second-pass colonoscopy divided by the total number of adenomas identified across both passes. Subgroup analyses were conducted based on adenoma size, location, and histological characteristics.

Secondary outcomes: The secondary outcomes included the polyp miss rate (PMR), ADR, adenomas per colonoscopy (APC), and withdrawal time. The PMR was calculated as the number of polyps detected during the second-pass colonoscopy divided by the total number of polyps detected across both passes. ADR was defined as the proportion of individuals undergoing a complete colonoscopy in whom at least one adenoma was detected, APC was determined by dividing the total number of adenomas detected by the total number of colonoscopies performed, and withdrawal time was measured as the duration required to withdraw the colonoscope while examining the colonic mucosa, excluding the time needed for biopsy or lesion excision.

Inclusion and exclusion criteria: Studies were included if they enrolled adults aged 18 years or older who underwent colonoscopy, while those that were not RCTs, did not report relevant outcomes, or had a sample size of fewer than 30 participants were excluded.

Selection process

Two independent reviewers (Wang SY and Gao JC) screened the search results based on predefined criteria. The screening process involved an initial review of titles and abstracts, followed by a full-text assessment of studies meeting the inclusion criteria. All screening decisions were documented, and any discrepancies were resolved through discussion, and there were no unresolved disagreements by the time of manuscript completion.

Data extraction

Data were independently extracted by Wang SY and Gao JC using standardized tables comprising study characteristics (author, country, year, and study design), patient characteristics (sample size, age, and sex), and outcome measures (AMR, PMR, ADR, APC, and withdrawal time). In cases where data were missing, the studies' corresponding authors were contacted, but no responses were received. Any discrepancies in data extraction were resolved through discussion with a third reviewer (Wu SD).

Study quality and assessment

The quality of the included studies was assessed using the Cochrane Risk of Bias tool, and the results are summarized in Figure 2.

Data synthesis and statistical analysis

Dichotomous outcomes were analyzed using odds ratios (OR) with 95% confidence interval (CI), while mean differences (MD) with 95%CI were used for continuous outcomes. The DerSimonian and Laird random-effects model was applied for all analyses. Given the skewed distribution of continuous variables in the included studies, this study applied the methods proposed by Luo *et al*[15] and Wan *et al*[16] to estimate mean values and standard deviations. Subgroup analyses were conducted to evaluate missed adenomas based on size (≤ 5 mm, 6-9 mm, and ≥ 10 mm), location (proximal colon and distal colon), and histological characteristics (sessile serrated lesions and advanced adenomas). To assess the sensitivity of ADR in evaluating CADe performance, subgroup analyses were performed for all detected adenomas, including ADR and first-pass ADR. Withdrawal time was also analyzed in subgroups based on first-pass and second-pass examinations.

Heterogeneity was assessed using Cochran's Q (χ^2) and I^2 statistics, whereby I^2 values of 25%, 50% and 75% indicated low, moderate, and high heterogeneity, respectively. Sensitivity analysis for the primary outcome (AMR) was performed using the leave-one-out method. Publication bias was evaluated using funnel plots.

The quality of evidence was graded using the Grading of Recommendations, Assessment, Development, and Evaluation methodology[17]. This meta-analysis adhered to the Preferred Reporting Items for Systematic Reviews and Meta-Analyses guidelines[18]. All statistical analyses were conducted using RevMan 5.4 (The Cochrane Collaboration, Copenhagen, Denmark). The meta-analysis was registered in PROSPERO (ID: CRD42024583571).

RESULTS

A total of 738 records were identified through the database search. After screening, five RCTs met the inclusion criteria, comprising a total of 1624 patients[19-23]. All five studies were tandem colonoscopy trials in which the CADe-assisted

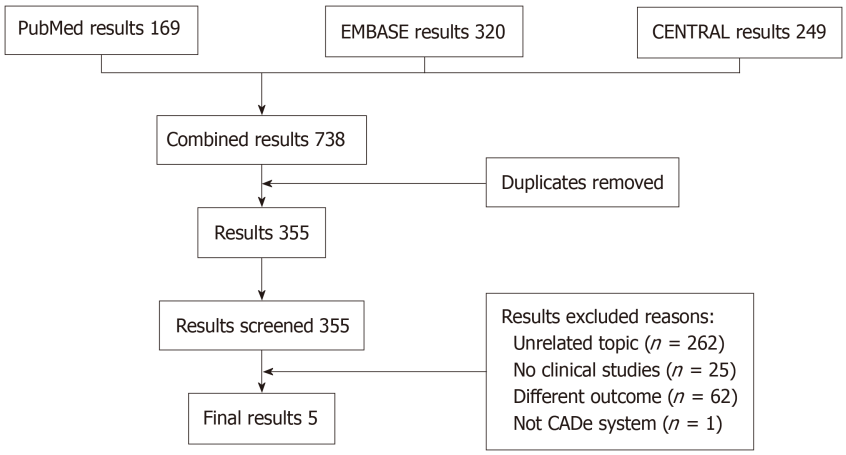

Figure 1 Study flow chart. CENTRAL: Cochrane Central Register of Controlled Trials; CADe: Computer-aided detection.

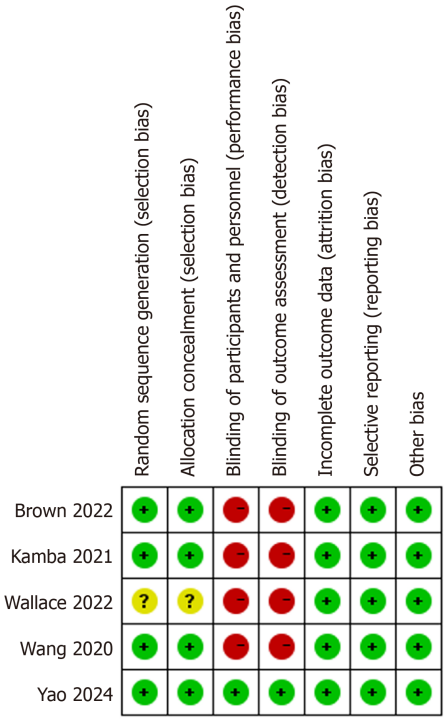

Figure 2 Study quality and assessment chart.

groups utilized the CADe system. However, one study incorporated an additional real-time assistance system, the CAQ system, which may have contributed to an increased false positive rate. Of these studies, three were conducted in Asia[19,20,23], one in North America[21], and one in Europe[22]. The key characteristics of these studies are summarized in Table 1.

Among the included studies, only one implemented a double-blind design, which was assessed as having a low risk of performance and detection bias[23]. The remaining studies used a single-blind design. In one study, the randomization method and the implementation of allocation concealment were not explicitly stated[22]. The risk of bias assessment for all included studies is presented in Figure 2.

AMR

A total of five studies were included in the analysis, all of which concluded that the CADe system significantly reduced AMR. We also observed that AMR was lower in the CADe-assisted group compared to the routine colonoscopy group (147/927, 15.9% *vs* 345/960, 35.9%; OR, 0.34; 95%CI: 0.26-0.45; $P < 0.01$). Heterogeneity was assessed as moderate (I^2 = 35%) (Figure 3A). No significant publication bias was detected in the funnel plot (Figure 3B). Sensitivity analysis demonstrated that the exclusion of the study by Glissen Brown *et al*[21] reduced heterogeneity to 0 (Figure 3C).

Table 1 Study characteristics, *n* (%)

Ref.	Year	Sample size	Age (mean years)		Gender (male)		Country	AI system	Endoscopists	Indication		Bowel preparation scale	
			CADe	Routine	CADe	Routine				CADe	Routine	CADe	Routine
Wang *et al* [19]	2020	369	47.72 ± 10.82	47.19 ± 10.38	93 (50.54)	86 (46.69)	China	CADe (EndoScreener)	Three experienced endoscopists	Screening: 58; ymptomatic: 107; Surveillance: 19	Screening: 55; Symptomatic: 117; Surveillance: 13	7.11 ± 1.40	7.19 ± 1.42
Kamba *et al*[10]	2021	355	61.63 ± 9.89	61.44 ± 10.01	136 (76.40)	136 (76.80)	Japan	CADe (Locally system)	Experts (> 5000 colonscopies) and non-experts (< 5000)	Screening: 88; Surveillance: 59; Other (FOBT positive): 31	Screening: 78; Surveillance: 68; Other (FOBT positive): 31	1-3: 166; 4-5: 5	1-3: 169; 4-5: 4
Glissen Brown *et al* [21]	2022	223	61.18 ± 9.83	60.51 ± 8.45	54 (47.79)	68 (61.82)	United States	CADe (EndoScreener)	_	Screening: 68; Surveillance: 45	Screening: 65; Surveillance: 45	9.00 (8.00-9.00)	9.00 (8.00-9.00)
Wallace *et al*[22]	2022	230	63.00 ± 8.20	64.60 ± 8.10	80 (68.97)	77 (67.54)	Italy, United Kingdom, and United States	CADe (GI-Genius)	Endoscopists (> 1000 colonscopies)	Screening: 41; Surveillance: 75	Screening: 41; Surveillance: 73	8.03 ± 1.27	8.08 ± 1.46
Yao *et al* [23]	2024	456	50.63 ± 12.25	49.85 ± 11.68	117 (51.54)	123 (53.70)	China	CADe + CAQ (EndoAngel)	8 novice endoscopists (< 5000 colonscopies) and 10 expert endoscopists (> 5000)	Screening: 145; Symptomatic: 60; Surveillance: 22	Screening: 146; Symptomatic: 64; Surveillance: 19	Inadequate (< 6): 31; Adequate (> 6): 196	Inadequate (< 6): 27; Adequate (> 6): 202

CADe: Computer-aided detection; CAQ: Computer-aided quality improvement; FOBT: Fecal occult blood test.

In the morphological subgroup analysis, all five studies provided data comparing AMR between the CADe-assisted and routine colonoscopy groups for sessile serrated lesions. The AMR was significantly lower in the CADe-assisted group (4/48, 8.3% *vs* 26/65, 40.0%; OR, 0.16; 95%CI: 0.05-0.50; $P = 0.001$), with heterogeneity assessed as low ($I^2 = 0$) (Figure 4A). However, for advanced adenomas, the difference between the CADe-assisted and routine groups was not statistically significant (7/47, 14.9% *vs* 27/58, 46.6%; OR, 0.35; 95%CI: 0.07-1.69; $P = 0.19$), and heterogeneity was moderate ($I^2 = 48\%$) (Figure 4B). Subgroup analysis based on adenoma size and location using data from two studies showed that in the ≤ 5 mm subgroup, the AMR was significantly lower in the CADe-assisted group compared to the routine colonoscopy group (OR, 0.33; 95%CI: 0.22-0.50; $P < 0.01$). However, no significant differences were observed in the 6-9 mm (OR, 0.67; 95%CI: 0.28-1.62; $P = 0.37$) or ≥ 10 mm subgroups (OR, 0.21; 95%CI: 0.04-1.07; $P = 0.06$). Heterogeneity in this analysis was low ($I^2 = 0$) (Figure 4C).

Regarding adenoma location, the AMR was significantly lower in the CADe-assisted group than in the routine group in both the proximal colon (OR, 0.48; 95%CI: 0.30-0.76; $P = 0.002$) and distal colon (OR, 0.20; 95%CI: 0.11-0.39; $P < 0.01$). Heterogeneity was low ($I^2 = 0$) (Figure 4D).

PMR, ADR, and APC

A total of five studies assessed the PMR, and all of them reported a significantly lower PMR in the CADe-assisted group compared to the routine colonoscopy group (330/1, 848, 17.9% *vs* 693/1, 863, 37.2%; OR, 0.35; 95%CI: 0.23-0.52; $P < 0.01$), and the heterogeneity was assessed as high ($I^2 = 85\%$) (Figure 5). Since sensitivity analysis revealed that the exclusion of any single study did not substantially reduce heterogeneity, no subgroup analysis was performed.

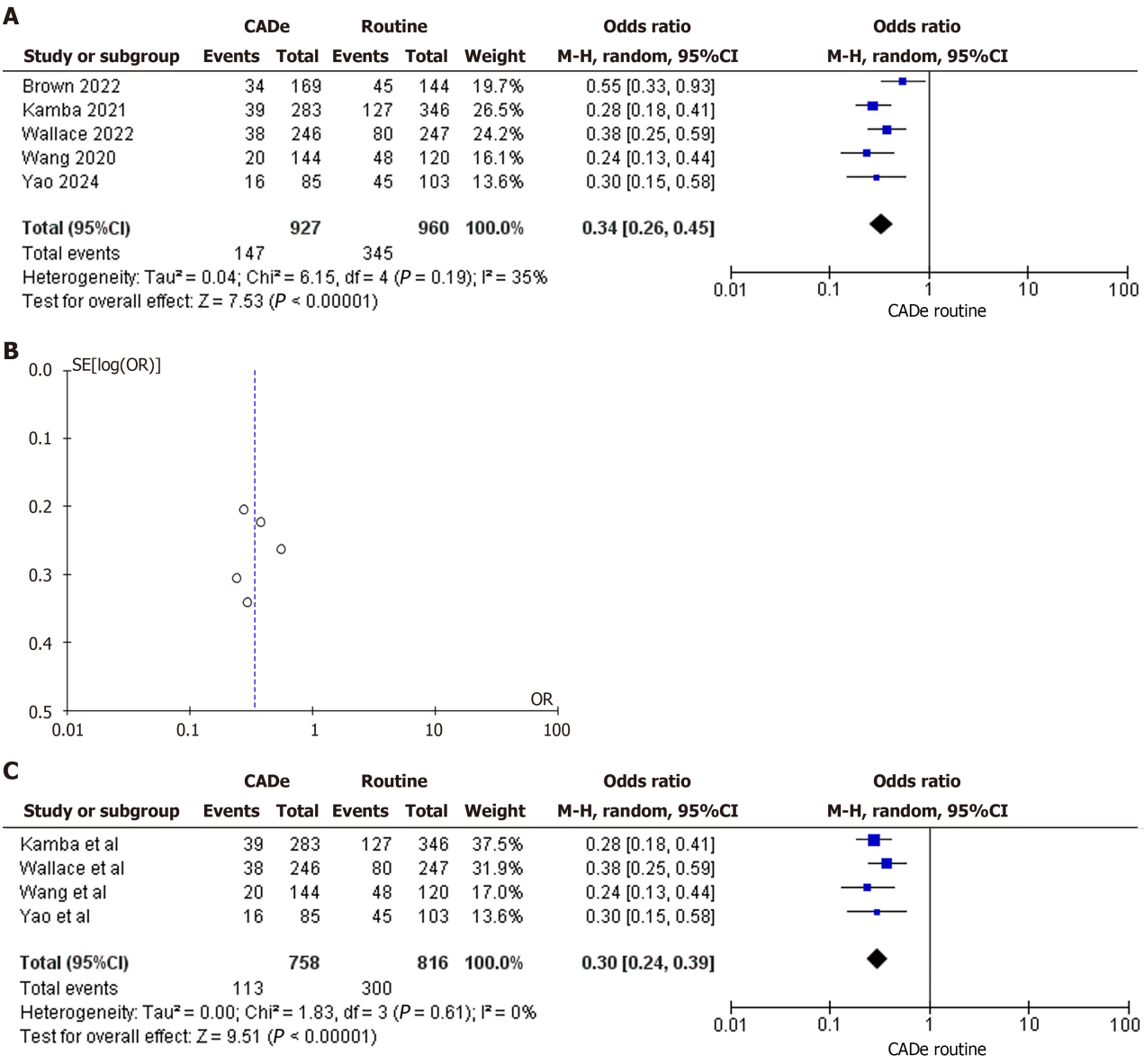

Figure 3 Forrest plots and funnel plot. A: Forrest plot showing adenoma miss rate for colonoscopy with *vs* without computer-aided detection (CADe) assistance for the included studies; B: Funnel plot showing associated publication bias; C: Sensitivity analysis of adenoma miss rate for colonoscopy with *vs* without CADe assistance for the included studies. CADe: Computer-aided detection; OR: Odds ratio.

For ADR, data from four studies were analyzed as one study did not provide relevant data. The results showed no significant difference between the CADe-assisted and routine colonoscopy groups (42.3% *vs* 41.3%; OR, 1.03; 95%CI: 0.79-1.34; $P = 0.83$; $I^2 = 18\%$) (Figure 6A). However, when all five studies were included, and first-pass ADR was specifically analyzed, the CADe-assisted group showed a significant improvement (43.2% *vs* 36.5%; OR, 1.37; 95%CI: 1.10-1.69; $P = 0.004$; $I^2 = 0$) (Figure 6B). Both analyses demonstrated low heterogeneity.

For APC, data from four studies were analyzed, and no significant difference was found between the CADe-assisted and routine colonoscopy groups (MD, 0.07; 95%CI: -0.12 to 0.25; $P = 0.47$; $I^2 = 24\%$) (Figure 7). The heterogeneity in this analysis was low.

Withdrawal time(s)

Since the calculation of the missed detection rate requires two separate colonoscopies, withdrawal times for both procedures were analyzed separately. The withdrawal time was measured in seconds, and data from four studies were included. No significant difference was observed between the CADe-assisted and routine colonoscopy groups for either the first procedure (MD, 33.53; 95%CI: -19.14 to 86.20; $P = 0.21$; $I^2 = 94\%$) or the second procedure (MD, 6.33; 95%CI: -24.69 to 37.35; $P = 0.69$; $I^2 = 89\%$) (Figure 8A and Figure 9). Both analyses demonstrated high heterogeneity. For the first procedure, heterogeneity was substantially reduced following the exclusion of the study by Glissen Brown *et al*[21] (Figure 8B). However, for the second procedure, heterogeneity remained high regardless of the exclusion of any single study.

A

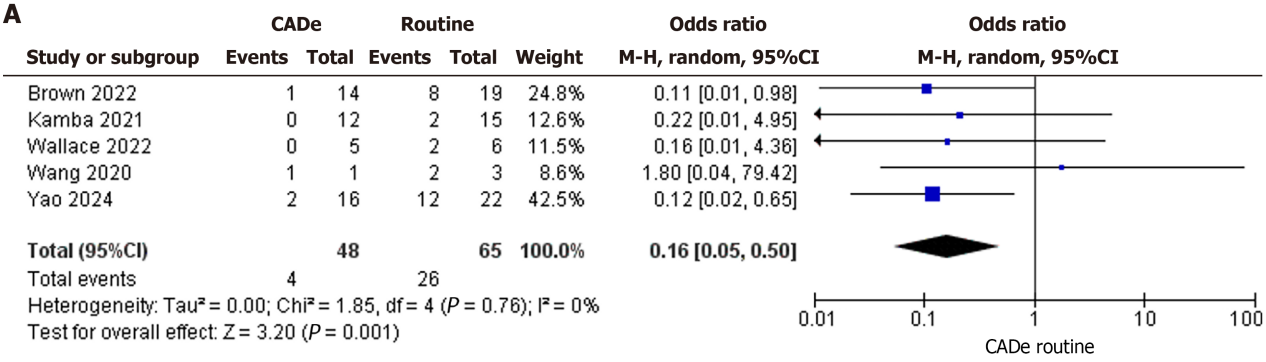
CADe
Routine
Odds ratio
Odds ratio
Study or subgroup Events Total Events Total Weight M-H, random, 95%CI M-H, random, 95%CI
Brown 2022 1 14 8 19 24.8% 0.11 [0.01, 0.98]
Kamba 2021 0 12 2 15 12.6% 0.22 [0.01, 4.95]
Wallace 2022 0 5 2 6 11.5% 0.16 [0.01, 4.36]
Wang 2020 1 1 2 3 8.6% 1.80 [0.04, 79.42]
Yao 2024 2 16 12 22 42.5% 0.12 [0.02, 0.65]
Total (95%CI) 48 65 100.0% 0.16 [0.05, 0.50]
Total events 4 26
Heterogeneity: Tau² = 0.00; Chi² = 1.85, df = 4 (P = 0.76); I² = 0%
Test for overall effect: Z = 3.20 (P = 0.001)
0.01 0.1 1 10 100
CADe routine

B

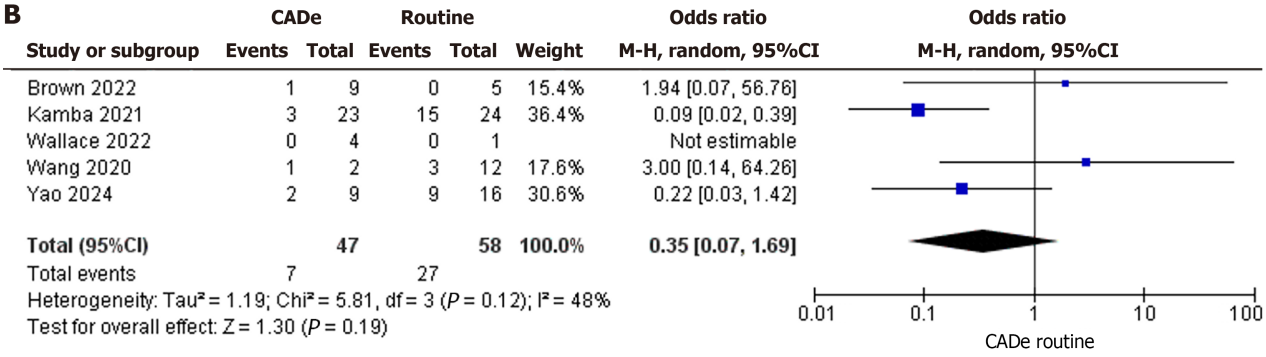
CADe
Routine
Odds ratio
Odds ratio
Study or subgroup Events Total Events Total Weight M-H, random, 95%CI M-H, random, 95%CI
Brown 2022 1 9 0 5 15.4% 1.94 [0.07, 56.76]
Kamba 2021 3 23 15 24 36.4% 0.09 [0.02, 0.39]
Wallace 2022 0 4 0 1 Not estimable
Wang 2020 1 2 3 12 17.6% 3.00 [0.14, 64.26]
Yao 2024 2 9 9 16 30.6% 0.22 [0.03, 1.42]
Total (95%CI) 47 58 100.0% 0.35 [0.07, 1.69]
Total events 7 27
Heterogeneity: Tau² = 1.19; Chi² = 5.81, df = 3 (P = 0.12); I² = 48%
Test for overall effect: Z = 1.30 (P = 0.19)
0.01 0.1 1 10 100
CADe routine

C

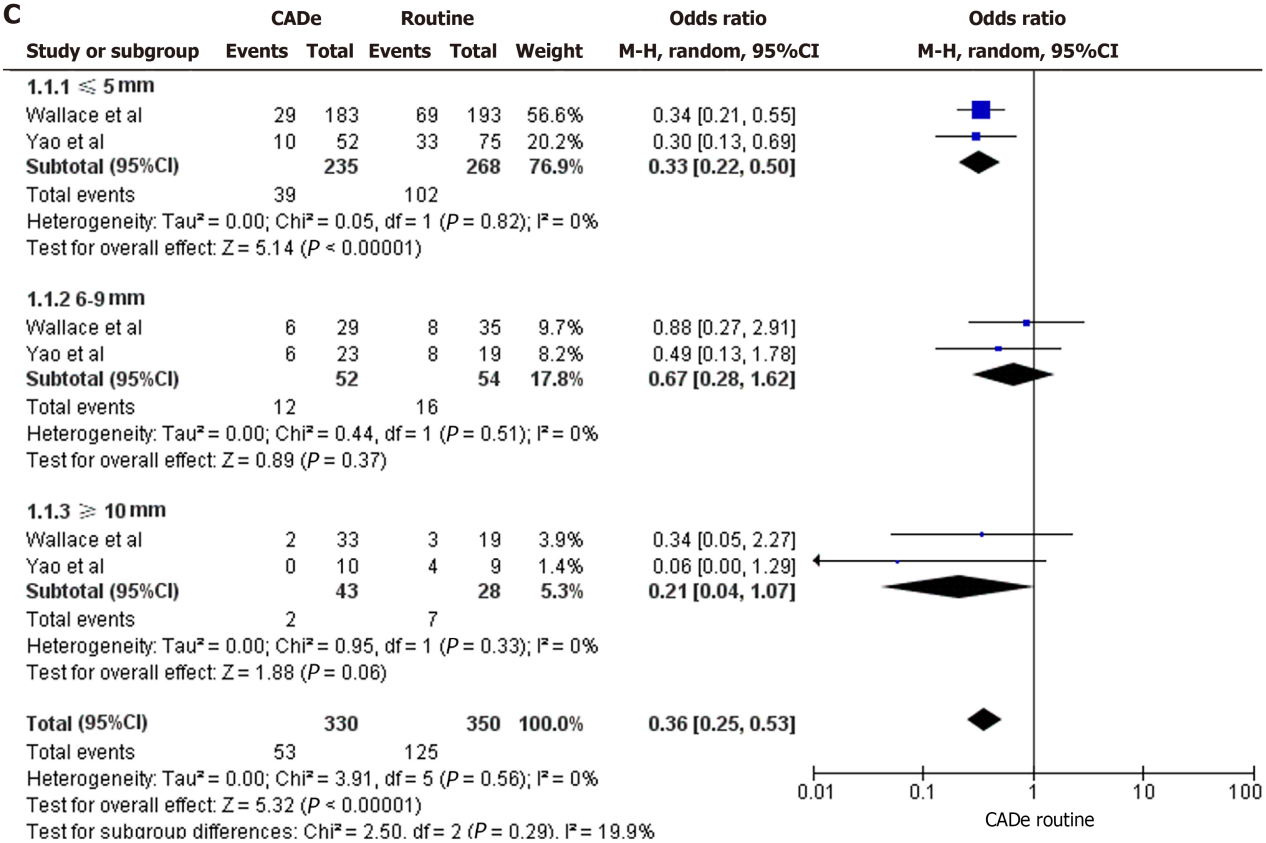
CADe
Routine
Odds ratio
Odds ratio
Study or subgroup Events Total Events Total Weight M-H, random, 95%CI M-H, random, 95%CI
1.1.1 ≤ 5 mm
Wallace et al 29 183 69 193 56.6% 0.34 [0.21, 0.55]
Yao et al 10 52 33 75 20.2% 0.30 [0.13, 0.69]
Subtotal (95%CI) 235 268 76.9% 0.33 [0.22, 0.50]
Total events 39 102
Heterogeneity: Tau² = 0.00; Chi² = 0.05, df = 1 (P = 0.82); I² = 0%
Test for overall effect: Z = 5.14 (P < 0.00001)
1.1.2 6-9 mm
Wallace et al 6 29 8 35 9.7% 0.88 [0.27, 2.91]
Yao et al 6 23 8 19 8.2% 0.49 [0.13, 1.78]
Subtotal (95%CI) 52 54 17.8% 0.67 [0.28, 1.62]
Total events 12 16
Heterogeneity: Tau² = 0.00; Chi² = 0.44, df = 1 (P = 0.51); I² = 0%
Test for overall effect: Z = 0.89 (P = 0.37)
1.1.3 ≥ 10 mm
Wallace et al 2 33 3 19 3.9% 0.34 [0.05, 2.27]
Yao et al 0 10 4 9 1.4% 0.06 [0.00, 1.29]
Subtotal (95%CI) 43 28 5.3% 0.21 [0.04, 1.07]
Total events 2 7
Heterogeneity: Tau² = 0.00; Chi² = 0.95, df = 1 (P = 0.33); I² = 0%
Test for overall effect: Z = 1.88 (P = 0.06)
Total (95%CI) 330 350 100.0% 0.36 [0.25, 0.53]
Total events 53 125
Heterogeneity: Tau² = 0.00; Chi² = 3.91, df = 5 (P = 0.56); I² = 0%
Test for overall effect: Z = 5.32 (P < 0.00001)
Test for subgroup differences: Chi² = 2.50, df = 2 (P = 0.29), I² = 19.9%
0.01 0.1 1 10 100
CADe routine

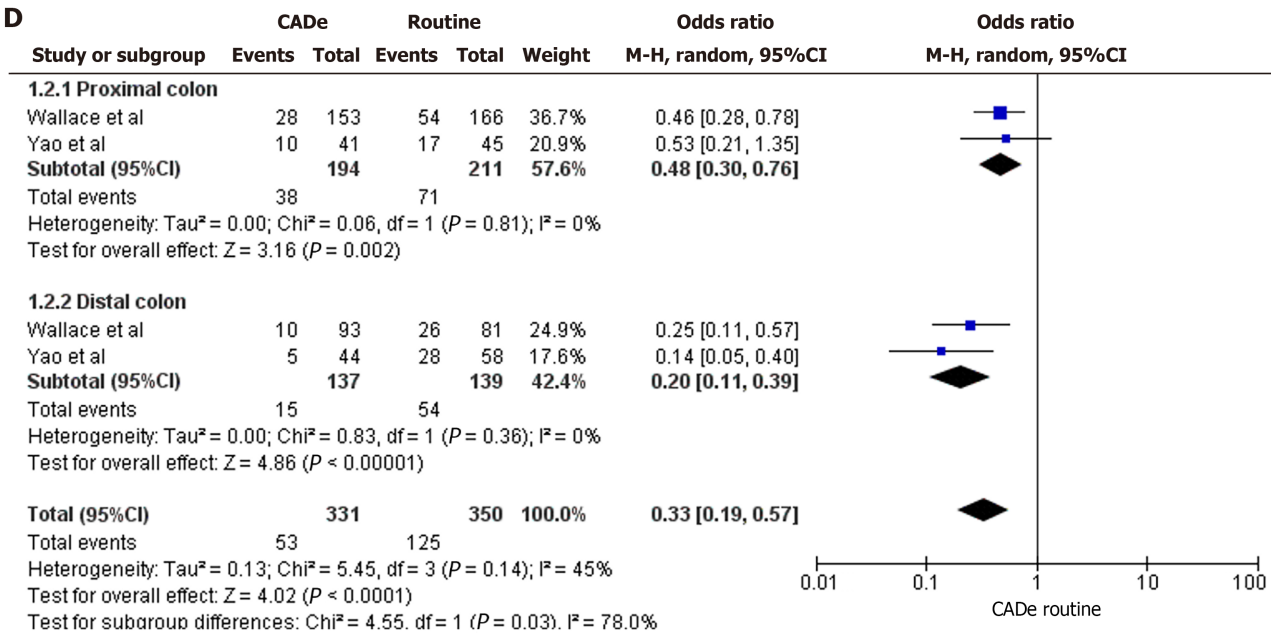

Figure 4 Forrest plots showing adenoma miss rate for colonoscopy with *vs* without computer-aided detection assistance. A: Sessile serrated lesions for the included studies; B: Advanced adenomas for the included studies; C: Size for the included studies; D: Location for the included studies. CADe: Computer-aided detection.

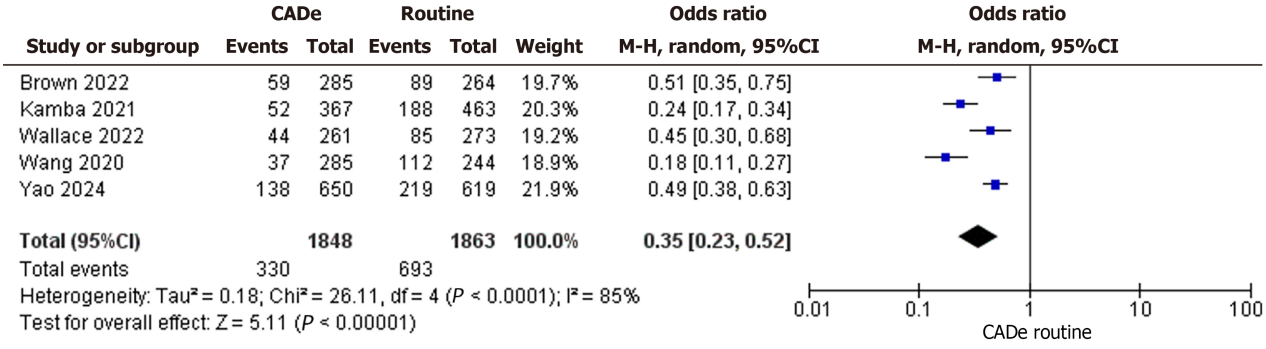

Figure 5 Forrest plot showing polyps miss rate for colonoscopy with *vs* without computer-aided detection assistance for the included studies. CADe: Computer-aided detection.

DISCUSSION

Previous meta-analyses have also reported favorable outcomes associated with AI-assisted colonoscopy. However, most studies have primarily focused on ADR, with AMR receiving only brief discussion and rarely being directly compared with ADR. The present analysis demonstrated a significant reduction in overall AMR with CADe assistance. However, its effectiveness was reduced in the ≥ 5 mm subgroup, which may be attributed to operator-dependent limitations during colonoscopy. Small and well-hidden adenomas are inherently difficult to detect with the naked eye, potentially explaining differences in CADe performance between advanced adenomas and sessile serrated adenomas. While advanced adenomas are typically ≥ 5 mm, routine colonoscopy generally achieves high detection accuracy. However, since this accuracy remains influenced by operator experience, the CADe system proved promising in mitigating this limitation by enhancing detection support[24].

The double-pass colonoscopy design used in the included studies might have influenced the observed ADR and APC, as the second examination inherently increases the likelihood of adenoma detection. To account for this effect, ADR from the first-pass examination was analyzed separately to provide a more accurate assessment of single-procedure ADR. Although first-pass ADR demonstrated statistically significant differences, regional variations in baseline ADR values and operator-related psychological factors may affect AI sensitivity in adenoma detection, making AMR a more reliable indicator of AI[25,26]. For instance, a study reported differences in adenoma detection sensitivity between Eastern and Western endoscopists (85.0% *vs* 75.8%)[27]. Additionally, even among endoscopists with an ADR value of 40%, adenomas have been found to be missed in approximately one-quarter of patients[28]. Despite its advantages, AMR may have limitations in fully evaluating the effectiveness of AI-assisted colonoscopy. Some studies suggest that missed adenomas

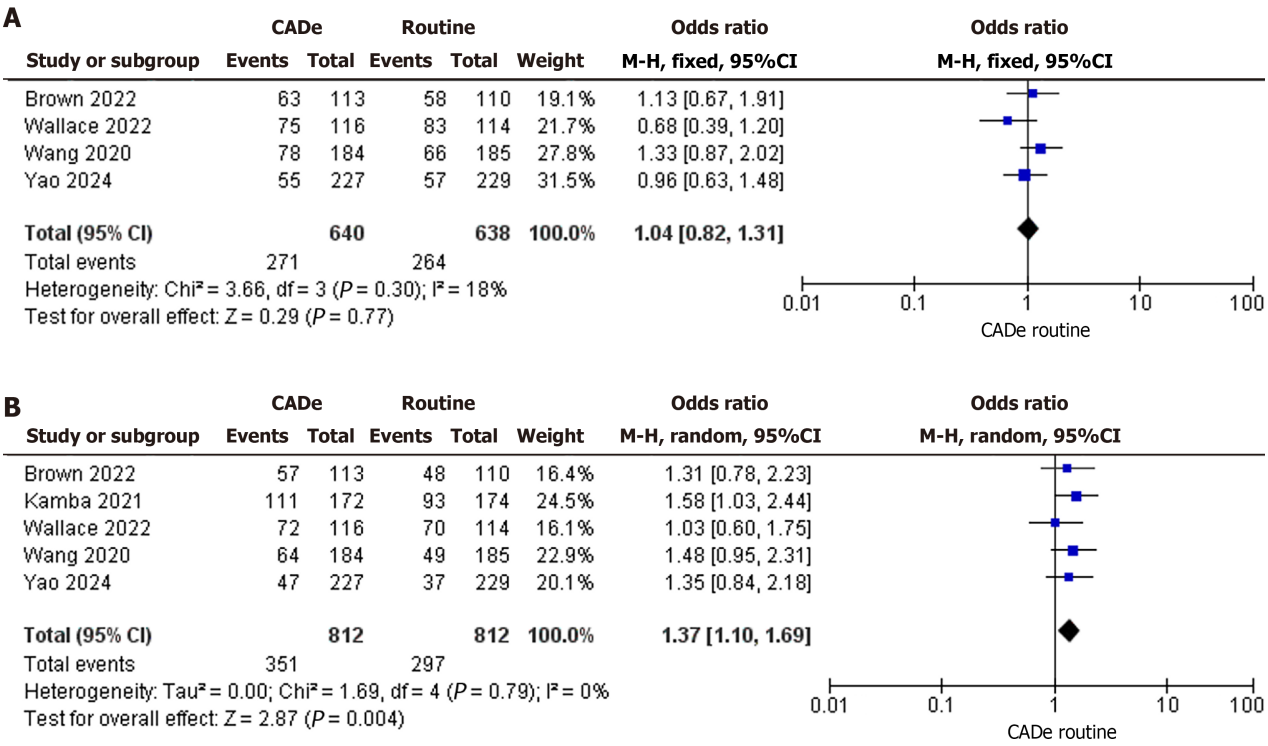

Figure 6 Forrest plots showing adenoma detection rate for colonoscopy with *vs* without computer-aided detection assistance. A: The included studies; B: The first pass for the included studies. CADe: Computer-aided detection.

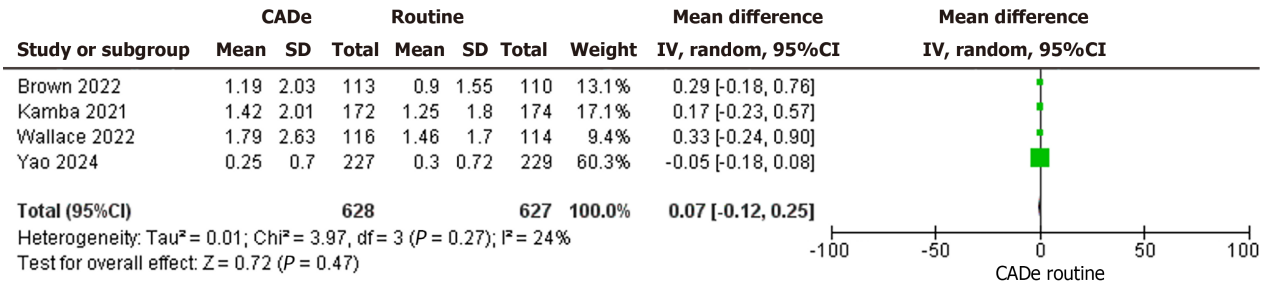

Figure 7 Forrest plot showing adenomas per colonoscopy for colonoscopy with *vs* without computer-aided detection assistance for the included studies. CADe: Computer-aided detection.

may result from inadequate mucosal exposure, and improving mucosal visualization through enhanced techniques or mechanical assistance may further reduce AMR[21,29]. Additionally, AI-assisted colonoscopy may not significantly lower AMR in cases of inadequate bowel preparation[30], indicating that AMR remains susceptible to external factors. No significant differences were observed in withdrawal times between the CADe-assisted and routine colonoscopy groups. Given that sufficient withdrawal time is associated with more thorough examinations and improved procedural safety, this finding suggests that AI assistance does not compromise procedural quality[31].

AI-assisted colonoscopy has certain limitations. First, AI does not guarantee perfect detection, as its performance depends on the system's training data and algorithms. While AI-generated findings often align with its predictive models, they may not fully reflect actual clinical scenarios, which may explain why AMR serves as a more sensitive indicator of colonoscopy performance[32]. Second, AI functions as a secondary reader, and its effectiveness remains dependent on the endoscopist's skill and technique, as the system operates under the endoscopist's guidance[33,34]. Despite these limitations, the benefits of AI-assisted colonoscopy outweigh the risks. AI supports endoscopists in maintaining consistent performance without fatigue, contributing to an overall improvement in ADR. However, an increase in adenoma detection may add to the medical burden on patients[35]. While AI-assisted colonoscopy raises individual healthcare costs, it has the potential to reduce CRC incidence, lower overall national healthcare expenditures, and alleviate pressure on medical insurance systems[36,37]. Moreover, AI-assisted colonoscopy has been shown to be cost-effective, with one study reporting an average savings of $57 per examination per patient in the United States[38]. In the long term, AI has the potential to improve colonoscopy by enhancing the speed and accuracy of lesion detection. Since CRC primarily develops from polyps or adenomas, identifying and removing these precancerous lesions represents a viable strategy for cancer prevention. However, due to time constraints, no studies have definitively confirmed the

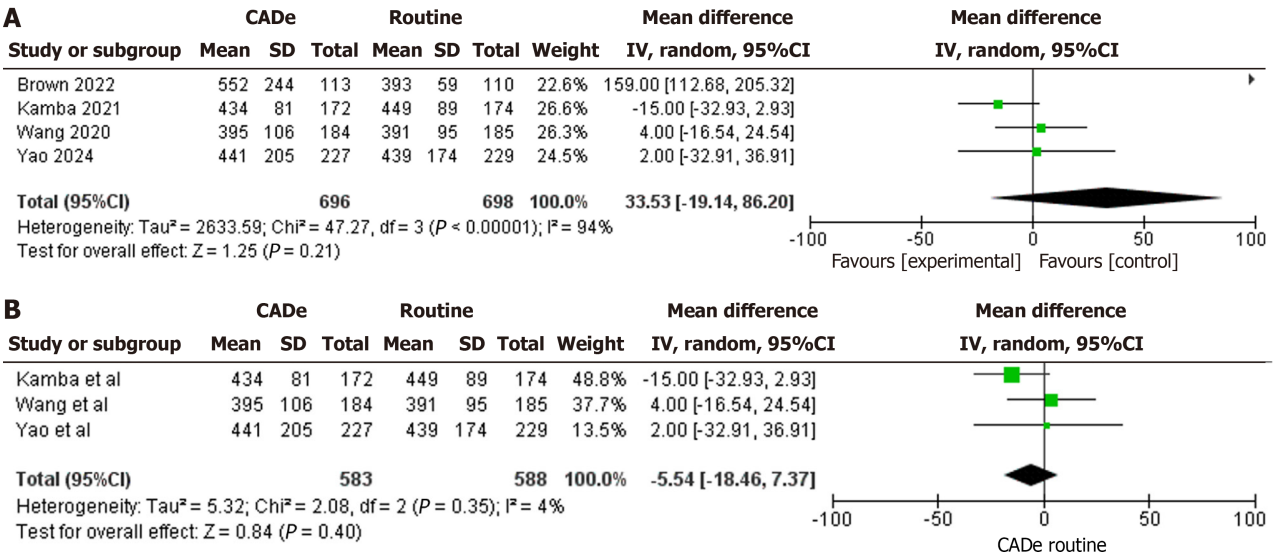

Figure 8 Withdrawal time for colonoscopy with *vs* without computer-aided detection assistance on first pass for the included studies. A: Forrest plot; B: Sensitivity analysis. CADe: Computer-aided detection.

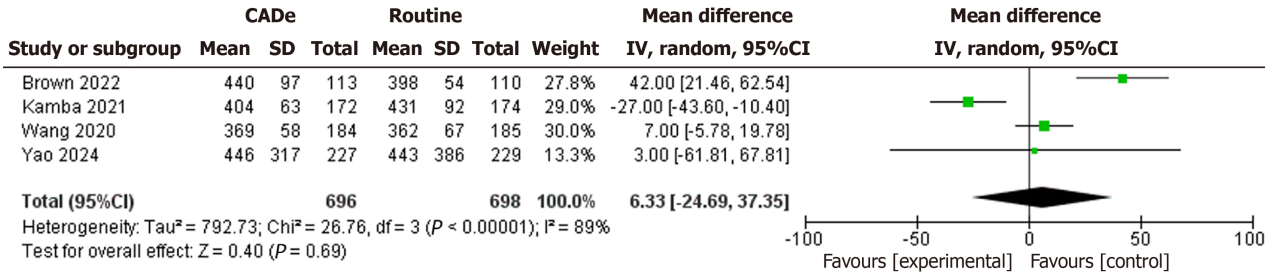

Figure 9 Forrest plot showing withdrawal time for colonoscopy with *vs* without computer-aided detection assistance on second pass for the included studies. CADe: Computer-aided detection.

long-term impact of AI-assisted colonoscopy on CRC prevention. Nonetheless, detecting more precancerous lesions is likely to contribute to more effective prevention strategies.

This study has several limitations. First, the relatively small number of included patients may limit the generalizability of the findings and may not fully reflect colonoscopy performance across the broader population. Additionally, all included studies were conducted in Northern Hemisphere countries, with a predominance in Asia. The effectiveness of AI-assisted colonoscopy in Western countries and the Southern Hemisphere remains uncertain and requires further clinical validation. Second, with the exception of one study, all included trials employed a single-blind design. This may have increased awareness among endoscopists, potentially influencing outcomes and limiting the generalizability of the results. Third, all studies utilized a tandem design, involving two consecutive colonoscopies performed within a short time frame, which does not reflect routine clinical practice. While CADe-assisted colonoscopy has demonstrated potential benefits, its clinical applicability should be further assessed through large-scale prospective studies to validate its effectiveness in real-world settings.

In recent years, continuous advancements in medical technology have driven the evolution of AI systems, leading to the development of strategies such as the dual AI approach[39]. This approach involves the simultaneous application of multiple AI techniques or the integration of AI with other endoscopic technologies to enhance ADR. One study reported that when AI was combined with the Endocuff, a device attached to the distal end of the colonoscope to improve mucosal exposure, ADR increased by 4.9% and PDR improved by 3.0%. Even after the removal of Endocuff, AI-assisted colonoscopy remained superior to standard colonoscopy, with significantly higher ADR (53.8% *vs* 46.3%, $P < 0.01$) and PDR (74.0% *vs* 54.2%, $P < 0.01$). However, the decrease in ADR and PDR after Endocuff removal suggests that the combination of AI and mechanical enhancement provides a greater diagnostic advantage than AI alone[40]. Beyond hardware innovations, ongoing improvements in AI algorithms have further enhanced detection capabilities. A study found that the YOLOv5s + BiFPN model exhibited superior accuracy and recall compared to the standard YOLOv5 algorithm, highlighting the potential of advanced AI models in colonoscopy[41]. The use of real-time assistive technology in AI-assisted colonoscopy has also gained increasing attention. One study demonstrated that integrating real-time assistive systems, such as the CAQ system, with AI significantly improved ADR (30.6% *vs* 21.27%, $P = 0.024$)[42]. The combined application of AI has shown promise in addressing challenges associated with detecting extrinsic adenomas. Although AI is increasingly being implemented in clinical practice, colonoscopy procedures are typically performed by

experienced endoscopists. Training in endoscopy requires extensive time and incurs significant costs. AI-assisted colonoscopy has been shown to enhance diagnostic accuracy among trainees. A retrospective study demonstrated that AI-assisted colonoscopy significantly improved the diagnostic performance of trainees, achieving an AMR comparable to that of experienced endoscopists[43]. This suggests that CADe-assisted colonoscopy may reduce training duration while facilitating a higher level of proficiency more rapidly. To date, CADe has been widely recognized for its ability to reduce human error and potentially lower the risk of colorectal lesions progressing to cancer. However, its implementation may also lead to an increased rate of unnecessary adenoma removal[44].

CONCLUSION

In conclusion, CADe-assisted colonoscopy offers significant advantages over standard colonoscopy, including improved ADR and a reduction in AMR. Additionally, it may alleviate the workload of endoscopists while enhancing procedural efficiency. Current evidence supports the clinical application of AI in colonoscopy, underscoring its potential to improve diagnostic accuracy and optimize workflow.

FOOTNOTES

Author contributions: Wang SL and Gao JC designed the research study; Wang SL, Gao JC, and Wu SD performed the research; Wang SL, Gao JC, and Wu SD analyzed the data and wrote the manuscript; all authors have read and approved the final manuscript.

Conflict-of-interest statement: All the authors report no relevant conflicts of interest for this article.

PRISMA 2009 Checklist statement: The authors have read the PRISMA 2009 Checklist, and the manuscript was prepared and revised according to the PRISMA 2009 Checklist.

Country of origin: China

ORCID number: Sheng-Yu Wang 0009-0002-1458-7458; Jia-Cheng Gao 0009-0006-9027-5412; Shuo-Dong Wu 0009-0000-0081-0204.

S-Editor: Li L
L-Editor: Wang TQ
P-Editor: Yu HG

REFERENCES

1 **Bray F**, Ferlay J, Soerjomataram I, Siegel RL, Torre LA, Jemal A. Global cancer statistics 2018: GLOBOCAN estimates of incidence and mortality worldwide for 36 cancers in 185 countries. *CA Cancer J Clin* 2018; **68**: 394-424 [PMID: 30207593 DOI: 10.3322/caac.21492] [Full Text]

2 **Kim ES**, Lee KS. Artificial intelligence in colonoscopy: from detection to diagnosis. *Korean J Intern Med* 2024; **39**: 555-562 [PMID: 38695105 DOI: 10.3904/kjim.2023.332] [FullText]

3 **Mehta A**, Kumar H, Yazji K, Wireko AA, Sivanandan Nagarajan J, Ghosh B, Nahas A, Morales Ojeda L, Anand A, Sharath M, Huang H, Garg T, Isik A. Effectiveness of artificial intelligence-assisted colonoscopy in early diagnosis of colorectal cancer: a systematic review. *Int J Surg* 2023; **109**: 946-952 [PMID: 36917126 DOI: 10.1097/JS9.0000000000000285] [FullText]

4 **Kudo SE**, Misawa M, Mori Y, Hotta K, Ohtsuka K, Ikematsu H, Saito Y, Takeda K, Nakamura H, Ichimasa K, Ishigaki T, Toyoshima N, Kudo T, Hayashi T, Wakamura K, Baba T, Ishida F, Inoue H, Itoh H, Oda M, Mori K. Artificial Intelligence-assisted System Improves Endoscopic Identification of Colorectal Neoplasms. *Clin Gastroenterol Hepatol* 2020; **18**: 1874-1881.e2 [PMID: 31525512 DOI: 10.1016/j.cgh.2019.09.009] [FullText]

5 **Ahmad OF**, González-Bueno Puyal J, Brandao P, Kader R, Abbasi F, Hussein M, Haidry RJ, Toth D, Mountney P, Seward E, Vega R, Stoyanov D, Lovat LB. Performance of artificial intelligence for detection of subtle and advanced colorectal neoplasia. *Dig Endosc* 2022; **34**: 862-869 [PMID: 34748665 DOI: 10.1111/den.14187] [FullText]

6 **Joseph J**, LePage EM, Cheney CP, Pawa R. Artificial intelligence in colonoscopy. *World J Gastroenterol* 2021; **27**: 4802-4817 [PMID: 34447227 DOI: 10.3748/wjg.v27.i29.4802] [FullText]

7 **Wang P**, Berzin TM, Glissen Brown JR, Bharadwaj S, Becq A, Xiao X, Liu P, Li L, Song Y, Zhang D, Li Y, Xu G, Tu M, Liu X. Real-time automatic detection system increases colonoscopic polyp and adenoma detection rates: a prospective randomised controlled study. *Gut* 2019; **68**: 1813-1819 [PMID: 30814121 DOI: 10.1136/gutjnl-2018-317500] [FullText]

8 **Levy I**, Bruckmayer L, Klang E, Ben-Horin S, Kopylov U. Artificial Intelligence-Aided Colonoscopy Does Not Increase Adenoma Detection Rate in Routine Clinical Practice. *Am J Gastroenterol* 2022; **117**: 1871-1873 [PMID: 36001408 DOI: 10.14309/ajg.0000000000001970] [Full Text]

9 **Hsu WF**, Chang WY, Kuo CY, Chang LC, Lin HH, Wu MS, Chiu HM. Effect of a novel artificial intelligence-based cecum recognition system on adenoma detection metrics in a screening colonoscopy setting. *Gastrointest Endosc* 2025; **101**: 452-455 [PMID: 39299304 DOI: 10.1016/j.gie.2024.09.019] [FullText]

10 **Wei MT**, Shankar U, Parvin R, Abbas SH, Chaudhary S, Friedlander Y, Friedland S. Evaluation of Computer-Aided Detection During Colonoscopy in the Community (AI-SEE): A Multicenter Randomized Clinical Trial. *Am J Gastroenterol* 2023; **118**: 1841-1847 [PMID: 36892545 DOI: 10.14309/ajg.0000000000002239] [FullText]

11 **Brand M**, Troya J, Krenzer A, Saßmannshausen Z, Zoller WG, Meining A, Lux TJ, Hann A. Development and evaluation of a deep learning model to improve the usability of polyp detection systems during interventions. *United European Gastroenterol J* 2022; **10**: 477-484 [PMID: 35511456 DOI: 10.1002/ueg2.12235] [FullText]

12 **Shao L**, Yan X, Liu C, Guo C, Cai B. Effects of ai-assisted colonoscopy on adenoma miss rate/adenoma detection rate: A protocol for systematic review and meta-analysis. *Medicine (Baltimore)* 2022; **101**: e31945 [PMID: 36401456 DOI: 10.1097/MD.0000000000031945] [FullText]

13 **Lou S**, Du F, Song W, Xia Y, Yue X, Yang D, Cui B, Liu Y, Han P. Artificial intelligence for colorectal neoplasia detection during colonoscopy: a systematic review and meta-analysis of randomized clinical trials. *EClinicalMedicine* 2023; **66**: 102341 [PMID: 38078195 DOI: 10.1016/j.eclinm.2023.102341] [FullText]

14 **Spadaccini M**, Menini M, Massimi D, Rizkala T, De Sire R, Alfarone L, Capogreco A, Colombo M, Maselli R, Fugazza A, Brandaleone L, Di Martino A, Ramai D, Repici A, Hassan C. AI and Polyp Detection During Colonoscopy. *Cancers (Basel)* 2025; **17**: 797 [PMID: 40075645 DOI: 10.3390/cancers17050797] [FullText]

15 **Luo D**, Wan X, Liu J, Tong T. Optimally estimating the sample mean from the sample size, median, mid-range, and/or mid-quartile range. *Stat Methods Med Res* 2018; **27**: 1785-1805 [PMID: 27683581 DOI: 10.1177/0962280216669183] [FullText]

16 **Wan X**, Wang W, Liu J, Tong T. Estimating the sample mean and standard deviation from the sample size, median, range and/or interquartile range. *BMC Med Res Methodol* 2014; **14**: 135 [PMID: 25524443 DOI: 10.1186/1471-2288-14-135] [FullText]

17 **Atkins D**, Eccles M, Flottorp S, Guyatt GH, Henry D, Hill S, Liberati A, O'Connell D, Oxman AD, Phillips B, Schünemann H, Edejer TT, Vist GE, Williams JW Jr; GRADE Working Group. Systems for grading the quality of evidence and the strength of recommendations I: critical appraisal of existing approaches The GRADE Working Group. *BMC Health Serv Res* 2004; **4**: 38 [PMID: 15615589 DOI: 10.1186/1472-6963-4-38] [FullText]

18 **Page MJ**, McKenzie JE, Bossuyt PM, Boutron I, Hoffmann TC, Mulrow CD, Shamseer L, Tetzlaff JM, Akl EA, Brennan SE, Chou R, Glanville J, Grimshaw JM, Hróbjartsson A, Lalu MM, Li T, Loder EW, Mayo-Wilson E, McDonald S, McGuinness LA, Stewart LA, Thomas J, Tricco AC, Welch VA, Whiting P, Moher D. The PRISMA 2020 statement: an updated guideline for reporting systematic reviews. *BMJ* 2021; **372**: n71 [PMID: 33782057 DOI: 10.1136/bmj.n71] [FullText]

19 **Wang P**, Liu P, Glissen Brown JR, Berzin TM, Zhou G, Lei S, Liu X, Li L, Xiao X. Lower Adenoma Miss Rate of Computer-Aided Detection-Assisted Colonoscopy vs Routine White-Light Colonoscopy in a Prospective Tandem Study. *Gastroenterology* 2020; **159**: 1252-1261.e5 [PMID: 32562721 DOI: 10.1053/j.gastro.2020.06.023] [FullText]

20 **Kamba S**, Tamai N, Saitoh I, Matsui H, Horiuchi H, Kobayashi M, Sakamoto T, Ego M, Fukuda A, Tonouchi A, Shimahara Y, Nishikawa M, Nishino H, Saito Y, Sumiyama K. Reducing adenoma miss rate of colonoscopy assisted by artificial intelligence: a multicenter randomized controlled trial. *J Gastroenterol* 2021; **56**: 746-757 [PMID: 34218329 DOI: 10.1007/s00535-021-01808-w] [FullText]

21 **Glissen Brown JR**, Mansour NM, Wang P, Chuchuca MA, Minchenberg SB, Chandnani M, Liu L, Gross SA, Sengupta N, Berzin TM. Deep Learning Computer-aided Polyp Detection Reduces Adenoma Miss Rate: A United States Multi-center Randomized Tandem Colonoscopy Study (CADeT-CS Trial). *Clin Gastroenterol Hepatol* 2022; **20**: 1499-1507.e4 [PMID: 34530161 DOI: 10.1016/j.cgh.2021.09.009] [FullText]

22 **Wallace MB**, Sharma P, Bhandari P, East J, Antonelli G, Lorenzetti R, Vieth M, Speranza I, Spadaccini M, Desai M, Lukens FJ, Babameto G, Batista D, Singh D, Palmer W, Ramirez F, Palmer R, Lunsford T, Ruff K, Bird-Liebermann E, Ciofoaia V, Arndtz S, Cangemi D, Puddick K, Derfus G, Johal AS, Barawi M, Longo L, Moro L, Repici A, Hassan C. Impact of Artificial Intelligence on Miss Rate of Colorectal Neoplasia. *Gastroenterology* 2022; **163**: 295-304.e5 [PMID: 35304117 DOI: 10.1053/j.gastro.2022.03.007] [FullText]

23 **Yao L**, Li X, Wu Z, Wang J, Luo C, Chen B, Luo R, Zhang L, Zhang C, Tan X, Lu Z, Zhu C, Huang Y, Tan T, Liu Z, Li Y, Li S, Yu H. Effect of artificial intelligence on novice-performed colonoscopy: a multicenter randomized controlled tandem study. *Gastrointest Endosc* 2024; **99**: 91-99.e9 [PMID: 37536635 DOI: 10.1016/j.gie.2023.07.044] [FullText]

24 **Song EM**, Park B, Ha CA, Hwang SW, Park SH, Yang DH, Ye BD, Myung SJ, Yang SK, Kim N, Byeon JS. Endoscopic diagnosis and treatment planning for colorectal polyps using a deep-learning model. *Sci Rep* 2020; **10**: 30 [PMID: 31913337 DOI: 10.1038/s41598-019-56697-0] [FullText]

25 **Barua I**, Vinsard DG, Jodal HC, Løberg M, Kalager M, Holme Ø, Misawa M, Bretthauer M, Mori Y. Artificial intelligence for polyp detection during colonoscopy: a systematic review and meta-analysis. *Endoscopy* 2021; **53**: 277-284 [PMID: 32557490 DOI: 10.1055/a-1201-7165] [FullText]

26 **Hann A**, Troya J, Fitting D. Current status and limitations of artificial intelligence in colonoscopy. *United European Gastroenterol J* 2021; **9**: 527-533 [PMID: 34617420 DOI: 10.1002/ueg2.12108] [FullText]

27 **Pecere S**, Antonelli G, Dinis-Ribeiro M, Mori Y, Hassan C, Fuccio L, Bisschops R, Costamagna G, Jin EH, Lee D, Misawa M, Messmann H, Iacopini F, Petruzziello L, Repici A, Saito Y, Sharma P, Yamada M, Spada C, Frazzoni L. Endoscopists performance in optical diagnosis of colorectal polyps in artificial intelligence studies. *United European Gastroenterol J* 2022; **10**: 817-826 [PMID: 35984903 DOI: 10.1002/ueg2.12285] [FullText]

28 **Kim NH**, Jung YS, Jeong WS, Yang HJ, Park SK, Choi K, Park DI. Miss rate of colorectal neoplastic polyps and risk factors for missed polyps in consecutive colonoscopies. *Intest Res* 2017; **15**: 411-418 [PMID: 28670239 DOI: 10.5217/ir.2017.15.3.411] [FullText]

29 **Antonelli G**, Badalamenti M, Hassan C, Repici A. Impact of artificial intelligence on colorectal polyp detection. *Best Pract Res Clin Gastroenterol* 2021; **52-53**: 101713 [PMID: 34172246 DOI: 10.1016/j.bpg.2020.101713] [FullText]

30 **Lui TKL**, Hui CKY, Tsui VWM, Cheung KS, Ko MKL, Foo DCC, Mak LY, Yeung CK, Lui TH, Wong SY, Leung WK. New insights on missed colonic lesions during colonoscopy through artificial intelligence-assisted real-time detection (with video). *Gastrointest Endosc* 2021; **93**: 193-200.e1 [PMID: 32376335 DOI: 10.1016/j.gie.2020.04.066] [FullText]

31 **Repici A**, Badalamenti M, Maselli R, Correale L, Radaelli F, Rondonotti E, Ferrara E, Spadaccini M, Alkandari A, Fugazza A, Anderloni A, Galtieri PA, Pellegatta G, Carrara S, Di Leo M, Craviotto V, Lamonaca L, Lorenzetti R, Andrealli A, Antonelli G, Wallace M, Sharma P, Rosch T, Hassan C. Efficacy of Real-Time Computer-Aided Detection of Colorectal Neoplasia in a Randomized Trial. *Gastroenterology* 2020; **159**: 512-520.e7 [PMID: 32371116 DOI: 10.1053/j.gastro.2020.04.062] [FullText]

32 **Tavanapong W**, Oh J, Riegler MA, Khaleel M, Mittal B, de Groen PC. Artificial Intelligence for Colonoscopy: Past, Present, and Future. *IEEE J Biomed Health Inform* 2022; **26**: 3950-3965 [PMID: 35316197 DOI: 10.1109/JBHI.2022.3160098] [FullText]

33 **Sinonquel P**, Eelbode T, Bossuyt P, Maes F, Bisschops R. Artificial intelligence and its impact on quality improvement in upper and lower gastrointestinal endoscopy. *Dig Endosc* 2021; **33**: 242-253 [PMID: 33145847 DOI: 10.1111/den.13888] [FullText]

34 **Komanduri S**, Dominitz JA, Rabeneck L, Kahi C, Ladabaum U, Imperiale TF, Byrne MF, Lee JK, Lieberman D, Wang AY, Sultan S, Shaukat A, Pohl H, Muthusamy VR. AGA White Paper: Challenges and Gaps in Innovation for the Performance of Colonoscopy for Screening and Surveillance of Colorectal Cancer. *Clin Gastroenterol Hepatol* 2022; **20**: 2198-2209.e3 [PMID: 35688352 DOI: 10.1016/j.cgh.2022.03.051] [FullText]

35 **Mori Y**, Wang P, Løberg M, Misawa M, Repici A, Spadaccini M, Correale L, Antonelli G, Yu H, Gong D, Ishiyama M, Kudo SE, Kamba S, Sumiyama K, Saito Y, Nishino H, Liu P, Glissen Brown JR, Mansour NM, Gross SA, Kalager M, Bretthauer M, Rex DK, Sharma P, Berzin TM, Hassan C. Impact of Artificial Intelligence on Colonoscopy Surveillance After Polyp Removal: A Pooled Analysis of Randomized Trials. *Clin Gastroenterol Hepatol* 2023; **21**: 949-959.e2 [PMID: 36038128 DOI: 10.1016/j.cgh.2022.08.022] [FullText]

36 **Liu P**, Wang P, Glissen Brown JR, Berzin TM, Zhou G, Liu W, Xiao X, Chen Z, Zhang Z, Zhou C, Lei L, Xiong F, Li L, Liu X. The single-monitor trial: an embedded CADe system increased adenoma detection during colonoscopy: a prospective randomized study. *Therap Adv Gastroenterol* 2020; **13**: 1756284820979165 [PMID: 33403003 DOI: 10.1177/1756284820979165] [FullText]

37 **Mori Y**, Kudo SE, East JE, Rastogi A, Bretthauer M, Misawa M, Sekiguchi M, Matsuda T, Saito Y, Ikematsu H, Hotta K, Ohtsuka K, Kudo T, Mori K. Cost savings in colonoscopy with artificial intelligence-aided polyp diagnosis: an add-on analysis of a clinical trial (with video). *Gastrointest Endosc* 2020; **92**: 905-911.e1 [PMID: 32240683 DOI: 10.1016/j.gie.2020.03.3759] [FullText]

38 **Areia M**, Mori Y, Correale L, Repici A, Bretthauer M, Sharma P, Taveira F, Spadaccini M, Antonelli G, Ebigbo A, Kudo SE, Arribas J, Barua I, Kaminski MF, Messmann H, Rex DK, Dinis-Ribeiro M, Hassan C. Cost-effectiveness of artificial intelligence for screening colonoscopy: a modelling study. *Lancet Digit Health* 2022; **4**: e436-e444 [PMID: 35430151 DOI: 10.1016/S2589-7500(22)00042-5] [FullText]

39 **Zhou G**, Xiao X, Tu M, Liu P, Yang D, Liu X, Zhang R, Li L, Lei S, Wang H, Song Y, Wang P. Computer aided detection for laterally spreading tumors and sessile serrated adenomas during colonoscopy. *PLoS One* 2020; **15**: e0231880 [PMID: 32315365 DOI: 10.1371/journal.pone.0231880] [FullText]

40 **Lui TK**, Lam CP, To EW, Ko MK, Tsui VWM, Liu KS, Hui CK, Cheung MK, Mak LL, Hui RW, Wong SY, Seto WK, Leung WK. Endocuff With or Without Artificial Intelligence-Assisted Colonoscopy in Detection of Colorectal Adenoma: A Randomized Colonoscopy Trial. *Am J Gastroenterol* 2024; **119**: 1318-1325 [PMID: 38305278 DOI: 10.14309/ajg.0000000000002684] [FullText]

41 **Li J**, Zhao J, Wang Y, Zhu J, Wei Y, Zhu J, Li X, Yan S, Zhang Q. A colonic polyps detection algorithm based on an improved YOLOv5s. *Sci Rep* 2025; **15**: 6852 [PMID: 40011590 DOI: 10.1038/s41598-025-91467-1] [FullText]

42 **Yao L**, Zhang L, Liu J, Zhou W, He C, Zhang J, Wu L, Wang H, Xu Y, Gong D, Xu M, Li X, Bai Y, Gong R, Sharma P, Yu H. Effect of an artificial intelligence-based quality improvement system on efficacy of a computer-aided detection system in colonoscopy: a four-group parallel study. *Endoscopy* 2022; **54**: 757-768 [PMID: 34823258 DOI: 10.1055/a-1706-6174] [FullText]

43 **Yamaguchi D**, Shimoda R, Miyahara K, Yukimoto T, Sakata Y, Takamori A, Mizuta Y, Fujimura Y, Inoue S, Tomonaga M, Ogino Y, Eguchi K, Ikeda K, Tanaka Y, Takedomi H, Hidaka H, Akutagawa T, Tsuruoka N, Noda T, Tsunada S, Esaki M. Impact of an artificial intelligence-aided endoscopic diagnosis system on improving endoscopy quality for trainees in colonoscopy: Prospective, randomized, multicenter study. *Dig Endosc* 2024; **36**: 40-48 [PMID: 37079002 DOI: 10.1111/den.14573] [FullText]

44 **Hassan C**, Bisschops R, Sharma P, Mori Y. Colon Cancer Screening, Surveillance, and Treatment: Novel Artificial Intelligence Driving Strategies in the Management of Colon Lesions. *Gastroenterology* 2025; S0016-5085(25)00478 [PMID: 40054749 DOI: 10.1053/j.gastro.2025.02.021] [FullText]

World Journal of Gastroenterology

Submit a Manuscript: https://www.f6publishing.com

World J Gastroenterol 2025 June 7; 31(21): 103184

DOI: 10.3748/wjg.v31.i21.103184

ISSN 1007-9327 (print) ISSN 2219-2840 (online)

LETTER TO THE EDITOR

Mechanisms underlying hepatocellular carcinoma progression through N6-methyladenosine modifications of long non-coding RNA

Ning Wang, Fei-Tian Min, Wei-Bo Wen, Huan-Tian Cui

Specialty type: Gastroenterology and hepatology

Provenance and peer review: Invited article; Externally peer reviewed.

Peer-review model: Single blind

Peer-review report's classification

Scientific Quality: Grade A, Grade A, Grade B

Novelty: Grade A, Grade B, Grade B

Creativity or Innovation: Grade A, Grade B, Grade B

Scientific Significance: Grade A, Grade A, Grade B

P-Reviewer: Bian YH; Ko CY; Miao J

Received: November 19, 2024

Revised: March 26, 2025

Accepted: April 22, 2025

Published online: June 7, 2025

Processing time: 199 Days and 18.9 Hours

Ning Wang, Fei-Tian Min, Wei-Bo Wen, Huan-Tian Cui, The First School of Clinical Medicine, Yunnan University of Chinese Medicine, Kunming 650000, Yunnan Province, China

Co-corresponding authors: Wei-Bo Wen and Huan-Tian Cui.

Corresponding author: Huan-Tian Cui, PhD, The First School of Clinical Medicine, Yunnan University of Chinese Medicine, No. 1076 Yuhua Road, Chenggong District, Kunming 650000, Yunnan Province, China. 1762316411@qq.com

Abstract

Hepatocellular carcinoma (HCC) is a highly lethal malignancy with limited treatment options, particularly for patients with advanced stages of the disease. Sorafenib, the standard first-line therapy, faces significant challenges due to the development of drug resistance. Yu *et al* explored the mechanisms by which lncRNA KIF9-AS1 regulates the stemness and sorafenib resistance in HCC using a combination of cell culture, transfection, RNA immunoprecipitation, co-immunoprecipitation, and xenograft tumor models. They demonstrate that N6-methyladenosine-modified long non-coding RNA KIF9-AS1 acts as an oncogene in HCC. This modification involves methyltransferase-like 3 and insulin-like growth factor 2 mRNA-binding protein 1, which play critical roles in regulating KIF9-AS1. Furthermore, KIF9-AS1 stabilizes and upregulates short stature homeobox 2 by promoting its deubiquitination through ubiquitin-specific peptidase 1, thereby enhancing stemness and contributing to sorafenib resistance in HCC cells. These findings provide a theoretical basis for KIF9-AS1 as a diagnostic marker and therapeutic target for HCC, highlighting the need for further investigation into its clinical application potential.

Key Words: Hepatocellular carcinoma; Stemness; Sorafenib resistance; Long non-coding RNA KIF9-AS1; Short stature homeobox 2; N6-methyladenosine

Core Tip: Yu *et al* present evidence showing that m6A-modified long non-coding RNA KIF9-AS1 drives the progression of hepatocellular carcinoma (HCC) and reveal novel molecular mechanisms underlying this process. The m6A modification, mediated by modification involves methyltransferase-like 3 and insulin-like growth factor insulin-like growth factor 2 mRNA-binding protein 1, stabilizes and upregulates KIF9-AS1 expression. In turn, KIF9-AS1 enhances the stability and expression of SHOX2 by promoting its deubiquitination *via* ubiquitin-specific peptidase 1, which strengthens stemness and contributes to sorafenib resistance in HCC cells. Future studies should further validate KIF9-AS1 as a potential diagnostic biomarker for HCC and explore its therapeutic applications in HCC treatment.

Citation: Wang N, Min FT, Wen WB, Cui HT. Mechanisms underlying hepatocellular carcinoma progression through N6-methyladenosine modifications of long non-coding RNA. *World J Gastroenterol* 2025; 31(21): 103184
URL: https://www.wjgnet.com/1007-9327/full/v31/i21/103184.htm
DOI: https://dx.doi.org/10.3748/wjg.v31.i21.103184

TO THE EDITOR

Hepatocellular carcinoma (HCC) is the most prevalent form of primary liver cancer, characterized by high global incidence and mortality rates. Several factors contribute to the development of HCC, including chronic infections with hepatitis viruses (such as hepatitis B and C), cirrhosis, alcohol abuse, and metabolic syndrome[1]. The prognosis for HCC is generally poor, with a low five-year survival rate. This is primarily due to the fact that HCC is often diagnosed at advanced stages, which delays treatment initiation[1,2]. A major challenge in HCC treatment is drug resistance, which refers to the ability of tumor cells to withstand chemotherapy, leading to chemotherapy failure and disease recurrence[3,4]. Research indicates that HCC cells evade drug effects through various mechanisms, such as inhibiting apoptosis, activating autophagy, promoting drug efflux, and undergoing epigenetic alterations[3,5]. Moreover, cancer stem cells are believed to play a pivotal role in the initiation, invasion, metastasis, and recurrence of HCC, with their presence closely linked to drug resistance[6,7]. Thus, effective therapeutic strategies for HCC must address the biological characteristics of the tumor, including stemness and drug resistance mechanisms, to enhance treatment efficacy and improve patient survival rates[8].

Non-coding RNAs, especially long non-coding RNAs (lncRNAs), play a critical role in the development of HCC. In 2014, Chen *et al*[9] conducted the first systematic review on the role of lncRNAs in liver cancer, elucidating their involvement in tumorigenesis *via* epigenetic regulation, transcriptional, and post-transcriptional modifications. Studies have demonstrated that lncRNAs influence key biological processes, such as proliferation, migration, and autophagy, by modulating various signaling pathways and gene expression[10]. Additionally, aberrant expression of lncRNAs (*e.g.*, HULC, MALAT1) is strongly linked to the onset and progression of HCC, making them potential novel biomarkers and therapeutic targets[9,11,12]. LncRNAs not only sustain stemness, thereby promoting tumorigenesis and progression[13], but alterations in the expression of specific lncRNAs can also enhance HCC's resistance to chemotherapy drugs[8,14]. Yao *et al*[15] demonstrated that LINC01189 enhances the chemoresistance of HCC cells by being regulated by hsa-miR-155-5p. During the same period, the interaction between the TGF-β/EMT pathway and lncRNAs was elucidated, with lncRNAs enhancing resistance to cisplatin and sorafenib *via* autophagy induction[16]. In 2022, Zhang *et al*[17] reported that LINC01132 enhances immunosuppression and drug resistance through the NRF1/DPP4 axis, and is significantly associated with the prognosis of HCC patients. Additionally, Wnt/β-catenin pathway-related lncRNAs, such as SNHG14 and FAM83H-AS1, have been shown to promote HCC progression by regulating macrophage polarization and the tumor microenvironment[18]. These findings indicate that the modified lncRNAs significantly contribute to regulating stemness and drug tolerance in HCC cells[19]. Gaining a deeper understanding of the role of lncRNAs in HCC will not only advance our knowledge of the molecular mechanisms underlying this disease but may also provide valuable insights for developing new therapeutic strategies.

Yu *et al*[20] offer valuable insights into HCC, with a particular focus on the role of m6A-modified lncRNA KIF9-AS1 in regulating stemness and sorafenib resistance. Sorafenib, a first-line therapeutic for HCC, faces significant challenges due to the development of drug resistance[21]. In their study, Yu *et al*[20] revealed the oncogenic role of KIF9-AS1 in HCC. Specifically, they found that KIF9-AS1 expression was upregulated in HCC tissues compared to normal liver tissues. Additionally, knocking down KIF9-AS1 inhibited HCC cell stemness and reduced sorafenib resistance. These findings suggest that KIF9-AS1 could serve as both a biomarker and a therapeutic target. However, further comprehensive evaluation and validation of KIF9-AS1-targeted therapies are required.

HOW KIF9-AS1 ENHANCES STEMNESS AND RESISTANCE TO SORAFENIB

Yu *et al*[20] demonstrated that the modification involves methyltransferase-like 3 (METTL3) and insulin-like growth factor 2 mRNA-binding protein 1 (IGF2BP1)-mediated m6A modification stabilizes and enhances the expression of KIF9-AS1, highlighting the critical role of METTL3, IGF2BP1, and m6A modification in HCC treatment. m6A, one of the most prevalent RNA modifications, regulates various biological processes, including gene expression, RNA stability, and translation[22]. METTL3, as an m6A methyltransferase, adds m6A modifications to RNA, while IGF2BP1, an m6A reader

protein, recognizes and binds to these modifications, influencing the stability and translation efficiency of target RNAs [23]. Numerous studies have shown that METTL3/IGF2BP1-mediated m6A modification promotes tumor cell proliferation, migration, and transformation[24,25]. However, it is important to acknowledge that other epigenetic mechanisms, such as DNA methylation and histone modifications, may also contribute to HCC drug resistance. Further research is needed to fully elucidate these epigenetic mechanisms and their impact on HCC drug resistance.

Yu *et al*[20] also explored the downstream regulatory mechanisms of KIF9-AS1 in HCC. They discovered that KIF9-AS1 enhances the stability and expression of short stature homeobox 2 (SHOX2) by promoting deubiquitination *via* ubiquitin-specific peptidase 1 (USP1). SHOX2, an oncogene implicated in tumor progression and metastasis, has been linked to several cancers, including lung, prostate, and breast cancer[26-28]. Furthermore, SHOX2 has been shown to contribute to drug resistance in lung cancer[26]. Elevated SHOX2 expression has been observed in HCC patients and is associated with tumor recurrence[29]. High expression of SHOX2 enhances the stemness phenotype of liver cancer cells, with the marker CD13 being highly expressed, endowing cells with proliferative, migratory, and adhesive capabilities. Further molecular mechanism studies have revealed that CD13 can interact with histone deacetylase 5 (HDAC5), inhibiting its ubiquitination and degradation, thereby enhancing the protein stability of HDAC5. This process leads to HDAC5-mediated deacetylation of lysine-specific demethylase LSD1, enhancing LSD1's activity[30]. LSD1, in turn, stabilizes the NF-κB subunit p65 protein and promotes its nuclear translocation by reducing the methylation level of p65, ultimately activating the transcription of downstream oncogenic genes of NF-κB[31]. This cascade reaction results in decreased sensitivity of tumor cells to sorafenib. Studies have shown that the combination of the CD13 inhibitor ubenimex with sorafenib can significantly inhibit tumor growth and reverse drug resistance[30]. Therefore, SHOX2 and CD13 can serve as a biomarker for predicting the prognosis of postoperative HCC patients and their responsiveness to sorafenib therapy.

USP1, a deubiquitinating enzyme, is abnormally expressed in various cancers, particularly in HCC, where its expression is significantly higher than in normal tissues. High USP1 expression correlates with increased tumor aggressiveness, metastasis, and reduced patient survival[32]. As a result, USP1 is considered a potential therapeutic target in HCC, and its value as a prognostic biomarker is widely recognized. Although SHOX2 is known to be a substrate for USP1-mediated deubiquitination, it remains unclear whether KIF9-AS1 regulates SHOX2 expression through USP1, or if other epigenetic modifications play a more prominent role. Further investigation is needed to clarify this relationship.

CLINICAL IMPLICATIONS

Yu *et al*[20] found that KIF9-AS1 upregulates the expression of SHOX2 through m6A modification, thus aiding in the specific diagnosis of early-stage HCC by detecting the epigenetic modification levels of m6A-related molecules KIF9-AS1 and SHOX2 in tumor tissues or blood. Furthermore, upregulated expression of KIF9-AS1 in clinical samples is significantly associated with poor overall survival in HCC patients. Moreover, high KIF9-AS1 expression in patients with advanced HCC strongly correlates with tumor-lymph node metastasis. Therefore, KIF9-AS1 can also serve as a biomarker for assessing the prognosis of HCC patients. As previously mentioned, KIF9-AS1 promotes the stemness characteristics of HCC cells by upregulating SHOX2, thereby enhancing resistance to sorafenib[30]. Detecting the levels of KIF9-AS1 and its downstream targets SHOX2 and CD31 in HCC patients will aid in predicting their response to sorafenib treatment. Correspondingly, adopting therapeutic measures targeting these markers is expected to optimize HCC treatment strategies and improve patient outcomes. Studies have shown that METTL3 inhibitors exert potent anti-cancer effects by reducing m6A modification function, potentially reducing drug resistance[33]. These findings suggest that KIF9-AS1 plays a key role in HCC progression, reinforcing its potential as both a biomarker and a therapeutic target. Currently, some m6A-related drugs have entered early-stage clinical trials, but the clinical translation of lncRNA applications still faces challenges such as specific recognition, optimization of delivery systems, and validation through large-scale clinical trials. Meanwhile, no significant association was observed between KIF9-AS1 expression and factors such as gender, age, or tumor size. In light of this, more direct experimental validation is needed to confirm its therapeutic potential, thereby promoting the development of precision medicine.

CONCLUSION

The study by Yu *et al*[20] not only elucidates the role of KIF9-AS1 in HCC but also provides a theoretical framework for developing new therapeutic strategies. As an m6A-modified lncRNA, KIF9-AS1 promotes stemness and sorafenib resistance in HCC by facilitating USP1-mediated deubiquitination of SHOX2. This finding highlights new potential targets for clinical treatment, which could improve the prognosis for HCC patients. However, Yu *et al*[20] did not fully elucidate the specific signaling pathways downstream of SHOX2, nor did they explore therapeutic strategies targeting the KIF9-AS1/SHOX2 axis or its therapeutic potential. Future research should focus on deepening the mechanistic investigation of the downstream pathways of SHOX2 and their causal relationship with HCC stemness. Utilizing single-cell sequencing or spatial transcriptomics technology could help dissect the cell-specific role of the KIF9-AS1/SHOX2 axis within the tumor microenvironment. Additionally, developing targeted intervention strategies, such as using m6A inhibitors (*e.g.*, targeting METTL3) or SHOX2 antagonists, and testing their efficacy in patient-derived or organoid models, could provide valuable insights.

FOOTNOTES

Author contributions: Wang N wrote the initial manuscript draft; Min FT did the literature review; Cui HT designed the overall concept and outline of the manuscript; Wen WB did literature review and critical revision of the manuscript; Cui HT contributed to the editing of the manuscript. All authors have read and approved the final manuscript. Both Wen WB and Cui HT have made crucial and indispensable contributions towards the completion of the project and thus qualified as the co-corresponding authors of the paper.

Supported by National Natural Science Foundation of China, No. 82405223; and Yunling Scholars Program, No. XDYC-YLXZ-2022-0027.

Conflict-of-interest statement: The authors declare that they have no conflicts of interest.

Country of origin: China

ORCID number: Ning Wang 0009-0002-1920-4727; Fei-Tian Min 0000-0002-0053-5561; Wei-Bo Wen 0000-0002-9303-7341; Huan-Tian Cui 0000-0002-0820-5436.

S-Editor: Li L
L-Editor: A
P-Editor: Yu HG

REFERENCES

1 **Block T**, Mehta AS, London WT. Hepatocellular carcinoma of the liver. *Cancer Biomark* 2010; **9**: 375-383 [PMID: 22112485 DOI: 10.3233/CBM-2011-0165] [FullText]
2 **Martínez-Chantar ML**, Avila MA, Lu SC. Hepatocellular Carcinoma: Updates in Pathogenesis, Detection and Treatment. *Cancers (Basel)* 2020; **12**: 2729 [PMID: 32977536 DOI: 10.3390/cancers12102729] [FullText]
3 **Lohitesh K**, Chowdhury R, Mukherjee S. Resistance a major hindrance to chemotherapy in hepatocellular carcinoma: an insight. *Cancer Cell Int* 2018; **18**: 44 [PMID: 29568237 DOI: 10.1186/s12935-018-0538-7] [FullText]
4 **Sun R**, Dong C, Li R, Chu H, Liu J, Hao D, Zhang L, Zhao B, Wang L, Zhang Y. Proteomic Analysis Reveals that EPHX1 Contributes to 5-Fluorouracil Resistance in a Human Hepatocellular Carcinoma Cell Line. *Proteomics Clin Appl* 2020; **14**: e1900080 [PMID: 32067389 DOI: 10.1002/prca.201900080] [FullText]
5 **Ul-Islam S**, Ahmed MB, Shehzad A, Ul-Islam M, Lee YS. Failure of Chemotherapy in Hepatocellular Carcinoma Due to Impaired and Dysregulated Primary Liver Drug Metabolizing Enzymes and Drug Transport Proteins: What to Do? *Curr Drug Metab* 2018; **19**: 819-829 [PMID: 29807513 DOI: 10.2174/1389200219666180529113818] [FullText]
6 **Xiao Y**, Lin M, Jiang X, Ye J, Guo T, Shi Y, Bian X. The Recent Advances on Liver Cancer Stem Cells: Biomarkers, Separation, and Therapy. *Anal Cell Pathol (Amst)* 2017; **2017**: 5108653 [PMID: 28819584 DOI: 10.1155/2017/5108653] [FullText]
7 **Zhou J**, Hu Z, Li Z, Yu P, Wu J, Zheng S. The role of liver cancer stem cells in donor liver allocation for patients with hepatocellular carcinoma. *Postgrad Med* 2013; **125**: 24-30 [PMID: 24200758 DOI: 10.3810/pgm.2013.11.2709] [FullText]
8 **Zhou Y**, Huang Y, Dai T, Hua Z, Xu J, Lin Y, Han L, Yue X, Ho L, Lu J, Ai X. LncRNA TTN-AS1 intensifies sorafenib resistance in hepatocellular carcinoma by sponging miR-16-5p and upregulation of cyclin E1. *Biomed Pharmacother* 2021; **133**: 111030 [PMID: 33378944 DOI: 10.1016/j.biopha.2020.111030] [FullText]
9 **Chen B**. [Role of long noncoding RNAs in hepatocellular carcinoma]. *Shijie Huaren Xiaohua Zazhi* 2014; **22**: 4762 [DOI: 10.11569/wcjd.v22.i31.4762] [FullText]
10 **Verma S**, Sahu BD, Mugale MN. Role of lncRNAs in hepatocellular carcinoma. *Life Sci* 2023; **325**: 121751 [PMID: 37169145 DOI: 10.1016/j.lfs.2023.121751] [FullText]
11 **Niu ZS**, Niu XJ, Wang WH. Long non-coding RNAs in hepatocellular carcinoma: Potential roles and clinical implications. *World J Gastroenterol* 2017; **23**: 5860-5874 [PMID: 28932078 DOI: 10.3748/wjg.v23.i32.5860] [FullText]
12 **Chen X**, Deng Y. [The role of competitive endogenous RNA in the development of hepatocellular carcinoma]. *Linchuang Gandanbing Zazhi* 2021; **37**: 1924-1928 [DOI: 10.3969/j.issn.1001-5256.2021.08.039] [FullText]
13 **Zhang X**, Zhu Y. Research Progress on Regulating LncRNAs of Hepatocellular Carcinoma Stem Cells. *Onco Targets Ther* 2021; **14**: 917-927 [PMID: 33603396 DOI: 10.2147/OTT.S289064] [FullText]
14 **Wei L**, Wang X, Lv L, Liu J, Xing H, Song Y, Xie M, Lei T, Zhang N, Yang M. The emerging role of microRNAs and long noncoding RNAs in drug resistance of hepatocellular carcinoma. *Mol Cancer* 2019; **18**: 147 [PMID: 31651347 DOI: 10.1186/s12943-019-1086-z] [FullText]
15 **Yao Y**, Shu F, Wang F, Wang X, Guo Z, Wang H, Li L, Lv H. Long noncoding RNA LINC01189 is associated with HCV-hepatocellular carcinoma and regulates cancer cell proliferation and chemoresistance through hsa-miR-155-5p. *Ann Hepatol* 2021; **22**: 100269 [PMID: 33059056 DOI: 10.1016/j.aohep.2020.09.013] [FullText]
16 **Zhang R**, Shi T, Wu Y, Zhang J, Zheng X. [The mechanism of autophagy inducing drug resistance of hepatocellular carcinoma]. *Linchuang Gandanbing Zazhi* 2024; **40**: 2315-2319 [DOI: 10.12449/JCH241128] [FullText]
17 **Zhang J**, Pan T, Zhou W, Zhang Y, Xu G, Xu Q, Li S, Gao Y, Wang Z, Xu J, Li Y. Long noncoding RNA LINC01132 enhances immunosuppression and therapy resistance *via* NRF1/DPP4 axis in hepatocellular carcinoma. *J Exp Clin Cancer Res* 2022; **41**: 270 [PMID: 36071454 DOI: 10.1186/s13046-022-02478-z] [FullText]

18 **Deldar Abad Paskeh M**, Mirzaei S, Ashrafizadeh M, Zarrabi A, Sethi G. Wnt/β-Catenin Signaling as a Driver of Hepatocellular Carcinoma Progression: An Emphasis on Molecular Pathways. *J Hepatocell Carcinoma* 2021; **8**: 1415-1444 [PMID: 34858888 DOI: 10.2147/JHC.S336858] [FullText]

19 **Manna D**, Sarkar D. Non-Coding RNAs: Regulating Disease Progression and Therapy Resistance in Hepatocellular Carcinoma. *Cancers (Basel)* 2020; **12**: 1243 [PMID: 32429062 DOI: 10.3390/cancers12051243] [FullText]

20 **Yu Y**, Lu XH, Mu JS, Meng JY, Sun JS, Chen HX, Yan Y, Meng K. N6-methyladenosine-modified long non-coding RNA KIF9-AS1 promotes stemness and sorafenib resistance in hepatocellular carcinoma by upregulating SHOX2 expression. *World J Gastroenterol* 2024; **30**: 5174-5190 [PMID: 39735272 DOI: 10.3748/wjg.v30.i48.5174] [FullText]

21 **Tang W**, Chen Z, Zhang W, Cheng Y, Zhang B, Wu F, Wang Q, Wang S, Rong D, Reiter FP, De Toni EN, Wang X. The mechanisms of sorafenib resistance in hepatocellular carcinoma: theoretical basis and therapeutic aspects. *Signal Transduct Target Ther* 2020; **5**: 87 [PMID: 32532960 DOI: 10.1038/s41392-020-0187-x] [FullText]

22 **Cusenza VY**, Tameni A, Neri A, Frazzi R. The lncRNA epigenetics: The significance of m6A and m5C lncRNA modifications in cancer. *Front Oncol* 2023; **13**: 1063636 [PMID: 36969033 DOI: 10.3389/fonc.2023.1063636] [FullText]

23 **Filippova JA**, Matveeva AM, Zhuravlev ES, Balakhonova EA, Prokhorova DV, Malanin SJ, Shah Mahmud R, Grigoryeva TV, Anufrieva KS, Semenov DV, Vlassov VV, Stepanov GA. Are Small Nucleolar RNAs "CRISPRable"? A Report on Box C/D Small Nucleolar RNA Editing in Human Cells. *Front Pharmacol* 2019; **10**: 1246 [PMID: 31780925 DOI: 10.3389/fphar.2019.01246] [FullText]

24 **Huang X**, Yang Z, Li Y, Long X. m6A methyltransferase METTL3 facilitates multiple myeloma cell growth through the m6A modification of BZW2. *Ann Hematol* 2023; **102**: 1801-1810 [PMID: 37222774 DOI: 10.1007/s00277-023-05283-6] [FullText]

25 **Cai J**, Cui Z, Zhou J, Zhang B, Lu R, Ding Y, Hu H. METTL3 promotes glycolysis and cholangiocarcinoma progression by mediating the m6A modification of AKR1B10. *Cancer Cell Int* 2022; **22**: 385 [PMID: 36476503 DOI: 10.1186/s12935-022-02809-2] [FullText]

26 **Li N**, Zeng Y, Huang J. Signaling pathways and clinical application of RASSF1A and SHOX2 in lung cancer. *J Cancer Res Clin Oncol* 2020; **146**: 1379-1393 [PMID: 32266538 DOI: 10.1007/s00432-020-03188-9] [FullText]

27 **Yang W**, Chen H, Ma L, Dong J, Wei M, Xue X, Li Y, Jin Z, Xu W, Ji Z. SHOX2 promotes prostate cancer proliferation and metastasis through disruption of the Hippo-YAP pathway. *iScience* 2023; **26**: 107617 [PMID: 37664594 DOI: 10.1016/j.isci.2023.107617] [FullText]

28 **Teng Y**, Loveless R, Benson EM, Sun L, Shull AY, Shay C. SHOX2 cooperates with STAT3 to promote breast cancer metastasis through the transcriptional activation of WASF3. *J Exp Clin Cancer Res* 2021; **40**: 274 [PMID: 34465361 DOI: 10.1186/s13046-021-02083-6] [FullText]

29 **Yang T**, Zhang H, Cai SY, Shen YN, Yuan SX, Yang GS, Wu MC, Lu JH, Shen F. Elevated SHOX2 expression is associated with tumor recurrence of hepatocellular carcinoma. *Ann Surg Oncol* 2013; **20** Suppl 3: S644-S649 [PMID: 23851611 DOI: 10.1245/s10434-013-3132-1] [FullText]

30 **Hu B**, Xu Y, Li YC, Huang JF, Cheng JW, Guo W, Yin Y, Gao Y, Wang PX, Wu SY, Zhou J, Fan J, Yang XR. CD13 promotes hepatocellular carcinogenesis and sorafenib resistance by activating HDAC5-LSD1-NF-κB oncogenic signaling. *Clin Transl Med* 2020; **10**: e233 [PMID: 33377659 DOI: 10.1002/ctm2.233] [FullText]

31 **Xiang QM**, Jiang N, Liu YF, Wang YB, Mu DA, Liu R, Sun LY, Zhang W, Guo Q, Li K. Overexpression of SH2D1A promotes cancer progression and is associated with immune cell infiltration in hepatocellular carcinoma *via* bioinformatics and in vitro study. *BMC Cancer* 2023; **23**: 1005 [PMID: 37858067 DOI: 10.1186/s12885-023-11315-1] [FullText]

32 **Zhao Y**, Xue C, Xie Z, Ouyang X, Li L. Comprehensive analysis of ubiquitin-specific protease 1 reveals its importance in hepatocellular carcinoma. *Cell Prolif* 2020; **53**: e12908 [PMID: 32951278 DOI: 10.1111/cpr.12908] [FullText]

33 **Moroz-Omori EV**, Huang D, Kumar Bedi R, Cheriyamkunnel SJ, Bochenkova E, Dolbois A, Rzeczkowski MD, Li Y, Wiedmer L, Caflisch A. METTL3 Inhibitors for Epitranscriptomic Modulation of Cellular Processes. *ChemMedChem* 2021; **16**: 3035-3043 [PMID: 34237194 DOI: 10.1002/cmdc.202100291] [FullText]

World Journal of Gastroenterology

Submit a Manuscript: https://www.f6publishing.com

World J Gastroenterol 2025 June 7; 31(21): 106057

DOI: 10.3748/wjg.v31.i21.106057

ISSN 1007-9327 (print) ISSN 2219-2840 (online)

LETTER TO THE EDITOR

Microbiota geography in the colorectal carcinoma microenvironment: A spatiotemporal atlas of colonic mucosal microbial niche reconstruction

Zong-Qiang Han, Li-Na Wen

Specialty type: Gastroenterology and hepatology

Provenance and peer review: Unsolicited article; Externally peer reviewed.

Peer-review model: Single blind

Peer-review report's classification

Scientific Quality: Grade A, Grade A, Grade A, Grade A, Grade C

Novelty: Grade A, Grade A, Grade B, Grade B, Grade B

Creativity or Innovation: Grade A, Grade B, Grade B, Grade B, Grade C

Scientific Significance: Grade A, Grade A, Grade A, Grade B, Grade B

P-Reviewer: Chen ZG; Wang LY; Wang W

Received: February 20, 2025

Revised: March 29, 2025

Accepted: April 18, 2025

Published online: June 7, 2025

Processing time: 106 Days and 20.5 Hours

Zong-Qiang Han, Department of Laboratory Medicine, Beijing Xiaotangshan Hospital, Beijing 102211, China

Li-Na Wen, Department of Clinical Nutrition, Beijing Shijitan Hospital, Capital Medical University, Beijing 100038, China

Corresponding author: Li-Na Wen, Associate Research Scientist, Department of Clinical Nutrition, Beijing Shijitan Hospital, Capital Medical University, No. 10 Tieyi Road, Yangfangdian Street, Haidian District, Beijing 100038, China. wenlina3074@bjsjth.cn

Abstract

A case-control study on the differences in colonic mucosa-associated microbiotas between patients with and without colorectal cancer (CRC) in the Indonesian population was recently published. The geographical distribution characteristics of the gut microbiota in the carcinogenic microenvironment are closely related to disease progression. Therefore, the results of that study are of great significance for determining the pathogenesis of CRC in the Indonesian region and for clinically diagnosing and treating CRC. While acknowledging the strengths of the study, its limitations should also be addressed. Future case-control studies of the gut microbiota based on specific populations should be further refined to provide more optimized guidance for clinical precision treatment.

Key Words: Microbiota; Colorectal cancer; Colon mucosa; Geography; Case control study

Core Tip: A clinical study from a specific Indonesian population showed that the colonic mucosal microbial composition differs significantly between patients with and without colorectal cancer at the genus and species levels. The combination of *Fusobacterium nucleatum* and *Bacteroides fragilis* may serve as a diagnostic biomarker for colorectal cancer. The area under the curve for combined diagnosis was 0.786 (95% confidence interval: 0.671-0.900), with 82.8% sensitivity and 50% specificity. Although the study yielded significant reference results, it was relatively limited in sample size, disease staging, dietary factors, and functional studies of the differential microbiota. Future research should improve on these aspects.

Citation: Han ZQ, Wen LN. Microbiota geography in the colorectal carcinoma microenvironment: A spatiotemporal atlas of colonic mucosal microbial niche reconstruction. *World J Gastroenterol* 2025; 31(21): 106057
URL: https://www.wjgnet.com/1007-9327/full/v31/i21/106057.htm
DOI: https://dx.doi.org/10.3748/wjg.v31.i21.106057

TO THE EDITOR

We read with great interest the study exploring the differences in diversity and composition of the colonic mucosa-associated microbiota between patients with and without colorectal cancer (CRC) in Indonesia[1]. This study investigated the spatiotemporal atlas of colonic mucosal microbial niche reconstruction in patients with CRC, with the expectation of providing new biomarkers and intervention targets for early diagnosis and personalized treatment of CRC in this region.

CRC is one of the most prevalent malignant tumors globally and the second leading cause of cancer-related deaths[2]. Its etiology and pathogenesis are highly complex[3]. The gut microbiota, as the key to decoding the "dark matter" of the gut, is a crucial tool for determining disease mechanisms[4]. In recent years, the role of the gut microbiota in CRC development and progression has become a research hotspot. The gut microbiota influences the pathological processes of CRC through various mechanisms, including modulating host immune responses, generating metabolic products, and affecting gut barrier function[5,6]. Studies have shown that certain specific bacterial communities (*e.g.*, *Fusobacterium nucleatum* and *Bacteroides fragilis*) are significantly enriched in patients with CRC and contribute to tumor development and progression by promoting tumor stem cell neogenesis, regulating cell proliferation and cell cycles, and inducing chemotherapy-resistance responses[7-10]. Additionally, short-chain fatty acids (such as butyrate) produced by metabolism of the gut microbiota play an important role in maintaining gut homeostasis and inhibiting tumor development, whereas some microbial metabolites (such as secondary bile acids) may have procarcinogenic effects[11-14]. Although numerous studies have revealed associations between the gut microbiota and CRC, microbial compositions differ significantly among populations from different regions, which may lead to heterogeneity in the CRC pathogenesis and biomarkers across populations[15]. For example, Pesoa *et al*[16] found that β-diversity differed significantly among populations from the United States of America, United Kingdom and Argentina and may be closely related to the geographic region of individuals. Therefore, research on the gut mucosal microbiota in specific populations (such as the Indonesian population) holds important scientific and clinical significance.

A comparison of colonic mucosal samples revealed significant differences in microbial diversity and composition between patients with and without CRC in Indonesia. The main findings were as follows: (1) Differences in microbial diversity: For α-diversity, the median Shannon index was higher in the CRC group than in the non-CRC group (3.28 *vs* 2.82, $P > 0.05$), indicating a tendency for increased richness and evenness of the microbial community in the CRC group, although the difference was not statistically significant. The Simpson index showed the opposite trend (0.050 *vs* 0.060, $P > 0.05$), also without statistical significance. For β-diversity, the two groups differed significantly at the genus ($P = 0.002$) and species ($P = 0.001$) levels, indicating that the overall microbial community structure in the colonic mucosa of CRC patients differed distinctly from that of non-CRC patients; (2) Differences in microbial composition: 38 phyla were identified, with *Firmicutes*, *Proteobacteria*, *Bacteroidetes*, and *Fusobacteria* being dominant. Although the relative abundance of each phylum did not significantly differ between the two groups, *Fusobacteria* and *Proteobacteria* were more abundant in the CRC group. 188 genera were identified, among which, *Fusobacterium*, *Faecalibacterium*, *Citrobacter*, *Prevotella*, and *Bacteroides* were the most common. The relative abundances of *Bacteroides*, *Campylobacter*, *Peptostreptococcus*, and *Parvimonas* were significantly higher in the CRC group, whereas the relative abundances of *Faecalibacterium*, *Haemophilus*, and *Phocaeicola* were higher in the non-CRC group. At the species level, the relative abundances of *Fusobacterium nucleatum*, *Bacteroides fragilis*, *Parvimonas micra*, *Peptostreptococcus stomatis*, *Enterococcus faecalis*, and *Campylobacter hominis* were significantly higher in the CRC group. Conversely, *Faecalibacterium prausnitzii*, *Haemophilus parainfluenzae*, and *Prevotella copri* were more common in the non-CRC group; (3) Exploration of potential diagnostic biomarkers: The potentials of *Fusobacterium nucleatum* and *Bacteroides fragilis*, both individually and in combination, were evaluated for diagnosing CRC. The areas under the curve were 0.727 for *Fusobacterium nucleatum* [95% confidence interval (CI): 0.600-0.853] and 0.735 for *Bacteroides fragilis* (95%CI: 0.607-0.862). The combined area under the curve was 0.786 (95%CI: 0.671-0.900). The combined diagnostic sensitivity was 82.8%, the specificity was 50%, the positive predictive value was 70.7%, and the negative predictive value was 66.7%; and (4) Other aspects: In the CRC group, the median age was higher (61 years *vs* 47 years, $P = 0.002$), and the proportion of men was higher (62.9% *vs* 41.7%) than in the non-CRC group. Regarding diet, 81.4% of participants consumed at least one serving of vegetables and fruits daily, and 78.2% had meat in their diet, but only 8.5% consumed 100-500 g of red meat daily.

These results provide a new perspective on the pathogenesis of CRC and offer important references for future diagnosis and treatment. The following advantages of the study strongly support the reliability and scientific nature of the results and lay a solid foundation for subsequent clinical applications and further research. (1) Rationality of the study design: The researchers used a case-control design, comparing the microbiota compositions of patients with and without CRC. This design effectively controls for confounding variables and provides more reliable results. In selecting the samples, the researchers excluded patients who had used antibiotics or probiotics or had special diets, ensuring the homogeneity of the samples; (2) Advanced technological application: In addition to 16S rDNA sequencing, the researchers used the Oxford nanopore technologies platform for sequencing. This third-generation sequencing technology generates longer sequence fragments, allowing more accurate species-level classification; (3) Focus on the Indonesian population: The results provide unique microbiota data for the Indonesian region, which is of great significance for understanding the differences in microbiotas across geographical regions and their relationship with CRC. Diet and lifestyle in Indonesia differ significantly from those of Western countries, which endow the study results with unique scientific value; (4) Scientific significance of the results: Microbiota compositions differed significantly between patients with and without CRC, especially at the genus and species levels, thus offering potential biomarkers for early diagnosis and prognosis assessment of CRC, with important clinical application value; and (5) Preliminary exploration of microbial functions: The study explored the potential mechanisms of certain microbes (such as *Fusobacterium nucleatum* and *Bacteroides fragilis*) in CRC. For example, *Fusobacterium nucleatum* may induce inflammatory responses and DNA damage by secreting the FadA protein, thereby promoting carcinogenesis, which provides direction for future functional studies.

Although this study yielded significant results by exploring the relationship between CRC and the colonic mucosal microbiota, providing valuable data support for subsequent research and clinical applications, the limitations in its research process must be addressed as they may impact the interpretation and application of the results. Thus, the process must be thoroughly analyzed and improved in future studies to further enhance the scientific nature and reliability of the research. The main bottlenecks that must be resolved are as follows: (1) Limitations in sample selection: The samples from the non-CRC group were derived from patients with gastrointestinal symptoms but no obvious tumors. This may have led to selection bias as other gastrointestinal diseases (*e.g.*, irritable bowel syndrome or microscopic colitis) may affect the microbiota composition. Moreover, an ideal control group should be healthy, asymptomatic individuals to exclude interference from other diseases with the microbiota; (2) Insufficient diagnostic criteria for non-CRC patients: The diagnostic criteria for the non-CRC group may have some subjectivity. For example, some patients may have had undetected early cancerous lesions, which may affect the accuracy of the results; (3) Insufficient sample size: Although a sample size of 59 was statistically sufficient, it was still relatively small, which may affect the universality and representativeness of the results. A larger sample size would enhance the reliability and applicability of the results; (4) Lack of longitudinal studies: This study was a cross-sectional study; thus, it could reveal no causal relationship between microbiota alterations and CRC progression[17]. Longitudinal studies allow better understanding the dynamic changes in the microbiota during cancer development; (5) Failure to consider other influencing factors: The study did not fully consider the impact of diet, antibiotic drugs, lifestyle, genetic factors, and other factors on the microbiota. These factors can significantly affect the microbiota composition, thereby influencing the research results. For example, the Indonesian diet is characterized by high fiber and low red meat content, which may impact the microbiota composition; (6) Complexity of the statistical analysis: Although appropriate statistical models were used, analysis of microbiota data is typically complex and often requires more refined statistical methods to address multiple comparisons and non-normal data distributions. Moreover, some results (*e.g.*, differences in the Shannon and Simpson indices) did not reach statistical significance, likely owing to the small sample size or large data variability; and (7) Lack of in-depth exploration of microbial functions: This study mainly focused on microorganism composition and did not investigate microbial functions and mechanisms of action in CRC. Future studies should consider combining techniques such as metabolomics and transcriptomics to further reveal the functional characteristics of the microbiota.

To create more rigorous evidence and promote clinical translation, a systematic improvement plan must be developed to address the existing bottlenecks. Future research should focus on optimizing the following six dimensions: (1) Increasing sample size and long-term follow-up: Future studies should expand the samples to include more CRC patients and non-CRC control populations. Long-term follow-up study designs should also be implemented to conduct regular microbiota testing for CRC patients to understand the trends in microbiota changes at different CRC stages; (2) Expanding study populations and disease controls: Similar studies should be conducted in different regions, incorporating populations with diverse ethnic backgrounds and lifestyles. Additionally, populations with other gastrointestinal diseases (*e.g.*, inflammatory bowel disease and intestinal infectious diseases) should be included as controls to more accurately assess the specificity of the CRC-associated microbiota; (3) In-depth functional analysis and mechanistic studies: Metagenomics techniques, in-depth sequencing and functional analysis of samples should be combined to comprehensively understand the functional characteristics of the microbiota. Additionally, *in vitro* experiments and animal models should be used to investigate interaction mechanisms between the microbiota and host immune system as well as intestinal barrier function; (4) Optimizing control group selection: As much as possible, healthy individuals without gastrointestinal symptoms should be selected as controls to minimize the impact of microbiota disturbances in the control group on the study results; (5) Detailed assessment of diet and other factors: More refined dietary survey methods should be used to quantify participants' dietary structures, and detailed information on medication history and lifestyle habits should be collected to assess the impact of these factors on the microbiota; and (6) In-depth exploration of diagnostic biomarkers: By combining multiple types of microbiotas, more effective diagnostic models should be constructed to improve the diagnostic sensitivity and specificity, and the current findings should also be compared with similar studies to contextualize the novelty of the proposed biomarkers. Moreover, biomarkers derived from non-invasive specimens such as the fecal microbiota, urine and blood should also be explored to enhance the convenience of specimen collection and diagnosis.

In summary, this study unveiled the spatiotemporal atlas of colonic mucosal microbial niche reconstruction, which serves as the microbial geography within the neoplastic microenvironment. It provided important foundational data for microbiota research in patients with CRC in Indonesia. Despite some limitations, the findings hold significant clinical implications and offer direction for future research. Future studies should further investigate the functions of the microbiota and their mechanisms of action in CRC based on local populations to provide new insights for early diagnosis and treatment of CRC.

FOOTNOTES

Author contributions: Wen LN designed the research and revised the letter; Han ZQ and Wen LN performed the research and analyzed the data; Han ZQ wrote the letter.

Supported by the Beijing High Level Public Health Technology Talent Construction Project, No. backbone-03-04.

Conflict-of-interest statement: All the authors report no relevant conflicts of interest for this article.

Country of origin: China

ORCID number: Li-Na Wen 0000-0001-6507-2978.

S-Editor: Wei YF
L-Editor: A
P-Editor: Yu HG

REFERENCES

1 **Darnindro N**, Abdullah M, Sukartini N, Rumende CM, Pitarini A, Nursyirwan SA, Fauzi A, Makmun D, Nelwan EJ, Shatri H, Rinaldi I, Tanadi C. Differences in diversity and composition of mucosa-associated colonic microbiota in colorectal cancer and non-colorectal cancer in Indonesia. *World J Gastroenterol* 2025; **31**: 100051 [PMID: 39991683 DOI: 10.3748/wjg.v31.i7.100051] [FullText]

2 **Patel SG**, Dominitz JA. Screening for Colorectal Cancer. *Ann Intern Med* 2024; **177**: ITC49-ITC64 [PMID: 38588547 DOI: 10.7326/AITC202404160] [FullText]

3 **Li Q**, Geng S, Luo H, Wang W, Mo YQ, Luo Q, Wang L, Song GB, Sheng JP, Xu B. Signaling pathways involved in colorectal cancer: pathogenesis and targeted therapy. *Signal Transduct Target Ther* 2024; **9**: 266 [PMID: 39370455 DOI: 10.1038/s41392-024-01953-7] [FullText]

4 **Aburto MR**, Cryan JF. Gastrointestinal and brain barriers: unlocking gates of communication across the microbiota-gut-brain axis. *Nat Rev Gastroenterol Hepatol* 2024; **21**: 222-247 [PMID: 38355758 DOI: 10.1038/s41575-023-00890-0] [FullText]

5 **Wong SH**, Yu J. Gut microbiota in colorectal cancer: mechanisms of action and clinical applications. *Nat Rev Gastroenterol Hepatol* 2019; **16**: 690-704 [PMID: 31554963 DOI: 10.1038/s41575-019-0209-8] [FullText]

6 **Wong CC**, Yu J. Gut microbiota in colorectal cancer development and therapy. *Nat Rev Clin Oncol* 2023; **20**: 429-452 [PMID: 37169888 DOI: 10.1038/s41571-023-00766-x] [FullText]

7 **Wang Q**, Hu T, Zhang Q, Zhang Y, Dong X, Jin Y, Li J, Guo Y, Guo F, Chen Z, Zhong P, Yang Y, Ma Y. Fusobacterium nucleatum promotes colorectal cancer through neogenesis of tumor stem cells. *J Clin Invest* 2025; **135**: e181595 [PMID: 39656543 DOI: 10.1172/JCI181595] [FullText]

8 **Wu QL**, Fang XT, Wan XX, Ding QY, Zhang YJ, Ji L, Lou YL, Li X. Fusobacterium nucleatum-induced imbalance in microbiome-derived butyric acid levels promotes the occurrence and development of colorectal cancer. *World J Gastroenterol* 2024; **30**: 2018-2037 [PMID: 38681125 DOI: 10.3748/wjg.v30.i14.2018] [FullText]

9 **Li B**, Wei Z, Wang Z, Xu F, Yang J, Lin B, Chen Y, Wenren H, Wu L, Guo X, Liu Y, Wei Y. Fusobacterium nucleatum induces oxaliplatin resistance by inhibiting ferroptosis through E-cadherin/β-catenin/GPX4 axis in colorectal cancer. *Free Radic Biol Med* 2024; **220**: 125-138 [PMID: 38657754 DOI: 10.1016/j.freeradbiomed.2024.04.226] [FullText]

10 **Qin Y**, Tong X, Mei WJ, Cheng Y, Zou Y, Han K, Yu J, Jie Z, Zhang T, Zhu S, Jin X, Wang J, Yang H, Xu X, Zhong H, Xiao L, Ding PR. Consistent signatures in the human gut microbiome of old- and young-onset colorectal cancer. *Nat Commun* 2024; **15**: 3396 [PMID: 38649355 DOI: 10.1038/s41467-024-47523-x] [FullText]

11 **Cheong YJ**, Trefely S. Divergent roles for propionate and butyrate in colorectal cancer epigenetics. *Nat Metab* 2025; **7**: 11-13 [PMID: 39789353 DOI: 10.1038/s42255-024-01186-6] [FullText]

12 **Dong J**, Wang B, Xiao Y, Liu J, Wang Q, Xiao H, Jin Y, Liu Z, Chen Z, Li Y, Fan S, Li Y, Cui M. Roseburia intestinalis sensitizes colorectal cancer to radiotherapy through the butyrate/OR51E1/RALB axis. *Cell Rep* 2024; **43**: 114407 [PMID: 38923460 DOI: 10.1016/j.celrep.2024.114407] [FullText]

13 **Cong J**, Liu P, Han Z, Ying W, Li C, Yang Y, Wang S, Yang J, Cao F, Shen J, Zeng Y, Bai Y, Zhou C, Ye L, Zhou R, Guo C, Cang C, Kasper DL, Song X, Dai L, Sun L, Pan W, Zhu S. Bile acids modified by the intestinal microbiota promote colorectal cancer growth by suppressing CD8(+) T cell effector functions. *Immunity* 2024; **57**: 876-889.e11 [PMID: 38479384 DOI: 10.1016/j.immuni.2024.02.014] [FullText]

14 **Caliceti C**, Punzo A, Silla A, Simoni P, Roda G, Hrelia S. New Insights into Bile Acids Related Signaling Pathways in the Onset of Colorectal Cancer. *Nutrients* 2022; **14**: 2964 [PMID: 35889921 DOI: 10.3390/nu14142964] [FullText]

15 **Govender P**, Ghai M. Population-specific differences in the human microbiome: Factors defining the diversity. *Gene* 2025; **933**: 148923 [PMID: 39244168 DOI: 10.1016/j.gene.2024.148923] [FullText]

16 **Pesoa SA**, Portela N, Fernández E, Elbarcha O, Gotteland M, Magne F. Comparison of Argentinean microbiota with other geographical populations reveals different taxonomic and functional signatures associated with obesity. *Sci Rep* 2021; **11**: 7762 [PMID: 33833357 DOI: 10.1038/s41598-021-87365-x] [FullText]

17 **Yachida S**, Mizutani S, Shiroma H, Shiba S, Nakajima T, Sakamoto T, Watanabe H, Masuda K, Nishimoto Y, Kubo M, Hosoda F, Rokutan H, Matsumoto M, Takamaru H, Yamada M, Matsuda T, Iwasaki M, Yamaji T, Yachida T, Soga T, Kurokawa K, Toyoda A, Ogura Y, Hayashi T, Hatakeyama M, Nakagama H, Saito Y, Fukuda S, Shibata T, Yamada T. Metagenomic and metabolomic analyses reveal distinct stage-specific phenotypes of the gut microbiota in colorectal cancer. *Nat Med* 2019; **25**: 968-976 [PMID: 31171880 DOI: 10.1038/s41591-019-0458-7] [FullText]

World Journal of Gastroenterology

Submit a Manuscript: https://www.f6publishing.com

World J Gastroenterol 2025 June 7; 31(21): 106530

DOI: 10.3748/wjg.v31.i21.106530

ISSN 1007-9327 (print) ISSN 2219-2840 (online)

LETTER TO THE EDITOR

Targeting the NAD+/SIRT1 axis: A metabolic strategy to overcome oxaliplatin resistance in colorectal cancer

Md Sadique Hussain, Vikash Jakhmola, Kavita Goyal, Arcot Rekha, Ayesha Sultana, Haider Ali, Gaurav Gupta

Specialty type: Gastroenterology and hepatology

Provenance and peer review: Invited article; Externally peer reviewed.

Peer-review model: Single blind

Peer-review report's classification

Scientific Quality: Grade A, Grade B, Grade B

Novelty: Grade A, Grade B, Grade B

Creativity or Innovation: Grade B, Grade B, Grade B

Scientific Significance: Grade A, Grade B, Grade B

P-Reviewer: Hasan N; Jin Y; Zhou Y

Received: February 28, 2025

Revised: March 21, 2025

Accepted: April 16, 2025

Published online: June 7, 2025

Processing time: 98 Days and 6.8 Hours

Md Sadique Hussain, Vikash Jakhmola, Uttaranchal Institute of Pharmaceutical Sciences, Uttaranchal University, Dehra Dun 248007, Uttarākhand, India

Kavita Goyal, Department of Biotechnology, Graphic Era (Deemed to Be University), Dehra Dun 248002, Uttarākhand, India

Arcot Rekha, Department of General Surgery, Dr. D.Y. Patil Medical College, Hospital and Research Centre, Pune 411018, Mahārāshtra, India

Ayesha Sultana, Department of Pharmaceutics, Sree Dattha Institute of Pharmacy, Hyderabad 501510, Telangāna, India

Haider Ali, Centre for Global Health Research, Saveetha Medical College, Saveetha Institute of Medical and Technical Sciences, Saveetha University, Chennai 602105, Tamil Nādu, India

Gaurav Gupta, Centre for Research Impact & Outcome-Chitkara College of Pharmacy, Chitkara University, Rajpura 140401, Punjab, India

Gaurav Gupta, Centre of Medical and Bio-allied Health Sciences Research, Ajman University, Ajman 13306, United Arab Emirates

Co-corresponding authors: Md Sadique Hussain and Gaurav Gupta.

Corresponding author: Md Sadique Hussain, PhD, Assistant Professor, Uttaranchal Institute of Pharmaceutical Sciences, Uttaranchal University, Prem Nagar, Dehra Dun 248007, Uttarākhand, India. sadiquehussain007@gmail.com

Abstract

Oxaliplatin resistance remains a significant clinical challenge in colorectal cancer (CRC), highlighting the urgent need to identify novel molecular targets for therapeutic intervention. Recent findings by Niu *et al* have elucidated the role of the NAD+/SIRT1 axis in mediating oxaliplatin resistance through metabolic reprogramming. Their study demonstrated that oxaliplatin-induced DNA damage activates PARP, resulting in NAD+ depletion and subsequent downregulation of SIRT1. This reduction in SIRT1 levels enhances glycolysis, as evidenced by increased expression of PKM2 and LDHA, thereby conferring a metabolic advantage to resistant CRC cells. Conversely, restoration of SIRT1 expression reverses resistance, while pharmacological inhibition of glycolysis effectively sensitizes cells to oxaliplatin. These findings underscore the therapeutic potential of targeting the NAD+/SIRT1 pathway as a metabolic vulnerability in CRC.

Future studies should investigate the clinical feasibility of combining SIRT1 agonists and glycolysis inhibitors with oxaliplatin to overcome drug resistance and improve patient outcomes.

Key Words: SIRT1; Glycolysis; Drug resistance; Colorectal cancer; Chemotherapy

Core Tip: Oxaliplatin resistance remains a major clinical challenge in colorectal cancer (CRC). This study underscores the critical role of the NAD+/SIRT1 axis in driving metabolic reprogramming that facilitates resistance. Oxaliplatin-induced DNA damage activates PARP, leading to NAD+ depletion and subsequent downregulation of SIRT1. This reduction in SIRT1 expression enhances glycolysis, marked by upregulation of PKM2 and LDHA. Notable, restoration of SIRT1 reverses resistance, while glycolysis inhibition sensitizes CRC cells to oxaliplatin. These findings suggest that targeting the NAD+/SIRT1 pathway, through SIRT1 agonists and glycolysis inhibitors, offers a promising metabolic strategy to overcome chemoresistance and improve therapeutic outcomes in CRC patients.

Citation: Hussain MS, Jakhmola V, Goyal K, Rekha A, Sultana A, Ali H, Gupta G. Targeting the NAD+/SIRT1 axis: A metabolic strategy to overcome oxaliplatin resistance in colorectal cancer. *World J Gastroenterol* 2025; 31(21): 106530
URL: https://www.wjgnet.com/1007-9327/full/v31/i21/106530.htm
DOI: https://dx.doi.org/10.3748/wjg.v31.i21.106530

TO THE EDITOR

I am writing to express my strong interest in the recent study by Niu *et al*[1], which elucidates the role of the NAD+/SIRT1 axis in mediating oxaliplatin resistance in colorectal cancer (CRC). The findings presented in this study are particularly compelling as they offer novel insights into metabolic reprogramming as a mechanism of underlying chemoresistance. The interplay between DNA damage repair, NAD+ metabolism, and SIRT1 activity reveals a complex regulatory network that may serve as a promising therapeutic target to overcome oxaliplatin resistance in CRC patients. Given the growing clinical burden associated with oxaliplatin resistance, the therapeutic implications of targeting the NAD+/SIRT1 axis merits further discussion and investigation[1].

CRC remains a major oncological challenge, with oxaliplatin-based chemotherapy forming the cornerstone of treatment for advanced-stage disease. However, the emergence of resistance to oxaliplatin presents a formidable obstacle, significantly compromising treatment efficacy and reducing patient survival[2]. Although multiple mechanisms have been implicated in oxaliplatin resistance—including enhanced DNA repair capacity, increased activity of drug efflux pumps, and alterations in apoptotic signaling—the role of metabolic reprogramming has been relatively underexplored [3]. The study by Niu *et al*[1] provides compelling evidence that oxaliplatin-induced NAD+ depletion *via* PARP activation leads to the downregulation of SIRT1 expression, triggering a metabolic shift toward glycolysis. This adaptive response, characterized by elevated expression of PKM2 and LDHA, confers a survival advantage that enables CRC cells to evade oxaliplatin-induced cytotoxicity[1].

While the study elegantly links SIRT1 downregulation to glycolytic reprogramming, the precise molecular mechanisms through which SIRT1 modulates glycolysis warrant further elucidation. It remains to be determined whether SIRT1 directly regulates glycolytic enzyme function *via* post-translational modifications, such as deacetylation, or whether its effects are mediated through upstream signaling pathways. For instance, previous studies have indicated that SIRT1 may deacetylate and destabilize transcription factors like HIF-1α, thereby indirectly suppressing glycolytic gene expression[4, 5]. Alternatively, SIRT1's role in activating AMPK and inhibiting mTOR signaling may intersect with key metabolic pathways critical for CRC cell survival under chemotherapeutic stress[6].

Importantly, the role of SIRT1 is context-dependent, influenced by both microenvironmental and genetic factors. While it may promote metabolic adaptation and chemoresistance in CRC, SIRT1 has also been shown to exhibit tumor-suppressive functions in other contexts. Therefore, a careful evaluation of potential off-target effects and CRC-specific molecular landscapes is essential to optimize the therapeutic targeting of the NAD+/SIRT1 axis.

Future investigations employing functional assays, such as chromatin immunoprecipitation to evaluate SIRT1's direct binding to the promoters of glycolytic enzymes, and enzyme activity assays following SIRT1 modulation will be crucial to determine whether SIRT1's influence on PKM2 and LDHA is direct or mediated through upstream regulators. Additionally, assessing the acetylation status of PKM2 and LDHA in oxaliplatin-resistant CRC cells could yield critical mechanistic insights.

Notably, prior studies have shown that SIRT1 agonists, such as resveratrol and SRT1720, exert anti-tumor effects in CRC models by modulating apoptotic pathways and cellular metabolism[7]. However, their specific impact on oxaliplatin resistance and glycolytic adaptation remains underexplored, highlighting the need for further investigation into SIRT1 modulation in this context.

The identification of SIRT1 as a key regulator of oxaliplatin resistance in this study aligns with growing evidence linking sirtuins to cancer metabolism and therapeutic resistance. SIRT1, an NAD+-dependent deacetylase, plays a pivotal role in maintaining genome stability, regulating apoptosis, and modulating cellular metabolism[8]. In the context of CRC, SIRT1 has been reported to exhibit dual functions, acting as either a tumor suppressor or an oncogene depending on the molecular and cellular context[9]. The current study suggests that NAD+ depletion, resulting from oxaliplatin-induced PARP activation, downregulates SIRT1 and enhances glycolytic activity, thereby promoting chemoresistance. Importantly, the finding that pharmacological activation of SIRT1 can restore oxaliplatin sensitivity underscores its potential as a viable therapeutic target.

An intriguing aspect of the study by Niu *et al*[1] is the elucidation of a link between DNA damage response (DDR) and metabolic adaptation. Oxaliplatin-induced DNA damage activates PARP, leading to NAD+ depletion and suppressing SIRT1 activity. This metabolic shift favors glycolysis over oxidative phosphorylation, mimicking the Warburg effect—a hallmark of cancer metabolism[10]. Notably, the study highlights how CRC cells exploit glycolysis reprogramming to survive chemotherapy-induced stress, thereby contributing to oxaliplatin resistance. The resensitization of resistant cells using glycolysis inhibitors, such as shikonin, underscores the therapeutic promise of targeting metabolic vulnerabilities in CRC[1].

While this study primarily addresses on oxaliplatin resistance, it raises an important question: Are SIRT1-mediated mechanisms also relevant to resistance against other platinum-based agents, such as cisplatin and carboplatin? Despite sharing the ability to induce DNA adducts, these agents differ in chemical structure, DNA-binding affinity, and associated repair pathways, all of which may influence how SIRT1 modulates cellular responses[11]. Cisplatin and carboplatin are extensively used in treating various malignancies—including ovarian, lung, and bladder cancers—where platinum resistance continues to pose a significant clinical challenge. Exploring the broader applicability of the NAD+/SIRT1 axis across different tumor types and platinum-based chemotherapeutics could inform the development of more effective combination strategies to overcome resistance.

Emerging evidence suggests that SIRT1 may similarly influence resistance mechanisms in other cancers. For instance, studies in ovarian and lung cancer models have implicated SIRT1 in regulating DDR, apoptosis, and metabolism—key processes involved in cisplatin sensitivity[12]. Therefore, future investigations should explore whether SIRT1 downregulation universally contributes to platinum resistance across tumor types. Integrating data from large clinical cohorts, such as The Cancer Genome Atlas (TCGA) and Gene Expression Omnibus, could yield correlative insights into SIRT1 expression patterns and patient outcomes following cisplatin or carboplatin treatment. Additionally, functional studies in preclinical models utilizing various platinum agents would help determine whether the NAD+/SIRT1 axis constitutes a generalized metabolic vulnerability in platinum-resistant cancers.

The clinical relevance of these findings is underscored by data from TCGA, which indicates that lower SIRT1 expression is associated with poorer overall survival in CRC patients undergoing adjuvant chemotherapy[13]. This suggests that SIRT1 expression levels could serve as a prognostic biomarker to predict oxaliplatin response. Future studies should aim to validate these observations in larger patient cohorts and assess the therapeutic potential of SIRT1 agonists in clinical settings.

From a translational perspective, the study raises important questions regarding the potential for therapeutic intervention targeting the NAD+/SIRT1 axis. The use of SIRT1 activators, such as CAY10602, in combination with oxaliplatin represents a promising strategy to enhance chemosensitivity[14]. Moreover, considering the role of PARP activation in NAD+ depletion, the combination of PARP inhibitors with SIRT1 agonists may enhance therapeutic efficacy. Although PARP inhibitors have primarily been explored in BRCA-mutant cancers[15], their ability to influence NAD+ metabolism suggests a broader application in overcoming chemoresistance in CRC. Future preclinical and clinical studies are warranted to evaluate the feasibility and effectiveness of such combination approaches.

While the study by Niu *et al*[1] provides valuable mechanistic insights, several areas warrant further exploration to fully harness the therapeutic potential of targeting the NAD+/SIRT1 axis in CRC. First, the molecular determinants governing the differential response of CRC cells to SIRT1 modulation need to be elucidated. Given SIRT1's dual role—as both a tumor suppressor and promoter depending on cellular and microenvironmental contexts—identifying predictive biomarkers (*e.g.*, NAD+ levels, PARP activity, metabolic profiles) will be essential for patient stratification and optimizing therapeutic efficacy.

Second, the interplay between SIRT1 and other key metabolic regulators, such as AMPK and mTOR, should be systematically investigated. These pathways converge on cellular energy homeostasis and stress responses, and may synergistically influence glycolytic reprogramming and drug resistance. A comprehensive mapping of these interconnected signaling networks would provide a more holistic understanding of the metabolic adaptations that drive oxaliplatin resistance.

Importantly, while the current study emphasizes the benefits of pharmacological SIRT1 activation in restoring oxaliplatin sensitivity, the therapeutic potential of SIRT1 inhibitors in combination therapy remains underexplored. Emerging evidence suggests that SIRT1 inhibition may exacerbate DNA damage, oxidative stress, and apoptotic signaling—mechanisms that could enhance oxaliplatin cytotoxicity under certain tumor conditions[14]. It is therefore imperative to evaluate the efficacy of SIRT1 inhibitors in in vivo models, particularly orthotopic CRC models that more accurately replicate the tumor microenvironment, including stromal fibrosis, hypoxia, and immune infiltration.

Future preclinical studies should assess critical endpoints such as tumor growth inhibition, metastasis suppression, and systemic toxicity profiles in response to combination therapy with SIRT1 inhibitors and oxaliplatin. Mechanistic analyses should also investigate whether SIRT1 inhibition amplifies DNA damage markers (*e.g.*, γH2AX), increases reactive oxygen species production, or enhances pro-apoptotic signaling in CRC cells. These insights would provide a rational basis for the dual targeting strategies and offer insight into the contextual benefits of either activating or inhibiting SIRT1. Collectively, such investigations will reinforce the translational relevance of NAD+/SIRT1 modulation

and support the development of more effective, biomarker-driven combination therapies in oxaliplatin-resistant CRC.

Conclusion

The study by Niu *et al*[1] offers a compelling framework for understanding the metabolic underpinnings of oxaliplatin resistance in CRC, and positioning the NAD+/SIRT1 axis as a promising therapeutic target. Integrating metabolic interventions with conventional chemotherapy holds significant potential to enhance treatment efficacy and overcome drug resistance. Future research should prioritize the clinical validation of these findings and the development of combinatorial therapeutic strategies aimed to improving patient outcomes for CRC patients. In light of the urgent need for innovative approaches to address chemoresistance, targeting metabolic vulnerabilities emerges as a promising and clinically relevant avenue for advancing CRC therapy.

FOOTNOTES

Author contributions: Hussain MS and Gupta G contribute equally to this study as co-corresponding authors; Hussain MS was responsible for conceptualization, data curation, writing – original draft; Jakhmola V was responsible for investigation, writing – original draft; Goyal K was responsible for formal analysis, investigation; Rekha A was responsible for data curation, writing – original draft; Sultana A was responsible for conceptualization, methodology, writing – original draft; Ali H was responsible for formal analysis, validation; Gupta G was responsible for conceptualization, supervision, writing – review & editing.

Conflict-of-interest statement: All the authors have no conflict of interest related to the manuscript.

Country of origin: India

ORCID number: Md Sadique Hussain 0000-0002-3554-1750; Ayesha Sultana 0000-0003-3773-6604; Gaurav Gupta 0000-0001-7941-0229.

S-Editor: Lin C
L-Editor: A
P-Editor: Yu HG

REFERENCES

1 **Niu JW**, Zhang GC, Ning W, Liu HB, Yang H, Li CF. Clinical effects of phospholipase D2 in attenuating acute pancreatitis. *World J Gastroenterol* 2025; **31**: 97239 [PMID: 39811501 DOI: 10.3748/wjg.v31.i2.97239] [FullText]
2 **Capdevila J**, Elez E, Peralta S, Macarulla T, Ramos FJ, Tabernero J. Oxaliplatin-based chemotherapy in the management of colorectal cancer. *Expert Rev Anticancer Ther* 2008; **8**: 1223-1236 [PMID: 18699761 DOI: 10.1586/14737140.8.8.1223] [FullText]
3 **Chen G**, Gong T, Wang Z, Wang Z, Lin X, Chen S, Sun C, Zhao W, Kong Y, Ai H, Yang H, Liu Y, Wu F, Kang J, Zhao S, Xiao X, Sun J, He A, Li Z. Correction to: Colorectal cancer organoid models uncover oxaliplatin-resistant mechanisms at single cell resolution. *Cell Oncol (Dordr)* 2022; **45**: 1169-1170 [PMID: 36422806 DOI: 10.1007/s13402-022-00728-y] [FullText]
4 **Joo HY**, Yun M, Jeong J, Park ER, Shin HJ, Woo SR, Jung JK, Kim YM, Park JJ, Kim J, Lee KH. SIRT1 deacetylates and stabilizes hypoxia-inducible factor-1α (HIF-1α) *via* direct interactions during hypoxia. *Biochem Biophys Res Commun* 2015; **462**: 294-300 [PMID: 25979359 DOI: 10.1016/j.bbrc.2015.04.119] [FullText]
5 **Lim JH**, Lee YM, Chun YS, Chen J, Kim JE, Park JW. Sirtuin 1 modulates cellular responses to hypoxia by deacetylating hypoxia-inducible factor 1alpha. *Mol Cell* 2010; **38**: 864-878 [PMID: 20620956 DOI: 10.1016/j.molcel.2010.05.023] [FullText]
6 **Li J**, Pan J, Wang L, Ji G, Dang Y. Colorectal Cancer: Pathogenesis and Targeted Therapy. *MedComm (2020)* 2025; **6**: e70127 [PMID: 40060193 DOI: 10.1002/mco2.70127] [FullText]
7 **Sonnemann J**, Kahl M, Siranjeevi PM, Blumrich A, Blümel L, Becker S, Wittig S, Winkler R, Krämer OH, Beck JF. Reverse chemomodulatory effects of the SIRT1 activators resveratrol and SRT1720 in Ewing's sarcoma cells: resveratrol suppresses and SRT1720 enhances etoposide- and vincristine-induced anticancer activity. *J Cancer Res Clin Oncol* 2016; **142**: 17-26 [PMID: 26055805 DOI: 10.1007/s00432-015-1994-2] [FullText]
8 **Pande S**, Raisuddin S. Molecular and cellular regulatory roles of sirtuin protein. *Crit Rev Food Sci Nutr* 2023; **63**: 9895-9913 [PMID: 35510883 DOI: 10.1080/10408398.2022.2070722] [FullText]
9 **Dong W**, Lu J, Li Y, Zeng J, Du X, Yu A, Zhao X, Chi F, Xi Z, Cao S. SIRT1: a novel regulator in colorectal cancer. *Biomed Pharmacother* 2024; **178**: 117176 [PMID: 39059350 DOI: 10.1016/j.biopha.2024.117176] [FullText]
10 **Barba I**, Carrillo-Bosch L, Seoane J. Targeting the Warburg Effect in Cancer: Where Do We Stand? *Int J Mol Sci* 2024; **25** [PMID: 38542116 DOI: 10.3390/ijms25063142] [FullText]
11 **Lokich J**. What is the "best" platinum: cisplatin, carboplatin, or oxaliplatin? *Cancer Invest* 2001; **19**: 756-760 [PMID: 11577818 DOI: 10.1081/cnv-100106152] [FullText]
12 **Luna A**, Aladjem MI, Kohn KW. SIRT1/PARP1 crosstalk: connecting DNA damage and metabolism. *Genome Integr* 2013; **4**: 6 [PMID: 24360018 DOI: 10.1186/2041-9414-4-6] [FullText]

13 **Guan J**, Zhang ZY, Sun JH, Wang XP, Zhou ZQ, Qin L. LITAF inhibits colorectal cancer stemness and metastatic behavior by regulating FOXO1-mediated SIRT1 expression. *Clin Exp Metastasis* 2023; **40**: 309-320 [PMID: 37266842 DOI: 10.1007/s10585-023-10213-x] [Full Text]

14 **Yousafzai NA**, Jin H, Ullah M, Wang X. Recent advances of SIRT1 and implications in chemotherapeutics resistance in cancer. *Am J Cancer Res* 2021; **11**: 5233-5248 [PMID: 34873458] [FullText]

15 **Pilié PG**, Gay CM, Byers LA, O'Connor MJ, Yap TA. PARP Inhibitors: Extending Benefit Beyond BRCA-Mutant Cancers. *Clin Cancer Res* 2019; **25**: 3759-3771 [PMID: 30760478 DOI: 10.1158/1078-0432.CCR-18-0968] [FullText]

World Journal of Gastroenterology

Submit a Manuscript: https://www.f6publishing.com

World J Gastroenterol 2025 June 7; 31(21): 106808

DOI: 10.3748/wjg.v31.i21.106808

ISSN 1007-9327 (print) ISSN 2219-2840 (online)

LETTER TO THE EDITOR

Outcome prediction for cholangiocarcinoma prognosis: Embracing the machine learning era

Arnulfo E Morales-Galicia, Mariana N Rincón-Sánchez, Mariana M Ramírez-Mejía, Nahum Méndez-Sánchez

Specialty type: Gastroenterology and hepatology

Provenance and peer review: Invited article; Externally peer reviewed.

Peer-review model: Single blind

Peer-review report's classification
Scientific Quality: Grade B, Grade B, Grade C, Grade C, Grade C
Novelty: Grade B, Grade C, Grade C, Grade C, Grade C
Creativity or Innovation: Grade C, Grade C, Grade C, Grade C, Grade C
Scientific Significance: Grade B, Grade C, Grade C, Grade C, Grade C

P-Reviewer: Huang X; Sarasa-Cabezuelo A; Wu H

Received: March 9, 2025
Revised: April 15, 2025
Accepted: May 12, 2025
Published online: June 7, 2025
Processing time: 91 Days and 1.9 Hours

Arnulfo E Morales-Galicia, Nahum Méndez-Sánchez, Faculty of Medicine, National Autonomous University of Mexico, Mexico City 04360, Mexico

Mariana N Rincón-Sánchez, Faculty of Medicine "Dr. Jose Sierra Flores," Northeastern University, Tampico 89337, Tamaulipas, Mexico

Mariana M Ramírez-Mejía, Plan of Combined Studies in Medicine, Faculty of Medicine, National Autonomous University of Mexico, Mexico City 04360, Mexico

Mariana M Ramírez-Mejía, Nahum Méndez-Sánchez, Liver Research Unit, Medica Sur Clinic and Foundation, Mexico City 14050, Mexico

Corresponding author: Nahum Méndez-Sánchez, Liver Research Unit, Medica Sur Clinic and Foundation, Puente de Piedra 150, Col. Toriello Guerra, Mexico City 14050, Mexico and Faculty of Medicine, National Autonomous University of Mexico, Mexico City 04360, Mexico. nmendez@medicasur.org.mx

Abstract

We read with great interest the study by Huang *et al*. Cholangiocarcinoma (CC) is the second most common type of primary liver tumor worldwide. Although surgical resection remains the primary treatment for this disease, almost 50% of patients experience relapse within 2 years after surgery, which negatively affects their prognosis. Key predictors can be used to identify several factors (*e.g.*, tumor size, tumor location, tumor stage, nerve invasion, the presence of intravascular emboli) and their correlations with long-term survival and the risk of posto-perative morbidity. In recent years, artificial intelligence (AI) has become a new tool for prognostic assessment through the integration of multiple clinical, surgical, and imaging parameters. However, a crucial question has arisen: Are we ready to trust AI with respect to clinical decisions? The study by Huang *et al* demonstrated that AI can predict preoperative textbook outcomes in patients with CC and highlighted the precision of machine learning algorithms using useful prognostic factors. This letter to the editor aimed to explore the challenges and potential impact of AI and machine learning in the prognostic assessment of patients with CC.

Key Words: Cholangiocarcinoma; Artificial intelligence; Liver tumor; Prognosis; Survival

Core Tip: Machine learning-driven preoperative risk stratification enhances surgical planning in intrahepatic cholangiocarcinoma. Huang *et al* demonstrated that the concept of the textbook outcome can be predicted preoperatively using artificial intelligence models, which outperform traditional prognostic methods. Their study underscored the importance of dynamic, data-driven approaches for improving disease-free survival and optimizing patient selection for curative resection.

Citation: Morales-Galicia AE, Rincón-Sánchez MN, Ramírez-Mejía MM, Méndez-Sánchez N. Outcome prediction for cholangiocarcinoma prognosis: Embracing the machine learning era. *World J Gastroenterol* 2025; 31(21): 106808
URL: https://www.wjgnet.com/1007-9327/full/v31/i21/106808.htm
DOI: https://dx.doi.org/10.3748/wjg.v31.i21.106808

TO THE EDITOR

Cholangiocarcinoma is a highly malignant and heterogeneous biliary tract cancer classified into intrahepatic, perihilar, and extrahepatic subtypes[1]. Among these, intrahepatic cholangiocarcinoma (ICC) is the second most common primary liver malignancy, accounting for 10%-15% of all primary liver cancers. Its incidence has been rising globally, particularly in regions with high HBV and hepatitis C virus prevalence, reflecting an increasing public health burden[2].

Despite advances in surgical and oncological care, ICC remains a challenging disease due to late-stage diagnosis and high recurrence rates. Surgical resection is the only curative option, yet long-term survival outcomes remain poor, with 5-year survival rates ranging between 20% and 40%. Even after curative-intent surgery, recurrence rates exceed 50% within 2 years, underscoring the need for improved preoperative risk stratification and outcome prediction[3]. Risk factors, which are conditions or exposures that increase the likelihood of developing ICC, include chronic liver disease, cirrhosis, primary sclerosing cholangitis, and liver fluke infections. These factors contribute to chronic inflammation, fibrosis, and malignant transformation of biliary epithelial cells and further complicate disease management[4,5].

One of the most critical challenges in ICC is the unpredictability of surgical outcomes, even when patients meet the criteria for resection[6]. Surgery remains the only curative therapeutic option for ICC, offering the best opportunity of prolonged survival by removing the main tumor and reducing the overall tumor burden[7]. Nevertheless, only a minority of patients are eligible for surgery because of the high frequency of advanced-stage disease at diagnosis and tumor unresectability at presentation. Achieving complete resection (R0) is crucial as it significantly improves disease-free survival (DFS) and overall survival, and thus surgical intervention is a cornerstone of ICC management[6].

Traditionally, oncological success has been evaluated according to metrics such as margin status and lymph node involvement[8]. Nonetheless, the concept of textbook outcome (TO), which incorporates multiple perioperative success indicators, has gained traction as a more holistic measure of surgical quality[9]. In their study, Huang *et al*[10] proposed that TO can be predicted preoperatively using machine learning (ML). This represents a paradigm shift in surgical planning.

To develop their model, they retrospectively analyzed 376 patients with ICC from four major medical institutions in China (2011–2017). Logistic regression identified key preoperative variables associated with TO, which were then used to construct an Extreme Gradient Boosting (XGBoost) model. To enhance interpretability, they applied the SHapley Additive exPlanations (SHAP) algorithm to visualize the contribution of each variable to the predictions of the model. The XGBoost package in R was used to build the prediction model, with 70% of the data randomly assigned to the training set and 30% to the validation set. The model was constructed using variables identified through logistic regression, such as Child-Pugh grade, Eastern Cooperative Oncology Group (ECOG) score, HBV status, and tumor size. The XGBoost model demonstrated strong predictive performance, yielding an area under the curve of 0.882 in the training group and 0.834 in the validation group, indicating high accuracy and robustness. Additionally, a Kaplan-Meier survival analysis was performed to compare the DFS between the TO-achieving and non-TO-achieving groups, highlighting the clinical relevance of the model in stratifying long-term outcomes (Figure 1).

The integration of artificial intelligence (AI) and ML in predictive oncology has transformed the landscape of clinical decision-making, surpassing traditional statistical methods by leveraging multidimensional datasets (Table 1). Unlike conventional prognostic models that rely on fixed clinical and pathological variables, ML algorithms process vast amounts of data, recognize intricate patterns, and dynamically adapt to patient-specific factors. These capabilities enhance risk stratification, surgical planning, and treatment optimization, making AI-driven models particularly valuable in refining preoperative assessments for ICC.

Several ML-driven approaches utilize diverse data sources, such as imaging, histopathological features, molecular markers, and electronic health records, to improve prognostic accuracy[9]. In this context, the model created by Huang *et al*[10] represents a significant advancement in AI-driven risk stratification for patients with ICC, demonstrating a high degree of predictive accuracy and clinical utility. Incorporating AI-driven decision support systems into surgical planning frameworks could further enhance predictive accuracy and clinical decision-making[11].

As AI and ML continue to evolve, their role in oncology will likely expand, shaping the future of precision medicine and personalized patient care. ML-driven approaches have already demonstrated potential in various domains, including early cancer detection, recurrence prediction, and treatment response monitoring[9]. The study by Huang *et al*[10] exemplified how ML can improve preoperative risk stratification for patients with ICC, setting the stage for further exploration and refinement of AI-assisted surgical planning. Future research should prioritize prospective validation,

Table 1 Machine learning approaches for preoperative risk stratification in intrahepatic cholangiocarcinoma

ML-driven approach	Description
Radiomics-based ML models	Extract imaging features from magnetic resonance or CT scans to predict tumor aggressiveness and microvascular invasion
Multiparametric clinical models	Integrate laboratory values, liver function scores, and tumor markers to assess perioperative risk
Hybrid AI models	Combine genomic, histopathological, and radiomic data to refine survival predictions and guide personalized treatment strategies

AI: Artificial intelligence; ML: Machine learning.

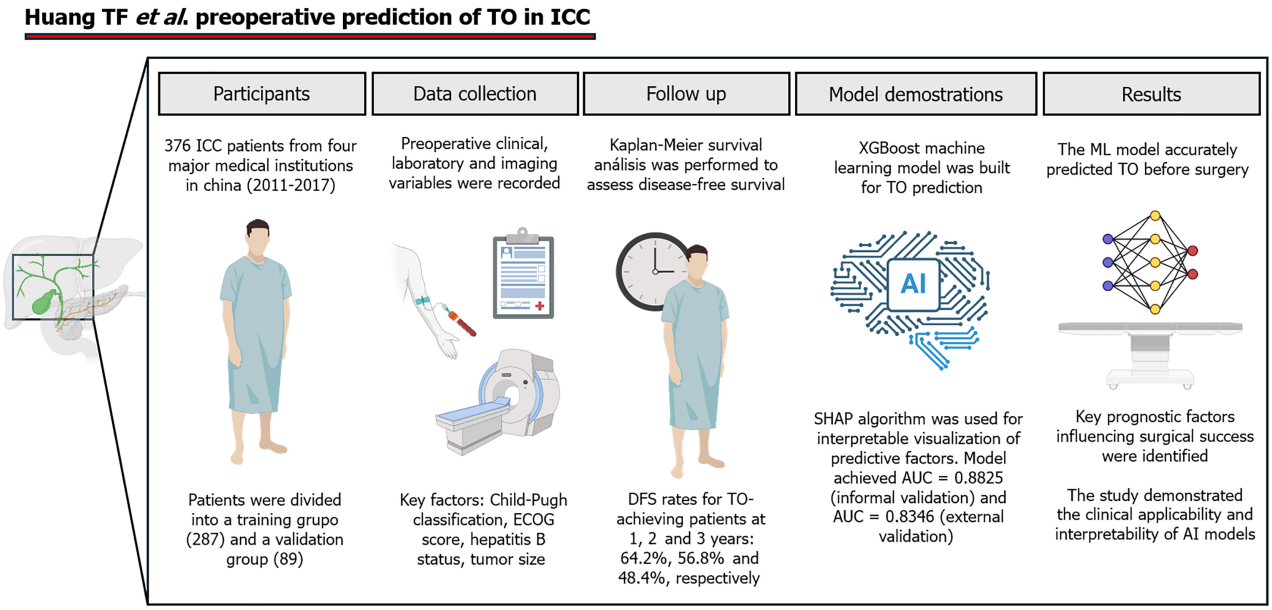

Figure 1 Machine learning for preoperative textbook outcome prediction in intrahepatic cholangiocarcinoma. Schematic representation of the study methodology, with details of participant selection, the data collection process, patient follow-up, development and demonstration of the machine learning model, and key findings. This study retrospectively analyzed a multicenter cohort of patients with intrahepatic cholangiocarcinoma and incorporated a comprehensive set of preoperative clinical, laboratory, and imaging variables. The machine learning model, constructed using Extreme Gradient Boosting, identified the Child-Pugh classification, Eastern Cooperative Oncology Group score, HBV status, and tumor size as the most influential predictors of textbook outcome. The application of SHapley Additive exPlanations provided enhanced interpretability, allowing for transparent risk stratification and clinical decision-making. The model demonstrated high predictive accuracy and achieved strong performance in both internal and external validation, which reinforced its potential as a valuable tool for improving surgical planning and optimizing patient outcomes in intrahepatic cholangiocarcinoma management[10]. AI: Artificial intelligence; DFS: Disease-free survival; TO: Textbook outcome; SHAP: SHapley Additive exPlanations; AUC: Area under the curve; ICC: Intrahepatic cholangiocarcinoma; XGBoost: Extreme Gradient Boosting; ML: Machine learning; ECOG: Eastern Cooperative Oncology Group.

integration with clinical decision-support systems, and continuous learning through real-time data incorporation to maximize the potential of AI in ICC management. This letter to the editor aimed to critically analyze the implications of AI-driven prognostic models in ICC, highlighting both their potential and the challenges that must be overcome for successful clinical integration.

CURRENT CHALLENGES IN CHOLANGIOCARCINOMA PROGNOSIS

One of the greatest challenges in the management of ICC is its high recurrence rate, which significantly affects long-term survival. Although surgical resection is the sole curative approach, more than 50% of patients develop recurrence within 2 years, even after R0 resection[2]. Factors that contribute to recurrence include tumor aggressiveness, microscopic residual disease, and the lack of effective adjuvant therapies[12]. Huang *et al*[10] emphasized that achieving a TO is strongly linked to better DFS as their study revealed that patients who met the TO criteria had significantly greater DFS rates at 1 year, 2 years, and 3 years. These findings underscore the need for early identification of high-risk patients and personalized perioperative strategies to reduce the risk of recurrence. Nevertheless, traditional preoperative risk stratification models remain limited as they rely on tumor size, nodal involvement, and margin status and fail to capture the complex biological behavior of ICC[9]. In response to these challenges Huang *et al*[10] proposed ML-based models as a

more accurate, data-driven alternative as they integrate multiple dynamic factors to improve perioperative predictions.

Tumor characteristics, histopathological features, and surgical parameters are key prognostic factors in ICC. Larger tumors (> 5 cm) are associated with higher recurrence rates and worse survival as they are more likely to invade vascular structures and lymph nodes[9]. Additionally, centrally located tumors pose greater surgical challenges and increase the risk of positive margins and postoperative liver failure[9]. Huang *et al*[10] confirmed that tumor size is one of the strongest predictors of TO, and larger tumors are significantly less likely to meet TO criteria. This observation reinforces the importance of early detection and aggressive management, including neoadjuvant therapies and meticulous surgical planning.

Histopathological factors such as perineural invasion and intravascular emboli further contribute to early recurrence and poor survival, but traditional prognostic models fail to integrate these microscopic tumor characteristics preoperatively[12]. The ML model developed by Huang *et al*[10] addressed this limitation and incorporated preoperative variables that are indirectly correlated with tumor aggressiveness.

Still, concerns remain regarding the interpretability of ML predictions as complex models often function as "black boxes", making it difficult for clinicians to understand how specific features contribute to outcomes. Techniques such as SHAP have been implemented to enhance model transparency, fostering clinical trust and supporting decision-making. SHAP is based on game theory and explains model predictions by quantifying the contribution of each feature. Other interpretability methods, such as LIME, counterfactual explanations, and saliency maps, also help make complex models more understandable, which is essential in clinical contexts where transparency is key to adoption.

Surgical and perioperative factors also play crucial roles in ICC prognosis. Achieving R0 resection is associated with significant improvements in survival, yet approximately 20% of patients with ICC have positive surgical margins due to the proximity of the tumor to vascular structure[9,10]. Postoperative complications, such as bile leakage and liver failure, further impact overall survival and recurrence rates[12]. Huang *et al*[10] proposed that TO should be used as a benchmark for surgical quality as their study revealed that patients with prolonged hospitalization and perioperative complications were less likely to achieve a TO. This reinforced the need for optimized perioperative care and enhanced recovery protocols. Their ML model accurately predicted TO in high-risk patients and offered opportunities for preoperative optimization to improve surgical outcomes.

Traditional ICC prognostic models have several limitations. First, they lack real-time predictive power as most are retrospective and cannot dynamically adjust to new patient-specific variables[9]. Second, they fail to capture multidimensional interactions since traditional tools do not account for the relationships among clinical, radiological, and molecular factors and limits their predictive accuracy[9,10]. Third, their generalizability is restricted as many scoring systems are developed from single-institution datasets, which reduces their applicability to broader patient populations. Additionally, AI models must address ethical concerns and the possibility of algorithmic errors that could influence high-impact clinical decisions. Regulatory approvals and physician training also represent critical barriers to widespread AI adoption in oncology[11].

Huang *et al*[10] challenged the validity of these conventional models by demonstrating the superiority of ML-based predictions. Their study revealed that ML models that integrate multiple preoperative factors (Child-Pugh classification, ECOG score, HBV status, and tumor size) were significantly more accurate than traditional statistical models in predicting TO. These findings highlighted the need for a paradigm shift in ICC prognostication, with a transition toward AI-enhanced risk assessment frameworks that offer greater predictive accuracy and individualized patient care. Moreover, comparisons with other hepatobiliary malignancies, such as hepatocellular carcinoma and pancreatic cancer, suggest that AI-driven prognostic applications may have broader implications in oncological risk assessment.

THE ROLE OF ML IN PROGNOSIS PREDICTION

ML has emerged as a transformative tool in predictive oncology, offering a data-driven approach to risk stratification and outcome prediction. Unlike traditional statistical models, ML algorithms can process vast amounts of multidimensional data, recognize complex patterns, and provide more precise risk estimations[9]. In ICC ML has the potential to revolutionize preoperative risk assessment by integrating clinical, radiological, and molecular parameters to predict surgical success, recurrence risk, and long-term survival[13]. Additionally, its ability to detect nonlinear relationships between prognostic factors allows for a more nuanced analysis compared with conventional regression models, uncovering subtle interactions that might otherwise be overlooked[14].

A comparable application of ML in oncology risk prediction was demonstrated in the study by Ke *et al*[15], who developed an ML-based model to predict early gastric cancer risk using a large-scale, population-based retrospective dataset. Their methodology integrated demographic, clinical, and biochemical variables to enhance early detection and stratification of high-risk individuals, which improved screening efficiency. Similar to the study by Huang *et al*[10] on ICC, Ke *et al*[15] emphasized the importance of ML-driven risk assessment, yet their focus was on early disease identification rather than surgical outcome prediction. Both studies highlighted the predictive power of ML algorithms. Huang *et al*[10] applied their model to perioperative decision-making, whereas Ke *et al*[15] used ML for preventive screening. These findings reinforce the versatility of AI in oncology and demonstrate its role not only in preoperative optimization but also in early cancer detection, which could be further refined with external validation and multicenter studies.

A similar approach has been explored for breast cancer prognosis and treatment outcome prediction as demonstrated by Zhang *et al*[16]. Their study applied ML models to multiomics data to enhance breast cancer survival predictions and integrated genomic, transcriptomic, and clinical variables for a more comprehensive prognostic assessment. While their findings highlight the potential of AI-driven models in oncology, challenges such as model generalizability, data bias,

and the need for external validation remain comparable with those discussed in ICC prognosis. Unlike the study by Huang *et al*[10], which focused on preoperative risk stratification using clinical and radiological data, Zhang *et al*[16] incorporated multiomics analysis and underscored how AI can adapt to different cancer types and datasets. This comparison emphasizes the growing applicability of AI in personalized oncology but reinforces the need for continued validation and refinement to ensure clinical reliability across various malignancies.

CHALLENGES AND CONSIDERATIONS IN AI ADOPTION

The integration of AI in medicine presents several challenges that must be addressed to ensure its effective and ethical implementation. One major concern is the complexity of AI algorithms, particularly deep learning models, which can obscure the decision-making process, raising transparency and reliability issues.

Trusting and effectively using AI in patient care depends on two key elements: Knowledge and experience. The more data and clinical exposure available, the better equipped health care professionals are to make informed decisions. Data are derived from evidence-based sources such as textbooks and peer-reviewed studies, whereas experience is gained through real-world patient outcomes, including medical records, lab results, and imaging[17-19]. The potential for bias in training data further complicates equitable treatment outcomes. To mitigate these risks, legal frameworks must define liability when AI-driven recommendations result in adverse outcomes[20].

Despite its potential, AI should complement rather than replace clinical expertise. Clinicians must oversee and interpret AI-generated recommendations, ensuring that they align with individual patient needs. AI integration should support, rather than hinder, clinical workflows and should enhance decision-making rather than dictate it[21]. The "black box" nature of many AI algorithms has raised concerns about transparency and clinical trust, prompting the use of explainable AI techniques, such as SHAP, that enhances model transparency by quantifying the contribution of each input feature to a given prediction, facilitating clinician understanding and supporting informed decision-making. Other interpretability methods like LIME, counterfactual explanations, and saliency maps also contribute to making AI outputs more accessible and trustworthy in clinical contexts.

A major limitation of current ML models lies in their generalizability. While retrospective studies offer valuable insights, external validation in independent cohorts, especially those representing different geographic and ethnic backgrounds, is essential to confirm the robustness and real-world applicability of these models. Without rigorous validation AI models risk producing biased or inaccurate outcomes, particularly for underrepresented populations[22]. Moreover, biases introduced by region-specific datasets can compromise the performance and fairness of AI-driven predictions in broader clinical applications.

Ethical and legal considerations are central to the safe implementation of AI in oncology. Issues such as algorithmic fairness, accountability, and the potential for AI-induced diagnostic errors must be rigorously evaluated to ensure responsible use in high-stakes clinical decision-making. Addressing these concerns is essential to promote trust, minimize harm, and uphold patient rights within an evolving technological landscape[23].

FUTURE DIRECTIONS AND CLINICAL INTEGRATION

AI technologies, particularly ML, are continuously advancing surgical practices by reducing errors, improving outcomes, and optimizing minimally invasive techniques that shorten hospital stays and lower complication rates[24]. Postoperative care also benefits from AI-driven predictive analytics, which anticipate potential complications or readmissions, enabling proactive interventions and personalized treatment adjustments[25].

A key advantage of AI is its role in risk stratification, leveraging large datasets from electronic health records, genetic information, and imaging to precisely identify high-risk patients. This allows multidisciplinary teams to tailor interventions and allocate resources efficiently, particularly in complex diseases such as cancer where personalized care is essential[26]. ML-based models have demonstrated their ability to predict lymph node metastasis in early-stage colorectal cancer, refining patient selection for more aggressive treatment strategies[27]. Similarly, ML algorithms using liver stiffness measurements show promise in predicting hepatocellular carcinoma risk, offering etiology-independent assessments that could be adapted for ICC surveillance[28]. AI also enhances disease progression prediction and treatment outcome forecasting, ensuring that high-risk patients receive prioritized attention[20].

To fully realize these benefits, ongoing efforts must focus on expanding and diversifying datasets to improve model generalizability and reduce bias. Large-scale, multi-institutional collaborations are necessary to develop more representative training datasets that capture variations in demographics, tumor biology, and treatment responses[18]. Additionally, real-world validation through prospective clinical trials is critical to confirm AI model performance outside of controlled settings. Establishing standardized evaluation frameworks will facilitate objective comparisons between AI tools, ensuring consistency across institutions[27]. Pilot testing and continuous monitoring must be integrated into clinical workflows, allowing AI systems to adapt to new data and evolving medical practices while maintaining safety and efficacy.

Huang *et al*[10] exemplified how ML-driven decision-making influences ICC management, particularly in preoperative TO prediction. Their model integrated tumor size, Child-Pugh classification, ECOG score, and HBV status to enhance risk assessment and surgical planning, demonstrating higher accuracy than conventional prognostic tools. By incorporating SHAP analysis, their AI-driven approach provided transparent and interpretable predictions, addressing a major barrier to AI adoption. This study underscored the potential of AI in refining surgical decision-making and optimizing patient

selection for resection, highlighting its clinical relevance in hepatobiliary oncology.

Successful AI implementation also requires structured clinician involvement throughout model development and validation. Engaging medical professionals in AI training processes and decision support system design ensures that models align with real-world clinical workflows. Interdisciplinary collaboration between data scientists, bioinformaticians, and clinicians is essential to refine algorithms based on expert input. The integration of dual safety mechanisms where AI provides insights but final decisions remain physician-led can help bridge the trust gap and facilitate seamless AI adoption in daily medical practice. Finally, regulatory frameworks should be updated to establish guidelines for AI integration, ensuring both patient safety and ethical accountability in AI-driven clinical decision-making[29].

CONCLUSION

The integration of AI and ML in ICC prognosis and management represents a significant advancement in oncological decision-making. Huang *et al*[10] demonstrated that ML-based models outperformed traditional prognostic tools, offering more precise and individualized risk stratification. Their findings confirmed the feasibility and clinical relevance of preoperative TO prediction, with direct implications for optimizing surgical candidacy and improving long-term outcomes. While their model exhibited strong predictive performance, its generalizability remains a key concern. Future efforts should prioritize diverse, multi-institutional data and real-world validation to enhance AI model reliability and clinical relevance. Interdisciplinary collaboration and updated regulatory frameworks are essential to ensure ethical deployment and meaningful integration into ICC care.

FOOTNOTES

Author contributions: Méndez-Sánchez N, Morales-Galicia AE, Rincon-Sanchez MN, and Ramírez-Mejía MM contributed to this paper; Méndez-Sánchez N designed the overall concept and outline of the manuscript; Morales-Galicia AE and Ramírez-Mejía MM contributed to the discussion and design of the manuscript; Méndez-Sánchez N, Morales-Galicia AE, Rincon-Sanchez MN, and Ramírez-Mejía MM contributed to the writing and editing of the manuscript, illustrations, and literature review.

Conflict-of-interest statement: All authors declare that they have no competing interests.

Country of origin: Mexico

ORCID number: Arnulfo E Morales-Galicia 0000-0003-2458-3573; Mariana M Ramírez-Mejía 0009-0005-6279-1527; Nahum Méndez-Sánchez 0000-0001-5257-8048.

S-Editor: Liu JH
L-Editor: Filipodia
P-Editor: Yu HG

REFERENCES

1 **Nathan H**, Pawlik TM, Wolfgang CL, Choti MA, Cameron JL, Schulick RD. Trends in survival after surgery for cholangiocarcinoma: a 30-year population-based SEER database analysis. *J Gastrointest Surg* 2007; **11**: 1488-96; discussion 1496 [PMID: 17805937 DOI: 10.1007/s11605-007-0282-0] [FullText]

2 **da Fonseca LG**, Izquierdo-Sanchez L, Hashizume PH, Carlino Y, Baca EL, Zambrano C, Sepúlveda SA, Bolomo A, Rodrigues PM, Riaño I, Boonstra A, Debes JD, Bujanda L, Carrilho FJ, Arrese M, Roa JC, Carrera E, Ferrer JD, Balderramo D, Oliveira CP, Banales JM. Cholangiocarcinoma in Latin America: a multicentre observational study alerts on ethnic disparities in tumour presentation and outcomes. *Lancet Reg Health Am* 2024; **40**: 100952 [PMID: 39655285 DOI: 10.1016/j.lana.2024.100952] [FullText]

3 **Saeed A**, Park R, Al-Jumayli M, Al-Rajabi R, Sun W. Biologics, Immunotherapy, and Future Directions in the Treatment of Advanced Cholangiocarcinoma. *Clin Colorectal Cancer* 2019; **18**: 81-90 [PMID: 30905548 DOI: 10.1016/j.clcc.2019.02.005] [FullText]

4 **Kelley RK**, Bridgewater J, Gores GJ, Zhu AX. Systemic therapies for intrahepatic cholangiocarcinoma. *J Hepatol* 2020; **72**: 353-363 [PMID: 31954497 DOI: 10.1016/j.jhep.2019.10.009] [FullText]

5 **Chinchilla-López P**, Aguilar-Olivos NE, García-Gómez J, Hernández-Alejandro KK, Chablé-Montero F, Motola-Kuba D, Patel T, Méndez-Sánchez N. Prevalence, Risk Factors, and Survival of Patients with Intrahepatic Cholangiocarcinoma. *Ann Hepatol* 2017; **16**: 565-568 [PMID: 28611259 DOI: 10.5604/01.3001.0010.0293] [FullText]

6 **Alaimo L**, Endo Y, Pawlik TM. ASO Author Reflections: Benchmarks in Liver Resection for Intrahepatic Cholangiocarcinoma. *Ann Surg Oncol* 2024; **31**: 4464-4465 [PMID: 38261125 DOI: 10.1245/s10434-024-14978-7] [FullText]

7 **Ruzzenente A**, Conci S, Valdegamberi A, Pedrazzani C, Guglielmi A. Role of surgery in the treatment of intrahepatic cholangiocarcinoma.

Eur Rev Med Pharmacol Sci 2015; **19**: 2892-2900 [PMID: 26241545] [FullText]

8 **de Jong MC**, Nathan H, Sotiropoulos GC, Paul A, Alexandrescu S, Marques H, Pulitano C, Barroso E, Clary BM, Aldrighetti L, Ferrone CR, Zhu AX, Bauer TW, Walters DM, Gamblin TC, Nguyen KT, Turley R, Popescu I, Hubert C, Meyer S, Schulick RD, Choti MA, Gigot JF, Mentha G, Pawlik TM. Intrahepatic cholangiocarcinoma: an international multi-institutional analysis of prognostic factors and lymph node assessment. *J Clin Oncol* 2011; **29**: 3140-3145 [PMID: 21730269 DOI: 10.1200/JCO.2011.35.6519] [FullText]

9 **Miao G**, Qian X, Zhang Y, Hou K, Wang F, Xuan H, Wu F, Zheng B, Yang C, Zeng M. An MRI-Based Radiomics Model for Preoperative Prediction of Microvascular Invasion and Outcome in Intrahepatic Cholangiocarcinoma. *Eur J Radiol* 2025; **183**: 111896 [PMID: 39732135 DOI: 10.1016/j.ejrad.2024.111896] [FullText]

10 **Huang TF**, Luo C, Guo LB, Liu HZ, Li JT, Lin QZ, Fan RL, Zhou WP, Li JD, Lin KC, Tang SC, Zeng YY. Preoperative prediction of textbook outcome in intrahepatic cholangiocarcinoma by interpretable machine learning: A multicenter cohort study. *World J Gastroenterol* 2025; **31**: 100911 [PMID: 40124276 DOI: 10.3748/wjg.v31.i11.100911] [FullText]

11 **Zhou SN**, Jv DW, Meng XF, Zhang JJ, Liu C, Wu ZY, Hong N, Lu YY, Zhang N. Feasibility of machine learning-based modeling and prediction using multiple centers data to assess intrahepatic cholangiocarcinoma outcomes. *Ann Med* 2023; **55**: 215-223 [PMID: 36576390 DOI: 10.1080/07853890.2022.2160008] [FullText]

12 **Xie H**, Hong T, Liu W, Jia X, Wang L, Zhang H, Xu C, Zhang X, Li WL, Wang Q, Yin C, Lv X. Interpretable machine learning-based clinical prediction model for predicting lymph node metastasis in patients with intrahepatic cholangiocarcinoma. *BMC Gastroenterol* 2024; **24**: 137 [PMID: 38641789 DOI: 10.1186/s12876-024-03223-w] [FullText]

13 **Meng A**, Zhuang Y, Huang Q, Tang L, Yang J, Gong P. Development and validation of a cross-modality tensor fusion model using multi-modality MRI radiomics features and clinical radiological characteristics for the prediction of microvascular invasion in hepatocellular carcinoma. *Eur J Surg Oncol* 2025; **51**: 109364 [PMID: 39536525 DOI: 10.1016/j.ejso.2024.109364] [FullText]

14 **Mi S**, Qiu G, Zhang Z, Jin Z, Xie Q, Hou Z, Ji J, Huang J. Development and validation of a machine-learning model to predict lymph node metastasis of intrahepatic cholangiocarcinoma: A retrospective cohort study. *Biosci Trends* 2025; **18**: 535-544 [PMID: 39631884 DOI: 10.5582/bst.2024.01282] [FullText]

15 **Ke X**, Cai X, Bian B, Shen Y, Zhou Y, Liu W, Wang X, Shen L, Yang J. Predicting early gastric cancer risk using machine learning: A population-based retrospective study. *Digit Health* 2024; **10**: 20552076241240905 [PMID: 38559579 DOI: 10.1177/20552076241240905] [FullText]

16 **Zhang ZY**, Wang QL, Zhang JY, Duan YY, Liu JX, Liu ZS, Li CY. Machine learning applications in breast cancer survival and therapeutic outcome prediction based on multi-omic analysis. *Yi Chuan* 2024; **46**: 820-832 [PMID: 39443311 DOI: 10.16288/j.yczz.24-156] [FullText]

17 **Mintz Y**, Brodie R. Introduction to artificial intelligence in medicine. *Minim Invasive Ther Allied Technol* 2019; **28**: 73-81 [PMID: 30810430 DOI: 10.1080/13645706.2019.1575882] [FullText]

18 **Sinz FH**, Pitkow X, Reimer J, Bethge M, Tolias AS. Engineering a Less Artificial Intelligence. *Neuron* 2019; **103**: 967-979 [PMID: 31557461 DOI: 10.1016/j.neuron.2019.08.034] [FullText]

19 **Choi RY**, Coyner AS, Kalpathy-Cramer J, Chiang MF, Campbell JP. Introduction to Machine Learning, Neural Networks, and Deep Learning. *Transl Vis Sci Technol* 2020; **9**: 14 [PMID: 32704420 DOI: 10.1167/tvst.9.2.14] [FullText]

20 **Keskinbora KH**. Medical ethics considerations on artificial intelligence. *J Clin Neurosci* 2019; **64**: 277-282 [PMID: 30878282 DOI: 10.1016/j.jocn.2019.03.001] [FullText]

21 **Liyanage H**, Liaw ST, Jonnagaddala J, Schreiber R, Kuziemsky C, Terry AL, de Lusignan S. Artificial Intelligence in Primary Health Care: Perceptions, Issues, and Challenges. *Yearb Med Inform* 2019; **28**: 41-46 [PMID: 31022751 DOI: 10.1055/s-0039-1677901] [FullText]

22 **Howard J**. Artificial intelligence: Implications for the future of work. *Am J Ind Med* 2019; **62**: 917-926 [PMID: 31436850 DOI: 10.1002/ajim.23037] [FullText]

23 **Hamet P**, Tremblay J. Artificial intelligence in medicine. *Metabolism* 2017; **69S**: S36-S40 [PMID: 28126242 DOI: 10.1016/j.metabol.2017.01.011] [FullText]

24 **Chen M**, Decary M. Artificial intelligence in healthcare: An essential guide for health leaders. *Healthc Manage Forum* 2020; **33**: 10-18 [PMID: 31550922 DOI: 10.1177/0840470419873123] [FullText]

25 **Gumbs AA**, Frigerio I, Spolverato G, Croner R, Illanes A, Chouillard E, Elyan E. Artificial Intelligence Surgery: How Do We Get to Autonomous Actions in Surgery? *Sensors (Basel)* 2021; **21** [PMID: 34450976 DOI: 10.3390/s21165526] [FullText]

26 **Zhou LQ**, Wang JY, Yu SY, Wu GG, Wei Q, Deng YB, Wu XL, Cui XW, Dietrich CF. Artificial intelligence in medical imaging of the liver. *World J Gastroenterol* 2019; **25**: 672-682 [PMID: 30783371 DOI: 10.3748/wjg.v25.i6.672] [FullText]

27 **Cheong C**, Kim NW, Lee HS, Kang J. Application of machine learning for predicting lymph node metastasis in T1 colorectal cancer: a systematic review and meta-analysis. *Langenbecks Arch Surg* 2024; **409**: 287 [PMID: 39311932 DOI: 10.1007/s00423-024-03476-9] [FullText]

28 **Lin H**, Li G, Delamarre A, Ahn SH, Zhang X, Kim BK, Liang LY, Lee HW, Wong GL, Yuen PC, Chan HL, Chan SL, Wong VW, de Lédinghen V, Kim SU, Yip TC. A Liver Stiffness-Based Etiology-Independent Machine Learning Algorithm to Predict Hepatocellular Carcinoma. *Clin Gastroenterol Hepatol* 2024; **22**: 602-610.e7 [PMID: 37993034 DOI: 10.1016/j.cgh.2023.11.005] [FullText]

29 **Whicher D**, Rapp T. The Value of Artificial Intelligence for Healthcare Decision Making-Lessons Learned. *Value Health* 2022; **25**: 328-330 [PMID: 35227442 DOI: 10.1016/j.jval.2021.12.009] [FullText]

Published by **Baishideng Publishing Group Inc**
7041 Koll Center Parkway, Suite 160, Pleasanton, CA 94566, USA
Telephone: +1-925-3991568
E-mail: office@baishideng.com
Help Desk: https://www.f6publishing.com/helpdesk
https://www.wjgnet.com